United States
Environmental Protection
Agency

Industrial Environmental Research
Laboratory
Research Triangle Park NC 27711

EPA-600 9-80-039d
September 1980

Research and Development

EPA

Second Symposium on the Transfer and Utilization of Particulate Control Technology

Volume IV. Special Applications for Air Pollution Measurement and Control

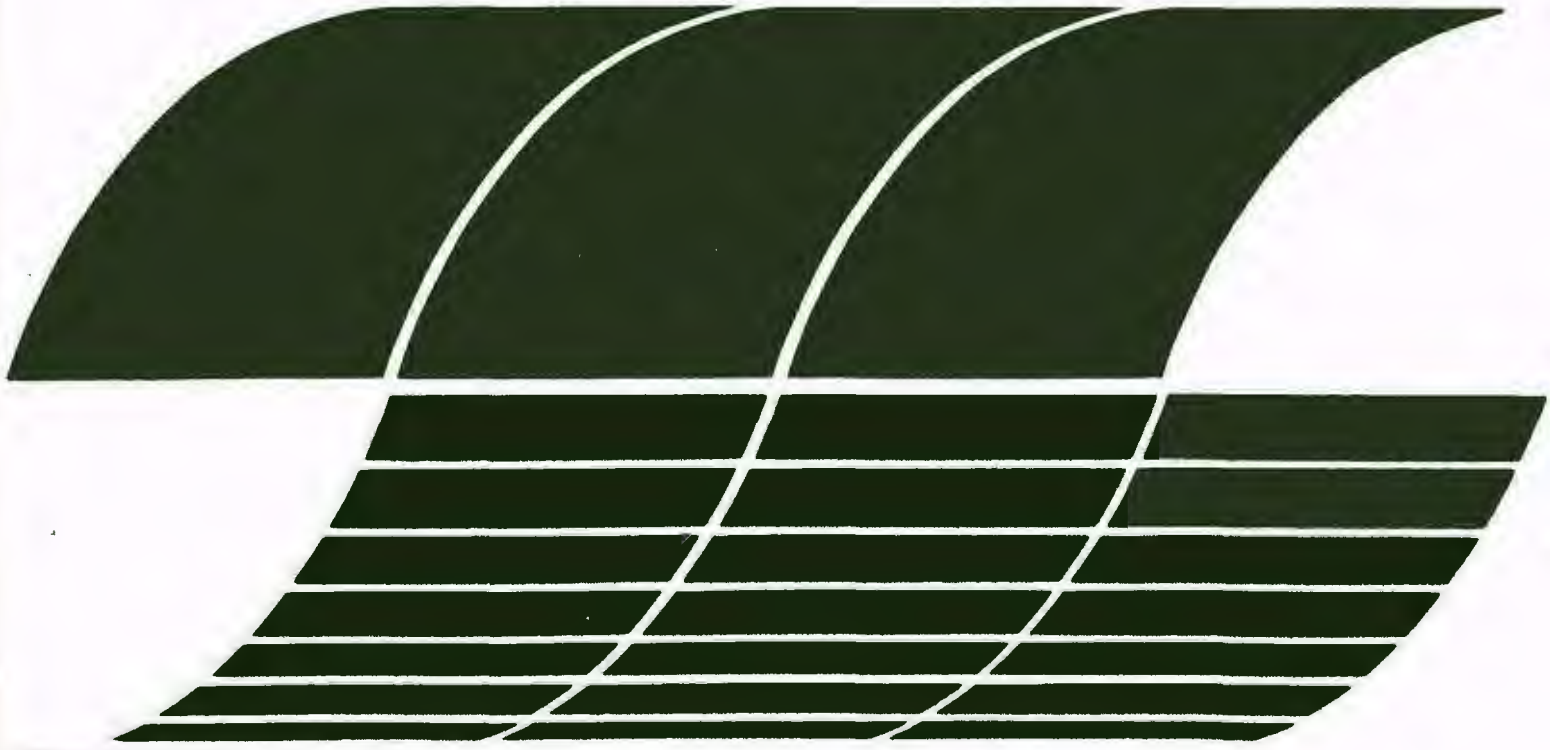

RESEARCH REPORTING SERIES

Research reports of the Office of Research and Development, U.S. Environmental Protection Agency, have been grouped into nine series. These nine broad categories were established to facilitate further development and application of environmental technology. Elimination of traditional grouping was consciously planned to foster technology transfer and a maximum interface in related fields. The nine series are:

1. Environmental Health Effects Research
2. Environmental Protection Technology
3. Ecological Research
4. Environmental Monitoring
5. Socioeconomic Environmental Studies
6. Scientific and Technical Assessment Reports (STAR)
7. Interagency Energy-Environment Research and Development
8. "Special" Reports
9. Miscellaneous Reports

This document is available to the public through the National Technical Information Service, Springfield, Virginia 22161.

EPA-600/9-80-039d
September 1980

SECOND SYMPOSIUM ON THE TRANSFER AND UTILIZATION OF PARTICULATE CONTROL TECHNOLOGY
VOLUME IV. SPECIAL APPLICATIONS FOR AIR POLLUTION MEASUREMENT AND CONTROL

by

F.P. Venditti, J.A. Armstrong, and Michael Durham

Denver Research Institute
P.O. Box 10127
Denver, Colorado 80210

Grant Number: R805725

Project Officer

Dennis C. Drehmel
Office of Energy, Minerals, and Industry
Industrial Environmental Research Laboratory
Research Triangle Park, NC 27711

INDUSTRIAL ENVIRONMENTAL RESEARCH LABORATORY
OFFICE OF RESEARCH AND DEVELOPMENT
U.S. ENVIRONMENTAL PROTECTION AGENCY
RESEARCH TRIANGLE PARK, NC 27711

DISCLAIMER

This report has been reviewed by the Industrial Environmental Research Laboratory-Research Triangle Park, North Carolina, Office of Research and Development, U.S. Environmental Protection Agency, and approved for publication. Approval does not signify that the contents necessarily reflect the views and policies of the U.S. Environmental Protection Agency, nor does mention of trade names or commercial products constitute endorsement or recommendation for use.

ABSTRACT

The papers in these four volumes of Proceedings were presented at the Second Symposium on the Transfer and Utilization of Particulate Control Technology held in Denver, Colorado during 23 July through 27 July 1979, sponsored by the Particulate Technology Branch of the Industrial Environmental Research Laboratory of the Environmental Protection Agency and hosted by the Denver Research Institute of the University of Denver.

The purpose of the symposium was to bring together researchers, manufacturers, users, government agencies, educators and students to discuss new technology and to provide an effective means for the transfer of this technology out of the laboratories and into the hands of the users.

The three major categories of control technologies - electrostatic precipitators, scrubbers, and fabric filters - were the major concern of the symposium. These technologies were discussed from the perspectives of economics; new technical advancements in science and engineering; and applications. Several papers dealt with combinations of devices and technologies, leading to a concept of using a systems approach to particulate control rather than device control. Additional topic areas included novel control devices, high temperature/high pressure applications, fugitive emissions, and measurement techniques.

These proceedings are divided into four volumes, each volume containing a set of related session topics to provide easy access to a unified technology area.

CONTENTS

Section B - Fugitive Emissions

Section C - Measurement and Analysis

VOLUME I

CONTROL OF EMISSIONS FROM COAL FIRED BOILERS

Section A - Electrostatic Precipitators

Section B - Fabric Filters

VOLUME II

ELECTROSTATIC PRECIPITATORS

Section A - Fundamentals

Section B - Operation and Maintenance

VOLUME II CONTENTS (Cont.)

Section B - Advanced Design

VOLUME II CONTENTS (Cont.)

VOLUME III

PARTICULATE CONTROL DEVICES

Section A - Scrubbers

Section B - Fabric Filters

Section C - Granular Beds

FUNDAMENTAL PARTICLE COLLECTION AT HIGH TEMPERATURE AND PRESSURE

by

Richard Parker and Seymour Calvert
Air Pollution Technology, Inc.
San Diego, California

Dennis C. Drehmel and James H. Abbott
U.S. Environmental Protection Agency
Industrial Environmental Research Laboratory
Research Triangle Park, North Carolina

ABSTRACT

High temperatures and pressures affect the physical mechanisms by which particles are removed from gas streams. In general, particles larger than a few tenths of a micrometer in diameter appear to be more difficult to collect at high temperature and pressure than at standard conditions. This prediction has been evaluated in a U.S. EPA-sponsored research project to obtain experimental data on the effects of high temperature and pressure on the collection mechanisms of inertial impaction, Brownian diffusion, and electrical migration. The results from the inertial impaction tests are presented here.

FUNDAMENTAL PARTICLE COLLECTION AT HIGH TEMPERATURE AND PRESSURE

INTRODUCTION

When designing, troubleshooting, or evaluating the performance of particulate control equipment, it is important to have a firm understanding of the physical mechanisms by which the particles are removed from the gas stream. This is especially true when the control device is to be used at high temperature and pressure (HTP) where current design models are unproven. In order to provide a rational basis for dealing with HTP particulate control equipment, a sound theoretical understanding of the HTP effects on particle collection mechanisms is essential.

We have made a thorough examination of the literature concerned with HTP effects on particle collection (Calvert and Parker, 1977). Although HTP particle collection has been of interest for over 30 years, no fundamental evaluation of the theory has been attempted. In general, conventional models for particle collection (valid at low temperatures and pressures) have been extrapolated to predict performance in HTP situations. Insufficient performance data are available to evaluate these models at HTP conditions, especially as a function of particle size.

Theoretical considerations and uncertainties have been presented previously (Calvert and Parker, 1977; Parker, et al. 1979). In this paper we present the results of the experimental test program and compare them with theoretical predictions.

EXPERIMENTAL PROGRAM

Test Facility

An experimental program to study fundamental particle collection mechanisms at high temperature and pressure is underway at A.P.T., Inc. under EPA sponsorship. The experiments will investigate the collection mechanisms of inertial impaction, Brownian diffusion, electrical migration, and cyclone separation at temperatures up to 1100°C and pressures up to 15 atm. Particles in the general size range of 0.5 to 10 μm are being considered.

A special high temperature and pressure test facility has been designed and constructed. This facility was described in a previous paper (Parker, et al. 1977).

Inertial Impaction Tests

High temperature and pressure nitrogen loaded with fly ash is passed through a specially designed inertial impaction test section. The test section is illustrated in Figure 1. It is essentially a single stage impactor placed between two flanges.

Particles are collected on a ceramic fiber substrate which is used to minimize particle bounce at the impaction plate. The substrate is removed and weighed after each test in order to complete the mass balance of particles and to check the overall efficiency determined from the inlet and outlet samples.

Isokinetic samples are taken at the inlet and outlet of the test section. The samples are collected on filters which can be washed and analyzed for particles.

The filter samples are removed after each test and are analyzed using an electronic particle counter (Coulter Counter Model TA-II) to determine the mass and size distribution of the fly ash collected on each filter. The sample probes are cleaned after each test and analyzed to determine the amount and size of particles deposited in each probe.

The data obtained from analysis of the inlet and outlet samples are used to determine an experimental penetration curve. The penetration curve is used to determine an experimental cut diameter. Experiments can be run at temperatures ranging up to 1100°C and pressures up to 15 atm.

The average particle density has been determined by comparing the calibrated cut diameter with the cut diameter measured using fly ash at standard temperature and pressure. The impactor characteristic impaction parameter was determined experimentally in the laboratory and is assumed to be independent of temperature and pressure.

Results

The results of the inertial impaction tests are presented in Table 1 and Figure 2. Table 1 shows the ratio of experimental to predicted cut diameters for various temperatures and pressures. The mean ratio is very close to 1.0 and does not exhibit any clear trends with temperature and pressure for temperatures to 800°C and pressures to 15 atm.

There is a lot of scatter to the data as shown in Figure 2. This is a result of many difficulties encountered in doing inertial impaction experiments at high temperatures and pressures. The major problem was finding a substrate suited to high temperature applications. We tried bare metal and ceramic fiber substrates.

Bare metal substrates resulted in excessive particle bounce as indicated in the typical penetration curve shown as Figure 3. No useful cut diameter data were obtained with bare metal substrates operating at high temperature. Bare metal substrates worked satisfactorily at room temperature. Jet velocities for these experiments ranged from 900 to 1200 cm/s.

Fiberfrax grade 970-C ceramic paper (0.25 mm thick) was used as the standard substrate material. It was necessary to pretreat the substrates by baking for 30 minutes at 200°C. This treatment burns off the organic binder so that a stable substrate weight can be maintained for high temperature tests. One consequence of the pretreatment is that without the binder, the substrate tears very easily and is difficult to handle.

Useful data were obtained using the ceramic substrates although the results were not as reproducible as we would have liked. Some typical penetration curves for ceramic substrates are shown in Figures 4, 5, and 6. The shape of these curves compares very closely with the calibration curves we have obtained using glass fiber substrates in conventional cascade impactors.

Conclusions

We did not detect any significant deviation from theoretical predictions within the experimental limitations of our apparatus. The major uncertainty is the extent to which particles adhere to or bounce from the substrate as a function of temperature. Particle bounce may be an important contributing factor to the scatter of the data.

The results of this study indicate that conventional inertial impaction theory can be used for high temperature and pressure performance predictions without substantial error. Fine particle sizing devices which are based on inertial impaction should be accurate at high temperatures and pressures provided the logistical problems of substrates, materials, and pressure seals can be solved.

HIGH TEMPERATURE/HIGH PRESSURE CASCADE IMPACTOR

A.P.T. has designed, built, and tested a unique cascade impactor for use in high temperature and pressure (HTP) gas streams.

The basic configuration is shown in Figure 7. The outside casing is a pressure vessel fitted together with two large flanges and sealed by a metallic "E" seal. There are eleven interchangeable stages. Six stages and a final filter are used at any one time. The interchangeable stages enable operation at flow rates from 24 to 472 cm^3/s (0.05 to 1.0 acfm). The stages are carefully polished to provide good metal-to-metal seals. Stages must be cleaned and the sealing surfaces lapped after each high temperature test in order to maintain good seals.

Two prototype A.P.T. HTP cascade impactors were built and tested in the laboratory and in the field. They are made of type 316 stainless steel. The "E" seal is made of Inconel X-750.

The laboratory experiments indicated that the stainless steel began to scale at temperatures of 800°C and higher. Also, the ceramic paper substrates eroded on the lower stages and exhibited weight loss during test runs. The ceramic paper worked well on the upper stages and as the final filter. Measured size distributions were in good agreement with measurements made using a conventional in-stack cascade impactor.

Field tests were carried out at the Exxon miniplant pressurized fluidized bed combustor (PFBC) facility. The impactors were operated at approximately 600°C for seven runs over a 2 week period. The impactors were heated externally and held at temperature for approximately 2 hours each run. Actual sampling times lasted about 7 or 8 minutes. Bare metal Inconel 600 shim stock was used for the substrate material. Fiberfrax ceramic paper (double thickness) was used for the final filter.

The impactor performed excellently and consistently. Some minor leakage between stages occurred, and some scaling occurred on the last run. The scale was magnetic and easily removed from the substrate without disturbing the sample. The nature of the PFBC fly ash was such that it readily adhered to the bare substrates. Microscope and Coulter counter analyses of substrate deposits revealed no evidence that particle bouncing had occurred.

The performance of the HTP cascade impactor was excellent and further validated the results obtained in the HTP inertial impaction experiments. Further improvements will involve material selection and designing to minimize the time and effort required to turn around the impactor between tests. We are confident that we have developed a very useful and economical device for measuring particle and size and mass concentration in high temperature and pressure gas streams.

ACKNOWLEDGEMENT

This work has been sponsored by the U.S. Environmental Protection Agency under contracts 68-02-2137 and 68-02-2183.

REFERENCES

1. Calvert, S. and R.D. Parker. Effects of Temperature and Pressure on Particle Collection Mechanisms: Theoretical Review. Air Pollution Technology, Inc., EPA-600/7-77-002, NTIS No. PB 264-203. January, 1977.

2. Parker, R., S. Calvert and D. Drehmel. Fundamental Particle Collection at High Temperature and Pressure. Symposium on the Transfer and Utilization of Particulate Control Technology: Volume 3, p. 367. EPA-600/7-79-044c. NTIS No. PB 295-228, February, 1979.

3. Parker, R.D., S. Calvert and D.C. Drehmel. High Temperature and Pressure Effects on Particle Collection Mechanisms. In: Proceedings of the EPA/DOE Symposium on High Temperature/High Pressure Particulate Control. Washington D.C., EPA 600/9-78-004, CONF-770970, September 20-22, 1977.

TABLE 1. COMPARISON BETWEEN PREDICTED AND EXPERIMENTAL CUT DIAMETERS

No. Data Points	Temperature, °C	Pressure, atm	$d_{p50}(expt)/d_{p50}(pred.)$	
			mean	std. dev.
9	26-33	1.2-1.4	0.96	0.30
6	102-124	1.2-1.5	1.05	0.08
2	202-208	1.2-1.3	1.22	0.02
1	313	1.4	0.99	--
5	491-535	1.3-2.0	1.17	0.20
1	699	1.1	1.17	--
2	797-816	1.1-1.2	0.99	0.30
1	96	3.0	0.84	--
6	28-34	5.1	1.03	0.23
2	103-106	5.1	1.20	0.35
3	26-31	10.2	0.98	0.09
1	100	9.8	1.09	--
1	100	14.9	0.88	--

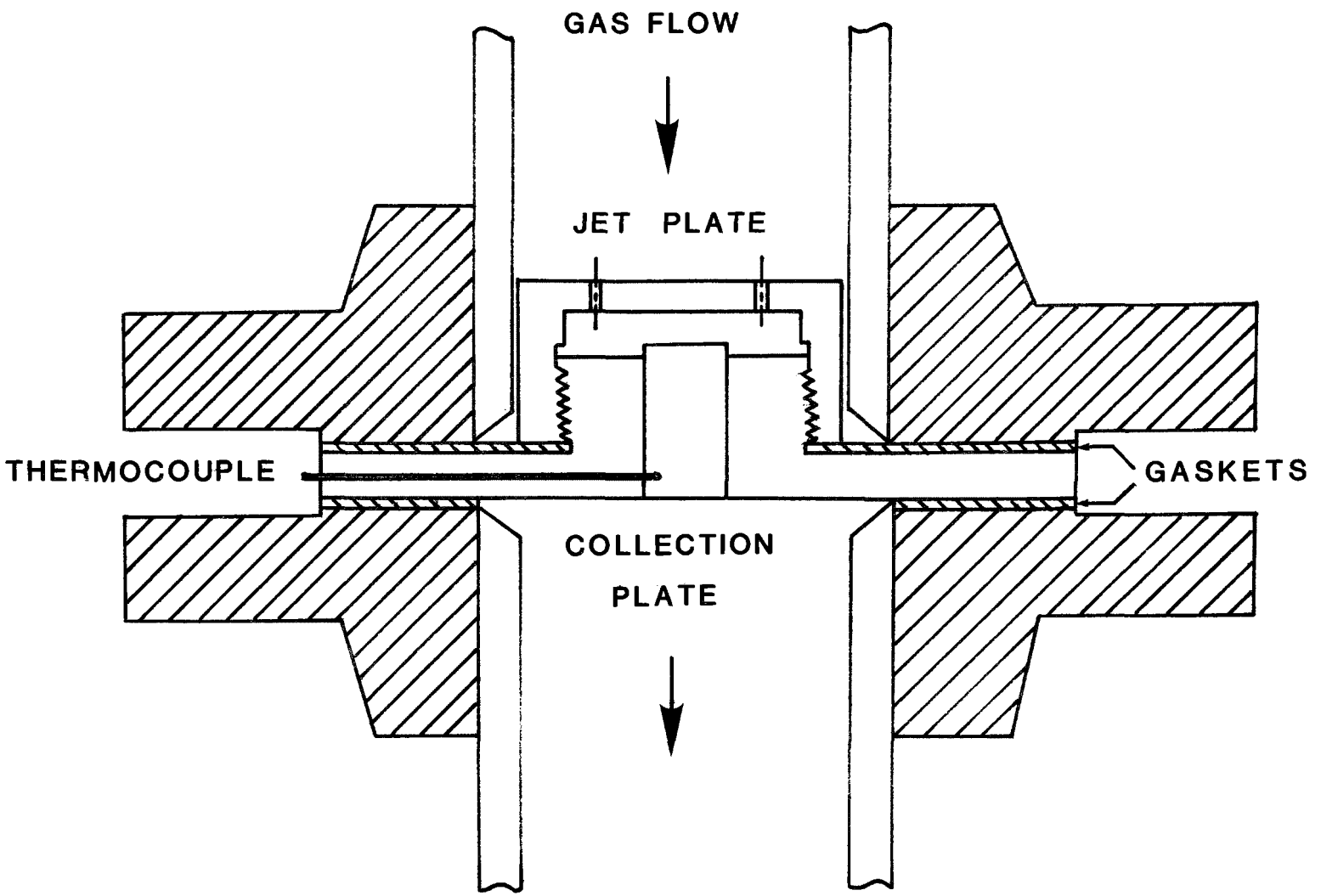

Figure 1. HTP single stage impactor.

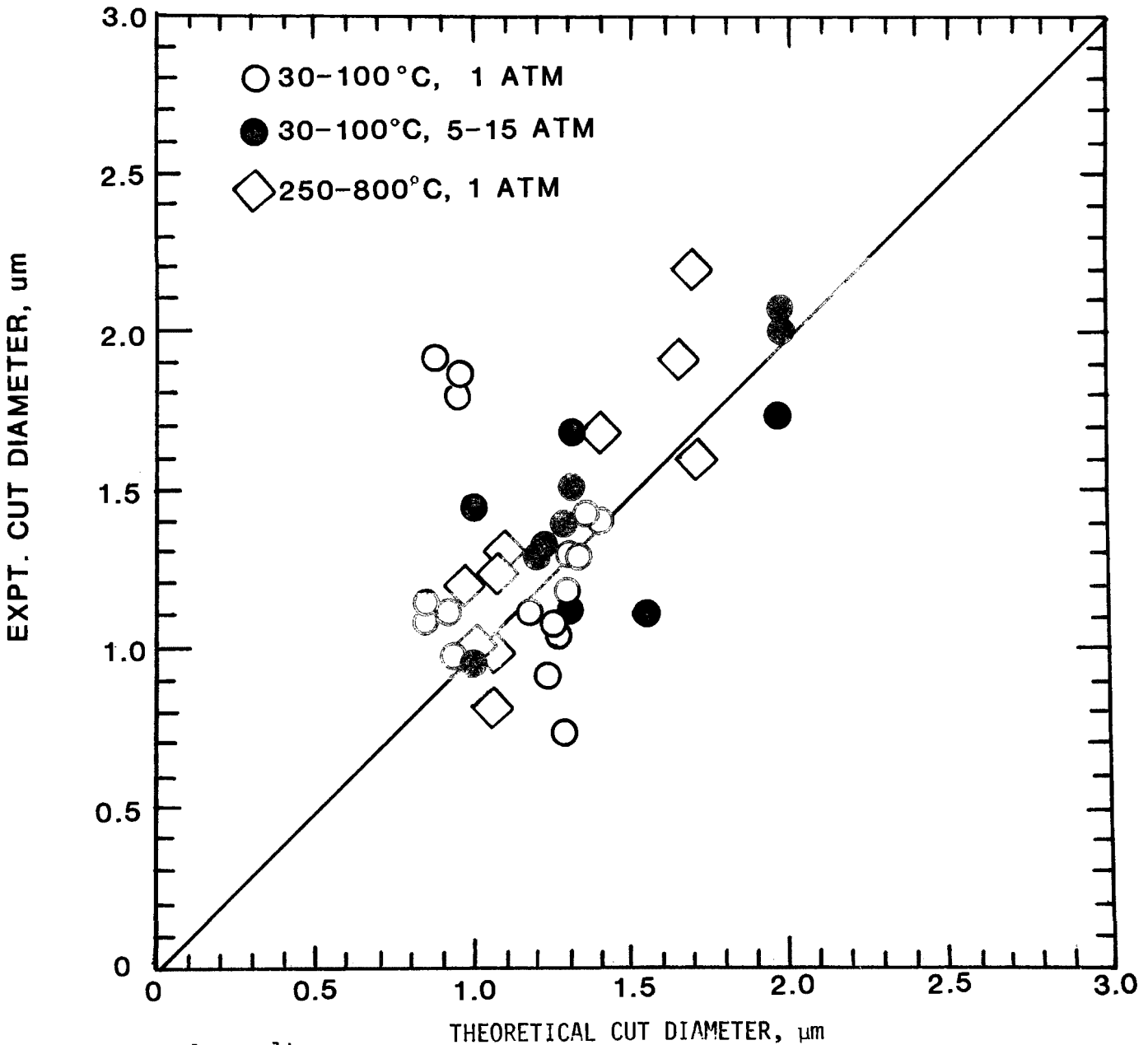

Figure 2. Experimental results.

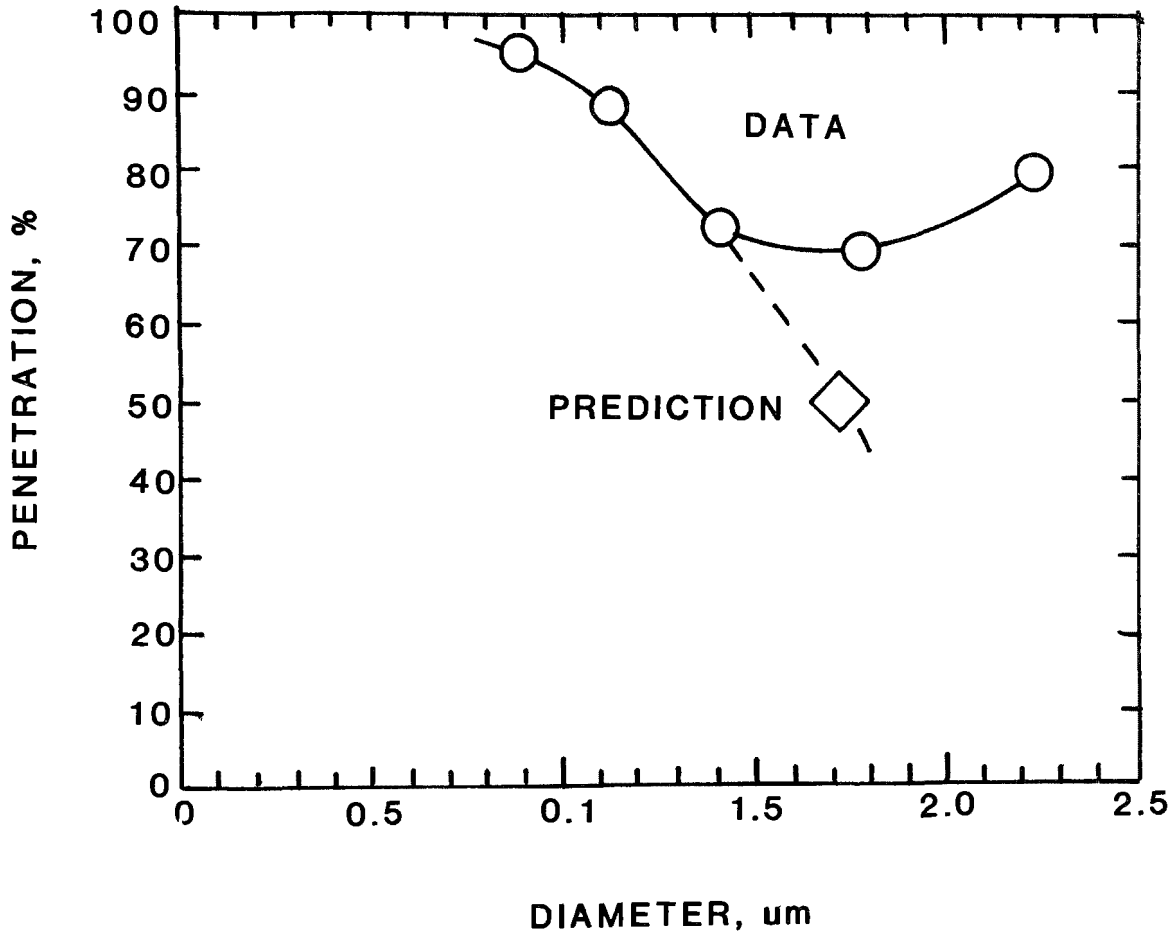

Figure 3. 500°C, 1 atm run with bare metal substrate.

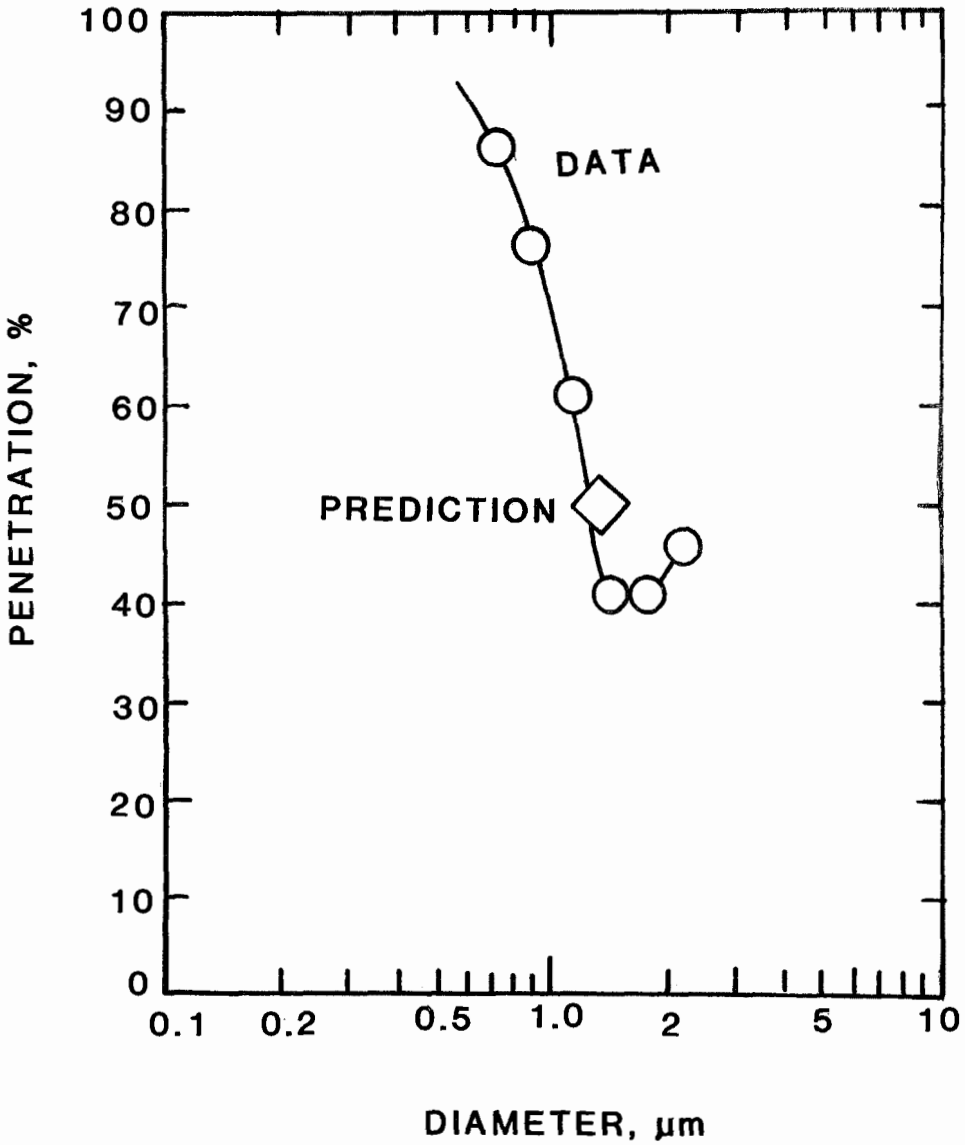

Figure 4. 100°C, 1 atm run with ceramic fiber substrate.

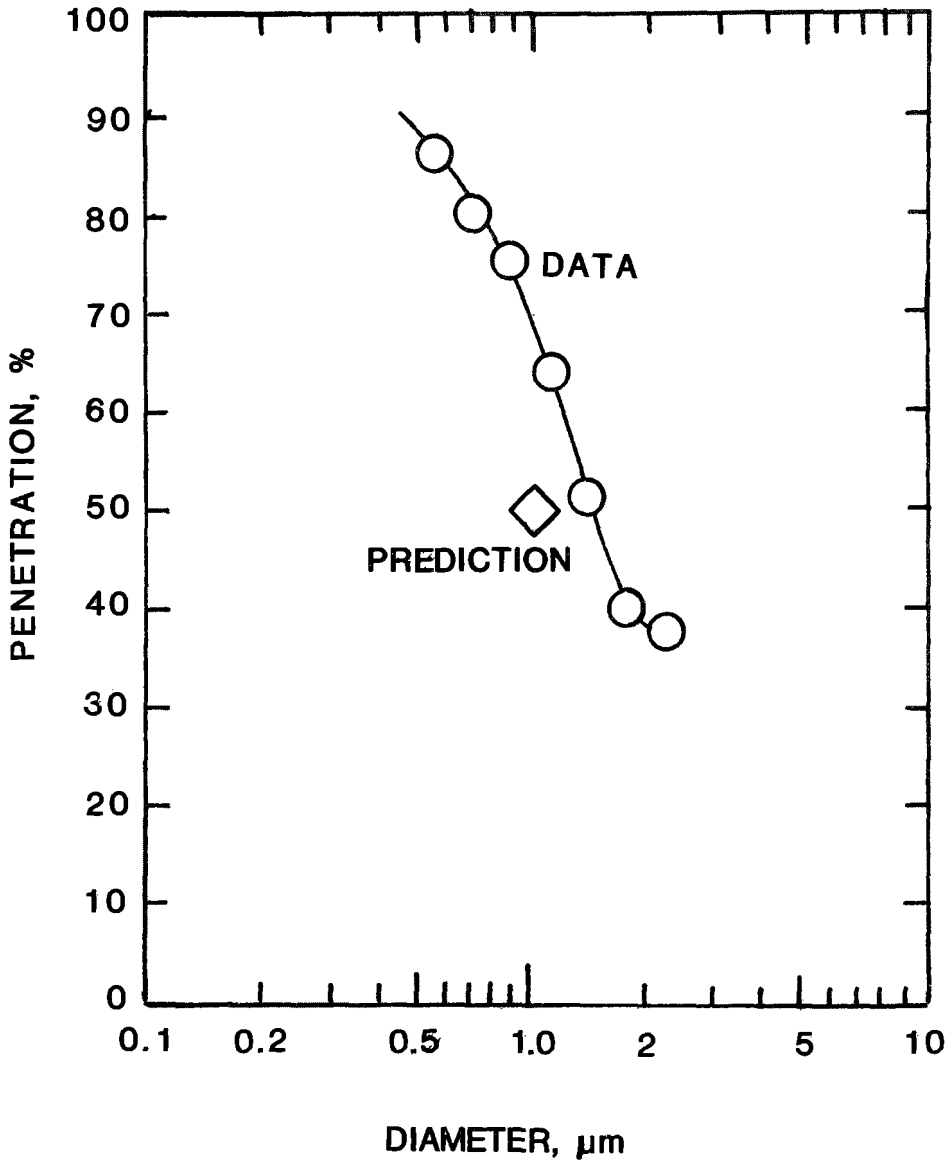

Figure 5. 100°C, 5 atm run with cermic fiber substrate.

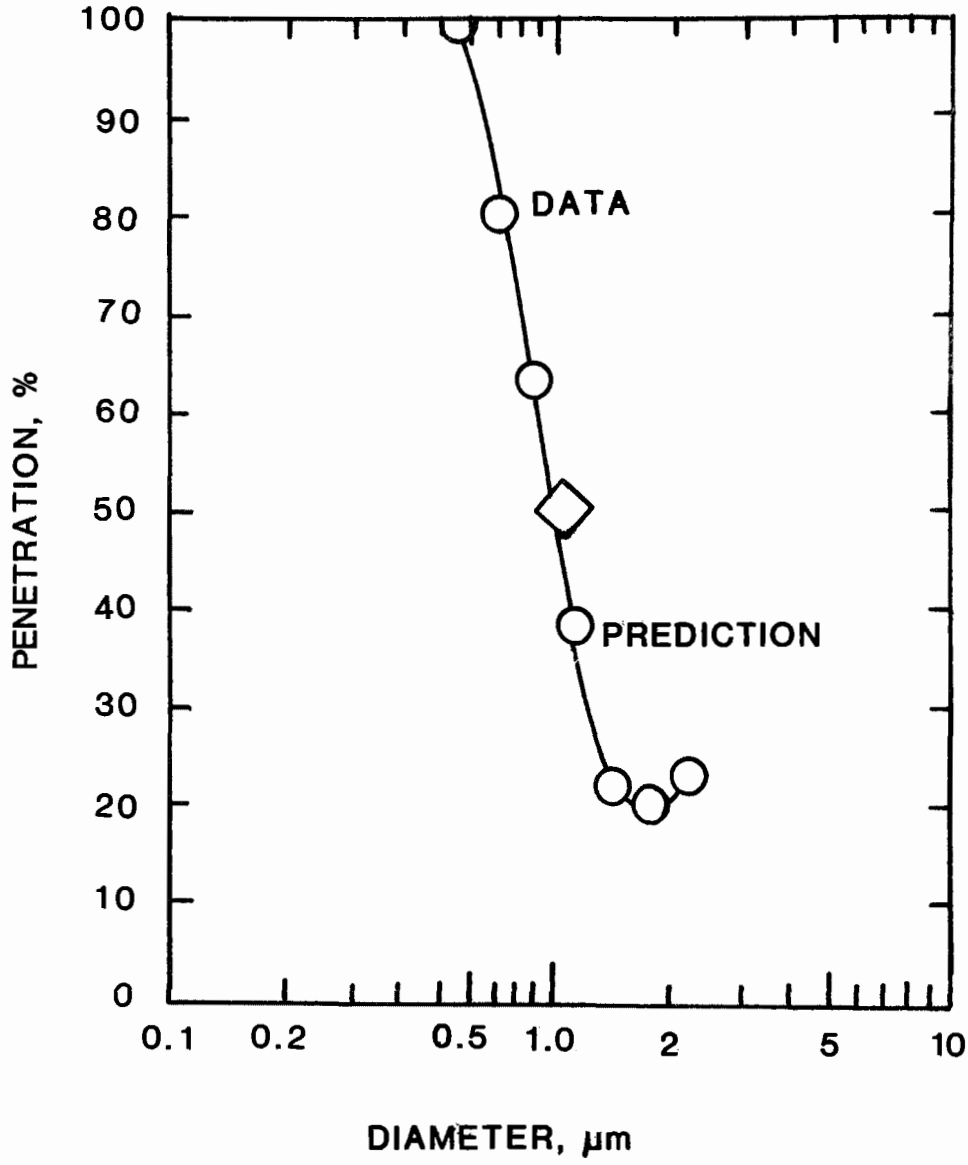

Figure 6. 500°C, 1 atm run with cermic fiber substrate.

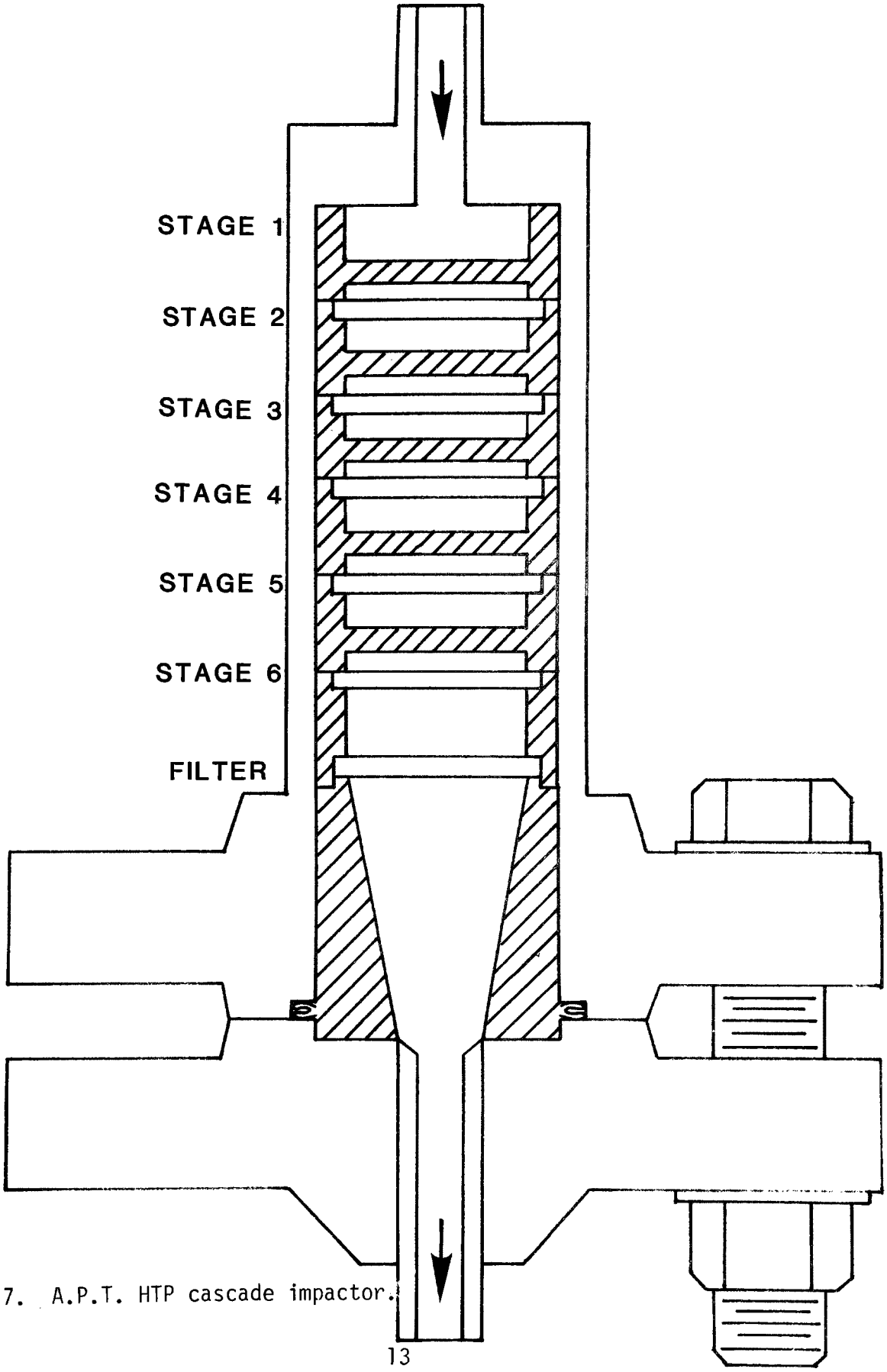

Figure 7. A.P.T. HTP cascade impactor.

PARTICULATE COLLECTION IN A HIGH TEMPERATURE CYCLONE

By:

Keh C. Tsao, C.O. Jen and K.T. Yung
College of Engineering & Applied Science
The University of Wisconsin--Milwaukee
Milwaukee, Wisconsin 53201

ABSTRACT

A new particle collection technique is analyzed and presented for its potential application in a high temperature, high pressure gas cleaning system. The technique is based on the collision and the agglomeration phenomena among the coal-ash particles when the cyclone is operated near the coal-ash fusion temperature. The percent increase of agglomeration rate is estimated by mathematical modeling for particles smaller than five microns diameter. Particulate collection efficiency with or without agglomeration is presented. Experimental results in a high temperature cyclone are presented. The output dust loading varied from 0.025 to 5 grains per cubic foot as the input dust loading is increased from 4 to 35 grains per cubic foot of gas flow.

PARTICULATE COLLECTION IN A HIGH TEMPERATURE CYCLONE

I. INTRODUCTION

The effective use of fluidized bed combustion products at high temperature and high pressure in a combined cycle plant depends on the particulate removal efficiency to an acceptable degree for the safe operation of gas turbines. Presently, there are numerous research and development projects involving cyclones, granular bed filters, molten salt scrubbers and other hybrid processes such as sonic agglomerators and charged filters in modified electrostatic precipitators.[1,2] However, some specific problems such as the effect of sticking of adherent particles and decreasing of collection efficiency at high temperature in clean-up apparatus result in making hot gas clean-up a major technical challenge. It was proposed that a new approach[3] utilizing the self-agglomeration phenomena[4] of carbon-ash particles near its fusion temperature to a modified multi-inlet, multi-pass cyclone be investigated. The combustion products, or the coal-ash particle-ladden gas, from the fluidized bed combustion boiler when passing a high temperature zone in the cyclone would enter momentarily a pseudo-molten state. The particles will coagulate, agglomerate and adhere together to form large particles. These larger size particles will subsequently be separated out under centrifugal action. Particulate removal efficiency of submicron particles could be increased further in the high temperature/pressure cyclone by the additional collection mechanism through collision of solid particles.

The goal of this paper is to report the continued progress on the analytical and laboratory results of particulate collection in a high temperature cyclone. The analytical study consists of: (1) the building of a mathematical model to simulate the particle collision phenomenon in a single gas stream for which the particles are of various sizes and concentration at differnt radial velocities, and (2) to estimate the degree of improvement of cyclone collection efficiency with and without particle collision and agglomeration phenomena. Laboratory findings of an experimental high temperature cyclone are also presented.

II. MATHEMATICAL FORMULATION

It is generally agreed that in a physical process and as a prerequisite of this study, the particle size and number distributions tend to be log-normal[5]. The number concentration of particles of diameter d, at time t, is

$$n(d,t) = \frac{N(t)}{\sqrt{2\pi}\, d \ln \sigma_m(t)} \exp\left[-\frac{1}{2}\left(\frac{\ln \frac{d(t)}{d_m(t)}}{\ln \sigma_m(t)}\right)^2\right] \qquad (1)$$

where N(t) = total number of particles at time t.
$\sigma_m(t)$ = standard deviation of log-normal distribution at time t, and

$$\sigma_m(t) = \exp\left[\ln\left(1+\frac{\sigma^2(t)}{\bar{d}^2(t)}\right)\right]^{\frac{1}{2}} \qquad (2)$$

$\sigma(t)$ = standard deviation at time t.
$\bar{d}(t)$ = particle mean diameter at time t.
$d_m(t)$ = log-normal mean diameter at time t.

The formulation of the mathematical model is based fundamentally upon the collision of elastic spheres as in the kinetic theory.[6] The number of elastic collisions between a group of large particles of diameter d_ℓ, concentration $n(d_\ell,t)$ and a group of small particles of diameter d_s, concentration $n(d_s,t)$ at time t is[6]:

$$n(d_\ell,t)\, n(d_s,t)\, v \sum_{s,\ell} \qquad (3)$$

where v = relative velocity between the two groups of particles, and

$\sum_{s,\ell} = \frac{\pi}{4}(d_\ell^2 + d_s^2)$, is the collision cross-sectional area.

For the tractability of the problem[7], assuming that the total number of inelastic collisions at time t is,

$$C(d_\ell,d_s,t) = \left[n(d_\ell,t)\, n(d_s,t)\right]^{\frac{1}{2}} v \sum_{s,\ell} \qquad (4)$$

and all particles have the same inlet tangential velocity, then the relative velocity v, Figure 1, in the cyclone becomes the difference of radial velocity of the large and small particles. That is,

$$v = V_r(d_\ell,t) - V_r(d_s,t)$$

$$= \frac{\rho_p Q^2}{72\mu_a w^2(\sqrt{r_2}-\sqrt{r_1})}\cdot\frac{1}{r^2}(d_\ell^2 - d_s^2) \qquad (5)$$

where r_1 = inner radius
r_2 = outer radius
w = inlet duct height
b = inlet duct width
Q = volumetric flow rate
μ_a = viscosity of air at operating temperature and pressure
ρ_p = mass density of solid particle.

Combining Equations (1), (2), (3), (4), and (5), we obtain

$$C(d_\ell,d_s,t) = (CONST)\cdot N(t)\cdot\frac{1}{r^2}\cdot(DIA) \qquad (6)$$

where

$$\text{CONST} = \frac{\sqrt{\pi}}{228\sqrt{2}\,\ln\sigma_m(t)\,(\sqrt{r_2}-\sqrt{r_1})^2}\,\frac{\rho_p}{\mu_a}\left(\frac{Q}{w}\right)^2 \tag{7}$$

$$DIA = \frac{d_\ell^4 - d_s^4}{(d_\ell\, d_s)^{\frac{1}{2}}}\exp\left\{-\frac{1}{4}\left[\left(\frac{\ln\frac{d_s}{d_m(t)}}{\ln\sigma_m(t)}\right)^2+\left(\frac{\ln\frac{d_\ell}{d_m(t)}}{\ln\sigma_m(t)}\right)\right]\right\} \tag{8}$$

Equations (7) and (8) are functions of cyclone geometry and particle size, respectively. In order to obtain the total number of collisions c(t) occuring at time t (take t = 0 at cyclone entrance), we need to integrate equation (8) for all small and large particles and $1/r^2$ term in equation (6) over the particle trajector traveled from r_1 to r_2 in the radial direction. Hence,

$$C(t) = N(t)\cdot(CONST)\cdot\int_{r_1}^{r_2}\frac{dr}{r^2}\int_{d_\ell>d_s}^{\infty}d(d_\ell)\int_0^{\infty}d(d_s)(DIA) \tag{9}$$

or

$$\frac{C(t)}{N(t)} = (CONST)\cdot\left(\frac{1}{r_1}-\frac{1}{r^2}\right)\cdot\int_{d_\ell>d_s}^{\infty}d(d_\ell)\int_0^{\infty}d(d_s)(DIA) \tag{10}$$

$$= (CONST)\cdot\left(\frac{1}{r_1}-\frac{1}{r_2}\right)\cdot(INT)$$

represents, at time t, the ratio of the number of collisions occuring to the number density of existing particles.[7]

III. COMPUTATIONAL RESULTS

For the cyclone under testing, Figure 2, the geometrical parameters are r_1 = 1.15 inches, r_2 = 1.905 inches, w = 1.70 inches and b = 0.75 inches. The operating parameters are pressure at 1.068 atmospheres, temperatures between 1650 to 2200°F, and volumetric flow rate between 13 and 25 cfm.

To carry out the numerical computation, we further assumed that the shape of the particle size distribution curve remains similar even though the number and size of the particles in the gas stream is changing. This is to say mathematically that $\sigma(t)/\bar{d}(t) = \sigma(0)/\bar{d}(0)$

and therefore σ_m is calculated to be 1.604 for $\bar{d}(t)$ = 10 μ , $\sigma(t)$ = 5 μ and $d_m(t)$ = 8.944 μ . Incorporating all the σ's and d's, we obtain the value of CONST to be 3.279×10^8 ft/sec.

Evaluation of DIA term is based on a fundamental premise that the removal efficiency of a conventional cyclone is 75% at 5 μ size particles. Smaller size particles must be agglomerated to form a new particle of diameter greater than 5 μ to be separated out. That is, in the computational process, when two particles adhere together, they shall have a diameter of $(d_\ell^3 + d_s^3)^{1/3} \geq 5\mu$.

The total number of collisions, at position r and time t, which would generate a new particle of a size greater than or equal to 5 μ among all the particles is to integrate the INT term with respect to all proper values of d_ℓ and d_s. For simplicity and a savings of computing time, we divided d_s into five size ranges: 0.1--0.5--1.0--2.1--3.0--3.968 μ and the corresponding size limits of d_ℓ are 5.0--4.97--4.90--4.87--4.61--3.969 μ . Particles of 100 μ size are considered to be the upper limit. Hence,

$$INT = \int_{0.1}^{0.5} d(d_s) \int_{5.0}^{100} d(d_\ell)(DIA) + \int_{0.5}^{1.0} d(d_s) \int_{4.97}^{100} d(d_\ell)(DIA)$$

$$+ \int_{1.0}^{2.1} d(d_s) \int_{4.90}^{100} d(d_\ell)(DIA) + \int_{2.1}^{3.968} d(d_s) \int_{3.0}^{100} d(d_\ell)(DIA)$$

$$+ \int_{3.968}^{3.969} d(d_s) \int_{3.969}^{100} d(d_\ell)(DIA)$$

$$= 5.1804 \times 10^{-10} \text{ ft}^3 \qquad (11)$$

Consequently $\frac{c(t)}{N(t)}$ = 69.44%. This fraction represents the formation of new particles through collision with a diameter greater than 5 μ . This value represents also the improvement of collection efficiency over the cyclone without collision agglomeration. Similarly, the computation process can be carried out for particles of mean diameter $\bar{d}(t)$ at 1 μ , 2 μ , etc. The cyclone collection efficiency $\eta(\bar{d},t)$ is computed by equation[5]

$$\eta(\bar{d},t) = 1 - \exp\left[- \frac{\rho_p Q \bar{d}^2 V}{36 \mu_a w (r_2 - \sqrt{r_1 r_2})(r_2 - r_1) 2\pi t} \right], \qquad (12)$$

or,

$$\frac{N(\bar{d},t)}{N(\bar{d},0)} = 1 - \eta(\bar{d},t) \qquad (13)$$

is the ratio of the number of particles remaining in the gas stream to the initial total number of particles at the cyclone entrance. Multiplication of $\frac{N(\bar{d},t)}{N(\bar{d},o)}$ by $\frac{C(\bar{d},t)}{N(\bar{d},t)}$ and by 0.75 for 5 μ particles, the increase of collection

efficiency due to collision and agglomeration $u(\bar{d})$ is

$$U(\bar{d}) = \frac{C(\bar{d},t)}{N(\bar{d},t)} \cdot \frac{N(\bar{d},t)}{N(\bar{d},0)} \cdot (75\%) \qquad (14)$$

Adding $u(\bar{d})$ to the original $\eta(\bar{d})$ gives the overall collection efficiency $\eta'(\bar{d})$ of a high temperature cyclone. The results are presented in Table 1 and graphically in Figure 3.

The computed cyclone efficiency is based on the particles' undergoing single collision. It is highly probable that a multiple collision process, fluid turbulence and pressure effect would increase further the collection efficiency in high temperature/pressure operations.

IV. EXPERIMENTAL FINDINGS

An experimental study was conducted to verify both the analytical indication and its practicability of cyclones operated at high temperature and pressure. The experimental set-up is shown schematically in Figure 4 and photographically in Figure 5. The set-up consists of a controllable high temperature gas burner, an experimental cyclone, coal-ash feeder and exhaust gas sampling train. Volumetric flow rate of air and gaseous fuel and temperatures were monitored. Coal-ash feed samples were preconditioned and sieved to sizes smaller than 38 μ. Filter papers were desicated and weighed on a micro-balance before and after sampling. Particles collected in cyclone hopper were weighed at the end of each test run. Experiments were carried out at various loading and in a temperature range of 1650 to 2250°F. The cyclone is operated slightly above atmospheric pressure.

Figure 6 shows the semi-log plot of the output duct loading versus input dust loading for 23 test runs. The output dust loading increases with input dust concentration. An enlarged insert is also shown for the cyclone performance at low particulate loading of incoming dust-ladden gas. The output dust loading can be lowered to 0.025 grains per cubic foot of gas flow after clean-up.

Figure 7 shows the experimental hopper collection efficiency which is defined as the mass ratio of ash particles collected in the cyclone hopper to that of ash mass fed into the cyclone. A collection efficiency of 92% is achieved in most of the test runs. The hopper collection efficiency is increased further and approaching the collection efficiency based on output dust loading measurements, if the weight of ashes lost in handling were excluded from the ash mass fed at the inlet. Table 2 lists all the test runs and their corresponding collection efficiency and operating conditions for the high temperature cyclone.

V. ACKNOWLEDGEMENT

The authors wish to express their appreciation for the grant support under ERDA University Coal Research Starter Grant Program. The project is also partially supported by the Department of Natural Resources, the State of Wisconsin under the Air Quality Program.

REFERENCES

1. EPA/DOE Symposium of High Temperature/Pressure Particulate Control, September 1977, Washington, D.C.

2. Wade, G.L., "Particulate Removal from Hot Combustion Gases," Proc. of 4th International Conference on FBC, Washington, D.C., 1975.

3. Tsao, K.C., Yung, K.T. and Bradley, J.F., "Multiple Jet Particle Collection in a Cyclone by Reheating FBC Products," 5th International Conference on FBC, Washington, D.C., Vol. III, p. 607, December 1977.

4. Tsao, K.C., Bradley, J.F. and Yung, K.T., "The Effect of Temperature, Particle Size and Time Exposure on Coal-Ash Agglomeration," Symposium on the Transfer and Utilization of Particulate Control Technology, Denver, Colorado, Vol. IV, pp. 441-456, May 1978.

5. Crawford, M., Air Pollution Control Theory, McGraw Hill, 1976.

6. Reif, F., Fundamentals of Statistical and Thermal Physics, John Wiley & Sons, 1969.

7. Yung, K.T., A Theoretical Investigation of Cyclone Collection Efficiency with Particle Collision, M.S. Thesis, The University of Wisconsin--Milwaukee, 1979.

TABLE 1

COMPUTED CYCLONE PERFORMANCE WITH AND WITHOUT AGGLOMERATION

$\bar{d}$ (μ)	1	2	5	10
$\eta(\bar{d}) = 1 - \frac{N(\bar{d},t)}{N(\bar{d},0)}$, (%)	5.37	19.81	75	99.5
$\frac{C(\bar{d},t)}{N(\bar{d},t)}$, (%)	1.42	28.07	75.63	69.44
$U(\bar{d},t) = \frac{C(\bar{d},t)\ N(\bar{d},t)}{N(\bar{d},t)\ N(\bar{d},0)}$. (75%) (%)	0.99	16.88	14.21	0.26
$\eta'(\bar{d}) = \eta(\bar{d}) + U(\bar{d})$, (%)	6.36	36.69	89.21	99.76
$\frac{\eta' - \eta}{\eta}$, (%)	18.4	85	18.9	0.2

TABLE 2

HIGH TEMPERATURE CYCLONE EFFICIENCY AND OPERATION CONDITION SUMMARY

Run #	Hopper Collect. Efficiency, %	Sampler Collect. Efficiency, %	Temp., °F	Run Time, Sec.
15	90.7	93.8	2100	300
16	86.7	93.0	2250	300
18	86.9	92.6	2250	300
21	88.2	93.3	2250	300
22	90.7	94.5	2200	300
24	84.2	93.1	1900	300
25	82.2	94.9	2050	300
27	84.7	96.9	1900	300
28	84.0	95.9	1950	300
30	81.9	98.4	1720	300
31	79.5	99.5	2000	300
32	93.2	99.6	2000	600
33	86.0	97.6	2000	600
36	83.2	98.7	2000	600
37	84.4	98.5	2000	600
38	85.9	98.8	2000	600
39	93.2	98.9	2000	600
40	88.6	98.9	2000	600
41	90.9	98.9	2000	1800
42	91.1	98.6	2000	1800
43	92.0	99.0	2000	1800
Average of	87.1 $\pm$ 3.9	96.8 $\pm$ 2.5		

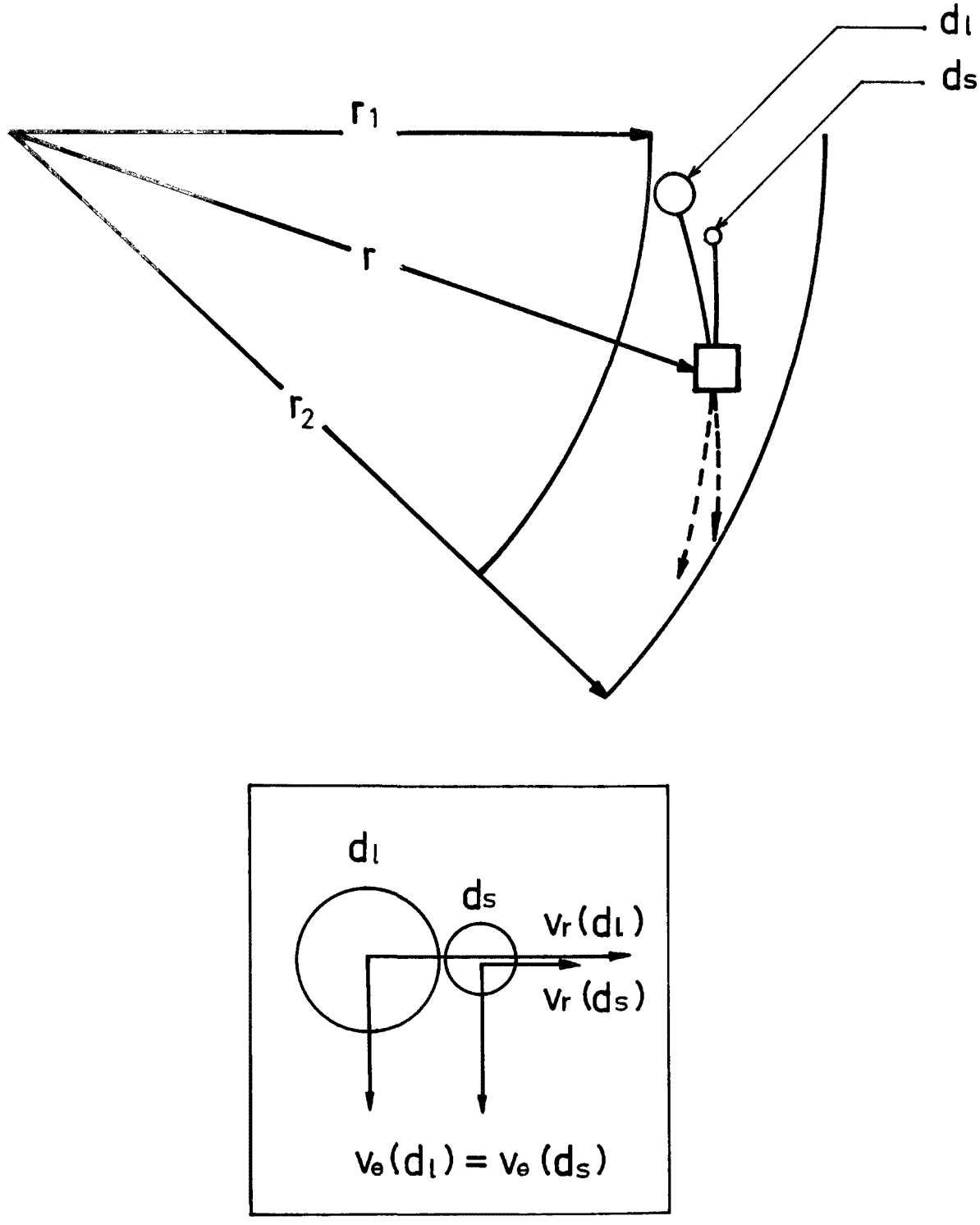

FIGURE 1. COLLISION DUE TO DIFFERENT RADIAL VELOCITIES OF PARTICLE

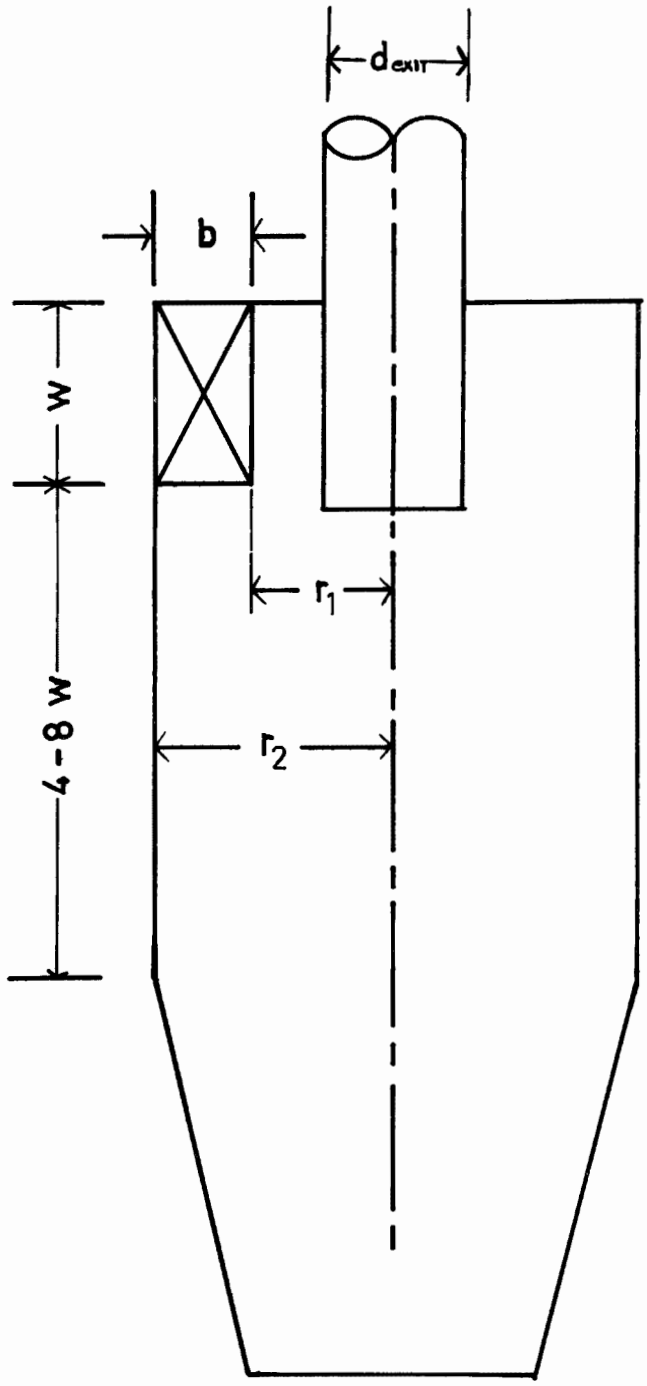

FIGURE 2. DIMENSION PARAMETERS OF CYCLONE

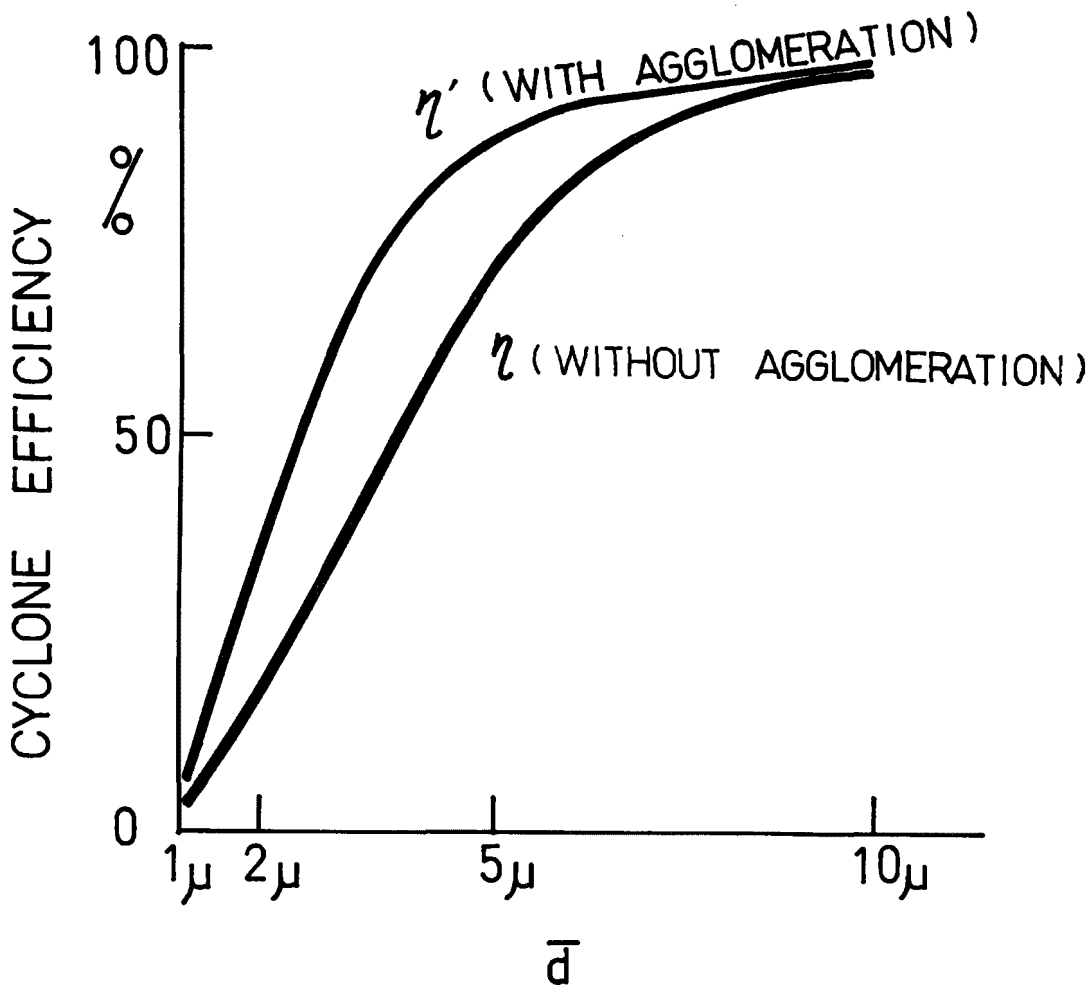

FIGURE 3. COMPUTED EFFICIENCY VS. PARTICLE MEAN DIAMETER

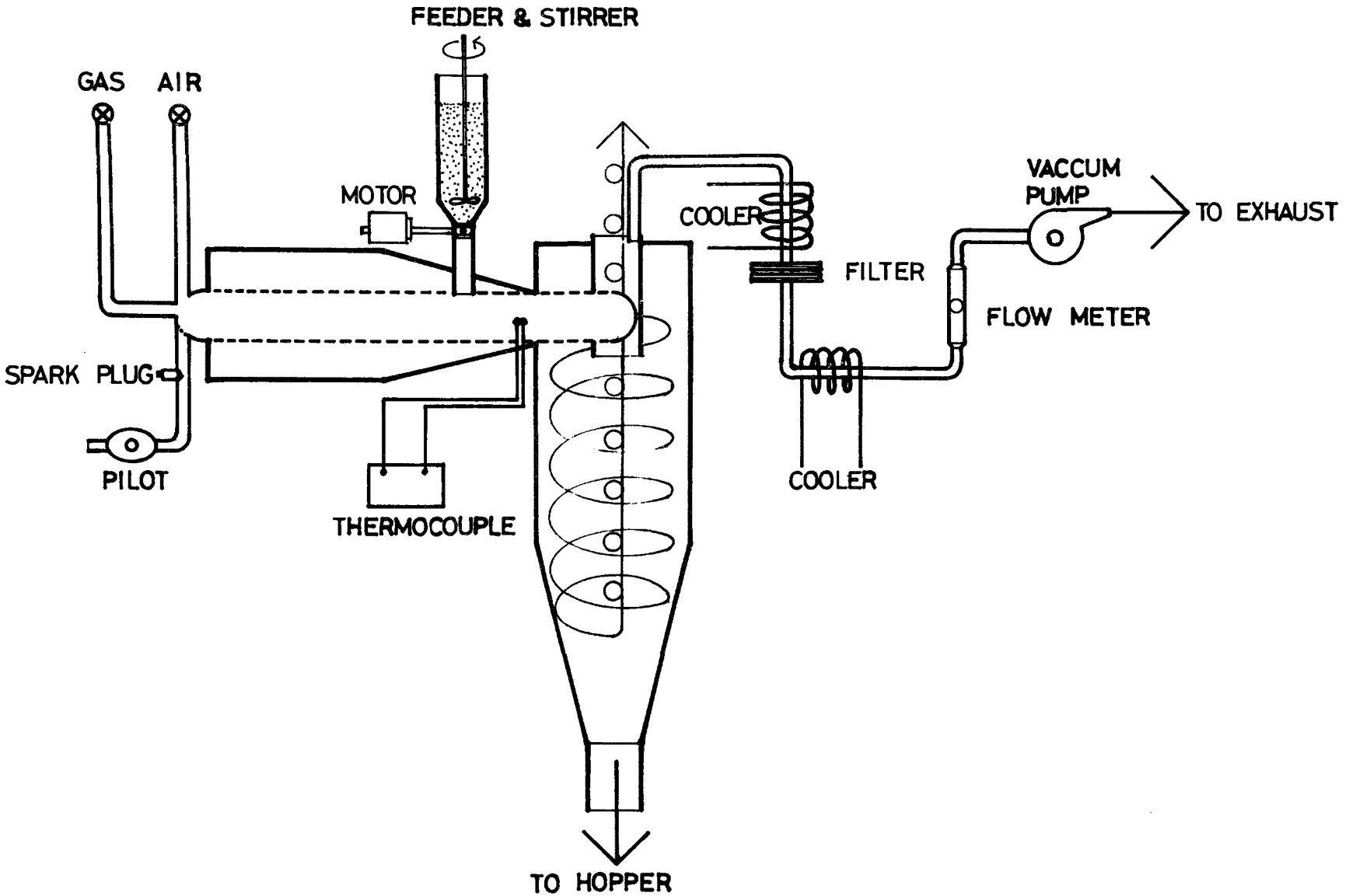

FIGURE 4 SCHEMATICS OF SET UP

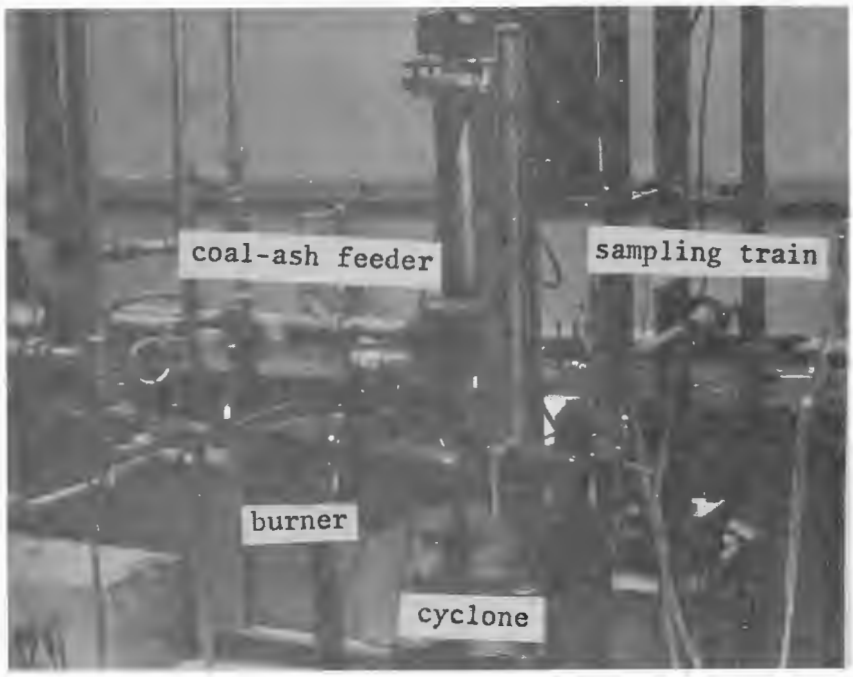

FIGURE 5. PHOTO OF TESTING SET-UP

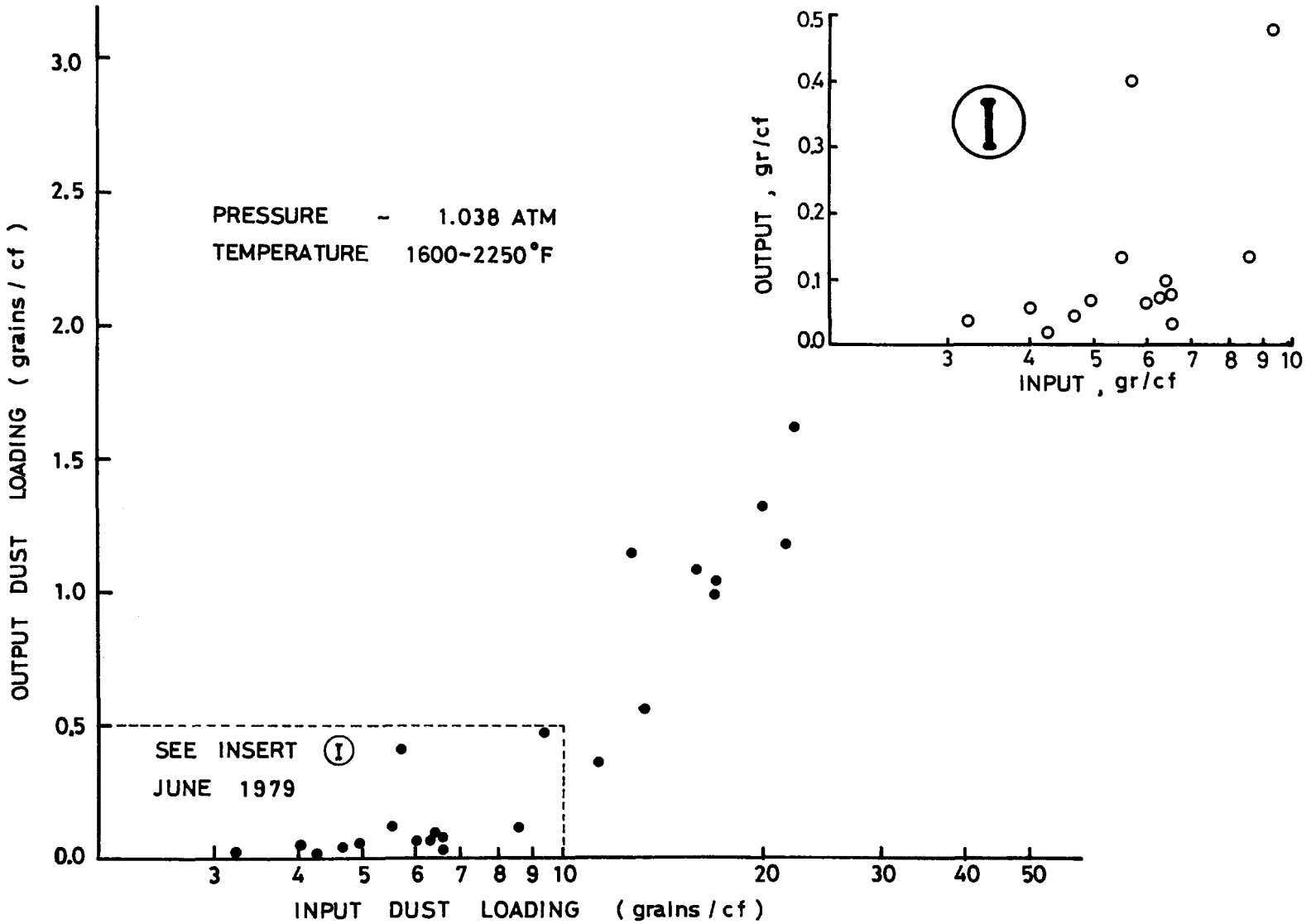

FIGURE 6 CYCLONE PERFORMANCE BASED ON OUTPUT DUST LOADING

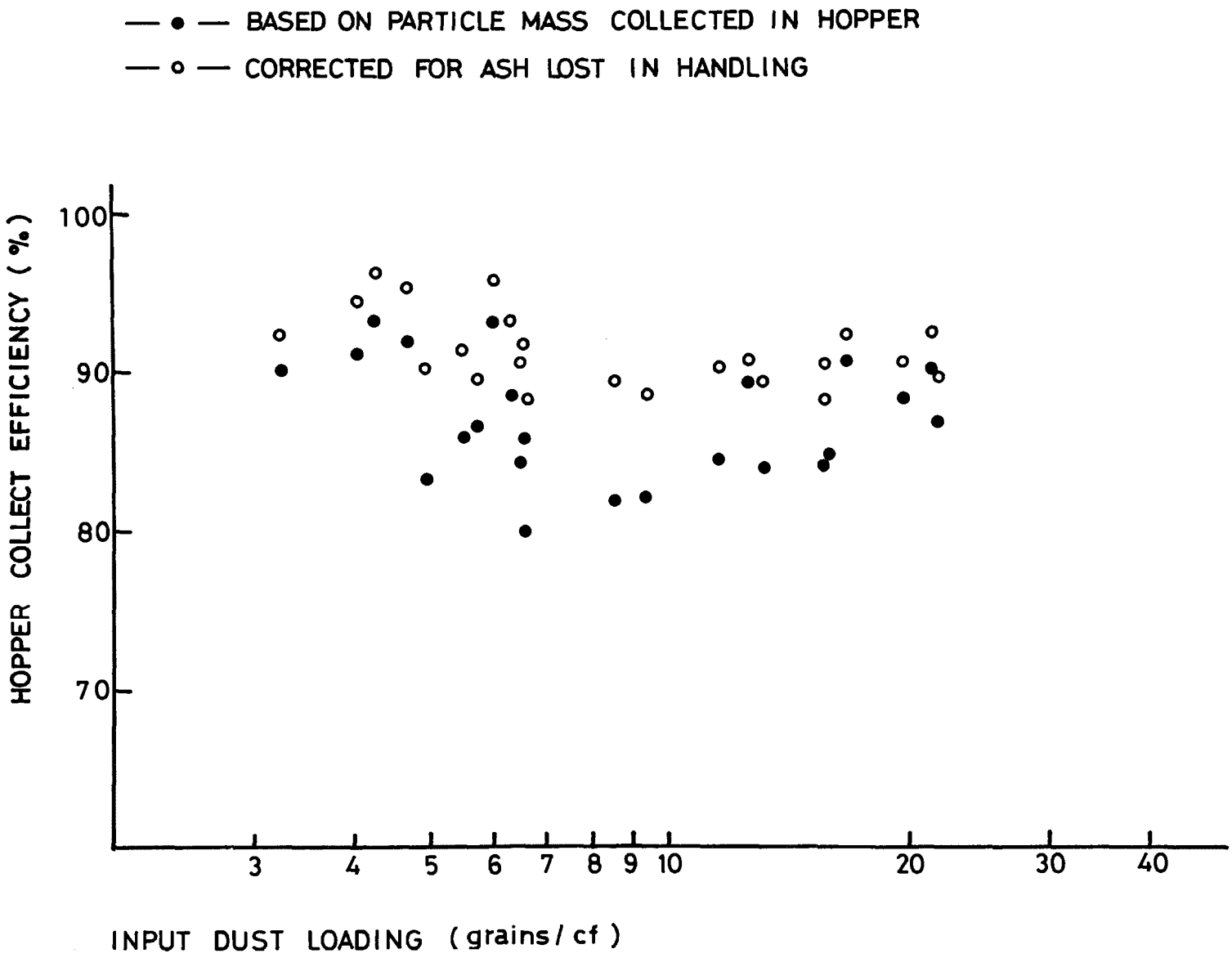

FIGURE 7 CYCLONE PERFORMANCE BASED ON ASH HOPPER COLLECTION

EVALUATION OF A CYCLONIC TYPE DUST COLLECTOR FOR HIGH TEMPERATURE HIGH PRESSURE PARTICULATE CONTROL

By:

M. Ernst
R. C. Hoke
V. J. Siminski
Exxon Research & Engineering
1900 E. Linden Ave.
Linden, N. J. 07036

J. D. McCain
Southern Research Institute
2000 9th Ave. South
Birmingham, Ala. 35205

R. Parker
Air Pollution Technology, Inc.
4901 Moreno Blvd. Suite 402
San Diego, CA 92117

D. C. Drehmel
Industrial Environmental Research
U.S. Environmental Protection Agency
Research Triangle Park, No. Carolina

ABSTRACT

The performance of conventional cyclones operating at temperatures up to 880°C and pressure up to 900 kPa on flue gas from a pressurized fluidized bed coal combustion unit was measured. The cyclones were very efficient, generally removing particulates to a level of 0.04 to 0.07 g/Sm^3 at the exit of a three stage cyclone system. Cyclone performance was measured using both a total filter and Coulter Counter technique and a cascade impactor to measure the particulates size distribution. The two methods gave comparable results.

INTRODUCTION

Pressurized fluidized bed coal combustion (PFBC) is a new direct combustion process which promises to provide an efficient, environmentally acceptable and economic method of using sulfur-containing coal to generate electricity. Coal is burned in a bed of fluidized calcium-based sorbent such as as limestone or dolomite. SO_2 formed in the combustion process is removed down to the required levels by reaction with the sorbent within the combustor. The heat of combustion is removed, in part, by steam coils immersed in the fluidized bed. The steam is used in conventional equipment to generate electricity. The immersed steam coils also reduce and control the temperature of the fluidized bed within the range of 850 to 950°C. The combustion is carried out at elevated pressure, generally in the range of 600 to 1000 kPa. The hot, high pressure, flue gas can then be expanded through a gas turbine, after suitable treatment to remove particulate matter, to generate additional electricity and increase the overall efficiency of the power generating cycle.

The successful development of the pressurized fluidized bed coal combustion process is dependent on the ability of particulate control devices to remove particulates from the hot combustor flue gas to very low levels. This must be done to assure that the expansion of the flue gas through a gas turbine does not cause damage to the turbine by erosion, corrosion, or deposition of solids on the turbine blades.

Studies are now under way to define the limits of particulate concentration and size distribution needed to prevent erosive damage to a gas turbine. Studies are also underway to characterize performance of a variety of particulate control devices which may be able to meet the limits imposed by the turbine requirements and environmental regulations.

PFBC particulate characterization and control studies are being carried out by Exxon Research and Engineering Company under contract to the U.S. Environmental Protection Agency (Contract 68-02-1312). The work is being done on a PFBC unit built and operated for the EPA by Exxon Research. Recently, the performance of cyclone separators, operating at high temperature (700-900°C) and pressure (9 atm), has been studied. These studies have determined the separation efficiency of cyclones and the concentration and size distribution of particulates in the flue gas leaving the cyclones. The particulate characterization technique used primarily by Exxon has been total filtration of an isokinetic sample followed by size analysis using a Coulter Counter.

Most recently a joint program was conducted with two other EPA contractors Southern Research Institute (SORI) and Air Pollution Technology Company (APT). In this program, a new high pressure, high temperature cascade impactor developed by APT was used to measure particulate size distribution in the flue gas entering and leaving the third stage cyclone on the PFBC unit. These data were also used to determine the cyclone capture efficiency. Data obtained by the total filter/Coulter Counter method and the cascade impactor were compared.

FIGURE 1

MINIPLANT THIRD CYCLONE DIMENSIONS

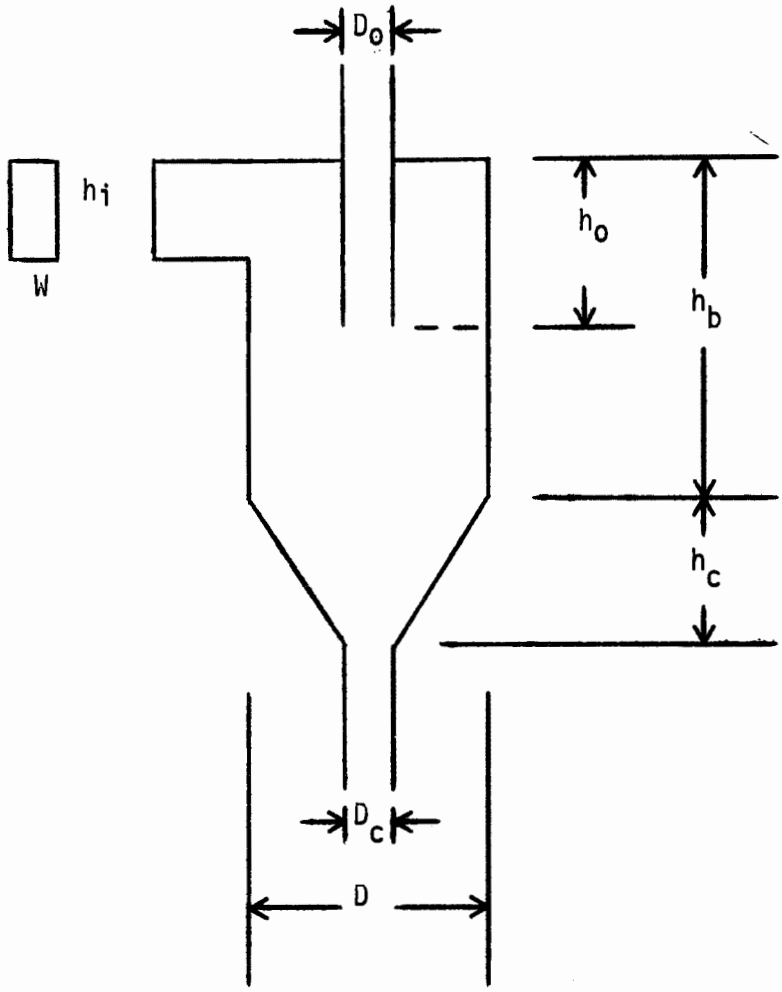

W	hi	h_o	h_b	h_c	D	D_o	D_c	
1.5	3.0	4.5	16	8	6.07	2.47	3.55	inches
3.81	7.6	11.4	41	20	15.4	6.27	9.02	cm

FIGURE 2

Tertiary Cyclone Fractional Efficiencies
From Coulter Counter and Mass Balances
(Runs 68-78)

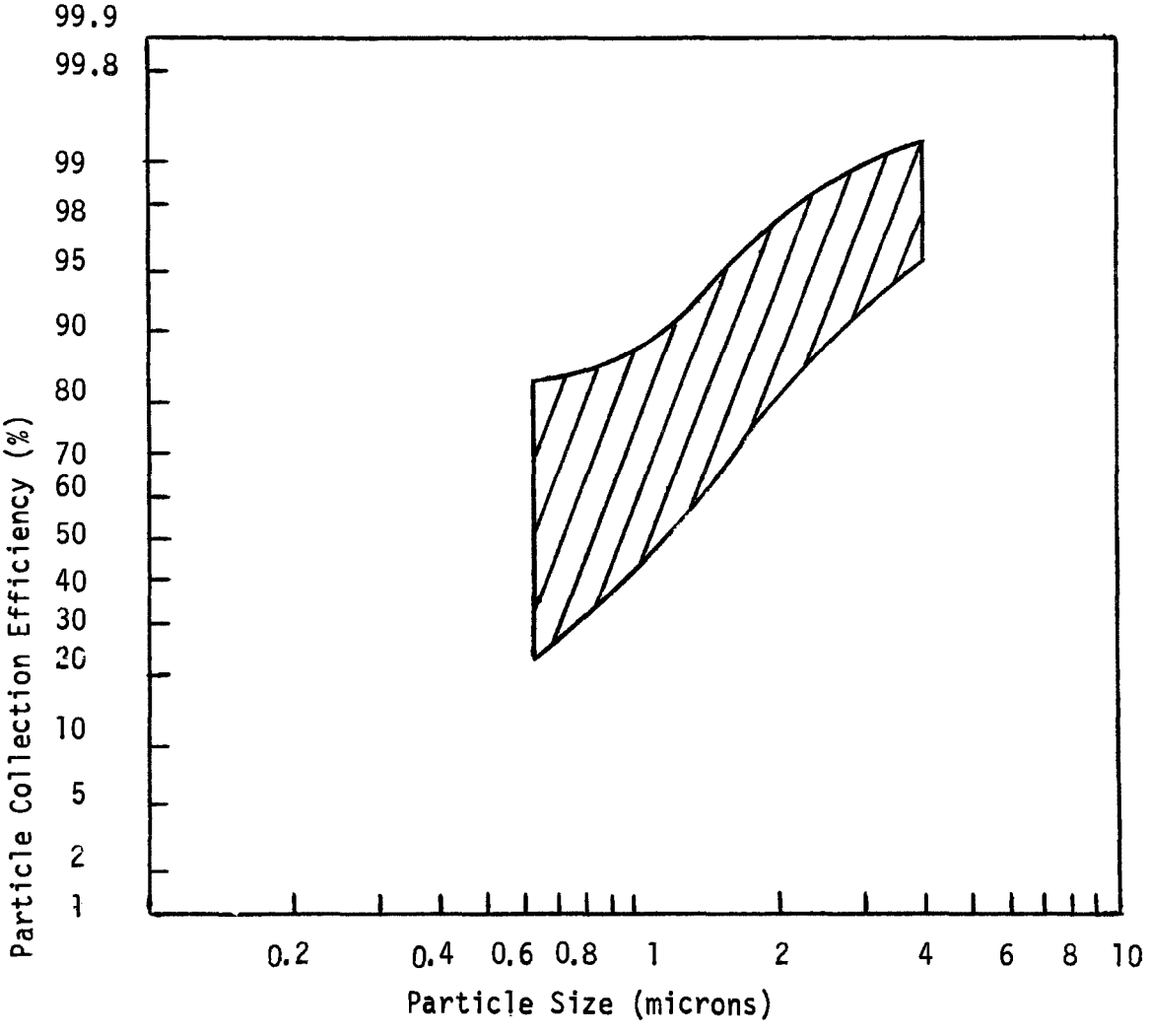

EXPERIMENTAL EQUIPMENT AND PROCEDURES

The PFBC "miniplant" process development unit used in this study consists of a combustor vessel refractory lined to an inside diameter of 33 cm. The overall height of the combustor is 10 m. Vertically oriented cooling coils are immersed in the bed. Coal and sorbent are premixed and injected pneumatically into the combustor through a single side-entering port 28 cm above the fluidizing grid. The maximum solid feed rate is approximately 160 kg/hr. The combustor is capable of operating at pressures up to 1000 kPa, at temperatures up to 1000°C, superficial gas velocities up to 3 m/s with expanded beds up to 6.1 m. The expanded bed height can be controlled at any level above 2.3 m by continuously withdrawing solids from the bed through a port located at that elevation. Flue gas exiting from the combustor passes through three cyclone separators. The solids collected in the first cyclone are returned to the combustor at a point 61 cm above the fluidizing grid. Solids collected in the second and third cyclones are removed through lock hoppers. Both cyclones are conventional tangential inlet cyclones designed and constructed by Exxon.

The third cyclone is located in a large pressure vessel. The flue gas can be sampled for particulates both before and after the cyclone. The dimensions of this cyclone are shown in Figure 1. The cyclone normally operates at 880°C, 1000 kPa pressure and inlet velocities of 50 m/s. Initially, during this study, isokinetic samples were taken with Balston total filters only on particulates in the gas exiting the cyclone. This sample gas was withdrawn through an isokinetic stationary probe at rates between 28 and 85 Sdm^3/min. This corresponds to probe sizes between 0.5 and 1.1 cm. This gas passed through an isolation valve and was allowed to cool to between 275 and 550°C before it reached the filter. After the filter, the gas was further cooled and passed through a water knock out before it was expanded through a needle valve and measured by a wet test meter. After the one to two hour sample was taken, the filter cartridge was weighed and particulates were removed from the filter cake for Coulter Counter size analysis.

The size distribution of the material captured by the cyclone was analyzed with a combination of a sonic sieve and the Coulter Counter. A mass balance was completed around the cyclone to determine inlet size and concentration. In this way cyclone fractional (grade) efficiencies were obtained under the assumption that there was no accumulation or attrition in the cyclone. The validity of these calculations has been confirmed with concurrent inlet and outlet samples and mass balance calculations.

As a further refinement on the particle sizing and concentration entering and exiting the cyclone, samples were taken with cascade impactors developed by Air Pollution Technology (APT). These samples were taken at approximate isokinetic rates through probes and nozzles which were permanently implanted within the inlet and outlet ducts of the tertiary cyclone. These probes and nozzles were continuously purged when sampling was not taking place. Heat traced, stainless steel, sample lines conveyed the samples from the ducts through two high temperature isolation valves to each impactor. Some loss of large particles

Table 1. IMPACTOR GEOMETRIES FOR MINIPLANT RUN 105 SAMPLING

	Cyclone Inlet			Cyclone Outlet		
Stage	No. of jets	Jet diameters (cm)	Cut * diameters (μmA)	No. of jets	Jet diameters (cm)	Cut * diameters (μmA)
1	24	0.118	7.9	24	0.118	2.8
2	24	0.0660	3.3	24	0.0914	1.9
3	24	0.0406	1.6	24	0.0660	1.1
4	18	0.0343	1.0	24	0.0406	0.53
5	7	0.0343	0.63	18	0.0343	0.34

* Typical Values
As operated in these tests.

Table 2. IMPACTOR SAMPLING CONDITIONS

	Cyclone Inlet	Cyclone Outlet
Sampling rate (at impactor conditions); cm^3/sec	38-41	283-349
Impactor Temperature; ^oC:	575-615	545-675
Impactor Pressure; kPa: (approximate)	580	560
Sample duration; minutes:	7	7

undoubtedly occurred in those lines and valves. The impactors were brought to a temperature of approximately 600°C by external heaters prior to each sampling run and maintained at that temperature throughout the run. Thermocouples located upstream and downstream of the impactors were used to measure gas temperatures through the impactors. The sampling systems were completed with heat exchangers to reduce the gas temperature, pressure letdown and flow control valves, moisture traps, and flow meters and dry gas meters for determining sampling rates and sample gas volumes. Details of the impactors and sample run conditions for the tests reported here are given in Tables 1 and 2.

RESULTS AND DISCUSSION

Particulates in the flue gas leaving the miniplant recycle cyclone pass through the two additional cyclones which remove over 99 % of the particulate matter. Mass balance calculations based on particulate material captured in the second and third cyclones and in the flue gas leaving the third cyclone are used to determine the particulate size and concentration at the exit of all three miniplant cyclones.

These measurements and calculations show that material captured by the second cyclone has a mass median particle size of 15 to 20 μm. The overall cyclone efficiency is about 95%. Material captured by the third cyclone has a mass median size of 3 to 5 μm. The overall efficiency of this cyclone is about 90%. Particulate concentration in the flue gas leaving the third cyclone is generally 0.04 to 0.07 g/Sm^3. The mass median size of the particulate ranges from 0.7 to 3 microns as determined by Coulter Counter. These results are summarized in Table 3.

Table 3. PARTICULATE CONCENTRATION AND SIZE MINIPLANT CYCLONE SYSTEM

Cyclone	Part. Conc. (g/Sm^3) Passing	Mass Median Size (Microns) Captured	Passing	Cyclone Efficiency
Recycle	10	-	20-25	-
Middle	0.4-0.6	20-25	3-5	~95
Final	0.04-0.07	3-5	0.7-3	~90

The third cyclone fractional efficiency is of greatest interest, since if a three stage cyclone system is used in a commercial PFBC system, the third stage must be very efficient to prevent damage to the gas turbine behind it. Results from a recent extended turbine materials test carried out by Exxon for the Department of Energy (contract EX-76-6-01-2452), indicated that the cyclone system may provide sufficient protection for gas turbines. (1).

Fractional efficiencies for the third cyclone have been tabulated for a number of miniplant runs. A sample of these fractional efficiencies is shown in Figure 2. Note that all of these fractional efficiencies were obtained by the mass balance technique with Coulter Counter size analysis. Some of the scatter can be attributed to varying operating conditions. The third cyclone was consistently between 60 and 85% efficient for particles having diameters of 1μm and 40 to 80% efficient for 0.6μm diameter particles. These efficiencies are higher than expected based on published cyclone performance models.

Measurement of the fractional efficiency of the tertiary cyclone with cascade impactors was suggested after conventional filtration sampling methods had indicated that the cyclone efficiency was higher than expected. The minimum particle size detectable by the Coulter Counter in this application was estimated to be approximately 0.6 μm. Thus the possibility existed that the fractional efficiency results shown in Figure 2 might have been biased by using the mass balance technique with incomplete size distributions. Further, the ultrasonic deagglomeration of particles prior to performing the Coulter analyses may have resulted in aerodynamically large agglomerates being measured by the Coulter Counter as individual primary particles. The magnitude of the possible errors in the fractional efficiency curves resulting from these biases are difficult to access.

Cascade impactors have been used for a number of years for determinations of control device fractional efficiencies over the size range from approximately 0.3 μm to 10 μm. Recent work at APT, has shown that cascade impactor performance at temperatures and pressures like those of the flue gas from the miniplant can be predicted to good accuracy by current theories. A pair of cascade impactors which were designed by APT, to operate at high pressures and temperatures was made available by the EPA for a series of independent test of the miniplant tertiary cyclone.

Inconel shim substrates were used for particle collection surfaces for each stage. Ceramic fiber backup filters were used to collect those particles which were not removed by the impaction stages. Qualitative verification of the performance of the impactors was obtained by Coulter Counter analyses (where applicable) and by electron microscopy of the various stage catches from typical runs. Previous experience by Exxon and the samples obtained during this joint program by Southern Research and APT showed that the particles, at the sampling conditions, were highly adhesive. This permitted valid impactor results to be obtained even though bare metal substrates were used. (Ceramic fiber substrates were on hand for use had this not been the case).

Figure 3 shows comparative results of size distributions of the particles in the tertiary cyclone exhaust stream obtained by Coulter analyses of filter catches from miniplant run 105 by Exxon and those obtained by means of cascade impactors during the same run by SORI and APT. Cyclone operating conditions are shown in Table 4.

Table 4. THIRD CYCLONE OPERATING CONDITIONS
(RUN 105)

Pressure	700 kPa
Temperature	635°C
Flow rate	14.6sm^3/min
Inlet velocity	36 m/sec
Pressure drop.	4 kPa

As seen, the cascade impactor results indicate a larger concentration of fine particles and a mass median particle size of about 1 micron, where the Coulter Counter mass madian particle size averaged 2 microns.

Electron micrographs of material captured on the various impactor stages indicated that, with the exception of the first stages, the particulate matter collected in the impactor stages was fine, non-agglomerated particulates. Electron microscopy also revealed that much of the areodynamically large particulate matter on the first impactor stage at the cyclone inlet was agglomerates of smaller particles. This agglomeration was insufficient to explain the high cyclone efficiencies.

These findings indicated that the results of the Balston filter/Coulter Counter method used by Exxon differred from cascade impactor results as expected, based on measurements made in other particulate systems. They also indicated that the Coulter Counter results were not being biased toward the finer particles by breakdown of agglomerates in the aqueous dispersing medium used in the Coulter Counter.

Figure 4 shows the fractional efficiency of the third cyclone during run 105 as calculated from; 1) the SORI/APT cascade impactor date, 2) the Exxon total filter/mass balance technique with Coulter Counter size analysis, 3) the Koch and Licht (2) (1977) cyclone fractional efficiency model. The impactor and the total filter/Coulter Counter efficiencies agree fairly closely except in the small particulate size range. The cyclone cut diameter (50% efficiency) of both measured efficiencies was approximately 0.7 microns. Therefore, the cyclone efficiency calculated from cascade impactor data substantially confirms the efficiency obtained from total filter/Coulter Counter data. However, the predicted fractional efficiency curve is significantly lower than the measured results. The Koch and Licht model, shown in Figure 4 comes closer to predicting miniplant third cyclone performance than other available models tested. The reason for the lack of agreement between the measured and predicted results is not understood at the present time. Many of the models are semi-empirical and based on data obtained with other particulate systems at lower temperatures and pressures.

Figure 3

Particle Size Distribution
Run 105 - Flue Gas Particulates

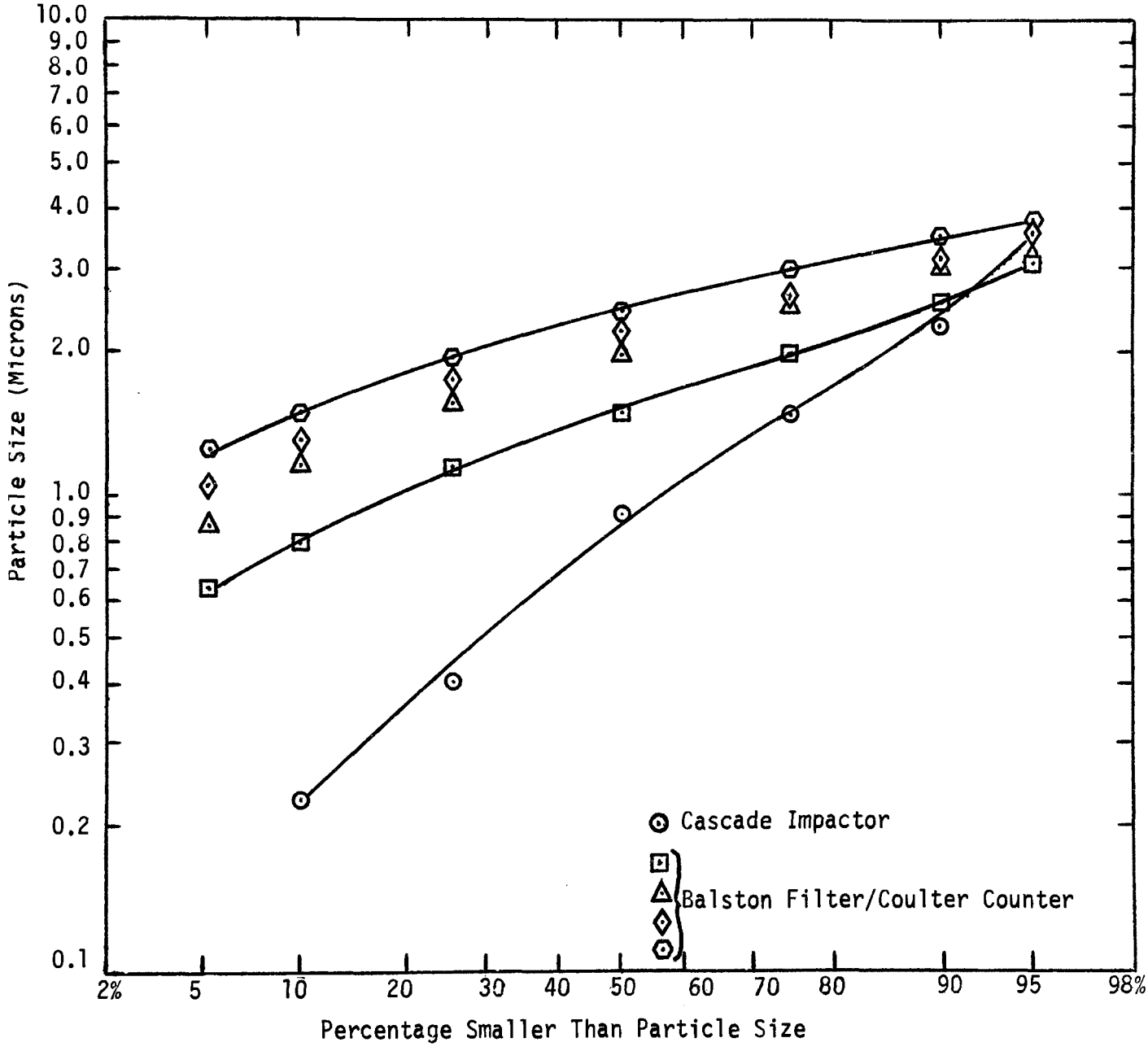

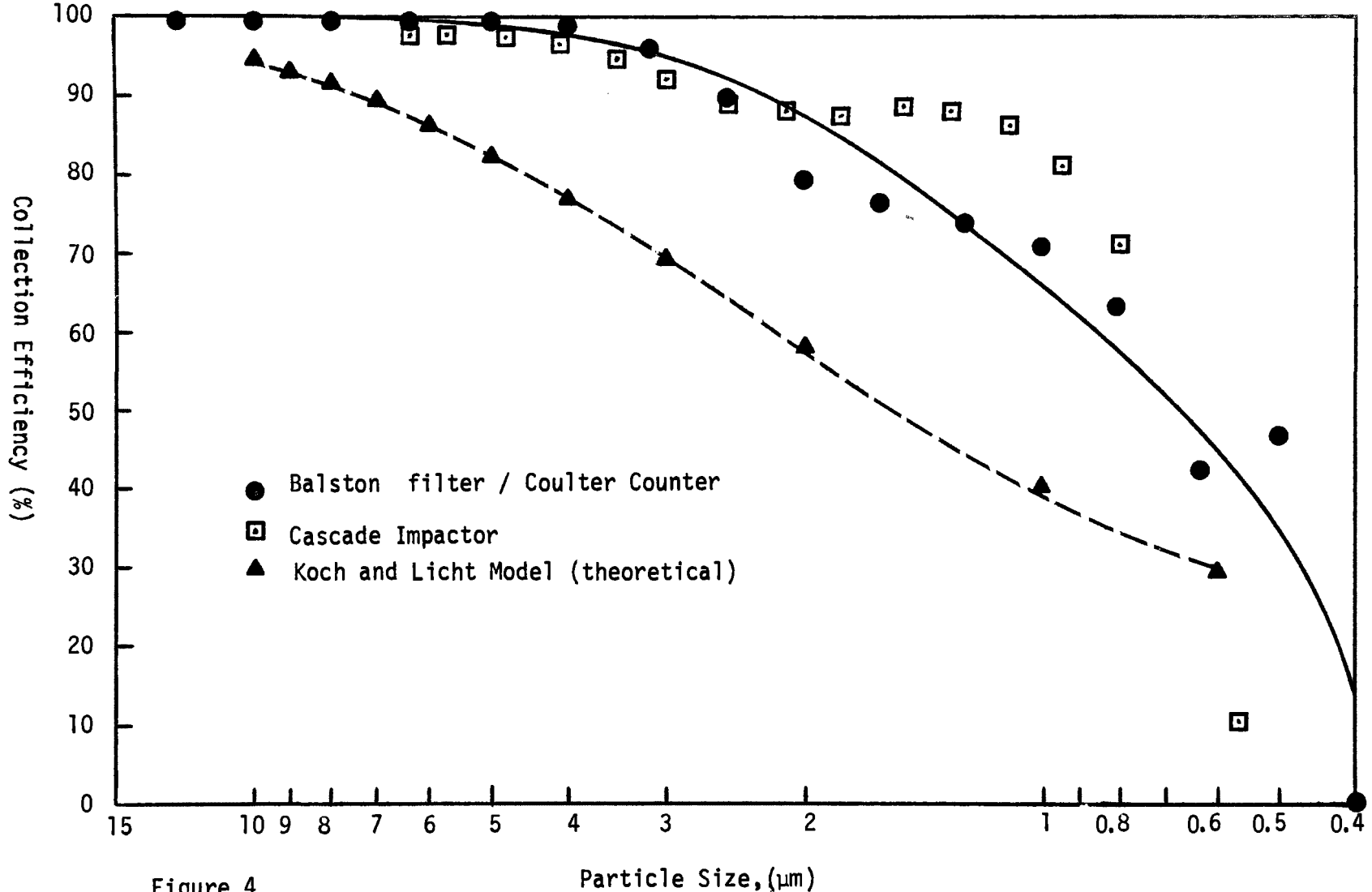

Figure 4

Fractional Cyclone Efficiency

(Run 105)

However, Knowlton and Bachovin (1977) (3) found that pressures up to 5.6 M Pa had little effect on cyclone performance, although their work was based on much higher dust loadings than the current study. Perhaps other effects, peculiar to the PFBC system such as the size and nature of the particulates, the operating temperature or pressure are responsible for the high efficiency. Additional work will be needed to explain the observed results.

CONCLUSION

A cyclone separator, removing fine particulates from the flue gas of the Exxon pressurized fluidized bed combustion unit, was shown to have very high separation efficiency. The efficiency was confirmed using two particulate measurement methods, a total filter/Coulter Counter technique and a cascade impactor. The measured efficiency is higher than that predicted by published correlations.

The cascade impactors did give a smaller size distribution than the total filter with Coulter Counter size analysis. This is similar to results from other systems and is due in part to the measurement range of the instruments. Therefore, the high fractional cyclone efficiencies obtained with Coulter Counter size analysis cannot be explained by deagglomeration during sample preparation.

The use of cyclones alone may be sufficient to protect gas turbines in the pressurized fluidized bed combustion system. However, further cyclone optimization and turbine material testing is required. Environmentally, cyclones have not yet met the new source performance standards (0.03 lbs/MBTU) set by the EPA. However, the improvement in performance required to accomplish this is small. Gas cleanup down stream of the gas turbine may be an attractive alternative to other forms of high temperature high pressure gas cleanup. To that end, tests with mobile electrostatic precipitator and mobile baghouse filter have recently been completed at Exxon by Acurex Corporation under EPA contract. If cyclones are insufficient to protect gas turbines, other more efficient cleanup devices must be developed.

REFERENCES

1. Nutkis, M.S., Pressurized Fluidized Bed Coal Combustion Exposure Testing of Gas Turbine and Heat Exchanger Materials. (Presented at Gas Turbine Conference & Exhibit & Solar Energy Conference. San Diego, Calif. March 1979) ASME Paper No. 79-GT-166.

2. Koch, W.H., and Licht, W., New Design Approach Boosts Cyclone Efficiency, Chem Eng. Nov. 7, 1977. P 80 ff.

3. Knowlton, T.M., and Bachovchin, D.B., The Effect of Pressure and Solids Loading on Cyclone Performance. Presented at A.I.Ch.E. 70th Annual meeting New York, N.Y. Nov. 1977.

CERAMIC FILTER TESTS AT THE EPA/EXXON PFBC MINIPLANT

By:

M. Ernst (Exxon Research and Engineering Company)
M. A. Shackleton (Acurex Corporation)

ABSTRACT

The performance of the Acurex ceramic bag filter operating at temperatures up to 880°C and pressures up to 930 kPa on particulate-laden flue gas from a pressurized fluidized bed coal combustion unit was shown on a slipstream of gas taken after the second stage cyclone. The particle concentration in the flue gas entering the filter was approximately 900 mg/m^3 with 50 percent of the particles finer than 3.5 μm. Filter outlet particle concentrations were typically 7 to 16 mg/m^3. Filter face velocities during the tests ranged from 2.6 to 6.0 m/min. The pressure drop across the filter was never allowed to exceed 12.2 kPa and could generally be maintained below 7.3 kPa before the start of a cleaning cycle. Immediately after a cleaning cycle, pressure drops were typically 0 to 1.0 kPa. The cleaning cycle was 20 to 40 seconds long and consisted of reverse flow and short pressure pulses. The cycle was initiated by sequence timer every 5 to 30 minutes. Three western and mid-western coals were used in the test program. Test periods ranged from 4.5 to 17 hours.

In general, these tests showed that the filter could achieve high efficiency collection and was able to stabilize pressure drop with the cleaning cycle. This was a significant achievement in the HTHP environment and indicates the ceramic fiber filter concept should receive further study to investigate longer term performance and scale-up for potential application as the final clean-up device for PFBC.

Presented for "The Second Symposium on the Transfer and Utilization of Particulate Control Technology", July 23-27, 1979 in Denver, Colorado.

CERAMIC FILTER TESTS AT THE EPA/EXXON PFBC MINIPLANT

INTRODUCTION

Pressurized Fluidized Bed Combustion (PFBC) of coal employed in a combined cycle process for steam and gas turbine power generation offers a potentially important new technique to lessen reliance upon liquid and gaseous fuels. In the gas turbine cycle energy is extracted from the hot high-pressure combustion gas by expanding the gas across a gas turbine. This gas which is typically at 850°C and 10 atm pressure contains large quantities of particles consisting of flyash and bed material. To protect the turbine components from erosion and corrosion, this particulate material must be removed before expansion across the turbine. There is a difference of opinion over what degree of efficiency must be achieved in this particulate removal (and over the significance of the role of alkali metal constituents in the gas stream) nevertheless, there is general agreement that a hot gas cleaning device is the major factor preventing commercialization of PFBC technology for power generation.

E. F. Sverdrup of the Westinghouse Research and Development Center analytically determined the tolerance of large turbines to particulate loading (i.e., Sverdrup (1978)[1]). Sverdrup's calculations indicate that cleaning of turbine expansion gas to a level of 4.6 mg/Nm^3 (0.002 grains/SCF) -- with all particles larger than 6 μm removed -- is currently the best estimated level of cleanliness needed for turbines. This analysis predicts a maximum blade erosion of 2.5 mm (0.10 inch) in 10,000 hours of operation. Tests at Acurex have shown high filter efficiencies resulting in a particulate loading considerably lower than Sverdrup's estimate of turbine requirements.

Nearly every type of particulate removal device has been proposed for high-temperature, high-pressure (HTHP) applications, including acoustic agglomerators, molten salt scrubbers, cyclones, granular beds, electrostatic precipitators, and ceramic filters. Professor E. Weber from the University of Essen has published a review paper entitled "Problems of Gas Purification Occurring in the Use of New Technologies for Power Generation" (i.e., Weber (1978)[2]). In this paper, he concludes that gravity and momentum force separators will not adequately remove particles from HTHP gas streams and will, therefore, be used only as precleaners. He also states that the required degree of cleaning can be achieved using fabric filters, and points out that fibrous ceramic materials are available which can withstand the temperatures expected in PFBC applications.

Granular bed filters have been considered the best available option for HTHP particulate control. However, tests at the Exxon Miniplant have shown that many problems remain to be solved before achieving high efficiency and long life in these devices (i.e., Hoke (1978)[3]). These problems involve achieving high collection efficiency and cleanability at reasonable pressure drop.

Many of the particle removal devices proposed for HTHP applications operate primarily through the mechanism of inertial impaction. These devices include all forms of cyclones, scrubbers and granular beds. Because gas viscosity increases with rising temperatures, the efficiency of all inertial devices is less at HTHP conditions than at room ambient conditions. Barrier filtration, on the other hand, is unique in that a theoretical basis exists to predict improved performance at high temperature and pressure conditions. This improvement results from using fine (3 μm) diameter ceramic fibers to construct the filter. Conventional filter media usually employ fibers 10 to 20 μm in diameter. The fine diameter fibers increase the filter efficiency enough to overcome the adverse effects of increased temperature (i.e., Shackleton, Kennedy (1978)[4]).

In August 1976, Acurex began an EPA-sponsored program to demonstrate the feasibility of employing available ceramic fibers in high temperature and pressure filtration. Under this two-year contract, the theory of barrier filtration was examined and a wide spectrum of ceramic papers, cloth and blanket felts were tested for filtration performance at room ambient conditions. A high temperature and pressure filter test rig was built. Promising media from room ambient tests were subjected to accelerated cleaning tests at HTHP conditions for 50,000 cleaning pulses. Ceramic blanket materials were shown to offer the greatest promise for further development. During 200 hour tests over a range of filter media face velocities (air-to-cloth ratio), SAFFIL alumina was judged to be the best commercially available material for filter application (i.e., Shackleton (1979)[5]). The filter media configuration employed is a loosely packed mat of fine fibers. Because the fibers are so small they achieve high collection efficiency even though the mat is not tightly held together. This porous "fluffy" mat of fibers is able to survive the mechanical stresses of cleaning because none of the fibers can exert large forces on each other because they are not firmly fixed in place. One of the test rig pressure vessels was modified to test a filter made from SAFFIL alumina on a slipstream at the Exxon PFBC Miniplant. This report presents the results of those tests.

TEST DESCRIPTION

To accomplish slipstream tests of the ceramic filter at the Miniplant, one of the existing test pressure vessels of the Acurex HTHP filter media test rig was modified. This modification consisted of changing the inlet location so that a dust hopper could be added to the vessel. In addition, an electronic control system was fabricated to operate the cleaning cycle. After modification, the single bag test unit could be operated automatically on a slipstream from the PFBC.

A cross section of the modified pressure vessel filter housing is shown in Figure 1. Hot, dusty inlet gas enters the unit from the side below the test filter. This gas impacts against a plate on the dust hopper. Heavy particles may remain in the hopper while others travel upwards to the filter element. The filter element was 10 cm in diameter by 45.7 cm long. A heater element surrounded the test filter and was used to maintain gas temperature in the test filter zone. After removal of particles by the test filter, hot gases exit the chamber through a pipe in the top of the vessel.

Figure 2 illustrates the installation of the test filter on a gas slipstream downstream of the Miniplant second stage cyclone. The electronic time sequencer controlled the operation of the cleaning cycle. Cleaning cycle parameters were adjustable but the basic cleaning sequence was as follows:

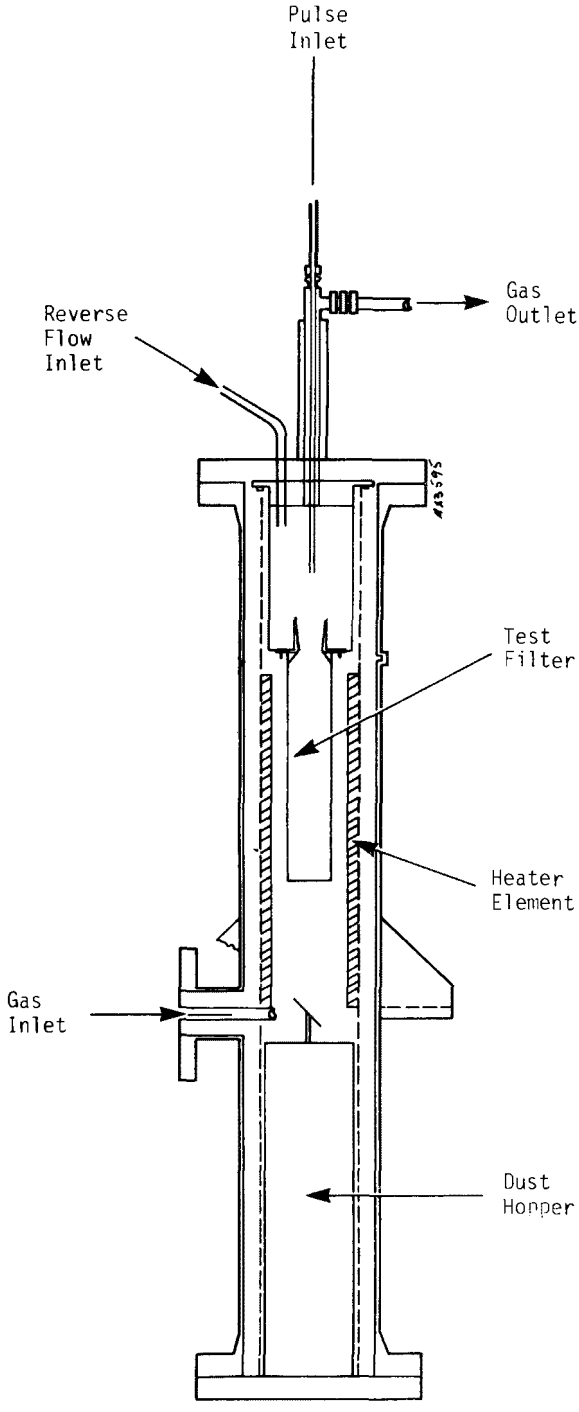

Figure 1. Filter housing pressure vessel cross section.

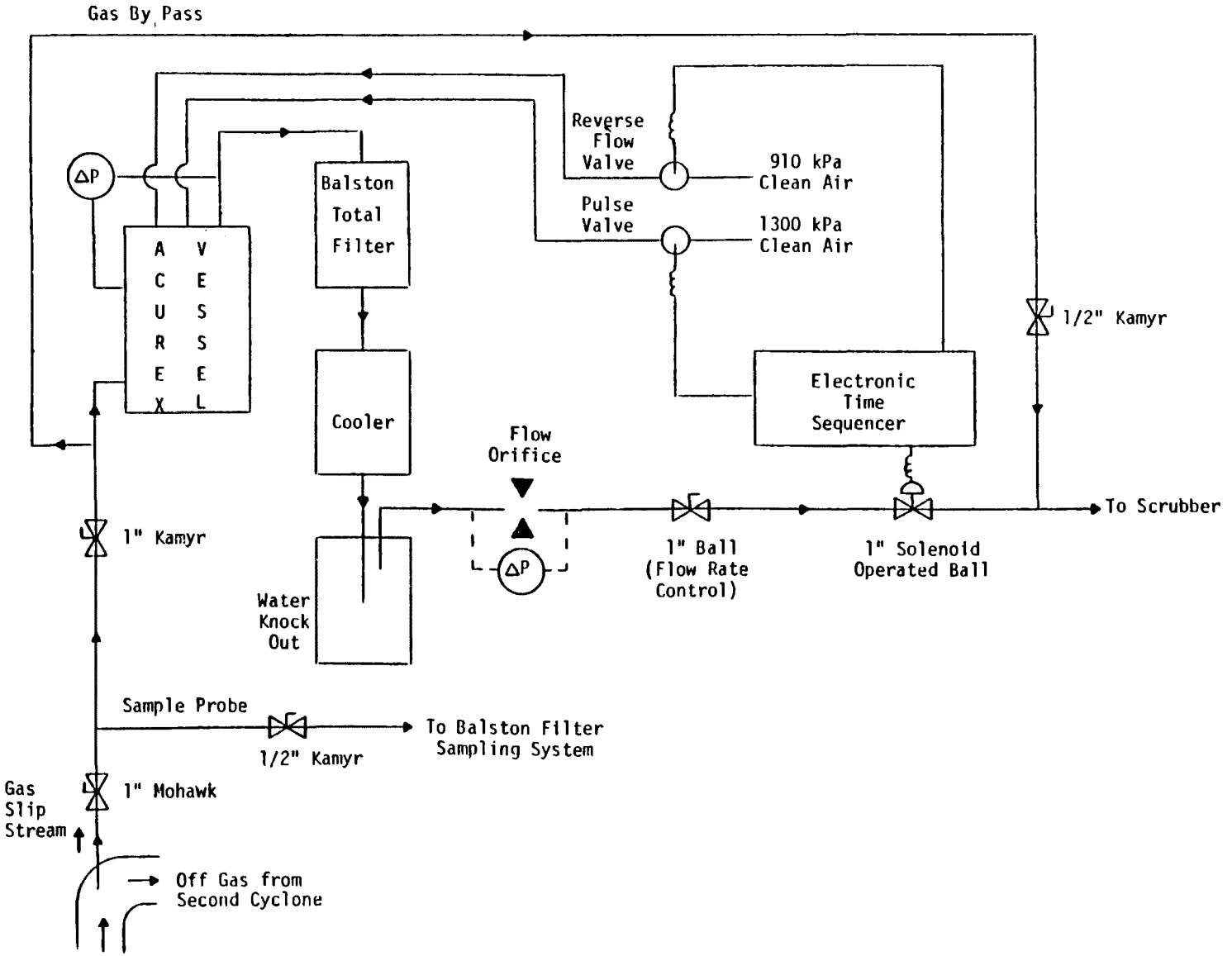

Figure 2. Acurex test filter installation schematic.

- Start on a timed interval by closing a solenoid valve downstream, taking the filter off-line
- Start a gentle reverse flow of unheated gas
- Release one or more cleaning pulses, (amplitude, duration and pulse interval are all adjustable)
- Wait several seconds for dust removed during pulsing to fall into the dust hopper
- Stop reverse flow
- Open the downstream solenoid valve, returning the filter to service

Figure 3 is a photograph of the filter unit installed at the Miniplant. The slipstream for the bag filter leaves the main flow duct through a 1-inch pipe. Two high-temperature valves, a 1-inch Mohawk ceramic gate valve and a 1-inch Kamyr ball valve, were used to isolate the filter from the PFBC. Hot gas entered the filter vessel at a point just below the bag, but above the dust hopper. Just before the filter vessel, a gas bypass line allowed extra gas to be withdrawn from the PFBC to maintain temperature in the inlet line. This bypass line was also used to preheat the inlet line prior to the start of filtration.

The filtered gas leaving the top of the filter pressure vessel cooled down to 440°C before it entered the Balston total filter shown in Figure 2. The weight gain of this filter was used to determine the outlet particulate concentration. The gas was further cooled and the water removed in a knockout vessel before it was measured through a flow orifice and expanded through a ball valve. Pressure drop across the ceramic filter was continuously measured and recorded. Inlet particulate concentration was measured by extracting a sample and passing it through a Balston total filter.

Various tests at the miniplant are assigned run numbers. Tests of the ceramic filter were accomplished in parallel to other tests at the miniplant. That is the filter tests were not the primary reason to operate the facility. The filters were evaluated during runs 82 through 96. Runs 82 to 85 were devoted to system shakedown. Typically, a run lasted for one working day. At the end of that time we changed test filters and began a new test the following day

Several problems with valves occurred during the shakedown runs 82 through 85. The Kamyr valve failed during run 83. It was removed and not replaced. The Mohawk valve bonnet leaked during run 84. That gasket was replaced with a copper gasket and the valve performed satisfactorily until the alumina gate cracked during run 93. The solenoid valve that shuts off the filtered gas flow during blow back failed during run 85. The teflon seat of this valve had become damaged by hot gas. The valve was replaced with a solenoid operated ball valve which functioned well for the remainder of the test. Otherwise, shakedown ran smoothly and was mainly used to optimize the cleaning phase of the filtration cycle.

TEST RESULTS

Pressure drop across the filter bags was recorded on chart paper and varied as a function of time in a manner typical for fabric filters. Figure 4 illustrates typical pressure drop and flow recordings. Baseline pressure drop was defined as the pressure drop of a bag at the start of the filtration cycle. Graphically this point corresponds to the first point in each cycle in Figure 4. Many filters were operated for several hours at baseline pressure drops close to

Figure 3. Acurex HTHP ceramic bag filter site.

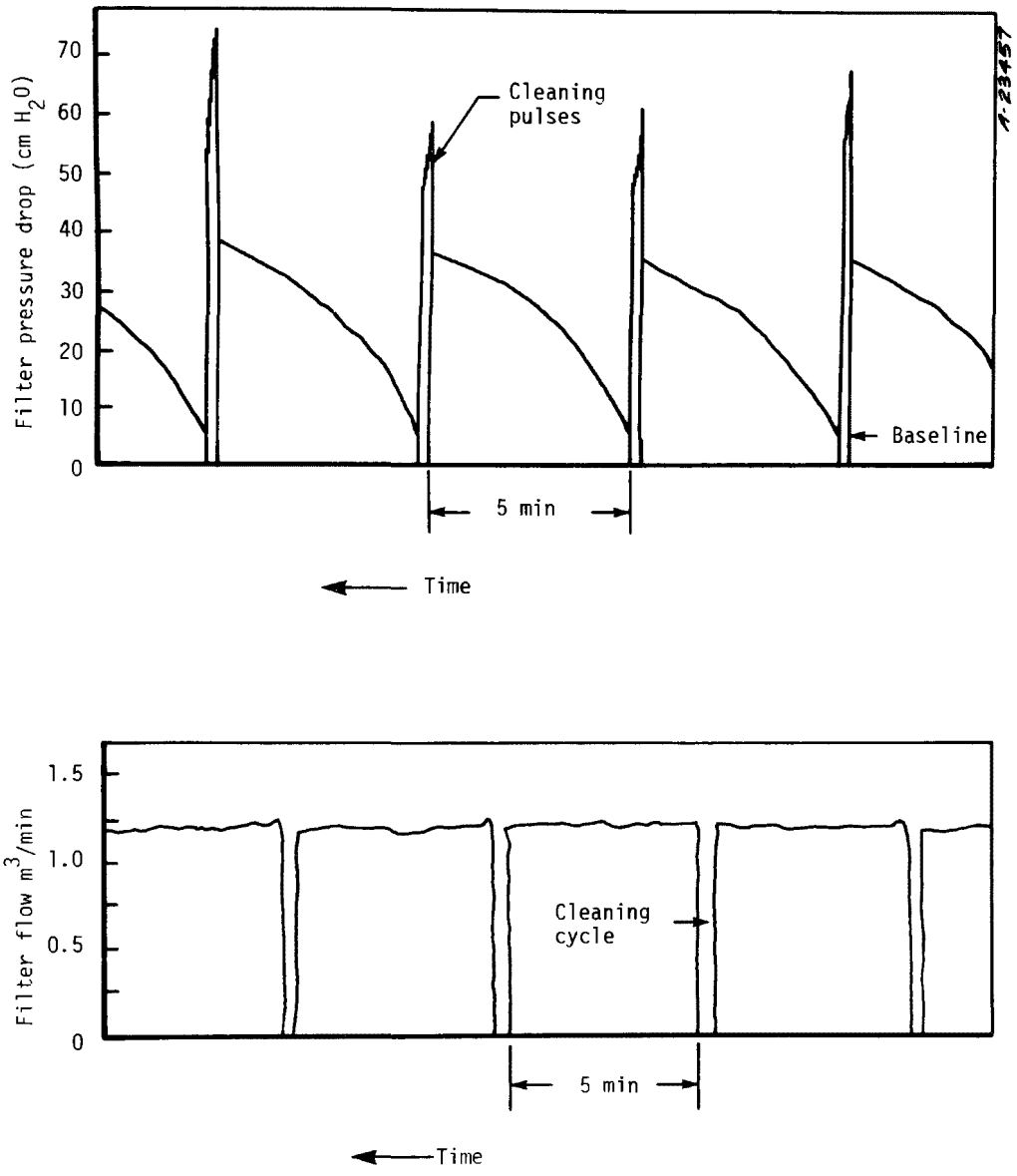

Figure 4. Acurex HTHP ceramic bag filter pressure drop and flow.

that for a new bag. The baseline pressure drop was always between 0.1 and 5.0 kPa, usually between 0.2 and 2.0 kPa. Pressure drops before cleaning were never allowed to exceed 14 kPa to reduce the chance of bag failure. High-pressure drops generally caused the inner filter support screen to bulge into the cage onto which the filter was fastened. Baseline pressure drops were slightly higher when filtering Champion coal than when filtering Illinois No. 6 coal under similar conditions. Outlet particulate loadings were slightly lower with Champion coal than with Illinois No. 6 coal. The overall influence of coal type was small, and could not be quantified from the relatively few tests completed at the Miniplant. Filter bags were used for from 4.5 to 19 hours. A summary of test conditions, pressure drops, and outlet particulate loadings is shown in Table 1.

Filtration efficiencies for the Acurex ceramic bag filter were generally over 90 percent, ranging from 96 to 99.5 percent. An exact filtration efficiency was difficult to determine because of problems in measuring the filter inlet particulate concentration. Filter inlet particulate concentration was measured or calculated by three methods: (1) Balston total filter catch on an extracted sample, (2) mass balance around the third Miniplant cyclone, (3) mass balance around the ceramic bag filter. The results obtained by these three techniques were not consistent as shown in Table 2.

The test filter inlet line (Figure 5) was 1-inch schedule 80 pipe taking a sample from a 4-inch schedule 5 pipe. Isokinetic flow would have been 1.15 Nm^3/min (41 SCFM). This flow was cooled from 800°C to 450°C before reaching the filter vessel. A bypass flow of 1.4-2.3 Nm^3/min (50 to 80 SCFM), in addition to the filtered gas, was drawn through the line to help maintain temperature near 800°C. The flow into the filter inlet line was therefore 200 to 300 percent isokinetic. The Balston total filter inlet sample (1/4-inch probe) was incorrectly operated isokinetically with respect to the filtered gas only, neglecting the bypass gas which was present at that point. Therefore, the Balston total filter samples were taken at only 30 to 50 percent isokinetic rates. For this particle size range and loading, isokinetic flow appears to be important, and this inlet loading may be treated as a lower limit of particle concentration.

The mass balance around the third Miniplant cyclone would have been a valid way to measure inlet concentration if the inlet sample of the ceramic filter had been taken under isokinetic conditions. This was not the case, and therefore this method of determining particulate concentration is not accurate.

A mass balance around the filter test vessel was attempted to resolve the inlet loading issue. Weight of the filter bags was not determined before exposure, so a tare of 0.2 Kg was assumed by weighing other unexposed bags. These inlet loadings, intermediate to the other two results, can still be considered low because of the multitude of places where particulates could have been lost during cleaning and dismantling operations. However, from these three calculation methods a reasonable estimate can be made of the actual inlet particulate concentration.

The bag filter outlet particulate concentration was determined by passing the entire filtered gas flow through a Balston total filter. The total particulate concentration was obtained by weighing the total filter before and

TABLE 1. ACUREX HTHP BAG FILTRATION SUMMARY

Run No.	Bag No.	Coal Type[4]	Outlet Load (g/m^3)	Flow Rate m^3/min	Face Velocity m/min	Average Temperature (°C)	ΔP (kPa) Baseline min	ΔP (kPa) Baseline max	ΔP (kPa) Max Before Cleaning	Filtration Cycle[6] Time (min)	Run Duration hrs
83	1	I	NA	1.42	4.0	NA	0	0.2	3.7	NA	4
84	1	I	NA	1.36	4.1	891	1.2	2.5	8.0	NA	3
85	2	I	0.0684	1.36	3.9	847	0	2.0	4.0	10	3.5
86	2[1]	I	0.0093	1.33	3.2	659	0	0.5	1.7	5	4.5
87.1	3	I	0.0146	1.70	4.0	635	0	0.2	1.0	5	3
87.2	3	I	0.0087	1.73	4.4	701	0	0.2	1.0	7	2.3
87.3	3	V	0.0027	1.81	4.5	679	0.2	0.2	1.7	15	3
88.1	3A	V	0.0205	2.01	5.4	762	0.4	0.5	2.5	20	2
88.2	3A	C	0.0137	2.27	6.0	752	0.5	3.0	6.5	20	2
88.3	3A[2]	C	0.0114	1.70	4.9	832	1.2	2.0	7.5	20	1
89.1	4	C	0.0226	1.84	5.1	801	0.1	0.1	5.0	20	1
89.2	4	C	0.0226	1.84	5.2	812	0.5	0.5	6.7	20	1
89.3	4	C	0.0226	1.42	3.9	791	0.5	2.0	7.7	20	1
89.4	4	C	0.0226	1.42	4.0	812	1.9	2.5	7.5	10	3
90	5	C	0.0089	1.42	3.9	790	0.1	2.0	7.5	5	5
91.1	5	C	0.0066	1.42	3.8	750	1.9	2.5	8.7	4	2.5
91.2	5	C	0.0034	1.42	3.8	757	2.5	3.7	9.5	4	3
91.3	5	C	0.0036	1.42	3.8	758	3.7	5.0	10.5	4	2.5
92.1	6	C	0.0059	1.13	3.1	762	0.2	0.5	5.2	10	3.3
92.2	6	C	0.0050	1.08	3.0	805	0.5	0.5	7.7	7	2.6
93.1	6	C	0.0071	0.99	3.1	787	0.2	0.5	3.5	5	3
93.2	6	C	0.0046	0.99	2.8	828	0.5	1.5	5.0	4	5
94	7[3]	C	0.0661	2.05	5.8	823	0.7	1.7	3.5	4	6
95	8	C	0.0116	1.84	5.1	797	0.5	5.0	11.2[5]	4	4.5
96.1	9	C	0.0157	1.10	2.8	693	0	0.5	6.5	10	3
96.2	9	C	0.0066	1.10	2.7	665	0.5	1.0	10.0	10	2
96.3	9	C	0.0066	1.10	2.7	665	1.0	2.5	8.7	5	1
96.4	9	C	0.0155	1.10	2.9	754	1.9	2.5	13.7[5]	5	3
96.5	9	C	0.0296	1.10	2.9	727	0	0.5	3.7	5	7
96.6	9	C	0.1870	1.10	2.6	648	0	0	0.5	5	2
96.7	9	C	0.2440	1.10	2.6	648	0	0	0.7	5	1

---

(1) Bag vacuumed prior to run.
(2) Pictured in Figures
(3) Double thickness ceramic filter material.
(4) Coal type "I" is Illinois No. 6
"V" is Valley Camp (Ohio)
"C" is Champion (Pennsylvania)
(5) Chart recorder limit exceeded.
(6) Time for filtration between cleaning cycles.

TABLE 2. ACUREX HTHP BAG FILTER INLET PARTICULATE LOADINGS

Run No.	Inlet Particulate Loading (g/m^3)		
	Sample by Balston Total Filter at Inlet	Calculated from Mass Balance Around 3rd Cyclone	Calculated from Mass Balance Around Filter
86	0.40	0.79	N/A
87.1	0.31	1.09	N/A
87.2	0.30	1.09	N/A
87.3	0.32	1.09	N/A
88.1	0.30	0.77	N/A
88.2	0.60	0.77	N/A
88.3	0.60	0.77	N/A
89.1	0.48	1.08	N/A
89.2	0.48	1.08	N/A
89.3	0.37	1.08	N/A
89.4	0.37	1.08	N/A
90	0.47	1.35	0.48
91.1	0.40	1.06	0.48
91.2	0.40	1.06	0.48
91.3	0.57	1.06	0.48
92.1		0.92	0.84
92.2		0.92	0.84
93.1	1.22	1.16	0.84
93.2	1.22	1.16	0.84
94	0.53	1.16	0.73
95	N/A	0.96	0.73
96.1	N/A	1.06	0.73
96.2	N/A	0.94	0.73
96.3	N/A	0.94	0.73
96.4	N/A	1.65	0.73
96.5	N/A	1.65	0.73
96.6	N/A	1.65	0.73
96.7	N/A	1.65	0.73

N/A = Not Available

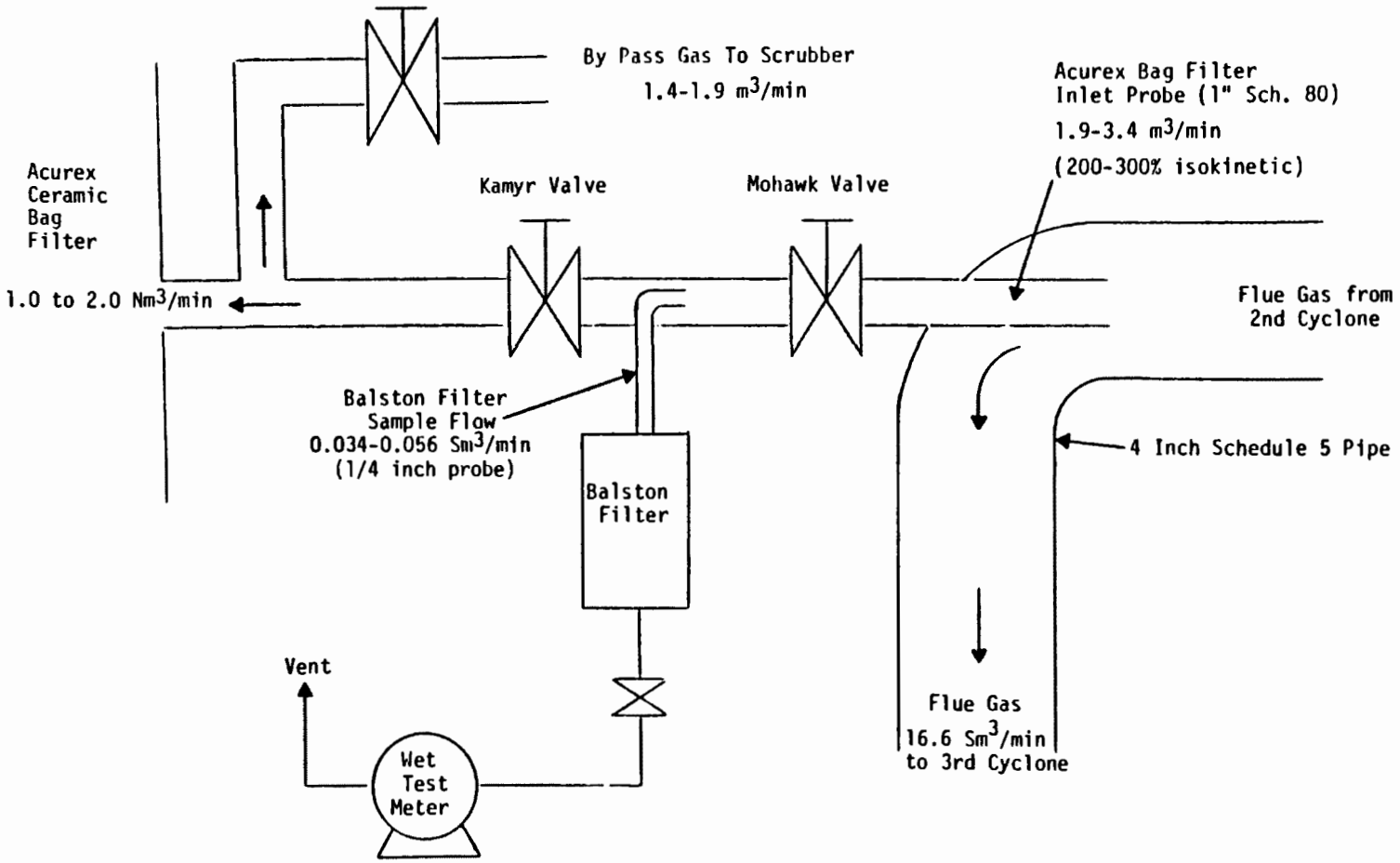

Figure 5. Acurex high-temperature ceramic bag filter gas inlet schematic.

after exposure. Overall ceramic bag filter efficiencies are shown in Table 3. These were calculated using the three methods of determining inlet concentration discussed previously. Despite some uncertainty in the inlet particulate concentrations, the collection efficiencies calculated by the three methods were generally in good agreement.

A size distribution of the outlet particulates could not be obtained. The amount of particulates on the Balston filter was so low that insufficient material was available for Coulter Counter analysis. The filters were washed off with Isoton II in an attempt to remove particulates without mechanical brushing. This method caused enough Balston filter material to be washed into solution to completely obscure the flyash particulates. A clean Balston filter, not exposed to any flyash but also washed with Isoton gave a sample which had a size distribution similar to that obtained from a used filter.

During the tests at the Miniplant, eight single and one double thickness bags were exposed to PFBC conditions. Most bags were exposed for 6 hours or more. Averaging the face velocity and exit particulate concentration over the first 6 hours of new bag exposure and plotting outlet loading as a function of face velocity provided the data shown in Figure 6. Bag number 4 results were not recorded on Figure 6 because of problems with the outlet filter. Bag number 7 was a double thickness bag (~2 cm). Nominally filter media thickness was about 1 centimeter. It was physically less distorted and its pressure drop was less than bag 8 which was run at similar conditions, but its filtration efficiency was much lower. The reason for the discrepancy is not known (it evidently had a leak). As seen in Figure 6, the particulate penetration of a bag increases with face velocity. The trend lines shown on the curve were selected by drawing a line through the Illinois No. 6 results which fell on a straight line. The data is not as precise as may be implied by this curve. One could easily make a claim for no correlation. In fact, an objective of off-line cleaning is to offset the increased penetration with velocity that is normally seen in filter tests. This data is interpreted to show little effect of coal type or of increased face velocity over the range tested.

Outlet loading plotted in Figure 6 was averaged over the first 6 hours of operation. Outlet loading actually decreased as a function of time in the same fashion that a conventional filter media test would show in similar tests under ambient conditions. This decrease as a function of time is shown as Figure 7. This bag was exposed to Champion coal at 775^{o}C for a total of 13 hours. Along with the decrease in filter particle outlet loading there was an increase in baseline pressure drop from 0.1 to 3.0 kPa as expected.

Examination of the filters after a test showed that the dust cake was deposited mostly on the surface of the filter media and the dust cake could be removed easily. Figure 8 shows bag number 3 immediately after removal from the filtration vessel. Figure 9 is a close up of the same bag after a strip was vacummed clean. This strip had the appearance of a virtually new bag indicating very little dust penetration into the media.

At the conclusion of the series of short runs, run 96, a long continuous test of the bag filter was attempted at conditions deemed optimum for extensive testing. Filtration commenced smoothly, however, the baseline pressure drop across the bag continued to increase during the first 6 hours of filtration. A

Run No.	Outlet Particulate Loading (g/m^3)	Collection Efficiency (%) Sampled by Balston Total Filter at Inlet	Calculated from Mass Balance Around 3rd Cyclone	Calculated from Mass Balance Around Filter	Average
86	0.0093	97.6	98.8	N/A	98.2
87.1	0.00146	95.2	98.7	N/A	97.0
87.2	0.0087	97.1	99.1	N/A	98.2
87.3	0.0027	99.1	99.8	N/A	99.5
88.1	0.021	93.0	97.3	N/A	95.2
88.2	0.014	97.7	98.2	N/A	98.0
88.3	0.011	98.1	98.5	N/A	98.3
89.1	0.023	95.3	97.9	N/A	96.6
89.2	0.023	95.3	97.9	N/A	96.6
89.3	0.023	93.9	97.9	N/A	95.9
89.4	0.023	93.9	97.9	N/A	95.9
90	0.009	98.1	99.3	98.1	98.5
91.1	0.007	98.3	99.4	98.6	98.8
91.2	0.003	99.1	99.7	99.3	99.4
91.3	0.004	99.4	99.7	99.2	99.4
92.1	0.006	--	99.4	99.3	99.3
92.2	0.005	--	99.5	99.4	99.4
93.1	0.007	99.4	99.4	99.2	99.3
93.2	0.005	99.6	99.6	99.5	99.6
94	0.066	87.6	94.3	90.9	90.9
95	0.012	N/A	98.8	98.4	98.6
96.1	0.016	N/A	98.6	97.8	98.2
96.2	0.007	N/A	99.4	99.1	99.2
96.3	0.007	N/A	99.4	99.1	99.2
96.4	0.016	N/A	98.6	97.9	98.3
96.5	0.030	N/A	97.4	95.9	96.7
96.6(1)	0.187	N/A	83.5	74.4	78.5
96.7(1)	0.244	N/A	78.4	66.6	72.5

N/A = Not Available

(1) Bag Failed

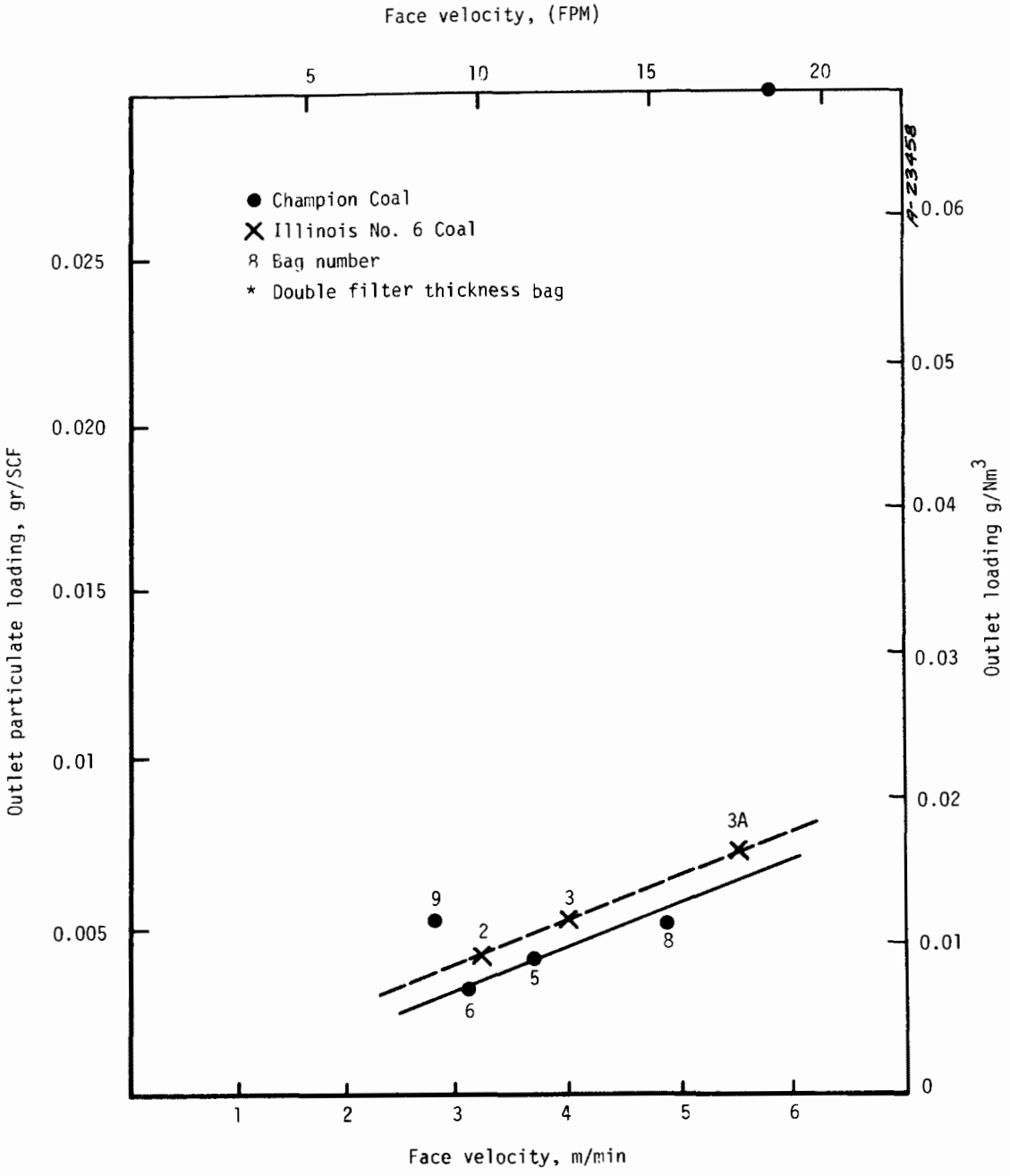

Figure 6. Acurex HTHP bag filter outlet loading vs. face velocity (averaged over first 6 hours of exposure).

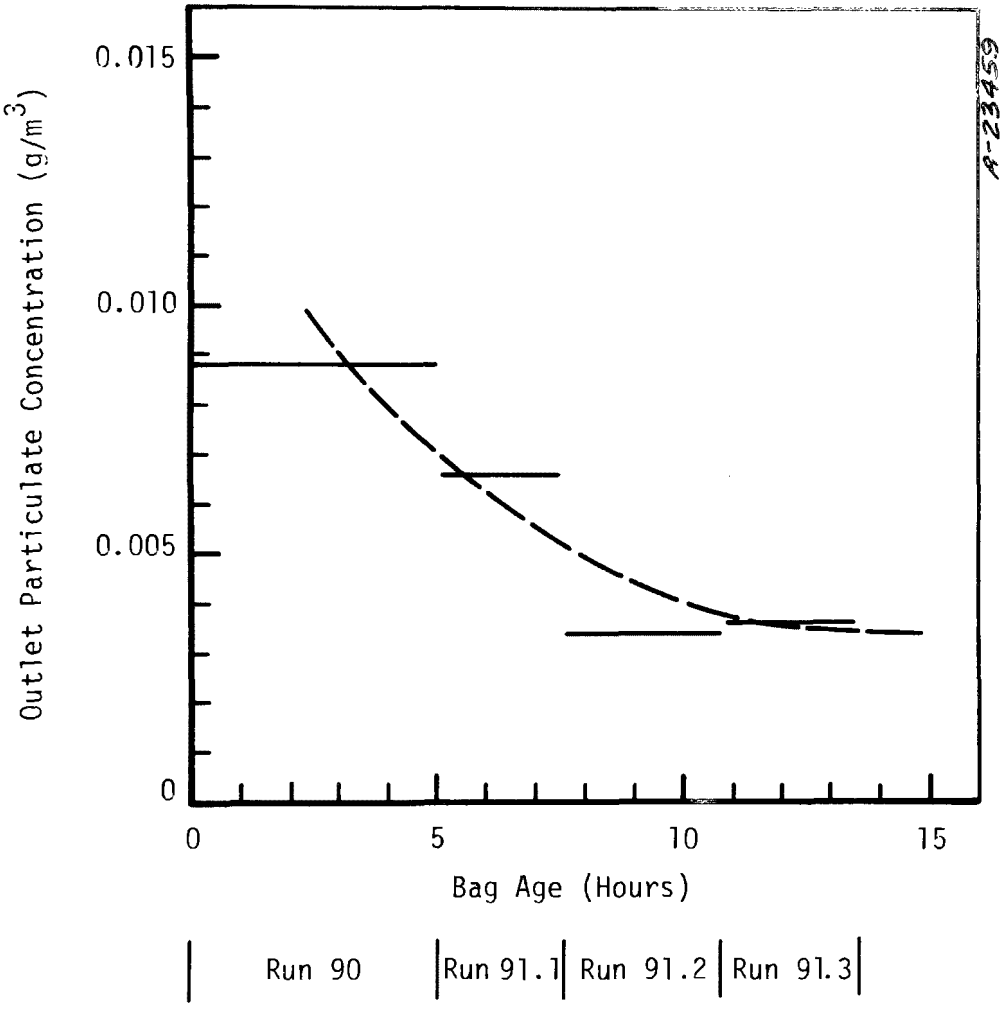

Figure 7. Acurex ceramic bag filter -- bag no. 5 particulate penetration history.

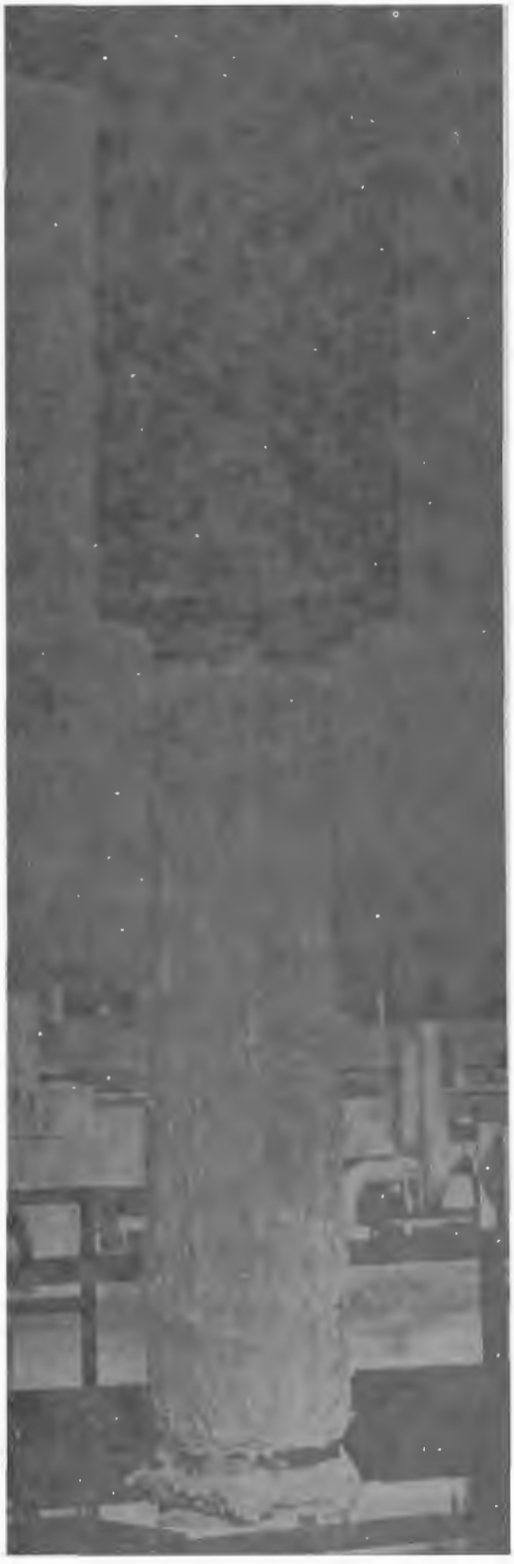

Figure 8. Ceramic filter bag (no. 3).

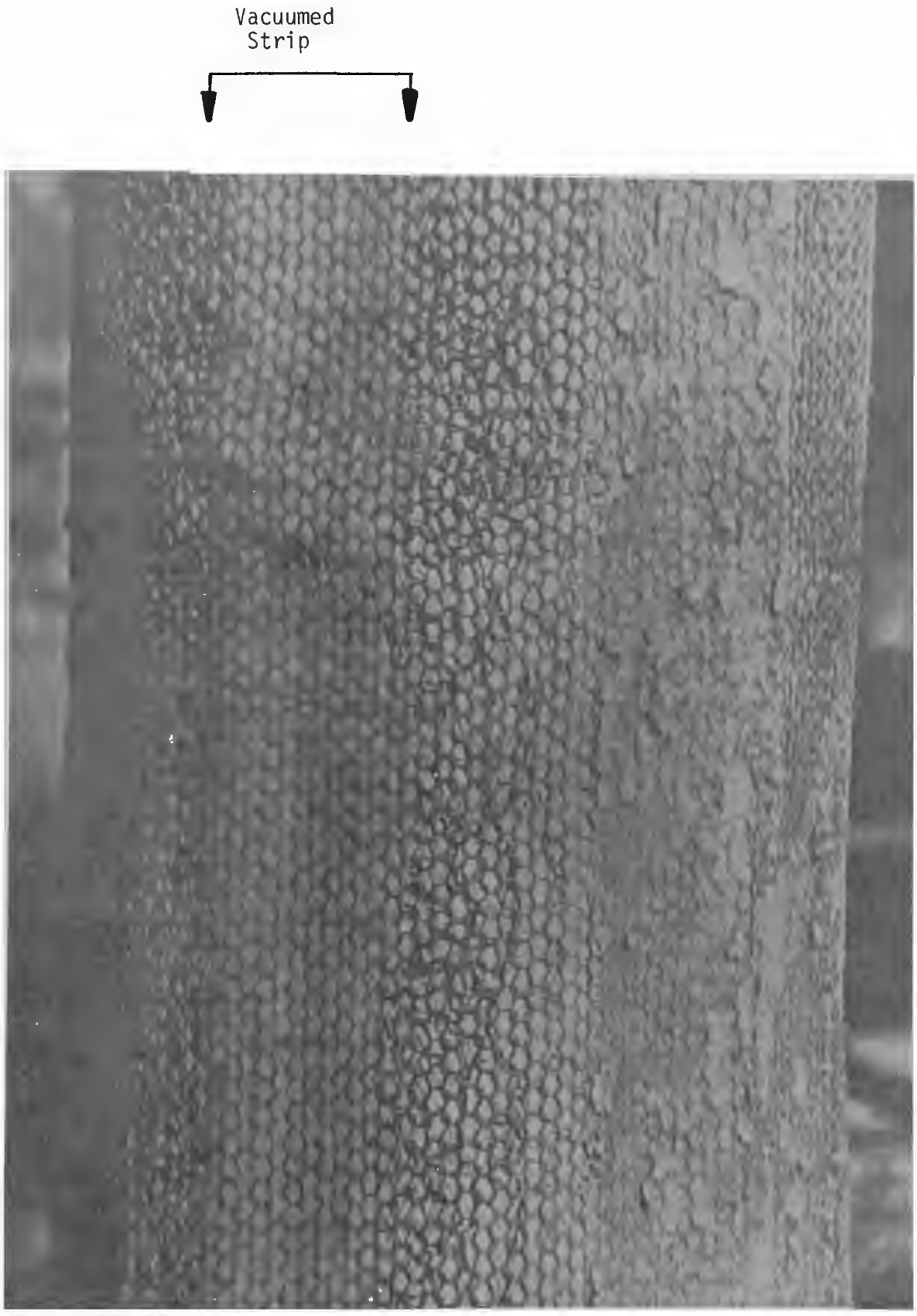

Figure 9. Ceramic filter bag (No. 3) closeup of vacuumed strip.

possible reason for this increase became clear at the conclusion of the run when it was discovered that the pressure regulator used to set the pressure of the reverse flush air was set only slightly higher than filter vessel system pressure. It is possible that a slightly higher combustor pressure could have reduced reverse flush air flow to a level too small to clean the filter effectivley. Since the reverse flush air flowrate was not measured, this hypothesis cannot be confirmed.

After 6 hours of filtration during run 96, a pressure drop of 12.5 kPa (50-in. Wc) across the filter was thought to be excessive for continued bag life. The vessel pressure was reduced to 300 kPa and a full high pressure pulse blow back was initiated into the lowered system pressure! This reduced the pressure drop almost back to the clean baseline condition (0.5 kPa, 2-in. Wc). However, outlet particulate concentration increased over the next 12 hours until it was almost identical to the inlet concentration. The run was terminated at that point. As expected, the bag had failed (see Figure 10). The bag failure prob- ably began with the high pulse pressure, low system pressure blow back, and was made worse by subsequent blow backs. The reason for the failure appeared to be hightemperature corrosion of the thin 304 stainless steel filter support screen.
The blown out appearance was probably caused by the high pressure pulse into the lowered system pressure environment.

High-temperature corrosion of the 304 stainless steel media support screen was accelerated when the thermocouple controlling the heater elements which maintain test temperature in the filter test zone came loose from the heater element surface early in the test. This caused the heater elements, which are capable of reaching 1200°C (2200°F) to heat the media support screen to temperatures in excess of the 815 to 870°C (1500 to 1600°F) planned for. It is recognized that corrosion of a metal support screen is a potential problem in long term applications. The metal support screens used in these tests were used only for ease of construction. Flexible woven ceramic fabric screens are available to perform this function for applications requiring greater corrosion resistance.

SUMMARY AND CONCLUSIONS

The Acurex high-temperature, high-pressure ceramic fiber filter system successfully completed a series of tests collecting flyash in a slipstream of gas downstream of the secondary cyclone at the EPA/Exxon PFBC Miniplant.

The filter was evaluated on the Miniplant during runs 82 through 96. Runs 82 through 85 were devoted to system shakedown. Actual evaluation of the filter started with run 86 and culminated with run 96, a 19-hour continuous filtration run.

During the tests, pressure drops of under 2 kPa were maintained for over 6 hours average duration at face velocities of 6.4 m/min with efficiencies of 95 to 99 percent.

These tests proved the ceramic filter was cleanable while subjected to flyash generated under PFBC conditions. High collection efficiency at high face velocity was also shown. In general, the test filter exhibited performance

Figure 10. Ceramic filter bag no. 9 after run 96.

similar to that which would have been expected from a filter unit operating under more common conditions.

High efficiency fine particle collection results from the use of small fiber diameter (3 μm nominal) in the filter media. The ability of the media to withstand cleaning stresses results from both fine fiber diameter and low solidity. The individual fibers are not held tightly together, and because of their low mass do not exert large forces on each other. Filter cleaning is enhanced through the use of fine fibers and off-line cleaning. The high collection efficiency of the fine fibers results in collection of particles near the surface of the media. Off-line cleaning prevents reintrainment of dust from the filter element being cleaned by adjacent filters. This permits the use of high face velocities also because it is reintrainment which limits air-to-cloth ratio in currently available pulse filter systems.

The ceramic filters are not inherently expensive. High temperature/pressure filters will cost more than standard filters, but primarily because of the pressure vessels, insulation requirements and the use of corrosion resistant alloys. These factors are present in all the components of a PFBC system. Compared to the costs of these components, the filter media cost is expected to be acceptable. The ceramic materials used for the filter media and the filtration concepts are applicable to high temperature, low pressure applications as well. This fact may create sufficient demand to lower costs still further and provide the benefits of high-temperature particle control to a wide spectrum of industry.

RECOMMENDATIONS

Testing of ceramic filters to date has been aimed at showing that these materials can be used for filtration purposes. This objective has been accomplished and it now seems clear that a practical high-temperature filter can be developed. Protecting gas turbines from the products of coal combustion in a PFBC is a difficult task and Acurex recommends that work on filtration using ceramic fiber media be resumed as quickly as possible. Component development, performance optimization, and verification of long term durability all need to be addressed for HTHP applications.

The ceramic filter may possibly be used as a "dry scrubber" by doping the dust cake with the appropriate chemicals injected into the upstream flow. The large surface area within the dust cake will enhance the scrubbing action. This may be a feasible means for removing vapor phase alkali metals or other gases from a PFBC and should be investigated experimentally.

A high-temperature filter in atmospheric pressure applications offers benefits of smaller size, less energy consumption, and lower cost. For example, heat recovery and subsequent energy savings may be enhanced with a high-temperature filter. The size of such a device could be reduced because the need for dilution air will not be as great. This capability, coupled with operation at high filter face velocity and heat recovery, could offer fine particle control at a lower total cost than is presently possible in other applications. There are also many process applications where a high-temperature filter could offer savings in energy, efficiency or product recovery.

REFERENCES

1. Sverdrup, E. F., D. H. Archer, and M. Menguturk. The Tolerance of Large Gas Turbines to 'Rocks,' 'Dusts,' and Chemical Corrodants. EPA-600/9-78-004, CONF-770970. pp. 14-32, March 1978.

2. Weber, E. Problems of Gas Purification Occurring in the Use of New Technologies for Power Generation. EPA-600/9-78-004, CONF-770970. pp. 249-277, March 1978.

3. Hoke, R. C., and M. W. Gregory. Evaluation of a Granular Bed Filter for Particulate Control in Fluidized Bed Combustion. EPA-600/9-78-004, CONF-770970. pp. 111-131, March 1978.

4. Shackleton, M., and J. Kennedy. Ceramic Fabric Filtration at Hig Temperatures and Pressures. EPA-600/9-78-004, CONF-770970. pp. 193-234, March 1978.

5. Shackleton, M. A., Extended Tests of Saffil Alumina Filter Media. EPA-600/7-79-112. May 1979.

HOT GAS CLEAN-UP BY GLASS ENTRAINMENT OF COMBUSTION BY-PRODUCTS

By

William Fedarko
Division of Fossil Fuel Utilization
Department of Energy
Washington, D.C. 20545

Arno Gatti and Louis R. McCreight
Space Sciences Laboratory
General Electric Company
Valley Forge Space Center
P.O. Box 8555
Philadelphia, PA 19101

ABSTRACT

The development and testing of a unique hot gas clean-up process is described. It utilizes waste glass at temperatures of 1800 to 2000 F to efficiently capture and dissolve the combustion by-products by several techniques. These include a cyclone, an impactor, and a bubbler section in the apparatus. Preliminary results indicate an apparent collection efficiency of 92 to 98% with preferential collection of the larger size particles. The process is continuous and yields a low solubility, dense glassy product showing extremely low leachability. This product is potentially useful in a wide variety of building and construction materials products having greater value than the usual fly or bottom ash.

HOT GAS CLEAN-UP GLASS ENTRAINMENT OF COMBUSTION BY-PRODUCTS

INTRODUCTION

The need for a clean-up process having both a very high clean-up efficiency and high temperature capability for use with coal derived fuel for gas turbines is well recognized as a very challenging problem. The process must permit high temperature (~ 1650 F -900 C or more) operation for reasons of maintaining acceptable system thermal efficiency as well as the ability to remove particles and preferably also vaporized species of various contaminants. Three types of problems arise in the turbines if these contaminants are not removed. These range from: (1) erosion caused by particles over about 5 microns diameter, (2) plugging due to deposition of fine particles, and (3) the most serious effect being from reaction of molten alkalis with the surface protective oxide coatings on metallic parts which may cause catastrophic corrosion.

Several processes for cleaning gases of particulates and vapors at low temperatures can be upgraded to higher temperature by the substitution of more refractory materials of construction. In general, they still retain any limitations that were evident at lower temperature as well as having some additional problems due to the high temperatures. These problems may include stickiness of the particles in some cases; ricochet, fracture and reentrainment in other cases, and lowered efficiency due to intermittent operation associated with the need for backflushing or rapping.

A novel process for overcoming many if not all of these problems is being studied. It involves the use of glass coated walls and discs, which are arranged to provide turbulent gas flow through a labyrinth or impactor-type path, to capture and dissolve the fly ash particles. A glass filled bubbler section is also provided as the last stage. The resulting glass fly ash mixture gradually flows to the bottom of the chamber, thus permitting continuous operation. The presence of the glassy coating which, at the operating temperatures of about 1652 to 2012 F (900 to 1100 C) are viscous or sticky leads to referring to the process as "The Sticky Wall Process." More importantly however, the viscous glass minimizes, if not eliminates, ricochet and reentrainment of the particles. Finally, the dense, vitreous, consolidated waste products are more easily disposable, less soluble, and perhaps useful as building materials.

The preliminary results of a demonstration of feasibility were described at the previous symposium of this series under the title "High Temperature Glass Entrainment of Fly Ash" Fedarko, et al (1979).[1]

In the current work a larger test unit has been designed, built, and operated briefly in several modes for checkout purposes. The principal advance in the current test equipment compared to the original laboratory units is the use of a large capacity dedicated air compressor which permits much longer runs at high pressures. The design and preliminary operation of this equipment is described in this paper.

Test Apparatus

The overall design approach for this test unit was to have it resemble, on a small scale, an ultimate clean-up unit which would fit into a coal combustor-to-gas turbine power train. The main test chamber is accordingly about 3.96 m by 762 mm (13 feet high by 30 inches diameter) shown as the central vertical section in Figure 1. It is heated by an oil burner at the righ-hand end of the horizontal tube. Fly ash and powdered glass as needed are fed from the tank just above the oil burner. Air for combustion and pressurization is furnished continuously by a 200 cfm air compressor currently operating at 100 psi but soon to be modified to provide 150 psi. The operating conditions give a predicted Reynolds Number of over 30,000 which should assure the desired turbulent flow among the impactor plates and discs. The hot gaseous effluents are then discharged through the elbow at the top left of the unit down through a water cooled scrubber which includes a fixed orfice to control the pressure in the unit. The steam and cooled combustion gases are then discharged through the 4-inch vent line on the left end of Figure 1 to a roof vent.

The test apparatus was designed and built in sections to facilitate lining, repair, or modifications of the internal sections. From the bottom up as illustrated in Figure 1, they include:

1. A reservoir to collect the fused glass-fly ash which slowly drains down from the walls and plates. It has a separate 6-inch drain port (not visible in Figure 1) for inspecting and removing the glassy waste during shut downs. A capability to do this during hot, high pressure operation was not deemed necessary at this time, although it would likely be in the future full scale equipment.

2. A centrifugal separator section for removing large particles immediately after injection with the oil burner flame.

3. The labyrinth or impactor plate section and the hot glass bubbler are in the tallest cylindrical section. These components were custom fabricated to shape of calcium aluminate bonded alumina ceramic materials which were chosen, after tests for compatibility with container glass of over 2500 F (1370 C).

4. The dome which includes: (a) a piston operated plug for use with the bubbler (to be described later), (b) an access port for intermittently loading more glass into and inspecting the bubbler and (c) the discharge elbow.

The pressure vessel is constructed of 7/16 inch (11.11 mm) and 1/2 inch thick (12.7 mm) low carbon steel to meet ASME requirements for 150 psi, 500 F operation and carries a "U" rating. It is lined with a total of about 5 inches (127 mm) of two grades of insulating firebrick (2600 F and 2000 F) which were specially contoured and

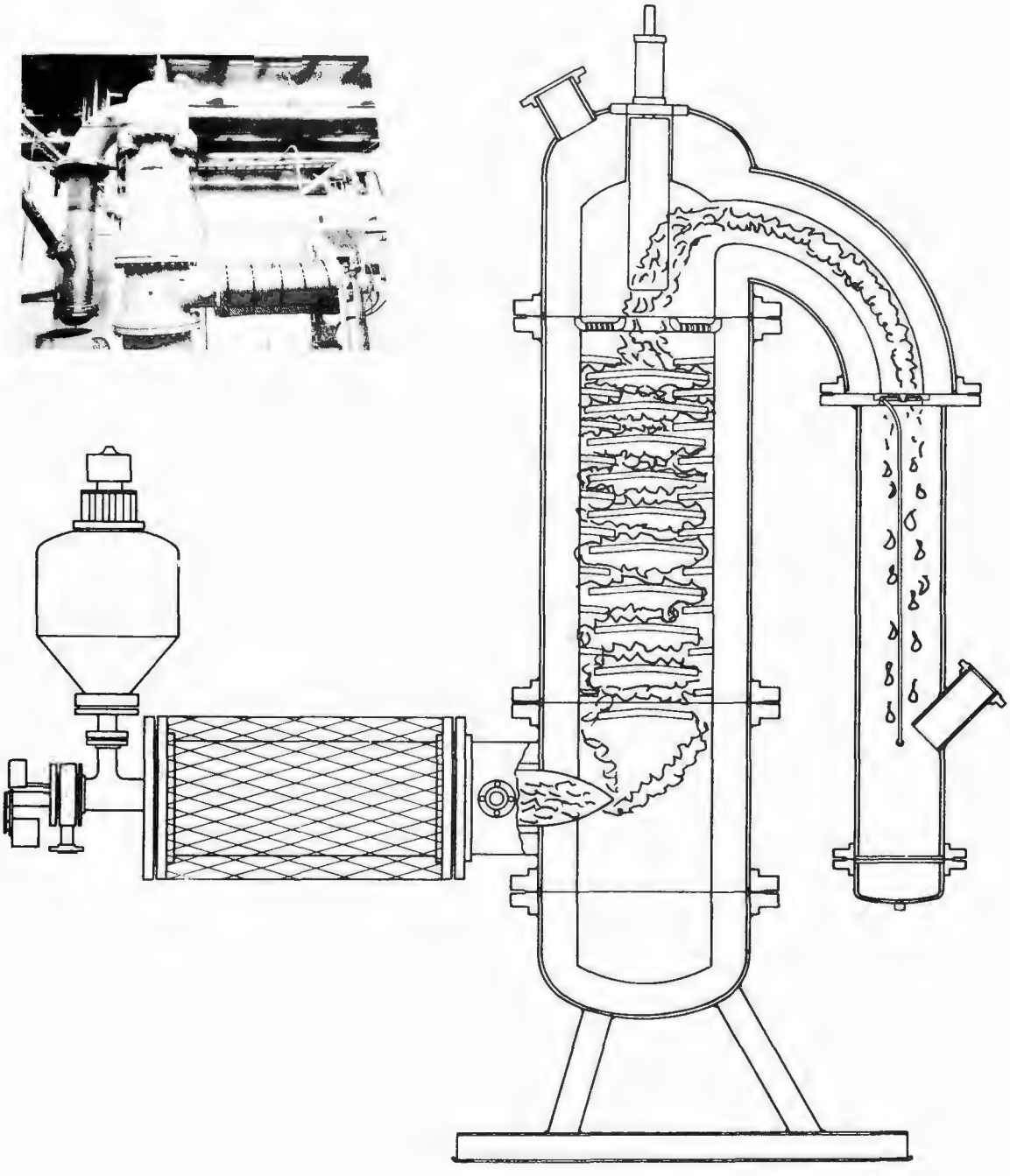

Figure 1. Overall view and schematic cross section of "Sticky Wall Process" hot gas clean-up test apparatus. Oil burner and fly ash feeder on extreme right of the photograph feed hot, dirty gas through horizontal pipe into centrifugal separator in lower portion of vertical cylinder where large particles are removed. Turbulent gases then pass upward among labyrenth of glass coated ceramic discs and exit through water-cooled orfice and scrubber. Excess drains into resorvoir at bottom of unit.

shaped to fit the vessel, backed by 1/4 inch (6.35 mm) of fibrous refractory insulation. The inside surfaces of the brick lining as well as the ceramic discs were coated with a layer of powdered amber container glass which was fused in place during the first hot operation.

Figures 2, 3, and 4 illustrate various steps and sections of the lining and assembly of the test sections. These and several other specific aspects of the apparatus will be described in the subsequent sections.

Fly Ash Feeder

The fly ash feeder is an in house design consisting of a pressure tank and air motor with a 10:1 gear reducer to drive a screw type auger using 4.5 to 45 psi air. It has been seperately (unpressurized) calibrated with a relatively coarse fly ash (from the No. 1 Exxon Miniplant Cyclone) consisting of 70% Illinois No. 6 plus 30% dolomite having particles from 2 to about 80 microns with a peak at about 30 microns, as measured with a Coulter Counter having a 140-micron orifice. Under those conditions, it provided 100 to 1220 grains per minute and has a capacity for up to 24 hour continuous runs even at the high feed rate. Some problems with moisture from the compressed air and the tendency of fine fly ash as well as the powdered glass to compact are being encountered when trying to feed those materials. Separate fluidizing air capabilities inside of the tank are being tried to overcome these problems.

Oil Burner

The oil burner is a modified version of a commercial unit designed and built by Voorheis Industries of Fairfield, NJ to have a capability for high pressure operation and a rather wide firing range. It can operate from about 500,000 to about 3.0×10^6 Btu using No. 2 fuel oil. Our usage to date has been at the low end of this range and using about 3 to 4 gal/hour to yield equilibrium temperatures of about 1800-1900 F (982 - 1037 C) in the test sections. The burner is fired through a four foot long pipe lined with 2 inches (50.87 mm) of a dense ceramic refractory chosen to promote uniform and complete combustion prior to the gases entering the test section.

Particle Collection Sections

Previous work in demonstrating the feasibility of this "sticky wall process" indicated: (1) the desirability for including a simple centrifugal or cyclone section to remove some of the largest particles as early as possible, (2) a tailored nonuniform spacing of the impactor or labyrinth plates, and (2) a bubbler section. The initial centrifugal section is illustrated in Figure 2 by a photo taken during construction of the test apparatus. The impactor plate particle collection section will be discussed next followed by a brief description of the bubbler.

In the previous feasibility demonstration work, a plastic model and later a refractory ceramic collector operating at atmospheric pressure, flow rates of 60 scfm

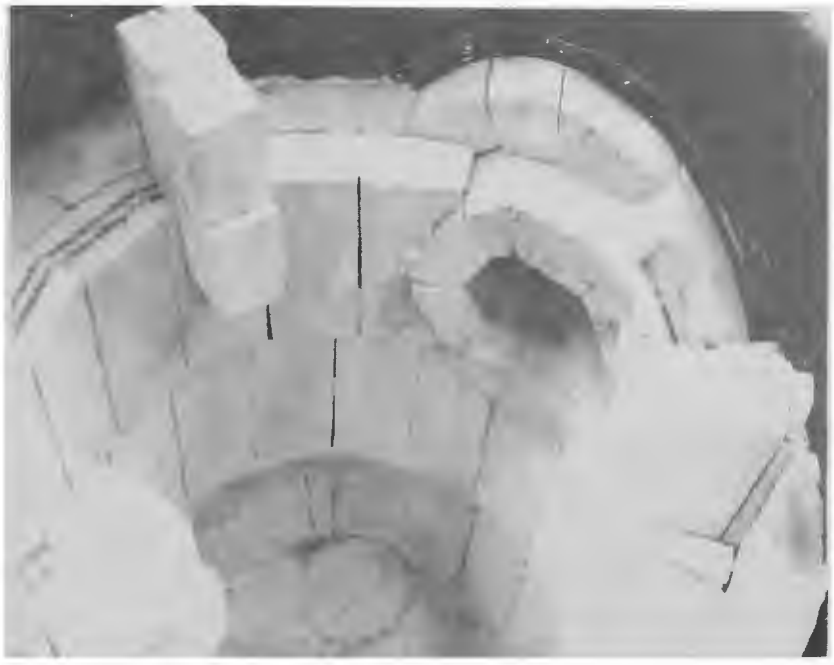

Figure 2. View through centrifugal separator and glass/fly ash reservoir during construction showing (from steel wall inward) fibrous insulation, 2000 F and 2600 F insulating brick prior to refractory cement and glass coating. Three notched insulating alumina bricks mounted on end are shown in place to support the lower two glass coated ceramic discs.

Figure 3. Top view of the upper discs with glass coating on them. One quadrant of the bubbler and two of the four silicon carbide resistance heaters are in place temporarily for the photograph.

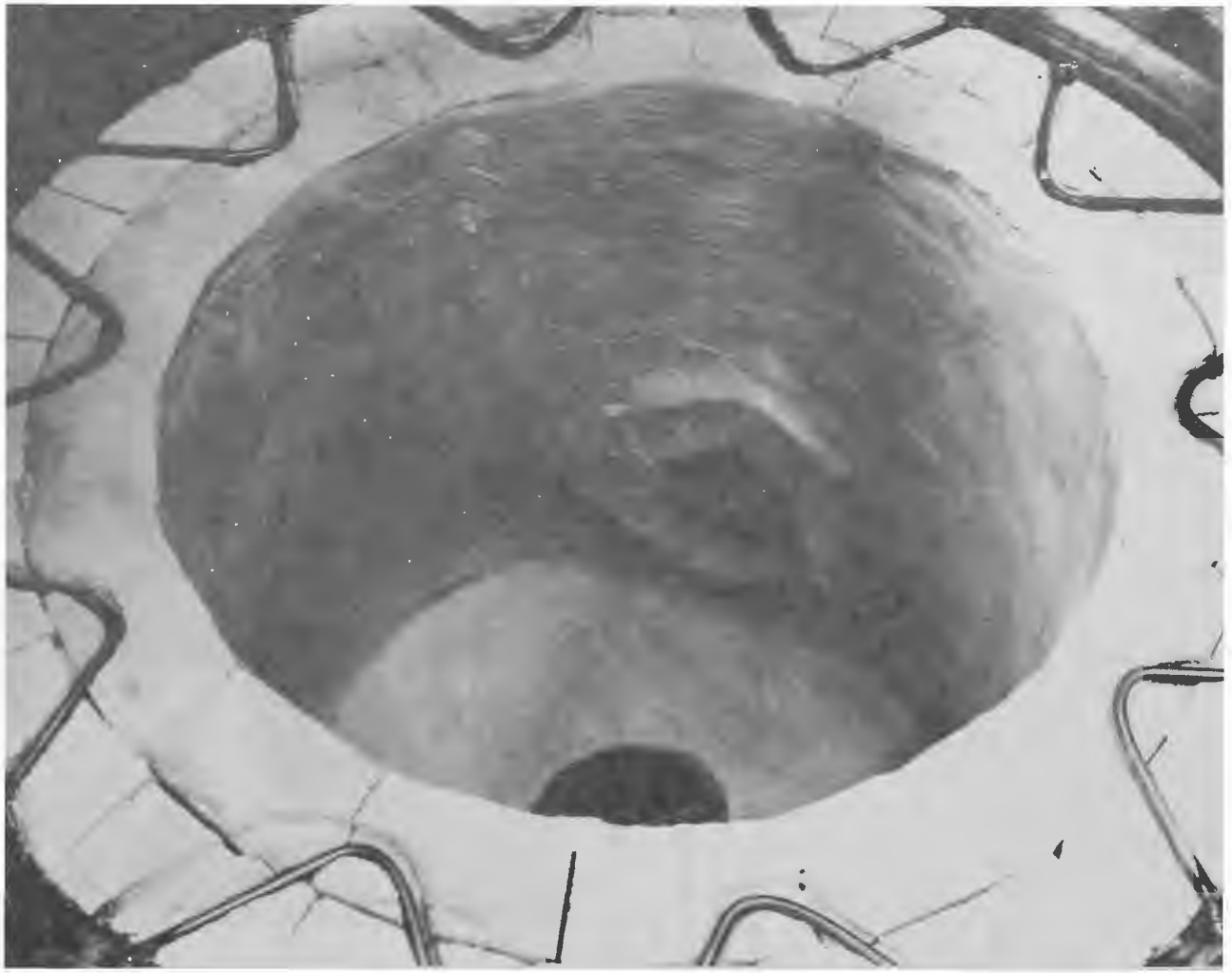

Figure 4. View inside the dome prior to installation. The exit hole for gases is visible on the side wall while the hole for the bubbler plug is partially visible in the lower center of the picture. This section is coated with a refractory cement but not powdered glass.

and at 6-8 (1.8-2.4 m) ft/sec gas velocity showed that each impactor subunit would collect about 50 percent of the dust passing through it. Each subunit was identical in dimensions to the others, the plastic duct had 14 subunits while the ceramic duct had 10 subunits. Figure 5 is a sketch of a typical subunit in either system. The design criteria used was to alternately vary the cross section of the device to promote turbulent flow and increase wall impact area significantly above that which would be provided by a straight wall device. A decrease in cross sectional area of 75% in any direction was arbitrarily chosen so that no severe pressure drop would be experienced. Data from both ducts showed that under those conditions of gas flow, particle density and subunit geometry, each subunit captured about 50% of the particles passing through it. (See Figure 6). The curve of Figure 7 was then generated using the information on hand that: (1) with the duct closed (i.e., zero area) 100% of the particles would be stopped, (2) with the duct open very few of the particles would be stopped and, (3) the measured point which occurred at 50% efficiency with 25% of the duct area open between scrubber plates. This curve was used to size the present duct. Also included in Figure 7 are the algebraic equations necessary to size the various discs and plates needed. As is seen, once D4 (inside pipe diameter) is fixed all the discs and plate sizes can be calculated with "less efficient" (i.e., less plate area, etc.) sizes and spaces used at the entrance end to lessen the tendency of the unit to clog in the larger diameter upper areas.

With this approach in mind, the present scrubber has been designed with ten subunits ranging from 35% "efficient" at the entrance end to 75% "efficient" at the exit end as determined by the design curve of Figure 7. Figure 8 is a schematic view of the internal plate, disk and spacing dimensions used in the scrubber with a total calculated "efficiency" of 99.95%.

Bubbler. The last step of the current hot gas clean up process is provided by a shallow layer of molten glass through which the gases pass. Figures 1 and 3 show this feature schematically and as partially complete during construction, respectively. Two features of this section require some discussion. First is the need for a separate control of the temperature in this section as a means of controlling (to lower) the viscosity of the glass. This is provided by four silicon carbide electrical resistance heaters shown partially installed in Figure 3 with the water-cooled copper power connectors. These are designed to provide up to 6 kW of additional heat. The other major feature of this system is the need to bypass the bubbler whenever desired but especially during startup when the glass would be cold and too viscous to pass the gases. This is provided by an axial plug which can be inserted and removed by an external air operated piston shown schematically in Figure 1.

Instrumentation

Several approaches to providing appropriate instrumentation both for the safe operation of the unit and to ascertain particle collection efficiency are being tested.

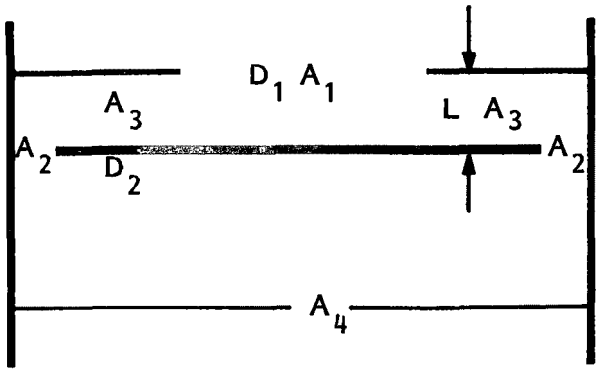

$$(1)\quad A_1 = \frac{\pi D_1^2}{4}\ , \qquad D_1 = \sqrt{\frac{A_1 \times 4}{\pi}}$$

$$(2)\quad A_2 = \frac{\pi}{4}(D_0^2 - D_2^2) = D_1^2 \qquad D_2 = \sqrt{D_0^2 - D_1^2}$$

$$D_2 = \sqrt{D_0^2 - \frac{A_1 \times 4}{\pi}}$$

$$(3)\quad A_3 = \pi D_1 h$$

$$A_1 = A_2 = A_3$$

$$\frac{\pi D_1^2}{4} = \pi D_1 h$$

$$(4)\quad h = \frac{D_1}{4}$$

Figure 5. Schematic of deflector plate geometry where A_4 is the duct area, while A_1, A_2 and A_3 are the areas the gas flows through.

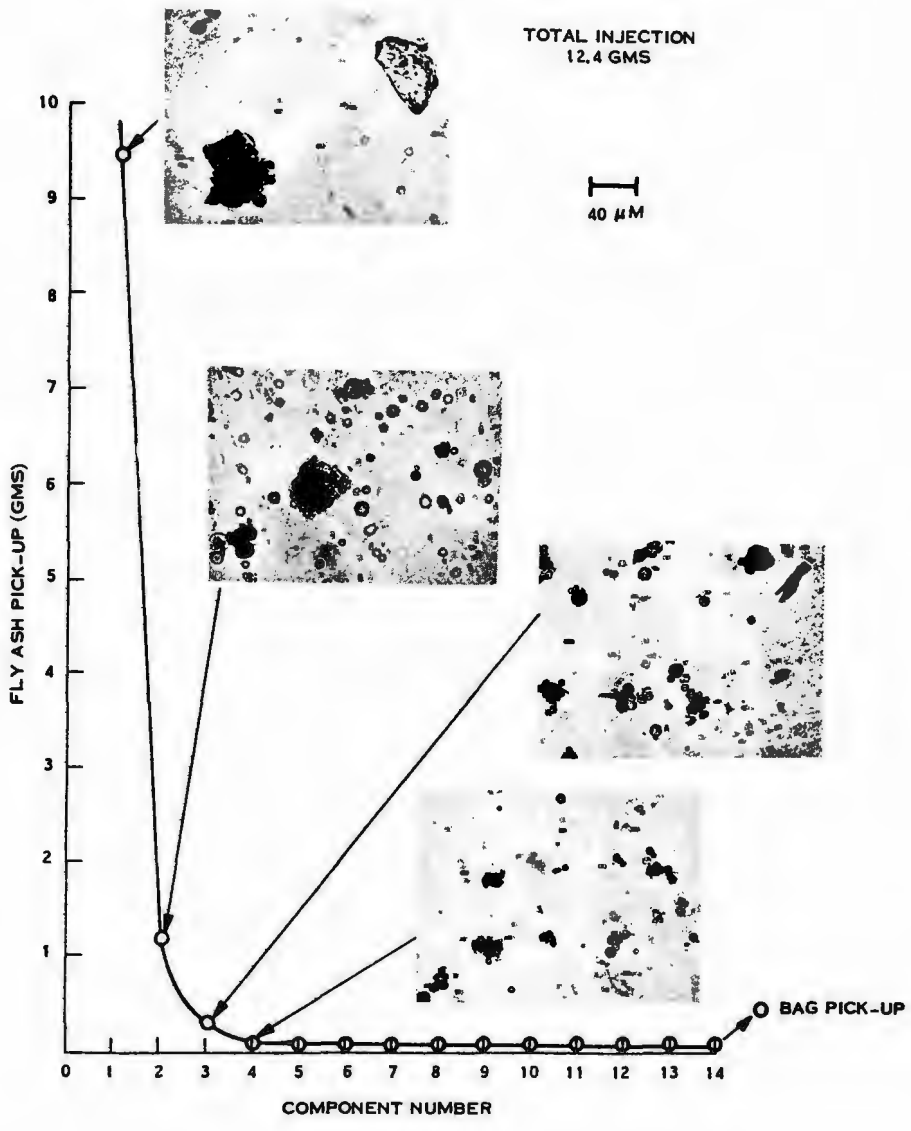

Figure 6. Fly ash pickup as a function of compartment number for plastic duct run during previous demonstration of feasibility phase of this program and photomicrographs of the largest particle detected for the first four compartments.

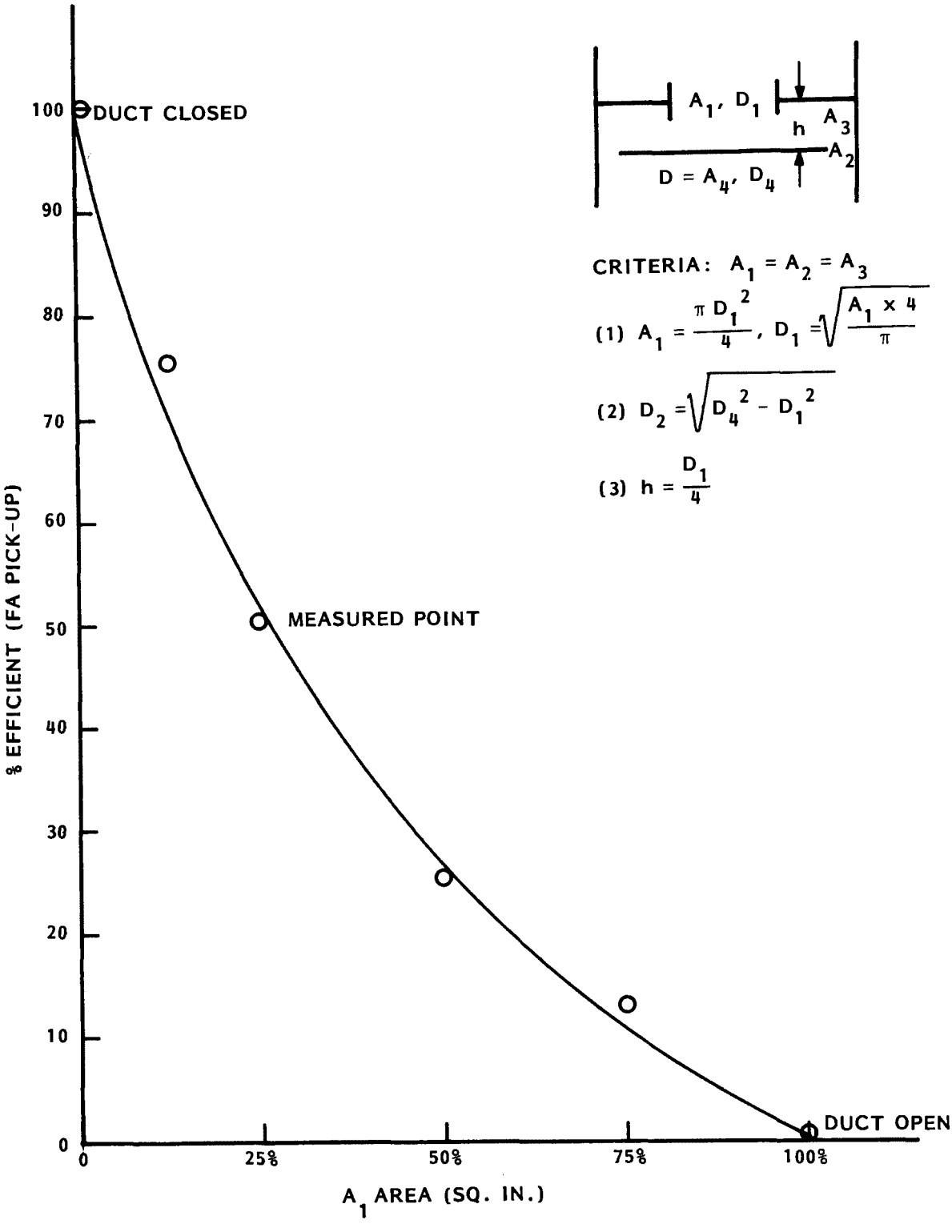

Figure 7. Curve of % efficiency of fly ash pickup vs hole-plate-space area developed from original data from bench scrubber.

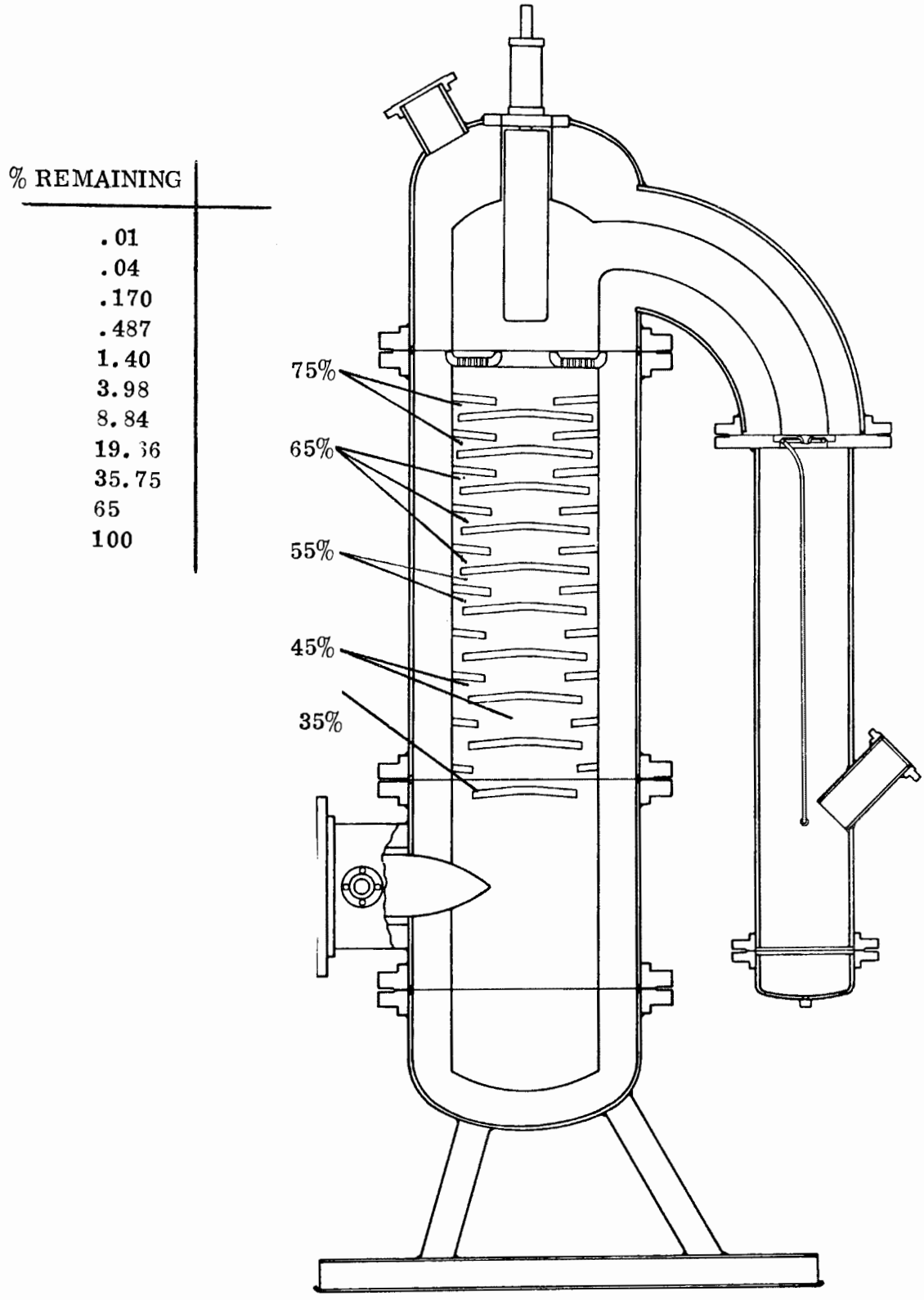

Figure 8. Schematic of present scrubber design showing calculated efficiency of each subunit and % fly ash remaining after passing each subunit.

Figure 9 shows the operator's console with most of the controls and instruments for operating the unit. These include numerous interlocks and safety controls. Only the air compressor and oil pump with their respective controls and pressure gages which are just out of the picture to the right of the doorway are not shown. Experimental data collection includes five internal and four surface temperature measurements plus three pressure measurements within the test chamber. The pressure measurement connecting tubes are equipped for nitrogen purging to keep them free of deposits.

Approaches to particle and vapor detection are shown in Figure 10. First the simplest is performed by collecting the water scrubber effluent for a finite time period, letting it settle, then by decanting and filtering to recover the particles for analysis. This is being done routinely. A pair of IKOR charge transfer process probes were obtained to hopefully detect the relative inlet and outlet particulate density continuously. They have not been satisfactory, especially at elevated temperatures, however some modifications are currently being developed by the manufacturer which will hopefully overcome these limitations. Finally, a high temperature particle and vapor sampling instrument is being completed and prepared for installation. The general instrument was described previously (Wang et al (1978))[2], incorporates a Southern Research Institute stage cyclone, (Smith and Wilson (1978))[3] however we have constructed this item from a machinable mullite ceramic. It is mounted inside of a furnace which heats it to about 2200 F (1204 C) in order to prevent condensation of the vapor species. These in turn are mounted in the high pressure chamber which is attached to the outlet instrument flange on the large elbow at the top of the unit. In operation, nitrogen is bled through the sample collection tube to prevent premature ingestion of sample. Turning off the nitrogen will permit ingress of the gas sample which will be further cleaned by the cyclone and a ceramic fiber filter, before it is cooled, to condense any vapor species. This apparatus is not quite operational, but should be by late summer of 1979.

TEST RESULTS

The initial runs reported herein were performed with the system previously described; they serve two purposes: (1) initial checkout of the operation of the system and (2) the obtaining of preliminary data which would be used to plan the future experiments and to modify sections of the system, as required. An example of a modification instituted as a result of initial results is the previously discussed separate fluidizing air capabilities being introduced into the fly ash feeder.

The fly ash samples used in these studies were obtained from the Exxon miniplant. The fly ash is the particulate residue collected in either cyclone number 1 (fly ash 1) or cyclone number 3 (fly ash 3) after burning a powdered mixture of 70% Illinois Number 6 coal and 30% dolomite in their fluidized bed combustor.

Two types of experiments were performed: (1) cold runs - the system was at room temperature, and (2) hot runs - the system was at temperature exceeding

Figure 9. Operator's console with both operating controls and some experimental data collection capability.

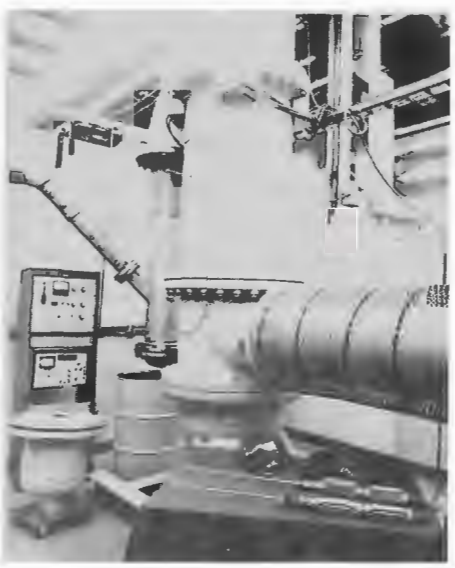

Figure 10. Shown are a number of instrumentation capabilities and approaches being evaluated. In the foreground are two IKOR change transfer-type probes for installation through the small (covered) flanges at the inlet and outlet of the test apparatus. The electronic console in the background is for use with them. The large heavy container in the lower left contains a high temperature ceramic cyclone and has provision for adding a vapor condensate trap through the small flange on the cover. It is to be mounted to the small flange just visible on the outlet elbow at the upper left. Finally, overall effluent samples are available by collecting the water from the bottom of the scrubber which otherwise drains into the 55-gallon drum in the background.

1832 F (1000 C). Initially the system was heated to a temperature exceeding 1000 C in order to completely fuze the glass that was painted on as the ceramics were assembled. It was observed after this first series of runs that the walls were not uniformly wetted; therefore, prior to reassembly of the system the ceramic refractories are to be pretreated with a process or modified glass composition now being tested.

During the first cold run relative particle density was determined with the pair of IKOR probes. The density measured at the outlet probe was considerably less than that measured at the inlet probe, indicating that particles were being collected in the system. Agreement between measurements made with the two probes was established by locating both probes at the inlet position and obtaining similar readings, at most less than a factor of two difference. Measurements were not able to be made when the system was hot as the probes were overloaded due to two factors: (1) temperature and (2) water droplets. A temperature of 1000 C was sufficient to give a very large signal as subsequently demonstrated in an electrically heated furnace without particles. Secondly, it was observed that water droplets from the combustion gases were depositing at the cool probe insulator, thus providing a low resistance path to ground. Modifications to the probe design and electronics are being investigated and will be incorporated as developments permit.

The water used to cool the hot exhaust gases in the scrubber is also used to collect the particles which pass through the system. The water/particle mixture continually drains into a large settling tank at the approximate rate of 2 liters per minute. Data on the effectiveness of the system for the removal of the fly ash particles are obtained by analysis of the water/particle mixture collected at specified intervals prior to its entry into the settling tank. The collected one minute sample is allowed to settle and cool to room temperature for at least 24 hours. Most of the liquid is decanted and the remainder filtered through paper having the reported capability of collecting particles greater than 0.5 mμ. Initial experiments indicated that the errors could amount to 0.2 gram. This amount could be a large fraction of the fly ash collected in one minute at low fly ash feed rates, therefore in later runs samples were collected for at least 15 minutes and for as long as one hour.

Based on these preliminary results, using a fly ash input between 0.5 and 5 grains per SCFM, it can be concluded that the system operating either cold or hot and using either fly ash has an apparent collection efficiency of 92 to 98%.

In addition to the overall system collection efficiency, the particle size distribution remaining after scrubbing is an important factor in determining the applicability of the system for hot gas clean-up. Typical Coulter Counter analysis (100 micron orifice) of fly ash 1 and fly ash 3 are shown in Figures 11 and 12, respectively. Samples of the fly ash obtained from the water-particle mixture were also analyzed after drying. These results are also shown in Figures 11 and 12. It is readily seen from this data, that the size distribution of these particles has been changed by the clean up system and that the particle size distribution of the fly ash passed by the system from both fly ash 1 and fly ash 3 are similar.

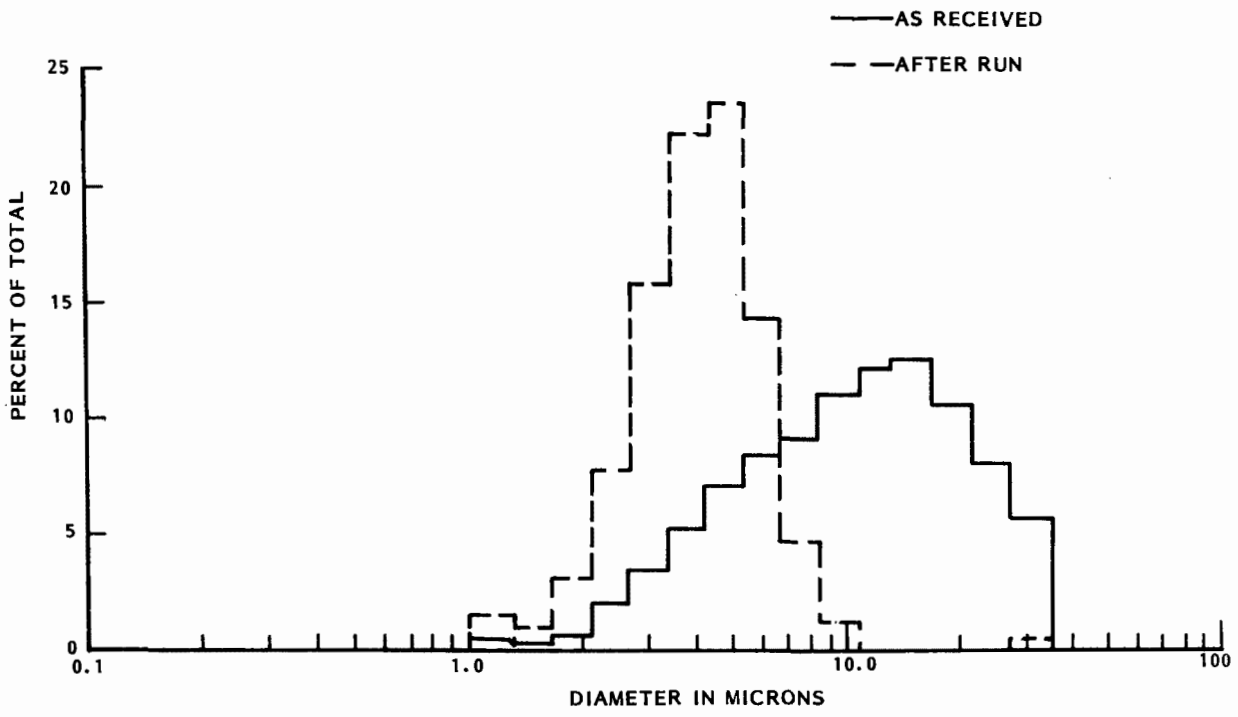

Figure 11. Coulter counter analysis of fly ash 1; —— as received, – – after run using 100 micron orfice.

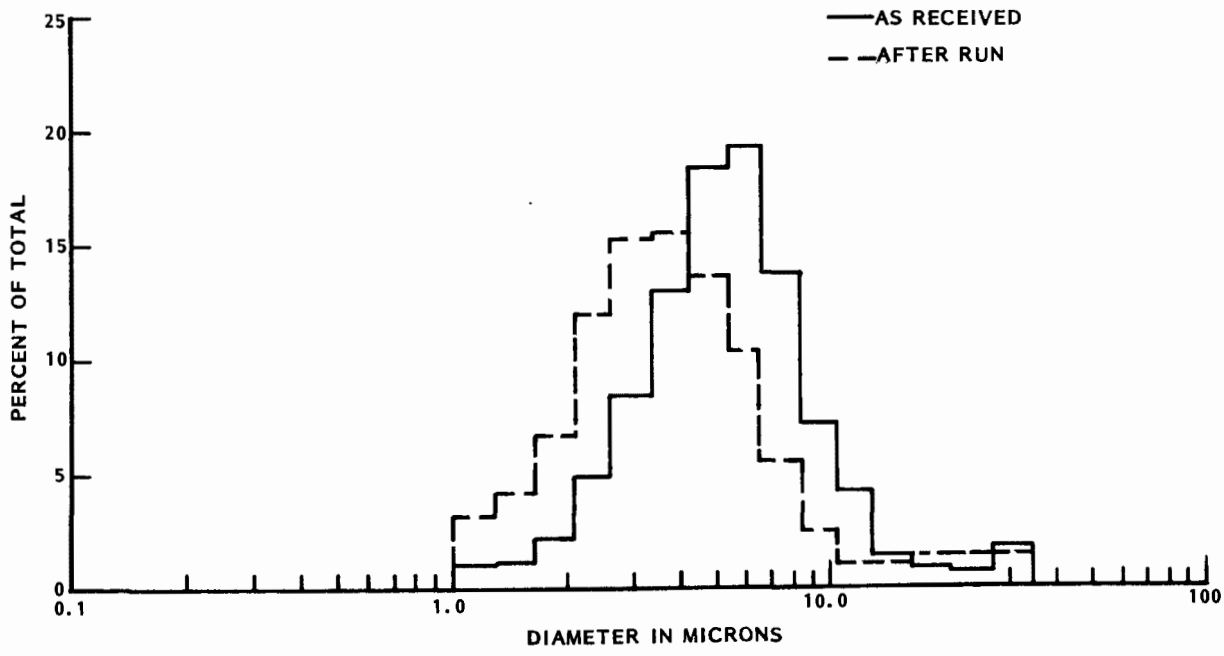

Figure 12. Coulter counter analysis of fly ash 3; —— as received, – – after run using 100 micron orfice.

LEACHATE STUDIES

The leachability of fly ash glass mixtures was investigated in two studies, one performed at the GCA/Technology Division, Svetaka and McGregor (1979)[4], and the other at the Pennsylvania State University, Komarneni (1979)[5]. The characterization of leachability is expressed in terms of the elemental and anion composition of the leachate.

In the GCA study the leachates were generated by two different procedures, the EPA Extraction Procedure was used for a survey of the elemental composition by Spark Source Mass Spectrography and for sulfate ion by Ion Chromatography, the ASTM Method A Extraction Procedure was employed for anion composition by Ion Chromatography. Selected results for the Spark Source Mass Spectrography analysis is given in Table 1 together with EPA proposed toxic substance guideline values. In Table 2 are the results for the anion analysis.

In the Pennsylvania State University study the samples were dry ground and sieved to < 200 mesh (< 75 μm) and one gram of sample was treated with 25 ml of deionized water (CO_2 buffered, $\sim$ pH 5.4) in sealed polyethylene containers at 176 F (80 C) for 3 days. The leachate solutions were analyzed by atomic absorption spectrophotometry, the results are given in Table 3.

As seen from these data, leachable elemental concentrations in the untreated fly ash samples are in much lower concentrations, much below the EPA guidelines, in the glass treated samples. In the case of the anion analysis, only sulfate and chloride were detected and only in the leachate from the untreated fly ash.

Table 1. Elemental Survey Results Spark Source Mass Spectrography

Element	Fly Ash	Leachate Concentration (mg/liter)			Guideline for Toxic Substance
		Fly Ash/Glass (70/30)	Fly Ash/Glass (30/70)	Glass	
Pb	(0.009)*	<0.025#	(0.007)	<0.002	0.50
Ba	0.34	0.04	0.007	0.019	10.0
Cd	0.0013	<0.0047	<0.006	<0.0004	0.10
Sr	2.5	0.010	0.01	0.11	-
As	0.060	<0.0019	0.0003	<0.0002	0.50
Cr	0.090	0.036	0.004	0.0015	0.50
Ti	0.50	0.009	0.012	0.006	-
Ca	85.	1.8	3.1	1.6	-
K	3.8	1.3	0.47	0.70	-
Si	3.5	0.55	0.21	1.1	-
Mg	85.	0.85	0.60	0.15	-
B	0.12	0.001	<0.0002	0.0018	-

* Values in parentheses indicate values measured but cannot be distinguished from values measured in the procedural blank.

\# The "<" symbol indicates an instrumental detection limit.

Table 2. Anion Analysis

Anion	Fly Ash	Sample		Glass	Extraction Blank
		Fly Ash/Glass (70/30)	Fly Ash/Glass (30/70)		
Sulfate[1] (ppm)	3260	<3	<3	<3	<3
Sulfate[2] (ppm)	590	<3	<3	<3	<3
Chloride[2] (ppm)	6	<1	<1	<1	<1
Fluoride[2] (ppm)	<1	<1	<1	<1	<1

1. EPA Extraction method
2. ASTM Extraction method

Table 3. Atomic Absorption Spectrophotometry
Elemental Analysis Results

Element	Glass	Sample		
		Fly Ash/Glass (30/70)	Fly Ash/Glass (70/30)	Crystallized* Fly Ash/Glass (70/30)
As (ppb)	90	33	20	20
Se (ppb)	21	10	< 5	< 5
Cr (ppb)	9	25	53	18
Ni (ppb)	< 1	< 1	< 1	< 1
Cd (ppb)	< 1	< 1	< 1	< 1
Pb (ppb)	< 10	< 10	<10	<10
Ca (ppm)	< 0.05	0.28	0.53	0.05
Na (ppm)	580	95	49	44
Si (ppm)	1200	213	96	88

* This sample was fused then recrystallized in preparation, all other samples vitreous.

CONCLUSIONS

A unique hot gas clean-up apparatus, currently under development, has been successfully checked out at temperatures in the range from 1800 to 2000 F (1000 to 1100 C). Leachability studies have been performed on fly ash glass mixtures. These studies have shown that the fly ash leachability is greatly reduced when combined with glass, either in the vitreous or crystalline state. Preliminary results indicate an apparent collection efficiency of 92 to 98 percent with preferential collection of the larger size particles.

ACKNOWLEDGMENT

The authors are pleased to acknowledge the extensive work of their associates in designing, building, and operating this test equipment, plus analyzing the results. They include: Robert Locker, Howard Semon, Robert Grosso, William Laskow, Al Zacharias and Drs. Harold Goldstein and Phillip Alley.

REFERENCES

1. Fedarko, W., Gatti, A. and McCreight, L. R., "High Temperature Glass Entrainment of Fly Ash," in Symposium on the Utilization of Particulate Control Technology, Vol. 3, EPA - 60017-79-044c, 1969. P. 395-404.

2. Wang, J. C. F., Boericke, R. R. and Fuller, R. A., "A High Temperature High Pressure Isokinetic/Isothermal Sampling System for Fossil Fuel Combustion Applications," Paper presented at the 1st International Symposium on Transfer and Utilization of Particulate Control Technology, Denver, Colorado, July 24-28, 1978.

3. Smith, W. E. and Wilson, Jr. R. R., "Development and Laboratory Evaluation of a Five-Stage Cyclone System," EPA - 600/7-78-008, January 1978.

4. Svetaka, P. S. and McGregor, K. T., Private Communication.

5. Komarneni, S., Private Communication.

THE A.P.T. PxP DRY SCRUBBER

FOR HIGH TEMPERATURE AND PRESSURE PARTICULATE CONTROL

By:

Ronald G. Patterson, Seymour Calvert,
and Mansoor Taheri

Air Pollution Technology, Inc.
San Diego, California 92117

ABSTRACT

The PxP scrubber is a device which may be used at high temperature for the collection of fine particles on larger particles, which can be cleaned and recycled. Electrostatic augmentation of the PxP scrubber has shown greater collection efficiency for fine particulates than for the non-augmented scrubber. Without electrostatic augmentation, particle collection is mainly by inertial impaction and to some extent by diffusion for smaller particles.

The effluent from a 500 ACFM coal-fired atmospheric fluidized bed combustor at 820°C is used as a source of particles for the PxP pilot plant.

THE A.P.T. PxP DRY SCRUBBER FOR HIGH TEMPERATURE AND PRESSURE PARTICULATE CONTROL

INTRODUCTION

High temperature and pressure (HTP) gas streams are encountered in developing advanced energy processes such as coal gasification and fluidized bed combustion. It is often economically desirable to utilize this gas stream directly by passing it through a gas turbine. To prevent the erosion and corrosion of turbine blades and heat exchanger tubes, it is necessary to remove the particulates before utilization. The Department of Energy[1] recently estimated particle cleanup requirements for gas turbines as follows:

Particle Size Range	Desired Mass Concentration	
	g/Nm^3	gr/SCF
0 - 3 μm	0.0199	0.0087
3 - 5 μm	0.002	0.001
5+ μm	0.0003	0.00012
Total	0.023	0.010

The elevated temperature and pressure conditions suggest that new devices for removal of fine particles may be necessary. Typical particle collectors used in fossil-fuel-fired power plants (electrostatic precipitators, scrubbers, fabric filters) generally operate at temperatures below 260°C and at low pressures. The suitability of these components at elevated temperatures and pressures may be limited. The A.P.T. dry scrubbing system, which we call the "E PxP" system (for electrostatically augmented particle collection by particles) is compatible with the special demands of HTP gas cleaning.

E PxP SYSTEM

The E PxP system for fine particle control utilizes relatively large particles as collection centers for the fine particles in the gas stream. The relatively large particles (collector particles) introduced to the gas stream can collect fine particles by mechanisms such as diffusion, inertial impaction, interception and electrophoresis. The larger size of the collector particles allows easier separation from the gas stream by devices such as cyclones and gravitational settling.

Figure 1 is a functional diagram of the process steps representative of the E PxP system. The functional phenomena represented on this diagram could occur concurrently or separately in several types of equipment.

The first step involves charging the particles in the gas stream with a corona discharge device. Collectors are introduced to the gas stream in the second step. This process can involve pneumatic or mechanical injection into the gas stream. The third stage involves contacting the collectors with the gas in the presence of an electric field in order to encourage the movement of the fine particles to the collectors. A venturi device can be used for the contactor which would be analagous to a venturi scrubber except that solid collectors are used instead of liquid drops.

The next process step is to remove the collector particles after sufficient exposure in the contactor to cause capture of the initial fine particles present in the gas. At this stage the large size and mass of the collector particles is utilized to separate them from the gas. A cyclone separator could be used for this step. Two streams are shown leaving the separator; the cleaned gas leaves the process at this point, and the second stream represents the flow of dirty collector particles to the next step. The final process involves either discarding the collector particles or cleaning them for recycling and disposing of the material collected from the gas stream.

Performance Prediction

The particle collection efficiency and pressure drop for an A.P.T. Dry Scrubber with co-current flow can be predicted with the same relationships that define electrophoretically augmented co-current wet scrubber performance. The theoretical performance of the PxP scrubber has been determined based on the venturi scrubber model of Yung, et al.[2] Figure 2 is a plot of particle penetration against particle size with collector/gas flow rate ratio as a parameter at a temperature of 870°C and 1,013 kPa.

Particle collection efficiency for the E PxP was predicted on the basis of inertial impaction only. No credit was taken for electrostatic augmentation beyond the assumption that it would prevent particle reentrainment and attrition particle losses.

The predicted penetration curves shown in Figure 2 have the following characteristics:

1. For a given set of operating conditions, the penetration decreases with increasing size of fine particles. This is expected since the collection mechanism is inertial impaction of fine particles on the collectors.

2. For a given size of collector particle and aerodynamic diameter of fine particle, the penetration decreases with increasing value of $(Q_p \rho_p / Q_G)$.

3. The pressure drop of the scrubber increases with increasing value of $(Q_C \rho_C / Q_G)$.

4. A similar dependence upon the gas velocity is apparent from the model of Yung, et al.[2]

5. For the 125 micron diameter collectors and a given fine particle aerodynamic diameter, the penetration increases with increasing gas temperature. This is the result of an increasing gas viscosity with temperature which reduces the effective inertia of the fine particles. In general high temperature and pressure particle collection has been found to be more difficult than at lower temperature and pressure as concluded in a report by Calvert and Parker.[3]

It can also be shown that collector particle diameter affects collection efficiency when other factors are held constant. The cut diameter (i.e., diameter of the particle which is collected at 50% efficiency) decreases as collector diameter decreases. Collection efficiency for particles larger than several microns in diameter varies in a more complex way, depending on flow and geometric parameter combination.

Phase I - Experimental Program

Experimental work has been done by A.P.T. at bench scale to determine fine particle collection efficiency in a PxP scrubber in order to confirm the predictions obtained from available mathematical models. Results of experiments with dibutylphthalate (DBP) aerosol at 20°C are reported in greater detail in an earlier paper (Calvert, et al.[4]).

The contactor and gravity separator used in these experiments are shown in Figure 3. Collectors entered the T-shaped contactor through the branch leg and were entrained by air entering through one of the (run) legs. The system gas flow enters either horizontally or vertically downward into the separator. Cleaned gas flows out of the branch of the separator T.

Particle penetration data for all runs with nickel and sand collectors are presented in Figure 4, a "cut power plot". The cut diameter is plotted against gas pressure drop in Figure 4. The line represents the relationship which is predicted and which has been confirmed by a number of field tests on large wet scrubbers. Agreement between the data points and the line is good.

The experimental apparatus was constructed of 316 SS after completion of the low temperature experimental program. This permitted operation of the system to 820°C. Particle penetration data at 650°C with nickel collectors are shown in Figure 5. Penetration of particles less than 1.0 μmA was less than predicted, possibly due to enhanced diffusional deposition.

Phase II - Experimental Program

A pilot plant was constructed to test the PxP system on a larger scale. A schematic of the Phase II experimental apparatus is shown in Figure 6.

An atmospheric fluidized bed coal combustor (AFBC) has been designed and constructed for providing a particulate source representative of advanced energy sources. The AFBC is designed to provide 14.2 Am^3/min of dirty gas at 820°C. Details of the major components of the AFBC were given by Calvert, et al.[5]

Preliminary results have shown that attrition of the sand collectors occurs at high temperature. A search for a more suitable collector particle has begun. The collector separator section of the dry scrubber will also be redesigned to provide more effective separation.

A bench scale E PxP is being designed as shown in Figure 1 to test electrophoretic augmentation in the dry scrubber system. Collector particles will be used on a once through basis for these experiments.

ENGINEERING EVALUATION

An engineering evaluation has been completed for an E PxP dry scrubber installed on a 710 MWe pressurized fluidized bed combined cycle (PFBC) power plant. The design specifications for the PFBC system were: plant size = 710 MW net power, number of gas turbines = 2, total inlet air flow per turbine = 345 kg/s, gas pressure at tertiary collector = 1,013 kPa, turbine inlet temperature = 870°C, net turbine power output = 66 MW/turbine.

E PxP Performance and Power Requirements

The particle size and mass concentration used in this evaluation were based on data from PFBC systems. The average size distribution had a d_{pg} (physical size) = 4.8 μm and σ_g = 3.2. The mass concentration was varied from 0.23 to 2.3 g/Nm^3.

When the particle size distribution and mass concentration of a PFBC source is known, it is possible to predict at what pressure drop an E PxP would be able to meet various cleanup requiements. The equation relating the fractional penetration for a specific particle diameter to the overall penetration is:

$$\overline{Pt} = \int_0^\infty P_{td}\, f(d_p)\, d(d_p) \qquad (1)$$

where $\overline{Pt}$ = overall penetration, fraction

P_{td} = penetration for particles with diameter, d_p, fraction

$f(d_p)$ = particle size frequency distribution

d_p = particle diameter, μm

Overall penetration of the E PxP Dry Scrubber was calculated from equation (1) for the average size distribution given. The gas velocity in the contactor was assumed to be 40 m/s. The results are shown in Figure 7. In Figure 7 the overall penetrations for the three particle diameter fractions of $d_p < 3$ μm, $3 < d_p$ 5 μm and $d_p < 5$ μm are plotted against pressure drop. These fractions were chosen based on the Department of Energy (DOE) gas turbine cleanup requirements previously presented.

Figure 7 indicates that if the inlet particle concentration were 2.3 g/Nm^3, a pressure drop of approximately 600 cm water would be required for an outlet concentration of 0.023 g/Nm^3. This emission rate will meet the turbine requirements for all particle size ranges. At lower inlet concentrations, lower pressure drops will be required to meet various emission requirements.

The turbine requirements are such that the mass concentration entering the turbine should be ≤ 0.023 g/Nm^3. The PFBC system has an overall thermal efficiency of 39.2%. Meeting the turbine requirements will produce air pollution emissions ≤ 0.007 $g/10^6$ J. This is approximately 50% of the new source performance standard (NSPS) of 0.013 $g/10^6$ J.

Capital and Operating Costs of E PxP

The estimated capital and operating costs and the "cost of electricity" (COE) for an E PxP Dry Scrubber installed on a 710 MWe PFBC system are given in Table 1. These estimates were determined according to the cost estimating ground rules developed as part of the "Energy Conversion Alternatives Study" (ECAS)[6] in terms of 4th quarter 1978 U.S. dollars. The E PxP Dry Scrubber is compared with three major types of granular bed filters (GBF).

The capital investment represents the installed cost based on a 65% availability factor and 18%/year cost of invested capital. The operating power costs for the E PxP and GBF systems include the following:

1. Pressure drop across the scrubber.
2. Heat loss to the surroundings.
3. Energy losses associated with collector cleaning.
4. Collector particle replacement.

For GBF systems there will be additional costs incurred from operating the compressor which is used either for cleaning or for pneumatic transport of solids. The "operating cost of electricity" (OCOE) is based on an electricity cost of 35 mills/kWh at the bus bar.

The estimated cost advantage of pressurized fluidized bed combustion over the ECAS reference cycle (conventional coal fired power plant with stack gas scrubber) amounts to 7.5 mills/kWe. The actual cost range would be several mills/kWe greater than this because of large increases in the fuel costs since the completion of the ECAS report. The estimated OCOE for the E PxP Dry Scrubber is less than 10% of the cost advantage for the PFBC power plant.

CONCLUSIONS

The experimental data for primary collection efficiency of the E PxP agree well with predictions based on a mathematical model which was first developed for wet scrubbers. Since the model was derived for the mechanism of particle collection by inertial impaction on spheres in a co-current scrubber, it is reasonable to expect it to fit the data. The E PxP A.P.T. Dry Scrubber system has the same primary collection efficiency/power relationship as the venturi type wet scrubber.

The overall efficiency of the E PxP system will depend on the reentrainment characteristics of the specific system in addition to the primary efficiency. Particle and collector properties, system geometry, flow rates and other parameters will influence reentrainment and collector particle attrition.

Research is continuing on the experimental evaluation of the E PxP system for HTP applications. The cost of electricity for the E PxP Dry Scrubber represents 10% of the cost advantage of a PFBC over a conventional power plant. Therefore, further development of the E PxP Dry Scrubber and PFBC systems is warranted. The work upon which this paper is based is supported by the U.S. Environmental Protection Agency.

ACKNOWLEDGEMENT

The work described in this publication was performed under Contract numbers 68-02-2164 and 68-02-3102 with the U.S. Environmental Protection Agency.

REFERENCES

1. Department of Energy, PRDA No. RA01-79ET15055. Exploratory Research, Development, Testing, and Evaluation of Systems or Devices for Hot Gas Cleanup. Issued April 4, 1979.

2. Yung, S.C., et al. Venturi Scrubber Performance Model. Air Pollution Technology, Inc. August 1977. EPA 650/2-75-021b. PB 271-515.

3. Parker, R. and S. Calvert. Alternatives for High Temperature/High Pressure Particulate Control. Air Pollution Technology, Inc. January 1979. EPA 600/7-79-019.

4. Calvert, S., et al. Fine Particle Collection Efficiency in the A.P.T. Dry Scrubber. Presented at the EPA/DOE Symposium on High Temperature/ High Pressure Particulate Control. Held in Washington, D.C. September 1977.

5. Calvert, S., et al. A.P.T. Dry Scrubber for Particle Collection at High Temperature and Pressure. Presented at the EPA Fine Particle Symposium. Held in Denver, Colorado. July 1978.

6. Sverdrup, E.F., et al. The Tolerances of Large Gas Turbines to Rocks, Dusts, and Chemical Corrodents. Proceedings of the EPA/DOE Symposium on High Temperature/High Pressure Particulate Control. September 1977. EPA 600/9-78-004.

Table 1. COST OF ELECTRICITY FOR HTP GAS CLEANUP ON A 710 MWe PFBC POWER PLANT.

System	Capital Investment 10^6\$*	$/kWe	CCOE mills/kWh	OCOE mills/kWh	COE mills/kWh
E PxP	7.2	10.2	0.3	0.4	0.7
Fixed Bed GBF	24.0	33.9	1.1	0.2**	1.3
Continuously Moving GFB	33.8	47.6	1.5	1.2**	2.7
Intermittently Moving GBF	59.4	83.7	2.7	0.9**	3.6

CCOE - Capital cost of electricity

OCOE - Operating cost of electricity

COE - Cost of electricity

*Based on 4th quarter 1978 U.S. dollars (Marshall & Stevens Index = 569.4).

**OCOE does not reflect the cost of collector particle replacement for these systems.

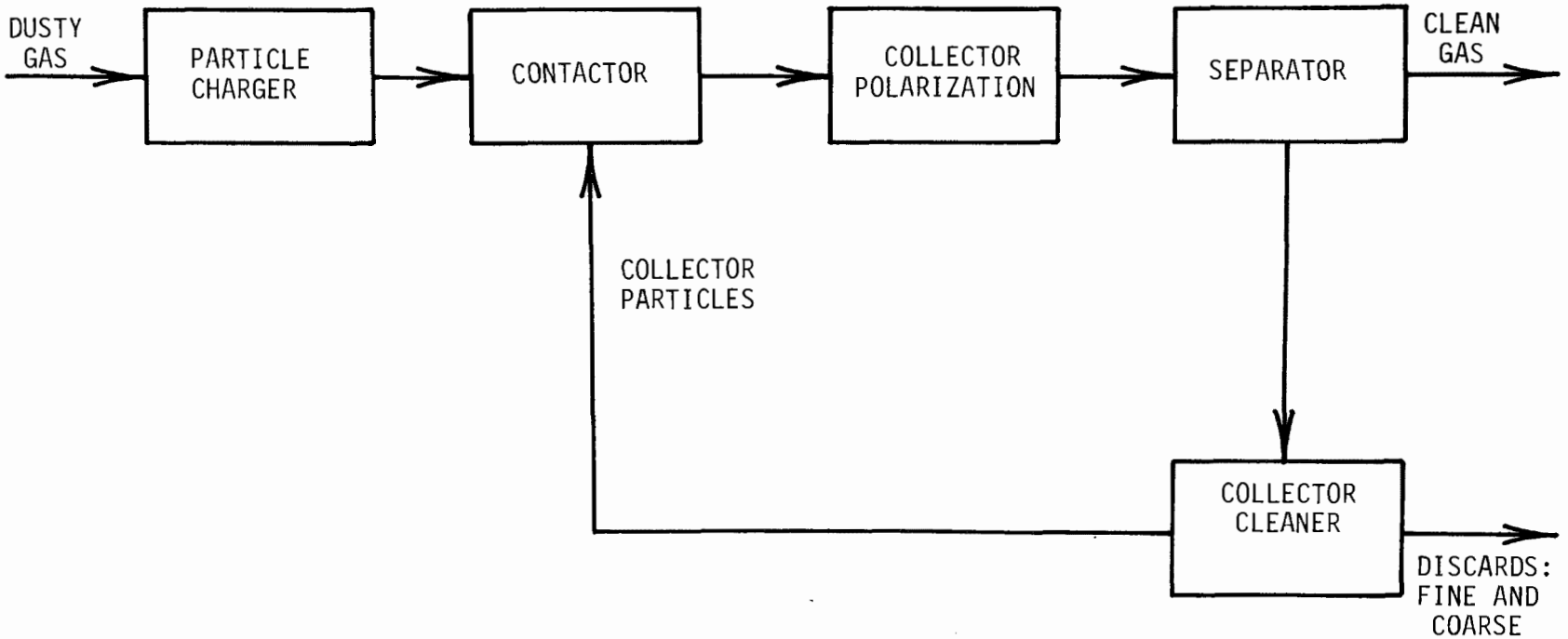

Figure 1. Schematic diagram of A.P.T. Dry Scrubber System.

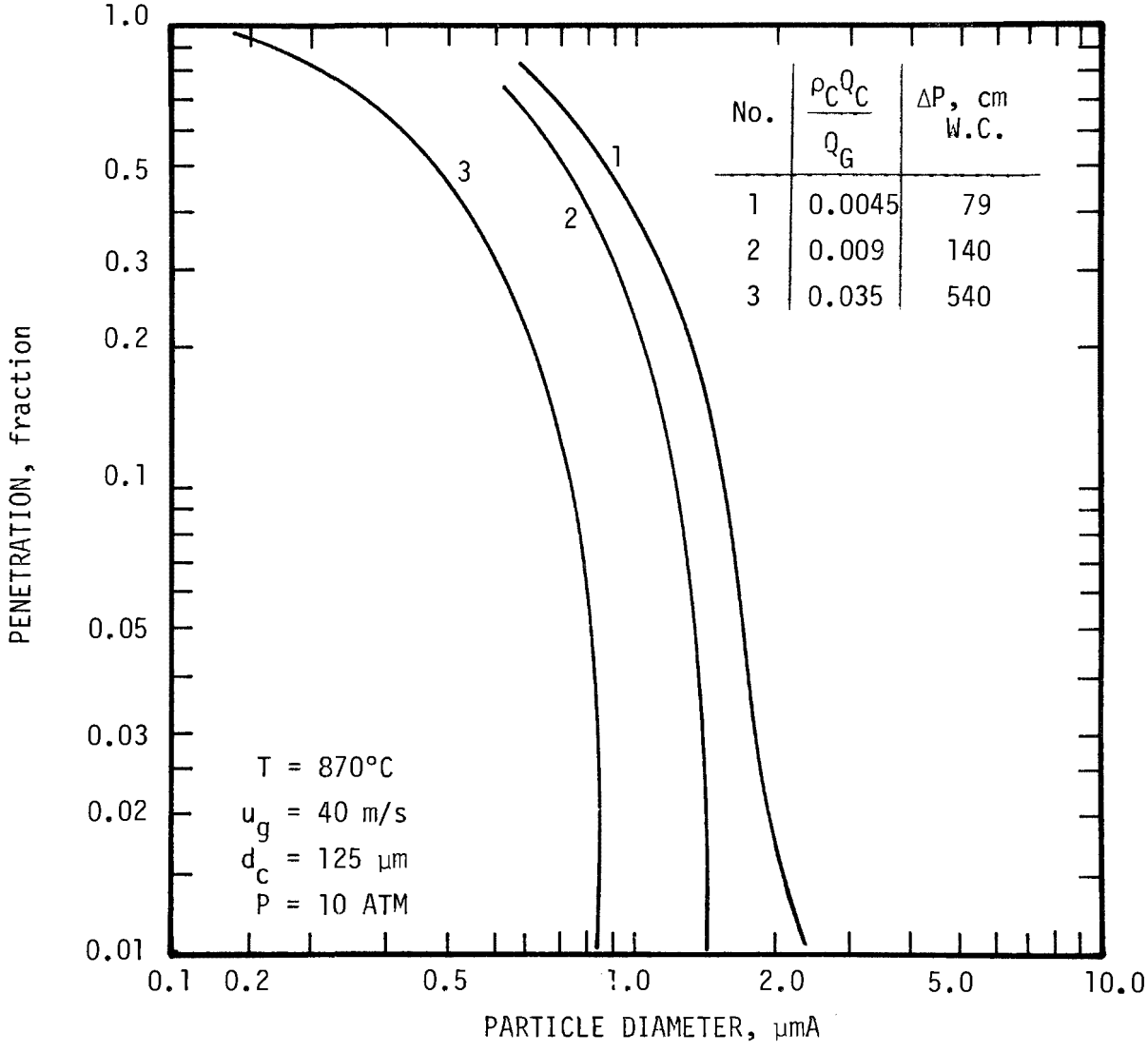

Figure 2. Predicted PxP performance.

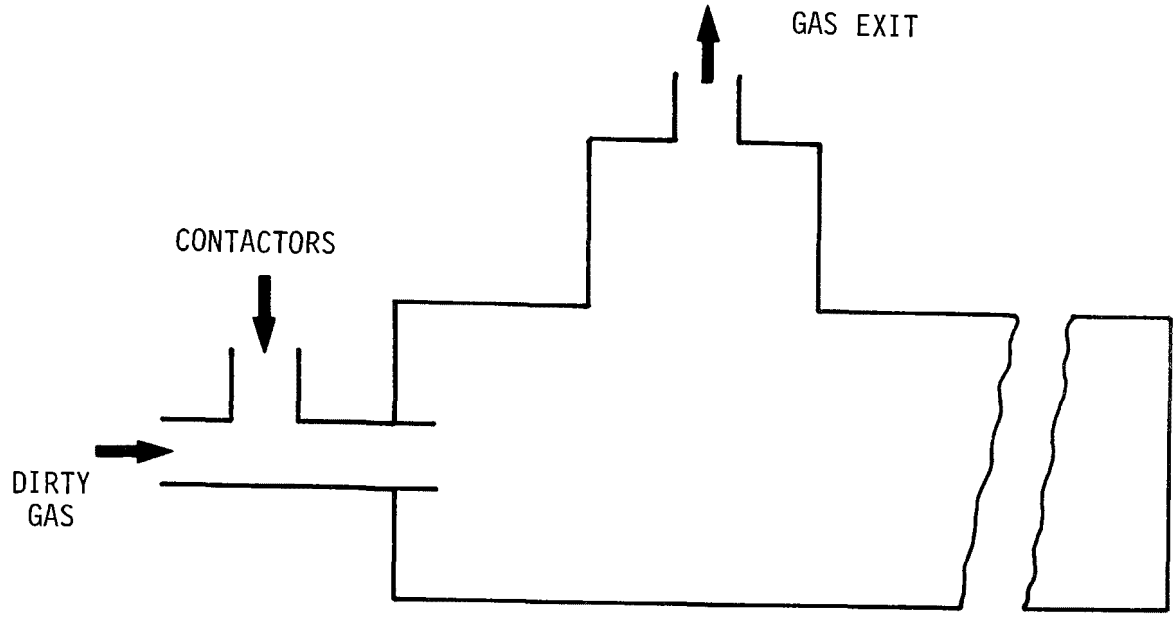

Figure 3. Contactor and gravity separator.

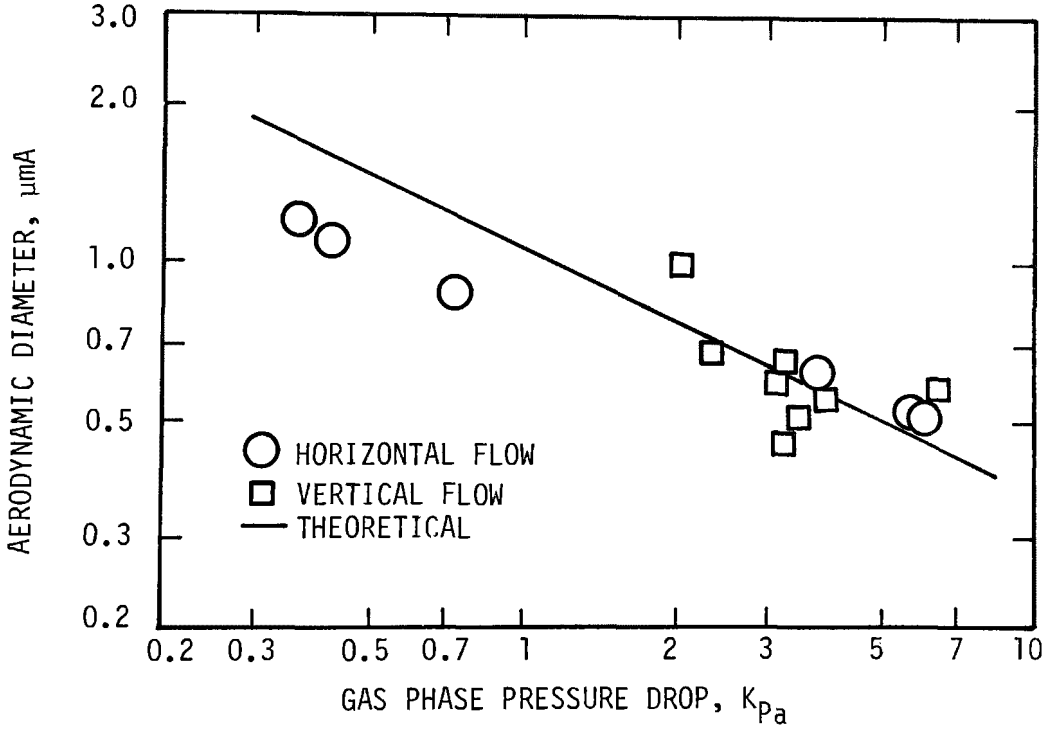

Figure 4. Comparison of particle collection characteristics of the A.P.T. Dry Scrubber with the A.P.T. cut/power relationship.

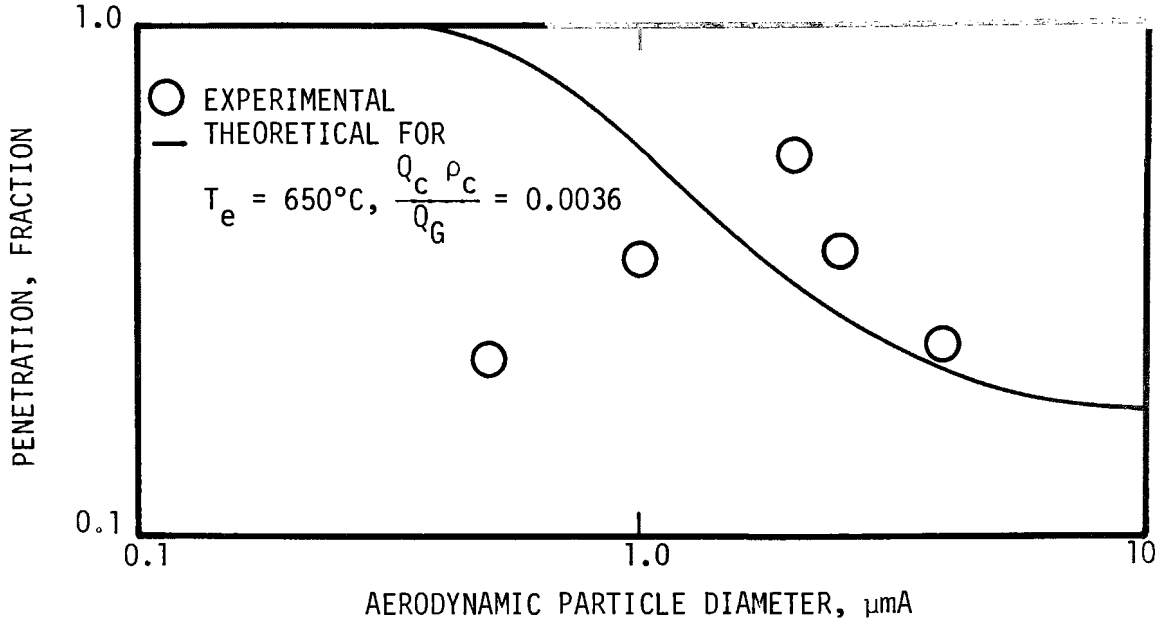

Figure 5. Particle penetration with nickel collectors.

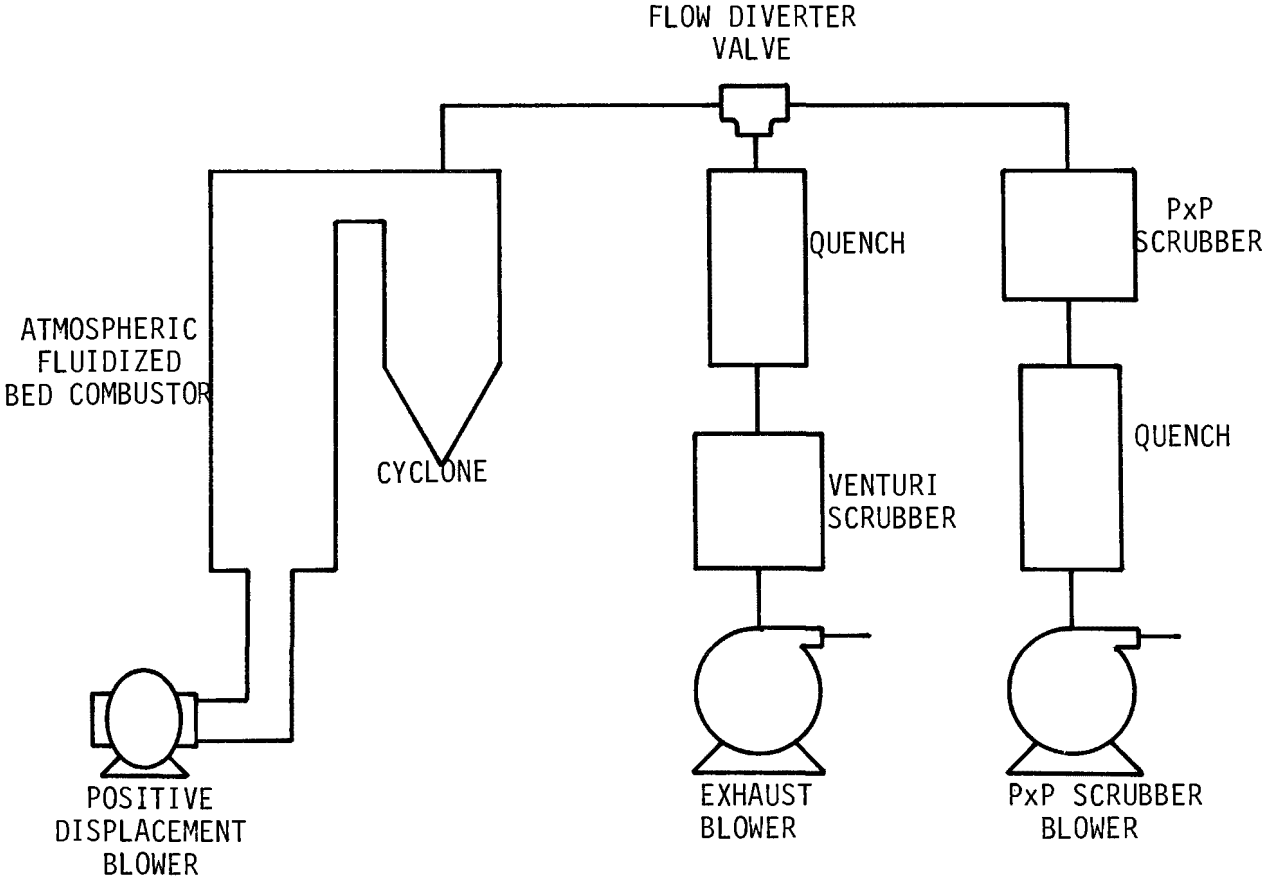

Figure 6. Phase II experimental apparatus.

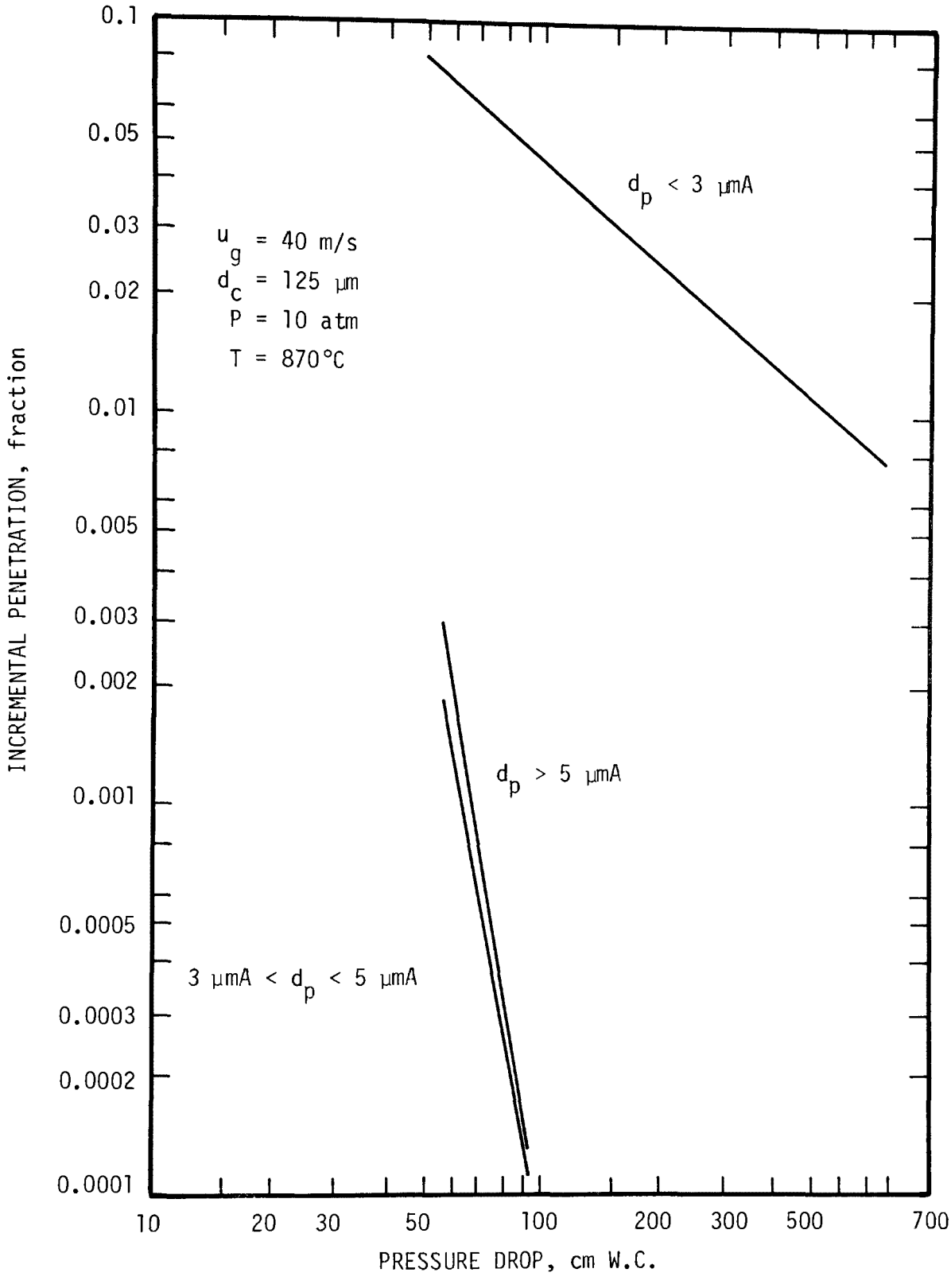

Figure 7. Predicted penetration for three size increments.

GAS CLEANING UNDER EXTREME CONDITIONS OF TEMPERATURE AND PRESSURE

E. Weber, K. Hübner, H. G. Pape, R. Schulz

In connection with the development of new technologies, like the metallurgical direct reduction process or coal conversion processes, it seems necessary and convenient to clean gases at temperatures up to 1000 ^{o}C and at pressures up to 20 bar and even higher.

Among the today known types of dust separators for the cleaning of gases at extreme conditions first of all mass force separators come into consideration which operate due to the centrifugal force principle. Their application depends mainly on the choice of suitable temperature and pressure resistant materials. It is well-known, however, that the centrifugal force separators are less appropriate for the precipitation of fine particles. In addition their efficiency deteriorates by the increasing of gas viscosity and by other effects /1/. It remains to be seen which claims for the gas purity will be enforced by the new technologies and what are the properties of dust. After that it can be decided whether or not mass force separators do offer a solution for the problems.

Contrary to mass force separators, high energy separators, namely electrostatic precipitators and wet scrubbers are known in principle to offer any desired efficiency of separation. Obviously these separators can be applicated at high temperatures and high pressures by suitable modifications / 2, 3, 4, 5 /.

Without change of the known physical separation effect new filtering media with sufficient temperature resistance have to be developed for filtering separators and wet seperators, whereas for the electrostatic precipitator it must be investigated what are the conditions of operation and which efficiency may be reached. Investigations concerning these subjects are carried

out in the Institute for Mechanical Process Engineering of the University of Essen. The efficiency of filtrating, electrostatic and wet separators is studied at extreme gas conditions and the apparata can be modified, according to the results. The investigations are sponsored by the German Ministry of Home Affairs and by the Ministry for Science and Technology. The authors wish to thank these authorities for their financial support.
This paper is concerned with actual results of the studies. There is a scale of fabric materials for the filtrating separation at high gas temperatures - extreme gas pressures are less important for the dust separation by fabrics. Fabrics which come into consideration are fibres of metal, carbon, alumina-silicate, quartz glass.
Figure 1 shows the field of application and the processibility and data about the fibre thickness. At present filter media made by metal fibres are already available. Their efficiency is quite similar to that of filter media used in the usual temperature range up to 350 ^{o}C. Until now, however, experiences about the durability of metal woven materials at high temperatures and in an oxidizing atmosphere are still missing. It must be supposed that the fine metal fibres will scale and corrode in presence of oxygen interfering the stability and efficiency. Further disadvantages are the high costs for the material from 300 to 500 $ per m^2 filter area and the relatively low temperature durability. Apparently metal fabrics can be used only in special cases. Carbon fibres too, are only applicable for particular purposes. The fibres show at least in reducing atmosphere a high temperature durability, but the felts made of carbon fibres have low mechanical stability. So it can be expected that the filtration and the cleaning of the filter is problematic for this material.
Besides that, filter media made of carbon are expensive. Alumina-silicate fibres - often called as ceramic fibres - do fulfil in principle all conditions of an advantageous filter medium. It is possible to produce thin fibres which are high temperature resistent, of good chemical durability and low costs. At present

one has not succeeded in manufacturing fibres of greater longitude from these materials. But this is necessary for the production of an endless thread as a basic material for multiple needled felts and woven materials. So it is only posible to manufacture alumina-silicate fibres to waddings, vleeces and single needled felts. Woven materials are only producible by means of metal core threads. Alumina-silicate felts are applicable for dust separation if certain apparative preconditions are fulfilled. These felts allow in principle high efficiencies, or low dust concentrations in the clean gas. It must be the subject of future investigations how to modify and to optimize these materials.

Besides alumina-silicates strongly improved quartz glass fibres seem suitable for a gas cleaning at high gas temperatures. It is an advantage of this fairly chemical resistant material, that it can be manufactured to filtering fabrics. Depending on the chemical composition the fibres may be temperature resistant up to 1000 ^{o}C. A further increase seems actually possible by incorporation of metal atoms into the fibre texture. From this point of view quartz glas fibres have been predominately investigated in studies about fabric filters. It must be taken care for the decrease in the mechanical strength with increasing temperatures. The tensile strength is sufficient, difficulties occur, however, with respect to the abrasion and buckling resistance. That is one reason why, at present, no double needled, i. e. strong felts, of quartz - fibre material are available. The application of quartz woven materials at high temperatures is possible in principle, as the investigations have already shown. Preconditions are some mechanical devices like fixings, holdings and supportings for the material in the filter. These requirements should be realizable. On the other hand a successful dust separation needs relatively strong woven materials, to have a maximum material stability and to avoid a displacement of the fabric structure during the filter's operation. Such dense and by that heavy fabrics are necessary because of another reason: In opposition to the filtration

at normal temperatures the high temperature filtration does occur at the start by the fabric itself and not by fibres at the surface of the material. Even if these preconditions are taken into consideration it can be expected that such fabrics would be available at low costs. For the basic studies a laboratory test facility was constructed operating at gas pressures up to 5 bar and temperatures up to 1000 ^{o}C. In connection with a gas burner even temperatures of 1400 ^{o}C can be reached. Figure 2 shows the scheme of the test facility. The filter media are studied in an electrical heated pressure vessel, in which the fabrics are installed in form of filter tubes. The cleaning can be carried out by pulse jet or mechanical means. Various kinds of dust like quartz or fly ash from power stations are added to the crude gas. The clean gas concentration is monitored discontinuously by well known sampling procedures. The superficial filtration velocity can be varied between 1.0 and 20.0 cm/s, i.e. gas to cloth ratios from 36 to 70 m^3/m^2h. Fig. 3 shows a view of the test plant.

In Fig. 4 the pressure drop of the clean high temperature filtration media is plotted as function of the superficial filtration velocity. The variation of the pressure drop is caused by different fibre strength, fabric texture and fabric strength.

Based on the previous considerations about the different types of fabrics, it can be expected that the materials G 1 to G 3 are not well applicable for the dust separation. This has been confirmed experimentally.The pressure drops of the more appropriate fabrics G 4 to G 7 do not much exceed that of filter materials for normal temperatures. Fig. 5 shows clean gas dust concentrations for various fabrics as a function of the superficial filtration velocity at different crude gas concentrations. The test dust consists of quartz particles sized below 30 µm and a mean diameter of 6.2 µm. Dependent on the filter material in some cases extremely low clean gas concentrations have been obtained. Different crude gas concentrations between 5 and 15 g/m^3 gas have negligible influence on the clean gas concentration.

Besides the properties and the amount of dust, specific factors caused by the woven materials influence mainly the filter efficiency. Varying these factors allows a more efficient dust separation which is not so strongly interfered by the magnitude of the superficial filtration velocity.
Fig. 6 shows the pressure drop of the dust loaden filter and different filter temperatures as functions of the filtration time. The initial pressure drop does not change after the jet pulse cleaning, because the applicated fabric has been already dust loaden over a long periode. The times of filter operation vary somewhat before the final pressure drop of about 2300 Pa is reached due to different dust concentrations in the crude gas. The investigations show that the cleaning of the fabrics can be carried out like that for normal temperature materials.
During the jet pulse cleaning the filter temperature decreases for a moment because of the use of cold air for the cleaning. The gas temperature at the filter inlet was always below the temperature in the interior of the filter because an additional heating was installed in the pressure vessel. Fig. 7 shows the dust loaden filter medium with parts of a filter cake. It can be summarized that the studied filter média allow in principle a fairly well dust separation at high pressures and high temperatures.
The development, however, including the manufacturing of suitable felts has not come to an end. Yet it can be expected that the necessary investigations can be finished successfully allowing a change from the laboratory to the industrial pilot scale.
In comparison with filtering separators a modification of dry electrostatic precipitators for their operation at high temperatures and pressures does not seem necessary besides the choice of suitable heat resistant materials. At present little is known about the behaviour of the factors influencing the electrostatic dust precipitation at high temperatures and high pressures. Thus it is unknown, whether or not a satisfying dust separation by electrostatic precipitators is possible at extreme conditions.
These factors are only known for gas temperatures up to about

350 °C and pressures of about 3 bar.

There is little understanding about the efficiency of electrostatic precipitators at temperatures of 1000 °C and high pressures. Even at normal temperatures the knowledge of the physics of separation has gaps. It can be stated in principle that the ion mobility which influences the sparkover voltage increases with temperature and decreases with growing pressure. It can be expected that electrostatic precipitators can operate only at high gas temperatures when there are high pressures too. In this case the difference between corona starting voltage and sparkover voltage is large enough. Quantitative data about this voltage difference as a function of the geometry of the precipitator and of kind and type of electrodes as well as of the amounts of dust and gas in the precipitator are still missing to a far extent. Besides this it is unknown which separation efficiency, respectively which migration velocities can be realized and what are the properties of adherence of the dust to be precipitated. Thus before planning larger units it is necessary to study these influences by experiment. For this purpose a single tube precipitator has been built, operating at pressures up to 35 bar and gas temperatures of up to 1100 °C. The duct width of the precipitator is variable between 50 and 250 mm and gas velocities up to 3 m/s in the duct can be reached. Fig. 8 shows the flow scheme of the test facility. The electrostatic precipitator was working stationary at first, allowing a discontinuous dust feed, too, in order to study the principal correlation between dust content and current-voltage characteristics. In the meantime the laboratory plant has been reconstructed for continuous operation with respect to dust and gas feed and the necessary dust monitoring equipment has been installed. The high voltage with a maximum value of 280 kV at 200 mA is supplied to the sparking electrode using fairly leakage proof insulators. Fig. 9 shows a photo of the test facility.

At present a lot of experiments, especially for discontinuous operation have been carried out. In the scope of this paper it shall be reported only about a few results of the investigations. Those were obtained with air at temperatures of up to 1050 °C

and pressures of up to 13 bar and a collecting tube diameter of 50 mm, operating the electrostatic precipitator without dust feed. Varying the duct width and the kind of gas changes the order of magnitude of the results, but led in principle to similar findings.

Fig. 10 shows typical examples for the pressure and temperature dependence of the current-voltage characteristics obtained with a sparking electrode diameter of 0.8 mm. In agreement with theoretical studies and experimental results of other authors / 6, 7 /, it is to be seen that the current-voltage characteristic becomes steeper with increasing gas temperatures, while the corona starting voltage and the sparkover voltage decrease. The curves' slope can increase as much that the two characteristic voltages become equal, inhibiting the operation of the electrostatic precipitator. In opposition to the influence of the temperature, an increase of the pressure flattens the current-voltage characteristics. The corona starting voltage and the sparkover voltage grow simultaneously. It exists a so-called critical pressure at which both voltages have the same value, even at high gas temperatures. The reason for this limiting pressure are two countercurrent effects. On one hand the declining mean free path of the gas molecules hinders the ionization by collision at increasing pressures. By that the sparkover voltage is increased. On the other hand the enhanced photo-ionization and the smaller ion diffusion facilitate the propagation of streamers. Above a certain gas pressure the second effect prevails. The sparkover voltage is lowered.

In Fig. 11 are the corona starting voltage and the sparkover voltage plotted as functions of the gas temperature for the same electrostatic precipitator device. It can be seen that the optimum range of operation of an electrostatic precipitator, i. e. the maximum difference between corona starting voltage and sparkover voltage, is shifted with raising pressure into the direction of higher gas temperatures.

Besides gas pressure and gas temperature other factors like the kind of gas, the geometric filter dimensions as well as type and shape of the electrodes take influence on the current-voltage characteristics. This has to be especially taken into account for the dimensioning of the apparata.
Fig. 12 shows as an example the corona starting voltage and the sparkover-voltage as a function of the temperature for two sparking wire diameters of 0.8 and 1.5 mm. The above defined optimum range of operation is apparently smaller for a sparking wire diameter of 1.5 mm. The difference between corona starting voltage and sparkover voltage declines too, almost at all gas temperatures.
In opposition to the results of the 0.8 mm sparking wire the electrostatic precipitator cannot be operated at pressures of 11 bar with a sparking wire of 1.5 mm.

First results for different gas and dust conditions show that in principle a high temperature and high pressure electrostatic precipitator may work successfully. At present, however, it is not known under which conditions a rapping of the filter for cleaning the electrodes is to be done.Such a rapping would cause high expenses with respect to the precipitators construction and to the choice of materials.
It remains to be seen, what are the future findings of the investigations and what possibilities will be found for the optimization of high pressure and high temperature electrostatic precipitators.
Scrubbing processes can be employed only when the washing liquids fulfil the following conditions.

1. The substances have to be in the liquid state at temperatures of about 500 ^{o}C. They should be sprayable and must have a low surface tension.
2. The vapour pressure of the melt should be negligible at least for temperatures up to 800 ^{o}C.

3. There should be formed no toxic or harmful compounds.

4. The melt has to be either loss-free reprocessable or convertable into products that can be led to disposal.

5. The costs for the used melt should be acceptable.

Considering possible metal melts, especially tin fulfils these preconditions, eventually with additional copper or aluminum.

To prevent a possible oxidation this medium can be only used in the case of reducing gas mixtures. Besides this the gas must be mainly free of chlorine and hydrogen chloride to avoid the formation of fugative tin chloride.
In contrast to metal melts it is possible to use inorganic salt melts as well in an oxidizing as in a reducing atmosphere. The mixtures of sodium-, potassium-, and calcium compounds, mainly hydroxides and/or carbonates can not only remove solids but even a large number of gaseous constituents.
For the investigated melts the dust separation is in principle comparable to the conventional wet scrubbing process, if one excepts chemical reactions by salt melts. Due to these findings it seems not necessary to modify the well-known principles of wet scrubbing for the high temperature gas cleaning.
Based on the prestudies a small laboratory test facility was constructed and after that a pilot plant, a flow scheme of which is shown in fig. 13.
This plant consists mainly of a liquid and a gas circuit. The gas or air can be circulated in the system by a high temperature fan. After dust loading the gas is passed to the scrubber tube and cleaned with liquid salt or tin. The formed liquid-solid particles are precipitated in the cyclone which follows the scrubber and reprocessed after that.
Besides solid particles gaseous constituents can be removed. The maximum gas flow rate of the plant is 360 m^3/h STP.

In the Venturi like scrubber gas velocities up to 30 m/s can be realized. The liquid circuits consists of the liquid tank with an inserted radial pump, the liquid feeding for the spray nozzles, and the liquid output from the cyclone with liquid reprocessing. The liquid flow is controlled by a manometer. The pump allows a delivery rate of 2 m^3/h.
Fig. 14 shows a view of the test facility.

Fig. 15 demonstrates the separation efficiency of the process. Clean gas concentrations are plotted as functions of the crude gas concentration at a constant liquid flow rate of 2.2 l/min. Parameters are the gas velocity in the scrubber between 11 and 28 m/s and the ratio of liquid to gas flow rate between 0.4 and 1.0 l/m^3 gas. The washing medium was a mixture of alkaline compounds. The dust was quartz with a mean particle diameter of about 3.5 µm. The characteristics of the figure are quite similar to that of the well-known conventional wet scrubbers using water as a washing medium. To a limit of at least 0.4 l/m^3 the influence of the gas velocity prevails that of the washing liquid flow rate. Finally it is well-known from conventional wet scrubbing processes that the dust concentrations in the crude gas and the clean gas show interdependence if other factors are kept constant.
The interdependence may be linear, as in this case.
It can be summarized from fig. 15 that dependent on gas velocity and liquid flow any desired clean gas concentration can be reached using alkaline compounds for the gas cleaning.

Fig. 16 shows the dust concentration as a function of the gas velocity at a constant crude gas concentration of 1.5 g/m^3 STP. Parameter is the liquid flow rate of 1.6 and 2.2 l/min. Again the curves show similarity to the conventional wet scrubbing. Remarkable are the reached low clean gas concentrations at relatively small gas velocities and thereby low power consumption. Similar results have been obtained with changed experimental parameters and other washing liquids.

A satisfying removal of gaseous constituents could be realized, too. For example SO_2-separation efficiencies of more than 90 % have been achieved depending on the amount of washing liquid and the content of SO_2 in the crude gas.

Good results were also obtained using tin as a washing liquid. A final judgement of scrubbing processes seems not possible at present. For this, it is still necessary to carry out further tests. But it can be expected that such processes offer a hopeful alternative for the high temperature and high pressure gas cleaning allowing the simultaneous removal of particles and gaseous pollutants.

Within the scope of this paper it was only possible to give a brief review about the possibilities of the high pressure and high temperature gas cleaning. For this purpose in principle filtering separators, electrostatic precipitators and special scrubbers come into consideration. But there are still remaining some questions about the technical realization of larger industrial plants. Although it seems possible to use all three processes for the high pressure and high temperature gas cleaning, it must be seen which process offers the lowest expenses.
Finally it shall be noticed that at the beginning of 1980 a special conference on high temperature and high pressure gas cleaning is held in the F.R.G.

The investigations and their results shall be reported in more detail.

Literature

(1) E. Weber — VDI-Bericht Nr. 322 (1978) S. 111/119

(2) - — EPA-600/7-79-044 a-d

(3) - — EPA-600/9-78-004

(4) J.P. Meyer, M.S. Edwards — ORNL/TM-6072

(5) E. Weber — Technische Mitteilungen 71 (1978),Nr.3,S.161/167

(6) C.C. Shale, W.S. Bowie, J.H. Holden, G.R. Strimbeck — Report of Investigations 6325, Bureau of Mines Bureau of Mines (1963)

(7) J.R. Bush, P.L. Feldman, M. Robinson — 71st. APCA Meeting

fibre material	temperature resistance °C	manufactured to	lowest diameter of the fibres µm
glass: normal	450	fabric, felt	2 - 5
glass: high converted	1000		
glass: high converted with after-treatment	1400		
alumina silicate	1200	fleece, felt	4 - 20
graphite: oxidizing atmosphere	400	fleece	8 - 15
graphite: reducing atmosphere	>2000		
metal	650	felt, fabric, fleece	4 - 10

Mechanische Verfahrenstechnik Universität Essen

Properties of high temperature resistant fibres

Figure 1

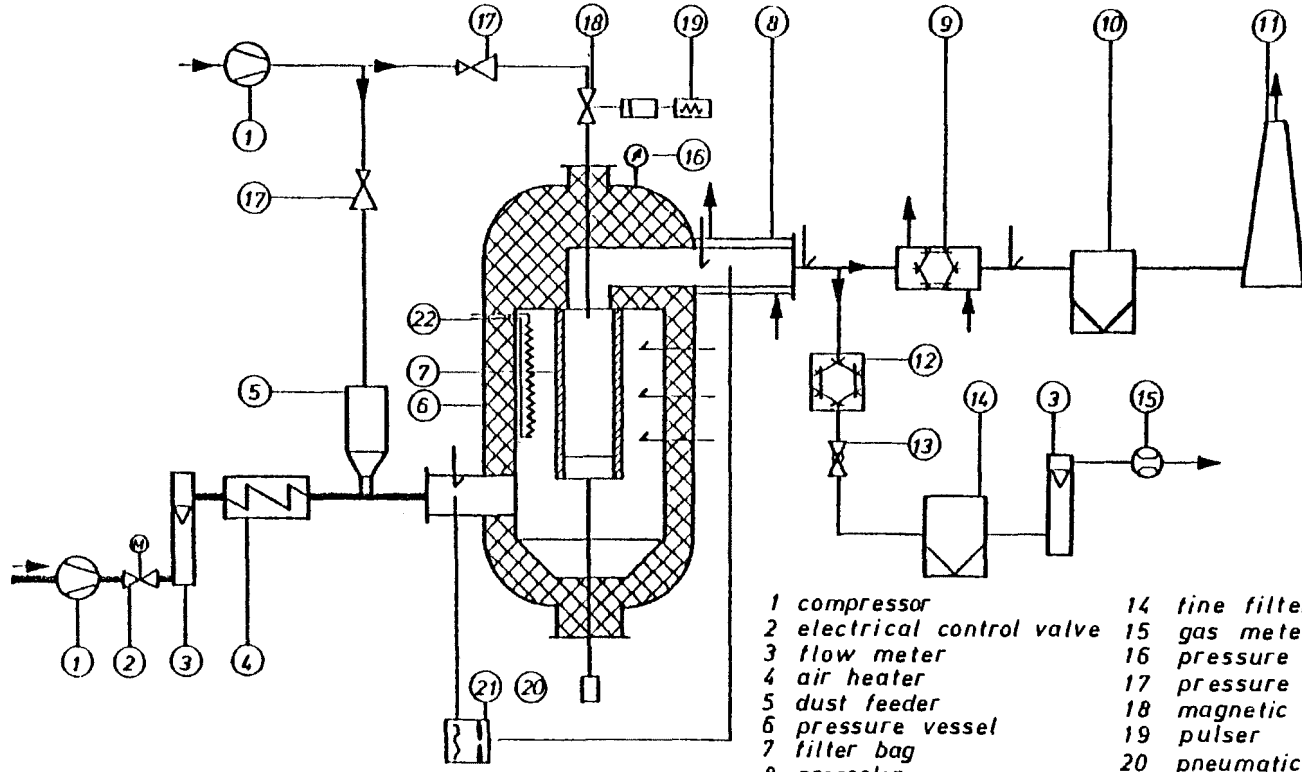

Mechanische Verfahrenstechnik Universität Essen	Flow scheme of the high pressure-high temperature fabric filter laboratory test facility	Figure 2

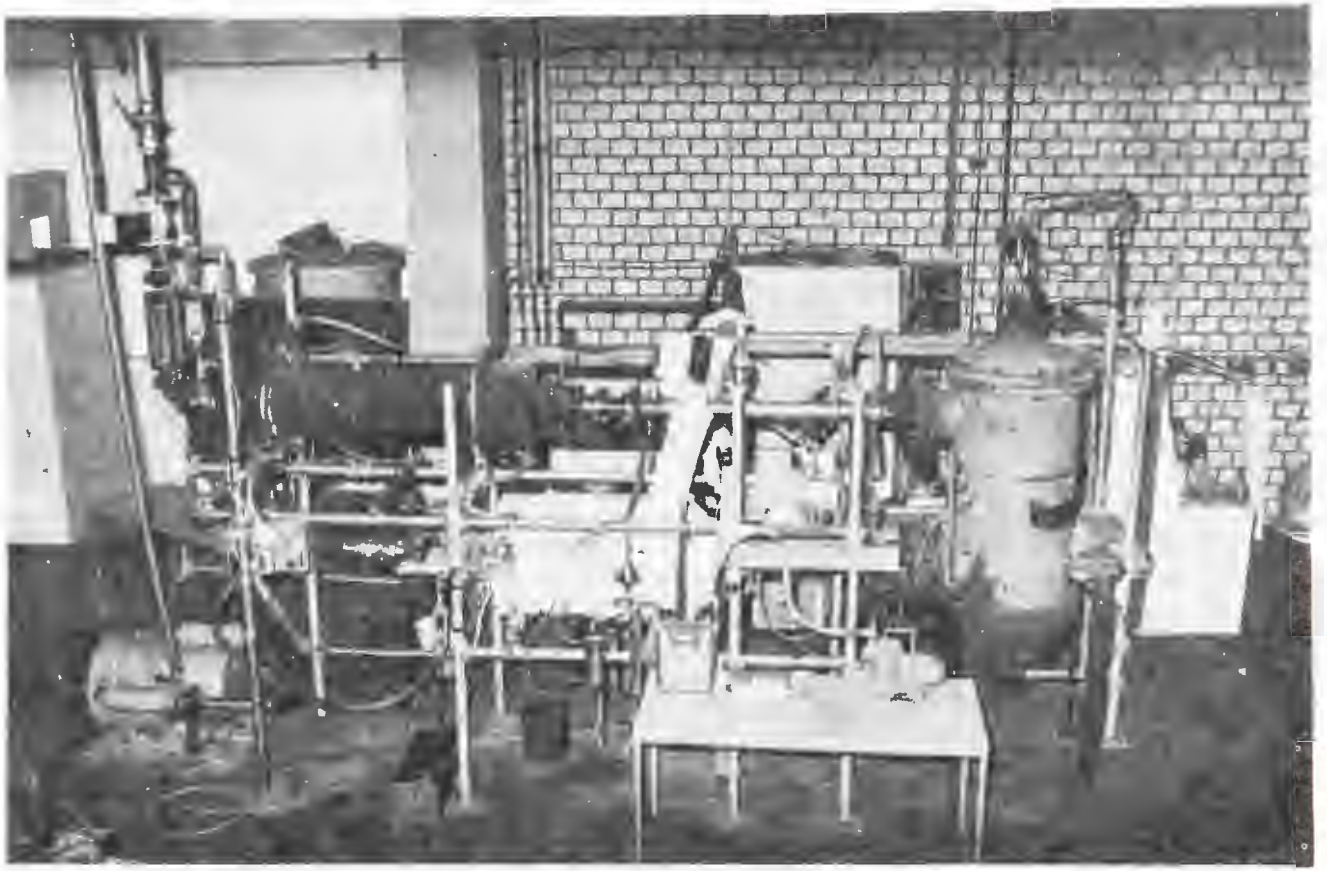

Mechanische Verfahrenstechnik Universität Essen	View of the high pressure-high temperature fabric filter test facility	Figure 3

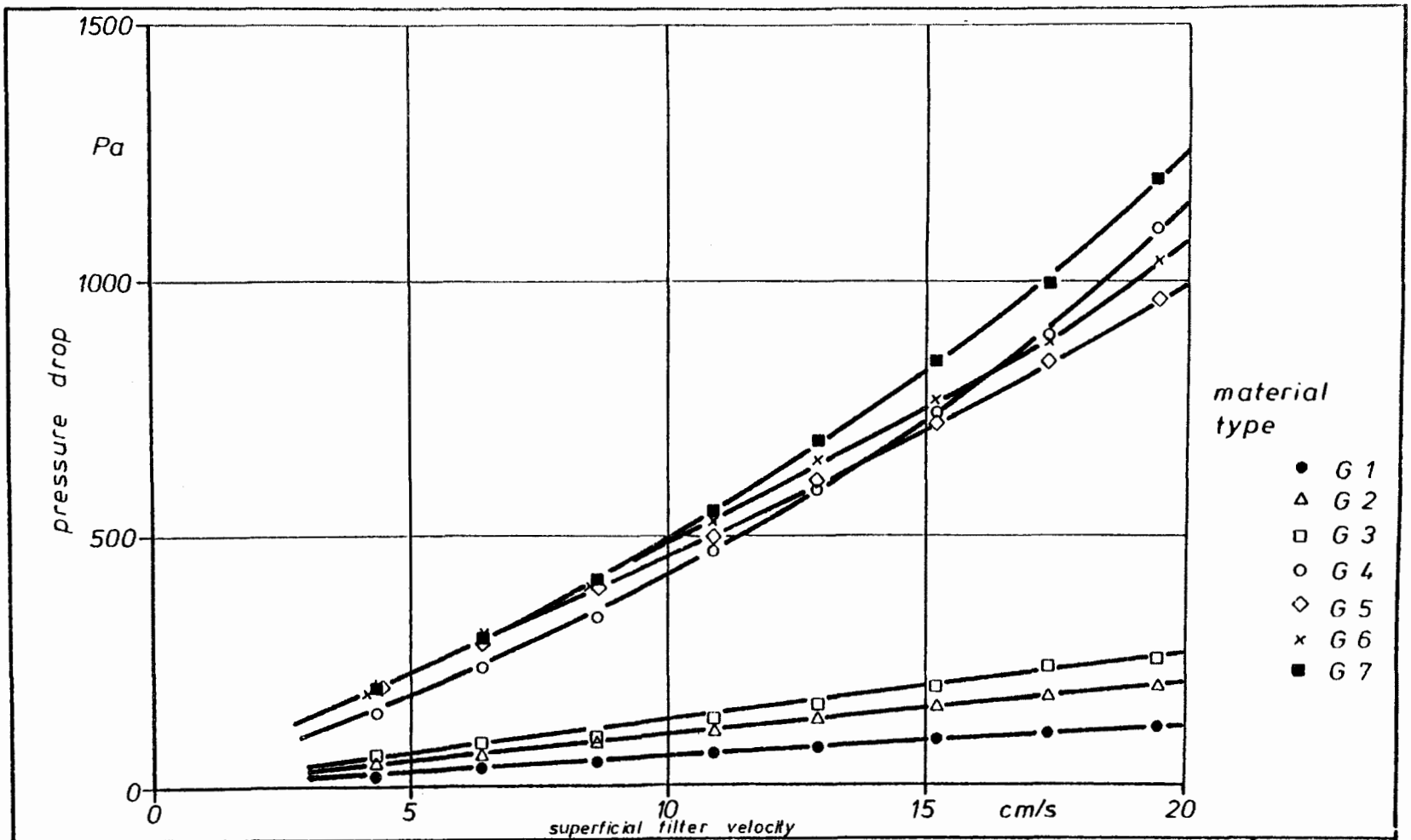

Mechanische Verfahrenstechnik Universität Essen	Pressure drop of clean fabrics versus superficial filter velocity	Figure 4

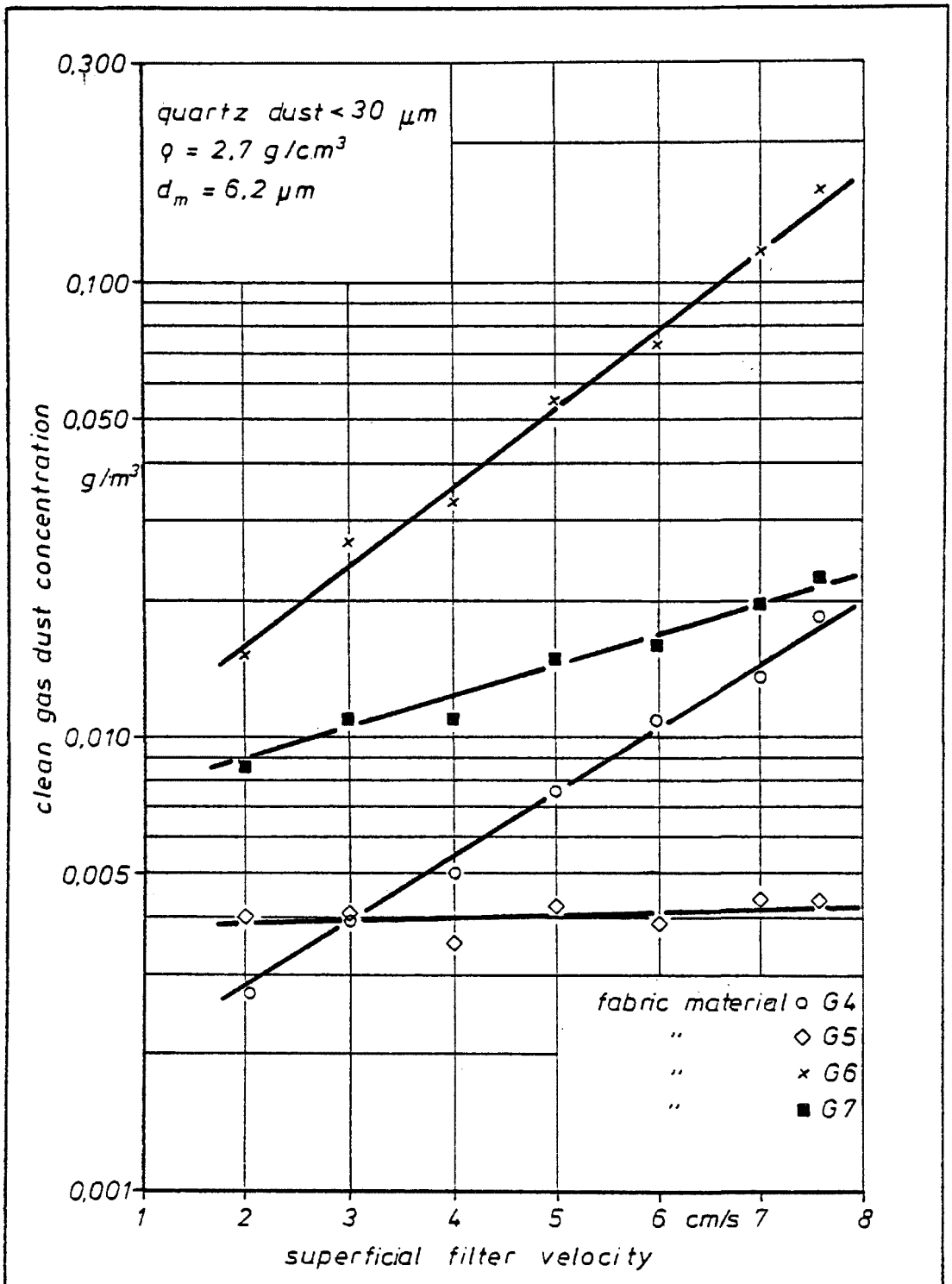

Mechanische Verfahrenstechnik Universität Essen	Clean gas dust concentration versus superficial filter velocity	Figure 5

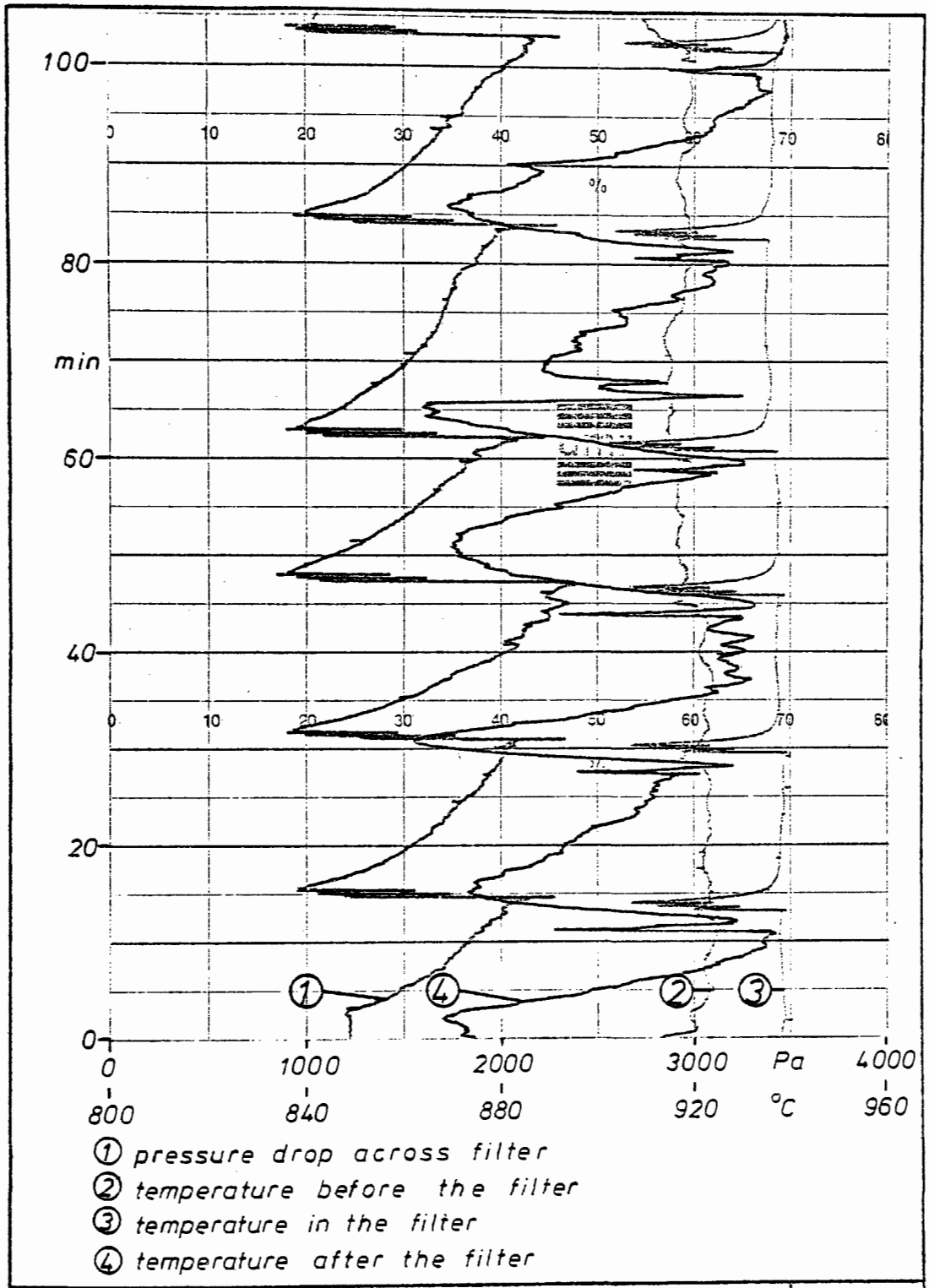

Mechanische Verfahrenstechnik Universität Essen	Filter pressure drop and filter temperature for quartz glass fabric	Figure 6

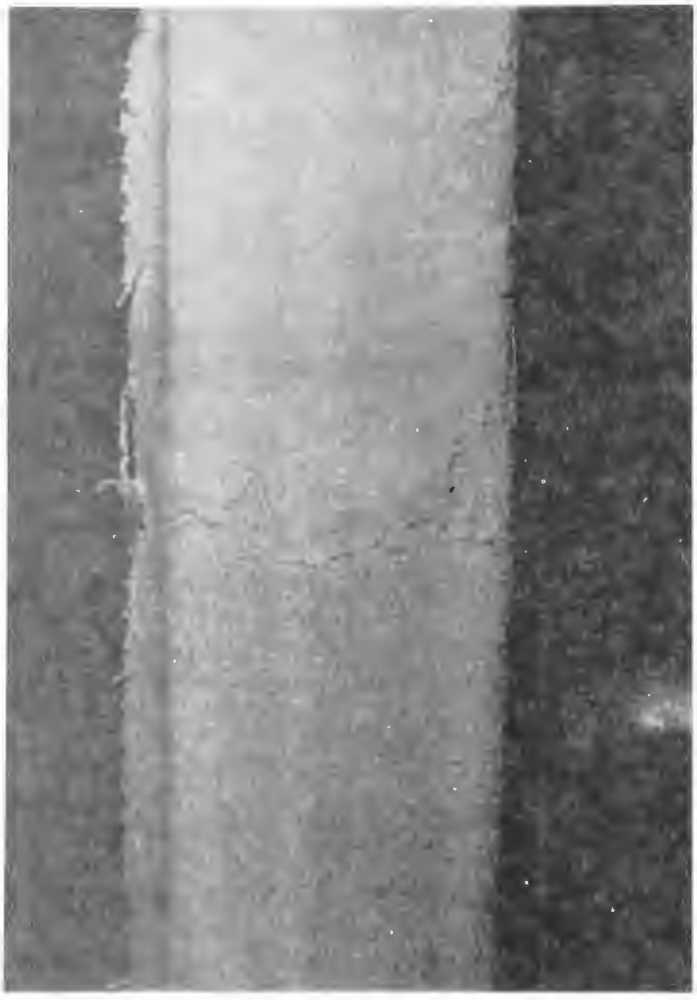

Mechanische Verfahrenstechnik Universität Essen	Loaden filter medium	Figure 7

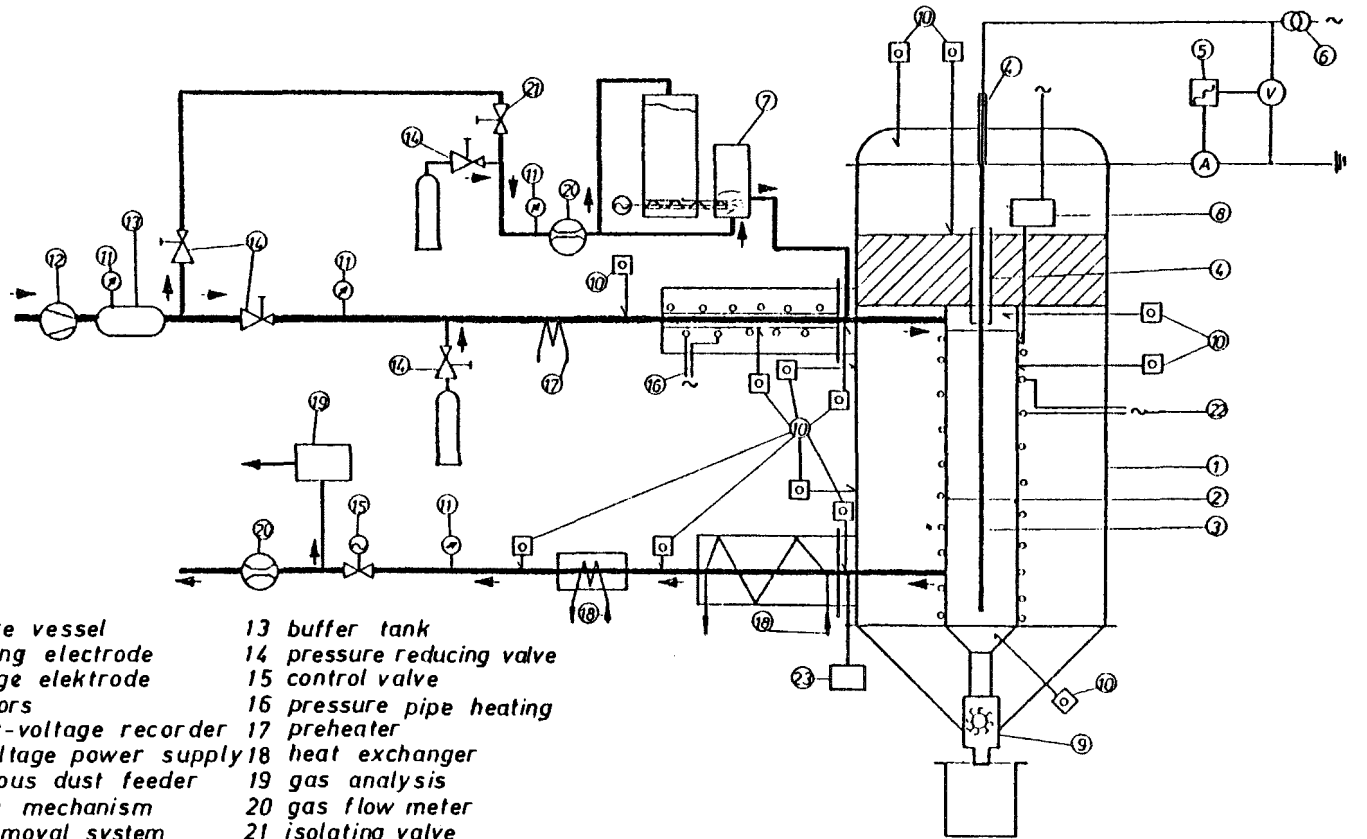

1 pressure vessel
2 collecting electrode
3 discharge elektrode
4 insulators
5 current-voltage recorder
6 high-voltage power supply
7 centinuous dust feeder
8 rapping mechanism
9 dust-removal system
10 thermocouples
11 pressure indicator
12 compressor
13 buffer tank
14 pressure reducing valve
15 control valve
16 pressure pipe heating
17 preheater
18 heat exchanger
19 gas analysis
20 gas flow meter
21 isolating valve
22 pressure vessel heating
23 dust measurement in the clean gas

Mechanische Verfahrenstechnik Universität Essen	Scheme of the high pressure and high temperature electrostatic precipitator test facility for continuous operation — Figure 8

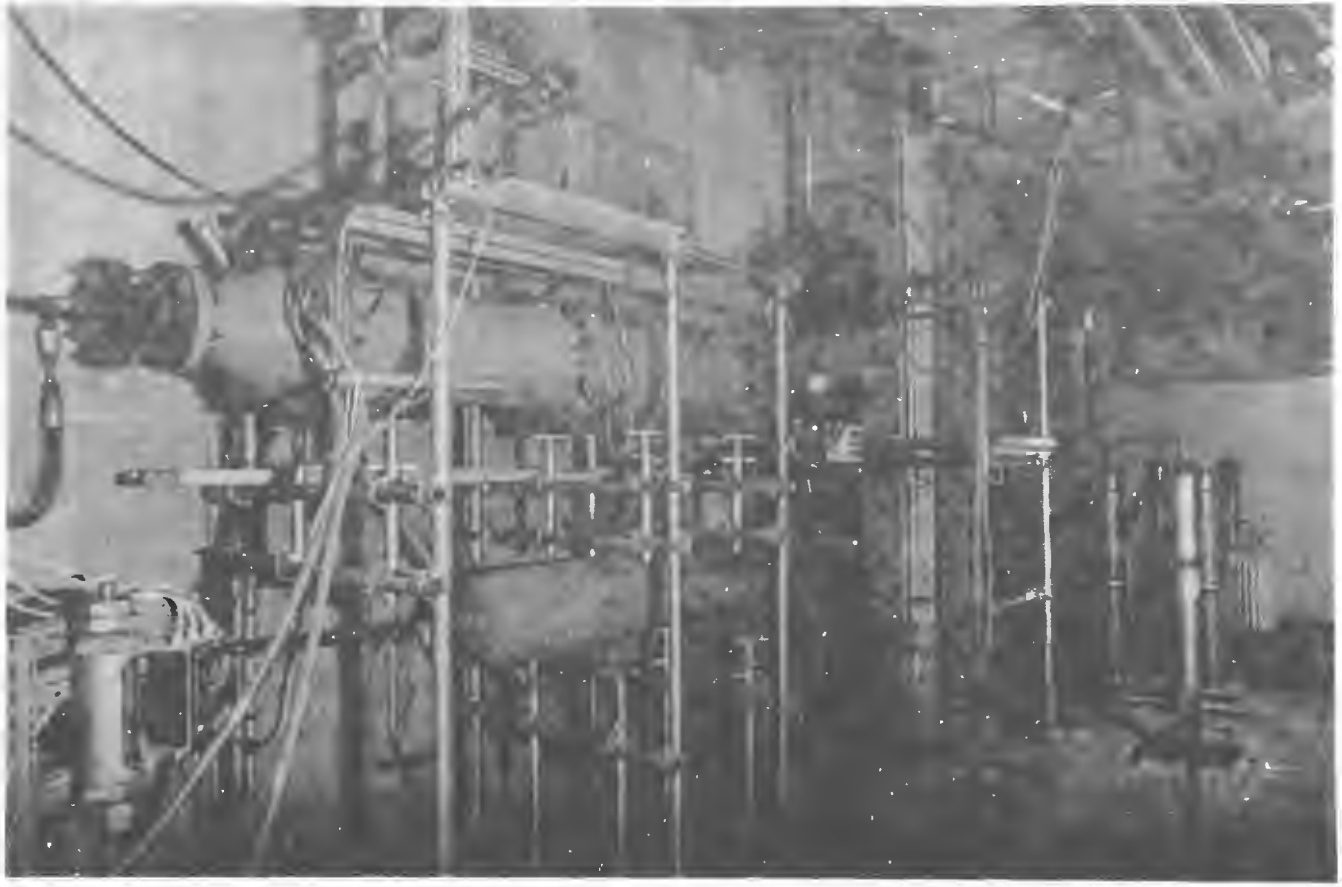

Mechanische Verfahrenstechnik Universität Essen	Test plant for high pressure and high temperature electrostatic precipitation	Figure 9

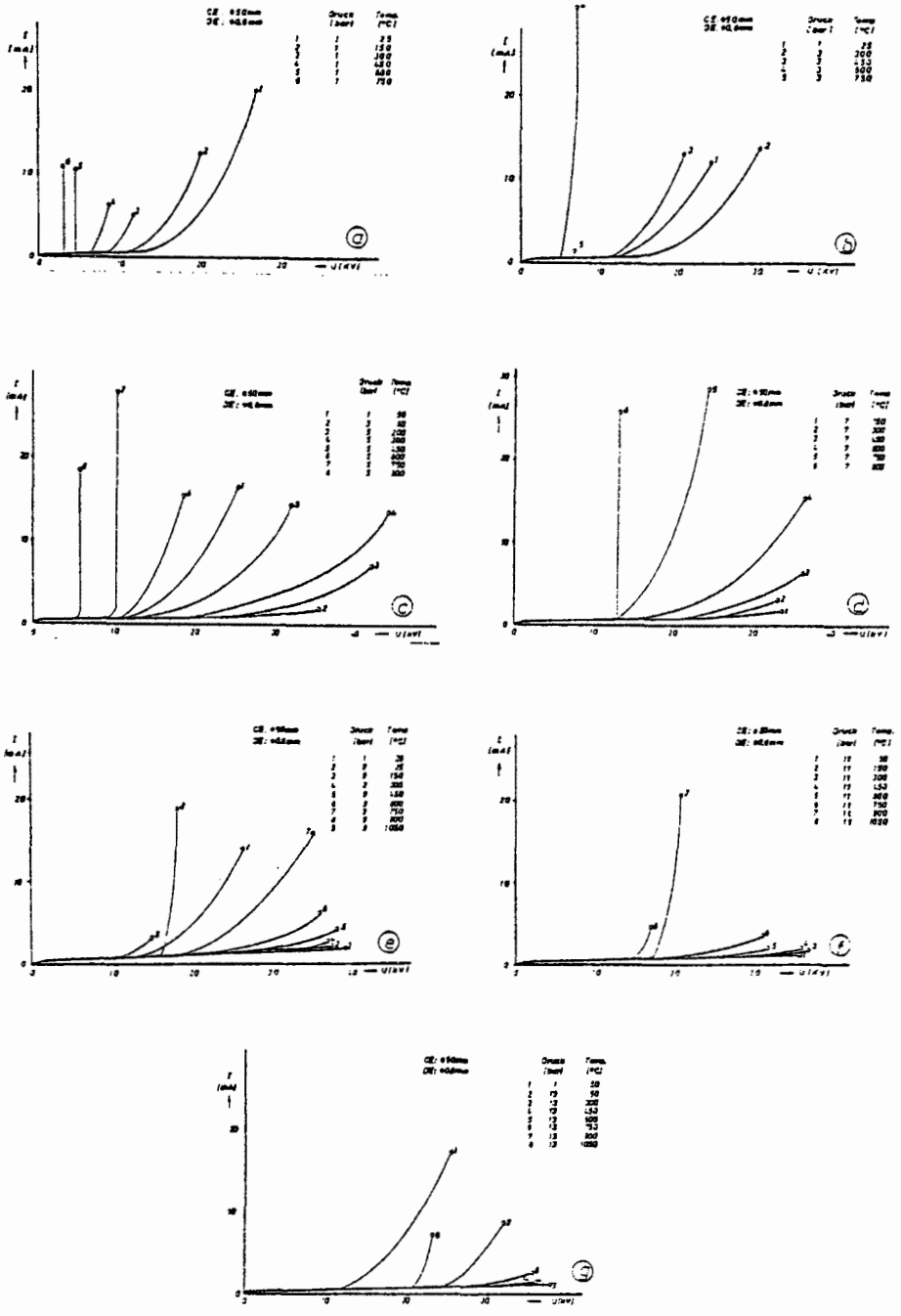

Mechanische Verfahrenstechnik Universität Essen	Current - voltage - characteris - tics (air)	Figure 10

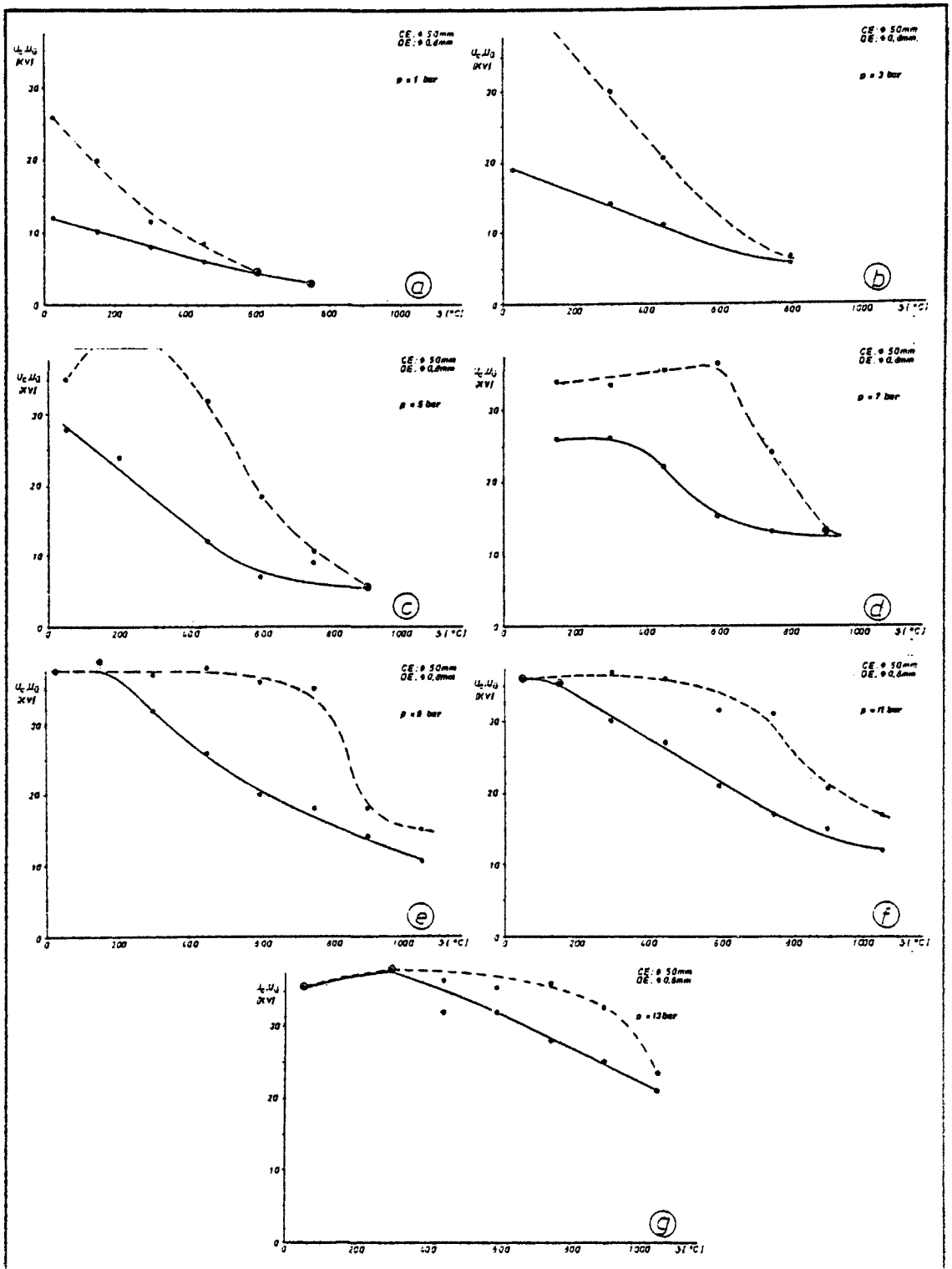

Mechanische Verfahrenstechnik Universität Essen	Corona-starting voltage and sparkover voltage as functions of the gas temperature	Figure 11

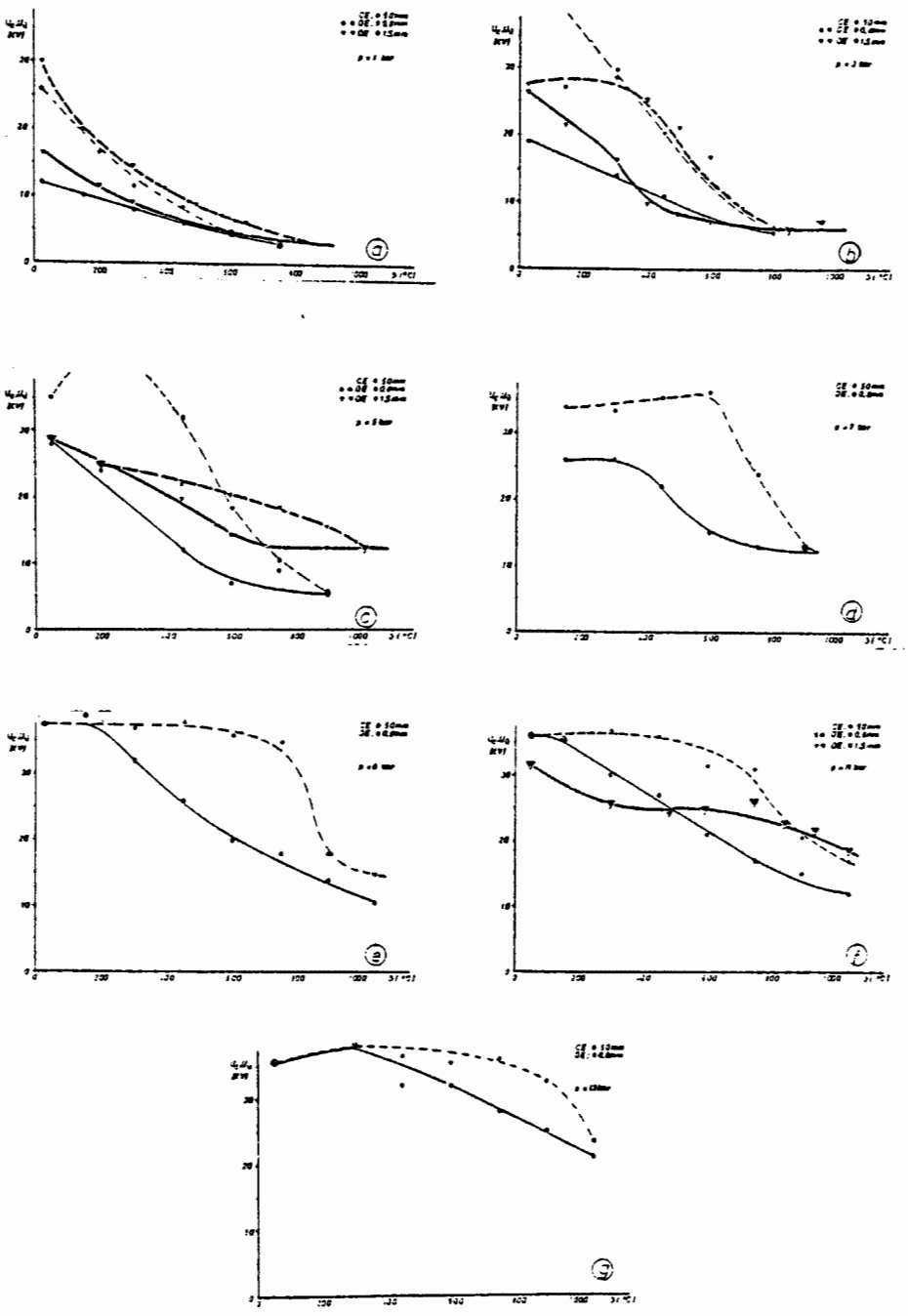

Mechanische Verfahrenstechnik Universität Essen	Corona-starting voltage and sparkover voltage as functions of the gas temperature	Figure 12

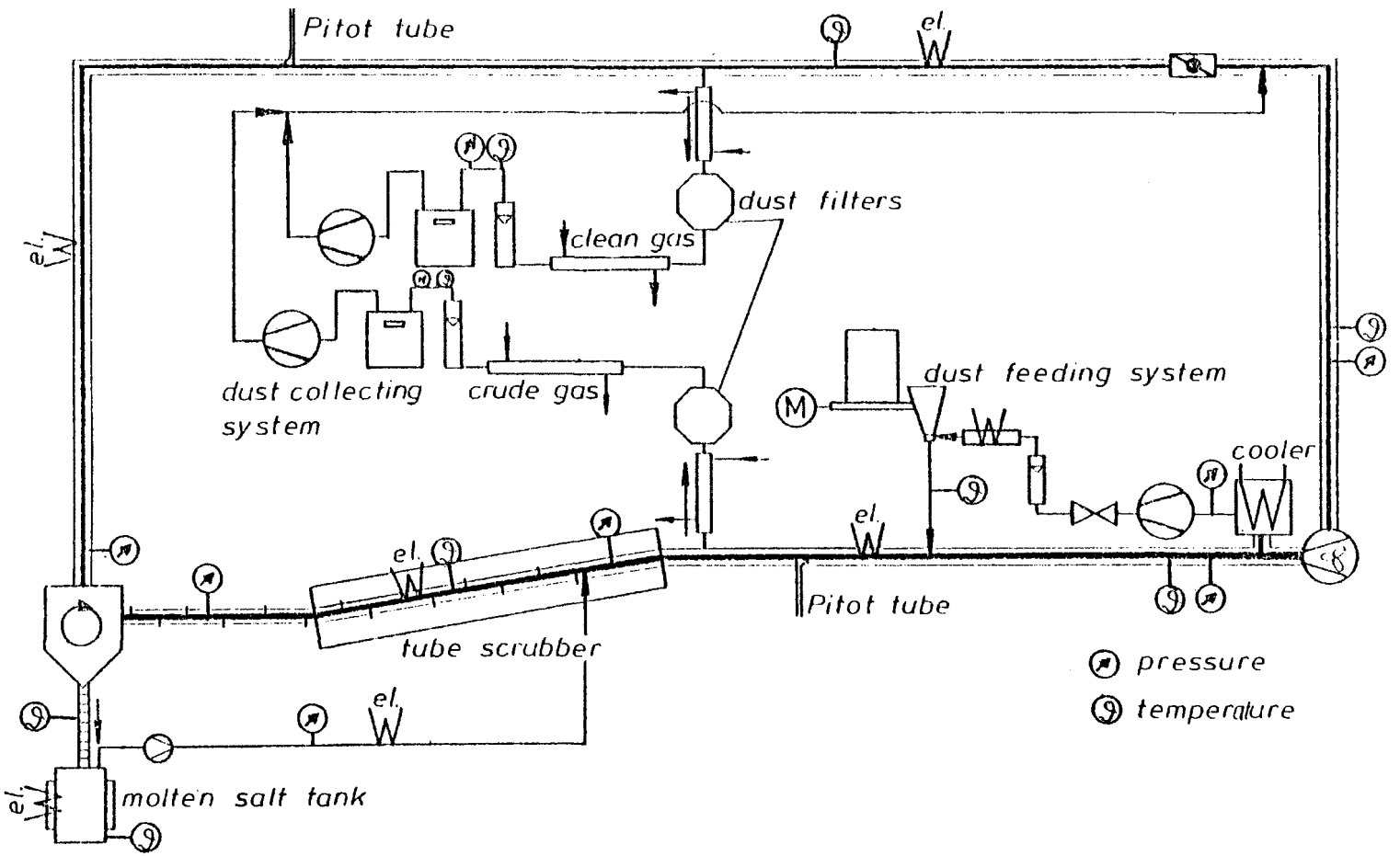

Mechanische Verfahrenstechnik Universität Essen

Scheme of the test plant

Figure 13

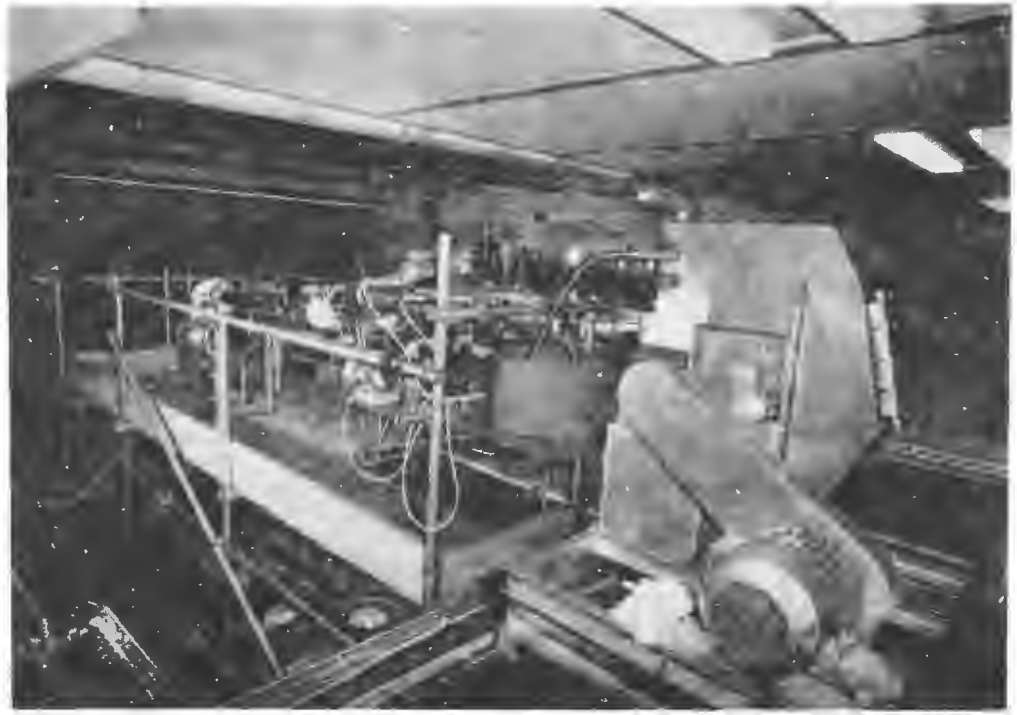

Mechanische Verfahrenstechnik Universität Essen	Semitechnical test plant for the high temperature gas cleaning by salt and metal melts	Figure 14

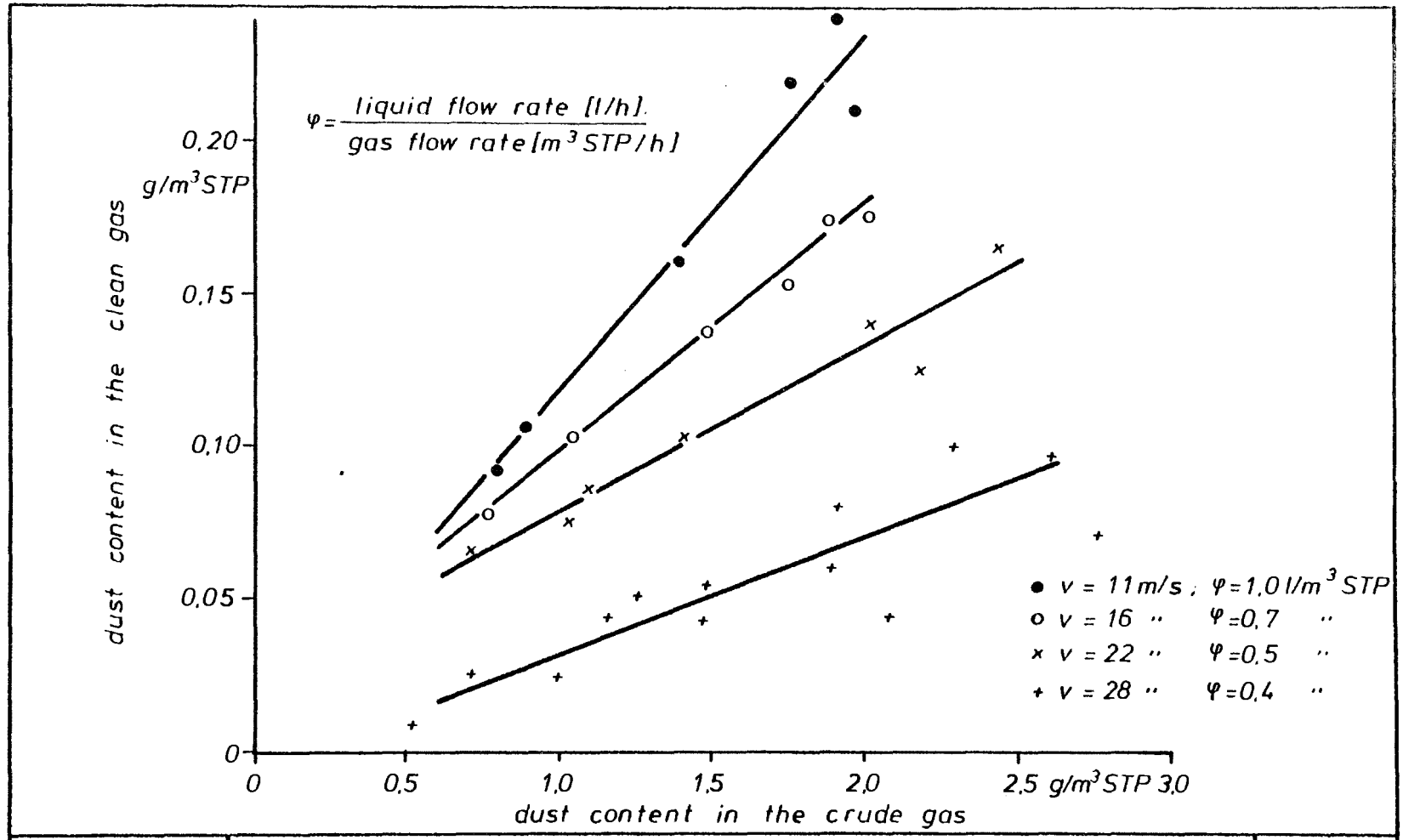

Mechanische Verfahrenstechnik Universität Essen	Clean gas contents at different gas velocities	Figure 15

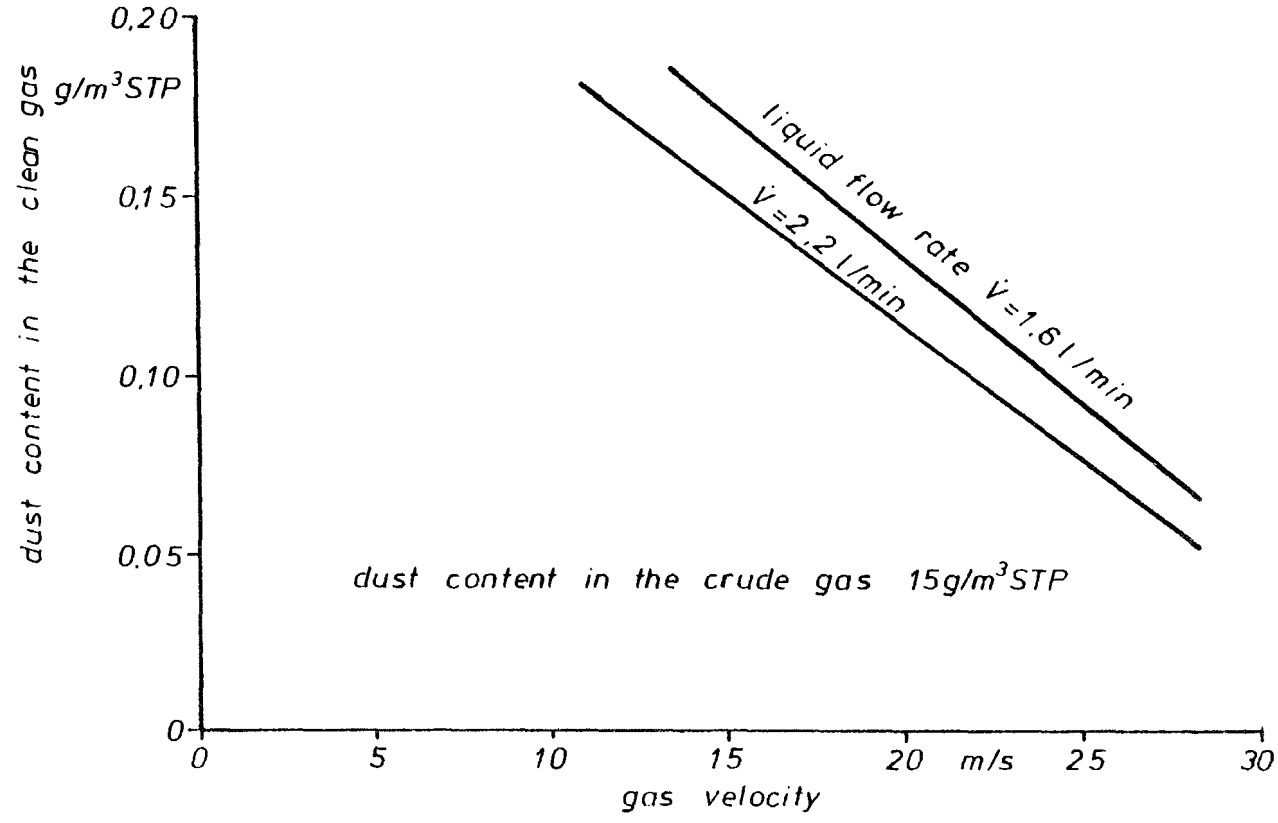

Mechanische Verfahrenstechnik Universität Essen	Clean gas dust content as a function of the gas velocity	Figure 16

PROGRESS ON ELECTROSTATIC PRECIPITATORS FOR USE AT HIGH TEMPERATURE AND HIGH PRESSURE

by

George Rinard, Donald Rugg
Robert Gyepes and James Armstrong
Denver Research Institute
Denver, Colorado 80208

ABSTRACT

Devices for hot gas cleaning are important to such processes as pressurized fluidized bed combustion and coal gasification. Some work has been done on the use of electrostatic precipitators (ESP's) for this application with promising results. However, there are many questions to be answered to determine if this technology is feasible. A review of past work at temperatures up to 1000°C (1832°F) and pressures up to 1 MPa (10 Atmospheres) is presented. The laboratory model high temperature, high pressure (HTHP) ESP presently under construction is also described.

PROGRESS ON ELECTROSTATIC PRECIPITATORS FOR USE AT HIGH TEMPERATURE AND HIGH PRESSURE

INTRODUCTION

The electrostatic precipitator (ESP) is one candidate apparatus for use as the tertiary collector in a pressurized-fluidized bed combustion (PFBC), combined cycle power plant. This application would require operation of the ESP at temperatures on the order to 1000°C and pressures of 1 MPa. EPS's in this range of temperature and pressure may also find application in coal gasification and MHD power generation. While some work has been done on ESP's operating under these conditions, the feasibility of commercial application of ESP's for use with PFBC is yet to be demonstrated.

Presently work is being conducted to determine the feasibility of ESP operation under these extreme conditions. The project is to design and build a high temperature pressure vessel and test ESP operations under flow conditions. Many of the technical problems to be overcome are in the materials that can be used for extended periods of time at the high temperature involved. Under the present schedule initial testing will start in December 1979.

BACKGROUND

All work to date on EPS's at high temperature and pressure, has been done utilizing cylindrical electrode geometry. Some of the earlier work on high temperature, high pressure (HTHP)-ESP's was done at General Electric (Koller and Fremont, 1950). In this work the negative corona characteristics of air and methyl chloride were determined over a temperature range of 20 to 500°C and pressures from 100 to 500 kPa. This work concluded that for a range of current densities of 68 to 680 nanoamperes/cm^2 the temperature and pressure has no effect on the corona discharge other than their effect on the density of the gas. Thus, the characteristics were uniquely determined by the relative density of the gas between the electrodes.

Several years later corona characteristics were measured at Princeton for both positive and negative corona for air and nitrogen at temperatures from 65 to 825°C and with pressures from 10 to 800 kPa (Thomas and Wong, 1958). At this time it was reported that positive corona characteristics were a function of gas density only. However negative corona characteristics were found to depend on the gas temperatures as well as gas density. In addition, pressure dependent instabilities were observed at high temperature for both polarities.

Shale's work (Shale et al., 1963) at the Bureau of Mines in 1963 also showed that negative corona depended on gas temperature as well as gas density. This work was done in a 5 cm diameter cylindrical type ESP for temperatures of 315°C to 815°C and pressure of 100 to 640 kPa, using negative discharge corona. The results indicate stable precipitator operation for the full range of

---

This work was supported under Grant R8059390-10 through the EPA Industrial Environmental Research Laboratory, Research Triangle Park, North Carolina.

pressure and temperatures up to 730°C. Above 730°C, operation was limited to pressures above atmospheric, because sparking occurred before corona could be generated at lower pressures. The length of the corona wire was 107 cm, the 5 cm diameter pipe section was 61 cm long. The current densities were in the range of approximately 3-5 microamps/cm^2. This is considerably higher than that normally encountered in low-temperature, atmospheric-pressure ESP's. An effective ion mobility was calculated from the experimental data and, with all else constant, was found to decrease with gas density, to increase with temperature, and to increase with field strength. The higher effective mobility, at higher temperatures and field strengths, was attributed to large components of electron current since the mobility of ions changes very little with these parameters.

At high temperatures Cooperman predicts high thermal ionization rates (Cooperman, 1964). Trace quantities of alkali metals could seriously affect ESP operation at temperatures above 800°C. However, Shale's conclusion concerning thermal ionization is that this should not be a problem over the range of temperatures and pressures considered.

A year later Shale repeated his earlier experiments (Shale et al., 1964), using positive discharge corona. The same procedure that was used for negative corona was used with the polarity reversed. This work showed essentially the same corona-start voltage for positive or negative corona, except that above 650°C, the negative corona-start voltage was considerably lower than that for positive corona. Sparkover voltage was considerably higher for negative corona below 200°C, at which temperature it was equal to that for positive corona. Above 200°C, sparkover voltage for negative corona was lower than that for positive corona, becoming about equal to the corona onset voltage at 800°C. The positive corona sparkover voltage, however, remained high at higher temperatures. From this result, Shale predicted that positive corona would be more efficient at high temperatures. He calculated that at 650°C a positive-corona ESP would have to be four times as large as a negative-corona ESP to achieve the same collection efficiency.

In 1969 Shale reported on a multitube, high-temperature, high-pressure ESP operating at 800°C and 640 kPa (Shale and Fasching, 1969). The equipment utilized a modified atmospheric gas-air combustor. The ESP, which was designed and constructed under contract with Research Cottrell was 1.5 m in diameter and 9.1 m high. There were 16 tube-type, collecting electrodes each 15.2 cm in inside diameter and 1.8 m long. Its SCA was 19.7 $m^2/(m^3/sec)$, with all tubes parallel with the gas flow. The power supply was 45 kv unfiltered dc (70 kv peak) at 250 ma. This supply would allow about one microamp/cm^2, which is lower than used in his earlier experiments but still high compared to atmospheric ESP's.

Shale found that he obtained higher collection efficiencies using negative corona. He obtained much higher currents with negative corona and operation was spark-limited. On the other hand positive current amplitudes were about 20% of those obtained with negative corona even though the voltage was considerably higher. He did not get sparking at the maximum positive voltages, which would indicate the maximum voltage was still too low. With the equipment available he was not able to operate in the high voltage positive corona

range where he predicted that collection efficiencies would be higher. The apparent reason for this is that he increased the size of the tubes from 5.1 to 15.2 cm but did not increase the power supply voltage sufficiently to be able to operate in the range where higher efficiency was expected for positive corona. The average measured efficiencies were 75 to 77 percent for positive corona and 91-96 percent for negative corona.

In 1971 a larger scale HTHP ESP was tested (Brown and Walker, 1971) by Brown at Research Cottrell; the temperature was as high as 940°C at pressures up to 1.05 MPa. The ESP was an 20.3 cm diameter, 4.6 m long pipe. The corona V-I characteristics and collection efficiencies agreed well with those obtained by Shale. Negative corona currents were much higher for a given voltage than positive corona currents, and negative corona collection efficiencies were much higher. Collection efficiencies for negative corona were as high as 91%, the SCA was about 37.4 $m^2/(m^3/sec)$.

Recent work on HTHP ESP's was also done at Research Cottrell by Feldman (1975, 1977). This work presents clean plate V-I corona curves for both polarities at temperatures up to 1093°C and pressures up to 3.5 MPa. The collector electrode was a 7.6 cm diameter tube. In this work negative corona appeared to provide higher sparkover voltages than positive corona; even in the range of temperature and pressure used by Shale and Brown.

A recent review of HTHP-ESP work in the Soviet Union is given by Val'dberg et al. (1977). This work covers the temperature range to 400°C and pressures of 100 to 600 KPa. The ESP's used were cylindrical and point-plane types. The cylindrical type used tubes 6.4, 9.9, and 14 cm in diameter and 49.8 cm long. The corona electrode was a strip-needle configuration, unlike the smooth round wire or twisted wires utilized by U.S. investigators. Their conclusions indicate once again that negative corona provides more efficient collection than positive corona. Another cylindrical ESP with a 15.2 cm diameter tube, 2.4 m long was tested on a blast furnace exhaust at 99.8% efficiency. The SCA was 19.7 $m^2/(m^3/sec)$. This ESP operated at a temperature of 250°C and a pressure of 300 KPa. The corona wire was operated at a negative voltage of 85 to 90 kv.

An HTHP-ESP experiment is being conducted in Essen, Germany (Weber, 1977). The apparatus consists of a recirculating pressure chamber, with provision for dust entrainment; it too is a cylindrical design.

The importance of hot gas cleaning is summarized in a recent EPA report (Parker et al., 1977). The importance of fluidized bed technology and hot gas cleaning to the power industry is summarized in the FBC workshop proceedings (ERDA, 1977). A theoretical review of important parameters relating to dust collection at HTHP is given in another report (Calvert et al., 1977). This report emphasizes that the behavior of these parameters in the range of temperature and pressure are only partially understood.

A review of HTHP-ESP work is given by Robinson (1971) who indicates that as pressure is increased a critical pressure may be reached where the sparkover voltage is lower than the corona onset voltage. The critical pressure is a function of corona electrode size and relative gas density. A range of operation suitable for PFBC-ESP's is given.

The results of this past work indicates stable operating regions for HTHP ESP's suitable for use with PFBC. There appears to be agreement that ESP's can be operated effectively at HTHP. The high temperature has a degrading effect on performance, but these effects are countered by increased pressure. If the corona characteristics are very nearly depending on density only, then at the pressures and temperatures under consideration one could expect two to three times the operating voltage that is normally found in a typical cold-side precipitator. There are questions as to how the gas density will affect its viscosity and, in turn, particle migration velocity. It is not clear what SCA's will be needed or how the sections should be subdivided mechanically and electrically. There is concern about ash resistivity and consistency at high temperature. There are uncertainties about thermal ionization particularly of those trace compounds with low ionization potentials that may occur in stack gas. The object of the present project is to test HTHP-ESP performance in the laboratory, using re-entrained fly ash, and to determine answers to these questions.

LABORATORY MODEL HTHP-ESP

A laboratory model HTHP-ESP system is presently being designed and is shown pictorially in Figure 1. The air compressor will supply 27.2 kg-mol/hr. at 1 MPa to the burner package. The burner is a specially designed high pressure unit capable of burning either methanol or No. 2 fuel oil. The burner has a maximum heating capacity of 244 J/s and a maximum turndown ratio of 4:1. Gases at temperatures up to 1000°C leaving the ESP will be cooled to 260°C before the outlet sampling port. Cooling will be accomplished by means of an air cooled jacket and cooling fins.

The planned pressure vessel is shown in Figure 2. It has a cool outside pressure shell. The hot gases enter near the bottom and exit near the top of this shell. The inside of the shell is lined with castable refractory. The chamber will be capable of accomodating collecting tubes up to 30 cm in diameter. The collecting tube will be supported by three rapping rods which will extend through the top of the pressure vessel.

The corona wire will be supported by means of an air cooled, one piece, high density alumina feedthrough. Cooling will be provided by means of cooling fins on the inside of the pressure shell and a water jacket outside. Radiation shields on the corona wire will help prevent radiant heat from reaching the high voltage feedthrough. The maximum design temperature for the high voltage feedthrough is 260°C.

The shell and flanges will be fabricated from carbon steel. The shell will be rolled from plate stock, and flanges will be butt welded ASA type. Sufficient insulation will be provided to maintain a maximum temperature of 110°C on all carbon shell components and welds. The collector tube will be 18 BWG (1.25 mm) type 310 stainless steel or equivalent. The corona wire will be Hastalloy X, and the radiation shields will be type 310 stainless steel. Other materials considered were Inconel, Tungsten and Incoloy. Inconel and Incoloy alloys do not have the creep strength required at 980°C and Tungsten oxidizes at temperatures above 425°C. The cooling section of the outlet will be type 316 stainless steel or Hastalloy X.

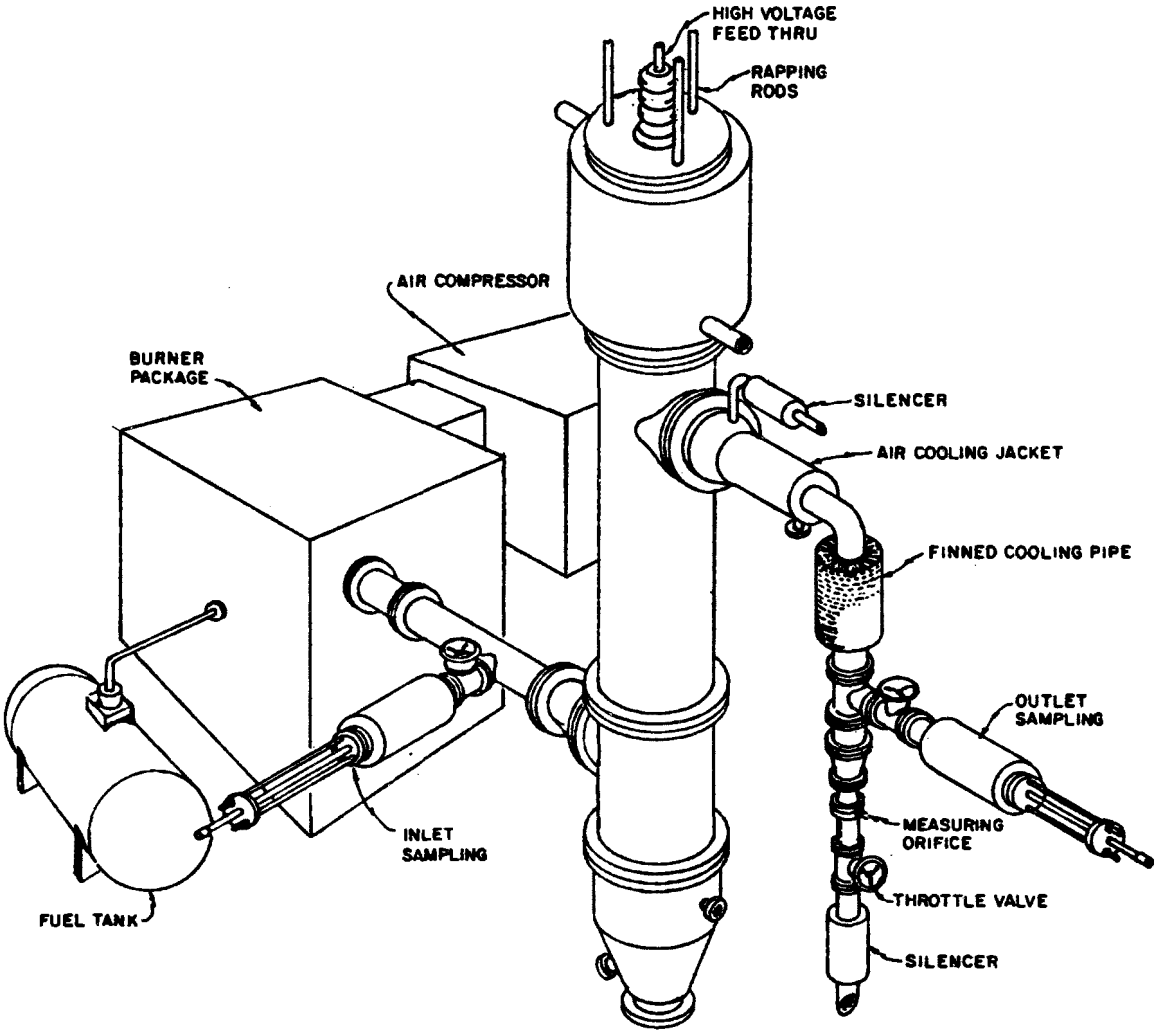

Figure 1. HTHP-ESP SYSTEM

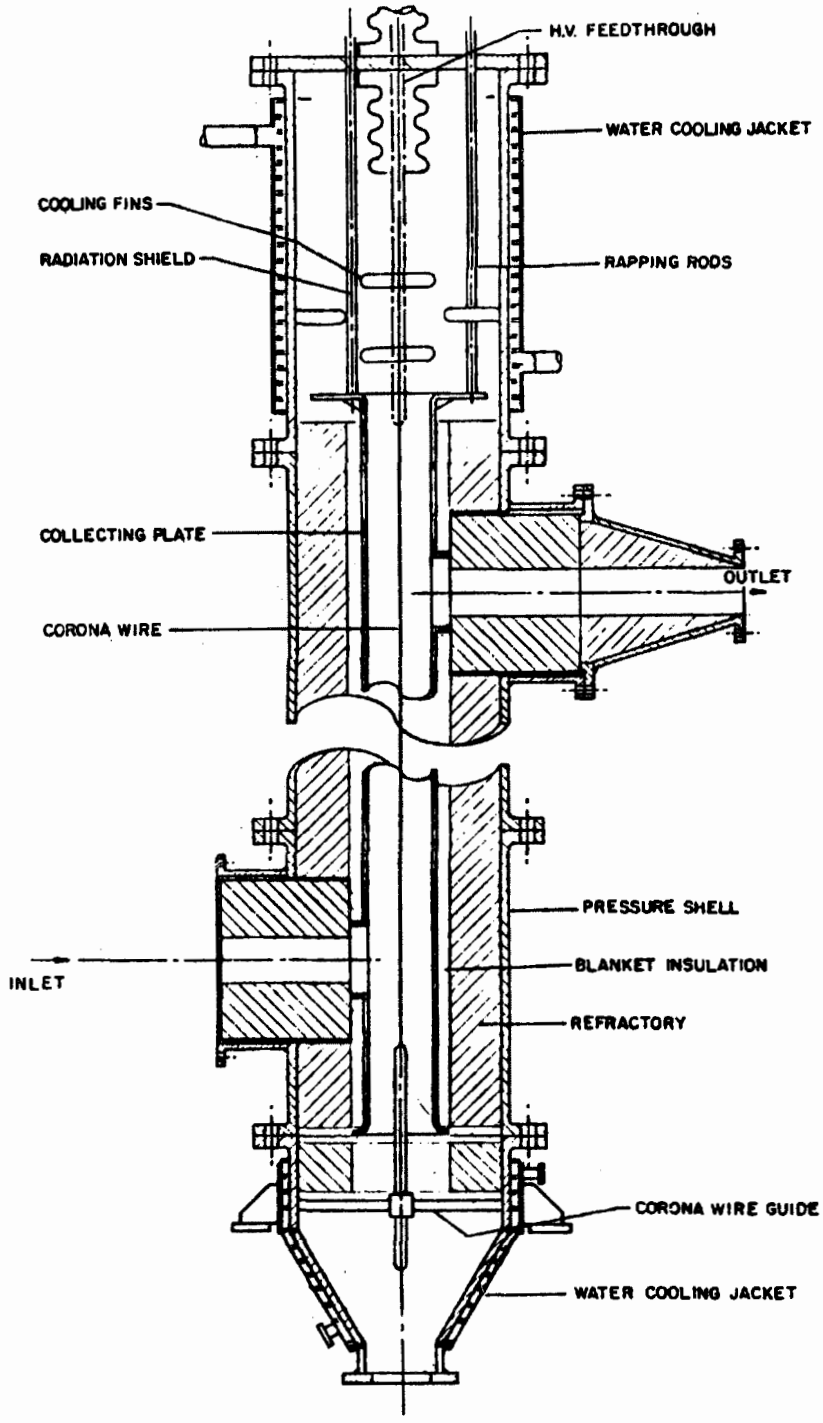

Figure 2. HTHP-ESP VESSEL

A cooling water system will be provided to cool the top and bottom of the precipitator vessel to a temperature level where the high voltage feedthrough can operate at a maximum temperature of 260°C. The system will consist of a cooling water jacket around the top of the vessel, a circulation pump, an air cooled heat exchanger and necessary piping and controls.

Laboratory tests were conducted to simulate the air flow and electrical conditions of the HTHP-ESP. For air flow modeling the following assumptions were made: the mean gas velocity through the ESP is 1 m/sec; the collector tube diameter is 29.2 cm and the gas pressure is 1 MPa. The Reynolds number was calculated to be,

$$Re = 1.4 \times 10^4.$$

To obtain the same Reynolds number for the half scale model at an ambient temperature of 21°C at Denver's altitude of 1.6 km required an average velocity of

$$\bar{v}_{scale} = 1.8 \text{ m/sec.}$$

Air velocity traverses were made at thirteen points along the length of the model including the hopper and high voltage feedthrough area. The velocity distribution had a normalized standard deviation of less than 10% in the collector tube three tube diameters from the inlet to one tube diameter before the outlet.

Smoke tests in the model indicated that essentially stagnant conditions existed in the hopper and high voltage feedthrough areas.

The results of the air flow modeling indicates that good quality air flow should exist in the HTHP-ESP.

The electrical modeling was done in a 23 cm diameter tube to determine if a lower corona wire guide would be required and to examine potential sparking problems at the inlet and outlet ports. The tests were performed at ambient conditions and the results extrapolated to indicate what could be expected at the relative gas densities of the HTHP-ESP.

The results of these tests indicate that a lower corona guide will be required to prevent pendulum action of the corona wire. To insure good electrical insulation of the guide, the hopper area, where the guide is located, will be water cooled.

The tests also show that sparking should not occur, with clean conditions below 200 kv. For a corona wire diameter of 0.635 cm the calculated negative corona onset voltage is 130 kv. It is expected to be possible to obtain corona current densities as high as 1 $\mu a/cm^2$.

While the electrical tests at ambient conditions should not be used to predict actual performance of the HTHP-ESP, they were done to help indicate practical parameters for the working unit.

REFERENCES

1. Koller, L.R., and H.A. Fremont. "Negative Wire Corona at High Temperature and Pressure." Journal of Applied Physics, 21:741-4, August 1950.

2. Thomas, J.B. and E. Wong. "Experimental Study of dc Corona at High Temperatures and Pressures." Journal of Applied Physics, 29:1226-30, August 1958.

3. Shale, C.C., W.S. Bowie, and J.H. Holden. "Feasibility of Electrical Precipitation at High Temperatures and Pressures." Bureau of Mines Report of Investigations RI 6325, 1963.

4. Cooperman, P. Commun. Electron., 75, 792, 1964.

5. Shale, C.C., W.S. Bowie, J.H. Holden, and G.R. Strimbeck. "Characteristics of Positive Corona for Electrical Precipitation at High Temperatures and Pressures." Bureau of Mines Report of Investigations RI 6397, 1964.

6. Shale, C.C, and G.E. Fasching. "Operating Characteristics of a High-Temperature Electrostatic Precipitator." Bureau of Mines Report of Investigations RI 7276, 1969.

7. Brown, R.F. and A.B. Walker. "Feasibility Demonstration of Electrostatic Precipitation at 1700°F." Journal of the Air Pollution Control Association, 21:617-20, October 1971.

8. Feldman, P.L. "Development of a High Temperature Electrostatic Precipitator." Progress Report of Cottrell Environmental Sciences to EPA Research Triangle Park, June 1975.

9. Feldman, P.L. "High Temperature, High Pressure Electrostatic Precipitator." EPA/ERDA Symposium on High Temperature/Pressure Particulate Control, Washington Hilton Hotel, Washington, DC, September 20-21, 1977.

10. Val'dberg, A.Y., V.V. Danilin, A.G. Lyapin, and V.M. Tkachenko. "Electrical Gas Cleaning at Higher Pressures." Second U.S./U.S.S.R. Symposium on Particulate Control, Environmental Protection Agency, Research Triangle Park, NC, September 26-29, 1977.

11. Weber, I.E. "Problems for Gas Purification Occurring in the Use of New Technologies for Power Generation." EPA/ERDA Symposium on High Temperature/Pressure Particulate Control, Washington Hilton Hotel, Washington, DC, September 20-21, 1977.

12. Parker, R., S. Calvert and D.C. Drehmel. "High Temperature and High Pressure Particulate Control Requirements." EPA-600/7-77-071, July 1977.

13. "Proceedings on the Fluidized Bed Combustion Technology Exchange Workshop, Vol. 1 and 2." Sponsored by ERDA and EPRI CONF-770447-P-1, April 13-15, 1977.

14. Calvert, S., R. Parker, and D.C. Drehmel. "Effects of Temperature and Pressure on Particle Collection Mechanisms: Theoretical Review." EPA-600/7-77-002, January 1977.

15. Robinson, M., "Air Pollution Control Part I." Edited by Werner Strauss, John Wiley, New York, 1971, pp. 283-298.

REDUCTION OF PARTICULATE CARRYOVER FROM A PRESSURIZED FLUIDIZED BED

By:

R. W. Patch
National Aeronautics and Space Administration
Lewis Research Center
Cleveland, Ohio 44135

ABSTRACT

A bench-scale fluidized-bed combustor was constructed with a conical shape so that the enlarged upper part of the combustor would also serve as a granular bed filter. The combustor was fed coal and limestone. Ninety-nine tests of about four hours each were conducted over a range of conditions. Coal-to-air ratio varied from 0.033 to 0.098 (all lean). Limestone-to-coal ratio varied from 0.06 to 0.36. Bed depth varied from 3.66 to 8.07 feet. Temperature varied from 1447 to 1905 F. Pressure varied from 40 to 82 psia. Heat transfer area had the range zero to 2.72 ft^2. Two cone angles were used. The average particulate carry-over of 2.5 grains/SCF was appreciably less than cylindrical fluidized-bed combustors. The carry-over was correlated by multiple regression analysis to yield the dependence on bed depth and hence the collection efficiency, which was 20%. A comparison with a model indicated that the exhaust port may be below the transport disengaging height for most of the tests, indicating that further reduction in carry-over and increase in collection efficiency could be affected by increasing the freeboard and height of the exhaust port above the bed.

REDUCTION OF PARTICULATE CARRYOVER FROM A PRESSURIZED FLUIDIZED BED

INTRODUCTION

The pressurized fluidized-bed combustor (PFBC) is being investigated by the Department of Energy, the utility industry, and several laboratories with the ultimate purpose of achieving clean coal combustion in high-efficiency central-station power plants. Not only must the flue gas meet EPA New Source Performance Standards for particulate and other emissions, but the power plant cycles require gas turbines to recover energy from the hot, pressurized flue gas, and these turbines will not tolerate large quantities of particulates in the gas driving the turbine. Also, the carry-over of unburned carbon must be reduced or recycled to achieve acceptable combustion efficiency. The state of the art at present in research PFBC's is to provide one to three stages of high-temperature cyclones and perhaps an additional clean-up device downstream. The solids from the high-temperature cyclones usually are recycled to the bed or go to a carbon burn-up cell to improve the combustion efficiency of the system. Unfortunately, the high-temperature cyclones frequently are not very reliable due to erosion and seal problems, as mentioned by Rollbuhler (1979)[1].

The primary purpose of the present program at Lewis is to test turbine blade materials in PFBC flue gas. It was also hoped that by making the combustor conical in shape so that the gas velocity at the top of the bed was greatly reduced, the particulate carry-over (solids loading) could be significantly reduced. Hence, the number of high temperature cyclones and carbon burn-up cells in a larger scale combustor could be reduced and the erosion of any remaining cyclones minimized. This appeared feasible because most of the combustion occurs near the bottom of a PFBC as evidenced by the axial temperature profile, and the top is mostly used for SO_2 adsorption, NO_x reduction, and possibly heat transfer tubes. Hence, the top, if enlarged, can serve as an in-bed granular filter for particulates. This paper is a report on this phase of the project and describes the first conical PFBC built anywhere.

APPARATUS

The Lewis PFBC is shown schematically in Figure 1 and has a conical shape to reduce the gas velocity at the top of the bed. The combustor has a carbon steel exterior lined with Kaowool insulation which, in turn, is lined with cast ceramic insulation.

The combustor is fed a mixture of coal and limestone (fuel). The coal and limestone storage hoppers feed metering screws which feed a blending auger. The blended fuel mixture flows from the blending auger to a fuel holding hopper at atmospheric pressure. The fuel holding hopper is used to pressurize the fuel up to bed pressure. The fuel is intermittently dumped at pressure into the pressurized fuel feed hopper. The fuel feed hopper feeds the bed continuously with the help of the fuel metering screw and a small supply of high pressure air as a transport medium.

The main air supply for the bed was dry air at ambient temperature monitored by a venturi flowmeter. It flowed into the bottom of the combustor through a distributor containing nine bubble caps, each with four 1/8 inch diameter holes.

The bed consisted mostly of limestone products and ash. The bed height was controlled by a discharge solids removal auger, which could be located at one of six ports at different heights. The removal auger was rotated continuously so that the bed level never exceeded its height.

Two geometries were used for the bed (Figure 2). For tests 1 to 29 the bed had a 3.40^{o} half angle, and the gas temperatures at the exhaust port were much lower than the bed temperatures. For tests 30 to 99 the upper side and top insulation were increased to minimize this heat loss. This reduced the bed half angle to 2.51^{o}.

To determine the amount of particulates in the flue gas, about one-fourth of the flow was bypassed through cyclone separator number 6 and a stainless steel mesh filter with a 0.5 micron nominal rating and then through a venturi flowmeter before venting to the atmosphere.

Additional details of the system and its instrumentation are given by Kobak (1979)[2]. The scale and general arrangement of the PFBC system can be seen from Figure 3.

EXPERIMENTAL PROCEDURE

A high-volatile coking bituminous coal from the Pittsburgh #8 seam was used in the tests described here. Typical ultimate and proximate analyses are given in Table 1. The coal was pulverized, and the -7 mesh fraction used without drying. It had an approximately 800 micron median diameter (50th weight percentile).

The limestone was from Grove City, Virginia, and had a size of -7 +18 mesh, yielding an approximately 1600 micron median diameter. The size distribution is given in Figure 4 and composition in Table 2. It was used without drying.

The bed initially consisted of the mixture of limestone products and ash left over from the bed of previous tests. This reduced the time required for the bed to reach chemical equilibrium during a test.

Each test was about four hours duration. Starting and operating procedures are given by Kobak (1979)[2]. During the last two hours the particulate loading of the exhaust gas was measured by means of separator number 6, the mesh filter, and the venturi flowmeter (Figure 1). The particulates from separator number 6 and the mesh filter were collected and weighed.

RESULTS AND DISCUSSION

The following sections give the test conditions, size distributions of particles, compositions of effluents, multiple regression analyses for

solids loading, filter efficiency, comparisons and explanation of solids loading, and bed pressure drop.

Test Conditions, Size Distributions and Compositions of Effluents

Ninety-nine tests were run. The first 29 had a cone half angle, a (symbols are given in Appendix A), of 3.4°; whereas, the last seventy had a cone half angle of 2.5° (see Figure 2). There were six other degrees of freedom in the experiment. Consequently, six other independent variables besides a were needed to specify a test condition. There are various possible ways of choosing these six. For this paper, the other six were coal-to-air ratio c, limestone-to-coal ratio L, bed depth D, heat exchanger area S, bed pressure p, and gas velocity at the bottom of the bed V_b. These seven independent variables are enough to determine the bed temperature T, the gas velocity at the top of the bed V_t, the coal feed rate w_c, the excess air ratio E, and the calcium-to-sulfur molar ratio C_s, so that the last five are not independent. The ranges and averages of the independent variables and of T, V_t, w_c, E, and C_s are given in Table 3.

The solids loadings of the flue gas exiting the top of the combustor can be expressed in units of grains per standard cubic foot of gas (S_t) or in units of pounds per million British thermal units from the coal (S_b). The ranges and averages of these quantities are also given in Table 3. The current New Source Performance Standard (NSPS) promulgated by EPA for large electric-utility boilers is given in Table 4. It can be seen that hot-gas clean-up would be needed to meet the NSPS, not to mention the requirements if a gas turbine were located downstream to recover energy from the pressurized flue gas.

An examination of the size distributions of the solids to and from the bed (Figure 4) gives an idea of what is taking place and the degree of attrition in the bed. The solids fed the bed are limestone and coal, but most of the coal burns away leaving coal ash. The particle size of the raw limestone is largest and narrowly distributed. Two curves are given for the coal ash. The right-hand curve is the distribution that would result if each coal particle contained one ash particle of the same weight fraction as the average for the coal. The left-hand curve was measured by dry and wet seiving coal ash produced by burning the coal at 1700 F for one hour in a laboratory furnace with adequate ventilation in a manner similar to Merrick and Highley (1974)[3]. The source of the solids removed from the bed was determined by using silicon as a tracer for coal ash and calcium as a tracer for limestone and is given in Figure 5 (only the average is shown for the minor constituents). The bed discharge was mostly limestone whereas the fly ash was mostly coal ash and char. Going back to Figure 4, it can be seen that there is appreciable attrition in the bed of limestone and perhaps coal ash.

Figure 6 shows the cumulative loading of the flue gas at the exit from the combustor in grains per standard cubic foot. The ordinate gives the loading by all particles up to the particle size given on the abscissa.

Loading and Filter Efficiency From Multiple Regression Analysis

The data from the 99 tests exhibited considerable scatter, and for the most part were not taken with the object of determining solids loading as a function of c, L, D, S, a, p, and V_b, but rather primarily with the object of determining gaseous emissions and combustion efficiency as functions of other sets of seven independent variables. To obtain maximum utilization of the data and confidence in the results, it was, therefore, necessary to use multiple regression analysis to correlate S_t and S_b with c, L, D, S, a, p, and V_b. This gave

$$S_t = 1.014 - 20.44L - 0.1140D + 0.5606S + 0.5498V_b + 73.89L^2 \quad (1)$$

$$S_b = 4.278 - 40.47L - 0.2316D + 1.243V_b + 146.3L^2 \quad (2)$$

The observed total solids loadings S_t and S_b are plotted versus equations (1) and (2), respectively, in Figures 7 and 8. Here the diagonal lines are the loci of perfect agreement.

If the reader wishes to use equations (1) and (2) where not all the independent variables L, D, S, and V_b are known, or if comparisons are to be made with a combustor of a different size so its value of S is not pertinent, the following relations from multiple regression analyses may be useful for estimating S and w_c for the conical PFBC:

$$S = 7.855 + 75.78c + 0.6197L + 0.125D - 0.008913T - 0.8183a + 0.04839p + 0.5312V_b \quad (3)$$

$$w_c = -49.57 + 241.2c + 5.019L + 0.08918D + 5.027S + 0.06709a + 0.4487p + 6.712V_b \quad (4)$$

It may be desirable to convert from coal-to-air ratio c to excess air ratio E. The stoichiometric value of c is 0.1004 for the coal used so

$$E = (0.1004/c) - 1 \quad (5)$$

It may also be required to convert limestone-to-coal ratio L to calcium-to-sulfur molar ratio C_s, which can be accomplished for the coal and limestone used by means of

$$C_s = 15.58L \quad (6)$$

By making use of equations (1) and (3) it is possible to predict conical PFBC solids loadings for test conditions of cylindrical PFBC's at other laboratories. In doing this the excess air ratio, bed depth, bed temperature, bed pressure, and gas velocity at the bottom of the bed were assumed to be the same for conical and cylindrical PFBC's. The average cone half angle of 2.77^o for the 99 tests was used for the conical PFBC. A comparison with the Leatherhead (1974)[4] PFBC is given in Table 5. The conical PFBC would have had 40 percent less solids loading. A comparison with the Argonne PFBC (using data from Montagna (1978)[5] and Swift (1979)[6]) is given in Table 6. The conical PFBC would have had 31 percent less solids loading.

Equation (1) may be used to produce a graph of solids loading and fractional collection efficiency of the top part of the fluidized bed considered as a filter. To do this, the average values of L, S, and V_b were assumed. The solids loading is shown in Figure 9 and decreases linearly with bed depth. If the lower 3.657 feet of the bed is regarded as the combustor and the part of the bed above 3.657 feet is regarded as the in-bed filter, the fractional collection efficiency η of the in-bed filter is readily calculated from

$$\eta(D) = 1 - S_t(D)/S_t(3.657) \qquad (7)$$

and is also shown in Figure 9. The maximum collection efficiency was 20 percent.

Explanation for Solids Loadings and In-Bed Collection Efficiency

A theoretical investigation comprising two phases was undertaken to attempt to explain the low filter efficiency of the in-bed filter. The first phase was based on a theoretical model and computer programs by Horio, et al (1977)[7] as modified by Patch (1979)[8].

The model is summarized briefly below:

It is assumed that "fast" bubbles are present (rising velocity of bubble greater than gas velocity in emulsion). Hence, the bubbles have clouds. The bubble size is given by the correlation of Mori and Wen (1975)[9] modified for a combustor of varying cross-sectional area. Char and limestone are assumed to be completely mixed. Plug flow of gas is assumed.

A spherical particle model is employed for coal combustion. Only the lean case is treated. The hydrogen and oxygen volatize immediately upon injection of coal into the combustor, not changing the diameter of the resultant char. The diameter is gradually reduced by burning with oxygen, with the rate determined by the surface rate of chemical reaction and gas diffusion. Ash particles break off as the char burns. Carbon, nitrogen, and sulfur in the char are assumed to be released or used at the same rate as the char burns.

Elutriation of char, ash, and limestone are treated differently. For char it is assumed that the combustor exhaust gas port is above the transport disengaging height, and one of three empirical correlations (Zenz and Weil (1958)[10], Kunii and Levenspiel (1969)[11], Wen and Hashinger (1960)[12]) may be selected for the elutriation rate. The fraction of ash elutriated is not calculated so it must be given as an input. The limestone is assumed not to elutriate.

For comparison between the model and experiment, five steady-state tests (no. 100-104) with a total duration of 20 hours and 7 minutes were run under the same conditions with a bed depth D of 4.657 ft., and results were averaged. Since the model calculates the burnable carbon entrained but not ash or limestone entrained, comparison was based on burnable

carbon entrained and is shown in Figure 10 for the three empirical elutriation correlations. Clearly the Horio et al model using the Zenz and Weil correlation agreed closest with experiment, but it predicted burnable carbon entrained more than an order of magnitude too low. In addition, the predicted diameter of the entrained burnable carbon was about a factor of three too high no matter which elutriation correlation was used (Figure 11).

To attempt to elucidate the discrepancies, comparisons were made between the model and tests 1 to 29 and are shown in Figure 12. Here it is significant that the calculated burnable carbon entrained fell off more rapidly with increasing bed depth than observed. Since increasing bed depth decreases freeboard (and exhaust port) height (see Figure 12) this divergence of trends would be explained if the combustor exit port were below the transport disengaging height so that bed material was being splashed into the exit port by bursting bubbles.

The second phase of the investigation was a comparison of empirical transport disengaging heights with the experimental freeboard and exit port heights. Unfortunately, no general empirical correlation of transport disengaging heights was available that did not require a special computer program. Three empirical correlations for cracking catalyst were available (Zenz and Weil (1958)[10], Amitin et al (1968)[13], and Fournol et al (1973)[14]) and are plotted in Figure 13 along with freeboard height. The correlations all tend to indicate the freeboard height was less than the transport disengaging height, especially for a bed depth of 8.073 ft. This condition could be further aggravated because coal ash tends to have a particle density less than cracking catalyst, so its transport disengaging height would be even higher than the correlations in Figure 13. Hence, it is believed that if the freeboard height (and combustor exhaust port height) were increased substantially, while holding bed depth constant, S_t would decrease and apparent filter efficiency would increase markedly.

Bed Pressure Drop

Bed pressure drop for tests 1-99 are shown in Figure 14. The dependence of bed pressure drop on bed depth was approximately linear as expected. When the bed depth was increased from 3.657 ft. to 8.073 ft., the pressure drop increased from about 0.6 psi to 3.2 psi, so the pressure drop attributable to the in-bed filter was about 2.6 psi.

There were three causes for the scatter in Figure 14. (1) When the limestone-to-coal ratio L was increased, the fraction of the bed which was limestone increased. The remainder of the bed was mainly ash. Since limestone is denser than ash, Δp increased. (2) When the air velocity at the bottom V_b was increased, the bubble fraction increased. Since the bubbles had very little weight, Δp decreased. (3) There was inherent experimental scatter, partly due to sampling error (only about eight readings were taken per test).

The bed pressure drop does not appear to present any significant application problem.

SUMMARY OF RESULTS

Use of a conical combustor shape to produce an in-bed filter resulted in from 31 to 40 percent less solids loading of the flue gas at the combustor exhaust port compared to cylindrical pressurized fluidized bed combustors at other laboratories. Solids loading at the exhaust port of the conical PFBC was found to increase linearly with gas velocity at the bottom of the bed and with heat transfer area, decrease linearly with bed depth, and had a parabolic dependence on limestone-to-coal ratio. This resulted in a filter efficiency of 20 percent for the deepest bed. Additional hot gas clean-up would be necessary to meet EPA New Source Performance Standards for large electric-utility boilers and for a gas turbine.

An investigation into the cause of the poor filter efficiency indicated that the combustor exhaust port was probably below the transport disengaging height. Hence, a marked improvement in filter efficiency can probably be expected if the freeboard is increased so the combustor exhaust port can be raised.

The pressure drop attributable to the in-bed filter was about 2.6 psi, which does not appear to present any significant application problem.

APPENDIX A - SYMBOLS

a	bed half angle (see Figure 2), deg.
B	fraction of burnable carbon entrained
C_s	molar ratio of calcium in limestone fed to sulfur in coal fed
c	coal-to-air ratio, as received weight basis
D	bed depth, ft
d	particle diameter, μm
E	excess air ratio
H	freeboard height, ft
L	limestone-to-coal ratio, as received weight basis
p	absolute pressure at top of combustor, psia
S	area of outside of heat exchanger and extractor tubes, ft^2
S_b	flue gas solids loading (particulate carry-over) at outlet of combustor based on higher heating value of coal, $lb/10^6$ Btu
S_t	flue gas solids loading (particulate carry-over) at outlet of combustor, wet gas basis, gr/SCF
T	bed temperature 1.22 ft above distributor, F
V_b	superficial velocity at bottom of bed, ft/sec
V_t	superficial velocity at top of bed, ft/sec
w_c	coal feed rate, as received basis, lb/hr
Δd	difference in particle diameter between two adjacent sieve sizes
Δp	bed pressure drop, psi
ΔW	weight of particles with diameters between two adjacent sieve sizes
η	fractional collection efficiency of filter

REFERENCES

1 Rollbuhler, R. J. Variable Operating Characteristics of a Conical Pressurized, Fluidized Bed Research Reactor. NASA TM report (to be published).

2 Kobak, J. A. Burn Coal Cleanly in a Fluidized Bed. Instru. and Control Systems. 52:29-32, January 1979.

3 Merrick, D., and J. Highley. Particle Size Reduction and Elutriation in a Fluidized Bed Process. AIChE Symp. Series. 70:366-378, January 1974.

4 Annonymous. Pressurized Fluidized Bed Combustion. National Research Development Corporation, (London). OCR-85-Int-1, July 1974.

5 Montagna, J. C., G. W. Smith, F. G. Teats, G. J. Vogel, and A. A. Jonke. Evaluation of On-Line Light-Scattering Opitcal Particle Analyzers for Measurements at High Temperature and Pressure. Argonne National Laboratory (Ill.). ANL/CEN/FE-77-7, 1978.

6 Swift, W. M. Personal communication. May 1979.

7 Horio, M., P. Rengarajan, R. Krishnan, and C. Y. Wen. Fluidized Bed Combustor Modeling. NASA CR-135164, 1977.

8 Patch, R. W. Preliminary Comparison of Theory and Experiment for a Conical, Pressurized Fluidized Bed Coal Combustor. NASA TM-79137, 1979.

9 Mori, S., and C. Y. Wen. Estimation of Bubble Diameter in Gaseous Fluidized Beds. Am. Inst. Chem. Eng. J. 21:109-115, January 1975.

10 Zenz, F. A., and N. A. Weil. A Theoretical-Empirical Approach to the Mechanism of Particle Entrainment from Fluidized Beds. AIChEJ 4:472-479, December 1958.

11 Kunii, D., and O. Levenspiel. Fluidization Engineering. New York, Wiley and Sons, 1969, p. 313-317 (Primary Source - S. Yagi and T. Aochi. Paper presented at the Soc. of Chem. Engrs. (Japan), Fall Meeting, 1955).

12 Wen, C. Y., and R. F. Hashinger. Elutriation of Solid Particles from a Dense-Phase Fluidized Bed. AIChE J. 6:220-226, June 1960.

13 Amitin, A. V., I. G. Martyushin, and D. A. Gurevich. Dusting in the Space Above the Bed in Converters with a Fluidized Catalyst Bed. Chem. Technol. Fuels Oils. 3:181-184, 1968.

14 Fournol, A. B., M. A. Bergougnou, and C. G. J. Baker. Solids Entrainment in a Large Gas Fluidized Bed. Can. J. Chem. Eng. 51:401-404, August 1973.

TABLE 1. ULTIMATE AND PROXIMATE ANALYSIS OF PITTSBURG #8 COAL

ULTIMATE ANALYSIS (DRY BASIS)	
CARBON	75.38%
HYDROGEN	5.14
NITROGEN	1.49
CHLORINE	0.01
SULFUR	1.99
ASH	8.38
OXYGEN	7.61
	100.00%

PROXIMATE ANALYSIS (AS RECEIVED)	
MOISTURE	2.12%
ASH	8.20
VOLATILE MATTER	37.41
FIXED CARBON	52.27
	100.00%

HIGHER HEATING VALUE
13274 BTU/LB

TABLE 2. COMPOSITION OF GROVE LIMESTONE BY WEIGHT (DRY BASIS)

LIME	53.97%
CARBON DIOXIDE	43.42
SILICA	1.17
MAGNESIA	1.16
ALUMINA	0.14
FERRIC OXIDE	0.11
SULFUR	0.08
BURNABLE CARBON	0.08
UNDETERMINED	-0.13
	100.00%

TABLE 3. RANGES AND AVERAGES OF VARIABLES IN CONICAL PRESSURIZED FLUIDIZED - BED COMBUSTOR

VARIABLE[a]	MINIMUM (AVERAGED OVER 4 HR TEST)	MAXIMUM (AVERAGED OVER 4 HR TEST)	AVERAGE OF ALL TESTS
COAL-TO-AIR RATIO, c	0.0334	0.0977	0.0616
LIMESTONE-TO-COAL RATIO, L	0.064	0.364	0.138
BED DEPTH, D, FT	3.66	8.07	5.34
HEAT TRANSFER AREA, S, FT^2	0	2.72	1.68
CONE HALF ANGLE, a, DEG.	2.51	3.40	2.77
BED PRESSURE, p, PSIA	39.7	82.2	72.5
GAS VELOCITY AT BOTTOM, V_b FT/SEC	2.20	8.58	4.39
BED TEMPERATURE, T, F.	1447	1905	1701
GAS VELOCITY AT TOP OF BED, V_t, FT/SEC	0.701	4.43	1.76
COAL FEED RATE, w_c, LB/HR	15.0	63.7	37.1
EXCESS AIR RATIO, E	0.028	2.01	0.630
CALCIUM-TO-SULFUR MOLAR RATIO, C_s	0.997	5.67	2.15
SOLIDS LOADING, S_t, GR/SCF	0.730	9.15	2.50
SOLIDS LOADING, S_b, LB/10^6 BTU	1.38	18.9	6.09
BED PRESSURE DROP, Δp, PSI	0.14	3.89	1.60

[a]SEE APPENDIX A FOR MORE COMPLETE DEFINITIONS

TABLE 4. COMPARISON OF SOLIDS LOADING AT COMBUSTOR EXIT AND NEW SOURCE PERFORMANCE STANDARDS FOR LARGE ELECTRIC UTILITY BOILERS

	SOLIDS LOADING S_b LB/10^6 BTU
MINIMUM (AVERAGED OVER 4 HR TEST)	1.38
MAXIMUM (AVERAGED OVER 4 HR TEST)	18.9
AVERAGE OF ALL TESTS	6.09
CURRENT EPA NEW SOURCE PERFORMANCE STANDARD	0.03

TABLE 5. COMPARISON OF SOLIDS LOADINGS AT COMBUSTOR EXIT WITH PFBC AT LEATHERHEAD (1974)[4] (USING EQUATIONS (1) AND (3) TO EXTRAPOLATE PFBC PERFRMANCE)

	EXPERIMENTAL QUANTITIES FOR CYLINDRICAL PFBC AT LEATHERHEAD (1974)[4]	PREDICTED QUANTITIES FOR CONICAL PFBC AT LEWIS (THIS PAPER)
EXCESS AIR RATIO, E	0.16	0.16
COAL-TO-AIR RATIO, c		0.0866
CALCIUM-TO-SULFUR MOLAR RATIO, Cs	2.03	2.03
LIMESTONE-TO-COAL RATIO, L		0.130
BED DEPTH, D, FT	4.1	4.1
BED TEMPERATURE, T, F	1740	1740
HEAT TRANSFER AREA*, S, FT^2		2.67
CONE HALF ANGLE, α, DEG.	0	2.77
BED PRESSURE, P, PSIA	87	87
GAS VELOCITY AT BOTTOM, V_b, FT/SEC	2.3	2.3
SOLIDS LOADING, S_t, GR/SCF	3.16	1.90

*FROM EQUATION (3)

TABLE 6. COMPARISON OF SOLIDS LOADINGS AT COMBUSTOR EXIT WITH PFBC AT ARGONNE (USING EQUATIONS (1) AND (3) TO EXTRAPOLATE CONICAL PFBC PERFORMANCE)

	EXPERIMENTAL QUANTITIES FOR CYLINDRICAL PFBC AT ARGONNE	PREDICTED QUANTITIES FOR CONICAL PFBC AT LEWIS (THIS PAPER)
EXCESS AIR RATIO, E	0.15	0.15
COAL-TO-AIR RATIO, c		0.0873
LIMESTONE-TO-COAL RATIO, L	0.562	0.562
BED DEPTH, D, FT	3	3
BED TEMPERATURE, T, F	1561	1561
HEAT TRANSFER AREA*, S, FT^2		2.88
CONE HALF ANGLE, α, DEG.	0	2.77
BED PRESSURE, P, PSIA	44.1	44.1
GAS VELOCITY AT BOTTOM, V_b, FT/SEC	3.28	3.28
SOLIDS LOADING, S_t, GR/SCF	23	15.9

*FROM EQUATION (3)

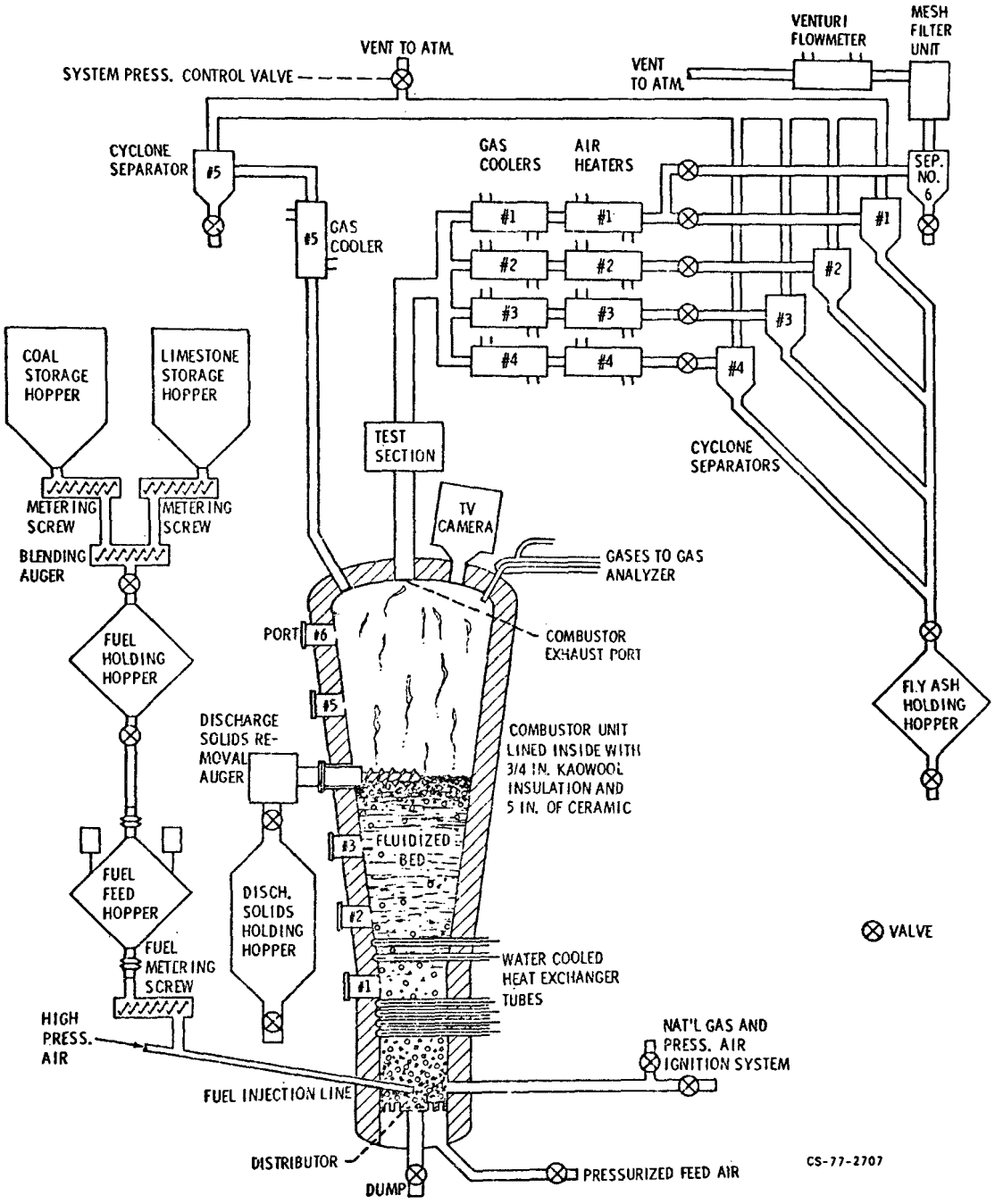

Figure 1 Schematic of LeRC pressurized fluidized bed combustor.

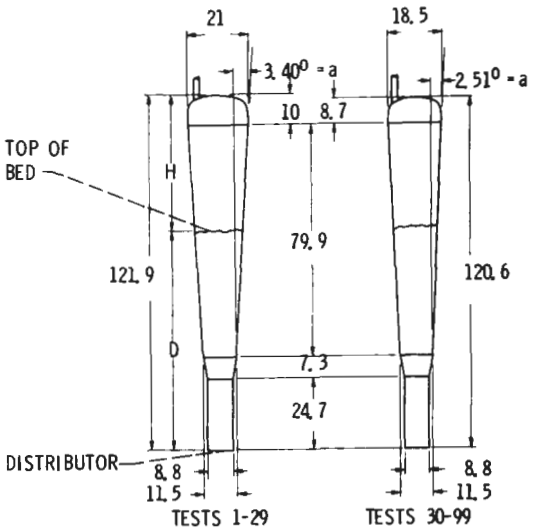

Figure 2 Two internal geometries of combustor (dimensions in inches except D and H; discharge solids removal auger and heat exchanger tubes omitted).

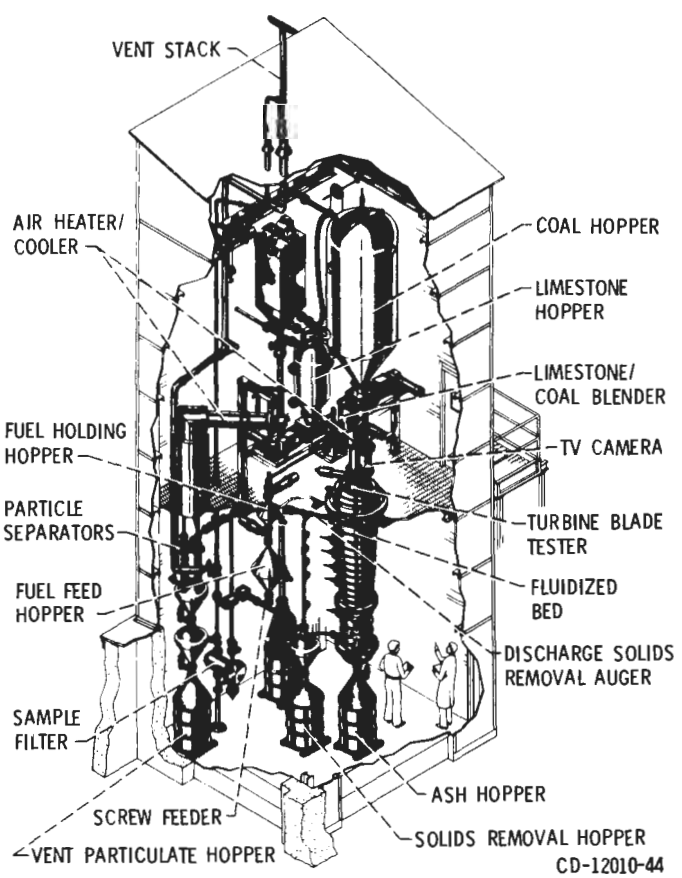

Figure 3 Artistic view of LeRC PFBC facility - combustion section.

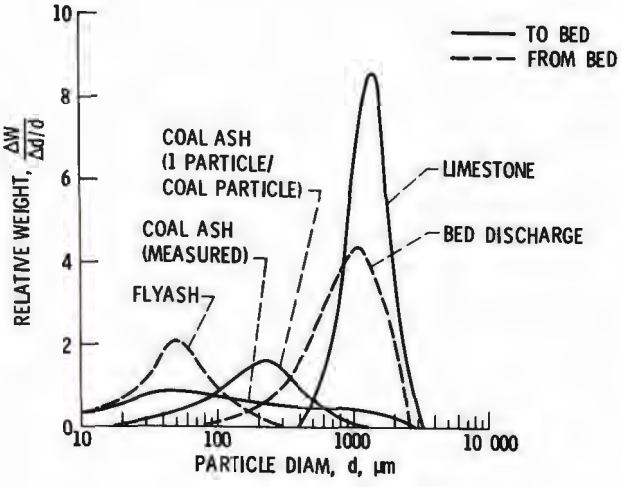

Figure 4 Solids size distributions.

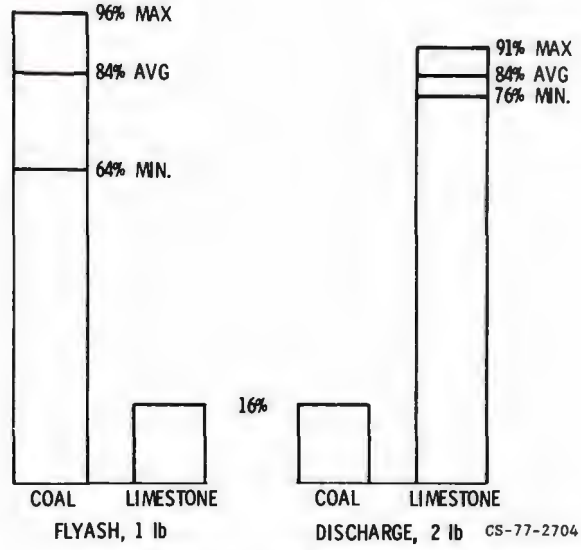

Figure 5 Source of solids removed from bed.

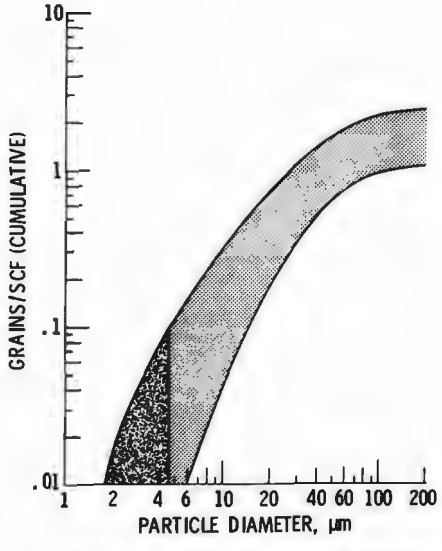

Figure 6 Particles in gases from combustor.

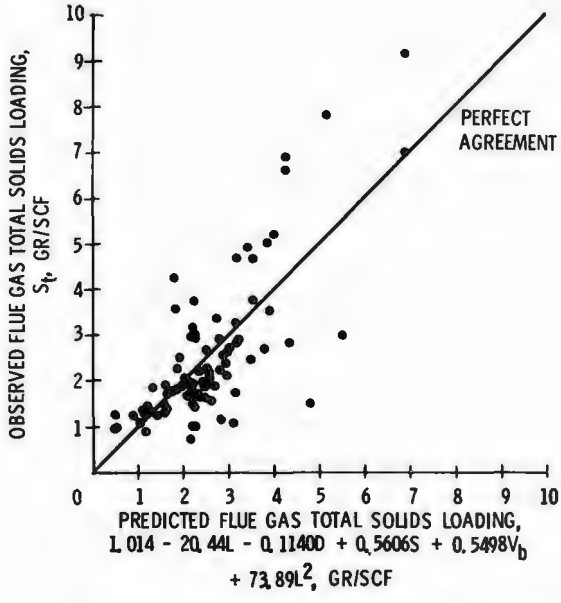

Figure 7 Comparison of observed flue gas total solids loading with predicted values.

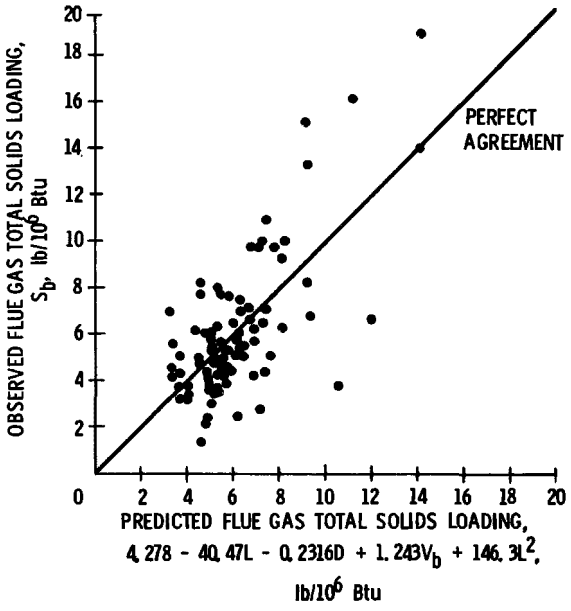

Figure 8 Comparison of observed flue gas total solids loading based on higher heating value with predicted values.

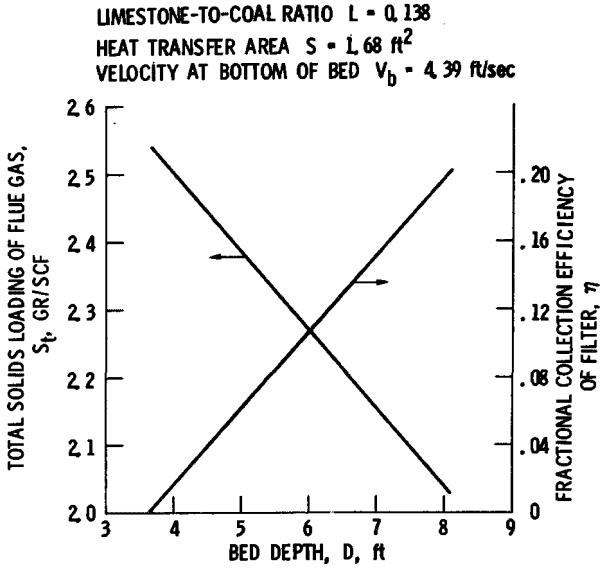

Figure 9 Total solids loading of flue gas at combustor exit and resulting filter efficiency.

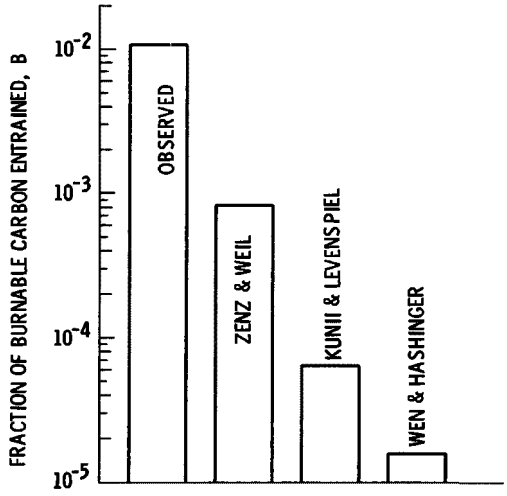

Figure 10 Comparison of burnable carbon entrained based on experiment and three elutriation correlations used in the model of Horio, et al. (1977)[7].

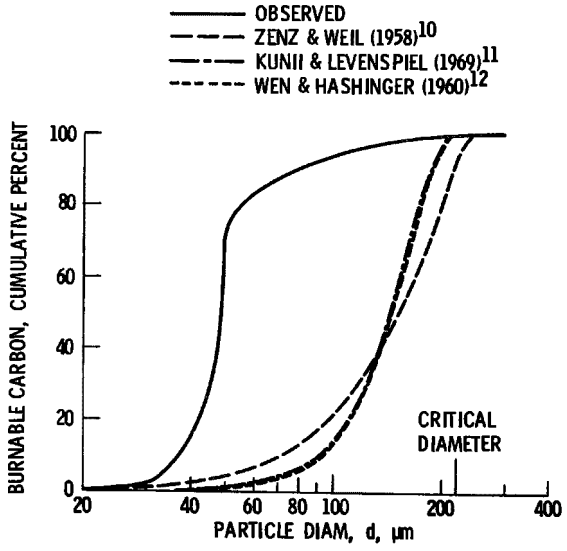

Figure 11 Comparison of calculated and observed size distribution of entrained burnable carbon. All calculations use the model of Horio, et al. (1977)[7] but with different elutriation correlations.

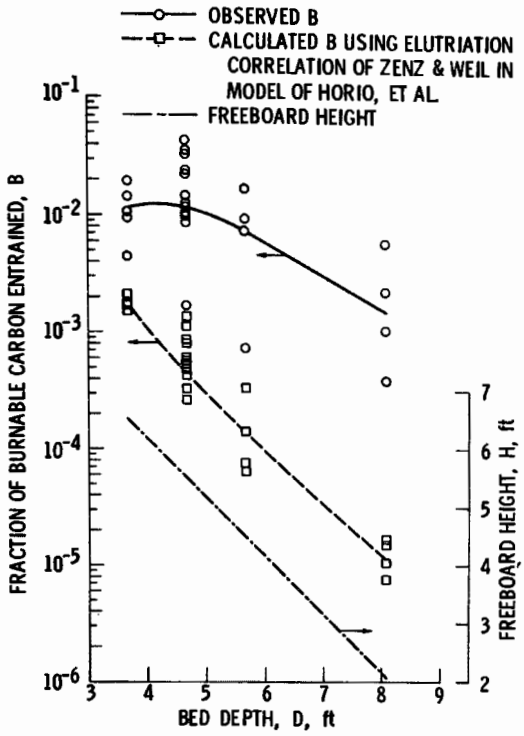

Figure 12 Effect of bed depth on entrained carbon.

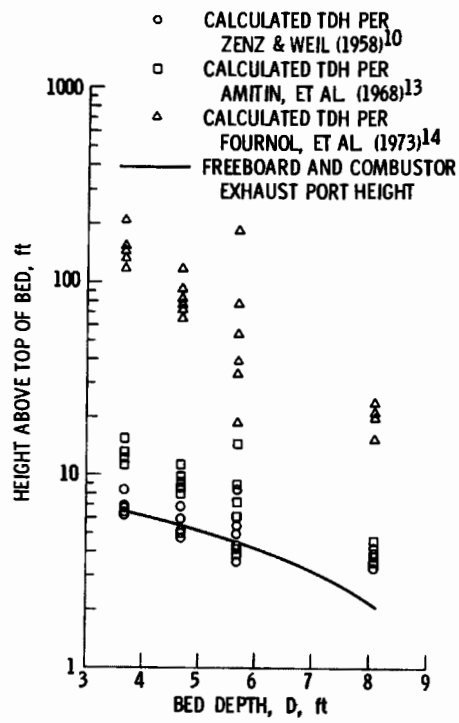

Figure 13 Comparison of calculated transport disengaging height (TDH) with combustor exhaust port height.

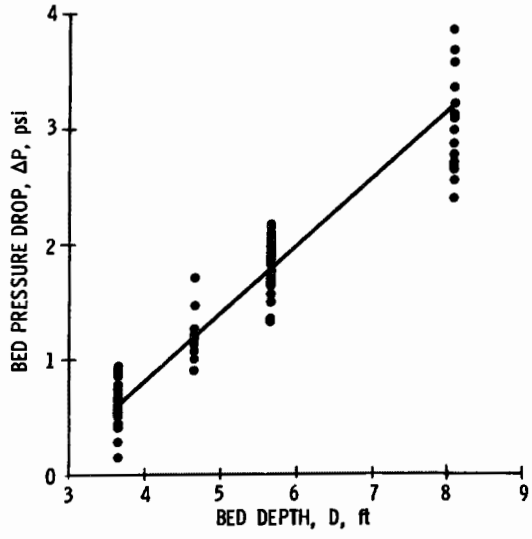

Figure 14 Dependence of bed pressure drop on bed depth.

COMPARATIVE ECONOMIC ANALYSIS OF SELECTED PARTICULATE CONTROL SYSTEMS FOR ADVANCED COMBINED CYCLE POWER PLANTS

By:

J. R. Bush
F. L. Blum
P. L. Feldman
Research-Cottrell, Inc.
Somerville, New Jersey 08807

ABSTRACT

Combined cycle power plants require particulate control to meet turbine specifications and to meet environmental regulation. Cost scenarios are presented, using both capital and operating cost estimates, for four particulate control systems that meet these requirements. Three scenarios use only high temperature, high pressure equipment - combinations of cyclones, granular bed filters and electrostatic precipitators - to collect all particulate before the gas turbine. The remaining scenario uses three stages of cyclones to collect all particulate above 5 microns prior to the gas turbine and conventional fabric filtration equipment to collect the fine particulate going through the gas turbine. Advantages and disadvantages of each system are discussed from both an economical and technical viewpoint.

INTRODUCTION

The use of gas turbine in advanced combined-cycle power plants is being planned and developed for use with coal as a fuel. These plants will burn coal at high temperatures (1500-1800^{o}F) and high pressures (6-20 atmospheres) in fluidized bed boilers and send the resulting flue gases to the turbine and waste heat recovery system. It is necessary to clean these gases of harmful, eroding, and corroding particulate prior to their entry into the gas turbine such that unwanted deposits do not form, that corrosion is reduced, and that unwanted down-time is avoided. This paper presents the comparative economics of four high temperature, high pressure (HTHP) particulate control systems and their importance to improving turbine reliability.

Pressurized fluidized bed (PFB) combustion is being incorporated into the overall design for an advanced combined cycle power plant. Two designs of the PFB combustor are considered: i) a water-cooled design in which steam is produced to drive a steam turbine, producing 2/3 of the plant power, the remaining being produced through the gas turbine (Figure 1) and ii) an air cooled design in which the heated air is combined with the cleaned flue gas prior to expansion in the gas turbine. A waste heat boiler after the turbine generates steam for 1/3 of the plant output as in Figure 2. Both designs are similar in that several PFB modules are used to drive the gas turbines. They differ in that in (i) the steam turbine is the base load for the plant, whereas in (ii) the gas turbines become the base load.

For a 600 megawatt power plant, the water cooled design (Figure 1) would use eight (8) PFB boilers to drive four (4) gas turbines, producing 200 megawatts of power. The steam produced in each boiler would be combined to drive one steam turbine producing over 400 megawatts. Sulfur dioxide is controlled within the PFB boiler through the addition of dolomite to the coal. Particulate control is required on the gases leaving each PFB boiler before the gases enter their respective turbines. Particulate loadings recommended for reliable turbine operation are sufficiently low that all environmental standards can generally be met without additional cleanup as shown in Table 1.

The air cooled design (Figure 2) is slightly different. The compressor delivers air to both the fluidized bed for coal combustion and to the clean heat transfer side in a 1/3 - 2/3 ratio. After being cleaned at high temperature and pressure, both hot gases are combined to reduce the particulate loading by a factor of 3 and thereby improve the turbine's reliability. Under conditions of minimal particulate control, sufficient to just meet the turbine specifications, an additional conventional cleanup system would be required to meet environments regulations. It is necessary to evaluate the costs associated with HTHP cleaning systems to evaluate a) both air and water-cooled designs and b) whether minimal cleaning followed by a conventional system at the stack is cost effective.

The purpose of this paper is to present four systems, one with a conventional system for fine particulate control, and their respective costs for a 600 megawatt power plant using PFB boilers and gas turbines.

Efficient particulate control at the high temperature and pressure is desired from several viewpoints: 1) turbine inlet loadings are reduced improving reliability; 2) HTHP gas volume is smaller resulting in a more compact system; 3) heat transfer in downstream waste heat recovery boiler is higher due to reduced build-up of deposits. There are several devices being developed for control: 1) conventional cyclones, 2) multicyclones, 3) tornado cyclones, 4) granular bed filters, 5) ceramic filters, 6) HTHP electrostatic precipitators and others. Of these designs, the cyclone designs are most advanced, however, experimental performance has been shown to be too low to meet adequate environmental standards without additional cleanup. Turbine specifications can be met at the expense of high pressure drop, especially with the air-cooled design which dilutes the final loading by a factor of 3.

Granular bed filters have higher efficiency than the cyclones but also have high pressure drops, have potential of plugging, have secondary air requirements for cleaning, and have recently been found to show long term deterioration in performance for fine particulate collection. Some of these problems are being solved and new designs will arrive that can improve the system.

Ceramic filters are still in the early stage of development. They promise high collection efficiencies, but suffer from plugging, high abrasion and tearing, and short bag life. Substantial work is still required before suitable materials produce a reliable life that is amenable to accurate cost analyses.

High temperature, high pressure electrostatic precipitators have low pressure drop, low power consumption, no moving parts or

plugging problems, and are the only device that results in higher collection efficiencies for a given size than at lower temperatures and pressures.

Of the equipment described, four systems comprised of combinations of cyclones, granular bed filters and electrostatic precipitators have been selected for a more detailed analysis. These are A) primary cyclone, secondary multicyclone, and tornado cyclone at high temperature and pressure, followed by a conventional baghouse system at the stack; B) primary cyclone, secondary multicyclone, and granular bed filter; C) primary cyclone and one HTHP electrostatic precipitator; and D) two high temperature high pressure electrostatic precipitators in series for maximum performance.

The costs derived for each system are based on a 600 megawatt design using eight (8) PFB boilers and 4 gas turbines. Shop fabrication is used where possible, and field erection/fabrication used as required. Costs for individual components are based on using Incoloy 800H for internals, refractory lined pressure vessels and ducting. Quotes have been obtained from some manufacturers, past published cost data has been updated where applicable, and estimates obtained from within Research-Cottrell for the various components and erection. The data base for the costs being presented is January, 1979.

HTHP PARTICULATE CONTROL SYSTEMS

The cyclone system (A), Figure 3, will be a modular design that splits the gases leaving the PFB boiler into three streams. Each stream will then have its own primary cyclone, secondary multicyclone, and tornado cyclone. Each of these will be mounted on the structure housing the PFB boiler and will have its own lock hopper and control instrumentation. Following the tornado cyclone, the three streams are united, combined with a stream from a second PFB boiler and sent to the gas turbine. This system is expected to achieve an overall 98-99% collection that meets minimum turbine requirements. Final fine particulate control will occur prior to the stack using a fabric filter system. The water cooled design will have an airflow similar to a conventional coal fired boiler, whereas the air cooled design will have 3 times the flow for a larger size and cost.

The second system (B), Figure 4, consists of a primary cyclone, a secondary multicyclone, and a granular bed filter. Again as in system A, the gas stream leaving the PFB boiler will be divided into three smaller equal streams to feed each individual system. After the granular bed filter the streams are combined, added to that from a second PFB boiler module and

sent to the turbine. Here, the granular bed filter is expected to, or can be developed to, meet environmental regulations as well as minimum turbine standards. Overall performance is expected to be near 99.5% to 99.8% with a corresponding total, pressure drop of 2 psi. Continued development and evaluation is required to improve performance and reduce pressure loss.

The third system (C), Figure 5, uses one primary cyclone and one HTHP electrostatic precipitator that handles the entire flow from the PFB boiler. This design reduces ductwork and reduces heat losses within the system. The overall pressure drop, mainly due to the cyclone, will be approximately 0.6 psi. This system is expected to yield an overall efficiency of 99.6 - 99.9% meeting both turbine and environmental requirements. Power consumption is low and will help to offset the large capital investment. As the precipitator pressure vessel is large, it requires its own supporting structure for erection. Again the gas flows from two PFB boilers will be combined to go to the gas turbine.

The fourth system for evaluation (D), Figure 6, is two HTHP electrostatic precipitators in series. Overall performance is expected to be 99.9+% efficiency that will substantially reduce the loadings to the gas turbines and should greatly increase the turbine's reliability by reducing deposition. As flyash does contain alkali sulphates, it is necessary tnat the loading be kept to a minimum to reduce corrosion. Capital costs are higher than in (C), but will yield a comparative cost basis for improving performance.

Each system has different advantages and disadvantages. The HTHP precipitator offers the lowest power consumption and thus improves overall plant thermal efficiency. The cyclone system is the most developed and ready for commercialization. The granular bed filter has the potential for added SO_2 removal, or as a sorbent for other gaseous species. Any recommendation must first be made on technical development and achievement of system objectives and second on economics. Although the first is not completely answered, it is necessary to look at the costs involved to direct final development towards cost effective systems.

COST EVALUATION

The cost of a cleanup system for particulate at high temperature and pressure is based on a 600 megawatt modular PFB boiler design using eight PFB boilers and 4 gas turbines. Capital cost estimates presented include shop fabrication, field fabrication where applicable, field erection, interconnecting ductwork, and supporting structure. All internal material and lining used Incoloy 800H. All pressure vessesl are refactory

lined and fabricated in accordance with ASME code, Section VIII, for unfired pressure vessels. All labor rates are based on a central U.S. location using January, 1979 rates, with escalation during construction estimated at 7%. Cost estimates have been checked against a) current quotes from manufacturers, b) updating past cost estimates using the chemical engineering construction cost index, and through independent cost estimates for various components. As each system is still developing, the cost estimates should be used as order of magnitude and only for comparative purposes.

Power consumption, maintenance and operating costs, and performance degradation have been estimated based on available data, manufacturers quotes, and on similar operating systems. Annual costs are based on 6¢/kwhr, the maximum expected for coal fired plants, and capital charges at 15% return rate on a 15 yr amortization schedule.

The reliability of the gas turbine to varied inlet loadings is not known very well as little data has been obtained. It is expected that at minimum conditions, forced outages could be as high as three times a year or as low as once a year. As loading decreases, particles deposition reduces, thus increasing turbine life and reliability. Thus systems B and C reduce the probability of a forced outage in addition to the scheduled outage to approximately one every two years. With the much lower loading associated with two precipitators (System D), outages should remain with that scheduled at one per year. Although cost estimates vary widely it is expected that scheduled maintenance will add 1 mill/kwhr to overall plant cost and that each forced outage will be slightly higher at 1.2-1.5 mil/kwhr.

The costs for each system, A, B, C, D, are shown in Table 2. The capital investments temperature control range from a low of 23.8 million dollars to a high of 51.9 million dollars for a 600 megawatt plant, or 39.7 to 86.5 $/kW installed. The annual power consumption will vary from 0.54% of the total plant output for the precipitator to 1.5% for the granular bed filter or for the cyclones and conventional system.

These figures result in a total annual cost in mils/kwhr ranging from a) 1.64 - 2.68 for the cyclone system (A), depending on the water cooled or the air cooled design, b) 2.34 for the granular bed filter system (B), c) 1.50 for the cyclone-precipitator system (C), and d) 2.31 for the two precipitator system (D). If one tries to incorporate savings on turbine maintenance due to reduction of forced outages, the net cost, using the cyclone system as a base, could vary from zero (0) for the cyclone-precipitator system, to 0.31 mil/kwhr for two precipitators, to 0.80 mil/kwhr for the granular bed filter system, to the maximum 1.64 - 2.68 mils/kwhr for the cyclone system.

These costs would be added, or included in the cost estimates made for the 600 megawatt plant using PFB boilers. Past estimates have ranged from an annual plant cost of 35 mils per kilowatt hour to 45 mils per kilowatt hour. New estimates are required in light of the rapidly changing energy picture.

CONCLUSIONS AND RECOMMENDATIONS

- The cost data show that a HTHP cyclone and HTHP electrostatic precipitator offer the lowest overall cost and minimum power consumption.

- The granular bed filter system has a similar annual cost to two HTHP electrostatic precipitators in series.

- Performance evaluation and cost of turbine maintenance and reliability as a function of inlet loading to the turbine is needed to fully evaluate the required HTHP particulate control systems.

- Expected annual costs range from 1.50 mills/kwhr to 2.34 mils/kwhr for the HTHP control systems.

- Investment costs vary from 51.7 $/kW to 80.5 $/kW depending on system and performance requirements.

- Finally it is recommended that development continue on all HTHP control systems that can meet all particulate control requirements and that will minimize power loss and power consumption.

REFERENCES

1. Bush, J. R., Feldman, P. L., and Robinson, M., "Development of a High Temperature High Pressure Electrostatic Precipitator",J. of Air Pollution Control Association, April, 1979.

2. Keairns, Archer, et al, "Fluidized Bed Combustion Process Evaluation, Phase II - Pressurized Fluidized Bed Coal Combustion Development", EPA-650/2-75-027-C, Sept., 1975.

3. Curtis Wright Corp., "Engineer Design, Construct, Test and Evaluate a Pressurized Fluidized Bed Pilot Plant using High Sulfur Coal for Production of Electric Power", FE-1726-17A, March, 1977.

4. Zakkag, Mitter, and Francesohi, "Recent Developments in Pressurized Fluidized Bed/Coal Combustion Research", 17th Aerospace Sciences Meeting, January, 1979.

5. Giranonti, Smith, Castello, Huber, and Horgan, "Evaluation of Coal-Fired Fluid Bed Combined Cycle Power Plant," 1977.

6. Schilling, Schreckenbert, and Wied, "A New Concept for the Development of Coal Burning Gas Turbine," ASME-78-GT-40, April, 1978.

7. Brooks and Peterson, "General Electric Pressurized Fluidized Bed Power Plant Status," General Electric, presented at Fifth International Conference on Fluidized Bed Combustion, December, 1977.

FIGURE 1

WATER COOLED PRESSURIZED FLUIDIZED BED

COMBINED CYCLE DESIGN CONCEPT

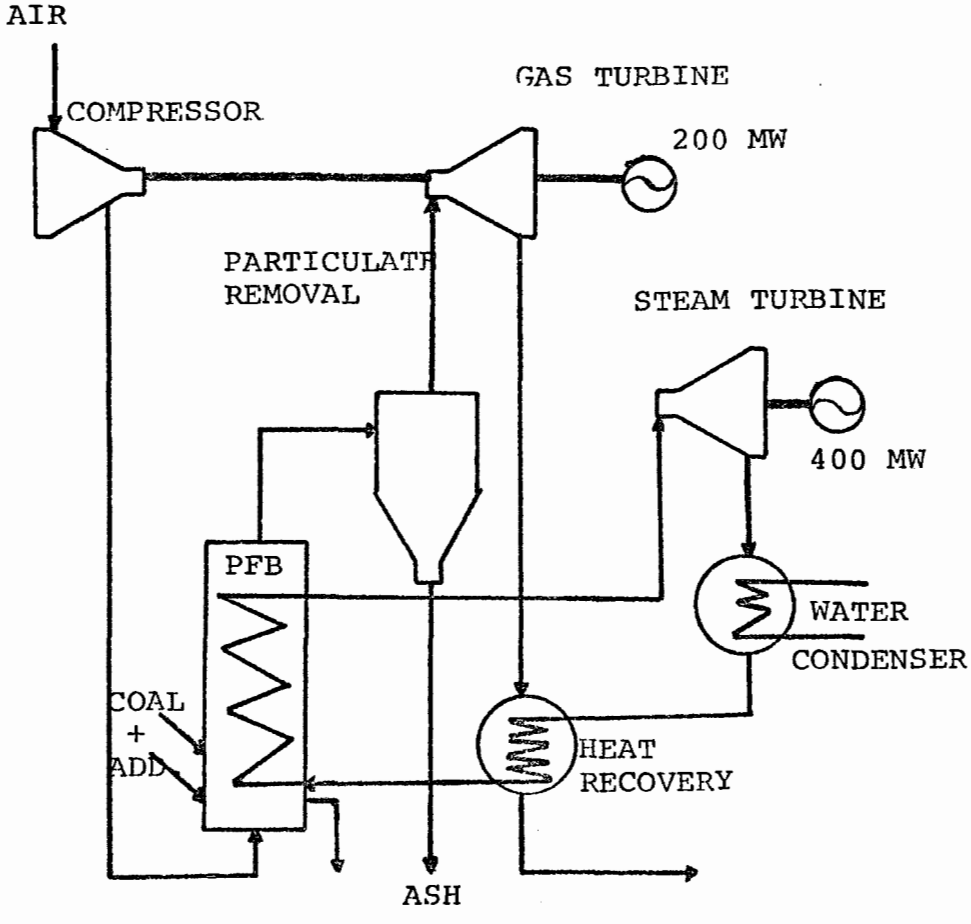

FIGURE 2

AIR COOLED PRESSURIZED FLUIDIZED BED COMBINED CYCLE DESIGN CONCEPT

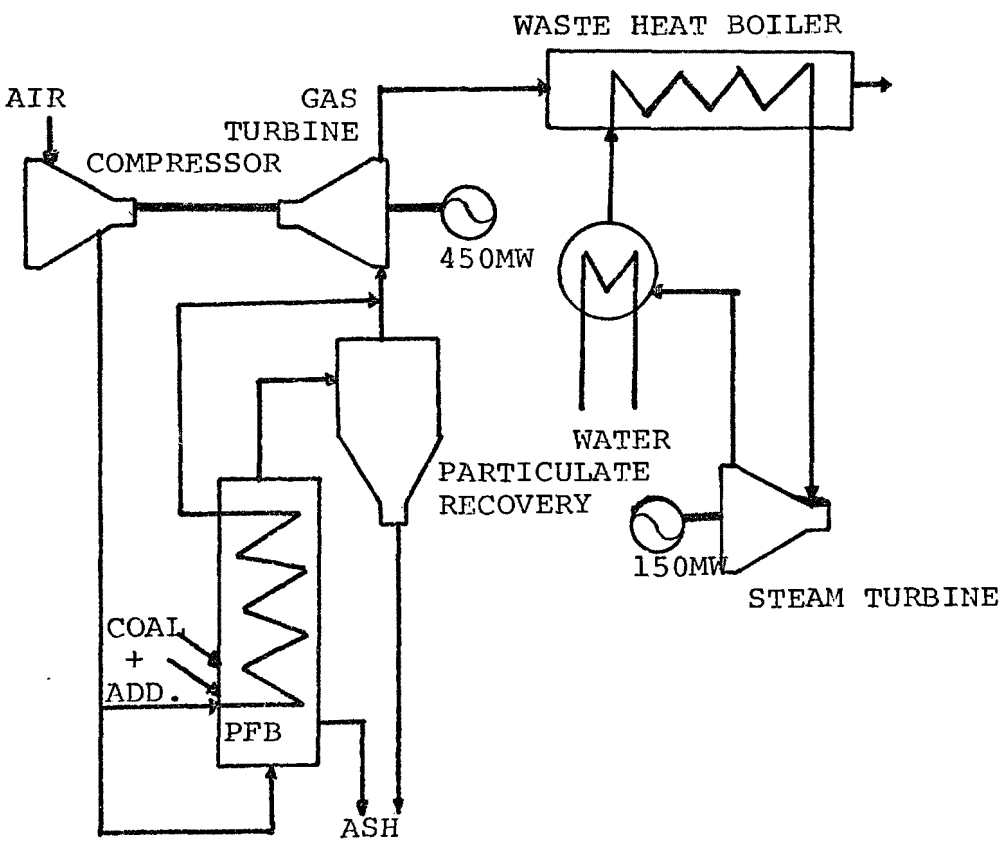

FIGURE 3
HTHP CYCLONE SYSTEM

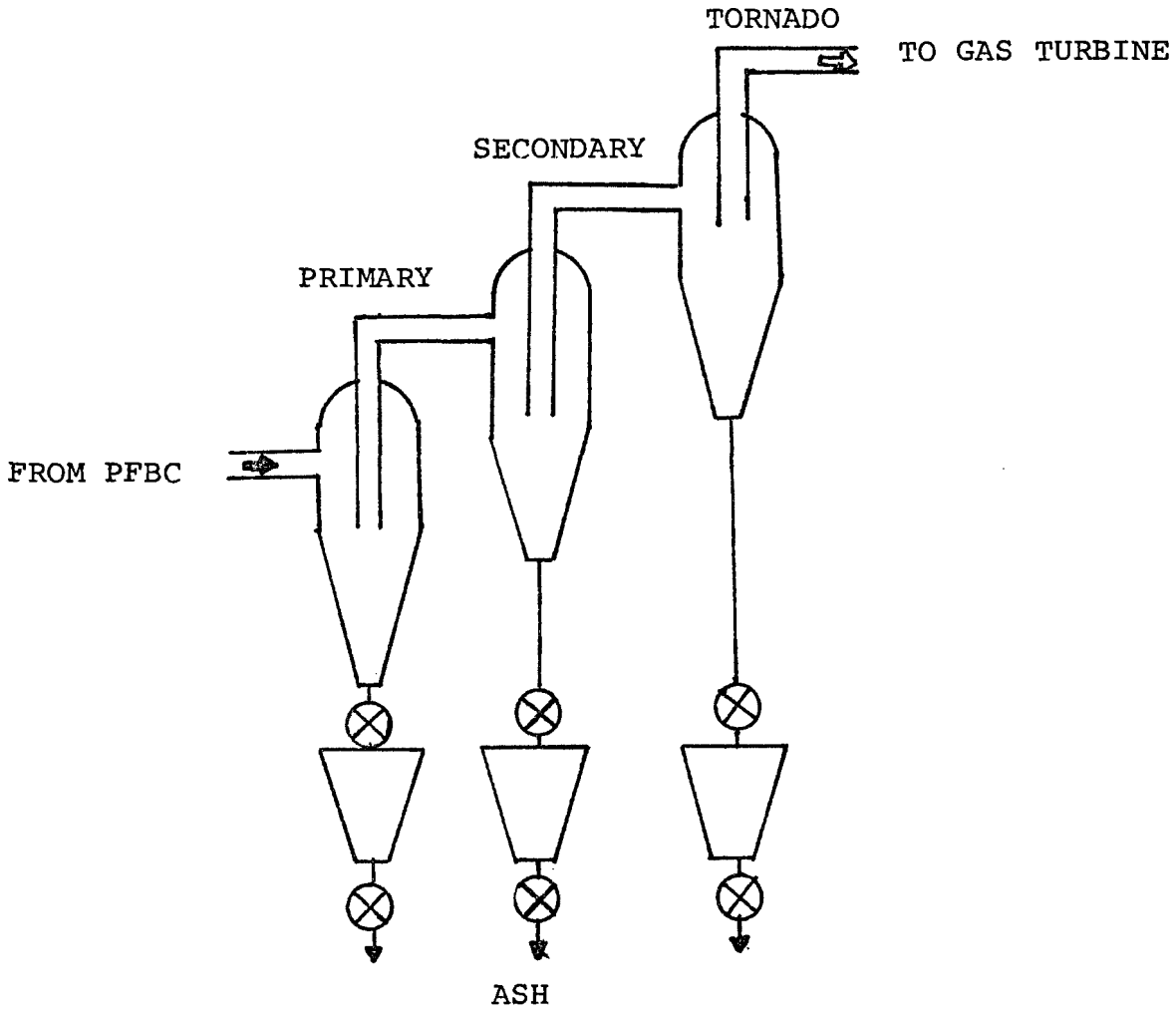

FIGURE 4

HTHP CYCLONE - GRANULAR BED FILTER SYSTEM

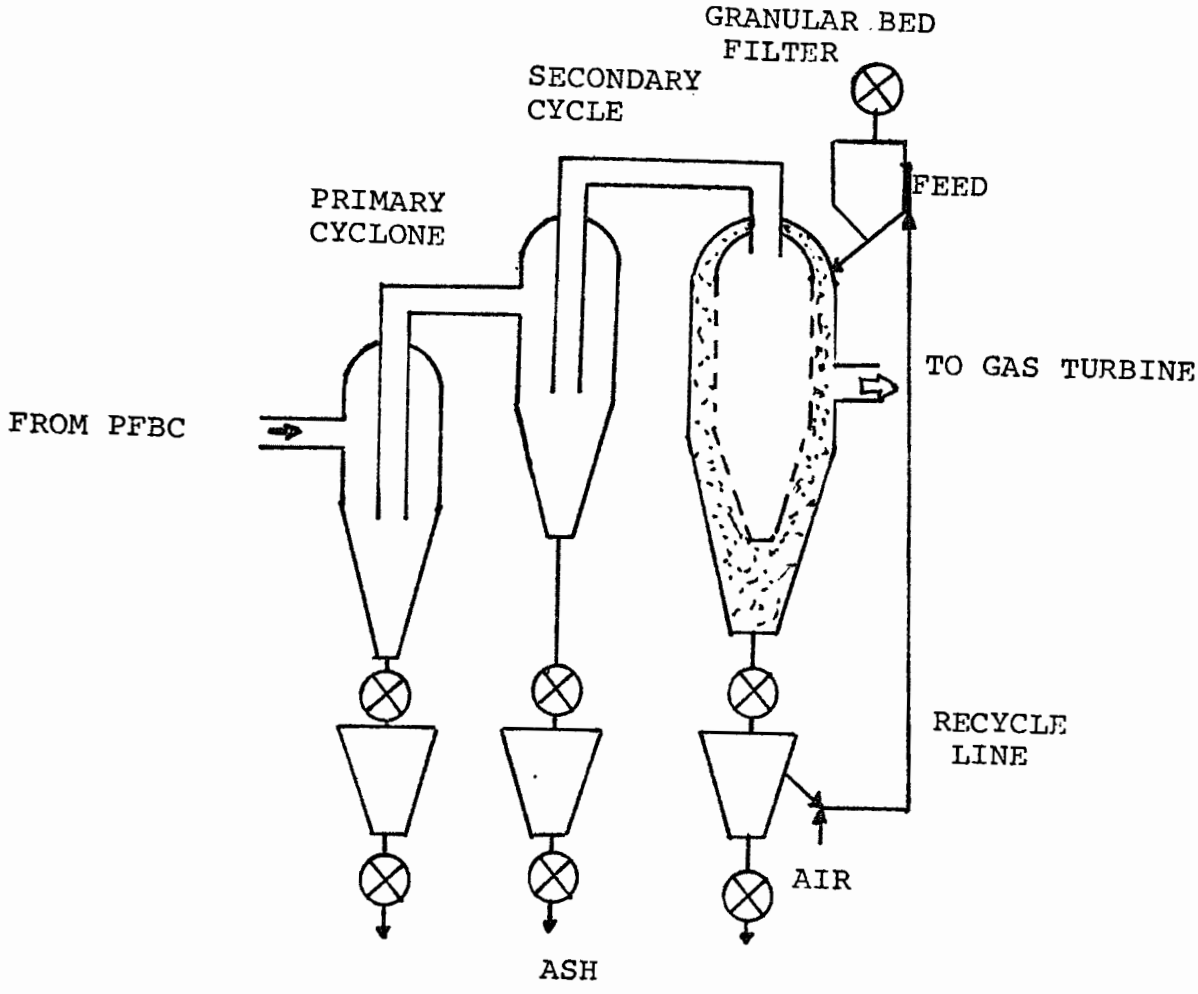

FIGURE 5

HTHP CYCLONE - PRECIPITATOR SYSTEM

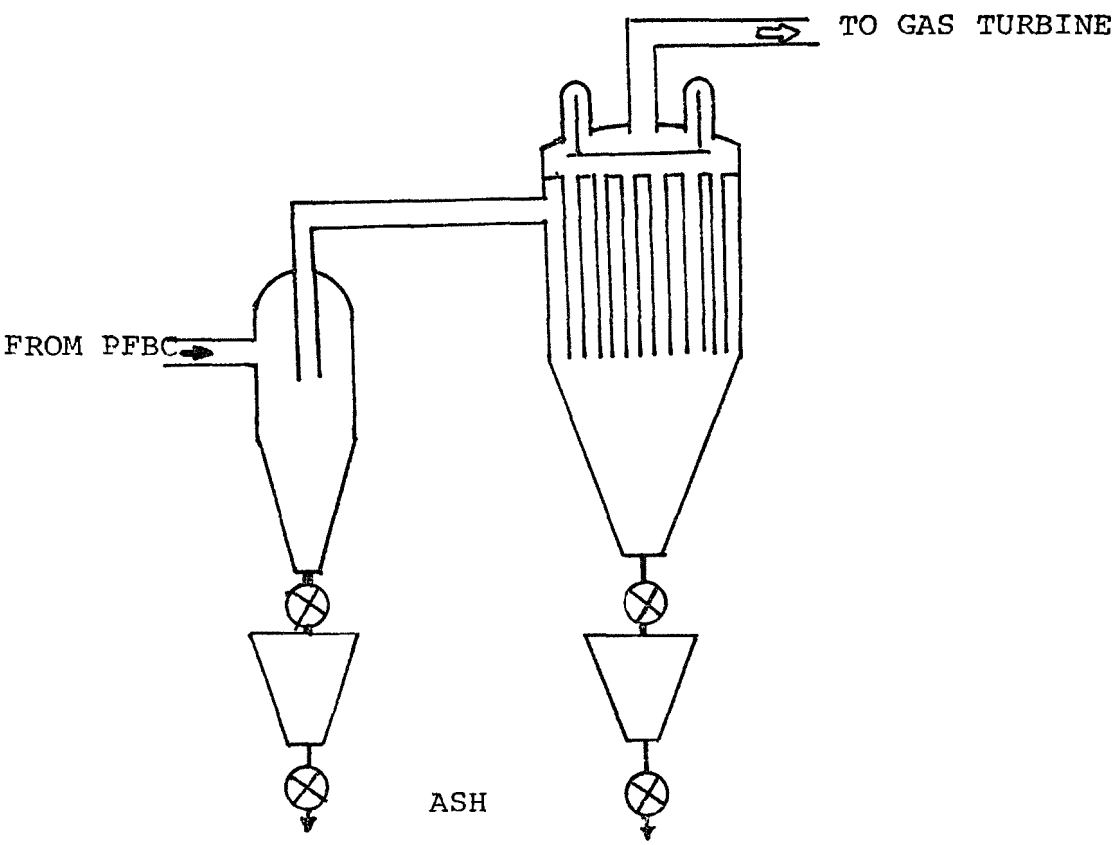

FIGURE 6

DUAL HTHP ELECTROSTATIC PRECIPITATOR

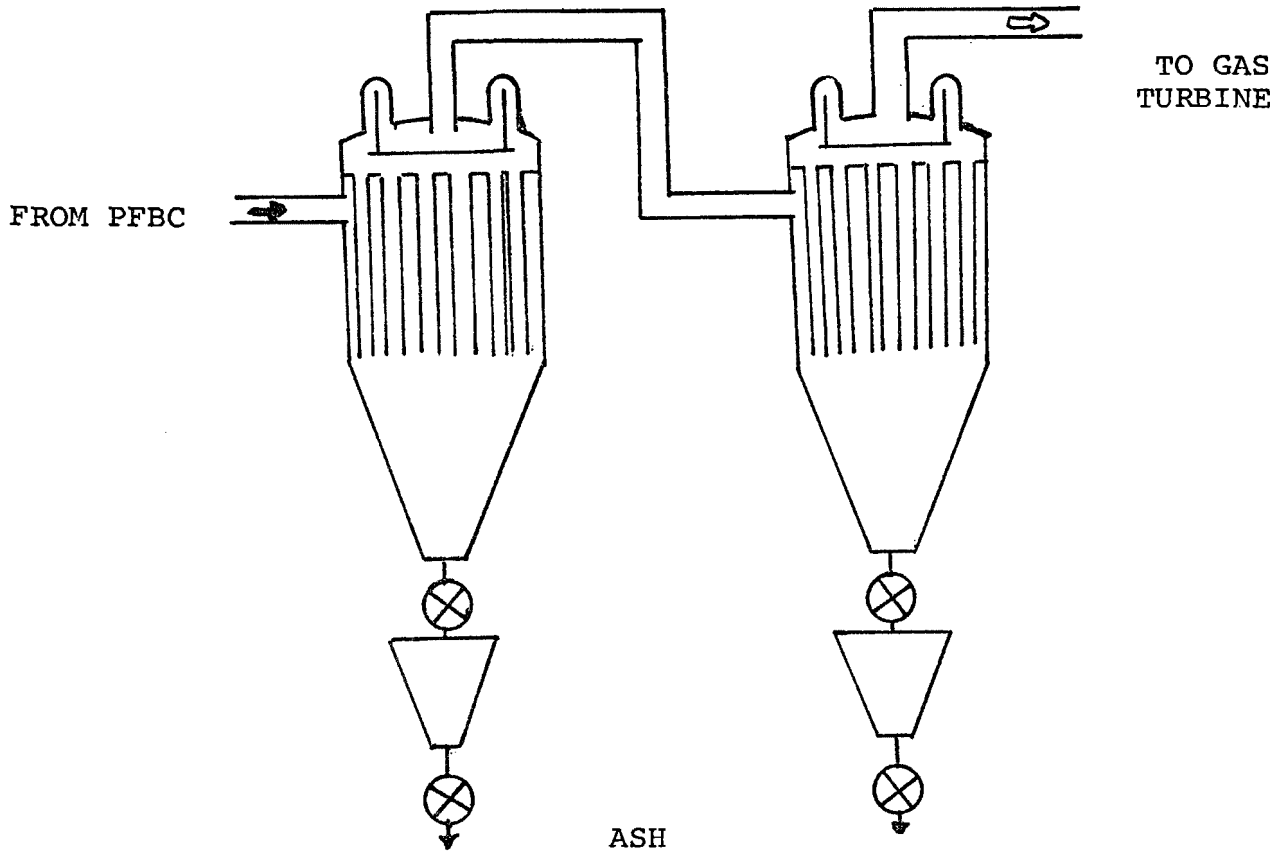

TABLE 1

PARTICULATE CONTROL REQUIREMENTS

AT HIGH TEMPERATURE AND HIGH PRESSURE

SIZE	MAX. LOADING TO TURBINE, GR/SCF	COMBINED TURBINE AND ENVIRONMENTAL LOADING GR/SCF
0-5μ	0.015 and up	0.0097 and up
5-10μ	0.005 to 0.010	0.002 to 0.0012
Total	0.08 to 0.125	0.0098 to 0.017
Efficiency based on inlet 10 gr/SCF:	98.8 - 99.2%	98.8 to 99.9%

TABLE 2

PARTICULATE CONTROL SYSTEMS COSTS

	SYSTEM			
	A	B	C	D
Installed Capital 10^6:	23.8 to 43.0	35.5	31.0	51.9
$/kW	39.7 to 71.7	59.2	51.7	86.5
Annual Power Required:				
106 kWhr equivalent:	56-72.2	72.2	26.1	28.0
% of plant output:	1.17-1.50%	1.50%	0.54%	0.58%
Annual Cost: mils/kWhr				
Capital charge:	0.85-1.53	1.27	1.10	1.85
Power @ 6¢/kWhr:	0.7-0.9	0.90	0.33	0.35
Operating & maintenance:	0.094-0.253	0.174	0.059	0.11
Total	1.64-2.68	2.34	1.49	2.31
Relative Turbine Maintenance Costs:	100% (Base)	-50%	-50%	-67%
(Approximate)mils/kWhr	(3.0)	(1.50)	(1.50)	(1.0)

CONCLUSIONS FROM EPA'S HIGH TEMPERATURE/ HIGH PRESSURE CONTROL PROGRAM

by

D. C. Drehmel and James H. Abbott
Industrial Environmental Research Laboratory
U. S. Environmental Protection Agency
Research Triangle Park, North Carolina 27711

ABSTRACT

Although particulate control equipment can be demonstrated to have high collection efficiency in some applications, extreme conditions of temperature, pressure, or both pose special problems. Aqueous scrubbers and filters using organic media have obvious temperature limitations. Electrostatic precipitators are commonly used on the hot side of the air preheated in power plants but performance at high temperatures such as 800°C is yet to be demonstrated. The need for control at extreme conditions arises in metallurgical operations and advanced energy processes. Consequently, EPA has conducted a program of research and development for control of particulates at high temperature and pressure.

Among the control devices given consideration in the program were cyclones, granular bed filters, dry scrubbers, molten scrubbers, electrostatic precipitators, ceramic bag filters, and other ceramic filters not of a bag configuration. Advantages and disadvantages of these devices involve parameters such as simplicity of operation, materials problems, inability to collect submicron particles, difficulty in regenerating the collection media, and the parameters related to cost including size and pressure drop. Since these advantages and disadvantages can be weighed differently according to the needs of a specific application, it is not possible to give universal conclusions. However, if the most important consideration is control of submicron particles, ceramic filters are foremost.

CONCLUSIONS FROM EPA'S HIGH TEMPERATURE/ HIGH PRESSURE CONTROL PROGRAM

Introduction

The Environmental Protection Agency (EPA) and its predecessor organizations have actively investigated improvements in airborne particulate control for 10 years. Five years ago it was recognized that extending the operating range of conventional devices to high temperature and high pressure would be necessary to provide abatement for a variety of industrial and advanced energy sources such as fluidized bed combustors and coal gasifiers. In addition it was recognized that stationary fuel combustion was the largest source category for particulate emissions.[1] Consequently, EPA focused its programs on fuel combustion and especially on power production and energy conversion. The objective of these programs was to demonstrate control technology to meet environmental standards concerning the ambient concentration of particles and the emission rate of particles from new sources. The current standard for power conversions states that new sources shall not emit more than 0.1 pounds of particulate matter for every million Btu's of thermal energy released (43 ng/J). It is expected that this standard will be lowered and future ambient air standards may apply to particles less than 15 μm. To meet this objective, EPA developed a program illustrated in Table 1. Particulate control at high temperature and pressure was thought to be possible with cyclones, ceramic filters, granular bed filters, non-aqueous scrubbers, and specially designed electrostatic precipitators. However, models predicted cyclones would be less than 50 percent efficient below 1 μm and data indicated poor efficiency even at 2.5 μm.[2] Since collection of fine particles was a pending subobjective to meet EPA standards, and cyclones demonstrated low potential for fine particle collection, no development of cyclones was planned. Development of the other approaches was planned as indicated in Table 1. The results of the progress along each path of Table 1 are the subject of this paper. Results of a field test of high temperature and pressure cyclones are also included for comparison.

Table 1. High Temperature/Pressure Control

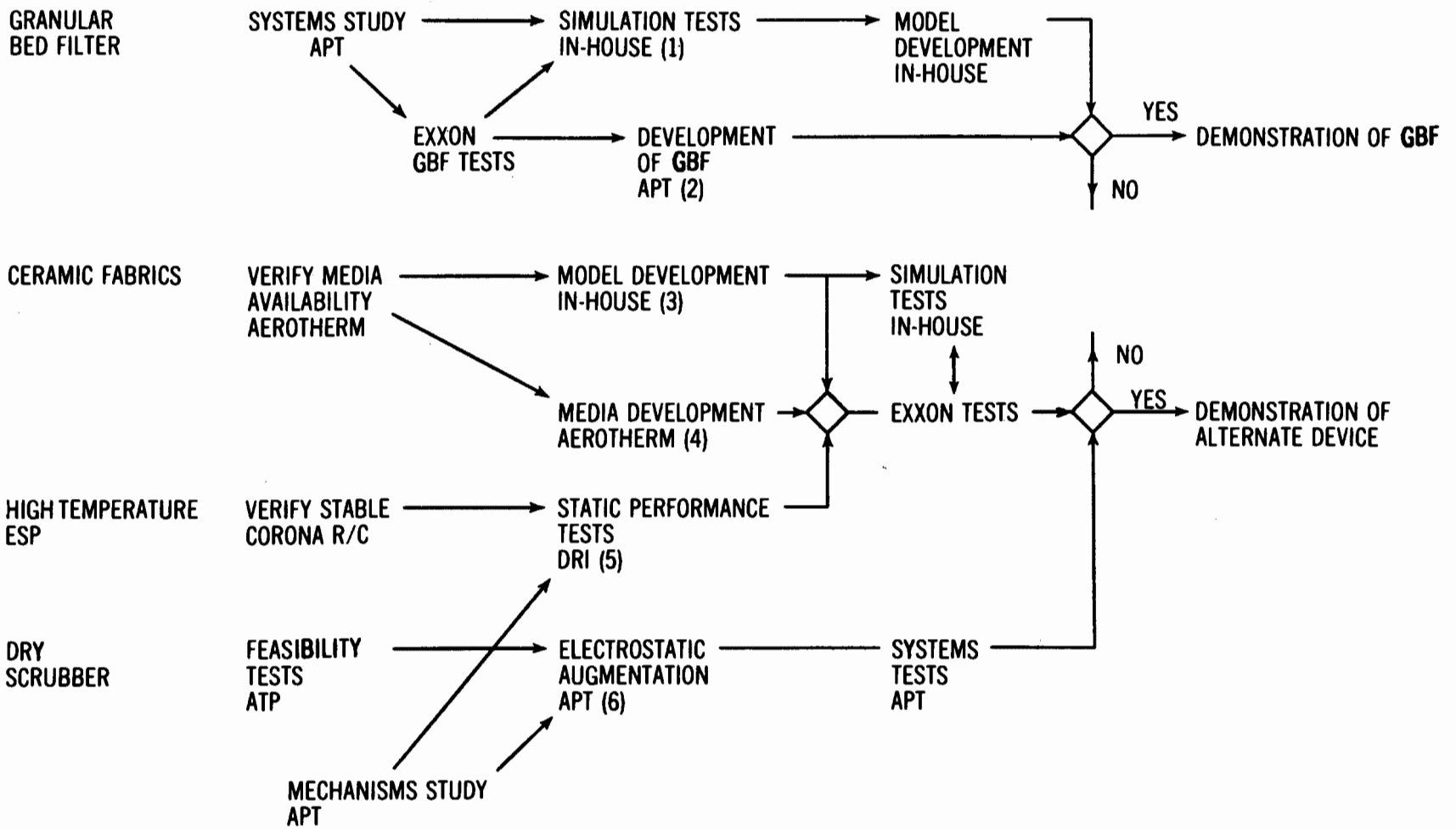

Granular Bed Filters (GBF) and Dry Scrubbers

Granular bed filters and dry scrubbers may be defined as any collection system comprised of stationary or moving discrete, relatively closely packed granules as the collection medium. With respect to motion of the granules, granular bed filters may be classified as moving or fixed bed filters. Dry scrubbers may be very similar to moving bed filters except that the gas stream may be accelerated before contacting the granules in order to maximize collection from impaction.

To evaluate granular bed filters and dry scrubbers, two contracts with Air Pollution Technology were initiated in 1976 (Contract 68-02-2164 in August and Contract 68-2-2183 in September). The purpose of these contracts was to assess the application of the APT dry scrubber and granular bed filters, as made by Ducon and Combustion Power Company (CPC), to the problem of particulate control at high temperature and pressure. The results of these contracts may be illustrated by comparing the APT, CPC, and Ducon control devices. These three devices give a range of design features available for collection of particulate on hard granules (see Table 2). At one end of the spectrum are fixed granular bed filters which rely on collection throughout the bed material until a layer or cake is formed. The cake provides greater filtration efficiencies especially for submicron particles. Optimizing the performance of the fixed granular bed filter requires a cleaning system which preserves some of the cake while preventing unacceptably high pressure drops. Moreover, it is essential that the cleaning systems not allow particulate to work its way through the bed either by insufficient cleaning or by motion of the granules.

At the other end of the spectrum is the dry scrubber which relies only on impaction for collection; a cake is never formed. In this case, the gas velocity is high to optimize impaction. Collection of submicron particles may be augmented by charging particles and granules with different signs. In 1978, EPA began work with APT, Inc. (Contract 68-02-3102) to verify the benefits of using electrostatics in dry scrubbers. Cold flow experiments confirm that penetration of submicron particles can be reduced by a factor of 4. Hot flow experiments will be completed in a year.

Table 2. Summary of Performance Information

	Device		
	Moving Granular Bed Filter (CPC)	Dry Scrubber (APT)	Fixed Granular Bed Filter (Ducon)
Superficial gas velocity, cm/s	20-80	3,000-6,000	45
Pressure drop, kPa	1.2-5.7	2-7	8(from prediction)
Bed depth, cm	20-40	NA	3.8
Granule diameter, cm	0.08-0.2	0.01	0.04
Efficiency at 1 μm,%	78	96	82
Efficiency at 6 μm,%	93	99	96

In the middle of the spectrum is the moving granular bed filter in which the granules move slowly enough to form a bed which acts like a filter. This device works partially by impaction and partially by filtration but cannot be optimized for either since the gas velocities are low and the bed is removed before a cake is formed. However, some designs using intermittently moving granular beds do establish and preserve the cake for better filtration.

The information in Table 2 is a quick comparison of the points in the spectrum discussed above. Pressure drops for all three devices tend to be the same. The APT dry scrubber has a very high gas velocity and no bed. The CPC moving granular bed filter has a low gas velocity and a thick bed. The Ducon filter has a low gas velocity and a thin bed. The thick bed is used with the CPC moving bed filter to ensure good filtration in the absence of cake filtration or high gas velocity for impaction collection. In the case of these data the APT dry scrubber gave the best performance. However, development of all these devices continues and it would be premature to conclude that efficiencies will not be improved. Both the APT and CPC devices can be augmented with electrostatic effects such as imposing a field or charging the particles, charging the granules, or both. Further development of the Ducon device will necessitate improved cleaning to avoid problems noted in tests at the Exxon Miniplant.[3] Tests at Exxon were terminated after a series of difficulties including plugging and rapid loss of acceptable filtration efficiency. Because of these results, further development of GBF's was ended early and points 1 and 2 on Table 1 were never reached.

Ceramic Filters

Two types of ceramic filters were investigated: 1) flat rigid filters,and 2) cylindrical bag filters. The first was made the subject of a Westinghouse contract (No. 68-02-1887) and the second, an Aerotherm contract (No. 68-02-2169). A number of rigid ceramic filters were tested including cubes comprised of thin filtering barriers separated by alternating layers of corrugations. The advantage of the filtering cube is that it has large surface area to volume ratios and has added strength to withstand mechanical and thermal stress. Using a limestone test dust

with a mass median diameter of 1.4 μm, the collection efficiency averaged 96.4 percent in experiments at temperatures from 360 to 815°C.[4] The disadvantage of the filtering cube is that the void spaces are small and could rapidly fill and plug with collected material. This would be especially true with tarry particles from coal gasification or sticky particles as encountered at the Exxon fluid bed combustor miniplant.

Ceramic bag filters were investigated with three basic media types: 1) woven ceramics,2) ceramic papers, and 3) ceramic felts. Tests with 0.3 μm particles showed that woven ceramics had low collection efficiencies, always below 50 percent, and ceramic papers and felts had high collection efficiencies, up to 99.5 percent.[5] Another advantage of ceramic felts was a loose, flexible structure which would provide the durability needed to withstand a miniumum lifetime of cleaning, typically requirimg several million cleaning cycles. For these reasons, it was decided to continue the program with development of the ceramic felt media (point 4 in Table 1) and to arrange tests at the Exxon fluid bed combustor miniplant. Under contract 68-02-2611, Aerotherm performed extended tests of Saffil* Alumina, a type of ceramic felt, and demonstrated that this media (as developed by Aerotherm) could be cleaned up to 50,000 times at 815°C and 9 atm. without damage to the ceramic bag filter.

Tests at the Exxon Miniplant were run under varying gas velocities through the bag and during combustion of two different coal types in the fluid bed combustor. It was found that coal type had little effect on filter performance. When superficial gas velocity was increased from 4 to 10 cm/s there was a slight decrease in efficiency from 99.4 to 98.6 percent. No problems with bag cleaning were encountered and residual pressure drops were always below 5 kPa (20 in. H_2O). In comparison to filters described in Table 2, this pressure drop is in the same range, superficial gas velocities are lower, and efficiencies are higher. The central remaining question for ceramic felt bag filters is the upper limit on bag lifetime. Although these bags are relatively inexpensive, trouble-free operation between scheduled outages would be necessary. Consequently, demonstration of long term bag lifetime is still required.

*ICI United States, Inc., Concord Pike and New Murphy Road, Wilmington, DE 19803

Electrostatic Precipitators

Under EPA Contract 68-02-2104, Research Cottrell was asked to verify the operability of electrostatic precipitators at high temperature and pressure. The objectives of this work were to define the temperature and pressure regions in which stable electrostatic precipitator operation is possible and to determine the suitability of electrostatic precipitators for particulate cleanup on advanced energy conversion processes. Electrostatic precipitators work by producing ions which charge the particles and cause the particles to migrate to the collection plate under the influence of an electric field. The ions are produced by corona discharge which will not be stable if sparkover conditions are reached. Research Cottrell did verify that stable corona was possible over the entire range of temperature and pressure combinations of advanced energy conversion processes. Research Cottrell also found that performance improved with increased temperature and pressure. This implies that satisfactory collection efficiencies could be attained. As an independent assessment, work was begun at Denver Research Institute (Grant 805939) to test an operating electrostatic precipitator at high temperature and pressure (refer to point 5 on Table 1). Results from this project will be available in a year.

Cyclones

Although no development of cyclones was undertaken, cyclones are of interest because of their simplicity. A field test of the testing cyclone at the Exxon Miniplant shows that in this case significant collection below 1 μm is possible. With a pressure drop of 3.7 kPa (15 in. H_2O), the collection efficiency at 1 μm was 80 percent; at 0.8 μm, 70 percent; and at 0.7 μm, 50 percent. Although these results are not unreasonable considering the pressure drop,[6] they do not fit available cyclone models which underpredict these efficiencies.[7] In light of the extremely sticky nature of the particles at the Exxon Miniplant, it is possible that the apparent collection of submicron particles is due to agglomeration into larger size regions. Further consideration of cyclones will have to be on an application by application basis.

Summary

A spectrum of granular collecting devices has been discussed in terms of three examples under development. Advantages of these differing approaches are:

APT Dry Scrubber

High collection efficiency possible from impaction and electrostatic attraction. Collecting granules are removed from the system for easy cleaning.

Ducon Fixed Bed Filter

High collection efficiency possible from cake filtration. Low attrition rates of bed material. Minimum energy requirement because of low heat loss and no bed recirculation power.

CPC Moving Granular Bed Filter

Collecting granules are removed from the system for easy cleaning. Electrostatic augmentation may provide high collection efficiencies.

In choosing between these alternatives, important considerations include cost, the adhesiveness of the particulate, and the importance of energy conservation. For example, if the particulate is sticky, a system which removes granules for easy cleaning will be necessary. On the other hand, if a fixed bed filter can be cleaned and removal of granules implies a high energy loss, cost considerations may favor the fixed bed filter.

A number of investigators have shown that high collection efficiencies are possible with ceramic filtration at high temperature (greater than 800°C) and/or high pressure (greater than 900 kPa). The recent work has tested both ceramic bags and rigid ceramic filters. Advantages of these different approaches are:

Ceramic Bag

High collection efficiency. Easy to clean. Resists failure because of thermal shock.

Rigid Ceramic Filter

High collection efficiency. Compact. Resists failure because of high pressure drop.

The endurance of both media is unknown. If the rigid ceramic filter can be used without clogging or thermal shock, it could be maintained in service for many years. However, ceramic bags are expected to have a limited life because of the less durable nature of the bag structure. Tests to date indicate that ceramic bags will easily survive up to 50,000 cleaning pulses or the equivalent of 1 year's light service.

Other devices considered are electrostatic precipitators and cyclones. Advantages of these are:

Electrostatic Precipitator

Very small pressure drop. High collection efficiency possible.

Cyclone

Simple. Available.

However, high temperature and pressure electrostatic precipitators need further development before application. Cyclones may be efficient in some cases, but generally low efficiency should be expected for fine particles.

A concluding comparison of all devices is given in Table 3. Selection of a device will depend primarily on the efficiency required and how soon the device is needed. Approaches such as the APT scrubber and the ceramic felt bag are the next to become available and offer higher efficiencies than commercial filters and cyclones. However, in comparison to filters, ceramic bags have low superficial velocities which may lead to large capital investment control units. Furthermore the APT dry scrubber still needs testing at the pilot scale.

Table 3. Comparison of High Temperature/Pressure Control Devices

Device	Superficial Velocity c/s	Pressure Drop kPa	Efficiency at 1 μm %	General Status
APT Dry Scrubber	3000-6000	2-7	96	bench
CPC Filter	20-80	1-6	78	commercial
Ducon Filter	45	8	82	commercial
Ceramic Bag	4-10	5	99	pilot
Electrostatic Precipitator	100-200	0.2	N/A	bench
Exxon Cyclone	N/A	4	80	commercial

References

1. Vandegrift, A. E. et al. "Particulate Pollutant Systems Study", EPA No. APTD0743, NTIS No. PB 203 128, May 1971.

2. Ciliberti, D. F. and B. W. Lancaster, "Performance of Rotary Flow Cyclones", AIChE J 22:2, p. 394, March 1976.

3. Hoke, R. C. et al. "Miniplant Studies of Pressured Fluidized-Bed Coal Combustion: Third Annual Report". EPA 600/7-78-069, NTIS No. PB 284-534, April 1978.

4. Drehmel, D. C. and D. F. Ciliberti, Paper #77-32.4, APCA Annual Meeting, Toronto, Canada, June 1977.

5. Drehmel, D. C. and M. S. Shackleton, Paper #17, Third Symposium on Fabric Filters for Particulate Control, Tucson, Arizona, December 1977.

6. Drehmel, D. C., Fine Particle Control Technology, JAPCA 27:138, 1977.

7. Parker, R. D., Private communication to D. C. Drehmel, 1979.

WATER SPRAY CONTROL OF FUGITIVE PARTICULATES: ENERGY AND UTILITY REQUIREMENTS

By

David P. Daugherty
David W. Coy
Research Triangle Institute
Energy & Environmental Research Division
Research Triangle Park, N. C. 27709

and

Dennis C. Drehmel
Industrial Environmental Research Laboratory
U. S. Environmental Protection Agency
Research Triangle Park, N. C. 27711

ABSTRACT

The efficiency and energy consumption expected from three fugitive control techniques--charged fog sprays, water sprays with additives, and building evacuation--are compared for applications in primary lead and copper smelters.

The control technique of charged fog water sprays is emphasized. These sprays enhance particulate collection by putting an electrostatic charge on fine water droplets. Available cost and energy consumption data were used to assess whether charged fog sprays are competitive.

Charged fog sprays were found to be less efficient than building evacuation, but also less expensive and less energy intensive by approximately a factor of 10. Charged fog sprays cannot replace conventional techniques in smelters such as secondary hooding or building evacuation because they are not suitable for the large volume, high temperature, turbulent air streams often encountered. They are better suited for smaller scale, localized emission sources, such as conveyor transfer points which contribute only a fraction of the fugitive particulate emissions.

WATER SPRAY CONTROL OF FUGITIVE PARTICULATES: ENERGY AND UTILITY REQUIREMENTS

BACKGROUND

Emissions from stacks and other so-called "point sources" have, in the past, been the main target of pollution control efforts. Windblown losses from storage piles, dust from material handling, fumes from hot metal transfer, and many other sources in the metals industry are not considered point sources. Instead, pollutants from these diffuse, nonducted sources are termed "fugitive emissions." This report compares three control techniques for fugitive emissions--charged fog sprays, water sprays with additives, and building evacuation--as they might be applied in lead and copper smelters.

Fugitive emissions from lead and copper smelters have serious impacts on more than just the total suspended particulate levels; they may also contain toxic metals for which separate ambient standards exist or are being contemplated. From admittedly rough base-data, estimates are made of the reduction of total suspended particulate emissions and the reduction of elemental lead emissions from smelters when fugitive control is applied. Primary lead and copper smelters were considered; secondary smelters were not.

The control technique of charged fog water sprays is emphasized in this report. These sprays enhance particulate collection by putting an electrostatic charge on fine water droplets. Building enclosure and evacuation is used as a basis with which water sprays are compared.

Several limitations on the scope of this project need to be mentioned. No sampling was done to measure fugitive emission rates or compositions; values used in the report are cited from prior publications. While use of charged fog sprays was discussed with plant engineers from smelters, no field trials were conducted. Instead, available cost and energy consumption data have been used to assess whether charged fog sprays can compete with other devices.

CHARGED FOG SPRAYS

Description of Operation

A spray of fine water droplets is a well-known means of dust removal. Various types of scrubbers rely on water droplets to sweep dust from the inlet gases, and water sprays have often been used in mining and material handling to reduce dust levels in the air. Charged fog sprays, as evaluated in this report, differ from conventional water sprays in that the droplets carry a charge of static electricity. Also, the droplets used for an electrostatic spray may be of a finer sizer. Since most fine particulates carry a natural electrical charge,[1] particle collection can be improved via electrostatic attraction if the water spray droplets

are charged to the opposite polarity. The charged water droplets then exert attractive forces on the oppositely charged particles and each droplet collects more particles as it travels through the dust-laden gas.

The water droplets in a spray may be electrostatically charged by several methods. Droplets may be charged via induction from a metal ring surrounding the spray (Figure 1a), via a charged needle in the spray (Figure 1b), or via direct electrical contact with the water (Figure 1c). In the third case, the spray nozzle must be insulated to prevent current leakage through the support structure or the water feedline. Hassler[2] has reported an autogenous charging method which does not require any voltage source. Droplet charges result from water-to-metal friction in a grounded spray nozzle (Figure 1d). While not requiring any voltage source, the method does require very pure, deionized water.

Collection Efficiency

Two areas important in evaluating sprays are collection efficiency and droplet evaporation. These areas have been treated by researchers in meteorology,[3-7] combustion[8,9] and spray drying.[10,11] For a detailed discussion of charged droplet collection, see the reports by Melcher and Sachar.[12,13]

For a single water droplet and a single dust particle, there are several forces acting simultaneously that affect the likelihood of particle capture. Fairly good theories exist which can predict how the various forces affect the efficiency of dust collection for well-controlled experimental conditions. In a practical application, the theories are less useful. Operating conditions vary, and it is very hard to choose representative values for many of the theoretical parameters: dust composition, loading, size, and charge; spray size and charge; ambient temperature and humidity; etc. The theory was used to project directional trends rather than to determine absolute values.

In an industrial application, the water spray droplets are charged and projected into the dusty gas stream. As the water droplets travel through the particulate cloud, they capture dust particles, and eventually settle out of the gas stream. Small particles which would otherwise remain suspended will settle out because they either have become attached to the larger water droplets or have agglomerated with other particles. Grover, et al.[7] determined the collision efficiency of a droplet/particle pair for the case of water droplets falling at terminal velocity through a stationary dust cloud. They calculated several cases while varying droplet size, humidity, electrical charge, etc. Cross-plots showing the effects of several variables are seen in Figure 2. These data can in principle be used to calculate overall collection efficiency of a spray.

The data in Figure 2 at first appear overwhelming, but on closer inspection several important conclusions can be drawn.

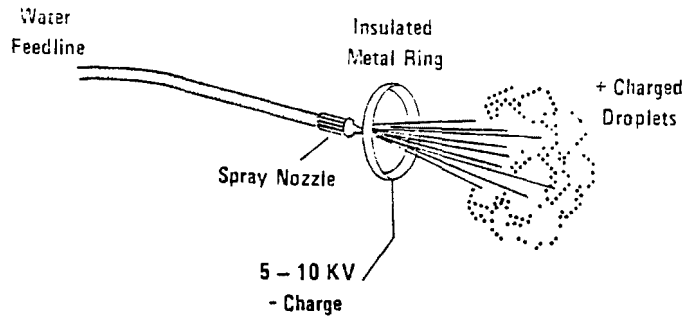

Figure 1a. Charge induced via metal ring.

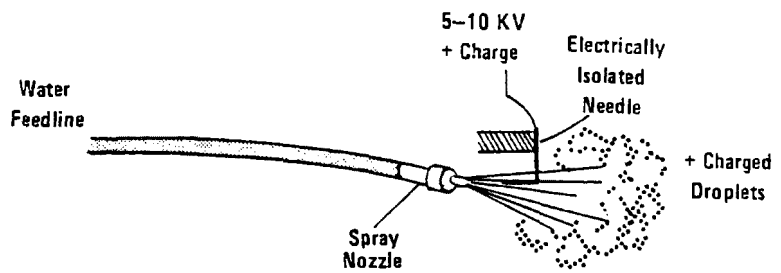

Figure 1b. Charging via needle.

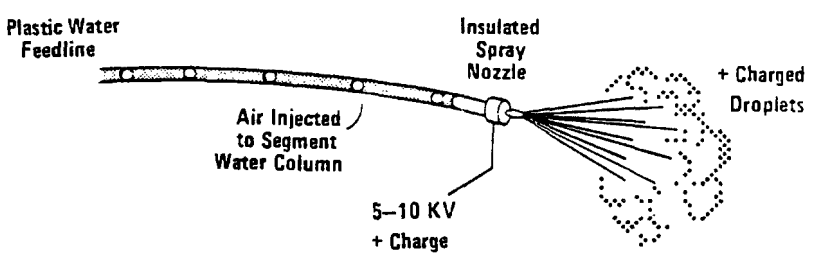

Figure 1c. Direct contact water charging.

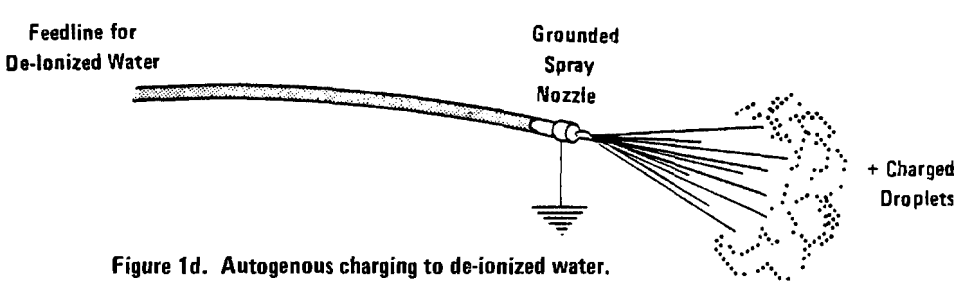

Figure 1d. Autogenous charging to de-ionized water.

Figure 1. Means of producing a charged water spray.

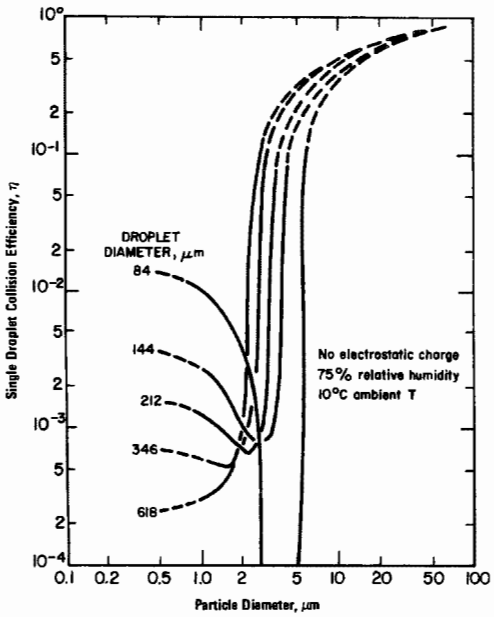

Figure 2a. Effect of droplet diameter on collision efficiency.

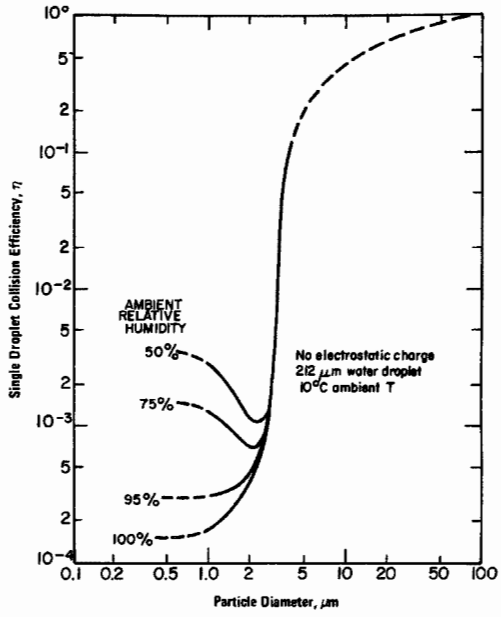

Figure 2b. Effect of relative humidity on collision efficiency.

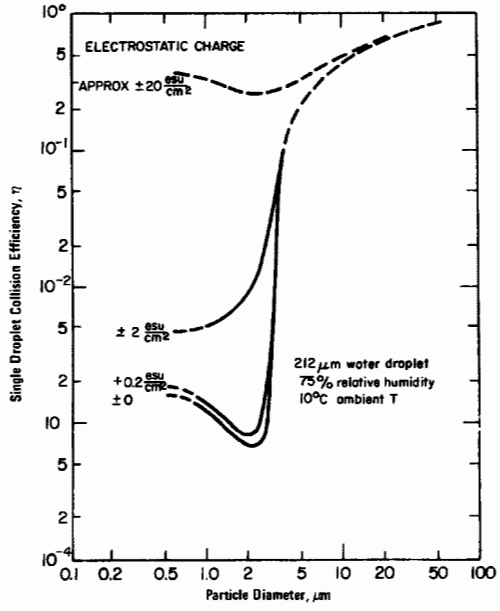

Figure 2c. Effect of electrostatic charge on collision efficiency.

Figure 2. Effects of particle size, droplet size, relative humidity, and electrostatic charge on collision efficiency.

Figure 2a shows how the collision efficiency is strongly dependent on particle diameter, decreasing from nearly 1.0 for 100 μm particles to a minimum value of about 0.001 for particles 2-3 μm in diameter. This minimum value in the collision efficiency curve implies that particles in the 2-3 μm size range, as are commonly found in smelters, will be much more difficult to collect than the larger particles. Notice also that for any given size particle, water droplet size influences the collision efficiency. Larger droplets tend to be more effective for larger particles while finer droplets are more effective for the submicron particles.

Figure 2b depicts how the ambient relative humidity affects the collision efficiency. For particles larger than about 3 μm, humidity has little effect, but for finer particles, drier environments theoretically improve the collision efficiency. In a real situation, the shorter droplet lifetimes at higher evaporation rates may override the collision efficiency improvements.

The most pertinent information in Figure 2 is that shown in Figure 2c--the effect of electrostatic charge on collision efficiency. For particle sizes typical in smelting applications (3 μm particles and 200 μm droplets) and for a particle of average excess charge (10e) and a strongly charged water droplet (2×10^8e), it is estimated that the collision efficiency curve will lie between the $Q = 2.0r^2$ and the $Q = 20r^2$ curves in Figure 2c.

There are two broad conclusions that are apparent from Figure 2c. First, the presence of electrostatic charges increases the collision efficiency for all size particles and eliminates the minimum around 2 μm. Secondly, charged sprays in industrial applications would have collision efficiencies roughly 5-10 times higher than uncharged sprays. Caution: these collision efficiencies are for single droplets only; they do not indicate that the overall collection of dusts by a spray will be 5-10 times higher. The relationship between single droplet collision efficiency and overall collection efficiency is presented next.

A relationship is needed between the collision efficiency and the other important variables such as flow rate, spray rate, system geometry, etc. In a paper on suppressing airborne coal dust, Cheng[14] presents such a relationship for overall efficiency of a water spray on a dust cloud:

$$E_o = 1 - \exp\left[\frac{-3\eta}{2D} \cdot \frac{Q_w}{Q_g} \cdot L\right]$$

where E_o = overall number of dust particles collected by the spray

η = single droplet collision efficiency as discussed above

D = droplet diameter

Q_w = water flow rate

Q_g = gas flow rate

L = a characteristic length which measures the length of the spray trajectory through the gas.

The equation is obviously an idealized version of the complex interaction between a spray and a moving dust cloud, but the form of the equation is instructive. By rearrangement, it is seen that log $1/(1-E_o)$ is directly proportional to η and to Q_{water} and inversely proportional to Q_{gas} when the droplet size and spray geometry are constant. These relationships were used to predict charged spray efficiencies from experimental results for uncharged commercial sprays.

Much of the experimental measurement of fine particulate removal by water sprays has been done by researchers attempting to reduce the level of respirable dusts in coal mines.[15] Uncharged sprays used in coal mining reportedly reduce respirable dust 20 to 60 percent with 30 percent seeming to be an average value.[16] By extrapolating 30 percent efficiency to a charged fog spray of equivalent geometry, water rate, and droplet sizes, a removal of about 80 percent of the respirable dust is predicted. Practically, the charged fog efficiency would not be as high because of much lower water application rates for charged fog sprays compared to conventional sprays. Lab scale experiments and limited commercial applications of charged fog sprays as cited by Hoenig[1] range mostly from 50 to 80 percent collection efficiency. This concurs with the above analysis.

There is an important limitation on the collection efficiencies cited so far--they have been in enclosed areas or on applications in moderately still air. Spray performance would not be anticipated to be very good for highly turbulent air streams which are often encountered in smelting for the following reasons.

The critical parameter in spray performance is the ratio of the spray rate to the volume of gas treated. For still air or confined spaces, the water droplets settle through the gas and collect and agglomerate particles. All together, the water from one small spray may be distributed through 2-4 m^3 of volume (30-100 ft^3). In an open, highly turbulent situation, both the dust particles and the water droplets would be dispersed outward and become more and more diluted into larger and larger volumes of gas. The effective volume of gas that must be treated is no longer just confined to the area around the spray, but also includes the entire area of turbulence which is greater by maybe a factor of 1,000 since volume goes up with the cube of distance. That is, if instead of being dispersed 1m (3 ft), turbulence disperses the particles and droplets 10 m (30 ft), the gas volume goes from 1 m^3 (9 ft^3) to 1000 m^3 (9000 ft^3). A second factor must also be considered in open, turbulent environments. When the water droplets that do collect particles eventually settle out of the air, the particulate will be spread over a large area and, in a sense, not be "collected" at all.

Another simplification in the above analysis has been that of no droplet evaporation. When sprayed into air, the small droplets formed by a charged fog device will evaporate unless the ambient air is saturated with water. In most cases of practical concern, the air is not saturated, and a droplet will completely evaporate after a certain period. The droplet lifetime determines the effective contact time between the spray and the dust-laden stream, and thus strongly influences the overall spray

efficiency. A short-lived droplet will disappear before collecting very many dust particles. Some work with charged fog sprays in high temperature enclosed systems is being done by Dr. Hoenig at the University of Arizona at Tuscon,[1] but at this time the results have not been analyzed.

The temperature and humidity of the ambient air are the two major variables affecting evaporation rate. Figure 3 depicts water droplet lifetime versus droplet diameter for three cases of practical significance: (a) 20°C (68°F), dry air which represents a plant compressed air supply; (b) 27°C (80.6°F) air with a relative humidity of 90 percent which represents a warm, moist environment; and (c) 170°C (338°F), dry air which represents the severe conditions around a copper converter or furnace taphole. Notice how, for a 200 μm droplet, the lifetime is of the order of 0.1 second for the high temperature (170°C) conditions. During such a short lifetime, the droplets can neither travel very far, nor encounter very many dust particles, and correspondingly poor dust collection would be expected under such conditions. Indeed a 100 μm drop falling at its terminal velocity in dry 170°C will only travel 7 cm (3 in.) before evaporating.

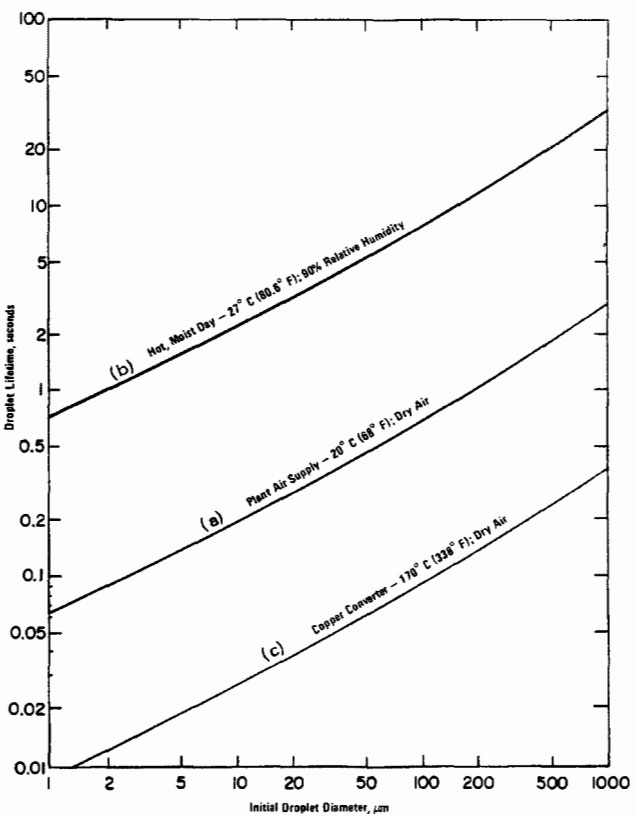

Figure 3. Lifetime of water droplets traveling at their terminal velocity.

To summarize the performance of charged fog sprays: (1) While uncharged sprays have a minimum in their collection efficiency at about 2 μm particle diameter, there is not any such minimum for charged sprays. Thus some improvement or collection of respirable dust is expected from charging. (2) The charged fog sprays are best suited to localized sources of dust suspended in a low velocity or stationary gas stream. (3) The combination of high temperatures and excessive gas turbulence rule out charged fog sprays for areas such as copper converter leakage or furnace taphole emission control. (4) At reasonable water application rates, the charged fog sprays are unlikely to have efficiencies approaching 90 percent. Maximum overall collection efficiencies on the order of 60 percent are more likely.

Cost and Energy Consumption

The total installed costs were estimated for three versions of charged fog sprays. The costs of a small charged fog spray, coverage area about 1 m by 2 m (2 ft by 6 ft) were based on information provided by the Ransburg Corporation. (At the time, Ransburg manufactured the only commercial charged fog device. Since then, Ritten Corporation, Ltd. has acquired the charged fog spray business from Ransburg.) Prices were predicted for a larger scale charged fog device, with a coverage area of approximately 2 m by 6 m (6 ft by 20 ft.). Such a device had not been commercialized and no sales prices was available. An air-atomized spray was estimated, as was a version of the larger charged fog spray which uses an integral high pressure water pump for hydraulic atomization. Also, estimates were made for a mobile version of the spray (no air source; D.C. battery powered) with an intermediate coverage area.

The total cost for a charged fog spray device consists of: (a) purchased equipment cost; (b) installation materials; (c) installation labor; (d) auxiliary equipment costs; and (e) indirect costs. The charged fog sprays themselves are the largest component of purchased equipment cost. Some additional investments is associated with auxiliary equipment needed for the fog sprays. A pro rata share of a plant air compressor (based on air consumption) is charged to each fog spray. Notice that the share of compressor costs is a large portion of the costs for air atomized systems. Table 1 summarizes the cost estimates for each spray type. A complete discussion of the estimate bases is in a report by Daugherty and Coy.[17]

In addition to the capital investment associated with operating a charged fog spray device, there are utility requirements such as electricity, water, and compressed air which must be considered. Table 2 summarizes the utility requirements for operation of a charged fog spray device converted to an equivalent kilowatt basis. By far the largest energy requirements are for the compressed air used to atomize and project the spray droplets. The energy required to charge the droplets is minor and is not representative of the total energy consumption of the charged fog device.

TABLE 1. SUMMARY OF TOTAL ESTIMATED COSTS FOR CHARGED FOG SPRAY DEVICE

Item	Cost per charged fog spray device			
	Small fog spray	Large fog spray (with air)	Large fog spray (no air)	Mobile fog spray
Purchased Equipment	$1,535	$ 2,454	$4,400	$2,400
Installation Materials	97	97	83	0
Total Materials	**1,632**	**2,551**	**4,483**	**2,400**
Installation Labor	318	318	292	75
Indirect Costs				
Construction Overhead	223	223	204	53
Engineering	228	357	628	336
Taxes and Freight	130	204	359	192
Total Indirects	**581**	**784**	**1,191**	**581**
Direct and Indirect Excluding Auxiliary Equipment	2,531	3,653	5,966	3,056
15% Contingency	380	548	895	458
Auxiliary Equipment	1,453	7,380	230	0
GRAND TOTAL	**$4,364**	**$11,581**	**$7,091**	**$3,514**

TABLE 2. ENERGY CONSUMPTION FOR OPERATING A CHARGED FOG SPRAY DEVICE

Item	Energy Requirement, Equivalent Kilowatts per Charged Fog Device	Basis for Calculations
Pumping Energy for Water		Water from centrifugal pump at 100 psig discharge pressure, except hydraulically atomized version has 600 psig reciprocating pump; 0.25 gpm for small fog spray; 2.5 gpm for large fog spray. Mobile fog spray assumed to have same requirements as hydraulically atomized large fog spray.
Small fog spray	0.02	
Large fog spray (air atomized)	0.16	
Large fog spray (hydraulically atomized)	1.59	
Mobile fog spray	1.59	
Compression Energy for Air		Air from plant air compressor discharging at 100 psig; 10 scfm for small fog spray; 50 scfm for large spray; no air required for hydraulically atomized version; assumed no air required for mobile fog spray.
Small fog spray	2.66	
Large fog spray (air atomized)	13.32	
Large fog spray (hydraulically atomized)	0	
Mobile fog spray	0	
Electrical requirements for charging		Charging requirement for small fog spray from manufacturer; requirement for large spray prorated by water consumption. Mobile spray requirement assumed equal to large fog spray.
Small fog spray	0.03	
Large fog spray (both versions)	0.30	
Mobile fog spray	0.30	
Total Equivalent Kilowatts		
Small fog spray	2.71	
Large fog spray (air atomized)	13.78	
Large fog spray (hydraulically atomized)	1.89	
Mobile fog spray	1.89	

WATER SPRAYS WITH ADDITIVES

It has been suggested that water sprays containing surface active agents would be more effective in collecting entrained dust than pure water sprays. The equipment for such a spray system would consist of hydraulic or air atomization spray nozzles, a reservoir and metering pump for injecting the additive into water, and the appropriate connecting piping. Sprays with additives have been successful in reducing dust emitted from conveyor belts and are used in quarries and mining operations.[18,19]

Reports conflict on whether additives improve particle collection by water sprays. Much of the conflict comes from a misunderstanding of the mechanisms working to reduce total particulate levels. There are two ways in which water suppresses particulate: (a) by wetting and immobilizing dust before it becomes airborne, and (b) by removing already suspended airborne particles.

To suppress dust formation, water is sprayed onto the surface of a solid material, for example, ore concentrate on a conveyor belt. The water ideally spreads into the interstices of the solid, and wets the surface of the fine particles. Thus, much of the dust adheres to the larger lumps of material. The wetted solid then has less tendency to generate dust as it is handled since the small, easily entrained particles have been immobilized. However, since water has a very high surface tension (roughly 70 dynes/cm), it often is not effective in spreading into the solid material and forming a water film around dust particles. Instead it "beads" on the solid surface and results in poor dust suppression. The high surface tension interferes with the wetting, spreading, and penetrating needed for control.

To improve the efficiency of suppression, various compounds known as surfactants, or wetting agents, are added to the water. Surfactants can reduce the surface tension to around 30 dynes/cm and improve the wetting and penetration of the water. The levels of surfactant needed to achieve such a surface tension reduction are very low--0.03 to 0.1 percent.

Water sprays can also be used to try to remove particles which have already become airborne. The droplets from a water spray collect and coalesce the fine entrained particles and increase their settling rate. It has been suggested that surfactants would improve particle removal for this case also by allowing the dust particle to penetrate the water droplet more easily. However, there is little evidence that this occurs. Most investigators report surfactants do little to suppress airborne respirable dust.[20] Walton and Woolcock[21] exposed equal size droplets to the same dust concentration; one droplet contained a wetting agent and the other did not. They found no significant difference in collection efficiency for the two drops. In a recent study, Woffinden, et al.,[22] reported only small effects on collection efficiency, if any, can be attributed to surface tension changes. Indeed, the effect of adding surfactant may be slightly unfavorable.[23]

In summary, water sprays with additives can be used to reduce dust entrainment from hard-to-wet solids, but have an advantage over conventional water sprays only for dusts which have not yet been suspended. Additives do not substantially improve the collection of particles which have already become airborne. Thus, they are not substitutes for charged fog spray applications. The addition of surfactants or other additives should be considered for such applications as conveyor belts and storage bins where the product is not water-sensitive and can be kept moist to reduce dust entrainment from the solid.

BUILDING EVACUATION

Description of Operation

One method of eliminating fugitive particulate emissions from smelting operations which are inside a building is to install ductwork on the building roof and large fans to draw the particulate-laden gases from the building and pass them through a collection device. A baghouse is the typical control device selected for building evacuation. Any fugitive particulates escaping inside the smelter building are collected by the evacuation system and the maximum overall control efficiency for fugitive emissions is quite high from 90 to over 95 percent.

While attractive from an environmental control viewpoint, building evacuation has several serious drawbacks. By enclosing the building, the emissions can only escape through the roof ducts and high levels of particulate, SO_2, etc., may build up inside in the workplace and cause occupational health concerns. An evacuation system may collect enough gas to sufficiently ventilate the <u>overall</u> workplace and yet still have unacceptable <u>local</u> pollutant concentrations because of "dead spots" in the air flow pattern. Figure 4 illustrates this effect. In smelting operations, such dead spots may create excessive temperatures as well as high pollutant levels in some locations.

A second drawback to building evacuation systems is the large airflow required and the attendant high energy consumption by the blower. Generally, the closer a hood to the emission source, the less evacuation air is required. For the particular case of building evacuation, the intakes are located far from the particulate sources and large volumes of air with low particulate loadings are collected.

Building evacuation systems have been successfully applied to electric arc furnace melt shops in the iron and steel industry.[24,25] One converter building in the copper industry has been fitted with a building evacuation system[26] although there are no known large building evacuation systems in the lead smelting industry. The evacuation system in the copper smelting plant has caused severe heat and SO_2 levels in the upper areas of the building. This may be due to inadequate fan volumes and the difficulty in designing for good air flow patterns in a retrofitted application.

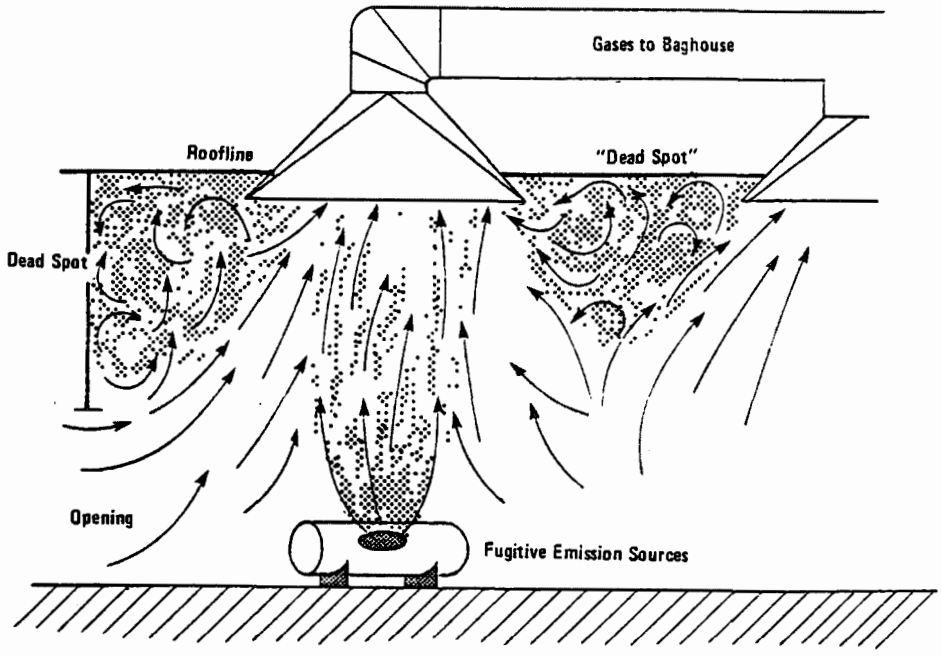

Figure 4. Schematic of "Dead Spots" in building evacuation system.

Cost and Energy Consumption

The Arizona Department of Health Services[26] considered building evacuation costs for a "typical," as defined by the U.S. Bureau of Mines,[27] 900,000 Mg/y (100,000 tons) per year copper smelter. They used 1.5 minutes per change for an air flow of 2,200 acfm.[28] They estimated an initial investment of $6,808,000 (3.09 $/acfm) and energy consumption of 6000 kW for a building evacuation system on a converter building. The costs and utilities for building evacuation in a lead smelter are similar to those for a copper smelter. However, it is felt that a larger volume of building space must be evacuated in a lead smelter. The evacuated building volume was assumed to be 150 percent of the building volume for copper smelting. Utility requirements were prorated directly by 1.5 to give 9000 kW while capital costs were prorated using the 0.6 power rule to give $8,683.000.

COMPARISON OF CHARGED FOG SPRAYS WITH BUILDING EVACUATION

The number of sprays needed to control all applicable fugitive emission sources was estimated for both copper and lead smelters. These quantities were used to estimate the cost and energy consumption of charged fog sprays applied throughout copper and lead smelters.

For application of charged fog sprays to a lead smelter, estimated capital investment totals $311,000. The energy consumption for the charged fog sprays in a lead smelter would be 417 kW. For building

evacuation, the estimated capital costs are $8,683,000 and the energy consumption is 9000 kW.

Capital investment (including installation and all auxiliary equipment) for application of charged fog sprays to a copper smelter is estimated to be $366,000. The energy consumption for the charged fog sprays in a copper smelter would be 450 kW. For building evacuation, the corresponding costs are $6,808,000 and the utilities usage is 6000 kW.

While both capital investment and energy consumption are higher for building evacuation, the reduction of total particulate and elemental lead emissions are also greater for building evacuation because of the higher collection efficiency and the larger number of sources covered by a building evacuation system. To compare obtainable reductions, Table 3 lists what are, by all accounts, rough estimates of the emission reductions expected from the application of charged fog sprays and those from the application of building evacuation. Several assumptions were made in compiling Table 3. The charged fog sprays were considered inapplicable for hot, turbulent areas such as molten metal transfer, lead sintering, and copper converter leakage. Building evacuation was not considered to be effective for reducing emissions from loading onto or out of storage

TABLE 3. COMPARISON OF CHARGED FOG SPRAYS WITH BUILDING EVACUATION

Item	Lead Smelting	Copper Smelting
Reduction in fugitive total particlate emissions		
by application of charged sprays	30%	20%
by application of building evacuation	45%	40%
Reduction in fugitive elemental lead emissions		
by application of charged sprays	40%	35%
by application of building evacuation	75%	65%
Estimated capital investment		
for application of charged sprays	311 k$	366 k$
for application of building evacuation	8,683 k$	6,808 k$
Electrical requirement		
for application of charged sprays	417 kW	450 kW
for application of building evacuation	9,000 kW	6,000 kW

piles. From fugitive emission estimates and typical composition data, the reduction of particulate and elemental lead emissions were made source-by-source and totaled.

Superficially, the figures in Table 3 indicate charged fog sprays to be a more cost-effective means for pollution control than building evacuation--10 to 20 k$ required for each percentage reduction in emissions by sprays versus 100 to 200 k$ required for each percent reduction by building evacuation. Similarly the electrical requirement is much lower for the charged fog sprays--15 to 30 kW for each percentage reduction versus 150 to 200 kW for the building evacuation system.

However, in spite of the apparent attractiveness of charged fog sprays, the authors feel that there are several practical problems which prevent them from supplanting building evacuation or secondary hooding as fugitive control techniques. The first and main objection is their limited applicability. Water sprays are only suitable when the process can tolerate water, when the emissions are from localized sources, when there is not a great deal of air turbulence, and when the air is not at high temperatures. These limitations rule out charged sprays for such major sources of fugitive emissions as converter leakage, sintering discharge, and metal tapping, pouring, and casting.

A second major limit on charged fog spray control is the collection of the agglomerated particles. It is usually assumed that once suspended particles collide with a water droplet, they are permanently removed from the atmosphere. This is a valid assumption for such applications as conveyor transfer points in moderately still air where the agglomerated dust settles out and is returned to the process. However, when particles, for example, from a railcar unloading station are contacted with spray droplets, they may settle out on the ground, dry out, and be reentrained. Particle control has only been temporary. The extent of this phenomenon is a major uncertainty for future large scale industrialized applications of charged fog sprays.

LOCALIZED HOODING

One control option not yet considered in this report is localized hooding at fugitive emission sources. Figure 5 shows two options for controlling emissions from a railcar unloading station--a curtain of charged fog sprays and a push-pull collection system. This application gives a direct comparison of charged fog sprays with another control technique on the same source. Using recommended push-pull design procedures[29] and assuming the same utility requirements and cost per cubic foot as was used for building evacuation, the following estimates were made: (a) 5.8 kW and $6,500 per lineal foot of opening for a push-pull system, and (b) 2.3 kW and $1,900 per lineal foot for the charged water spray curtain. Neglecting the potentially serious problem of particle reentrainment after spray evaporation, the charged sprays could in theory collect about half of the fugitive dust less expensively and with less

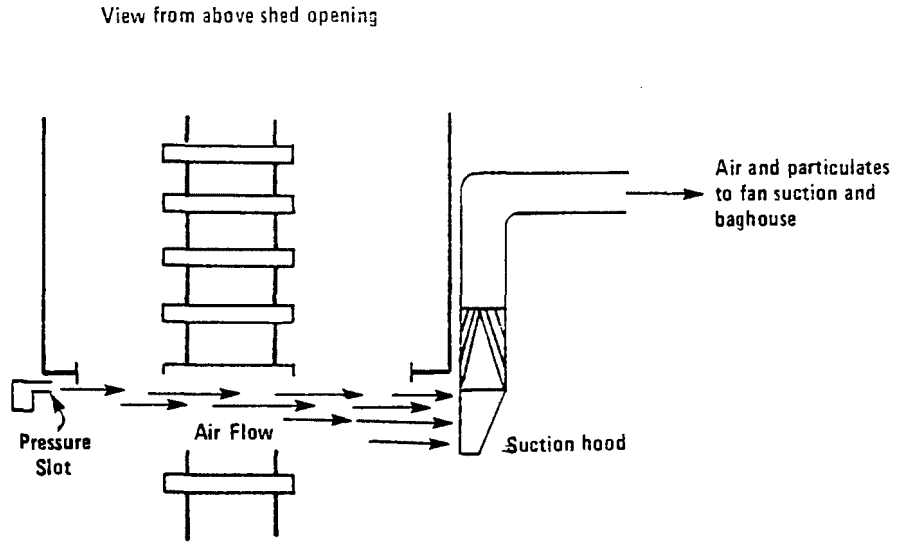

Application of push-pull local hooding.

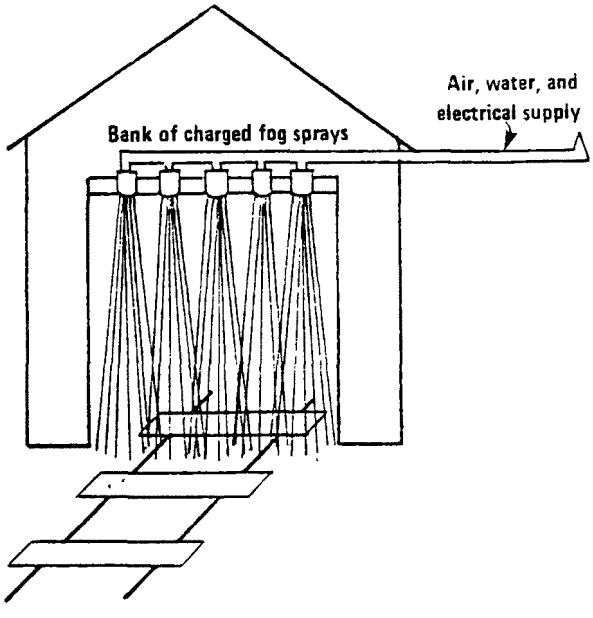

Application of charged fog spray curtain.

Figure 5. Push-pull local hooding versus charged fog spray curtain.

energy than local hooding. However, it is pointed out that the sprays can never collect more than about half the particulate. If greater efficiency is needed, some other control method must be used regardless of any extra expense.

EPILOGUE

Building evacuation and charged fog sprays have been treated as either/or control techniques. It makes more sense to consider them as complementary control devices instead of mutually exclusive techniques. For high temperature, large scale turbulent emissions, either building evacuation or secondary hooding is required to collect the fugitive emissions. Charged fog sprays are better suited for smaller, localized emission sources. Two applications for which charged sprays may be particularly advantageous over other controls are: (a) mobile sources such as front-end loaders where any other type of control is impossible, and (b) areas where personnel exposure must be reduced without impeding access to equipment such as sanders or grinding wheels.

REFERENCES

1. Hoenig, S. A., Use of Electrostatically Charged Fog for Control of Fugitive Dust Emissions, U. S. Environmental Protection Agency, EPA-600/7-77-131, NTIS No. PB 276-645/AS, November 1977.

2. Hassler, H. E., "A New Method for Dust Separation Using Autogenous Electrically Charged Fog," Journal of Powder and Bulk Solids Technology, v.2, n.1, pp. 10-14, Spring 1978.

3. Shafrir, U., and T. Gal-Chen, "A Numerical Study of Collision Efficiencies and Coalescence Parameters for Droplet Pairs and Radii up to 300 Microns," Journal of the Atmospheric Sciences, v.28, pp. 741-751, July 1971.

4. Slinn, W. G. N., and J. M. Hales, "A Reevaluation of the Role of Thermophoresis as a Mechanism of In-and Below-Cloud Scavenging," Journal of the Atmospheric Sciences, v.28, pp. 1465-1471, November 1971.

5. Lai, Kuo-Yann, et al., "Scavenging of Aerosol Particles by a Falling Water Drop," Journal of the Atmospheric Sciences, v.35, pp. 674-682, April 1978.

6. Wang, P. K., and H. R. Pruppacher, "An Experimental Determination of the Efficiency with Which Aerosol Particles are Collected by Water Drops in Subsaturated Air," Journal of the Atmospheric Sciences, v.34, pp. 1664-1669, October 1977.

7. Grover, S. N., et al., "A Numerical Determination of the Efficiency with Which Spherical Aerosol Particles Collide with Spherical Water Drops Due to Inertial Impaction and Phoretic and Electrical Forces," Journal of the Atmospheric Sciences, v.34, pp. 1655-1663, October 1977.

8. Ranz, W. E., "On the Evaporation of a Drop of Volatile Liquid in High-Temperature Surroundings," Transaction of the ASME, pp. 909-913, 1956.

9. Ranz, W. E., and W. R. Marshall, Jr., "Evaporation from Drops," Chemical Engineering Progress, v. 48, pp. 141-173, 1952.

10. Marshall, W. R., Jr., "Evaporation from Drops and Sprays," Atomization and Spray Drying, Chemical Engineering Monograph Series No.2, v.50, 1954.

11. Masters, I. Spray Drying, 2nd ed. John Wiley and Sons, New York, 1956.

12. Melcher, J. R., and K. S. Sachar, "Charged Droplet Technology for Removal of Particulates from Industrial Gases," Rep. No. APTD-0868, NTIS No. PB 205-187, August 1971.

13. Melcher, J. R., and K. S. Sachar, "Charged Droplet Scrubbing of Submicron Particulate," U. S. Environmental Protection Agency, EPA-650/2-74-075, NTIS No. PB 241-262, August 1974.

14. Cheng, L., "Collection of Airborne Dust by Water Sprays," Industrial Engineering/Chemistry, Process Design and Development, v.12, n.3, pp. 221-225, 1973.

15. Walton, W. H., and A. Woolcock, "The Suppression of Airborne Dust by Water Sprays," International Journal of Air Pollution, v.3, pp. 129-153, 1960.

16. Courtney, W. G., and L. Cheng, "Control of Respirable Dust by Improved Water Sprays," Respirable Dust Control, Proceedings: Bureau of Mines Technology Transfer Seminars, U. S. Bureau of Mines Information Circular No. IC/8753, U. S. Department of the Interior, Washington, DC, pp. 92-108, 1977.

17. Daugherty, D. P., and D. W. Coy. Assessment of the Use of Fugitive Emission Control Devices. U. S. Evnironmental Protection Agency, EPA-600/7-79-045, NTIS No. PB 292-748, Cincinnati, OH. 85 pp, February 1979.

18. Johnson March Corporation, Dust Control News, vol.1, Philadelphia, PA, Fall 1978.

19. Emmerling, J. E., and R. J. Seible, "Dust Suppression with Water Sprays During Continuous Coal Mining Operations," U. S. Bureau of Mines Report of Investigation 8064, Washington, DC, 1975.

20. Kobrick, T., "Water as a Control Method, State-of-the-Art, Sprays and Wetting Agents," Paper in Proceedings of the Symposium on Respirable Coal Mine Dust, Washington, DC, November 3-4, 1969, Bureau of Mines IC 8458, pp.123-133, 1970.

21. Walton, W. H., and A. Woolcock, "The Suppression of Airborne Dust by Water Spray," International Journal of Air Pollution, v.3, pp. 129-153, 1960.

22. Woffinden, G. J., et al., Effects of Interfacial Properties on Collection of Fine Particles by Wet Scrubbers, U. S. Environmental Protection Agency, EPA-600/7-78-097, NTIS No. PB 284-073, Washington, DC, June 1978.

23. Emory, S. F., and J. C. Berg, "Surface Tension Effects on Particle Collection Efficiency," Appendix to Reference 22.

24. Kaercher, L. T., and J. D. Sensebaugh, "Air Pollution Control for an Electric Furnace Melt Shop," Iron and Steel Engineer, pp. 47-51, May 1974.

25. Research Triangle Institute, "Trip Report: Crucible, Inc., Midland, PA," Research Triangle Institute, Research Triangle Park, NC, August 4, 1977.

26. Billings, C. H., "Second Annual Report on Arizona Copper Smelter Air Pollution Control Technology," Arizona Department of Health Services, Phoenix, AZ, April 1978.

27. Hayashi, M. et al., Cost of Producing Copper from Chalcopyrite Concentrate and Related to SO_2 Emission Abatement, U. S. Bureau of Mines Report of Investigations No. RI/7957, U. S. Department of the Interior, Washington, DC, 1974.

28. Personal communication with C. H. Billings, Arizona Department of Health Services, Phoenix, AZ, November 1978.

29. American Conference of Governmental Industrial Hygienists, Industrial Ventilation, 9th ed., Edward Brothers, Inc., Ann Arbor, MI, 1966.

THE CONTROL OF DUST USING CHARGED WATER FOGS

By:

Stuart A. Hoenig
Department of Electrical Engineering
University of Arizona
Tucson, Arizona 85721

ABSTRACT

In the past year the emphasis has been on the development of new electrostatic technology to reduce fugitive dust emissions. An electrostatic fence designed to reject dust while permitting ventilation air to flow in and out of a plant has been demonstrated. A system for pushing acid fume toward a collector has been demonstrated; the collector operates electrostatically and is quite effective in removing the fumes from the air. The same system has been tested with lead fume and proved to be quite effective.

Arrangements have been made to install a spinning cup fog thrower on a front loader and an industrial sweeper. We hope that the fog dispensing systems will significantly reduce the dust generated by this type of industrial machinery.

Another corona discharge system, for destruction of germs and toxic organic materials, has been demonstrated and we plan a series of tests in a medical environment.

An electrostatic flow enhancement system designed to improve the efficiency of a standard dust hood has been demonstrated and we are negotiating to install a unit of this type in a hood on campus.

The studies of the improved dust cyclone are continuing; we have been making further improvements with the hope of obtaining better efficiency. We are looking at techniques for raising the efficiency of low energy wet scrubbers. The addition of charged fog has made some improvement and we hope to add an ionizer to provide further gains.

THE CONTROL OF DUST USING CHARGED WATER FOG

INTRODUCTION

The University has been involved for some four years in a series of programs to develop new devices for control of industrial dust, fume and smoke. One technique, the use of charged water fog to induce agglomeration and fall-out of dust, has reached the commercial stage. The Ritten Corporation, Ltd. of Ardmore, Pennsylvania is marketing Fogger I, II and III. A variety of applications have been demonstrated, with permanent installations in foundries, cement plants and copper smelters. The details of fog application to some fifty different dusts and the methods of measurement have been reviewed in Hoenig (1977)[1] and (1979)[2].

A dust controlled hand grinder/sander system has been developed and tested at a major automobile company laboratory for control of lead dust during the sanding of solder filler. The results have been most satisfactory in that the air at the workman's breathing level was below the allowed OSHA minimum at all times during the grinding process. The units will be marketed by the ARO Company of Bryan, Ohio. The details of the design and testing at the University of Arizona were reviewed in Hoenig (1979)[2].

In the last year we have begun a study of the use of charged fog to suppress dust and SO_2 under simulated smelter stack conditions. Other investigations have involved the use of charged fog to improve dust collection in reverse flow cyclones and to suppress dust raised by industrial sweepers and front loaders, Hoenig (1979)[2].

Another area of interest has been the development of improved dust/smoke collection systems. Based on electrostatic techniques the details of this work will be discussed below.

RECENT DEVELOPMENTS

Cyclone Improvements

Our major interest in this period has been the demonstration of new techniques to reduce fugitive respirable dust, fume and smoke. One program has involved the improvement of conventional reverse flow cyclones by the addition of charged fog and certain mechanical modifications. Typical results are shown in Figure 1 where we have plotted the University of Arizona data versus the best Stairmand Cyclone results. This data was taken on one of the most difficult materials to handle, cotton trash, and demonstrates the potential for

improvement of dust cyclones. A complete discussion of the apparatus, test procedure, etc., was given in Hoenig (1979)[2]. At present we are testing other cyclone modifications that promise even greater improvements. It is worth noting that cyclones are low cost, simple, low pressure drop devices that can operate over a wide range of temperatures. If they could be improved to "catch" fine particulates by some sort of "add on" system the effect on fugitive dust emission control costs would be significant.

Electrostatic Technology

Another area of interest has been electrostatic hoods and screens that might be used to collect smoke/dust in areas where conventional hoods are precluded by crane movements or other manufacturing obstacles. The major advantages of a purely electrostatic system is the fact that it can be designed with chain mail mesh and a series of rings much like a hoop skirt. This allows the unit to be folded up or collapsed when the crane comes by. In Figure 2 we show a system of this type with smoke from burning C_2H_2. On the left the power is "off" while on the right the power is "on". It is clear that when the power is "on" the smoke is compressed and carried out of the top of the hood. We anticipate that a hood of this type with an attached elephant trunk to carry off the fume would be most useful in many industrial environments. It is worth noting that while the hood operates at some 15,000 volts ALL EXPOSED METAL SURFACES ARE AT GROUND POTENTIAL.

Another system of this type is an electrostatic screen designed to "push" or "pull" smoke and dust from the point of generation to an area where a permanent control system can be installed. The system is built up from a number of phonograph needles (corona points) and a grounded metal screen. The point to screen discharge produces a strong ion current and a significant "electric wind".

One application, to control of acid fume from a hot dip tank, is shown as a scale model in Figure 3. The fumes are generated by an acid reaction in the baking dish; the screen on the right is a "pusher", the one on the left is a "puller". In the upper photograph the power is "off" and on the bottom it is "on". When the power is "on" the fumes are pushed to the left and deposited on the left hand collector screen. In a large scale industrial system the deposited material would be periodically washed off with a spray of detergent solution. It is worth noting again that in an industrial system all exposed surfaces would be at ground potential and that appropriately designed insulators, Hoenig (1979)[2], would allow the system to operate even in a "wet, acid" environment.

There are a number of other applications of this system including the collection of lead fume which has been a severe problem in the non-ferrous industry. Initial studies indicate that the lead fume is carried over to the collector and deposited for later removal by water sprays. A larger test system is under construction.

These electrostatic systems have other uses; in one test a small (76.2 mm ID by 267 mm long) unit was challenged with bacillus subtilis at a flow rate of 30 l/min. The effluent gas from the system was bubbled through sterile

water to collect the bacteria; the water was sampled after a five minute run and analyzed microscopically for bacteria. After a five minute run with the power "off" the bacteria content was some 2800 per ml; after a similar run with the power "on" (-9000 V at 0.5 mA) the bacteria level was zero. This suggests that the corona discharge was effective in destroying bacteria and as such might have applications in hospital ventilation systems or recombinant DNA facilities where it is important that toxic materials be effectively destroyed.

In another test the same system was exposed to a flow of methyl parathion as a typical example of a cholinesterase reducing pesticide/nerve gas. With the system "off" some 12 micrograms of parathion was collected in a benzene solution after five minutes of operation. With the power "on" the parathion level was less than 0.1 microgram (the limit of detection).

In both these applications it is important to note that the corona discharge system does not have the pressure drop of conventional fabric or charcoal filters; with proper design the electric wind actually "pushes" the flow through the system. Electric wind velocities as high as 650 to 1000 FPM (198 to 305 m/min) have been observed and other applications of this technology will be discussed below.

Another application of the corona system involves collection of oil smokes not easily precipitated by conventional equipment. In Figure 4 we show a typical system operating on oil smoke. With a two element unit at 15,000 volts the reduction in oil smoke, at a flow velocity of some 300 FPM (91 m/min), was over 95%. A large scale test of this system on tinter frame oil smoke in a cotton mill is under way at the moment. Once again we would suggest that in a commercial installation the collection plates could be washed by a detergent spray when cleaning was required. The use of shielded insulators, Hoenig (1979)[2], allows the system to operate for many hours in heavy smoke before any voltage breakdown occurs. Since the corona discharge is generated by points instead of wires the stored energy is quite small and there is little danger that the system will explode or catch fire.

One of the problems with fugitive dust is its escape via open windows in industrial plants. Ideally the entire plant should be vented through a baghouse but in many cases this can be prohibitively expensive. We have been looking at systems that might allow windows to be used for ventilation while at the same time preventing the escape of dust. In Figure 5 we show a simple high voltage dust control system that might be installed in a factory window. When the system is off and dust (AC Fine) is blown against the screen the dust passes through the screen quite easily. When the power is on the dust is repelled even at a velocity of some 650 FPM (198 m/min).

The effect depends upon the generation of electrons by the corona discharge. These electrons move outward in the electrostatic field generated by the corona points and charge dust particles approaching the system. These charged particles are then repelled by the field of the corona points. As a result the airflow through the screen is almost unaffected while the approaching dust particles are strongly repelled.

We are considering a system of this type for application at factory windows or fan exhausts that are important for ventilation. The addition of an electrostatic screen would prevent the dust leakage that results in EPA citations while at the same time permitting the airflow needed for temperature or humidity control.

Another electrostatic system of interest has involved an airflow generator for use on a fan driven hood. Hoods are widely used in industry but the aerodynamic design is such that the intake velocity at the edge of the hood is usually too low and collection is poor. We have designed an electrostatic wind device for installation at the edge of the hood to increase the velocity in this critical area. Testing of this system has just begun but the results are encouraging. A photograph of the system is shown in Figure 6. On the left side the electrostatic system is "off" and the smoke (ammonium chloride) is being drawn in by the fan alone at a velocity of some 30 FPM (9.1 m/min). In the right hand photograph the electrostatic system is "on" and the flow velocity has risen to some 82 FPM (25 m/min).

One advantage of a system of this type is that it can be an "add-on" to an existing hood of almost any size and is therefore more likely to be used in industry than the larger electrostatic hoods and curtains that would require special facilities and equipment. It should be noted that the application discussed above made use of a hood with a rather low inlet velocity. In an industrial hood with a higher (100 FPM) inlet speed we would expect to make use of several electrostatic screens in series to increase the net velocity.

Tagging Smelter Dust

As part of our work with local industry we have helped to develop a system for marking industrial dust as it goes up the stack so that it can be distinguished from windblown particulates of similar size and chemical composition. The technique involves a high temperature gas burner and spraying system. The sprayers dispense a lithium acetate solution into the flame to provide a cloud of lithium particles. Preliminary tests in the campus Anaconda Stack Simulator indicate that the particles "stick" to the stack dust and are easily identified by atomic absorption or flame spectrometry. The system will allow the company in question to demonstrate what fraction of the local dust is windblown versus stack generated.

Improvement of Wet Scrubber Operation

Discussions with industrial air pollution control personnel have indicated that many fugitive dust citations are due to poor operation of typical low energy wet scrubbers. Our own experience with a 300 ACFM Buffalo Forge unit indicated that it does not adequately collect the fine material (below 5 micrometers). Since these units are widely used it was of some interest to see if the charged fog technology might be used to agglomerate the fine particulates before they got to the scrubber and thereby increase scrubber efficiency.

For this test an induction charging system similar to the Ritten Fogger I was placed some fifteen feet upstream of the scrubber to permit a contact time of some 2.2 seconds. The dust coming from the scrubber was sampled under a

variety of conditions and the results are shown in Figure 7. There was a significant improvement with charged fog and we suggest that techniques of this type might find a place in the control technology of wet scrubbers.

Another technique might involve charging the dust before it gets to the scrubber since many studies, Loffler (1978)[3] and Reid (1978)[4], have indicated that charging increases collection efficiency. For this purpose we constructed a 75 point corona source that fits in the 12 inch diameter pipe ahead of the wet scrubber. Experiments with this system have just begun but it appears that this system is effective and that the contact time is not nearly as long as that required for the charged fog generator.

The Spinning Cup Fog Thrower

This system consists of a rapidly rotating cup to break liquid water into fine droplets, a series of fans to provide an air flow to push the droplets in the proper direction plus the necessary power supplies, motor, etc., needed to operate the system. This fog throwing device is unique in that it can accept water with a high solids content without clogging and is capable of scaling up or down over a vast range.

The details of the work to date have been reported in Hoenig (1979)[2]. Here we shall simply note that arrangements have been made to mount a unit of this type on a front loader and an industrial sweeper. The unit will be "on" only during the loading and unloading cycles suggesting that some 8 to 10 gallons of water will be needed during an 8 hour shift. All power for the motor oil will be taken from the 12 V DC system on the loader. On-off control will be actuated by the regular vehicle hydraulic system.

Industrial Application of the Charged Fog System

One interesting application of the larger (Fogger II) units involves the suppression of dust under industrial conditions where high temperatures and heavy dust flows are involved. In Figure 8 we show a smelter application; on the top the fog is "off" and there is a heavy flow of dust into the smelter while on the bottom the Fogger II is "on" and the dust is completely suppressed.

REFERENCES

1. Hoenig, S. A. Use of Electrostatically Charged Fog for Control of Fugitive Dust Emissions. EPA-600/7-77-131, November 1977. Available from NTIS, Springfield, Virginia 22161.

2. Hoenig, S. A. Fugitive and Fine Particle Control Using Electrostatically Charged Fog. EPA-600 7-79-078, March 1979. Available from NTIS, Springfield, Virginia 22161.

3. Löffler, F. The Influence of Electrostatic Forces for Particle Collection in Fibrous Filters. In: Novel Concepts, Methods and Advanced Technology in Particulate-Gas Separation, Ariman, T. (ed.). Notre Dame, The Center for Continuing Education, University of Notre Dame, 1978. p. 206-236.

4. Reid, D. L. Electrostatic Capture of Fine Particles in Fiber Beds. In: Novel Concepts, Methods and Advanced Technology in Particulate-Gas Separation, Ariman, T. (ed.). Notre Dame, The Center for Continuing Education, University of Notre Dame, 1978. p. 305-319.

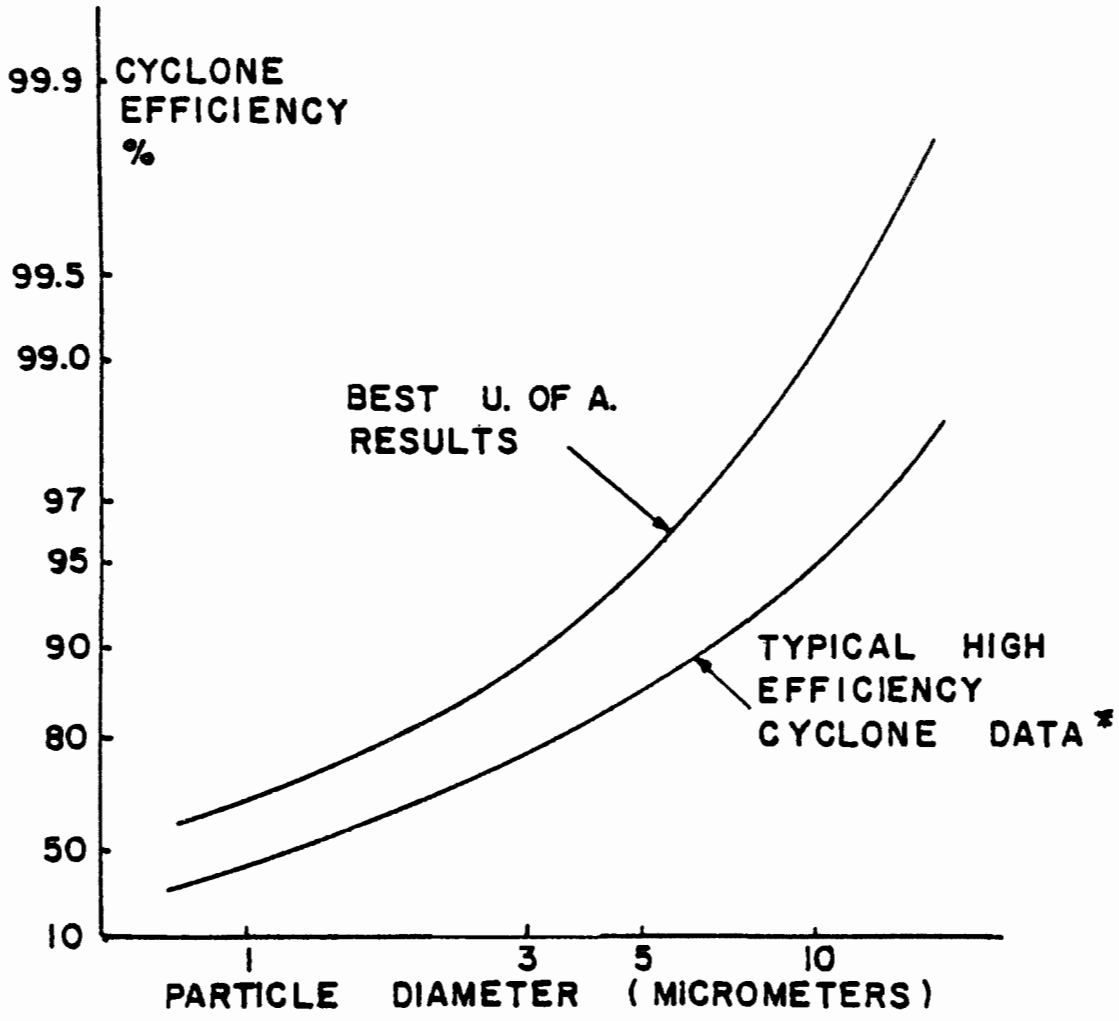

Figure 1 Improvement of cyclone efficiency with cone and charged fog, operating on cotton trash.

*W. Strauss, Industrial Gas Cleaning, Pergamon Press, 1975.

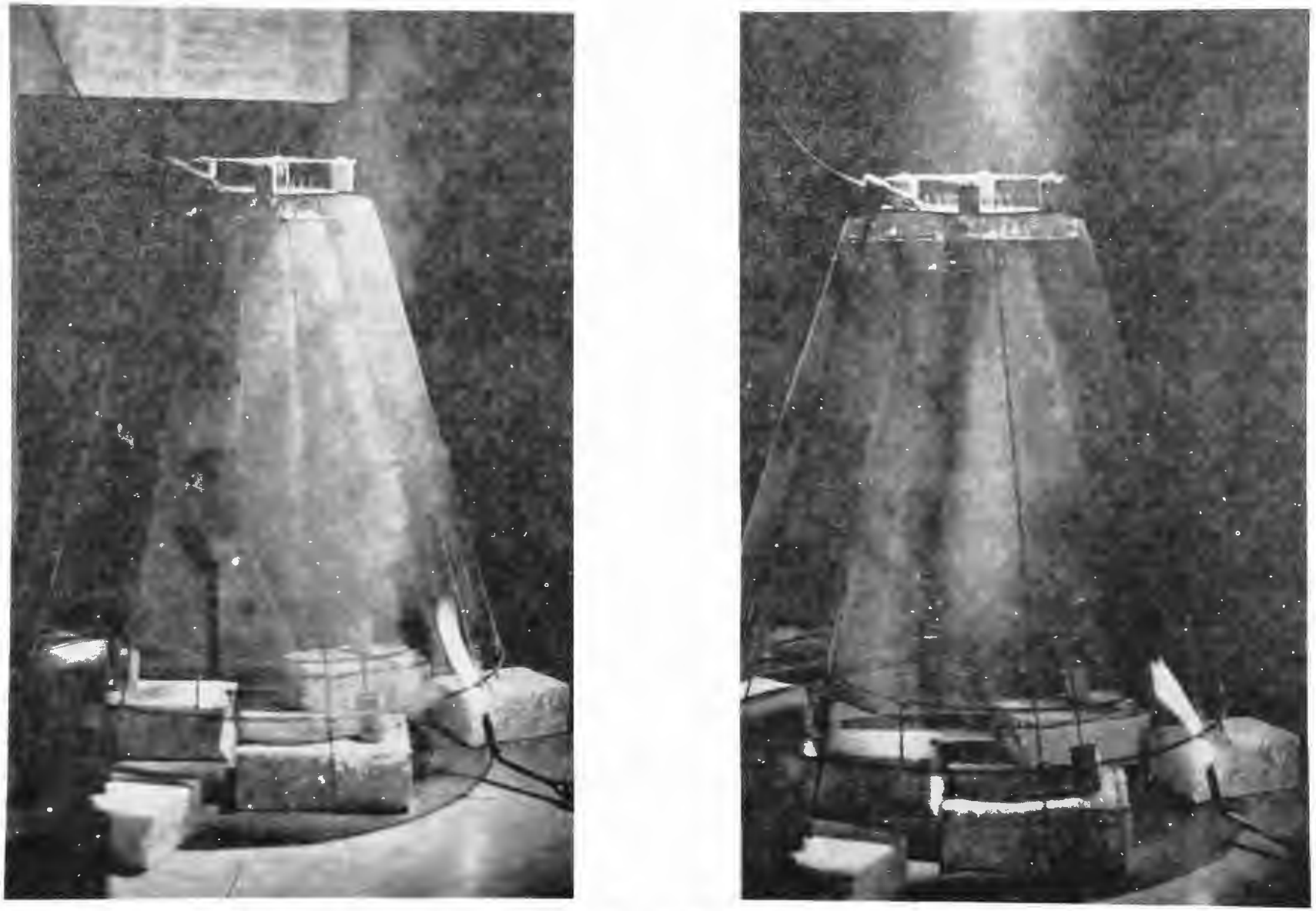

Figure 2 Model of experimental electrostatic hood in operation. Left: With electrostatic field "off", the smoke rises <u>through</u> the cones. Right: With field "on", the smoke is drawn into the space <u>between</u> the cones and carried out the top of the system.

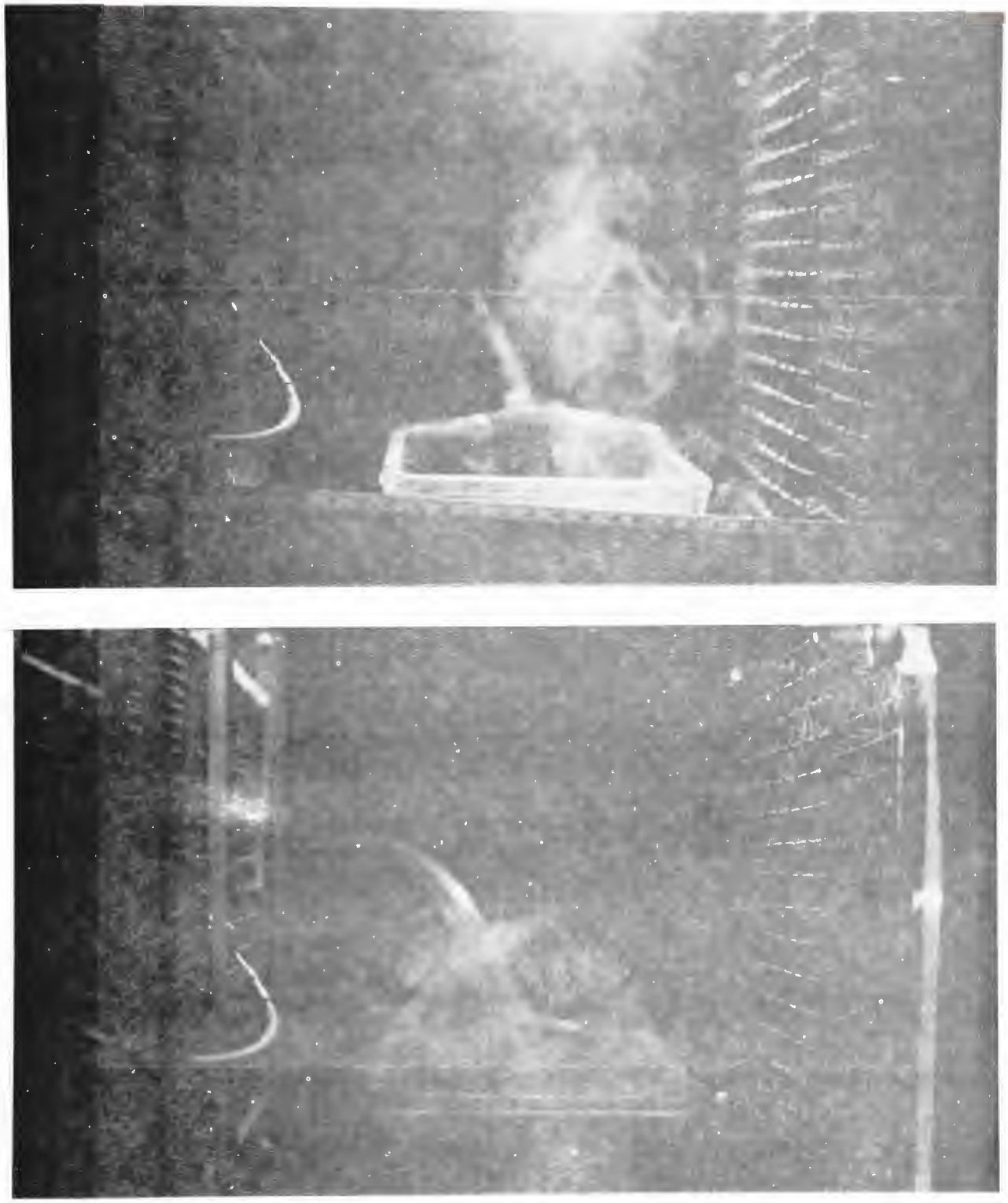

Figure 3 Electrostatic dust pusher-puller system operating on acid fume. Top: System with power "off". Bottom: System with power "on"; acid fumes are pushed to left and deposited on left hand collector screen.

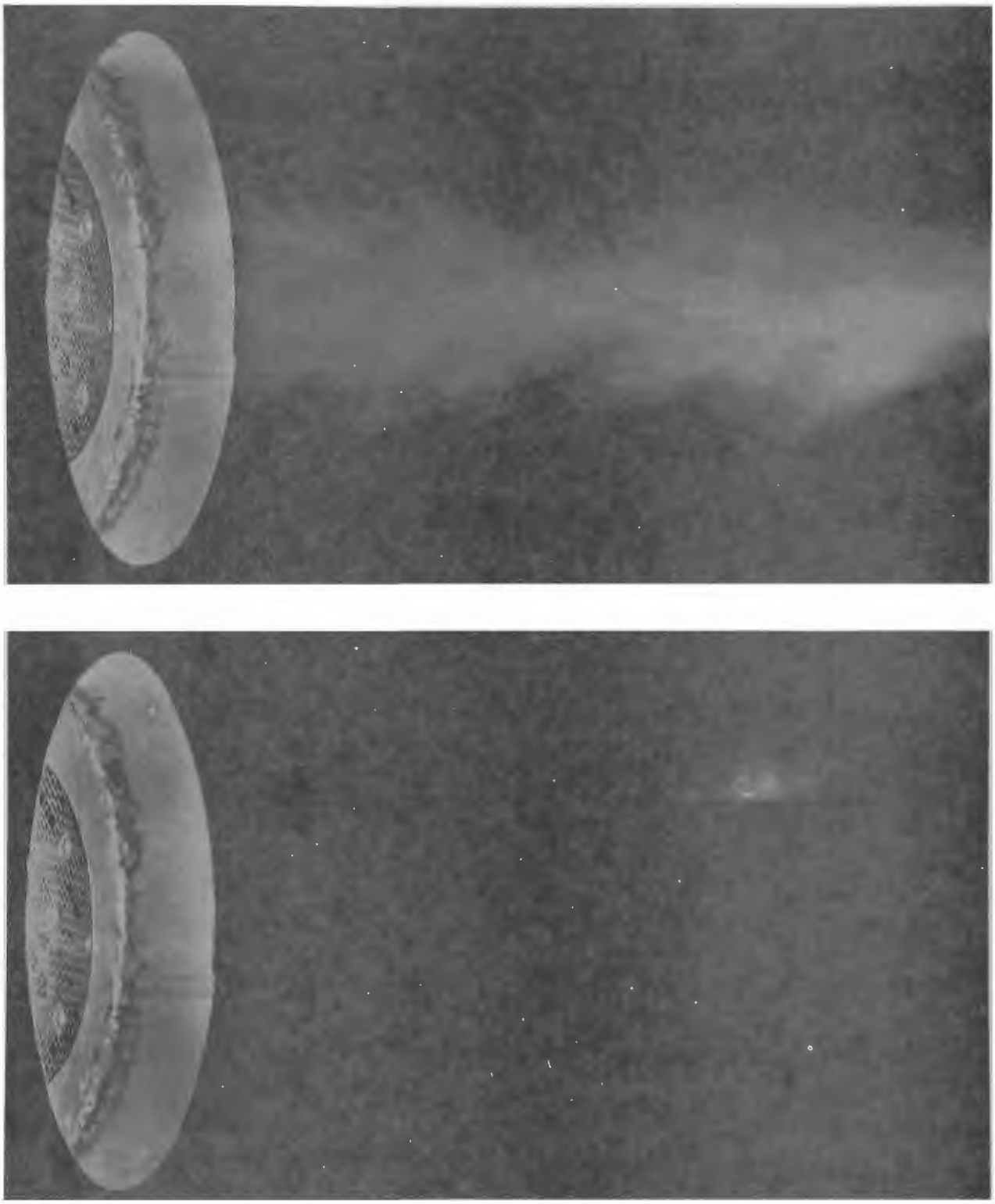

Figure 4 Electrostatic oil mist collector system operating on mineral oil smoke. Top: System is "off". Bottom: System is "on". Two element unit at 15,000 volts; flow velocity 300 FPM (91 m/min).

Figure 5 Electrostatic dust pusher operating on AC Fine. Right: With power "off" dust blows through the screen. Left: With power "on" dust is repelled while allowing air to pass through metal screen; velocity 650 FPM (198 m/min).

Figure 6 Electrostatic hood flow enhancement system operating on ammonium chloride smoke. Left: With system "off" smoke is drawn in by fan alone at velocity of 30 FPM (9.1 m/min). Right: With system "on" flow velocity is now 82 FPM (25 m/min).

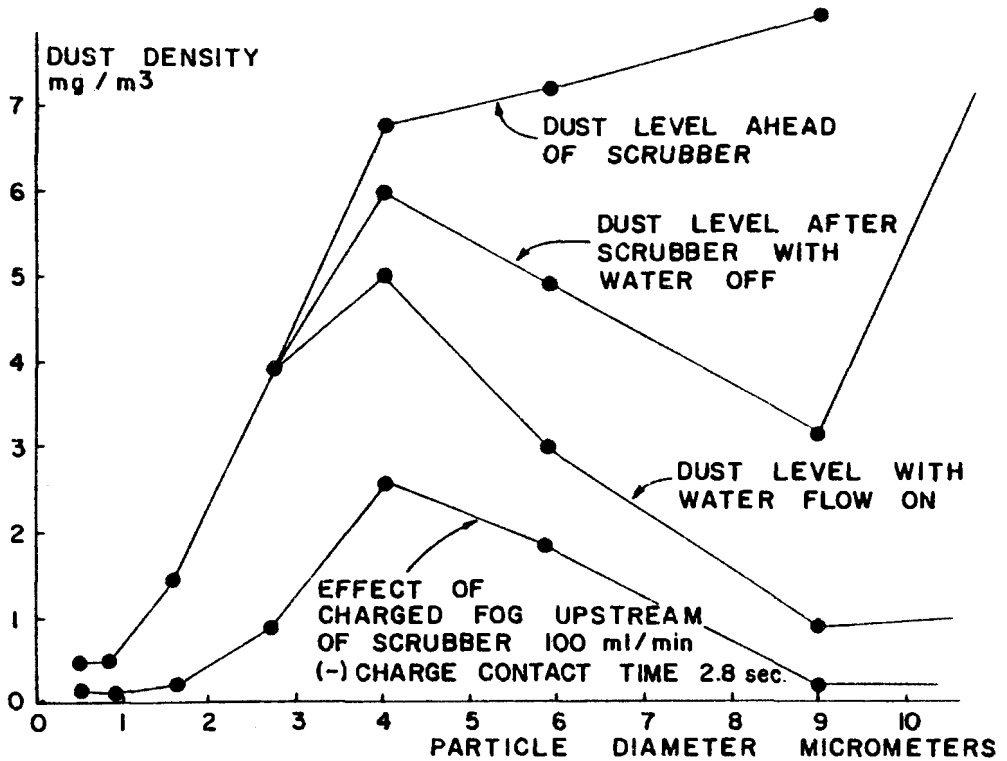

Figure 7 Data showing effects of applying charged fog ahead of 300 ACFM Buffalo Forge wet scrubber. Contact time: 2.2 seconds.

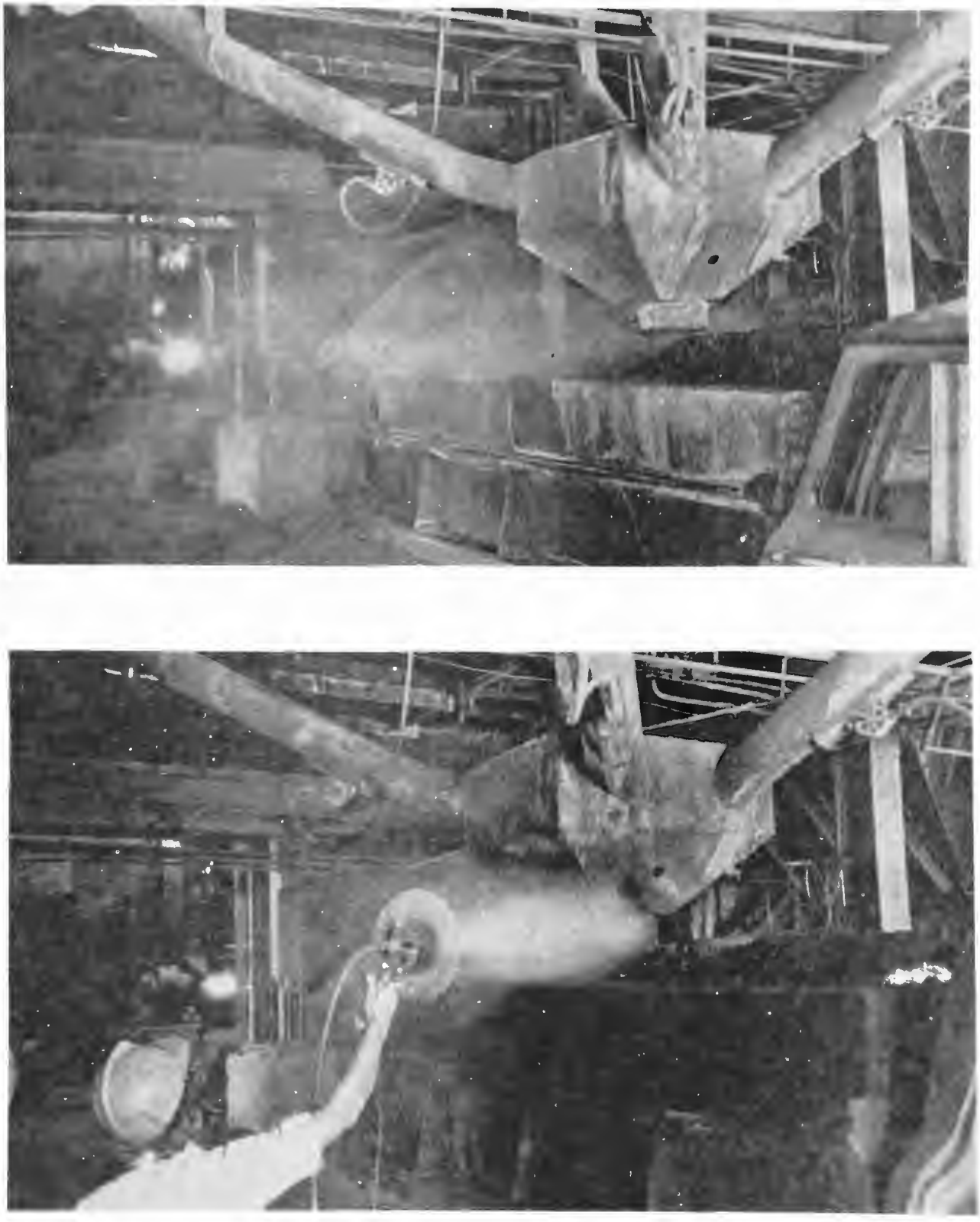

Figure 8 Use of charged fog for control of smelter dust. Top: Fog is "off". Bottom: Fog is "on" and dust is completely suppressed.

SPRAY CHARGING AND TRAPPING SCRUBBER FOR FUGITIVE PARTICLE EMISSION CONTROL

By:

Shui-Chow Yung and Seymour Calvert
Air Pollution Technology, Inc.
San Diego, California 92117

and

Dennis C. Drehmel
Industrial Environmental Research Laboratory
Environmental Protection Agency
Research Triangle Park, North Carolina 27711

ABSTRACT

The control of fugitive emissions with electrostatically charged water sprays was evaluated both theoretically and experimentally. Theoretical calculations show that collection is better than 90 percent for all particle sizes in a charged-particle/charged-drop system.

Experiments were performed on a 225 m^3/min bench-scale apparatus to verify the theory and the feasibility of collecting fugitive particles with charged water spray. The effects of charge levels on drops and particles, water injection methods, drop size, gas velocity, and liquid-to-gas ratio on collection efficiency were determined experimentally. The results of the experiments and the comparison between theory and data are presented.

SPRAY CHARGING AND TRAPPING SCRUBBER FOR FUGITIVE PARTICLE EMISSION CONTROL

INTRODUCTION

Fugitive emissions are air pollution emissions which have not passed through a stack or duct. They are diffuse and typically come from many small sources as opposed to a single large emitter. Fugitive particle emissions tend to be site-specific; open operations, storage and disposal of materials and wastes, incompletely controlled point sources, and poor housekeeping provide maximum potential for their release.

There are two major methods in controlling fugitive emissions. The first method involves stabilizing the dust to keep it from dispersing. It is predominantly a preventive measure rather than capture and separation. A commonly used stabilization technique is wet suppression using sprays of water or water plus a wetting agent. Such spraying generally requires a low first cost, but provides only temporary dust control. The nature of the dust producing activity determines whether sprays will give effective stabilization for only a few hours or several days. The technique can only apply to sources which can tolerate the addition of water.

The second method involves the controlled disposal of fugitive dust that is entrained in a gas stream. Fugitive emissions are gathered and conveyed to conventional control devices. This approach is the permanent way to control fugitive process emissions (FPEs) because it precludes the redispersal of dust which can occur if stabilization is used or if the controlled particles are deposited on the ground.

The overall effectiveness of controlled disposal is determined by how well the system gathers the FPEs as well as by the particle collection efficiency. Typical FPE gathering systems are either secondary hooding at the local source of emissions, or total building enclosure and evacuation. High energy and capital investment are required in controlling FPEs by this method, especially when there are many small, diffuse emission sources. In addition, secondary hooding may not be efficient. For example, a Pierce-Smith converter in a copper smelter equipped with a fixed or secondary fugitive hooding will capture at the most a small percentage of the fugitive emissions created during the charging of matte or slagging, or blister copper pouring (Craig, et al., 1979).

A much simpler and cheaper method for controlling fugitive emissions is by diverting the FPE into a control device located near the source. The SCAT scrubber (Spray Charging and Trapping Scrubber) is such a system. It minimizes the apparatus required to contain, convey, and control the FPE.

SCAT SYSTEM

The SCAT system uses air curtains and/or jets to contain, convey, and divert the FPEs into a charged spray scrubber which is located near the source. Figure 1 shows one of the many possible designs. It has the following features which suit it to FPE control.

1. Minimum use of solid enclosure (hooding).
2. Air curtain(s) and/or air jet(s) applied to divert, contain, and convey the FPE.
3. Charged sprays of water or aqueous solutions to collect FPE and to aid in moving and containing the air being cleaned.
4. Trapping of collected dust and disposal so as to prevent redispersion.
5. Minimum size of scrubber and entrainment separator section.
6. Minimum consumption of water.
7. Portability.

An air curtain involves the use of one or more high velocity air streams flowing as a sheet. The air sheets are produced by one or more air jets which issue from nozzles of circular or rectangular cross section. The high velocity air streams will push and entrain FPEs plus some additional air and carry them away from the source. At some convenient distance downstream, charged water is sprayed cocurrently into the gas stream to remove the entrained dust. After sufficient contacting distance to effect capture of the particles present in the gas, water spray drops are removed with a low pressure drop entrainment separator. For drop collection a zigzag baffle type entrainment separator might be used, depending on the mist elimination and pressure drop requirements. The cleaned gas stream leaves the entrainment separator at this point.

The water from the entrainment separator can be passed through a separation process, such as a filter, to remove the collected dust particles. The water may then be recycled and the dust may be disposed of in such a way as to prevent its redispersion. Alternatively, a blowdown stream of dirty liquid may be directed to a disposal system.

The construction of the SCAT is very simple; therefore, the capital investment will be low. Containing fugitive emissions with air curtains and/or a series of barriers could be very cost effective. The air curtains could also be used to deflect the wind, thus minimizing the volume of air to be cleaned.

The use of air curtains permits open access to the source. Some of the potential applications include:

1. Transfer points on conveyor belts
2. Loading and unloading of materials
3. Coke oven pushing operation

4. Sand preparation, molding, pouring operations in iron foundries.
5. Mixing and pelletizing, slag cooling, and slag granulation processes in primary lead smelting operation.
6. Preparation of anodes. Crushing, screening, and mixing of raw material, for the preparation of anodes in an aluminum production plant
7. Sand, gravel, and asphalt batching.

The SCAT scrubber system has three important steps: (1) contain and convey the fugitive emissions to the spray zone with air curtain(s) and/or air jet(s); (2) collect the particles with charged water sprays; and (3) remove the water drops. To generate design information quickly, the air curtain and the charged spray scrubber were studied individually in separate bench scale device before being combined.

AIR CURTAIN STUDY

An air curtain is a sheet of air blown either by a jet or out of a slot at high speed. The principle of the air curtain was first applied in 1904 by Theophilus van Kemmel (Herndon, 1964). He took out a patent to seal an entrance from outside weather. Since 1916, the device has been vastly developed. Two main types of air curtains exist today: with recirculation, (i.e., with a return duct arranged in push/pull configuration) and without. In either case, the flow may be vertical or horizontal. But each type may also vary in type of fan, jet velocity, depth, and direction of curtain.

Today, simple to elaborate air curtains up to 27.4 m (90 ft) wide and 4.6 m (15 ft) high are widely used in industrial plans, mainly to provide constant access or to isolate a warm interior from the cold outdoors or vice versa. Air curtains can also be used to contain and convey dusty gases. For example, a non-recirculating horizontal air curtain is used at the Quebec Iron and Titanium Smelter in Sorel to separate two ambients: one building in which molten slag cars are quenched with water (which produces large volumes of steam and fumes) from the main working area (Grassmuck, 1969). The total air volume handled is 2,720 m^3/min (9,600 CFM) over a great width but a normal height. At Naoshima Island, Japan, the Naoshima Smelter of Mitsubishi Metal Corporation uses an air curtain system to collect and convey the fugitive emissions from a copper converter into a hood (Uchida et al., 1979).

The design of a SCAT system requires information on several parameters of the jet stream; the jet expansion angle, air reentrainment ratio, mixing of particles in the curtain, effect of crosswind, and effect of hot sources. The jet expansion angle and particle mixing determine the overall cross-sectional dimensions of the SCAT, the air entrainment ratio determines the volumetric flow rate, and the crosswind and heat effect dictate the placement of air curtains and sprays. These parameters are currently being studied.

Theory

Even though air curtains have been widely used, there is little published information on their design and aerodynamics. However, the air curtain approximates a two-dimensional free jet for which there is much information, both theoretical and experimental, available in the literature.

A jet of air will mix at its periphery with the surrounding air so that, with increasing distance from the nozzle, the volume of air flow constantly increases and the velocity decreases. The mixing action is due to simple turbulence rather than an effect of negative static pressure. Air from the surrounding mass moves inward to the periphery of the expanding stream for its full length to replace that entrained into motion by mixing. Continuance of the motion is due solely to the momentum of the air jets.

The flow field produced by a two-dimensional jet exhausting into still surroundings can be broken into two regimes. Where the jet exits from the nozzle, as shown schematically in Figure 2, regions of turbulent mixing are formed at either edge of the slot. The width of the turbulent mixing region expands in the downstream direction, so that it encroaches both on the external still air and on the non-turbulent potential core region between the two mixing layers. At the point where the two mixing layers meet, the potential core disappears, and the potential core region, or regime I of mixing, undergoes a transition to regime II in which turbulent flow is encountered all the way across the jet. The potential core length is usually very short; therefore, the jet becomes completely turbulent at a short distance from the point of discharge.

The mixing model just described is idealized. The ideal two-dimensional jet has no characteristic length, which means not only that the fluid viscosity and jet velocity completely specify the whole flow, but also that a characteristic Reynolds number for the whole flow cannot be defined. This in turn implies that all two-dimensional jets are dynamically similar. Under this condition, the centerline velocity and jet width can be found from equations of motion.

A truly two-dimensional flow is difficult to realize experimentally, because the physical necessity of limiting the length of the slot (L on Figure 2) unavoidably introduces three-dimensional end effects into the flow. A true two-dimensional flow can only be approximated, and this only through the use of a suitably high aspect ratio, L/w on Figure 2. The maintenance of two-dimensionality also limits the downstream distance over which the jet may be measured. Van der Hegge Zijnen (1958) states that the slot jet will approximate the true two-dimensional case in the plane of symmetry perpendicular to the slot if the downstream distance is not longer than 2L.

It can be shown from equations of motion that in the self-preserving region, in which the profiles of velocity and shear stress exhibit similarity, the centerline velocity ratio, u_{Gc}/u_{Gj}, varies as $(x/w)^{-0.5}$. Figure 3 shows the data of Albertson (1950), Van der Hegge Zijnen (1958), Miller and Comings (1957), and Heskestad (1965). As can be seen, the center line velocity exhibits an $x^{-0.5}$ decay over some region.

For turbulent regions and slot nozzles, McElroy (1943) suggested the following equations in determining the velocity profile:

$$\frac{u_{Gc}}{u_{Gj}} = 2.45\left(\frac{x}{w}\right)^{-0.5} \quad (1)$$

$$\frac{u_{Gc}}{u_{Gx}} = 2.5 \quad (2)$$

These two equations could be used at a distance up to 6 slot lengths from the nozzles.

The air entrainment ratio can be deduced from the principle of the conservation of momentum. The total rate of air flow in the stream is related to the primary air flow issuing from the nozzle by:

$$u_{Gj}^2 \; A_j = u_{Gx}^2 \; A_x \quad (3)$$

Since volumetric flow rate is equal to the product of uA:

$$\frac{Q_{Gx}}{Q_{Gj}} = \frac{u_{Gj}}{u_{Gx}} = 1.02\left(\frac{x}{w}\right)^{0.5} \quad (4)$$

Experiment

Figure 4 shows the system for air curtain and air flow experiments. It actually is a small scale SCAT scrubber system without the drop charger. It consists of two sections. Each is 1.8 m x 1.8 m x 1.2 m (6 ft x 6 ft x 4 ft), and is mounted on casters.

One section consists of water spray nozzles (36 spaced 30.5 cm center to center on a square pattern) and an optional zigzag baffle entrainment separator. Distributors and nozzles for air curtains are mounted on the other section.

The mounting of the sections on casters permits easy change of spacing between the spray and the air curtain and rapid adjustment to wind direction.

Figure 5 shows the velocity profile of one curtain at various locations and u_{Gj} = 30.5 m/s. The height of the curtain was 1.8 m (6 ft) and nozzles were 2.54 cm x 2.54 cm openings. The distance between the nozzles was 2.54 cm.

Figure 6 shows the air entrainment ratio. The ratio was calculated by integrating the areas under the curves in Figure 5 and then multiplying them by the curtain height. Predictions by equation (4) are also shown in Figure 6. The measured entrainment ratio is close to prediction.

The measured jet expansion angle was about 35° which is close to that measured by Tuve and Priester (1944).

CHARGED SPRAY SCRUBBER STUDY

Theory

For a spray system, collection by drops is the principal collection mechanism. Particle penetration for a given size particle is given by:

$$Pt_d = \exp\left[-\frac{3}{2}\frac{Q_L}{Q_G}\frac{1}{d_{ds}}\int_o^z \eta dz\right] \tag{5}$$

If the particles are uniformly distributed throughout the approaching gas stream, the single drop collection efficiency, η, equals the ratio of the area swept clean to the cross-sectional area of the drop. The area swept clean by the drop can be determined from the particle trajectory. The trajectory of a particle can be predicted from Newton's law of motion if the initial position, velocity, and applied forces are specified. If the trajectory of the particle intersects the surface of the drop, it will be removed from the gas stream.

When considering only the viscous and electrostatic forces, the equation of motion for an aerosol particle can be expressed, in vector form, as:

$$\vec{F}_v + \vec{F}_e = m_p \frac{d\vec{u}_p}{dt} \tag{6}$$

In dimensionless form, it becomes:

$$K_p \frac{d\tilde{U}_G}{dT} = (\tilde{U}_G - \tilde{U}_p) + K_e \tilde{f}_e \tag{7}$$

By considering only the viscous and inertial forces, Langmuir and Blodgett (1946) solved equation (7) for potential flow and Herne (1960) for both the potential and viscous flows. His calculations for potential flow are close to Walton's and Woolcock's (1960) experimental data. Calvert (1970) approximated the Walton and Woolcock data by:

$$\eta = \left(\frac{K_p}{K_p + 0.7}\right)^2 \tag{8}$$

There is no analytical solution to equation (7) when simultaneously considering the inertial, viscous, and electrostatic forces. George and Peohlein (1974), Nielsen (1974), and Nielsen and Hill (1976b) solved equation (7) numerically on a digital computer for the collection of fine particles by a single spherical collector and presented the results in graphical form.

The collection efficiency of the charged spray scrubber will depend on several parameters; e.g., drop size, liquid/gas ratio, charge level on particles and drops, and relative velocity between particle and drop. A sensitivity analysis of these variables i presented in the following paragraph for inertialess particles.

When the inertial impaction parameter, K_p, is much less than 1, the particles can be considered as inertialess. This situation arises when the particle is small or the relative velocity between the drop and the particle is small. For the collection of a charged particle by an oppositely charged collector, considering only the Coulombic force, Kraemer and Johnstone (1955) and Nielsen and Hill (1976a) gave the following equation for the single drop collection efficiency.

$$\eta = -4 K_c$$

$$= -\frac{4 q_d q_p C'}{3 \pi^2 \varepsilon_o \mu_G u_o d_{dA}^2 d_p} \qquad (9)$$

Substituting equation (9) and $d_s = u_o dt$ into equation (5) and carrying out the integration gives:

$$Pt_d = \exp\left[\frac{2}{\pi^2}\left(\frac{Q_L}{Q_G}\right)\frac{q_d q_p C' t}{\varepsilon_o \mu_G d_{ds} d_{dA}^2 d_p}\right]$$

$$= \exp\left[-\frac{t}{\tau}\right] \qquad (10)$$

where

$$\tau = \frac{\pi^2}{2}\left(\frac{Q_L}{Q_G}\right)\frac{\varepsilon_o \mu_G d_{ds} d_{dA}^2 d_p}{q_d q_p}$$

= scrubber time constant, s

The efficiency of the charged spray scrubber can be interpreted in terms of the scrubber time constant. The smaller the time constant, the higher the collection efficiency for a given scrubber residence time. The time constant decreases with increasing liquid/gas ratio, charge on drops and particles, and with decreasing drop size. The relative importance of the liquid/gas ratio and charge levels is about the same. The most important parameter is drop size. The efficiency of the scrubber will increase dramatically with decreasing drop size. Equation (10) also shows that electrostatic augmentation becomes more important with decreasing particle size.

When there is inertial force, the above analysis is still informative. In addition to those mentioned variables, the relative velocity between drop and particle also plays an important role. Electrostatic force is more effective when the relative velocity is low. However, lower relative velocity will lead to a lower impaction parameter which decreases the efficiency due to inertial impaction.

Experiment

Figure 7 shows a sketch of the charged spray scrubber system. In order to enable us to make good measurements, it is much more elaborate than the prototype SCAT will be.

The system was made in sections jointed by flanges. The scrubber was made of thin aluminum sheets and supported on PVC frames in order to permit electrical current measurements. The cross-section of the scrubber is 0.91 m x 0.91 m (3 ft x 3 ft). The overall length, including the blower, is about 11 m (36 ft).

The scrubber system consists of a flow straightening section, an inlet particle sampling section, a particle charging section, a spray section, an entrainment separator, and an outlet sampling section. It should be noted that all sections except the spray and entrainment separator section will not be included in an industrial installable SCAT system. The inclusion of the sections in the bench scale device is for the purpose of studying various combinations of components and to provide for good particle sampling and electrical measurement.

The particle charger section consisted of two rows of corona wires. Wire diameter was 0.18 mm (0.007 in.). The spacing between wires within the same row was 6.5 cm (2.5 in.). The ground electrodes were 1.3 cm (0.5 in.) diameter aluminum tubing.

The overall length of the spray section was 2.44 m (8 ft) including two spray banks. The water was charged by induction. The nozzles and water feed lines were kept at ground potential. A high voltage grid assembly was placed in front of the nozzles to charge the water drops. This arrangement not only simplified the construction by eliminating a complicated electrical isolation system but also gave a higher charge level on drops.

Data

In the SCAT scrubber system, drops are charged by induction. Drops are charged by grounding the nozzles and by applying a high voltage to a grid assembly which is located at a short distance downstream from the nozzles. The distance between the nozzle plan and the grid plan can be adjusted to give maximum charge to the drops.

In the present study, drop charge was measured by the following three techniques.

1. Monitoring the current output from the power supply. The measured current divided by the measured liquid flow rate gives charge to mass ratio for the drops.

2. The scrubber and water lines are electrically isolated from the ground. The nozzles are grounded through an ammeter. The measured current divided by the water flow rate gives charge to mass ratio for the drops.

3. A drop collector is placed in the scrubber. The collector collects the drops and their charges which are measured by leaking it to the ground through an electrometer. Thus, by monitoring the current and sampling time, and measuring the amount of water collected, the charge level can be calculated.

Method 3 is considered to be most accurate, Method 2 is second, and Method 1 is least accurate. Method 1 gives the total energy consumption in charging the water. It includes the charge carried away by the drops and line loss or leakage. In performing the cost analysis, power supply output will be used as the basis for energy consumption and either Method 2 or Method 3 will be used to determine the charge level on drops.

Figure 8 shows the measured charge level on drops by Method 3. Nozzles were Bete P-48 and the spacing between the grid plane and the nozzle plane was 1.3 cm (0.5 in.). Curve "A" is for a water flow rate of 9.5×10^{-4} m^3/s (15 GPM) and a pressure of 450 kPa (50 psig) at the nozzle. Curve "B" is for water flow rate of 7.2×10^{-4} m^3/s (11.5 GPM) and a pressure of 380 kPa (40 psig). The drop diameter, which was measured and sized with a photographic technique was about 240 μm.

Both curves show a maximum at 10 kV. When the applied voltage to the grid was below 10 kV, the measured drop charge to mass ratio was about the same for the three measurement techniques. When the applied voltage increased above 10 kV, power supply current output increased rapidly while the measured charge level by Method 3 decreased. This is illustrated in the following table for a water flow rate of 9.5×10^{-4} m^3/s (15 GPM).

Applied Voltage (kVDC)	Power Supply Output (mA)	Measured Charge Level (C/g)	Total Drop Current (mA)	% of Power Supply Output
-10	-0.5 to -0.6	$+5.8 \times 10^{-7}$	0.55	100
-12	-0.8 to -0.9	$+5.3 \times 10^{-7}$	0.50	59
-15	-2.0	$+3.4 \times 10^{-7}$	0.32	16
-16	-2.6 to -3.0	$+2.5 \times 10^{-7}$	0.26	9.3
-20	Sparks			

It is possible that at applied voltage about 10 kV, corona discharge occurred at the edge of the liquid sheet. At a larger nozzle/grid spacing, a higher voltage can be applied to the grid without causing corona discharge.

The measured drop charge is in good agreement with that reported by Pilat et al. (1974). In their experiment, drops were charged by induction with the high voltage terminal connected directly to the nozzle. They used Spraying Systems Fogjet 7N4 nozzles which produce 50 μm dia. drops. At an applied voltage of 5 kV, the measured charge level was 5.6×10^{-7} C/g.

The collection efficiency of the charged spray scrubber was determined by simultaneously measuring the particle size distribution and mass concentration at the inlet and outlet of the scrubber. Figure 9 shows the results for charged-drop/uncharged-particle and neutral-drop/uncharged-particle. Scrubber operating conditions were the same. One spray bank was used. Superficial gas velocity was 2.9 m/s (9.5 ft/s) and the liquid/gas ratio was 4×10^{-4} m^3/m^3 (3 gal/mcf).

As can be seen from Figure 9, the collection efficiency of the spray scrubber improves by charging the water. The improvement is more with submicron particles. For particles with diameters larger than 3 μmA, charging the water has no effect on efficiency.

CONCLUSIONS

A simple technique for controlling fugitive emissions is described. The technique involves the use of air curtains and air jets to contain and convey the emissions into a nearby spray scrubber.

The collection efficiency of a spray scrubber was investigated experimentally. The collection efficiency could be improved by charging the water or both the particles and the water.

Air curtains have been used in industries to contain dust but no carefully performed study has been reported in the literature. A pilot plant has been built by A.P.T. to study various aspects of air curtains. Experiments are currently underway.

ACKNOWLEDGEMENT

The work upon which this paper is based was performed pursuant to EPA contract No. 68-02-3109.

REFERENCES

1. Albertson, M.L., et al. Diffusion of Submerged Jets. Transactions ASCE, 115: 143-164, 1950.

2. Calvert, S. Venturi and Other Atomizing Scrubbers, Efficiency and Pressure Drop. AIChE J. 16: 392-396, 1970.

3. Craig, A.B., et al. Present and Future Control of Particulate Emissions in the Primary Nonferrous Metals Industry. Paper presented at the Control of Particulate Emissions in the Nonferrous Metals Industries Symposium. Monterey, California, March 1979.

4. George, H.F. and G.W. Poehlein. Capture of Aerosol Particles by Spherical Collectors, Electrostatic, Inertial, Interception and Viscous Effects. Env. Sci. and Tech., 8: 46-49, 1974.

5. Grassmuck, G. The Applicability of Air Curtains as Air Stoppings and Flow Regulators in Mine Ventilation. Paper presented at the 71st Annual General Meeting, Canadian Institute of Mining and Metallurgy, Montreal, Canada, April 23, 1969.

6. Herndon, C.L. Preliminary Studies of Air Curtains for Refrigerated Warehouses, T.N.N.-573, U.S. Naval Civil Engineering Lab., Port Hueneme, CA, January 1964.

7. Herne, H. International Journal of Air Pollution. 3: 1-3, 26-34, 1960.

8. Heskestad, G. Hot-Wire Measurements in a Plane Turbulent Jet. J. of Applied Mechanics. 32: 721-724, 1966.

9. Kraemer, H.F. and H.F. Johnstone. Collection of Aerosol Particles in the Presence of Electrostatic Fields. Ind. and Eng. Chem. 47: 2,426-2,434, 1955.

10. Langmuir, I. and K.B. Blodgett. Army Air Forces Tech. Rpt. 5418, 1946.

11. McElroy, G.E. Air Flow at Discharge of Fan-Pipe Lines in Mines. Part II. U.S. Bureau of Mines Report of Investigation 3730, November 1943.

12. Miller, D.R., and E.W. Comings. Static Pressure Distribution in the Free Turbulent Jet. J. of Fluid Mechanics. 3: 1-16, 1957.

13. Nielsen, K.A. Effect of Electrical Forces on Target Efficiencies for Spheres, Eng. Research Inst. Tech. Report 74127, Iowa State Univ., 1974.

14. Nielsen, K.A. and J.C. Hill. Collection of Inertialess Particles on Spheres and Electrical Forces. Ind. Eng. Chem. Fund. 15: 149-157, 1976a.

15. Nielsen, K.A., and J.C. Hill. Capture of Particles on Spheres by Inertial and Electrical Forces. Ind. Eng. Chem. Fund. 15: 157-163, 1976b.

16. Pilat, M., et al. Collection of Aerosol Particles by Electrostatic Droplet Spray Scrubber. Env. Sci. and Tech. 8: 360-362, 1974.

REFERENCES (continued)

17. Tuve, G.L. and G.B. Priester. Control of Air-Streams in Large Spaces. Heating, Piping & Air Cond., ASHVE Journal, January 1944.

18. Uchida, H., et al. Processing of Copper Smelting Gases at Naoshima Smelter. Paper presented at the Control of Particulate Emissions in the Primary Nonferrous Metals Industries Symposium. Monterey, California, March 1979.

19. Van der Hegge Zijnen, B.G. Measurements of the Velocity Distribution in a Plane Turbulent Jet of Air. Applied Scientific Research. Section A. 7: 250-276, 1958.

20. Walton, W.H. and A. Woolcock. Aerodynamic Capture of Particles. E.G. Richardson, editor. Pergamon Press, Oxford, England, 1960.

NOMENCLATURE

A_j = total area of nozzle cross section, m

A_x = cross-sectional area of jet stream at "x" meters downstream from nozzle, m

C' = Cunningham slip correction factor, dimensionless

d_{dA} = drop surface mean diameter, m

d_{ds} = drop Sauter mean diameter, m

d_p = particle diameter, m

$\vec{F}_e$ = electrostatic force, N

$\vec{F}_v$ = viscous force, N

f_e = spatial dependence of the electrostatic force in terms of dimensionless coordinates

K_c = Coulombic force parameter, dimensionless

$$K_c = \frac{q_d\, q_p\, C'}{3\, \pi^2\, \varepsilon_o\, \mu_G\, u_o\, d_d^2 d_p}$$

K_e = electrostatic force parameter, dimen

K_p = inertial impaction parameter, dimensionless

m_p = particle mass, kg

Pt_d = penetration for particle diameter, d_p, fraction

Q_G = volumetric gas flow rate, m^3/s

Q_{Gj} = volumetric gas flow rate at nozzle exit, m^3/s

Q_{Gx} = average gas flow rate at "x" meters downstream from nozzle, m^3/s

Q_L = liquid volumetric flow rate, m^3/s

q_d = charge on drops, C

q_p = charge on particle, C

U_G = dimensionless gas velocity, dimensionless

NOMENCLATURE (continued)

$\tilde{U}_p$ = dimensionless particle velocity, dimensionless

u_{Gc} = centerline gas velocity, m/s

u_{Gj} = gas velocity at nozzle exit, m/s

u_{Gx} = average jet velocity at "x" meters downstream from nozzle, m/s

u_o = upstream particle drop relative velocity, m/s

u_p = particle velocity, m/s

T = dimensionless time, dimensionless

t = time, s

w = slot width, m

x = distance from nozzle, m

Z = coordinate, m

Greek

η = single collector collection efficiency, fraction

μ_G = gas viscosity, Pa.s

ε_o = dielectric constant of free space, F/m

τ = time constant, s

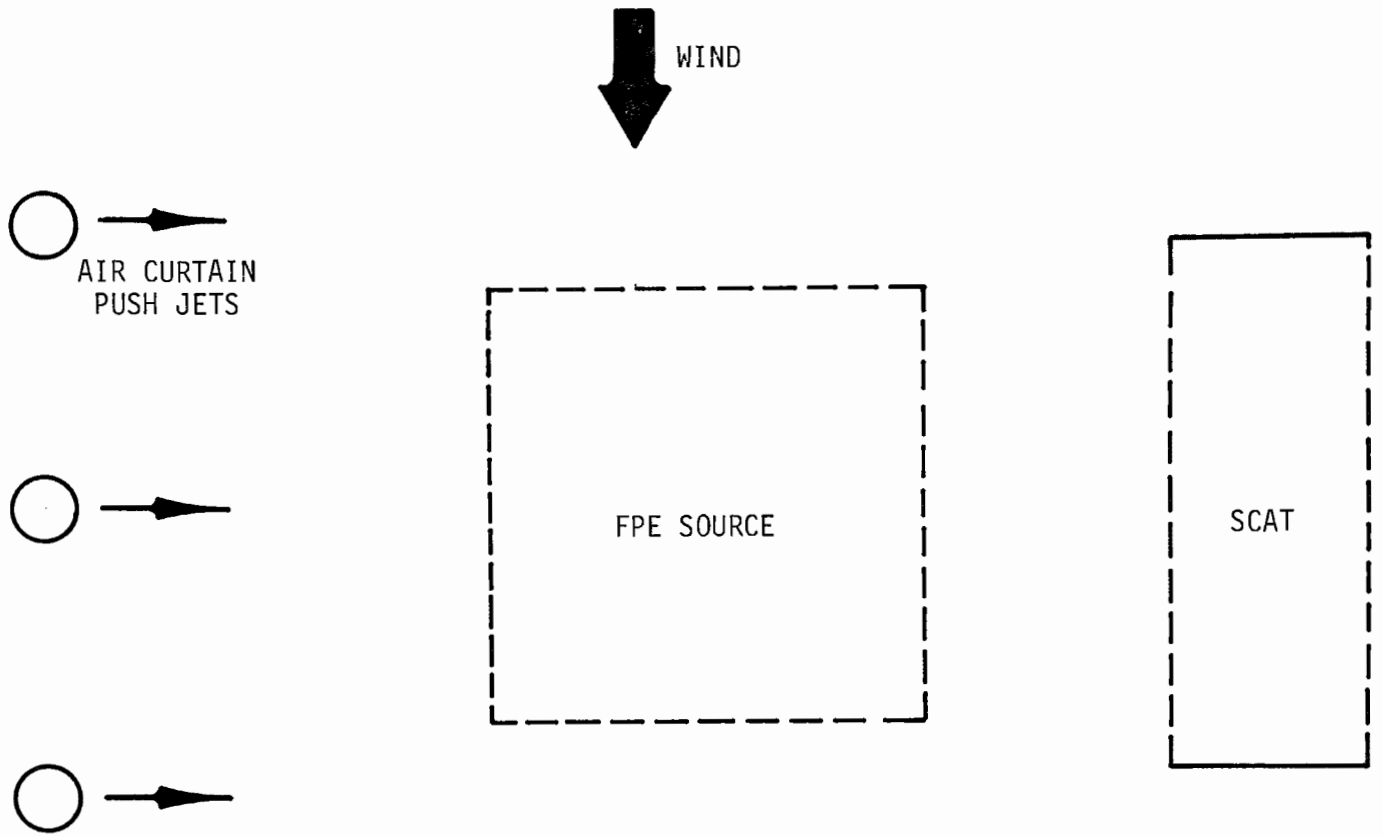

Figure 1. Example of SCAT system arrangement.

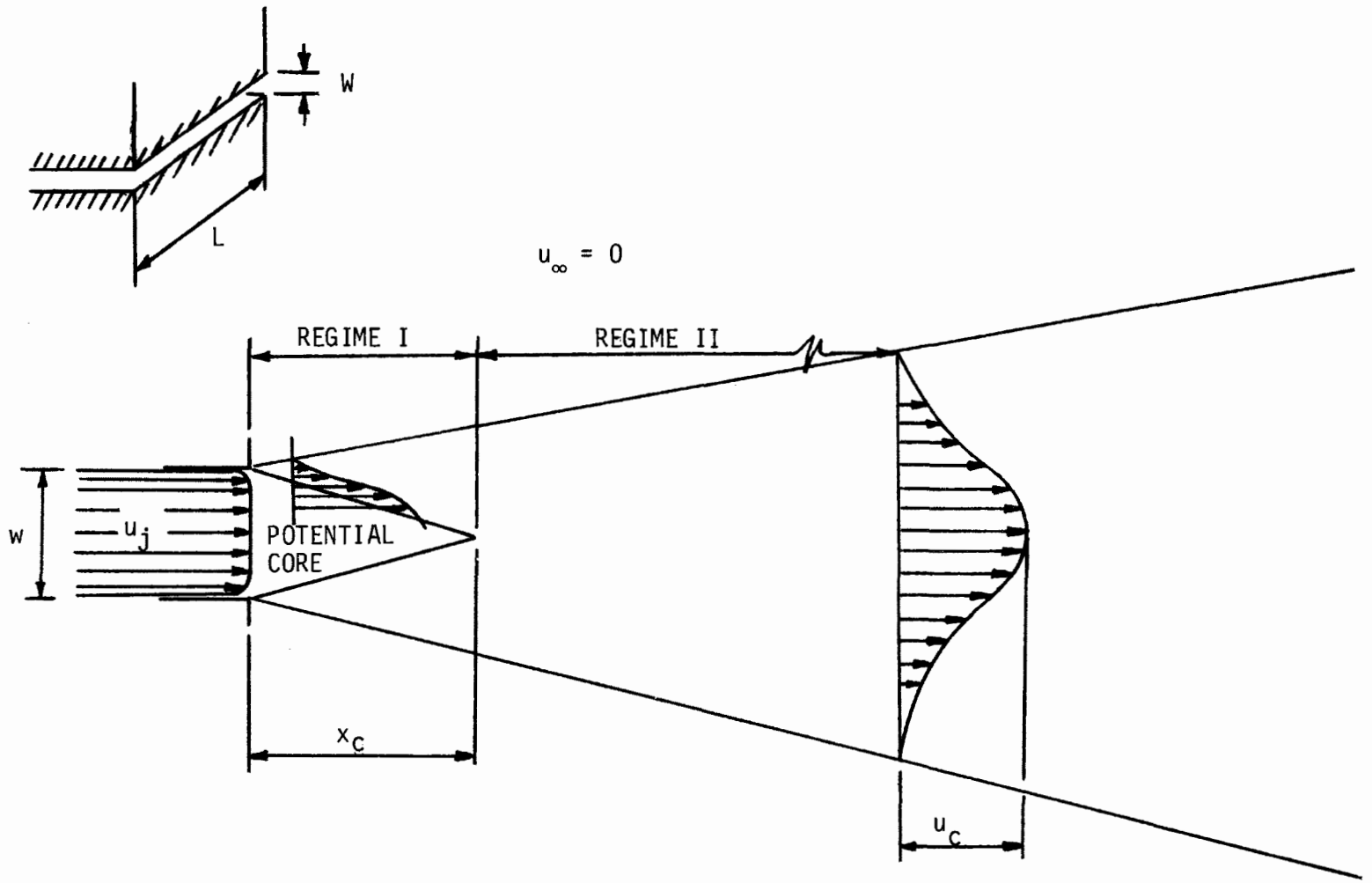

Figure 2. Two - dimensional jet with gas external velocity.

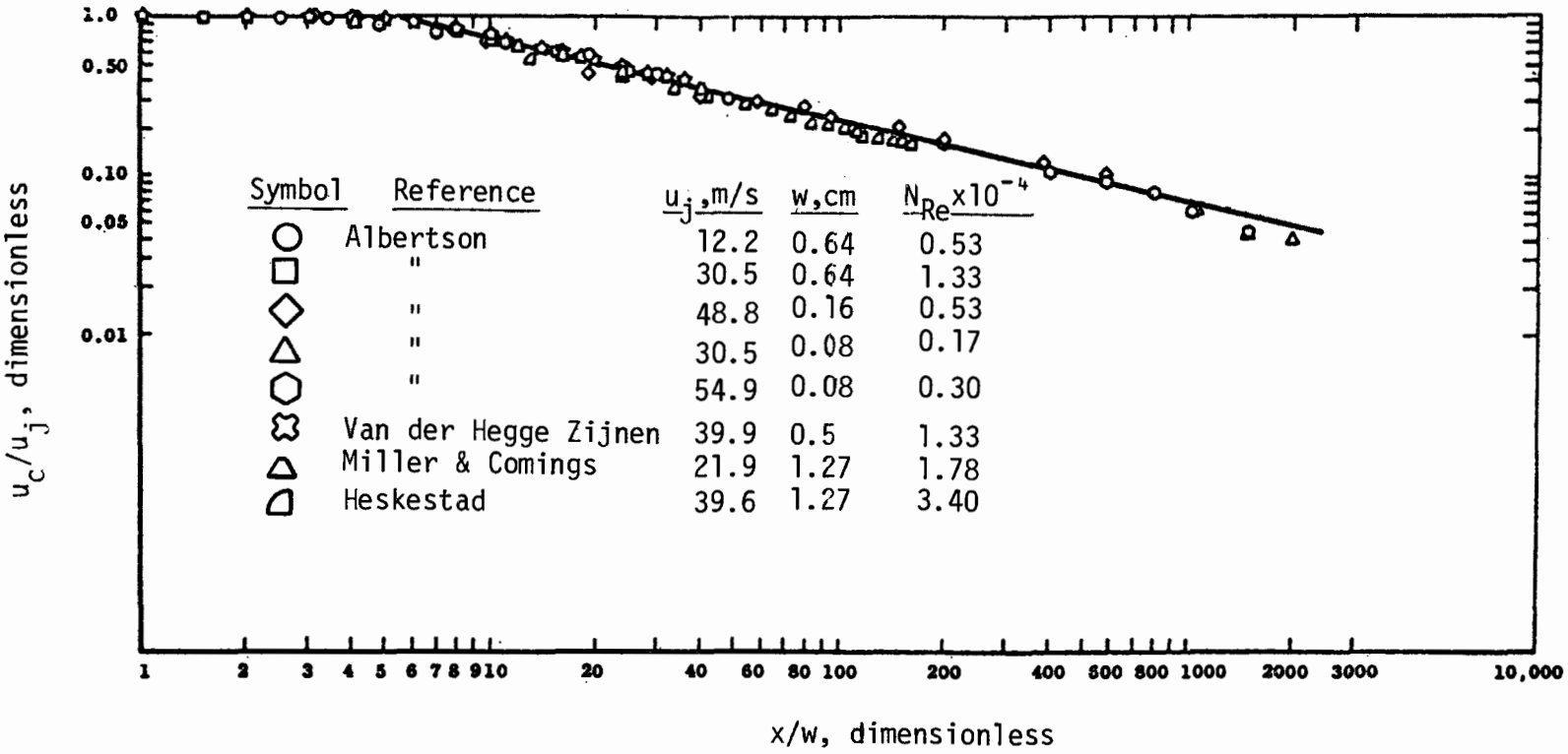

Figure 3. Axial decay of centerline velocity ratio, two-dimensional jet into still air.

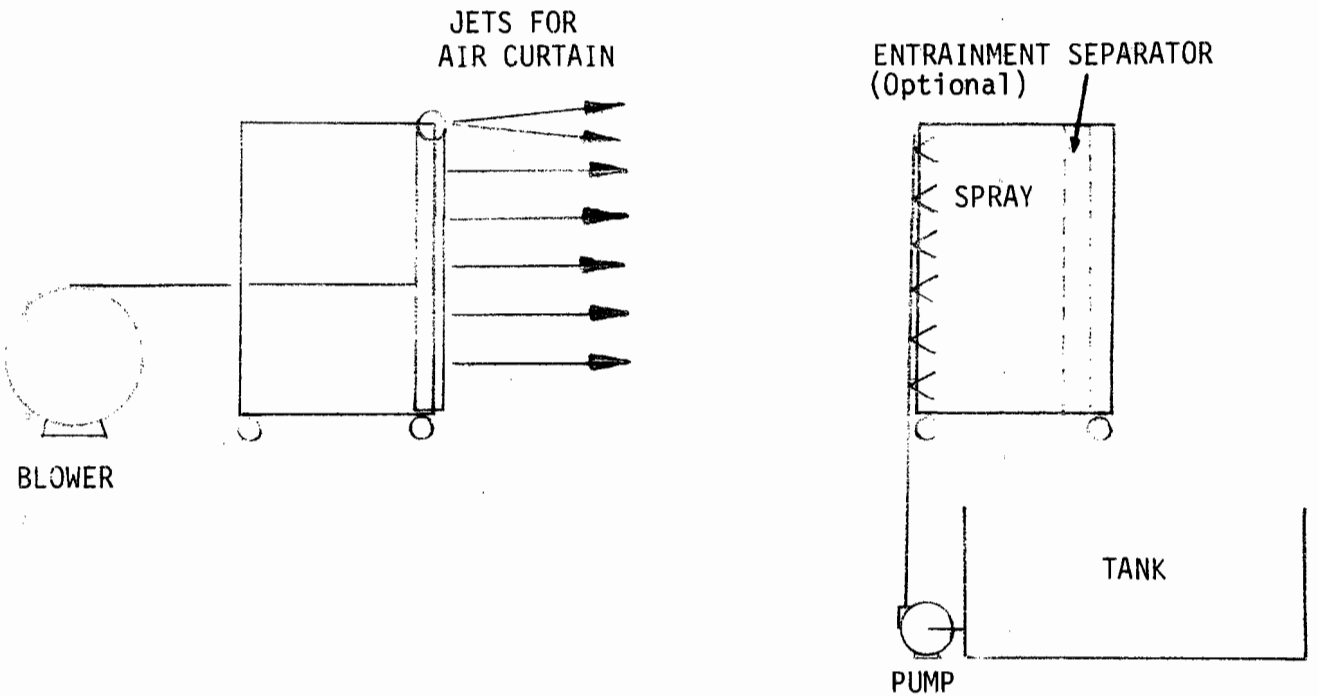

Figure 4 . Apparatus for air flow study.

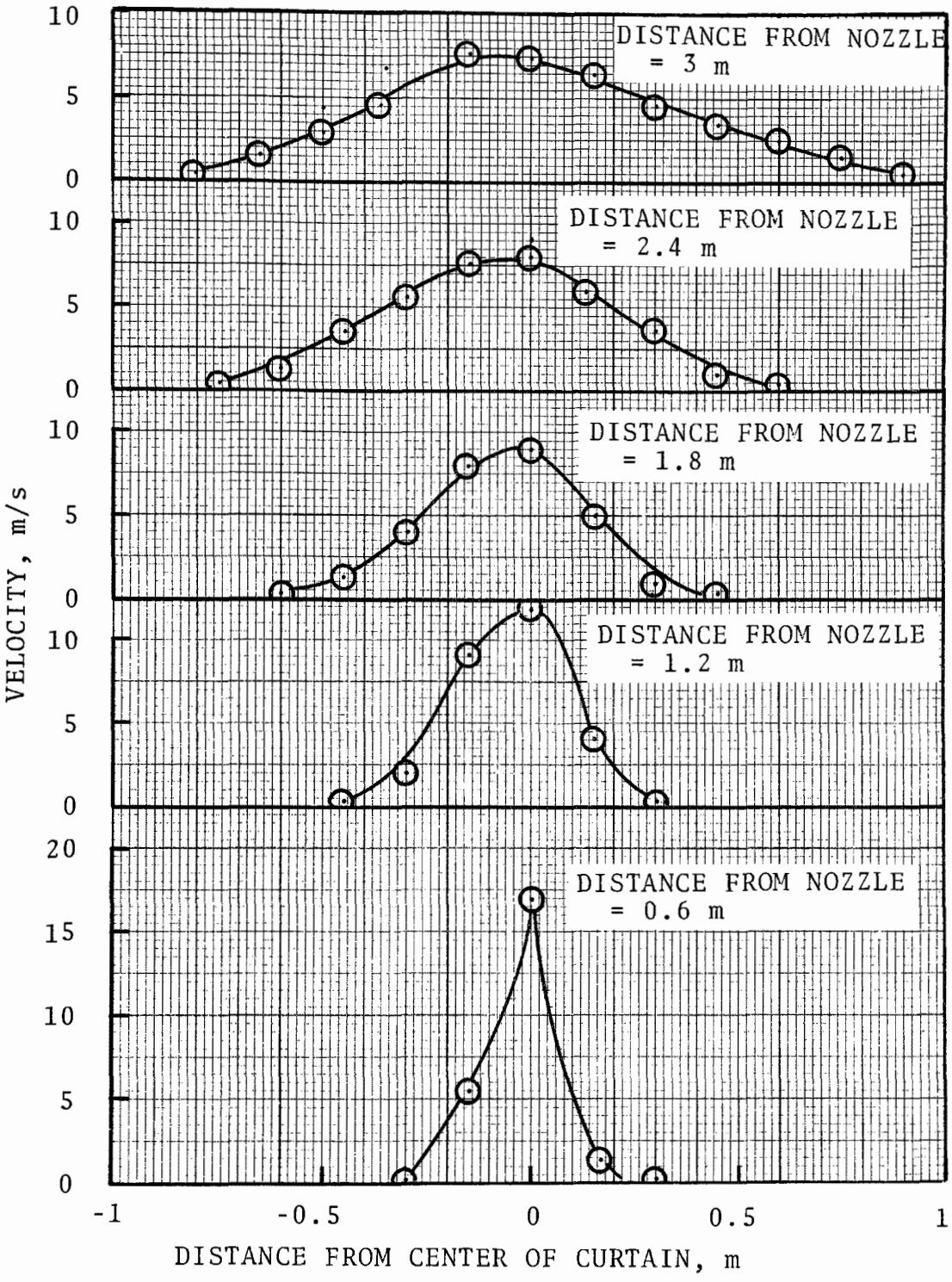

Figure 5. Experimental velocity profile.

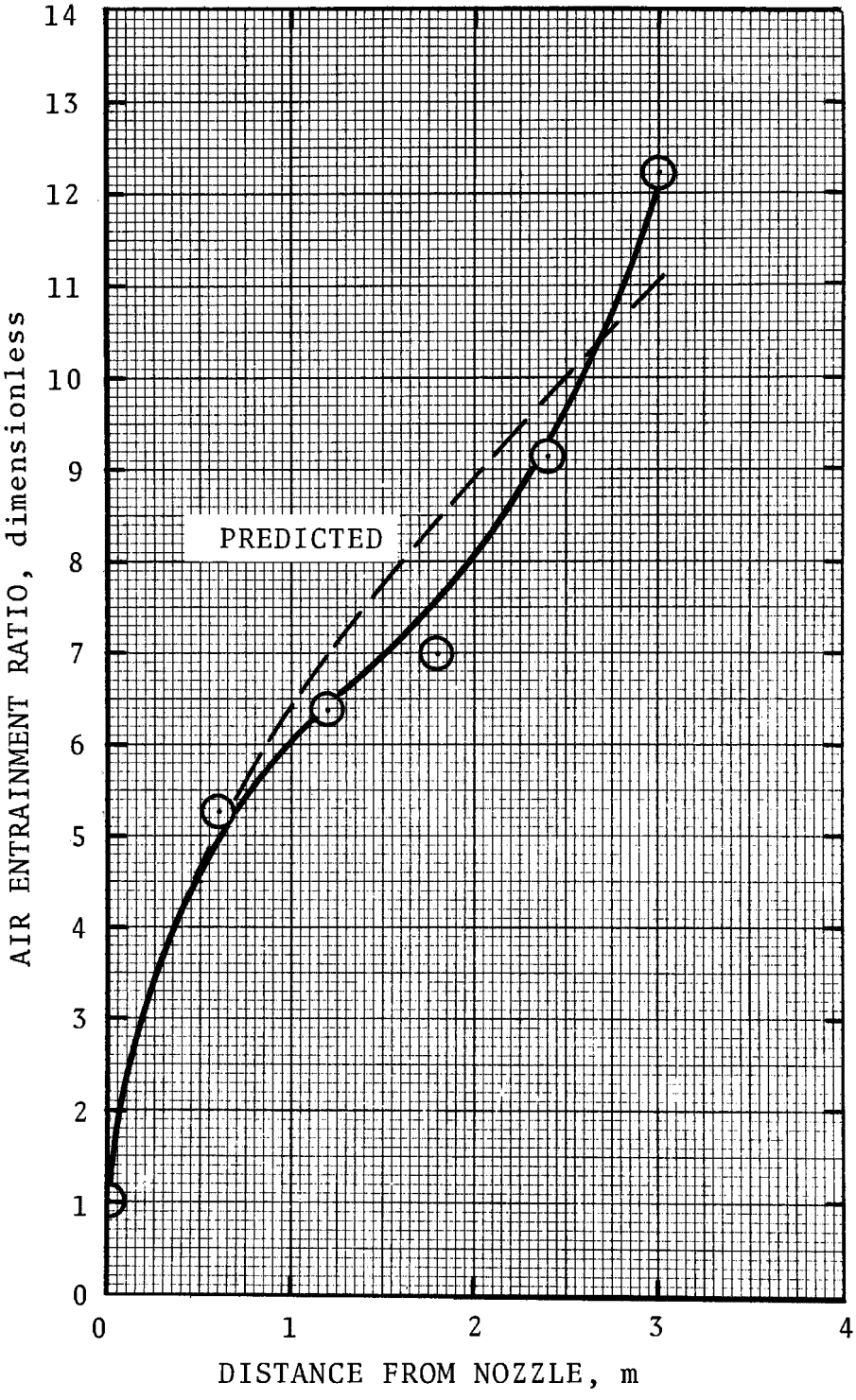

Figure 6. Measured and predicted entrainment ratio.

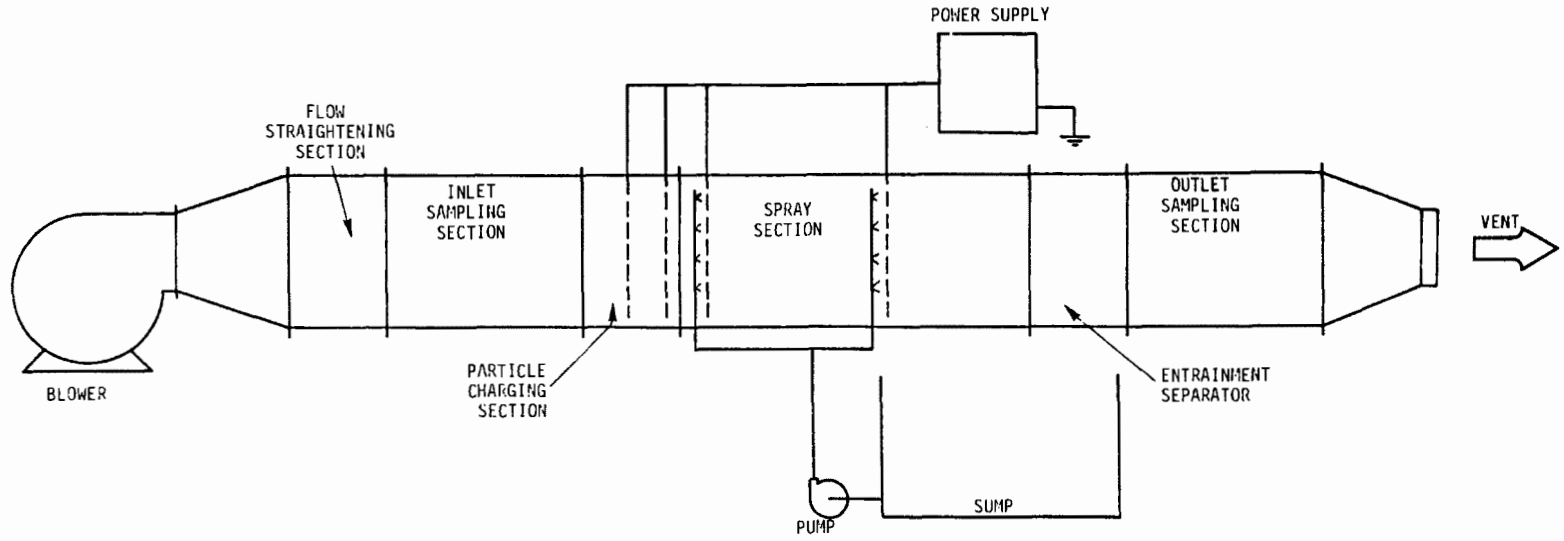

Figure 7. Experimental apparatus for studying charged spray section of SCAT scrubber.

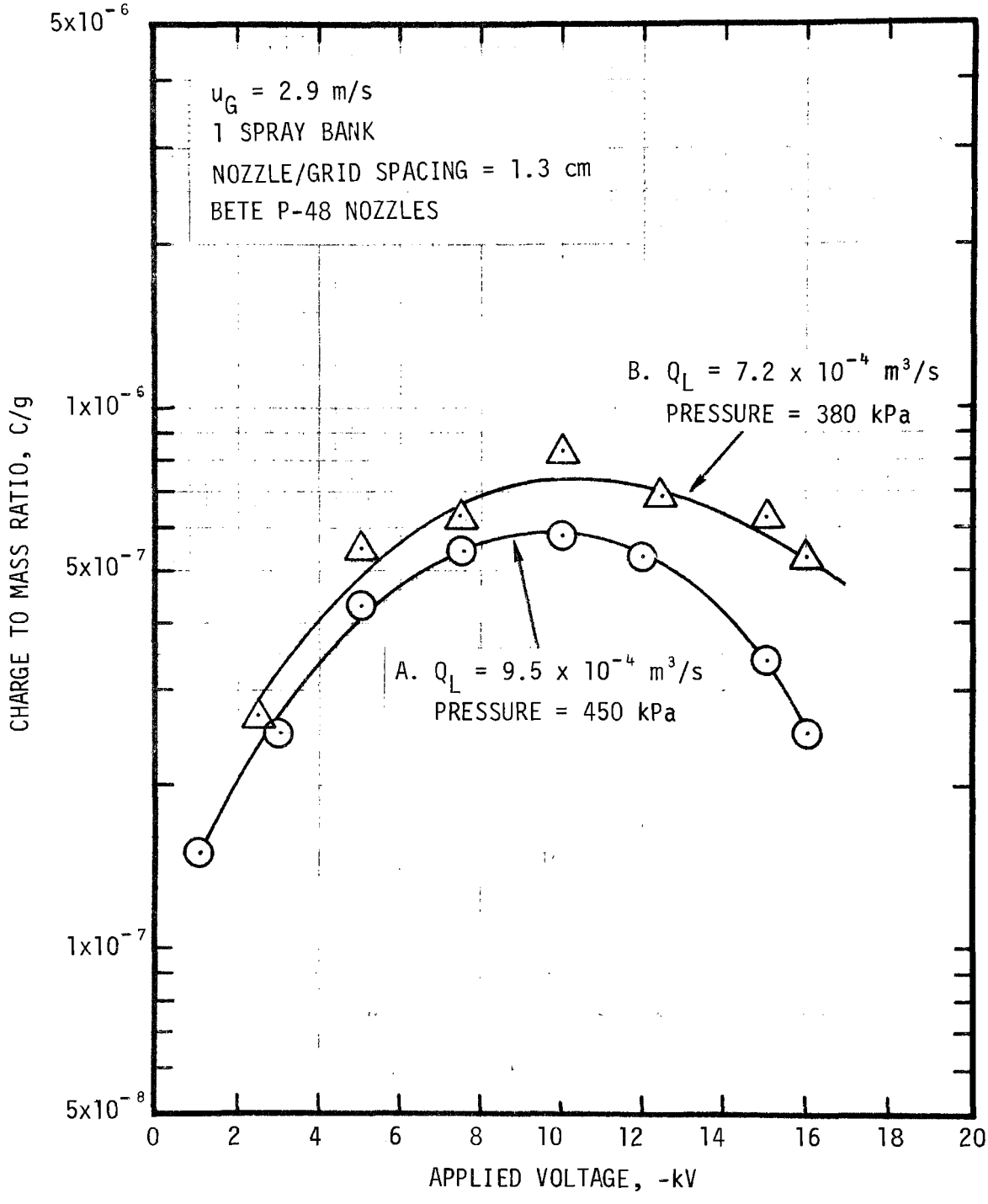

Figure 8. Measured charge level on drops.

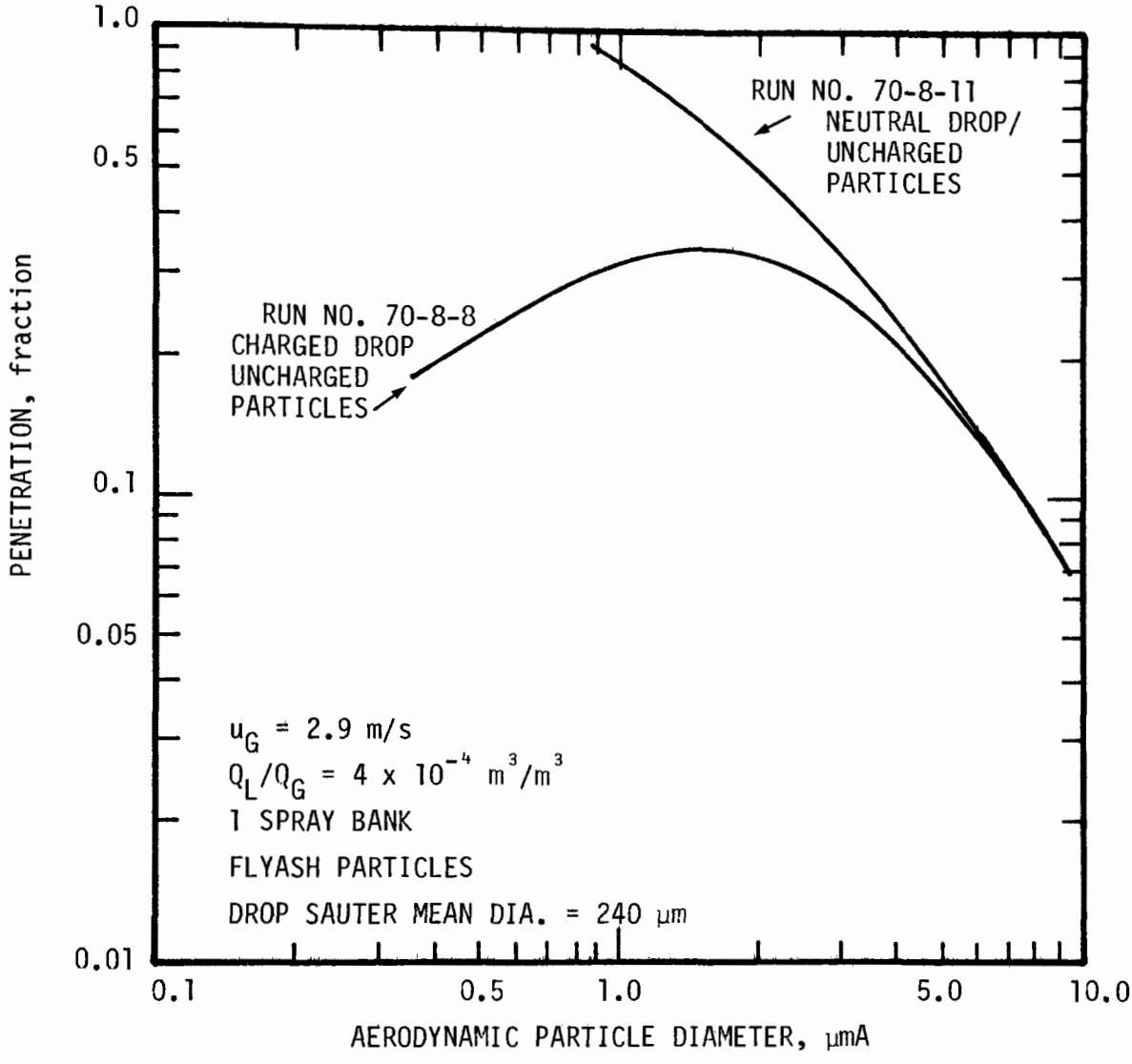

Figure 9. Experimental penetration of the SCAT scrubber.

CONTROL OF WINDBLOWN DUST FROM STORAGE PILES

Chatten Cowherd, Jr.
Midwest Research Institute
Kansas City, Missouri 64110

ABSTRACT

This paper presents a strategy for developing more reliable estimates of the efficiencies of preventive methods for the control of windblown dust from aggregate storage files. The strategy is dependent on the availability of an experimentally verified emission factor equation which relates the particulate emission rate to wind speed, pile surface properties, and pile shape factors. The control efficiency is determined by field measurements of the changes in emission factor parameters effected by the control method. Such measurements are far less difficult to perform than direct measurements of reductions in pile emissions. A simplified emission factor equation developed from measurement of windblown dust from agricultural fields is used to illustrate the strategy.

An experimental technique for emission factor development entailing the use of a portable wind tunnel and isokinetic sampling system is described. Coal pile emissions data obtained by this technique are found to be in good agreement with the simplified equation after refinements are made for wind speed dependence. The experimental technique coupled with the analysis of wind flow patterns around storage piles forms the basis for development of an improved emission factor equation from which reliable estimates of control efficiency can be made.

INTRODUCTION

Wind erosion of open storage piles is a recognized source of particulate air pollution associated with the mining and processing of mineral aggregates, both metallic and nonmetallic. Preventive methods for control of windblown emissions from raw material storage piles consist of wetting, chemical stabilization and enclosures. Table 1 lists literature sources which describe these methods and their applicability.[1-6] Physical

stabilization by covering piles with less erodible aggregate material and/or vegetative stabilization are seldom practical control methods for raw material storage piles.

As indicated in Table 1, most of the commonly cited control efficiency values for the practical control methods listed above are estimates. Presumably these estimates are based on visual observations of plume generation and opacity under windy conditions. In one case, control efficiency values for chemical stabilization methods are based on laboratory wind tunnel experiments.[6] However, since these experiments entail questions about the representativeness of the test surface properties in comparison to exposed storage pile surfaces, the absolute values of the measured efficiencies may not be applicable to storage piles.

QUANTIFICATION TECHNIQUES

The scarcity of quantitative control efficiency data for storage piles appears to be attributable to the difficulty of measuring windblown dust emissions from storage piles using conventional sampling techniques. If quantification techniques were readily applicable, control efficiency values could be determined by comparing measured emissions from untreated and treated piles of the same geometry and under the same wind conditions. It would also be essential to document the specific level of control, e.g., application intensity and time since application.

Upwind-downwind sampling[7] has been the most common method employed to measure windblown suspended particulate emissions from a given weight or volume of stored aggregate. This method relies on the use of an atmospheric dispersion model to back-calculate the emission rate which produces the pattern of particulate concentrations measured in the vicinity of the test pile. Because of the technical problems involved, calibration of the dispersion model is usually not performed.

The errors associated with this application of the upwind-downwind method may be substantial. Usually the test pile is represented either as a virtual point source or as a uniformly emitting area source. Wind conditions are assumed constant and unaffected by the presence of the pile. These assumptions increase the possibility of error in the calculated emission rate beyond the range (a factor of three)[8] usually associated with the use of an uncalibrated dispersion model applied to the simpler case of unobstructed dispersion from an easily represented source.

An alternative approach to this problem is to uncouple the analysis of wind flow pattern from the relationship of suspended particulate emission rate to wind speed. Wind flow patterns around basic storage pile configurations can be determined as a function of approach wind velocity either by

TABLE 1. REPORTED EFFICIENCIES FOR CONTROL OF WIND EROSION OF STORAGE PILES

Control Method	Reported Efficiency (%)	Reference (Year)*	Method of Determination
Watering - periodic sprinkling	50	2 (1976) 3 (1977)	Ref. 1 (1973) - estimate Ref. 2 (1976) - estimate
Watering - wind-activated sprinkler system	80	4 (1978)	Estimate
Chemical wetting agents or foam	90	3 (1977)	Estimate
Continuous chemical spray onto input material	90	2 (1976) 3 (1977)	Vendor brochure - estimate
Surface crusting agents	Up to 99	4 (1978)	Ref. 6 (1974) - wind tunnel tests
Enclosure	95 to 99	3 (1977)	Estimate
Storage silos	100	4 (1978)	Estimate
Vegetative windbreak	30	4 (1978)	Estimate
Low pile height	30	4 (1978)	Estimate

* Reference 5 cites References 3 and 4.

physical modeling or by full-scale measurements.[9] The basic relationship rate of windblown dust emissions to the physical parameters which enter into the wind erosion process may be determined by in situ measurements of emissions from isolated areas on representative test pile surfaces.

The physical principles underlying wind erosion of agricultural land has been the subject of field and laboratory investigation for a number of years. This research has focused on the movement of total soil mass, primarily sand-sized aggregates, as a function of wind and soil conditions.[10,11] Wind tunnels have been used commonly in these investigations to measure soil loss under controlled wind conditions. Only relatively recently, however, have field measurements been performed in an effort to quantify fine particle emissions produced by wind erosion (e.g., Gillette).[12,13]

EMISSION FACTOR EQUATION

Cowherd et al.[14] have proposed a predictive equation to calculate annual average suspended particulate emissions generated by wind erosion of exposed, flat, or rolling terrain. The equation relates the total rate of wind erosion to the following field and climatic parameters:

$$E = 3{,}400 \frac{\left(\frac{e}{50}\right)\left(\frac{s}{15}\right)\left(\frac{f}{25}\right) V}{\left(\frac{PE}{50}\right)^2} \quad (1)$$

where

E = emissions of suspended particulate, i.e., particles smaller than 30 μm in Stokes diameter based on a particle density of 2 to 2.5 g/cm^3 (lb/acre/year)

e = surface erodibility or potential annual loss rate for a wide, unsheltered, isolated field with a bare, smooth surface based on the percentage of erodible dry aggregates (particles smaller than 0.84 mm in diameter) as determined from the fraction passing through a 20-mesh screen (relationship in Reference 15) (tons/acre/year)

s = surface silt content, defined as particles smaller than 75 μm as determined by dry sieving through a 200-mesh screen (%)

f = percent of the time that the wind velocity, measured at 1 ft above the surface, exceeds the nominal wind erosion threshold value of 12 mph (5.4 m/sec)

V = fractional value reflecting reduction of wind erosion due to vegetative cover (equals 1.0 for bare soil)

PE = Thornthwaite's Precipitation Evaporation Index[16] used as a measure of average surface moisture content.

The proportionality constant of 3,400 in the above equation was calculated using data developed by Gillette[17] for an eroding agricultural soil in west Texas. The constant is based on a friction velocity (measure of surface shear stress) of 25 cm/sec (the wind erosion threshold of the test soil), a particle density of 2.5 g/cm^3, and a field length of 2/3 km.

EXPERIMENTAL VERIFICATION

In order to check the applicability of Equation 1 to a coal storage pile, a testing program was conducted by Cowherd et al.[18] which entailed the use of a portable wind tunnel developed by Gillette.[19] The wind tunnel consisted of a two-dimensional 5:1 contraction section, an open-floored test section, and a roughly conical diffuser. The test section of the tunnel was placed directly on the surface to be tested (15 cm x 2.4 m), and the tunnel centerline air flow was adjusted to predetermined velocities up to 27 m/sec (60 mph), as measured by a pitot tube at the downstream end of the test section.

An emissions sampling module was designed and fabricated for use with the pull-through wind tunnel in measuring particulate emissions and particle size distributions generated by wind erosion. As shown in Figure 1, the sampling module was located between the tunnel outlet hose and the fan inlet. The sampling train, which was operated at 34 m^3/hr (20 cfm), consisted of a tapered probe, cyclone precollector, parallel-slot cascade impactor, back-up filter, and high volume motor. Interchangeable probe tips were sized for isokinetic sampling at cross-sectional average velocities of 7, 12, 17, and 27 m/sec within the tunnel test section.

Testing was performed on the upper flat surface of the coal pile--on both undisturbed (crusted) and disturbed sections. A test surface was disturbed, i.e., the thin crust was crushed, by walking over it with a twisting action.

In order to determine the quantity and textural properties of each material being eroded, samples of the loose surface material were removed from an area adjacent to the test surface before each test series and from the test surface subsequent to each test series. The samples were obtained by manually sweeping the surface with a small broom. Further detail on the testing program is presented elsewhere.[18]

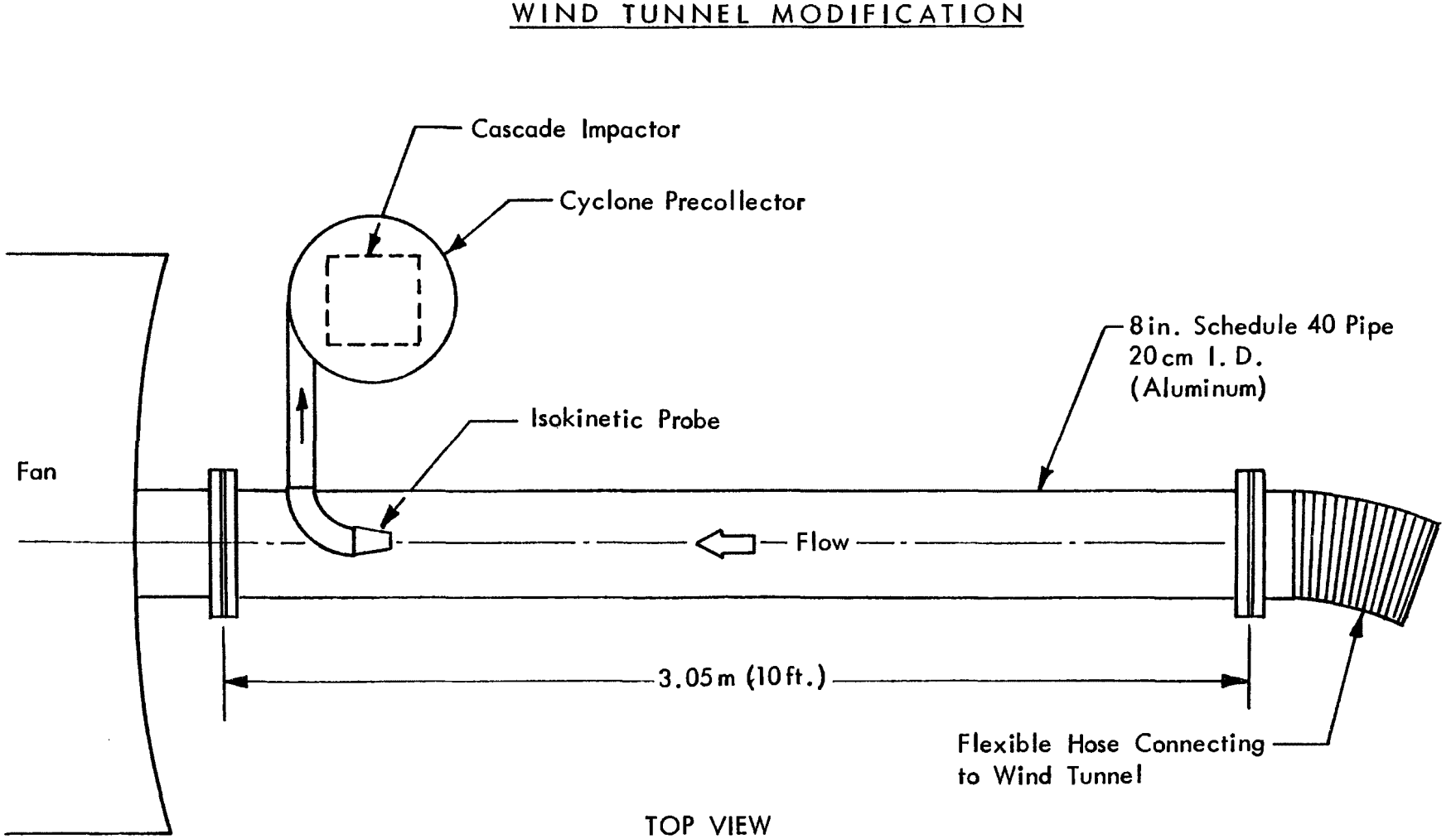

Figure 1. Emissions sampling module for portable wind tunnel.

The measured wind tunnel erosion rate for a disturbed (uncrusted) coal surface was found to compare within 20% of the value predicted by Equation 1 when the following adjustments were made:

1. Friction velocity: The equation was modified for the increased friction velocity (U_*) of the test as compared to 25 cm/sec using the following relationship for the test soil:[20]

$$E \sim (U_*)^{9.67} \quad (2)$$

2. Field length: In separate wind tunnel experiments, Gillette[13] has shown that avalanching of the total mass of particulate generated from erosion of a flat surface of loose material is limited to the first portion of the tunnel length. Thus, a field length factor of 1.0 was used in place of the value of 0.85 that was incorporated into Equation 1.

Although it is likely that erodibility of coal with a density of about 1.0 g/cm^3 is greater than soil with a density of 2.5 g/cm^3, no data were available to correct for this difference.

ESTIMATION OF CONTROL EFFICIENCY

Equation 1 can be used to estimate the efficiency of controls applied to raw material storage piles. This entails measurement of the effects of the specific control method on the parameters which enter into the equation, rather than the much more difficult measurement of the reduction in particulate emissions.

For example, wetting of the pile surface increases the moisture content which is represented in Equation 1 by the Precipitation-Evaporation Index. Techniques for measurement of surface moisture are presented in Reference 18.

In checking the moisture levels of the storage pile surface, the diurnal variation of surface moisture in the absence of moisture addition must be taken into account. The daytime variation of surface moisture is illustrated in Figure 2, based on measurements of moisture levels in coal and taconite pellet piles. Under dry summertime conditions at a test site in Ohio, storage pile moisture levels were found to correlate with weighted precipitation over four days previous to the moisture measurement.[18]

The control efficiency afforded by chemical stabilization of the pile surface may be estimated by measuring the reduction in loose silt on the pile surface, using the techniques for sample collection, reduction, and analysis presented in Reference 18. Chemical stabilizers act to bind suspendable fines to non-erodible coarse particles on the pile surface. In the wind tunnel experiments described above, the natural surface crust on a dormant,

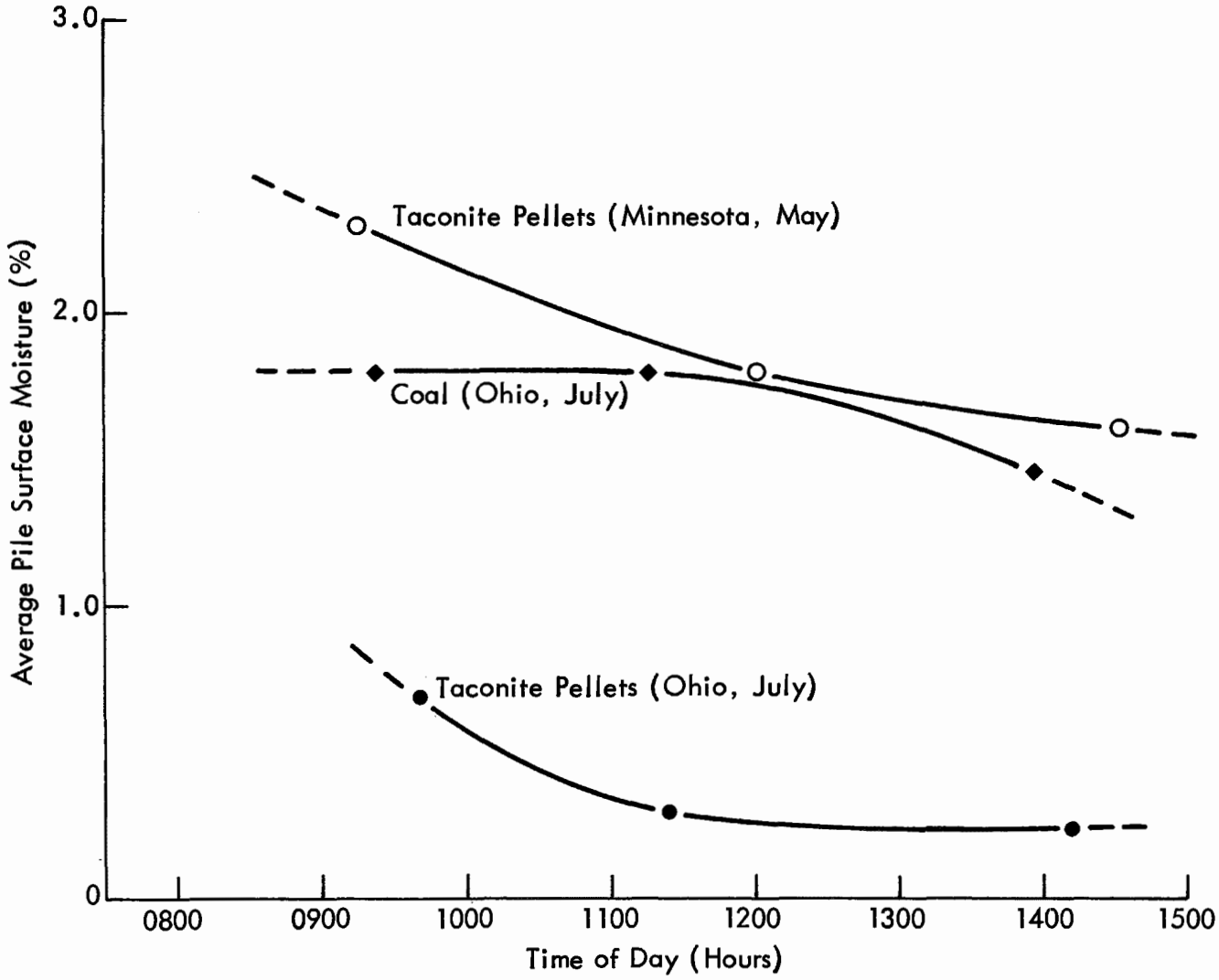

Figure 2. Observed storage pile surface moisture versus time of day.

compacted coal pile was found to reduce the erosion rate by roughly an order of magnitude for tunnel centerline wind speeds exceeding the threshold for the crusted surface (approximately 13 m/sec).[18]

The effect of total or partial enclosures or windbreaks is to reduce the wind speed over the pile surface. An analysis of wind flow patterns around basic pile configurations (at 1 m above the pile surface) is useful in estimating unprotected pile exposure for a range of approach wind speeds measured at a reference height of 10 m. The control efficiency associated with the use of windbreaks may be estimated by measuring the wind flow distribution at various points 1 m above the protected pile surface. However, this is not a straightforward determination because of the complex dependence of suspended particulate emission rate on wind speed above the threshold value.

CONCLUSIONS

In spite of the numerous recent literature sources presenting data on preventive methods for control of windblown dust from storage piles, most of the reported control efficiency values are estimates based on visual observation. These data are traceable to a few primary literature sources. The lack of quantitative data appears to be related to the difficulty measuring wind-generated emissions from storage piles using conventional upwind/downwind sampling techniques.

A predictive emission factor equation developed from measurements of windblown dust from agricultural fields may be used as a tool for better estimating the efficiencies of storage pile controls. This equation has been partially verified against direct measurements of windblown dust from an uncrusted surface of a coal storage pile using a portable wind tunnel coupled with an isokinetic particulate sampling system. The strategy for using the predictive emission factor equation to estimate a control efficiency entails the measurement of the change in parameters which enter into the wind erosion process rather than the more difficult measurement of the reduction in windblown dust emissions.

The usefulness of this approach is directly related to the reliability of the predictive emission factor equation. Refinements to the existing equation were required to achieve good agreement between measured emissions of windblown dust from the uncrusted surface of the test coal storage pile and the generation rate predicted by the equation. These refinements indicate the need for modification of the equation especially as related to the wind speed dependence of the emission rate.

The portable wind tunnel and associated sampling apparatus described in this paper constitute an effective means to define better the relationship of dust emissions generated by wind erosion of industrial aggregates to the influencing parameters and the applicability of previous research on soil erosion. These relationships coupled with an analysis of wind flow patterns around basic storage pile configurations form the basis for development of an improved predictive emission factor equation for storage pile wind erosion, incorporating pile shape parameters. The improved equation can be used to develop reliable estimates of efficiencies for preventive emission controls including those which entail reduction of surface wind speed.

ACKNOWLEDGEMENT

The work upon which this paper is based was performed in part pursuant to Contract No. 68-02-2609 with the U.S. Environmental Protection Agency.

Factors for Conversion to Metric Units

1 lb	= 0.454 kg
1 ft	= 0.305 m
1 mile	= 1.61 km
1 acre	= 0.00405 km^2
1 short ton	= 0.907 metric tonnes
1 mph	= 0.447 m/sec
1 cfm	= 1.70 m^3/hr
1 lb/acre	= 0.112 g/m^2

REFERENCES

1. Anonymous, "Investigation of Fugitive Dust--Sources, Emissions, and Controls," prepared by PEDCo Environmental for U.S. Environmental Protection Agency under Contract No. 68-02-0044, Task 9, May 1973.

2. Anonymous, "Evaluation of Fugitive Dust from Mining," Task 2 Report, prepared by PEDCo Environmental for U.S. Environmental Protection Agency under Contract No. 68-02-1321, Task 36, June 1976.

3. Anonymous, "Technical Guidance for Control of Industrial Process Fugitive Particulate Emissions," EPA-450/3-77-010, prepared by PEDCo Environmental for U.S. Environmental Protection Agency, Research Triangle Park, NC, March 1977.

4. Bohn, R., T. Cuscino, Jr., and C. Cowherd, Jr., "Fugitive Emissions in Integrated Iron and Steel Plants," EPA-600/2-78-050, U.S. Environmental Protection Agency, Research Triangle Park, NC, March 1978.

5. Currier, E. L., and B. D. Neal, "Fugitive Emissions at Coal-Fired Power Plants," paper No. 79-11.4 presented at Annual Meeting of the Air Pollution Control Association, June 1979.

6. Boscak, V., and J. S. Tandon, "Development of Chemicals from Suppression of Coal Dust Dispersion from Storage Piles," paper presented at Fourth Annual Environmental Engineering and Science Conference, Louisville, KY, March 1974.

7. Kolnsberg, H. J., "Technical Manual for Measurement of Fugitive Emissions: Upwind/Downwind Method for Industrial Sources," EPA-600/2-76-089a, U.S. Environmental Protection Agency, Washington, D.C., 1976.

8. Turner, D. B., "Workbook of Atmospheric Dispersion Estimates," AP-26, U.S. Environmental Protection Agency, Research Triangle Park, NC, 1970.

9. Loo, S. L., J. Tyrrel, and A. C. Chen, "Research on Measurement and Control of Windblown Dust from Storage Piles," Quarterly Report prepared for U.S. Environmental Protection Agency under Grant No. R805969-01-0, December 1978.

10. Bagnold, R. A., The Physics of Blown Sand and Desert Dunes, Methuen, London, 1941.

11. Chepil, W. S., and N. P. Woodruff, "The Physics of Wind Erosion and Its Control," in: Advances in Agronomy, Vol. 15, A. G. Norman (Ed.), Academic Press, New York, NY, 1963.

12. Gillette, D. A., and I. H. Blifford, Jr., "Measurement of Aerosol Size Distributions and Vertical Fluxes of Aerosols on Land Subject to Wind Erosion," J. of Applied Meteorology, 11, 1972, p. 977.

13. Gillette, D., "A Wind Tunnel Simulation of the Erosion of Soil: Effect of Soil Texture, Wind Speed, and Soil Consolidation on Dust Production," Atmospheric Environment, 12, 1978, p. 2309.

14. Cowherd, C., Jr., C. M. Maxwell, and D. W. Nelson, "Quantification of Dust Entrainment from Paved Roads," EPA-450/3-77-027, U.S. Environmental Protection Agency, Research Triangle Park, NC, July 1977.

15. Woodruff, N. P., and F. H. Siddoway, "A Wind Erosion Equation," Soil Science Society of America Proceedings, 29, 1965, p. 602.

16. Cowherd, C., Jr., K. Axetell, Jr., C. M. Guenther (Maxwell), and G. Jutze, "Development of Emission Factors for Fugitive Dust Sources," EPA-450/3-74-037, U.S. Environmental Protection Agency, Research Triangle Park, NC, June 1974.

17. Gillette, D. A., "Production of Fine Dust by Wind Erosion of Soil: Effect of Wind and Soil Texture," Proceedings of the 1974 Symposium on Atmospheric-Surface Exchange of Particulate and Gaseous Pollutants, 1976.

18. Cowherd, C., Jr., R. Bohn, and T. Cuscino, Jr., "Iron and Steel Plant Open Dust Source Fugitive Emission Evaluation," EPA-600/2-79-103, U.S. Environmental Protection Agency, Research Triangle Park, NC, May 1979.

19. Gillette, D., "Tests with a Portable Wind Tunnel for Determining Wind Erosion Threshold Velocities," Atmospheric Environment, 12, 1978, p. 1735.

20. Gillette, D. A., "On the Production of Soil Wind Erosion Aerosols Having the Potential for Long Range Transport," paper presented at the International Symposium on the Chemistry of Sea-Air Particulate Exchange Process, Nice, France, 1973.

THE CONTRIBUTIONS OF OPEN SOURCES TO AMBIENT TSP LEVELS

By:

John S. Evans and Douglas W. Cooper
Harvard School of Public Health
Boston, Massachusetts 02115

ABSTRACT

We estimate that open sources (roads, fields, construction, etc.) contribute 400 x 10^6 tons/year of particles to the atmosphere in the U.S. Total U.S. point and area source particulate emissions are approximately 20 x 10^6 tons/year. Proposed open source control strategies cannot be assessed rationally without considering the influences of characteristic differences in patterns of location, particle size distributions, and emission heights of these two major source types, open sources and point sources. Simple physical and statistical models indicate that although open sources contribute less per ton of emissions to monitored TSP concentrations than point sources, due to their vast emission rates they account for a greater fraction of ambient mass concentration than point sources. Further analysis indicates that although open source control programs seem attractive on the basis of the cost-effectiveness of emissions reductions, and in some cases may be necessary to local compliance efforts, they may not provide an economically attractive means of achieving widespread reductions in ambient TSP levels.

THE CONTRIBUTIONS OF OPEN SOURCES TO AMBIENT TSP LEVELS

INTRODUCTION

Although over the last few years vast sums have been spent on the control of air pollution from point sources, in many areas of the United States the primary air quality criteria for total suspended particulates (TSP) are not being met. Figures 1 and 2 indicate the extent of non-compliance and the severity of the problem. Figure 1 shows that while there are violations of the annual TSP standard in every region of the country, widespread violations of both the annual and daily maximum TSP standards are most prevalent in the Southwest.[25] Figure 2 presents two alternative measures of the severity of a state's TSP problem. For each state we have calculated the arithmetic mean of both the geometric annual mean and the 90th percentile concentration reported by all of the TSP monitors in the state, using 1976 SAROAD data.[27] On the basis of this analysis it appears that most states which have high average geometric annual mean concentrations also have extremely high 90th percentile concentrations. The most severe TSP problems seem to be concentrated in two rather distinct regions, the Ohio River Valley and the Southwest.

Traditionally, it has been assumed that point sources (e.g., utility combustion, cement manufacture, metal processing) were the dominant anthropogenic sources of atmospheric particles. The notion was that while open sources, those sources too large in extent to be controlled by enclosure or ducting (such as unpaved roads, agricultural tilling, construction activities, surface mining...) might emit significant quantities of dust, the impact of these emissions would be highly localized and sporadic. Recently this belief has come to be questioned.

THE EVIDENCE FROM AIR SAMPLING

Table 1, from the work of Lynn et al. (1976),[28] indicates that approximately 65% of the mass collected by high-volume samplers in 14 U.S. cities under study was of mineral origin. The mineral component of TSP, consisting largely of quartz, calcite, hematite, and feldspars, is commonly attributed to wind erosion, resuspension of soil, quarrying, cement manufacturing, iron and steel processing, and fuel combustion (fly ash)(Dzubay(1979)).[8] The microscopy techniques used by Bradway and Record (1976)[1] permitted enough resolution of the mineral component so that fly ash could be excluded from it. Hematite (which might be primarily due to industrial emissions) accounted on the average for only 15% of the mineral component in these 14 cities (Lynn, et al.).[28] Several other studies of the composition of the ambient aerosol (and its sources) are of interest:

i. Microscopic analysis of high-volume filters collected on twenty days with TSP levels above 130 $\mu g/m^3$ in Evansville, Indiana, indicated high contributions

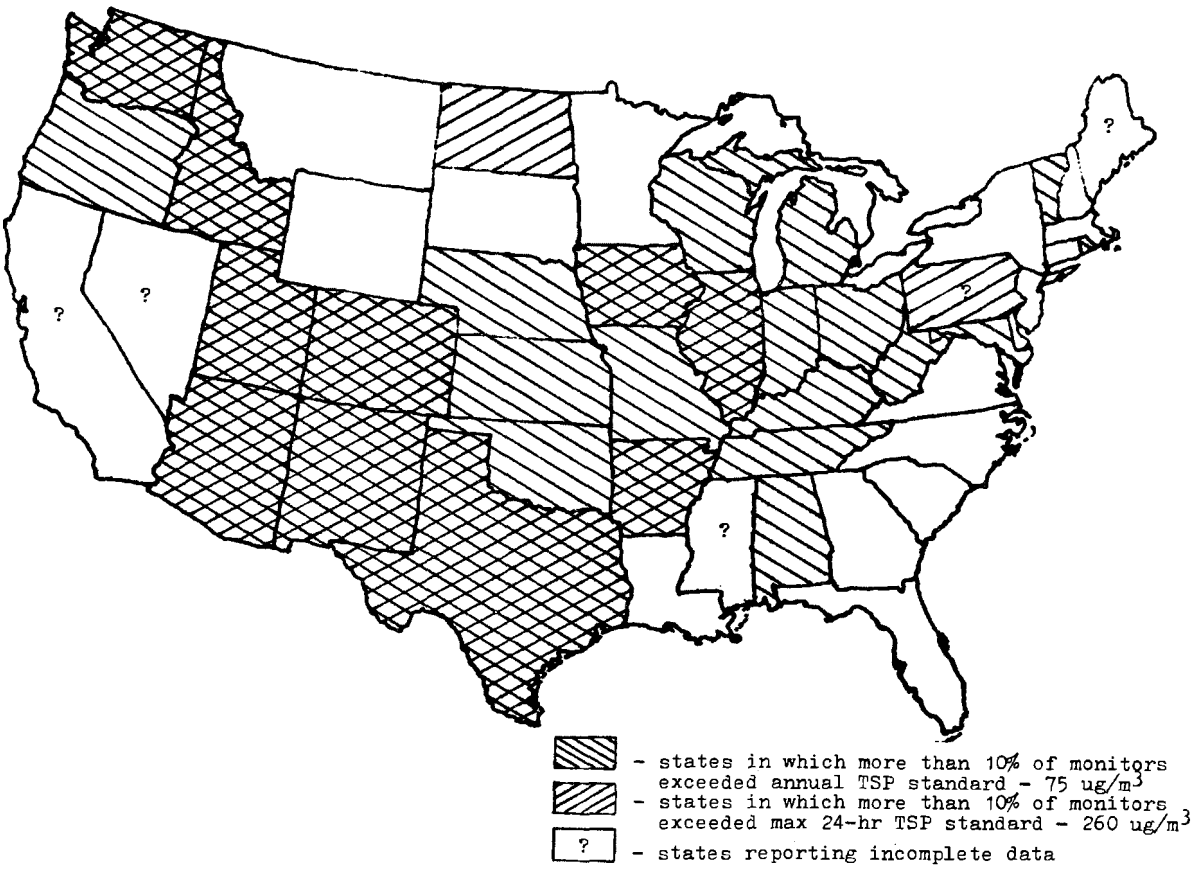

Figure 1. Noncompliance With Primary TSP Standards - 1977

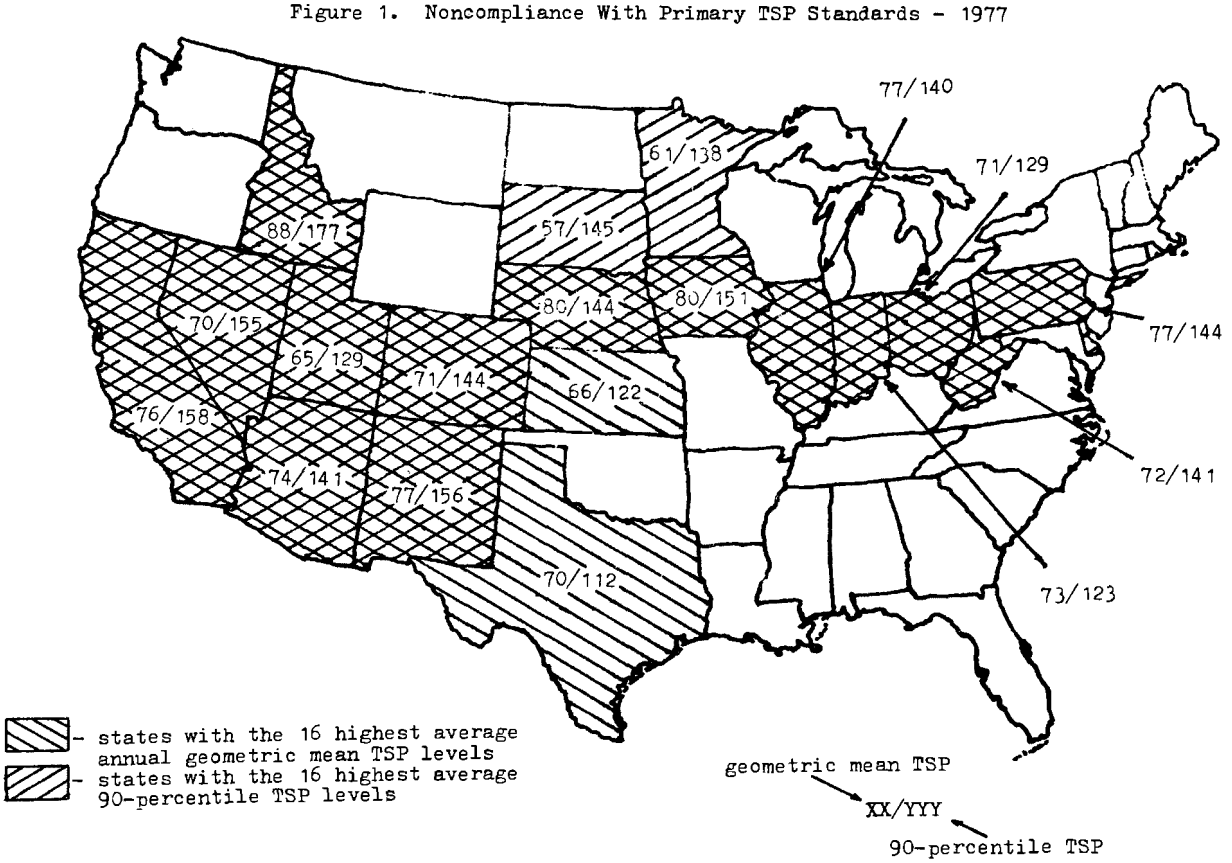

Figure 2. Severity of Ambient TSP Levels - 1976

Table 1. COMPOSITE SUMMARY OF MICROSCOPIC ANALYSIS IN 14 CITIES, $\mu g/m^3$ *

City	Minerals		Combustion products		Biological material		Miscellaneous	
	Average	Range	Average	Range	Average	Range	Average	Range
Heavily industrialized								
Cleveland	51	28-85	40	10-70	1	<1-5	8	tr-22
Birmingham[a]	66	14-90	22	2-86	2	0-8	10	0-50
Philadelphia[a]	64	6-93	33	6-89	1	0-10	2	0-30
Baltimore[a]	69	52-88	25	11-61	3	<1-11	3	0-26
St. Louis	75	21-99	21	1-79	<1	0-5	4	0-10
Cincinnati	51	24-88	44	9-84	1	<1-5	4	<1-20
Moderately industrialized								
Chattanooga	36	3-96	35	8-78	16	0-90	13	0-45
Denver	81	62-97	7	1-19	1	0-7	11	0-32
Seattle	60	30-96	27	1-62	3	tr-24	10	<1-40
Providence	64	28-92	22	4-68	1	0-5	13	0-35
Lightly industrialized								
Washington, D.C.	70	39-87	23	5-49	5	<1-47	2	<1-25
Oklahoma City	88	63-99	8	1-31	<1	<1-4	4	<1-30
Miami[b]	79	75-83	9	7-12	<1	<1	12	10-15
San Francisco	52	29-73	29	10-50	3	tr-10	16	0-35
All cities	65	3-99	25	1-89	3	0-90	7	0-50

[a] Excludes analyses of NASN site filters

[b] Analyses of NASN site filters only

* from Lynn, D. A. et al, National Assessment of the Urban Particulate Problem, EPA-450/3-76-024, (1976).

(approximately 60% by weight) of "alluvial dust." Among these data strong positive correlations existed between wind speed and TSP, and between wind speed and TSP of alluvial origin (Mukherji, et al. (1978)).[5]

ii. Hopke et al. (1976)[3] found, through factor and cluster analyses, that a "crustal factor" accounted for over 50% of the total variance in their data set, which consisted of the measured concentrations of 18 elements from over ninety samples collected at seven locations in Boston.

iii. Gaarenstroom et al. (1977)[4] demonstrated with factor analysis that at an urban monitor in Phoenix a "soil factor" explained 53% of the variance in a data set consisting primarily of measured elemental concentrations. For a similar data set taken at a desert location 60 miles outside of Phoenix this "soil factor" explained only 38% of the variance. Total particulate mass was heavily weighted (.84 in the urban location and .73 in the remote location) in both "soil factors." These heavy weights indicate high correlation between total mass and the "soil factor."

iv. Applying the chemical element balance method to elemental data from dichotomous samplers at ten RAPS sites in St. Louis, Dzubay (1979)[8] found that crustal shale and limestone accounted for 43% of total mass, 83% of the coarse fraction (2.4 μm ≤ aerodynamic diameter < 20 μm) and 9.8% of the fine fraction (aerodynamic diameter < 2.4 μm).

v. The results of Richard and Tan (1977),[9] who used microscopy, indicated that about 70% of the total mass collected by high-volume samplers in the Phoenix area consists of particles with diameters greater than 20 μm. Open sources (and fugitive industrial sources) emit much larger particles, on the average, than traditional point sources.

vi. Hammerle and Pierson (1975)[7] found that less than 30% of the mass of Fe, Ti, and Ca (all possibly of soil origin) collected on membrane filters in Pasadena was due to particles with aerodynamic diameters less than 1.5 μm, while about 80% of the total mass of Pb and Br was in this small size fraction. The percentage of Fe in the small size fraction was found to be negatively correlated with wind speed (as might be expected for soil dust), and positively correlated with precipitation. On the basis of a chemical element balance they estimated that 20% by weight of the particles collected were "soil dust."

vii. Using the chemical element balance method, Gartrell and Friedlander (1975)[2] have estimated that 19.8 $\mu g/m^3$ (23% of total mass) and 15.1 $\mu g/m^3$ (9% of total mass) of TSP collected in samples from Pasadena and Pomona, California was "soil dust."

viii. Examining the relative abundance of various elements in impactor samples collected in South Florida, Hardy et al. (1976)[6] concluded that urban enrichment of the large-particle size fraction may be attributed to soil dust.

On the basis of these estimates it would appear that open sources contribute significantly to measured TSP concentrations, particularly on days with high winds, offsetting the decrease in concentrations of material from traditional sources with relatively constant emission rates. Although open sources contribute primarily to the large size fraction, their impact on respirable/inhalable particulate concentrations is not negligible. In the remainder of this paper we estimate open source emission rates, and explore their relationships with measured TSP concentrations in an attempt to assess the necessity and practicality of open source controls.

OPEN SOURCE EMISSION RATES

One of the primary reasons for the current uncertainty as to the significance of open sources of TSP has been the unavailability of emissions estimates or acceptable methods for the estimation of emissions rates. Although Chepil, Woodruff and Siddoway(1965)[23] and others began working in the 1930's on the problem of estimating agricultural soil losses due to wind erosion, only recently has the relevance of their work to air pollution been recognized. Handy (1975)[18] and his colleagues at Iowa State University also made some early estimates of soil transport by the wind and more recently have published estimates of dust fallout near unpaved roads. Throughout the literature there are scattered discussions of the importance of other open sources; however, the first comprehensive discussions of the open source problem are those of Cowherd et al. (1974)[15,17](1976),[16] Jutze and Axetell (1974),[19] and Carpenter and Weant (1977).[22] Cowherd and his colleagues at Midwest Research Institute developed methodologies for the estimation of emissions from agricultural tilling, paved and unpaved roads, construction activities, and dirt airstrips. They noted that the wind erosion equation of Woodruff and Siddoway (1965)[23] might be adapted to permit estimation of dust emissions due to wind erosion of agricultural land.

Carpenter and Weant at Research Triangle Institute used NEDS data for emissions from dirt roads, landings and takeoffs from dirt airstrips, and agricultural tilling (based upon the work of Cowherd), and on emissions from open burning, agricultural slash burning, and coal refuse fires, in conjunction with data on conventional point and area sources, to demonstrate that in most (146) of the 150 AQCR's which violated TSP standards in 1976, over 50% of all emissions were from open sources. Jutze and Axetell, of PEDCo Environmental Specialists, estimated the emissions rates from unpaved roads, construction activities, agricultural wind erosion and tilling, tailings piles, aggregate storage piles, and feedlots for five AQCR's in the states of New Mexico, Nevada, Arizona, and California. As part of their study, field sampling programs were conducted to develop emission factors for unpaved roads, agricultural tilling, and construction activities.

Supplementing the methodology of Cowherd et al. with estimates of the emissions factors for forest fires and prescribed agricultural burning (Yamate et al.(1975)[24] and Ward et al.(1976)),[21] surface mining (Ochsner and Blackwood (1977)),[29] and tailings piles (Amick (1974)),[11] we developed the formula shown in Table 2 for estimating total annual open source emission rates for any region of interest. In order to estimate the total open source emissions rates for each state, we collected data, applicable to the mid-1970's, for each of the climatic, geologic, and economic factors which appear in the formula. The development of the formula and data base is described in detail in Evans et al. (1978).[10] Our open source emissions estimates are summarized in Table 3. These estimates indicate that nationally the largest open sources, in descending order, are: unpaved roads (319 x 10^6 tons/yr), construction activities (27 x 10^6 tons/yr), and wind erosion of cropland (23 x 10^6 tons/yr). Total U.S. open source emissions are estimated to be approximately 410 million tons per year. As a point of comparison, total point source emissions in the U.S. in the mid 70's were estimated to be about 20 million tons per year (CEQ(1976)).[14] On the basis of these estimates alone

Table 2. FORMULAS FOR ESTIMATING OPEN SOURCE EMISSION RATES

agricultural tilling emissions	where:
$E_A = (1.1\, S_a(s_i/5.5)/(PE/50)^2)(H)(T_1)/2000$	S_a - agricultural soil silt content (%) s_i - implement speed (mph) PE - Thornwaite's PE index H - acreage of harvested cropland T_1 - number of tillings per year = 3
agricultural wind erosion emissions	
$E_W = (.025\ I\ K\ C\ L'V')(H)/100$	I - soil erodibility index (tons/acre/yr) K - surface roughness C - climatic factor L' - unsheltered field width factor = 1.0 V' - vegetative cover factor
construction activity emissions	
$E_C = (1)(D)(E)(M)$	D - duration (months) E - extent (acres/10^6 \$) M - construction expenditure (10^6 \$)
forest fire emissions	
$E_F = (150\ F_F)(B)/2000$	F_F - available fuel (tons/acre) B - acres burned in wildfires
prescribed burning emissions	
$E_P = (50\ F_P)(P)/2000$	F_P - available fuel (tons/acre) P - acres burned in prescribed fires
surface coal mining emissions	
$E_M = ((1.7\ T_{me}) + (0.06\ T_{mw}))/2000$	T_{me} - tons mined in Eastern U.S. T_{mw} - tons mined in Western U.S.
other surface mining emissions	
$E_S = (2)(T)/2000$	T - tons handled at surface mines
paved road emissions	
$E_R = (0.013)(M_{Pr} \times 10\, U_r + M_{Pu} \times 10\, U_u)/2000$	M_{Pr} - miles of paved rural roads M_{Pu} - miles of paved urban roads U_r - rural use factor - vehicle miles/mile U_u - urban use factor - vehicle miles/mile
unpaved road emissions	
$E_u = (0.65\ S_r(\frac{s}{40})(\frac{d}{365}))(M_{ur} \times U_r + M_{uu} \times U_u)/2000$	S_r - road surface silt content (%) s - vehicle speed (mph) d - number of dry days/year M_{ur} - miles of unpaved rural roads M_{uu} - miles of unpaved urban roads U_r - rural use factors - vehicle miles/mile U_u - urban use factors - vehicle miles/mile
tailings pile emissions	
$E_T = (0.133\ C)(A)$	C - climatic factor A - acres of tailings piles
total open source emissions	
$E_O = E_A + E_W + E_C + E_F + E_P + E_M + E_S + E_R + E_u + E_T$	

Table 3. OPEN SOURCE EMISSIONS RATE ESTIMATES (10^3 TONS/YR)

State	Tilling	Wind Erosion	Construction	Wild Fires	Prescribed Fires
AL	5.30	47.5	273.	102.00	15.60
AK	0.10	0.0	59.	646.80	0.00
AZ	117.00	713.1	139.	28.50	5.20
AR	14.60	159.3	141.	94.50	4.10
CA	126.00	3945.8	4854.	218.80	21.20
CO	158.00	881.6	117.	25.00	0.50
CT	0.50	4.1	333.	1.00	0.00
DE	0.60	8.6	10.	0.05	0.04
FL	5.00	92.2	766.	316.60	71.90
GA	8.45	91.5	455.	41.30	54.30
HI	2.30	0.0	62.	0.00	0.00
ID	88.80	987.8	24.	544.00	45.40
IL	151.00	1721.4	1415.	11.40	0.00
IN	52.40	842.6	773.	8.90	0.00
IA	142.00	2077.7	253.	1.90	0.00
KS	239.00	4769.0	245.	65.80	0.00
KY	15.10	122.1	270.	62.50	0.00
LA	14.40	90.7	870.	73.00	16.60
ME	1.20	10.4	87.	2.50	0.00
MD	2.10	44.6	128.	1.40	0.00
MA	0.50	6.4	1260.	8.40	0.00
MI	21.20	410.7	743.	7.70	0.30
MN	99.30	1610.6	452.	30.80	0.00
MS	12.90	71.9	138.	78.60	12.70
MO	61.70	858.8	346.	119.80	0.00
MT	200.00	1264.1	31.	99.60	52.90
NE	306.00	5218.9	197.	20.00	0.00
NV	68.00	1157.1	22.	14.80	0.00
NH	0.40	0.5	69.	0.46	0.00
NJ	1.60	15.7	844.	23.50	1.50
NM	50.30	842.3	61.	19.90	1.40
NY	20.10	149.6	1462.	6.00	0.00
NC	6.30	118.2	640.	75.10	8.80
ND	292.00	3553.3	80.	0.47	0.10
OH	44.20	822.8	1365.	5.20	0.00
OK	89.00	1177.9	332.	115.80	0.00
OR	39.40	48.2	212.	196.50	21.60
PA	21.60	81.6	2090.	12.90	0.00
RI	0.10	0.9	82.	0.70	0.00
SC	4.30	54.0	177.	43.60	29.10
SD	210.00	3119.6	39.	4.80	0.00
TN	10.90	41.2	333.	27.70	0.00
TX	386.00	5000.7	3760.	19.10	6.20
UT	78.40	653.4	203.	10.00	0.00
VT	1.90	8.1	17.	0.20	0.00
VA	5.30	71.0	212.	5.60	3.90
WA	14.60	64.3	447.	164.30	56.80
WV	2.84	5.6	215.	74.20	0.00
WI	49.00	663.1	218.	6.90	0.00
WY	56.30	638.8	59.	8.30	0.00

Table 3. (CONT'D)

State	Extraction: Coal	Extraction: Other	Tailings	Paved Roads	Unpaved Roads
AL	16.9	39.3	1.1	149.	3760.
AK	0.6	127.0	0.0	11.	1990.
AZ	0.2	187.0	156.7	92.	9740.
AR	0.4	38.0	1.0	73.	9340.
CA	0.0	171.0	141.5	803.	27530.
CO	0.2	33.8	17.0	89.	10080.
CT	0.0	15.1	0.4	117.	320.
DE	0.0	2.4	0.0	23.	70.
FL	0.0	235.0	2.6	386.	7010.
GA	0.0	54.6	1.3	212.	7010.
HI	0.0	9.0	0.0	26.	80.
ID	0.0	17.8	30.9	30.	4120.
IL	49.5	104.0	5.5	370.	7960.
IN	20.2	58.1	2.6	229.	6450.
IA	0.5	49.4	4.8	104.	11310.
KS	0.6	28.5	22.5	78.	14330.
KY	116.6	36.6	2.1	146.	4380.
LA	0.0	24.5	0.4	121.	3790.
ME	0.0	5.4	0.2	43.	710.
MD	2.0	30.5	0.8	154.	710.
MA	0.0	25.7	0.5	182.	680.
MI	0.0	139.0	6.7	345.	8830.
MN	0.0	216.0	20.4	139.	11560.
MS	0.0	18.2	0.2	81.	4260.
MO	3.9	56.1	19.3	175.	10330.
MT	0.4	33.9	11.6	28.	773.
NE	0.0	16.9	2.8	56.	10610.
NV	0.0	36.8	142.2	21.	4890.
NH	0.0	6.8	0.0	32.	1250.
NJ	0.0	44.9	1.8	304.	1950.
NM	0.3	42.5	44.0	48.	10640.
NY	0.0	75.6	10.0	414.	5160.
NC	0.0	57.1	2.0	220.	3860.
ND	0.0	5.1	1.5	17.	8800.
OH	38.6	95.9	6.3	403.	3820.
OK	2.0	32.0	6.5	123.	11860.
OR	0.0	45.0	1.4	83.	12110.
PA	68.4	90.7	4.0	424.	10100.
RI	0.0	3.2	0.1	36.	390.
SC	0.0	24.3	0.6	126.	1350.
SD	0.0	12.4	5.3	24.	6370.
TN	6.4	56.0	1.5	191.	4380.
TX	0.0	116.0	25.9	476.	28640.
UT	0.2	55.8	118.0	42.	5410.
VT	0.0	5.3	0.7	18.	1180.
VA	29.2	58.7	3.9	214.	2340.
WA	0.1	38.1	0.7	137.	6710.
WV	87.1	14.6	1.2	60.	3920.
WI	0.0	53.9	2.9	176.	3310.
WY	0.6	17.9	5.9	19.	2440.

it would seem that open sources might warrant further consideration. Proposed open source control strategies cannot be assessed rationally without considering the extent to which characteristic differences in patterns of location, particle size distributions, and emission heights of these two major source types (point sources and open sources) affect the contribution to TSP values per ton of emissions.

THE CONTRIBUTIONS OF OPEN AND POINT SOURCES TO TSP LEVELS

An evaluation of the impact of application of various control methodologies to a single specified open source, such as a particular mine, field, or stretch of unpaved road, would require site-specific dispersion calculations, but a basic assessment of the general relationship between open source emission rates and ambient TSP levels may be conducted without the benefit of site-by-site dispersion calculations. For example, using states as the unit of observation, and specifying semi-theoretical relationships ("models") linking source emissions and ambient concentrations, readily available meteorological and aerometric data may be used to estimate model parameters empirically. Although these models are not intended to supplant more traditional dispersion calculations, they may economically provide information useful to those faced with the determination of efficient and equitable courses for national policy.

Using our own estimates of open source emissions rates, published estimates of point source emission rates(E.P.A."point" and "area" sources are considered as point sources)(U.S. E.P.A. (1976))[26] and climatological and aerometric data for 1976 (U.S. E.P.A. (1978) [25] and Holzworth (1972)[34]), we have explored the contributions of open and point sources to measured TSP levels. Our data are summarized in Table 4. (The state-by-state data will be made available on request.) Three models have been considered:

Model 1 - Rollback

$$TSP = a_{10} + a_{11}E_o + a_{12}E_p + a_{13}TSP_a + a_{14}P \qquad (1)$$

Model 2 - Modified ADTL

$$TSP = a_{20} + a_{21}\left[\frac{E_o/A}{u}\right] + a_{22}\left[\frac{E_p/A}{u}\right] + a_{23}TSP_a + a_{24}P \qquad (2)$$

Model 3 - Simple Box

$$TSP = a_{30} + a_{31}\left[\frac{E_o}{(H\cdot u)\sqrt{A}}\right] + a_{32}\left[\frac{E_p}{(H\cdot u)\sqrt{A}}\right] + a_{33}TSP_a + a_{34}P \qquad (3)$$

where:
- TSP = station-averaged annual geometric mean TSP level ($\mu g/m^3$)
- E_o = total open source emission rate (10^3 tons/yr)
- E_p = total point source emission rate (10^3 tons/yr)
- TSP_a = perimeter-weighted, adjacent states station-averaged annual geometric mean TSP ($\mu g/m^3$)

Table 4. REGRESSION INPUTS

Input	Mean	Standard Deviation
TSP	58.8	12.9
E_o	8150.	7815.
E_p	307.	359.
P	110.6	34.3
TSP_a	55.7	10.0
$E_o/H \cdot u\sqrt{A}$	2.26	1.35
$E_p/H \cdot u\sqrt{A}$	0.120	0.136
A	72.3	87.8
u	9.2	1.40
H·u	64.9	10.2

Table 5. REGRESSION RESULTS

Factor: Model	constant a_{i0} ($t_{a_{i0}}$)	open sources a_{i1} ($t_{a_{i1}}$)	open sources a_{i2} ($t_{a_{i2}}$)	adjacent TSP a_{i3} ($t_{a_{i3}}$)	precipitation a_{i4} ($t_{a_{i4}}$)	R^2 (R^2_{adj})
Rollback	47.	0.00029	0.011	0.29	-0.094	39
(i=1)	(3.7)	(1.2)	(2.5)	(1.7)	(-1.7)	34
ADTL	49.	0.35	4.4	0.33	-0.15	42
(i=2)	(4.0)	(1.9)	(2.5)	(2.0)	(-3.1)	36
Box	50.	2.2	29.	0.32	-0.15	42
(i=3)	(4.0)	(1.9)	(2.5)	(1.9)	(-3.1)	37

Table 6. EXAMINATION OF RESIDUALS

model	overprediction		underprediction	
	state	standardized residual	state	standardized residual
rollback	(1) Wyoming	-2.8	Idaho	+3.2
	(2) Montana	-1.9	West Virginia	+1.7
	(3) North Dakota	-1.5	Nebraska	+1.4
box	(1) Wyoming	-2.6	Idaho	+3.6
	(2) Montana	-1.6	Nebraska	+1.5
	(3) North Dakota	-1.5	W. Virginia	+1.5

P = precipitation, number of days with rain (≥.01 inch) or snow (≥1 inch) per year
A = state area (1000 miles^2)
u = mean surface wind speed (mph)
H·u = mean annual (morning + afternoon/2) mixing height times mean annual wind speed averaged through mixing height (100 m^2/s)

The rollback model was chosen because of its simplicity and its history of application in air pollution policy determination (deNevers and Morris (1973)).[30] The other two were selected because they are somewhat more physically realistic, accounting at least partially for the effects of wind speed, mixing height, and state area. In the rollback model source contributions to TSP are assumed to be proportional to their emission rates. In the modified ADTL model, TSP concentrations are assumed to vary proportionally with emission rate per area and inversely with mean wind speed. In the box model source contributions to TSP are proportional to emissions rates and inversely proportional to the volumetric flow rate of dilution air (Hanna (1971) [31] and Benarie (1978)).[33] We have modified each of these models slightly, allowing for transport of particles from adjacent states and for the atmospheric cleansing effect of precipitation.

The results of ordinary least squares analyses of these data, cf. Table 5, indicate that even these simple models are descriptively useful. In Table 5 each empirical coefficient (e.g., a_{ij}) is reported along with its t-statistic; i.e., $t_{a_{ij}}$. The empirical coefficients reported are multipled by the appropriate terms to yield the full empirical model. For example, the full rollback model would be:

$$TSP = 47.0 + 0.00029\ E_o + 0.011\ E_p + 0.29\ TSP_a - 0.094\ P \qquad (4)$$

The t-statistics are indicators of the likelihood that an empirical coefficient at least as large as the one reported could have arisen by chance if the true coefficient were zero. Mathematically, the reported t-statistics are found simply by dividing the empirical coefficients, a_{ij}, by an estimate of their standard error; i.e.,

$$t_{a_{ij}} = \frac{a_{ij}}{s_{a_{ij}}} .$$

(The t-statistics are distributed with n - (k + 1) degrees of freedom; where n is the number of observations and k is the number of variables.) Thus, the larger the absolute value of the t-statistic the less likely that the true coefficient is zero. With 45 degrees of freedom, t values of 1.68 and 2.69 would be significant at the .05 and .005 levels respectively in a one-tailed test. In addition, the coefficient of determination, R^2, and the adjusted R^2 is reported for each model. The R^2 indicates the fraction of the variance in TSP which is accounted for by the model. The adjusted R^2, or corrected coefficient of determination, is a better measure of the adequacy of the model, which accounts for the use of degrees of freedom by the introduction of more independent variables. In addition to examining the coefficients individually, using the F-statistic we may explore the possibility that all of the true coefficients are zero. The F is mathematically equivalent to

$$\frac{n - (k + 1)}{k} \cdot \frac{R^2}{1 - R^2},$$

and is distributed with k and n - (k + 1) degrees of freedom. An F value of 4.27 is significant at the 0.01 level for 4 and 45 degrees of freedom. Complete discussions of these statistical parameters are found in standard statistical texts, for example, those by Armitage, Wonnacutt and Wonnacutt, and Draper and Smith. Several features of these results should be noted. First, the sign of each empirical coefficient is in agreement with intuition. Second, in each equation point sources contribute more to TSP, per ton of emissions, than open sources. This would be expected as a result of the differences in particle size distributions and patterns of source location of these two source classes. Third, the coefficients of adjacent state TSP and precipitation seem to be reasonably stable. Finally, note that the explanatory power (as indicated by the adjusted R^2) of the models increases slightly with increasing physical sophistication of the model.

Although, as outlined above, many aspects of the results are encouraging, none of the models have impressive R^2 values. The relatively low R^2 may be due to improper specification of the model; i.e., specification of a linear relationship rather than a quadratic; failure to account for important variables; errors in the estimation of data; or simply due to the use of highly aggregated data. A side effect of the limited explanatory power of the models is a large constant term. It is not proper to consider the constant as "background." Rather it is a "catch-all," combining the influence of inadequate models and data bases with the effects of sources which have not been accounted for, for example, industrial fugitive sources, sources of secondary aerosols.

Often an analysis of the residuals from the regression is a useful tool for uncovering specification errors. Most commonly a plot of standardized residuals versus predicted values is visually inspected. The standardized residual is simply the observed value minus the predicted value divided by the square root of the mean square residual. The mean square residual is the average value of the square of the difference between the observed and predicted values. Such an analysis failed to reveal irregularities in our models. In addition to this simple visual analysis of residuals, we examined statistically the relationships between standardized residuals and several included and excluded independent variables in an attempt to detect second order effects and to identify new variables for subsequent inclusion. It is also useful to examine in detail the cases yielding the largest residuals. Occasionally such an analysis will reveal errors in data collection, data transcription, and/or inadequacy of models. The three largest positive and three largest negative standardized residuals from the rollback and box models are presented in Table 6. (For brevity, we omit further consideration of the ADTL model, which performed very similarly to the box model.)

No transcription errors were evident in the data for these six states. However, the physical proximity of the three consistently most overpredicted states is suggestive of some systematic deficiency in the data base and/or model.

Reflection upon the assumptions inherent in these approaches and upon the adequacy and accuracy of the data base revealed several potential sources of error. Among them:

i. In the box model we assume that each state may be represented as a box with a square base. The states are not squares.

ii. We are using as a dependent variable the station-averaged geometric mean annual TSP concentrations. Spatially-averaged arithmetic annual mean concentrations would be more appropriate.

iii. Arithmetic mean annual wind speed, rather than the mean annual resultant wind, is used to characterize dilution potential in the ADTL model.

iv. The influence of errors in measurement/estimation of data upon the empirical coefficients and regression statistics has not been evaluated.

v. The dependent variable, TSP, is not estimated with constant variance. States vary both in the variability of TSP levels within the state and the number of monitors employed to characterize TSP levels. Thus the least squares assumption of homoskedasticity is violated.

These problems are discussed in detail in a technical appendix to this paper, which will be made available. Here, we simply note that the empirical regression coefficients and the estimates of the standard errors of the coefficients, and therefore indirectly the accompanying t-statistics, are biased in the presence of measurement errors and heteroskedasticity, respectively. The combined effect of these problems is to underestimate the absolute values of the coefficients, overestimate their standard errors, and thus underestimate their t-statistics.

Using the empirical coefficients from the rollback and box models and the emissions estimates from Table 4 we may gain some insight into the contributions of point and open sources to ambient TSP levels. The average contributions of each term in the models to statewide TSP levels is found by inserting the mean values of the variables into the models. For the rollback and box models we have:

Rollback Model:

$$TSP = 47 + 0.00029\ E_o + 0.011\ E_p + 0.29\ TSP_a - 0.09\ P \qquad (5)$$

Box Model:

$$TSP = 50 + 2.2\left(\frac{E_o}{Hu\sqrt{A}}\right) + 29\left(\frac{E_p}{Hu\sqrt{A}}\right) + 0.32\ TSP_a - 0.15\ P \qquad (6)$$

The average contributions ($\mu g/m^3$) of each of the terms is as follows (rollback, box): unexplained (47,50), open (2.4,4.9), point (3.4,3.5), adjacent states (16.2,17.8), precipitation (-10.4,-17.0).

The large influences of adjacent state TSP and precipitation frequency, and the dominating "unexplained" term are at first troublesome. However, the adjacent states' contribution of between 16 and 18 $\mu g/m^3$ probably reflects primary aerosol background. The precipitation term includes any influence of rainfall on soil moisture and, indirectly, open source emission rates, which are not properly accounted for in the open source emissions rates, as well as the atmospheric cleansing effect of precipitation. The "unexplained" term has been discussed previously. It is possible to redistribute this "unexplained" constant among the independent variables by simply applying least squares regression methods to models without constants, i.e., rollback:

$$TSP = a_{11} E_o + a_{12} E_p + a_{13} TSP_a + a_{14} P \qquad (7)$$

The least squares estimate of the parameters in this equation are:

$$TSP = \underset{(1.58)}{0.0041} E_o + \underset{(1.84)}{0.0091} E_p + \underset{(8.15)}{0.834} TSP_a + \underset{(1.22)}{0.050} P \qquad (8)$$

Table 7 presents the results of calculations of the contributions of open and point sources to TSP in each state, using equations (5) and (6). (The computer output has been truncated to two decimal places.)

An examination of the data in Table 7 indicates that the ten states in which open sources contribute the smallest percentages to TSP are clustered in the South and Southeast. The ten states with the largest percentage open source contributions are all west of the Mississippi River.

THE CONTRIBUTION OF ROAD DUST TO TSP

Although it would be desirable to determine the contribution of each source category (e.g., agricultural tilling, surface mining, utility combustion) to measured TSP levels, an inspection of the full correlation matrix, Table 8, reveals a great deal of collinearity. For example, paved road emissions are highly correlated with construction emissions (+0.889), incineration emissions (+0.800), and vehicle exhaust emissions (+0.924); point source combustion emissions are highly correlated (+0.767) with industrial emissions; and unpaved road emissions are highly correlated with agricultural tilling emissions (+0.630), construction emissions (+0.688), and vehicle exhaust emissions (+0.691). The numbers in parentheses are correlation coefficients,

$$r = \frac{\Sigma(x_1-\bar{x}_1)(x_2-\bar{x}_2)}{\sqrt{\Sigma(x_1-\bar{x}_1)^2\Sigma(x_2-\bar{x}_2)^2}} \cdot \qquad (9)$$

In large samples from bivariate normal populations, the standard error of r is approximately $(1-r^2)/\sqrt{n}$.

With such severe collinearity and such a small data set (50 observations) it would be impractical to attempt to derive meaningful coefficients for each of the 15 emissions categories. Rather than generating 15 unstable and/or un-

Table 7. ESTIMATED MINIMUM OPEN AND POINT SOURCE CONTRIBUTIONS TO STATEWIDE TSP ($\mu g/m^3$)

State	Rollback Model		Box Model	
	open sources	point sources	open sources	point sources
AL	1.26	13.03	3.39	9.24
AK	0.66	0.26	0.14	0.01
AZ	3.19	1.28	2.68	0.28
AR	2.80	1.44	6.69	0.90
CA	10.77	5.92	11.12	1.61
CO	3.25	2.57	2.70	0.56
CT	0.22	0.49	4.72	2.74
DE	0.03	0.42	1.78	6.06
FL	2.46	2.59	5.16	1.43
GA	2.26	3.79	5.06	2.23
HI	0.05	0.56	1.01	2.92
ID	1.53	0.51	2.02	0.17
IL	3.36	10.33	7.97	6.44
IN	2.41	6.63	8.61	6.24
IA	3.98	4.32	8.85	2.53
KS	5.63	2.27	7.21	0.76
KY	1.48	5.98	4.66	4.95
LA	1.42	4.70	4.15	3.61
ME	0.24	0.62	0.83	0.55
MD	0.30	1.28	3.42	3.78
MA	0.61	1.26	8.48	4.57
MI	3.02	8.01	6.38	4.46
MN	4.05	2.10	6.12	0.83
MS	1.36	2.07	4.30	1.72
MO	3.39	4.16	5.96	1.92
MT	0.69	0.64	0.42	0.10
NE	4.69	3.34	6.57	1.23
NV	1.81	1.32	1.77	0.34
NH	0.38	0.18	4.71	0.60
NJ	0.90	1.43	11.93	4.96
NM	3.35	1.45	2.20	0.25
NY	2.06	3.13	4.45	1.76
NC	1.42	5.22	3.69	3.58
ND	3.64	0.93	5.55	0.37
OH	1.88	22.51	5.53	17.39
OK	3.90	1.56	6.08	0.64
OR	3.59	1.20	5.78	0.51
PA	3.68	9.81	8.66	6.07
RI	0.14	0.17	13.86	4.42
SC	0.52	2.17	2.23	2.46
SD	2.79	0.65	5.09	0.31
TN	1.44	4.63	4.45	3.76
TX	10.99	6.63	4.34	0.69
UT	1.87	0.85	2.04	0.24
VT	0.35	0.18	4.34	0.61
VA	0.84	4.93	2.62	4.06
WA	2.15	1.88	5.14	1.18
WV	1.25	3.37	6.51	4.61
WI	1.28	4.21	2.88	2.30
WY	0.92	0.89	0.91	0.23

Table 8. CORRELATION MATRIX - INDEPENDENT VARIABLES

Key:

c2 = E_A	c8 = E_S	point sources:
c22 = E_W	c9 = E_R	c13 = combustion
c4 = E_C	c10 = E_u	c14 = industrial
c5 = E_F	c11 = E_T	c15 = incineration
c6 = E_P	c29 = P	c16 = transportation
c7 = E_M	c28 = TSP_a	c17 = miscellaneous

	c2	c22	c4	c5	c6	c7
c22	0.922					
c4	0.267	0.394				
c5	-0.201	-0.122	0.224			
c6	-0.059	-0.106	0.049	0.293		
c7	-0.137	-0.140	0.099	0.245	-0.168	
c8	0.083	0.123	0.469	0.363	0.217	0.008
c9	0.036	0.192	0.889	0.246	0.131	0.167
c10	0.630	0.707	0.688	0.207	0.029	-0.053
c11	0.203	0.246	0.275	-0.028	-0.023	-0.135
c13	-0.151	-0.127	0.231	0.097	-0.113	0.499
c14	0.205	0.262	0.463	0.194	-0.042	0.356
c15	0.102	0.257	0.737	0.168	0.056	0.135
c16	0.271	0.356	0.928	0.253	0.107	0.085
c17	0.176	0.157	0.282	0.126	0.068	0.160
c29	-0.506	-0.513	-0.107	-0.042	-0.033	0.157
c28	0.397	0.359	0.078	-0.244	-0.183	0.169

	c8	c9	c10	c11	c13	c14
c9	0.593					
c10	0.468	0.542				
c11	0.367	0.164	0.386			
c13	0.178	0.426	-0.037	-0.167		
c14	0.290	0.542	0.366	0.005	0.767	
c15	0.437	0.800	0.436	0.199	0.453	0.560
c16	0.370	0.924	0.691	0.187	0.342	0.574
c17	0.092	0.259	0.323	-0.077	0.342	0.537
c29	-0.163	0.004	-0.477	-0.504	0.244	-0.125
c28	0.039	0.050	0.433	0.436	0.049	0.182

	c15	c16	c17	c29	c28	c23
c16	0.698					
c17	0.146	0.395				
c29	-0.138	-0.065	-0.094			
c28	0.192	0.058	0.171	-0.432		

interpretable coefficients, we grouped several source categories together in order to investigate the relative and absolute contributions of emissions from unpaved roads, the single largest source of particulate emissions, in comparison to all other point and open sources. Table 9 summarizes the data which was used in these final analyses, and the results of ordinary least squares regression applied to these data.

The relative magnitudes of the coefficients a_{11}, a_{12}, and a_{13} are the relative contributions to TSP (as modeled) per ton of emissions for the open sources except unpaved roads (E_{o-u}), unpaved roads, and the point sources. Thus the rollback model indicates that unpaved road emissions are about one-fiftieth as effective (per ton emitted) in contributing to TSP readings as are point sources and about one-third as effective as are other open sources. A similar interpretation holds for a_{21}, a_{22}, and a_{23}. The box model indicates somewhat greater effectiveness of unpaved road emissions: they are about one-twentieth as effective as point sources and about half as effective as other open sources. Given that the emissions from unpaved roads are about twenty times as great as those from point sources, unpaved road emissions seem to make a contribution to ambient TSP levels of the same magnitude as the contribution from point sources. The modeling results indicate that for paving of unpaved roads in general to be cost-effective, the cost per ton of emissions prevented would have to be more than an order of magnitude less expensive than point source controls. For specific cases, however, such as urban unpaved roads, the impact of the unpaved road emissions on urban TSP readings might be much higher than average, so that the paving of such roads might be cost-effective even when the cost per ton of emissions reduction is similar to the cost of controlling point sources.

CONCLUSION

The current TSP levels are well above National Ambient Air Quality Standards in many areas of the U.S. Both on the basis of inferential analyses of the chemical and elemental composition of TSP and our emission rate estimates and modeling, it appears that well over 50% of the ambient TSP in many regions are the result of open source emissions. Although in certain cases, open source controls may be necessary to comply with NAAQS, widespread reduction of ambient TSP levels by control of emissions from open sources may not be economically attractive in light of the relatively low contributions of these emissions to measured TSP levels per ton emitted.

We are currently conducting a study which has as its goal an analysis of the economics of open source control. Several of the open source emissions rate estimates are being revised, and advanced statistical techniques are being applied to our data in an effort to further resolve the importance of specific classes of open sources.

Table 9. EMPIRICAL ESTIMATION OF ROLE OF UNPAVED ROADS

Model 1 - Rollback[a]

$$TSP = a_{10} + a_{11}E_{(o-u)} + a_{12}E_u + a_{13}E_p + a_{14}TSP_a + a_{15}P$$

Model 2 - Box

$$TSP = a_{20} + a_{21}\frac{E_{(0-u)}}{H \cdot u\sqrt{A}} + a_{32}\frac{E_u}{H \cdot u\sqrt{A}} + a_{23}\frac{E_p}{H \cdot u\sqrt{A}} + a_{24}TSP_a + a_{25}P$$

Coefficients

	a_{i0} ($t_{a_{i0}}$)	a_{i1} ($t_{a_{i1}}$)	a_{i2} ($t_{a_{i2}}$)	a_{i3} ($t_{a_{i3}}$)	a_{i4} ($t_{a_{i4}}$)	a_{i5} ($t_{a_{i5}}$)	R^2 (R^2_{adj})
Rollback	46.6	0.0006	0.0002	0.011	0.30	-0.093	39
(i=1)	3.6	0.4	0.3	2.4	1.7	(-1.7)	(32)
Box	48.4	3.6	1.6	28.	0.33	-0.15	42
(i=2)	(3.8)	(1.1)	(0.9)	(2.3)	(1.9)	(-2.9)	(36)

Data Summary

variable	mean
$E_{(o-u)}$	1778
E_u	6372.
E_p	307.
$E_{(o-u)}/(H \cdot u)\sqrt{A}$	0.64
$E_u/(H \cdot u)\sqrt{A}$	1.71
$E_p/(H \cdot u)\sqrt{A}$	0.120

[a] E_{o-u} = total open source emissions minus unpaved road emissions.

KNOWLEDGMENTS

appreciate the support of the EPA through its grant No. R 805294010 (under . Dennis C. Drehmel) and of the U.S.P.H.S. through grant No. 5 D04 AH 01475.

FERENCES

. Bradway, R.M., and F.A. Record. National Assessment of The Urban Particulate Problem: Vol II - Particle Characterization, EPA-450/3-76-025. U.S. E.P.A., Research Triangle Park, NC 27711, 1976.

2. Gartrell, G. Jr., and S.K. Friedlander. Relating Particulate Pollution to Sources: The 1972 California Aerosol Characterization Study. Atmospheric Environment. 9(3):279-299, 1975.

3. Hopke, P.K. et al. The Use of Multivariate Analysis to Identify Sources of Selected Elements in the Boston Aerosol. 10(11):1015-1025, 1976.

4. Gaarenstroom, P.D., S. P. Perone, and J.L. Moyers. Application of Pattern Recognition and Factor Analysis for Characterization of Atmospheric Particulate Composition in Southwest Desert Atmosphere. Environmental Science and Technology. 11(8):795-800, 1977.

5. Mukharji, S. et al. Rural Fugitive Dust Impact on an Urban Area. (Presented at the 71st Annual Meeting of the Air Pollution Control Association, Houston, 25-30 June 1978).

6. Hardy, K.A. et al. Elemental Constituents of Miami Aerosol as a Function of Particle Size. Environmental Science and Technology. 10(2): 176-182, 1976.

7. Hammerle, R.H. and W.R. Pierson. Sources and Elemental Composition of Aerosol in Pasadena, Calif., by Energy-Dispersive X-ray Fluorescence. Environmental Science and Technology. 9(12):1058-1068, 1975.

8. Dzubay, T.G. Chemical Element Balance Method Applied to Dichotomous Sampler Data. Submitted for publication in the Annals of the New York Academy of Sciences, 31 Jan 1979.

9. Richard, G. and R. Tan. Implemental Plan for Suspended Particulate Matter in the Phoenix Area: Volume I. Air Quality Analysis. EPA-450/3-77-021a. U.S. E.P.A., Research Triangle Park, NC, 1977.

10. Evans, J.S., et al. Setting Priorities for the Control of Particulate Emissions from Open Sorces. (Presented at the 1st Annual Symposium on the Transfer and Utilization of Particulate Control Technology, Denver, Colorado, 24-28 July 1978).

11. Amick, R.S., K. Axetell, Jr., and D.M. Wells. Fugitive Dust Emission Inventory Techniques. (Presented at the 67th Annual Meeting of the Air Pollution Control Association, Denver, Colorado, 9-13 June 1974).

12. Blackwood, T.R. and Peters, J.A.. Relative Impacts of Open Sources of Emissions. Presented at the Symposium on Fugitive Emissions, Hartford, Conn., May 16-19, 1976.

13. Chepil, W.S. Soil Conditions that Influence Wind Erosion. U.S. Department of Agriculture. Washington, D.C., Technical Bulletin Number 1185, 1958.

14. Council on Environmental Quality. Environmental Quality: The Seventh Annual Report of the C.E.Q. U.S.G.P.O., Washington, D.C., 1976.

15. Cowherd, C., C.M. Guenther , and D.D. Wallace . Emissions Inventory of Agricultura l Tilling, Unpaved Roads and Airstrips, and Construction Sites. EPA-450/3-74-085, U.S. E.P.A., Research Triangle Park, NC, 1974.

16. Cowherd, C., and O. Mann. Quantification of Dust Entrainment from Paved Roads. (Presented at the 69th Annual Meeting of the Air Pollution Control Association, Portland, Oregon, June 27-July 1, 1976).

17. Cowherd, C., K. Axetell, C. Guenther, and G. Jutze. Development of Emission Factors for Fugitive Dust Sources. EPA-450/3-74-037. U.S. E.P.A., Research Triangle Park, NC, 1974.

18. Handy, R., K. Hoover, K. Bergman, and D. Fox. Unpaved Roads as Sources for Fugitive Dust. Transportation Research News, 1975.

19. Jutze, G.A., and K. Axetell. Investigation of Fugitive Dust - Sources, Emissions, and Controls. EPA-450/3-74-036a. U.S. E.P.A., Research Triangle Park, NC, 1974.

20. Thornthwaite, C.W. The Climates of America According to a New Classification. The Geographical Review. 21:633-655, 1931.

21. Ward, D.E., C.K. McMahon, and R.W. Johansen. An Update on Particulate Emissions from Forest Fires. (Presented at the 69th Annual Meeting of the Air Pollution Control Association, Portland, Oregon, June 27-July 1, 1976).

22. Carpenter, B.H., and G.E. Weant, III. Particulate Control for Fugitive Dust. EPA 600/7-78-071, U.S.E.P.A.. Research Triangle Park, NC, April 1978.

23. Woodruff, N.P., and F.H. Siddoway. A Wind Erosion Equation, Soil Science Society Proceedings. 29(5):602-608, 1965.

24. Yamate, G., W. Stockham, W. Vatnunk, and C. Mann. An Inventory of Emissions from Forest Wildfires, Forest Managed Burns, and Agricultural Burns. (Presented at the 68th Annual Meeting of the Air Pollution Control Association, Boston, MA, June 15-20, 1975).

25. U.S. Environmental Protection Agency. National Air Quality, Monitoring, and Emissions Trends Report, 1977. EPA-450/2-78-052. U.S. E.P.A., Research Triangle Park, NC, 1978.

26. U.S. Environmental Protection Agency. 1973 National Emissions Report, EPA-450/2-76-007. U.S. E.P.A., Research Triangle Park, NC, 1976.

27. U.S. Environmental Protection Agency. Air Quality Data - 1976 Annual Statistics. EPA-450/2-78-009. U.S. E.P.A., Research Triangle Park, NC, 1978.

28. Lynn, D.A., G.L. Beane, R.C. Galkiewicz, and R.M. Bradway. National Assessment of the Urban Particulate Problem: Volume I - Summary of National Assessment. EPA-450/3-76-4024. U.S. E.P.A., Research Triangle Park, NC, 1976.

29. Ochsner, J.C. and T.R. Blackwood. Fugitive Emissions from Chemical Fertilizer Mining. (Presented at the 2nd Symposium on Fugitive Emissions: Measurement and Control, Houston, TX, 23-25 May 1977).

30. deNevers, N.H., and J.R. Morris. Rollback Modelling - Basic and Modified. (Presented at the 66th Annual Meeting of the Air Pollution Control Association, Chicago, IL, 24-28 June 1973).

31. Hanna, S.R. A Simple Method of Calculating Dispersion from Urban Area Sources. J. Air Pollut. Control Assoc. 21(12):774-777, 1971.

32. Holzworth, G.C. Mixing Depths, Wind Speeds, and Air Pollution Potential for Selected Locations in the United States. J. of Applied Meteorology. 6(12):1039-1044, 1967.

33. Benarie, M. Short Communication: The Simple Box Model Revisited. Atmospheric Environment. 12:1929-1930, 1978.

34. Holzworth, G.C. Mixing Heights, Wind Speeds, and Potential for Urban Air Pollution Throughout the Contiguous United States. AP-101. U.S. E.P.A., Research Triangle Park, NC, 1972.

FUTURE AREAS OF INVESTIGATION REGARDING THE PROBLEM OF URBAN ROAD DUST

by

Edward T. Brookman
TRC-THE RESEARCH CORPORATION of New England
Wethersfield, CT 06109

and

Dennis C. Drehmel
Industrial Environmental Research Laboratory
U.S. Environmental Protection Agency
Research Triangle Park, NC 27711

ABSTRACT

In a number of metropolitan areas of the country, failure to attain national primary air quality standards for total suspended particulates (TSP) has fostered a detailed reexamination of the nature of the urban TSP problem. Reentrained dust from paved streets and other traffic-related emissions are now recognized as major sources of TSP in urban areas. While numerous reports and studies have examined this subject, some significant aspects of urban road dust have not been studied in enough detail, if at all. Examples of this are the effects of gutters and pavement composition and shape. This paper discusses those areas of the urban road dust problem that are felt to require further attention and outlines the priorities with which the data should be obtained.

FUTURE AREAS OF INVESTIGATION REGARDING THE PROBLEM OF URBAN ROAD DUST

INTRODUCTION

Failure to attain the national primary air quality standards for total suspended particulates (TSP) in a number of metropolitan areas of the country has fostered a detailed reexamination of the nature of the urban TSP problem. While TSP control strategy development has routinely included an analysis of the contributions of traditional point and area sources superimposed on a constant background level, adequate consideration has not been given to the contributions of nontraditional dust sources. Reentrained dust from paved streets and other traffic-related emissions have now been recognized as major sources of suspended particulates in urban areas and a potential leading cause of TSP concentrations in excess of the ambient air quality standards. To attain these standards, a thorough knowledge of the contribution of urban road dust to ambient TSP levels is required.

While the subject of urban road dust and its numerous offshoots has been discussed and studied in literally hundreds of reports, there are still many questions left unanswered. Has every area that relates to urban road dust been studied thoroughly? What areas require further study? What areas have not been studied at all? Do these areas contribute to the problem significantly enough to warrant study? If so, with what priority should the desired information be obtained?

To answer these questions, a search and review of the existing literature relating to all aspects of urban road dust was conducted. The aim of the review was to define the informational gaps in urban road dust research and evaluate these gaps as to their relative importance with regard to improvement of air quality. This paper presents the results of that review.

SUBJECTS RELATING TO URBAN ROAD DUST

To better understand the areas requiring further research, a general overview of the subjects associated with urban road dust is warranted. In dealing with the subject of urban road dust, there are five major areas that need to be addressed. They are:

- The means by which the material comprising urban road dust is deposited on the road surface.
- The variables that affect the surface loading once the material is deposited on the road.
- The physical and chemical nature of the deposited material.

- The impact of the material on its surroundings.
- The methods of removal or control of the material.

The specific topics that fall under these five generic areas are discussed below.

Methods of Deposition

The origins of the material comprising urban road dust are quite varied. Natural processes and the activities of humans both contribute to the surface loadings. The primary methods of deposition have been identified as the following:

- Motor vehicles
- Sanding and salting
- Pavement wear
- Litter
- Biological debris
- Wind and water erosion from adjacent areas
- Atmospheric pollution fallout.

These methods are depicted in Figure 1.

Motor vehicles contribute materials in a number of different ways. Tire wear, settleable exhaust, wear of brake and clutch linings, corrosion and abrasion of panels and undercoatings, mud and dirt carryout from unpaved areas and construction sites, and truck cargo spills all deposit particulate matter. Lubricants, coolants, hydraulic fluids, and oil leaks deposit organic material.

Sanding and salting deposit particulate material on the street on only a few occasions per year. However, a good deal of this material remains on streets for long periods of time due to street cleaning schedules and inefficiencies.

Pavement wear and decomposition contribute various types of particles to the street surface loading. These include asphalt, cement, aggregate, expansion joint compounds, and fillers.

Litter is comprised of cans, bottles, broken glass, plastic, tobacco, etc. Some of this material is reduced in size until it is no longer recognizable as a specific object and contributes to the overall surface loading.

Biological debris includes leaves, grass clippings, sticks, insect parts, and animal waste. Again, this debris can be reduced to small size by the actions of vehicle traffic and merge with the overall particulate loading.

1 MOTOR VEHICLES
- **a** TIRE WEAR
- **b** EXHAUST
- **c** BRAKE & CLUTCH LININGS
- **d** MUD & DIRT CARRYOUT
- **e** TRUCK SPILLS
- **f** CORROSION & ABRASION OF PANELS & UNDERCOATINGS
- **g** LUBRICANTS, COOLANTS, HYDRAULIC FLUIDS, OIL

2 SANDING & SALTING

3 PAVEMENT WEAR

4 LITTER

5 BIOLOGICAL DEBRIS

6 WIND & WATER EROSION FROM ADJACENT AREAS

7 ATMOSPHERIC FALLOUT

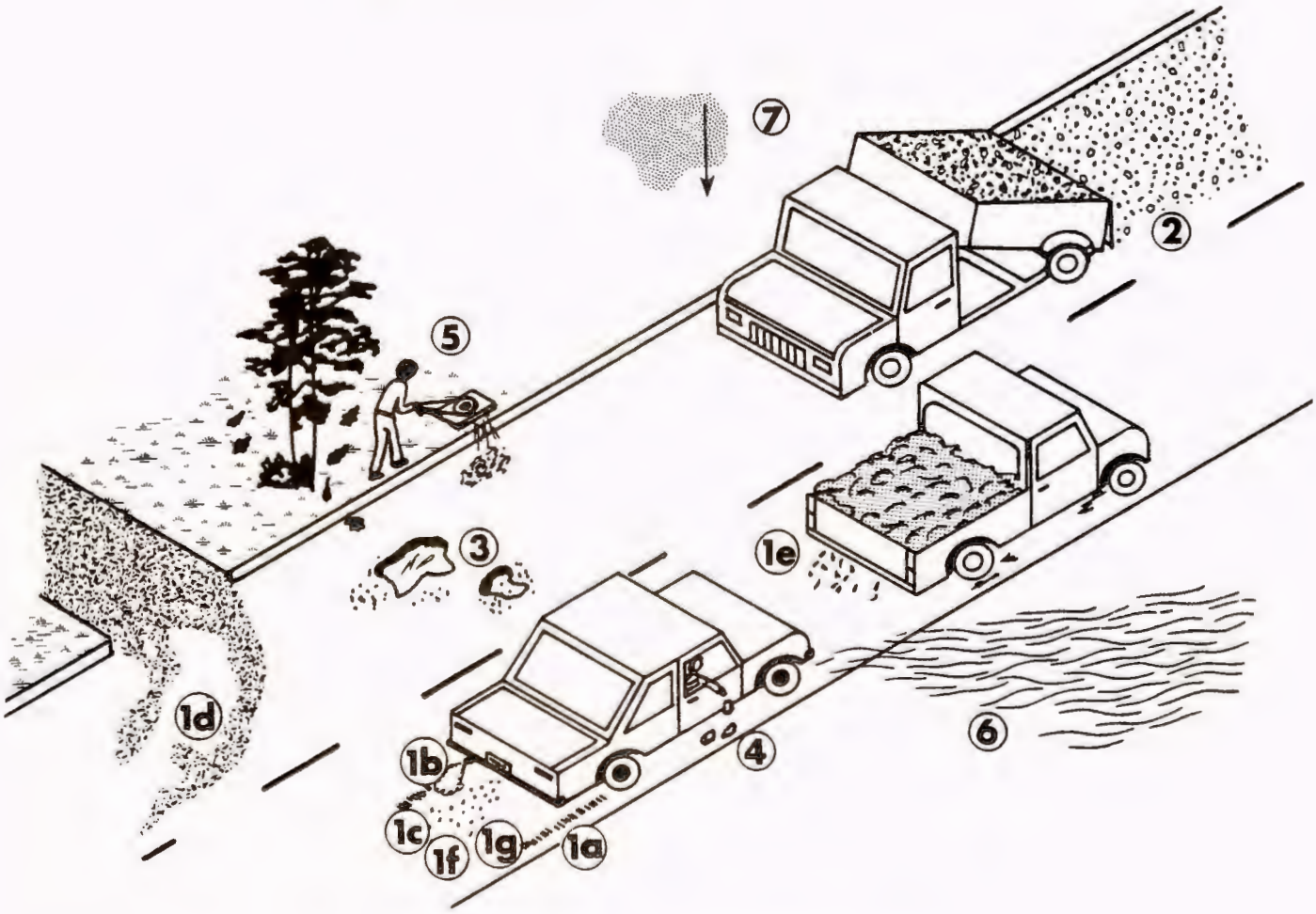

Figure 1. Methods of deposition.

Soil adjacent to roadways can become part of the street surface loading due to wind and water erosion. This is particularly true in more arid areas and areas lacking curbs, sidewalks, roadside vegetation, or other inhibiting agents.

Finally, atmospheric fallout of dust and particulate pollutants from other areas contributes to road dust. This material can originate from remote industrial and agricultural sources and be transported over long distances to the road surface via air currents.

Variables Affecting Road Dust Loadings

Any variation in one of the deposition processes just described affects the amount of material accumulating on the street. In addition, once the material has been deposited on the street surface, other processes can affect the surface loading. These include:

- Meteorological conditions
- Vehicle traffic
- Roadway configuration
- Pavement composition

Meteorological conditions play a very significant role in the variability of surface loadings. Rain will flush the streets and remove a significant portion of the road dust. Snow will cover the dust and prevent it from becoming resuspended. Ice and the freeze/thaw cycle contribute to pavement wear. Fog and dew add moisture and inhibit resuspension, and wind speed, mixing depth, and atmospheric stability can affect the quantity of dust that becomes reentrained.

Vehicles are not only sources of road dust, they also affect the loadings through several mechanisms. The speed, size, volume, and mix of vehicles (e.g., trucks vs. cars) passing over the pavement affect turbulence and resulting dust suppression. Speed variations (idling, stop and start, free flowing) affect emission loadings. Engine conditions are important since a cold engine exhausts more particulate matter than a warm one under the same conditions. Even parked cars can adversely affect road dust to the extent that they hinder street cleaning effectiveness.

Roadway configuration provides another set of variables that affects the amount of road dust that accumulates on the streets. The physical layout of the road (e.g., road slope, gutters and sewers, cobblestones, grooves in the pavement), and conditions alongside the street surface, such as curbing size and shape, vegetation, embankments, buildings and medians, are all important factors. Elevated roads impose still another set of conditions (e.g., wind exposure) that affect surface loadings.

Lastly, the pavement composition itself affects the surface loadings. Different types of surfaces wear at different rates, and some are more easily cleaned than others. The type of resurfacing material used, the

frequency of its application, and pothole patching practices all can affect dust formation and deposition and cleanability.

Physical and Chemical Nature of Road Dust

Another realm of study concerning urban road dust deals with the physical and chemical nature of the particulate material. The physical aspect is basically particle size and shape. The chemical aspect relates to material composition.

Suspendability of road dust is of paramount importance since this is the principal aspect that relates to human health. If none of the surface material became suspended, there would be no particulate air pollution problem. The quantity of material suspended by any of the mechanisms previously discussed depends primarily on particle size. Particle size also affects the amount that remains suspended to become part of the TSP background and the amount that falls out of the atmosphere within a short distance from the roadway.

The chemical nature of the road dust determines whether or not the material is of a hazardous nature to its surroundings (e.g., toxic to man, harmful to vegetation and water supplies). It also helps establish the origins of the dust and can point the direction towards effective controls.

A variety of measurement and examination techniques are used to determine the physical and chemical nature of the material deposited on street surfaces. Filter analyses can help to determine particle size distributions, shape, and chemical characteristics as well as relative concentration. Hi-vols and dustfall buckets are used to measure ambient concentration levels and fallout rates. Impactors are used to measure TSP levels and size distributions. Tracer and wind tunnel studies are used to help determine fallout rates, trajectories, and emission factors.

Road Dust Impact

The primary impact of road dust is on the land, air, and water in the immediate area of the roadway. Vegetation, soils, and animal biota are all affected, with the salt and lead components of the dust causing particular harm. These and other harmful pollutants can enter water resources via flushing, leaching, and runoff; thus causing a water pollution problem. The impact on air quality, the contribution to urban TSP levels, has prompted most of the reports written on the subject of road dust. The major concern seems to be ambient TSP concentrations rather than toxic effects. Not only are local urban areas impacted, but the environment can be adversely affected at great distances due to long range atmospheric transport.

Removal/Control Methods for Urban Road Dust

Removal and/or control of urban road dust can be separated into two relatively distinct categories. The first involves the control or elimination of the sources of urban road dust. The second involves the removal and control of the dust after it has accumulated on the street surface.

The sources of urban road dust were discussed previously. The sources readily adaptable to control measures are construction sites, unpaved areas, and truck cargo spills. The amount of road dust originating from these sources can be reduced by paving, chemical stabilization, tire scrapers, wheel washes and the wetting or covering of loaded trucks. Most other sources are not really amenable to controls per se. Reductions in the amount of sand and salt applied, the number of vehicles on the roads, and the amount of litter deposited can reduce surface loadings. A reduction in the use of sand and salt can be affected by improved snow plowing techniques, utilization of a road surface texture or coating that minimizes ice adhesion, or pavement heating. Washing the sand before application removes the fines which can become resuspended and leaves the coarse particles which are necessary to prevent skidding. Improvements in pavement wearability, automobile degradation, and gasoline additives could likewise reduce loadings; but these steps cannot really be classified as specific control methods.

Once the material has accumulated on the streets, it is removed via a number of mechanisms. These include:

- Reentrainment
- Wind erosion
- Displacement
- Rainfall runoff to a catch basin
- Street cleaning methods.

These are illustrated in Figure 2.

Two of these removal methods, rainfall and wind erosion, are natural phenomena and are thus highly sporadic and not reliable as control methods. Reentrainment and displacement are related to vehicle speed, size, mix, and volume. Street cleaning methods include sweeping, vacuuming, flushing, coating and resurfacing, and various combinations of these methods. These methods vary in cost and effectiveness. Effectiveness is largely a function of frequency and timing (e.g., sand and salt should be removed as soon as possible during thaw periods).

RESEARCH GAPS

Approximately 75 reports and papers were reviewed in order to determine to what extent the various areas associated with urban road dust have been investigated. Of the five generic areas described in the previous section, three have been reasonably well studied and discussed in the liter ature. These are the methods of deposition, the physical and chemical

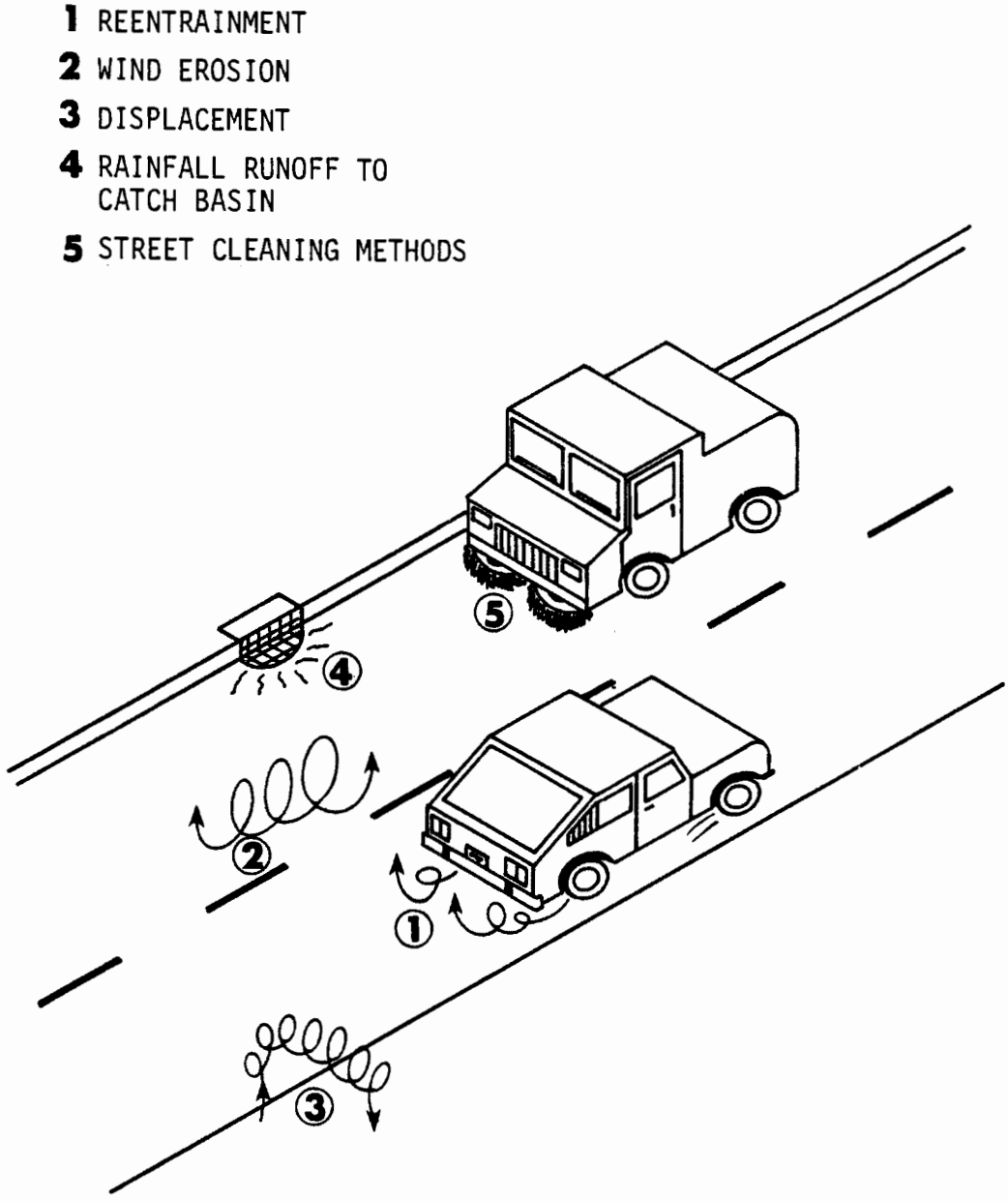

Figure 2. Methods of removal.

nature of the road dust, and the impact of the road dust. There are only a few specific topics that do not appear among the references reviewed. Under methods of deposition, truck cargo spills and the corrosion and abrasion of panels and undercoatings were not analyzed. No information was found on the use of wind tunnels in modeling road dust emissions. All other areas were addressed.

The variables affecting road dust loadings, one of the other two generic categories discussed previously, were essentially ignored in the literature. Mention is frequently made as to the quantitative aspects of these variables, but very little actual data is available. In particular, information on the effects of vehicle mix, volume, and speed was not found. Pavement and roadway configuration and its affect on surface loadings and reentrainment is an area almost completely ignored. Not only are hard data unavailable, but discussion on the possibility of its importance is lacking as well. Pavement composition is another topic only briefly mentioned in the literature.

Many of the subjects pertaining to removal/control methods, the fifth generic category, were thoroughly discussed, but several topics were not covered at all. Mention is made of control methods for carryout sites, unpaved areas and truck spills, but little hard data are available. The effectiveness of washing sand to remove fines was not studied. Although removal methods are fairly well covered, with some actual field data, the studies have been limited to existing methods of control. Information on the development of new types of street cleaners is lacking.

EVALUATION OF RESEARCH GAPS

After reviewing the pertinent literature on the subject of urban road dust, it is apparent that the basic analysis of the problem itself has been thorough. The methods by which material is deposited on the streets and the rates at which this deposition occurs have been reasonably well defined. Table 1 presents deposition rates for various processes. It is recognized that these rates can vary considerably, but it is felt that the relative magnitude of the process rates, in relation to the others, is representative. The few information gaps in the research regarding deposition, notably truck cargo spills and undercoating abrasion, would seem of low priority since they contribute very little to the surface loading according to this table. The chemical and physical nature of road dust has been well studied and documented. Results for the various constituents, such as lead, salt, and rubber, and for various size ranges are available for a number of land-use categories and highway types. Finally, the impact of the road dust on the surrounding environment is well recognized. The effect of various road dust constituents on nearby land, water, and vegetation and the contribution to ambient TSP levels is basically understood and quantified.

Table 1. DEPOSITION PROCESSES

Source	Constituents	Typical deposition rate, kg/curb-km/day	Range, kg/curb-km/day
1. Mud and dirt carryout	Soil from construction sites, unpaved parking areas, etc.	28.2	Extreme
2. Litter	Cans, bottles, broken glass, cigarette butts, plastic, other debris	11.3	Extreme
3. Biological debris	Leaves, grass clippings, sticks, animal droppings, insect parts, etc.	5.6	Extreme
4. Ice control compounds	Sand, salt, cinders, calcium chloride	5.6	0-16.9
5. Dustfall	Atmospheric fallout	2.8	0.6-7.0
6. Pavement wear and decomposition	Asphalt, cement, aggregate, expansion joint compounds and fillers	2.8	1.4-42.3
7. Vehicle-related			
-Tire wear	Rubber	2.8	1.7-14.1
-Brake and engine component wear	Metals, lubricants, brake and clutch linings	1.4	0.6-7.0
-Settleable exhaust	Combustion products, fuel additives	0.6	0.3-2.8
8. Spills	Sand, dirt, chemicals	No data; est <0.6	
9. Erosion (runoff and blowing) from adjacent areas	Soil	5.6	Extreme
TOTAL		67.6	

Source: Axetell and Zell (1977)

On the other hand, the variables affecting road dust loadings and removal/control methods have not been given adequate coverage in the literature. These areas are discussed in the following sections.

Variables Affecting Surface Loadings

Although the basic concepts of the mechanisms and rates of deposition of materials on street surfaces and the chemical and physical makeup have been well documented, the variables affecting the loadings, which could be of considerable importance for future air quality improvement, have not received much attention. As discussed previously, these variables are meteorology, vehicles, pavement and roadway configuration, and pavement composition. The suggested priorities for studying the parameters under these variables are as follows:

1. Pavement and Roadway Configuration -

   Several studies have touched on the possible effects of pavement and roadway configuration, but studies specifically aimed at defining these effects have not been made. Some of the results briefly mentioned in these studies are: curbing reduces reentrained dust by a factor of four, curbing height is significant, sidewalks and vegetation reduce soil erosion, and roadways with surrounding embankments have less impact on the immediate area than elevated roadways.

   Sartor and Boyd (1972) determined the distribution of surface material across a typical street. Their results are presented in Table 2. Since the majority of the surface loading material accumulates within 0.15 meters of the curb, a redesigned curb and gutter could potentially facilitate surface material collection and subsequent removal by flushing and/or vacuuming.

   Other aspects of pavement and roadway shape, such as the effects of medians, guard rails versus barriers, shoulder stabilization, grooves, and crown and bank slopes, should be studied since they show a potential for reduced or redistributed surface loadings. The impact of nearby buildings should also be examined.

2. Pavement Composition -

   One study found a large difference between surface loadings on asphalt and those on concrete roadways. Whether this relates to pavement erosion or cleaning or both is not known and should be examined. Should one material prove to be more effective in reducing air pollution, this information could easily be applied to resurfacing and new roadway construction.

Table 2. DISTRIBUTION OF SURFACE MATERIAL ACROSS A TYPICAL STREET*

Street location, distance from curb	Normal weight of material, % of total
0 - 0.15 m	78
0.15 - 0.30 m	10
0.30 - 1.02 m	9
1.02 m - 2.44 m	1
2.44 m to center line	2

Source: Sartor and Boyd (1972)

*The numbers presented in this table represent the average results of tests conducted on urban streets in several different cities.

3. Vehicles -

Many of the effects of vehicles, such as volume, speed, and size, are already well recognized. Other effects, such as mix and speed variations, could be relatively easy to assess. Additional research should be performed in these areas. Another possible research area is the distribution of vehicles on a highway. As pointed out in Table 2, most of the surface loading is near the curb. Reduced reentrainment may occur if the use of lanes with curbs is somehow restricted. Engine temperature, while perhaps important, would be difficult to control and thus its study should be of low priority.

4. Meteorology -

Rain, snow, fog and dew, wind speed, mixing depth, and atmospheric stability can affect surface loadings and the amount of reentrainment to varying degrees. Even though the magnitudes of these effects may not be defined, such definition would seem of low priority since humans have essentially no control over such phenomena.

Control of Sources

Perhaps of greater importance than the study of the variability of surface loadings is the study of removal/control methods. Many of the concepts discussed above will merely serve to prevent the already present road dust from becoming reentrained. The material must still be effectively removed from the street surface or, better still, prevented from being deposited in the first place.

To evaluate the priorities for the prevention of material deposition, Table 1 can again be utilized. According to the information presented in the table, mud and dirt carryout accounts for about forty percent of the material deposited on roadways. There are many suggested and tested methods for the control of dust and dirt from construction sites and unpaved areas, such as wheel washes, oiling, paving, immediate cleanup of tracked-out material, chemical stabilization, wetting or covering of loaded trucks, and tire scrapers. These methods should be examined in further detail and other potentially acceptable measures should be evaluated.

The contributions to road dust from litter and biological debris are also significant. However, aside from public awareness programs and littering fines, little can be done in this area to prevent deposition.

Erosion of material from adjacent areas is important, but further study of this does not seem valuable. Control methods, such as sidewalks, vegetation and chemical stabilization, are already known and all that is required is their implementation.

Another deposition source of similar magnitude to erosion and biological debris is the application of ice control compounds, mainly sand and salt. This is an area where further research is needed. The effect of sand washing has not really been evaluated and could be significant. Improved plowing methods, the use of a hydrophobic substance, and other similar methods of reducing sand and salt use have been studied, but further analysis is warranted.

The contributions to surface loadings from motor vehicles seem to be of minor importance compared with some of the other deposition processes. Since the contributions from vehicles have been fairly thoroughly studied, further study would not seem productive at this time.

The other two processes of minor importance are dustfall and pavement wear. Nothing much can be done to prevent dustfall and so no study is necessary. Pavement wear should be studied to some extent, at least with respect to asphalt versus concrete, but this should have a relatively low priority.

Removal Methods

The third area in which further research is needed is road dust removal methods. Once the material is on the street, it must be removed efficiently. The removal processes, discussed previously, are reentrainment, wind erosion, displacement, rainfall runoff, and street cleaning methods. Table 3 presents some typical removal rates for these processes.

Two of these processes, reentrainment and displacement, are directly related to vehicular movement. These have been fairly well studied already and information obtained from the studies of the variables affecting surface loadings will provide helpful knowledge in these areas. One additional study area should be the reduction of vehicle-induced turbulence.

Wind erosion and rainfall runoff are natural processes. These are well understood and not easily controllable and further study is not warranted.

The final process, street cleaning, is one on which a great deal of work has been performed. Dozens of studies have been conducted which evaluate street cleaning programs and sweeper effectiveness. However, these studies have almost exclusively centered on existing street cleaning methods and practices and the results have primarily shown that such existing practices are relatively ineffective. Research should first be carried out to see whether the current methods can be made effective either through a revised cleaning cycle (e.g., daily and/or immediately after sanding and salting) or through improvements to existing equipment. Research should then center on developing new street cleaning methods with much greater removal efficiencies.

An additional high priority item which would fall into this category would be the development of an effective street dust loading measurement

Table 3. URBAN ROAD DUST REMOVAL PROCESSES

Process	Typical rate of removal from street surfaces, kg/curb-km/day	Assumptions incorporated
Reentrainment	28.2	For 10,000 ADT; net removal rate = 4.5 g/VMT*
Displacement	11.3	Estimated from dustfall rate just beyond curb
Wind erosion	5.6	Force of same magnitude as reentrainment, but only operative 20% of time
Rainfall runoff	14.1	Removal efficiencies of 50% for rain of 0.25-1.27 cm and 90% for rain of >1.27 cm
Sweeping	9.9	Average efficiency of removal = 50%; weekly cleaning

*ADT: Average Daily Traffic VMT: Vehicle Miles Traveled

Source: Axetell and Zell (1977)

procedure. Such a technique should be accurate, representative of a significant length of street, repeatable, and capable of being performed by technician-level personnel. A method should also be developed that could link street loadings to the resuspension rate.

RECOMMENDATIONS

The research needs described above can be summarized by separating them into high, medium, and low priority categories. The high priority items are those that either have the potential of providing fairly immediate air quality improvement or are necessary prior to further research studies. The medium priority items are those that are felt to have potential, but require time to develop and implement. Some of these also depend on the results of the high priority research. The low priority items are those that have not been fully researched to date, but whose impact is assumed to be relatively minor. Table 4 presents the priority categorization.

It is recommended that future areas of investigation regarding the problem of urban road dust be conducted according to this prioritization. This will help to produce the desired information in the most effective manner.

REFERENCES

1. Axetell, K. and J. Zell. Control of Reentrained Dust from Paved Streets. U.S. Environmental Protection Agency, Kansas City, MO. EPA 907/9-77-007. NTIS No. PB 280-325. August 1977.

2. Sartor, J.D. and G.B. Boyd. Water Pollution Aspects of Street Surface Contaminants. U.S. Environmental Protection Agency, Washington, D.C. EPA-R2-72-081. NTIS No. PB 214-408. November 1972.

Table 4. RESEARCH PRIORITIES

High Priority:

- Determination of the effects of more frequent street cleaning and cleanup immediately after application of sand and salt utilizing existing technology
- Analysis of control methods for mud and dirt carryout sites and truck spills
- Improvement of existing street cleaning equipment
- Development of a standard procedure for determining street loadings
- Development of a method to link street loading to resuspension rate
- Study of ways to reduce the amount of sand and salt applied to street surfaces including sand washing, plowing improvement and development of hydrophobic substances
- Study of curbing effects: size, shape and relationship with gutter design, need to pave or stabilize shoulders

Medium Priority:

- Development of new methods of street cleaning
- Further study of the effects of vehicle speed, size, mix, speed variations and volume
- Study of asphalt versus concrete surface loadings
- Study of crown and bank slope effects
- Study of redesigned road surfaces such as grooves or grids
- Study of the effects of sidewalks and vegetation
- Study of reducing vehicle induced turbulence
- Study of meteorological effects

Low Priority:

- Determination of the effects of vehicle distribution on roadways
- Study of median effects, guard rails versus barriers
- Study of cut, at-grade and fill section roadways
- Study of building effects along roadways
- Study of vehicle engine temperature effects

STATUS OF CONNECTICUT'S CONTROL PROGRAM FOR TRANSPORTATION-RELATED PARTICULATE EMISSIONS

By:

John H. Gastler
H. Ledger Chamberlain
Connecticut Department of Transportation
Wethersfield, Connecticut, 06109

Material prepared for Connecticut's 1979 State Implementation Plan (SIP) submittal indicates that transportation related sources contribute more than half of total suspended particulates (TSP) emissions.

The SIP's conclusions are strikingly different from earlier estimates of TSP attributable to the transportation sector. The conclusions mandate additional measurements and analyses to document source contributions.

Of greater importance is the development of TSP control measures because Connecticut's ability to maintain an adequate transportation system and to accommodate stationary source, commercial and industrial growth are affected.

Possible control measures must consider control of exhaust emissions, a source control program, and control of re-entrained road dust having characteristics of a fugitive emissions control program.

Current programs are discussed and analyzed where sufficient data exists. Technical methodology and administrative responsibilities are discussed. Insights of future program needs are presented.

STATUS OF CONNECTICUT'S CONTROL PROGRAM FOR TRANSPORTATION-RELATED PARTICULATE EMISSIONS

Connecticut is a small state whose air quality problems are unique. Consequently, the state has had to adopt aggressive programs to evaluate and cope with these problems. One of these aggressive programs involves total suspended particulates (TSP) attributable to transportation facilities.

The unique character of Connecticut's air quality problems, including the sources of its violations of the TSP standards, spring from its geographic location, its history as an early industrial state, and its present pattern of development. The provisions of the 1977 Clean Air Act Amendments require that the State Implementation Plan (SIP) be revised and approved by July 1, 1979. The revised SIP will play a critical role not only in meeting air quality standards, but also in shaping Connecticut's future industrial, commercial, and transportation growth.

Connecticut, the southern-most of the New England states, is an integral part of the northeast megalopolis which stretches from northern Virginia and Washington D.C. to the southern New Hampshire suburbs of metropolitan Boston. Connecticut, lying directly northeast of New York City, is in the core of this megalopolis. Weather systems frequently travel from a southwesterly direction. Such systems can be responsible for the transport of upwind-generated pollutants into Connecticut.

Since its colonial days of the 17th and 18th centuries Connecticut has been a producer and distributor of consumer goods. Mills were built on swift-flowing streams and roads wound through river valleys and along the shoreline. Although energy sources changed, many of these early industries grew and flourished. Entering the 20th century Waterbury dominated the brass industry, New Britain became known as the Hardware City and Hartford was an early home of the machine tool and automobile industries, as well as becoming an insurance capitol.

Today, Connecticut is fighting to retain industry. Many companies have found it more economical to move to new modern facilities rather than refurbish older plants. Sometimes the new facilities are built in the state, but competition from other states and overseas is intense. The fear has been expressed that air quality considerations can weaken Connecticut's competitive position.

The principal cities in Connecticut have never grown much beyond 150,000 population and now are experiencing declining populations, while suburban towns continue to grow. Much of the state could now be characterized as a series of contiguous suburban areas. Although Connecticut's transportation system has some multi-modal characteristics over 90% of its transportation network serving this suburban complex is oriented toward highways and motor vehicles.

The revision of the SIP has caused many segments of Connecticut's society to focus attention on air quality. An extensive monitoring system has been in place for TSP since the early 1970's. An early and aggressive program to control industrial pollutants has resulted in a measurable improvement in TSP levels. The primary standard was violated at only one location in 1978.

Connecticut's TSP monitoring network operated by the Connecticut Department of Environmental Protection (DEP) consists of 43 HiVol sampling sites throughout the state. Some sites are also equipped with other types of particle measuring devices. TSP standard violations have been measured or projected at many of these monitoring stations. After accounting for local anomalies it was determined that the entire state of Connecticut is noncompliance for the secondary standard, but that only the city of Waterbury and vicinity is noncompliance for the primary standard.

The situation has improved dramatically in recent years. The number of measured violations of both the primary and secondary standard, as well as their severity, has decreased substantially (Table 1). However, the fact remains that the entire state is officially in violation of the standards and must implement control strategies to achieve them by 1982.

Table 1. Number of Measured TSP Standard Violations, 1971 - 1977. (ConnDEP (1975, 77, 78)[1])

Year	Number of Sites Monitored	Primary Violations	Secondary Violations
1971	53	21	34
1972	55	13	27
1973	65	5	11
1974	73	0	12
1975	72	3	14
1976	62	1	18
1977	43	2	15

The goal of the SIP is to demonstrate attainment and maintenance of the primary standard by 1982 and the secondary standard as soon as practicable. Moreover, Connecticut's SIP revision policy is to achieve an "accommodative SIP". As the term implies, an accommodative SIP is a blueprint for not only achieving the standards, but further reducing emissions to achieve a margin available to accommodate growth. The goal of an accommodative policy is to seek attainment of the TSP secondary standard in all areas so that new industries could be permitted to use Reasonably Available Control Technology (RACT) rather than Lowest Achievable Emissions Reduction (LAER).

The emissions inventory prepared by the DEP for the SIP revision indicates that 51% of TSP emissions were attributable to transportation sources in 1976. See Figure 1. This inventory was compiled using available data and making estimates and assumptions where reliable data was not available. In the case

of motor vehicles, the emission factors used for inventory calculations are summations of three component factors:

- exhaust or tailpipe emissions;
- tire wear emissions; and
- reentrained road dust.

Tailpipe emissions consist primarily of carbon particles and large aggregates of unburned, heavy hydrocarbon molecules. Vehicles burning leaded gasoline also emit lead-containing particles through their exhaust systems.

Tire wear emissions are composed of particles of rubber and other tire constituents, produced by friction between the tire and the roadway surface.

Reentrained road dust consists of particulate matter of any origin which accumulates on or near the roadway and is forced into suspension by the combined turbulent forces of the moving vehicle and natural air currents.

The emission factors used in the inventory calculations are contained in Table 2. These factors were also used in computer modeling of source contributions to monitored TSP concentrations around the state.

Table 2. Vehicular TSP Emission Factors (Units: Grams Per Vehicle Mile Traveled)(SIP (1979)[2])

Year	Tailpipe	Tire Wear	Reentrainment	Total
1976	0.37	0.20	0.68	1.25
1982	0.25	0.20	0.68	1.13
1987	0.21	0.20	0.68	1.09

A determination that a state or region is not in compliance with a particular ambient air quality standard, in this case TSP, can have profound economic, social, and legal implications. This is particularly true in Connecticut where stationary sources as a group have already been controlled to a high degree. Additional controls would exhibit a high cost/benefit ratio, in an area which is presently at a competitive economic disadvantage relative to other areas of the country.

Imposition of severe control measures on individual citizens runs the risk of infringing on their legal rights as well causing social and economic hardship. Yet the control of large stationary sources and of small citizen-operated sources are closely interrelated, and must be treated as such in developing pollution abatement strategies. For these reasons, determinations of compliance with a standard and their supporting analyses must be definitive and technically incontrovertable.

Connecticut's SIP and its treatment of the state's TSP situation has generated considerable controversy. We in the transportation sector are skeptical about the accuracy of certain assumptions and procedures used in assessing Connecticut's TSP levels and particularly the transportation impact.

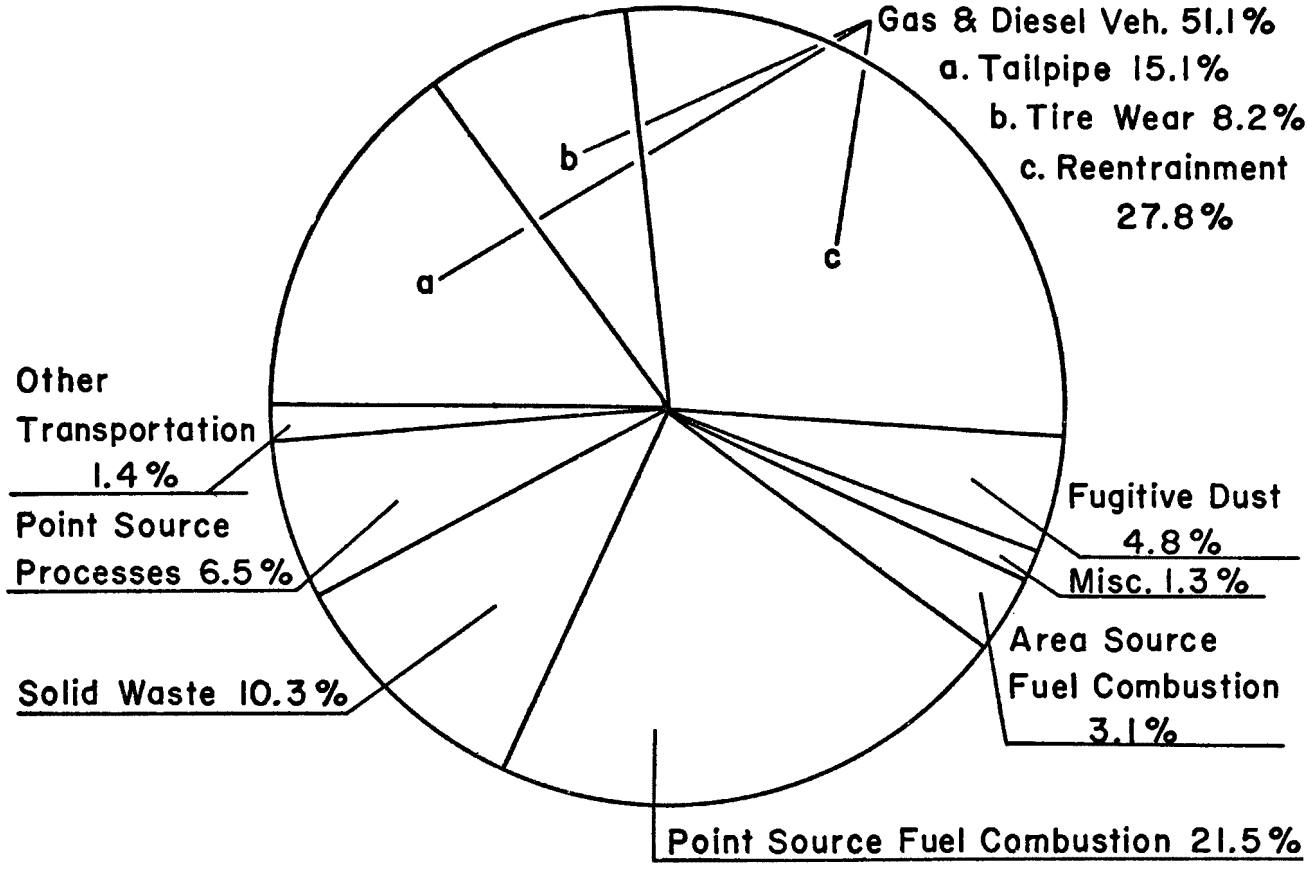

Figure 1 RELATIVE PARTICULATE CONTRIBUTION BY SOURCE CATEGORY-1976 SIP (1979) 3)

We recognize that there is a problem and that transportation makes a significant contribution to that problem. We accept that reduction of transportation related TSP offers an opportunity to achieve an accommodative SIP. However, it is our belief that the levels of TSP attributed to transportation sources have been overstated.

Due to the effectiveness of Connecticut's early control programs for stationary sources, transportation is responsible for a larger percentage of the TSP problem than in other areas having less stringent controls. Also, the costs associated with available transportation control measures may be significantly less prohibitive and growth restrictive than squeezing another round of TSP control out of the stationary source sector. For these reasons the Connecticut Department of Transportation (ConnDOT) has become one of the first state transportation departments to take an aggressive stance on TSP analysis and control.

Several elements of the analysis of the overall TSP levels led us to question the accuracy of the TSP monitoring procedures. Due to the number of monitoring stations, the decentralized character of their placement and limits on DEP's staffing, the majority of the samplers only operate every sixth day. A few samplers in critical areas operate every third day. The samplers are only tended once in each sampling cycle, resulting in filters being exposed to particle laden air for two or five days, depending on the length of the cycle. The particles which settle onto the filter during this period, known as passive sampling, introduce a significant positive error into the TSP measurements. This passive sampling error is acknowledged by DEP, but is not accounted for in evaluating the state's air quality.

A passive sampling correction should be applied to all existing and future TSP measurements if present sampling procedures and schedules remain in effect. Sampling studies have been conducted by DEP at one of its Hartford monitoring stations in order to quantify this error. The relationship developed was tested at other monitoring stations and exhibited good correlations. Further refinement and validation of this relationship should receive high priority.

A better way to achieve an accurate picture of the state's TSP situation would be to eliminate the source of passive sampling. Regardless of how well a correction relation is validated there will always be some error introduced into the measurements. Recently, samplers have been marketed which automatically cover the sample filter when the instrument is not operating. DEP has purchased several of these instruments and is in the process of acquiring more. It will be some time, however, before all monitoring stations in the state are so equipped. ConnDOT endorses this effort to modernize equipment and eliminate passive sampling error.

Passive sampling error is a significant factor. Initial studies presented in the SIP indicated that 5% to 28% of the total sample weight is attributable to passive sampling. Correcting for this error has been referred to by some, somewhat in jest, as a 20% control strategy. The implications to air quality standard compliance are obvious. In Connecticut, for example, there were no primary and eight secondary short-term TSP standard violations measured in

1977, the last year for which published data is readily available (ConnDEP (1978)[4]). Correcting these measurements by using DEP's correction relationship reduces the total number of secondary violations to three. Two of these are marginal and would require minimal additional emissions controls.

In summary, passive sampling error should be eliminated or, at the very least, accounted for. This would result in a more accurate portrayal of Connecticut's air quality, and result in less stringent control requirements for the state's citizens and industries.

Location of monitoring sites has led to questions about whether or not the measurements are representative of the air quality in an area. Two EPA designations apply to TSP monitoring sites for transportation sources. Zone A sites are close to and under the local influence of the roadway source and are therefore unrepresentative of an area's ambient air quality. The situation is analogous to placing an ambient monitor in the plume from an industrial or power plant chimney, in close proximity to its orifice. Zone B sites are acceptable for ambient measurements, being far enough from the roadway to be outside it direct influence (Federal Register 5).

A few of the sites in Connecticut's monitoring network are Zone A sites. The downtown site in the city of Waterbury, location of the state's highest TSP readings, has been thus classified by EPA. The argument has been put forth that a large portion of the area in a city such as Waterbury is classified as Zone A and thus that a Zone A monitoring site is representative of the entire city.

A monitoring study was conducted by DEP to better define the problem in Waterbury and to determine how well the permanent monitoring station represented the city. Seven samplers including the two permanent monitoriing stations were placed at various points in the city. Three were classified Zone A, the remainder classified Zone B. The study showed that all of the Zone B sites in the downtown area yielded significantly lower measurements than all of the Zone A sites (SIP(1979)[6]). The use of monitoring sites which are unduly influenced by a limited number of TSP sources leaves questions concerning the true magnitude of the particulate problem in Connecticut.

Atmospheric transport of air pollution has been a long standing problem whose significance has only recently been acknowledged. This recognition, however, has generally been restricted to ozone and its precursors. Recent evidence illustrates that other pollutants including TSP are transported considerable distances and do not respect political boundaries.

Connecticut has long recognized the existence and implications of pollutant transport. The New York City/Northern New Jersey industrial complex is a tremendously large source of all pollutants. The inventoried sources of particulates in this area emit several times as much pollution as the entire state of Connecticut, transportation sources included. As mentioned earlier, Connecticut is situated such that prevailing weather patterns carry large amounts of pollution into the state. This occurs by both the mechanisms of air mass transport and the urban plume effect.

Both monitoring and modeling studies have been conducted in an attempt to quantify the transport phenomenon. Monitoring has shown that the vast majority of days with highest TSP concentrations exhibit prevailing southwesterly winds. This is well illustrated by the pollution roses in Figure 2. Wind data from Newark were chosen for this illustration because they have been shown to better represent weather patterns typical of the New York City area and across Connecticut than other weather stations in the area. The pollution rose for Bridgeport in southwestern Connecticut exhibits similar characteristics. Meteorological data from New Jersey and Massachusetts were used in addition to those from Connecticut in the monitoring study in order to minimize local peculiarities.

A computer modeling study indicated that as much as 60% of the short term TSP concentrations in the southwest corner of the state can be attributed to transport when winds are from a southwesterly direction. The transport portion of TSP levels decreased with increasing distance from New York (SIP(1979)[8]).

Regardless of the precise magnitude of the amount of transported material, the implications are obvious. Additional control programs must be imposed on the state than would be required if the amount of transport were less. Connecticut must make up for emissions over which it has no control. This puts Connecticut's industries and businesses at a competitive disadvantage relative to those elsewhere. The resultant economic problems will be further compounded by a cut-off of federal funds should the air quality standards not be attained.

ConnDOT recommends that the studies of transport of both ozone and particulates which are underway be continued and refined on a higher priority basis. This is necessary to quantify this significant transport phenomenon and determine its magnitude. From this information, Connecticut's actual and equitable pollution control requirements can be determined and included in the 1982 SIP revision. The data might be used as evidence in persuading other states to implement more effective control programs. A possible secondary outgrowth of these studies would be the establishment of a regional approach to air pollution modelling and control.

The uncertainty concerning the portion of the TSP problem attributable to mobile sources springs from lack of agreement over the magnitude and characteristics of vehicular particulate emissions. Before outlining reservations concerning the analysis of mobile source emissions contained in the SIP, it would be instructive to present an illustration of the magnitude of the problem with which we are confronted.

Consider a 500 megawatt power plant operating at 38% thermal efficiency. The boilers of this plant, operating at capacity, require a thermal input of approximately 4500×10^6 BTU/hr. Assuming that the plant conforms to the Connecticut existing source emission standard of 0.20 lb/10^6 BTU, the plant will emit approximately 900 lb/hr of particulates, or 10.8 tons/day. Now consider an expressway carrying 40,000 vehicles per day. Assuming a vehicular emission rate of 1.2 gm/veh mi, see Table 2, a one mile long section of this highway emits 0.053 tons/day of particulates. It can be seen that it

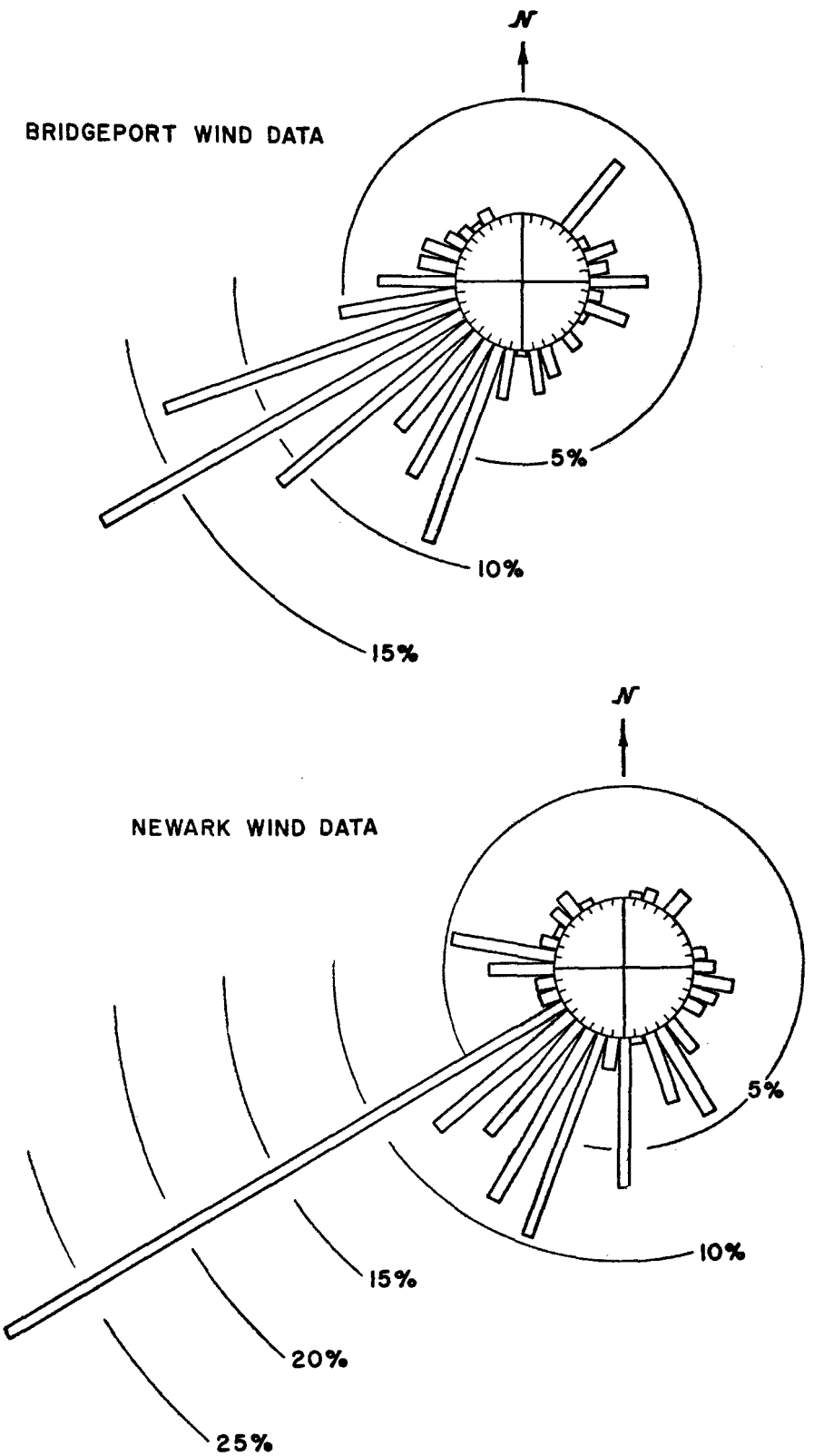

FIGURE 2 TSP POLLUTION ROSE

10 HIGHEST READINGS AT ALL CONNECTICUT MONITORING SITES
1975 - 1977 (SIP (1979) 7)

would take a 204 mile section of highway to equal the particulate emissions from a power plant which conforms to applicable emissions standards.

Individually, emission factors contained in Table 2 seem rather insignificant and not worth worrying about. Even when applied to a concentration of vehicles such as an expressway the emissions appear relatively small. However, it must be remembered that even a small state such as Connecticut contains thousands of miles of roads, which daily accumulate millions of vehicle miles of travel (VMT). Viewed in this light, it should be apparent that we in the transportation sector are facing a considerable problem; one whose relative importance is increasing as stationary source control improves.

The earlier perception of mobile source particulate emissions as a relatively minor problem is part of the reason that they have not been addressed until recently. Another reason is that mobile source emissions are generally more difficult to quantify than those from stationary sources.

The number of stationary sources subject to emission control is limited in number and fixed spatially. On the other hand, the number of motor vehicles is very large. Herein lies a large part of the problem faced by transportation planners attempting to quantify and control pollution from transportation sources.

The emission characteristics of stationary sources operating under various conditions may be determined quite accurately by source testing. There is little guesswork and few assumptions necessary in determining emissions at any time. In many cases the emission factors themselves reflect some operating parameters, e.g. mass of emissions per quantity of thermal input. There is no need, particularly for large sources, to average various sources to develop composite emission factors.

The determination of mobile source emission factors is more complex. Individual vehicles can be sampled to determine their emissions characteristics. However, there are millions of other vehicles, each with different emissions characteristics and each operating under constantly changing conditions. All of these emissions must be "averaged" into a composite emission factor which represents the average vehicle on the road.

Many estimates must be made. These include vehicle type and age mix, and percentages of vehicles operating under various conditions. These assumptions are based on analyses of historical trends and present sampling.

The emission factors for mobile sources are commonly expressed as mass of emitted pollutant per distance traveled (grams/vehicle mile or kilometer traveled). Some others have found limited application, but these are the most widely used units. This factor, as currently used in Connecticut does not account for any vehicle operating parameter.

TSP emission factors for transportation sources are affected by a number of parameters. Some parameters, such as vehicle type mix or ambient temperature, can often be assumed to be constant. Such factors either have a minor influence on emission rates or, by virtue of their characteristics, lend themselves to the assumption of a constant overall value. Other parameters, however, have a significant effect on vehicular emissions and require a

different composite emission factor for each value of the parameter. Vehicle speed is a typical example. Depending on the pollutant, emissions can vary by more than an order of magnitude for normally encountered speed ranges.

Presently all three components of the emission factor used in the SIP calculations are assumed to be constant, regardless of operating parameters. A small decrease in the tailpipe emission component is assumed for each analysis year to account for the phase-out of leaded gasoline, but otherwise assumes constant operating conditions. Consequently, all three components of vehicular emissions have been related only to VMT. This oversimplification would indicate that only a reduction in VMT is a valid strategy.

The emission factors for other pollutants are influenced by parameters such as vehicle speed, vehicle operating conditions and the mix of vehicle age and type. It is reasonable to expect that exhaust particulate emissions would be similarly affected. The emission of lead particles, which constitute a significant portion of exhaust particulates, is proportional to fuel consumption and thus vehicle speed (EPA (1977)[9]). It is evident that total particulate tailpipe emissions would be influenced by vehicle speed, at least to the extent of accounting for variations in lead emissions. Diesel-powered vehicles emit more particulates than gasoline-powered vehicles, indicating an influence of vehicle type mix. Engine efficiency influences emissions, indicating variations with vehicle age mix and the presence or absence of inspection/maintenance programs. Other probable influencing factors include: engine design; whether the vehicle is accelerating, decelerating, cruising at constant engine RPM's or idling; and whether the vehicle is in cold-start or hot stabilized mode of operation.

The tailpipe component of vehicular particulate emissions is probably the easiest to quantify. Sampling of the vehicle tailpipe can be done, similar to stack sampling on a stationary source. However, the parameters outlined above complicate the establishment of a composite emission factor or range of factors.

Procedures exist which can overcome this difficulty, but additional data must be obtained and reported. The EPA's Federal Test Procedure is presently used to determine and update vehicular emissions of CO, NOx and NMHC. Tailpipe particulate sampling has been done, but not to a large extent. The particulate emission factors contained in EPA's AP-42, from which the Connecticut SIP emission factors were obtained, do not reflect the influences outlined above. Thus the technology and standard procedure exist. These must be used to establish tailpipe emission factors as soon as possible.

Although tailpipe emissions constitute less than one-third of the vehicle generated particulates, their control is necessary. Exhaust emissions contain small, respirable particles which pose a more significant threat to human health. As noted earlier, lead-containing particles may constitute a significant portion of exhaust particles, often in excess of 10%. These particles, produced by high temperature alteration of lead anti-knock compounds, are a health hazard because of their chemical toxicity. Lead control is now governed by a separate Ambient Air Quality Standard adopted in October, 1978. Similarly,

proposals have been advanced to differentiate between and control respirable TSP.

The federally-mandated reduction of lead compounds in gasoline will reduce lead emissions and produce a corresponding reduction in overall particulate exhaust emissions provided no particle-producing additives are substituted. Although this lead phase-out is having and will continue to have a beneficial effect on mobile source particulate emissions, this was not the primary impetus for its implementation. Lead poisons the catalytic converters used for control of CO and NMHC, which were considered a more critical problem than lead or particulate emissions.

Several states are implementing vehicle inspection/maintenance programs in the interest of air pollution control. Through scheduled, usually annual, inspections some assurance that vehicle engines are tuned well and that pollution control devices are operating properly can be gained. These programs are not directed at particulate control however they do have a beneficial effect. Improving overall engine efficiency will substantially reduce particulate exhaust emissions.

ConnDOT annually proposed or supported legislation which led to establishing a mandatory inspection/maintenance program in 1981. A limited, voluntary system is scheduled to be in operation in 1980. The inspection portion of the program may be conducted by the state itself, by private contractors, or by licensed individual service stations. After considering the various alternatives and the experiences of other states, it was decided that Connecticut's system would be operated by a private contractor.

There are various engine modifications and add-on devices which can reduce particulate exhaust emissions significantly. Connecticut has no plans for requiring engine modifications or installation of particulate control devices. This is a matter for federal regulation. Legal and jurisdictional questions, and practical problems of implementation and enforcement make this strategy generally infeasible for an individual state to implement.

The assumption of a constant tire wear emission factor is no more reasonable that a contant factor for exhaust emissions. Major factors which can influence road/tire friction include acceleration and deceleration characteristics, vehicle speed, roadway surface roughness, tire rubber characteristics and tire loading. The tire wear emission factor component should reflect the most important of these factors.

Implicit in the SIP tire wear emission factor is the assumption that all of the mass worn off tires is in the form of particles small enough to be considered suspendable. Recent studies have shown this not to be the case. The preponderance of the emissions is in the form of larger particles, with small quantities of gas. Suspendable particles constitute approximately 5% of the total mass emitted (Cadle and Williams (1978)[10]). The precise percentages, of course, may vary somewhat in practice and should be refined by further experimentation. However, the assumption that all particles are suspendable introduces a significant over-estimation of the mobile source contribution to ambient TSP levels.

Sampling the wear products of a rolling tire is more difficult than sampling tailpipe emissions. However, a technical method for conducting controlled measurement studies has been demonstrated (Cadle and Williams (1978) [11]). The method used in these studies has the ability to test tire wear under different operating conditions, such as vehicle load, speed and surface roughness. We recommend that this procedure or some similar measurement method be approved by EPA and incorporated into the Federal Test Procedure. The studies which have been conducted could be expanded, resulting in the development of a viable set of emission factors.

As long as rubber tires are used on motor vehicles particles will be emitted by tire wear. Reducing vehicular travel is the most direct method to reduce tire wear emissions. Smoother roadway surfaces could reduce it somewhat, but safety considerations place limits on pavement smoothness. Use of tires with improved wear characteristics is perhaps a feasible means to reduce this emissions component. Connecticut has no strategies, active or planned, directed at control of tire wear emissions.

Reentrained road dust emissions are so variable that a constant emission factor is unrealistic. Studies have indicated an influence from vehicle operating parameters, roadway surface loading, "dirt" characteristics, and meteorological parameters. Again the major factors should be reflected in a set of emission factors, rather than relying on a single factor for all conditions.

The reentrainment component of vehicular emissions is by far the most difficult to quantify adequately. By the very nature of the problem, closely controlled laboratory experimentation is not feasible and ambient studies to date have been woefully inadequate.

A wide range of values has been reported by various researchers ranging from 0.8 gms/mi to 77.0 gms/mi (SIP (1979)[12]). The studies taken as a group amply demonstrate the difficulties in defining reentrainment factors.

Perhaps an outgrowth of the complexity of the system in question is that there is little agreement on how to go about sampling such a system. There are probably as many different methods as there are researchers in the field. Some have placed HiVOL samplers at various distances downwind of a roadway and at different heights. The disparities in their results are not surprising because, by virtue of particle settling, they are measuring different things. Some researchers have used upwind samplers in addition to those placed downwind while others have not. Sampler height placement ranges from one meter to the top of buildings. Some researchers have chosen not to monitor meteorological parameters.

This confused and confusing situation should be remedied as soon as possible so that uniform efforts to establish true emission rates may proceed. This is the largest component of vehicular particulate emissions and the one most subject to controversy. Guidelines on sampling procedures should be developed in the near future.

There are a great variety of methods and strategies which can be implemented to control the reentrainment of road dust. Most of these can be classified either as prevention of particle deposition on roadway surfaces or removal of deposited matter.

Prevention of deposition can cover a wide range of practices. The most difficult task is control of atmospheric particle fallout. Gravity settling of suspended particles can account for a significant portion of the material deposited on the roadway surface. Reduction of ambient TSP concentrations will generally decrease the amount of deposition. This may be accomplished through source control of particulate emissions, including those from mobile sources. As mentioned earlier, Connecticut is a leader in air pollution control, particularly of stationary sources. Thus, the implementation of this indirect strategy has been in effect for several years.

Vehicles which travel on unpaved areas such as roads, parking lots, and construction areas contribute to the material available for reentrainment. Particles, mostly composed of mineral matter, adhere to vehicles traveling in these areas and are deposited later on paved roadway surfaces. This mechanism, commonly known as vehicular carryout, can result in locally significant contributions to the roadway surface loading, particularly in wet weather. Control of carryout is accomplished by paving or stabilizing the surfaces of these unpaved areas, where practical. Connecticut has no unpaved roads on its state system. A few lightly-travelled town roads remain unpaved. Local ordinances often require that large parking areas be paved. As elsewhere, however, these actions have resulted for reasons other than controlling air pollution.

A related and often simultaneous mechanism of particle deposition is vehicle spillage. This occurs when a truck which hauls particulate or particulate-producing matter is overfilled or when air resistance erodes exposed surfaces of the matter being transported. This can cause significant local increases in the surface loading of a roadway, especially in the vicinity of construction projects or sand and gravel operations. Installation of control devices, such as retractable fabric covers, on appropriate trucks and prevention of overfilling can minimize this problem. These controls have been in effect in Connecticut for approximately ten years but better enforcement of existing regulations is needed. ConnDOT construction and maintenance specifications require covering loaded trucks. Enforcement of these specifications is carried out by the operating units.

Large amounts of particle matter may be deposited on roadway surfaces by storm runoff. This may be controlled by physical alterations to the roadway which will prevent material from being washed or tracked onto the roadway. These alterations will either prevent runoff water from inundating the roadway or removing it rapidly without allowing it to dissipate its energy. Such alterations may take the form of curbs, culverts, hydraulically efficient catch basins, or similar structures. These measures have been implemented extensively in Connecticut, and have a strong, beneficial effect on air pollution control.

A significant source of particulate matter is sanding and salting operations during winter ice and snow storms. Although large amounts of sand and salt are deposited on roadways during storms, the magnitude of the contribution of this mechanism to overall reentrainment is unclear. Since these operations take place

only a limited number of times during the winter months, it has been theorized that the overall impact is small. Preventive control would obviously take the form of reducing the amount of both salt and sand to the minimum required for motoring safety.

The efficiency of sanding and salting operations may also be increased to better utilize the amount of material used. This can be accomplished through the use of automatically-fed spreaders, resulting in more even distribution and lower material consumption than is obtained with conventional driver-controlled spreaders. Connecticut has decreased its total usage of salt and sand in recent years and reduced the ratio of salt to sand in consideration of economy and water quality. That policy is now being evaluated as a control measure. Purchase of automatic spreaders is being considered by ConnDOT to replace equipment which is normally phased-out every year.

Despite efforts to control it, some particulate matter will inevitably be deposited on roadway surfaces. Reduction of reentrainment requires that the material be removed, usually by means of water flushing and sweeping. The latter may take the form of rotating broom sweeping, air blast sweepers, or vacuums. Little data is available on the absolute or relative effectiveness of each of these methods in reducing TSP emissions. Water flushing has been shown by one study to increase reentrainment during several days immediately following the operation (Bradway et.al.(1978)[13]).

As in many locations, roadway cleaning operations have been going on in Connecticut for a long time. Many of the larger municipalities periodically clean the gutters on city streets. ConnDOT sweeps all major state roads each spring, primarily to remove and reclaim sand spread during winter snow storms. The state operations and the majority of those on the municipal level are accomplished using rotating broom sweepers which collect the material. A few municipalities have vacuum cleaning devices; these are used primarily for removing fallen leaves during the autumn.

Perhaps as important as the particle emission rates from motor vehicles is the size/density distribution of these particles. The uncertainty of this distribution introduces potential errors of the same magnitude as the potential errors in emission factors. There is evidence that a portion of the particles emitted by motor vehicles are large enough to settle out of suspension rapidly and do not contribute to ambient TSP concentrations. Accurate accounting for particle settling in concentration calculations is necessary to evaluate transportation emissions and prepare an accurate inventory of an area's air quality.

The EPA has recommended an emission factor for reentrained dust of 5.15 grams per vehicle mile. The DEP correctly assumed that a portion of this is not suspendable. Assuming that the entire mass is in suspension would result in transportation completely overwhelming all other sources. Monitored data tells us this is not the case.

In Connecticut the procedure used to date has been to assign a portion of vehicle emissions as suspendable and a portion as settleable. In early calculations non-rigorous assumptions were made. Better information regarding

particle size distributions for each emission component is needed. ConnDOT has worked to develop a model which would account for particle settling. If these efforts are successful, a realistic picture of actual conditions could be obtained. This would obviate the necessity of using a separate, suspendable emission factor, and eliminate uncertainty as to the definition of what is suspendable and what is not.

A basic weakness in the current approach is that particulate emissions are not generally divisible into suspendable and non-suspendable fractions with a discrete dividing point. Most emissions cover a continuum of particle sizes, the fraction that is "suspendable" depending largely on the distance from the source. Granted, some particles may remain suspended indefinitely, but this type of artificial approach has tremendous potential for error. Attempting to define a suspendable particulate fraction without knowing the size distribution of the emitted particles and without having defined the mechanisms of deposition leaves a weak foundation on which to base regulatory decisions.

There are presently no readily-available predictive models which can be used to calculate the profile of concentrations resulting from a transportation line source. The most popular highway line source models, HIWAY (Zimmerman and Thompson (1975)[14]) and CALINE -2(Jones and Wilbur (1976)[15]) are both Gaussian models based on conservative gaseous dispersion over flat, open terrain. Neither is acceptable for analysing the deposition and dispersion characteristics of non-homogeneous particles in typical urban/suburban flow fields, characterized by everything but flat, open land.

Chemical analysis of monitored samples could and should be expanded. Such analysis furnishes valuable information and could be used to better demonstrate contributions from motor vehicles. Presently in Connecticut, the samples are analysed for several metals, total nitrates and sulfates, ammonium, acidity and benzene-soluble organics. This analysis gives some valuable insights but does not firmly establish the transportation contribution.

Lead, for which Connecticut samples are presently analysed, has been proposed as a tracer for vehicular particulate emissions. Connecticut would seem to be a favorable location for this use, as there are no overwhelming stationary sources of lead in the state. However, the results of past monitoring do not support the use of lead as a tracer. Annual average concentration trends of lead and TSP bear little resemblance to each other at most monitoring stations in the state. The graph in Figure 3 shows these trends at a typical station. As can also be seen from the graph, generally increasing traffic trends have not been reflected in either lead or TSP concentrations. Thus lead has dubious value as a tracer of mobile source particulate emissions. Furthermore, the phase-out of leaded gasoline will tend to reduce its potential usefulness over time.

Recently some of Connecticut's monitored samples have been analysed for mineral substances. Silicates and some other mineral constituents have been suggested as indicators of transportation related particulates. The implication is that all mineral particles detected in TSP samples are the product of vehicle reentrainment. This is not necessarily the case. Operations such as agricultural plowing, construction, or various natural sources may account for significant portions of mineral particles at any given sampling station. Thus, the assumption is premature and suspect without knowledge of a particular site.

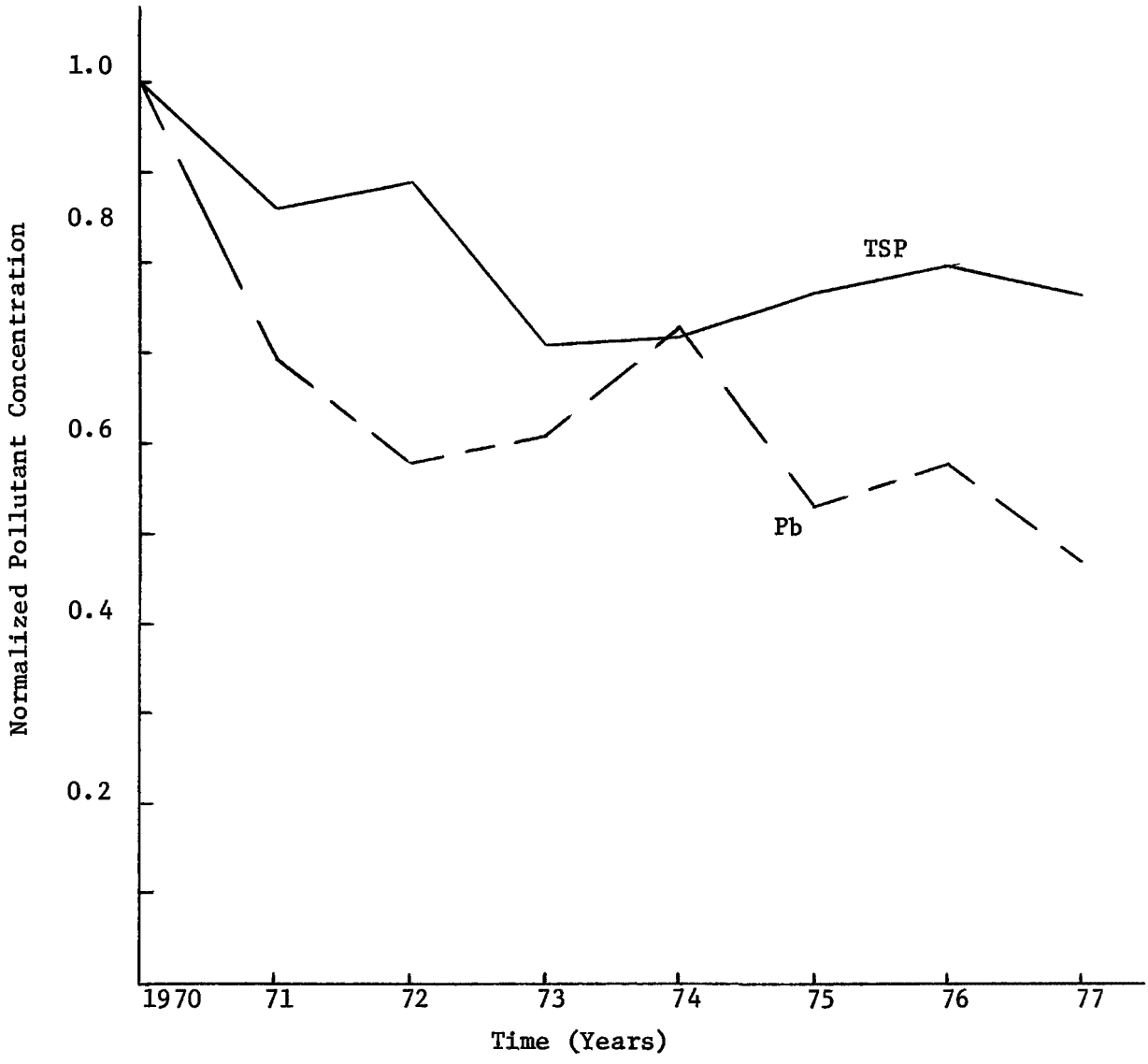

Figure 3. TSP and Lead Concentration Trends at a Typical Monitoring Site (ConnDEP(1978)[16])

Particular tire constituents or some other substance which is relatively unique to vehicular emissions might be used as a tracer. However, great care must be exercised in interpreting and utilizing the results, acknowledging the limitations of the use of any such tracer.

The state of Connecticut is involved in a number of additional studies and programs which are designed to better define the mobile source particulate problems and to implement measures to alleviate them.

Much of this effort is focused on the city of Waterbury. This is the site of the state's only primary standard violation. There are currently several monitoring studies being funded by EPA in an effort to determine the sources of the high TSP levels and the particle characteristics. The first of these studies is an attempt to determine the amount of traffic-generated TSP at the permanent monitoring site in downtown Waterbury. One hour average TSP concentrations will be compared with corresponding traffic counts on streets surrounding the site.

The particle size character of the TSP in Waterbury is being addressed in a second monitoring effort. Dichotomous samplers have been placed at the permanent monitoring site and at several other points. The respirable and non-respirable fractions of suspended particulates will thereby be obtained. DEP also hopes to obtain an indication of the mobile source contribution to total particle concentrations in the area from this study.

A third study, being conducted by a consultant, is a comparison of meteorology inside and outside the Naugatuck River valley, in which Waterbury is situated. This study is designed to identify the role of climatic effects in accounting for the high TSP levels in the area.

The final study is a continuation of one which was started in 1978. This is an attempt to determine the spatial distribution of TSP concentrations and their sources in the city of Waterbury. The original study, which was briefly discussed earlier, used seven HiVol samplers in the downtown area; no definite conclusions were reached. The continuation of the 1978 study is using a much larger number of samplers scattered throughout the city.

Much of the monitoring for the four studies has already been completed. With the exception of the consultant meteorological study, all of the monitoring is being performed by DEP.

ConnDOT is coordinating closely with DEP in the analysis and interpretation of the data.

ConnDOT presently has the capability for ambient pollution monitoring in the form of a fully equipped mobile monitoring unit. This unit is used in preparing air quality assessments for highway project environmental impact statements and/or collecting data for other transportation programs as is deemed necessary. Since mobile source particulates are a relatively recent concern, ConnDOT's monitoring capability has not included particulates. However, the Department has recently acquired two HiVol samplers to supplement its existing monitoring capacity. These monitors are initially being used in

a study to determine the emissions from pavement recycling operations. After this study is completed these samplers will be used in various traffic-related monitoring studies.

A consortium of municipal, regional, and state agencies recently received a grant from the Department of Housing and Urban Development and several other federal agencies to carry out an air quality and economic development technical demonstration project. The project is to be conducted principally by the municipalities and regional planning agencies in the lower Naugatuck River valley, with the state agencies providing technical assistance. The City of Waterbury has been designated the lead agency.

The purpose of the grant is to stimulate economic development in this somewhat depressed area, while minimizing the impact of this development on the area's air quality. The project is in the planning and negotiation stages at present, so the precise objectives and procedures of the study have not yet been established. However, monitoring and modeling of transportation-related TSP and determination of "off-sets" policy will be prime considerations of the air quality portion of the study.

A joint ConnDOT/DEP TSP monitoring study is presently being formulated, as a possible outgrowth of the air quality/economic development technical demonstration project. The purpose would be to determine the effect of roadway maintenance operations on dust reentrainment emissions. Monitoring would be conducted on a control section of highway which had been subjected to salting and sanding, vacuum cleaning, rotary brush sweeping and other similar operations.

A further commitment to TSP control will be made a part of Connecticut's Indirect Source program. This is a state program which is applicable to transportation facilities. Proposed regulation changes in the revised SIP mandate the consideration of TSP and lead emissions and promulgate strong incentives for developing technical methodologies for both analysis and control of transportation related particulates.

Connecticut is steadily expanding programs, other than those discussed above, directed at control of vehicle-generated air pollutants. These programs are aimed at reduction in automobile use, particularly for low occupancy use and during work trip congestion. For several years ConnDOT has provided alternatives to private automobile use. Operating subsidies have been paid to the Penn Central Railroad, now Conrail, in order to maintain rail commuter service in areas of the state served by passenger rail lines. Intracity bus service has been operated by the state in several of the largest municipalities, resulting in expanded and improved service. Express bus service between central business districts in several large cities and fringe area collector parking areas has been very successfully implemented. One-hundred twenty-two commuter parking lots have been constructed at expressway interchanges and other convenient points throughout the state. These lots are intended to be meeting points for carpools and other ride-sharing operations. Several of the lots are served by express or intracity buses. Promotion of ride-sharing has included computer carpool matching, providing assistance to businesses in establishing and encouraging carpool programs, and financing a limited number

of vanpools. All of these alternatives have specific benefits in addition to air pollution control, but the evolution to a multi-modal system will produce significant air quality improvements. Other benefits of reduced VMT, such as reduced traffic congestion and fuel savings, have also been major considerations.

To date, Connecticut has not adopted a program of automobile use disincentives. Such measures are under consideration and could be implemented should the need arise.

The measurements and analyses recommended in the preceeding few pages are not frivolous academic exercises. They constitute a necessary attempt to gain an understanding of phenomena which will affect all of us. The information gained will more clearly define the sources and magnitude of the TSP problem and may prevent the imposition of unnecessary control measures.

REFERENCES

1. Axetell, K., and Zell, J. Control of Reentrained Dust From Paved Streets. EPA Publication No. EPA-907/9-77-007, August 1977.

2. Bradway, R.M., Record, F.A., and Belanger, W.E. Monitoring and Modeling of Resuspended Roadway Dust Near Urban Arterials. Transportation Research Record 670. National Academy of Sciences. 1978.

3. Cadle, S.H., and Williams, R.L. Gas and Particle Emissions From Automobile Tires in Laboratory and Field Studies. J. Air Poll. Control Assoc. 28:502-509, May 1978.

4. Connecticut Department of Environmental Protection. Connecticut Air Quality Summary - 1975.

5. Connecticut Department of Environmental Protection, Connecticut Air Quality Summary - 1976. March 1977.

6. Connecticut Department of Environmental Protection. Connecticut Air Quality Summary - 1977. June 1978.

7. Connecticut Department of Environmental Protection. State Implementation Plan For Air Quality. June 22, 1979.

8. Connecticut Department of Transportation. Connecticut Master Transportation Plan 1979. December 1978.

9. Cowherd, C., Maxwell, C.M., and Nelson, D.W. Quantification of Dust Reentrainment From Paved Roads. EPA Publication No. EPA-450/3-77-027. July 1977.

10. Federal Register, August 7, 1978 (Vol. 43, No. 152, pp. 34892-34934)

11. Fitzpatrick, M.W., and Law, D.A. Automatic Controls for Salt & Abrasive Spreaders. Transportation Research Record 674, National Academy of Sciences. 1978.

12. Jones, K.E., and Wilbur, A. A User's Manual For the CALINE-2 Computer Program. FHWA Report No. FHWA-RD-76-134, August 1976.

13. U.S. Environmental Protection Agency. Control Techniques for Lead Air Emissions. November 1977.

14. Zimmerman, J.R., and Thompson, R.S. User's Guide For HIWAY, A Highway Air Pollution Model. EPA Publication No. EPA-650/4-74-008, February 1975.

NEW CONCEPTS FOR CONTROL OF FUGITIVE PARTICLE EMISSIONS FROM UNPAVED ROADS

by

T. R. Blackwood
Monsanto Research Corporation
Dayton, Ohio 45407

and

D. C. Drehmel
Industrial Environmental Research Laboratory
U. S. Environmental Protection Agency
Research Triangle Park, NC 27711

ABSTRACT

An analysis of the forces that produce emissions from unpaved roads shows that if fine material can be reduced or moisture increased, emissions will be reduced. Instead of collecting emissions, this new approach would decrease the emissions by reducing the fine material or by making minor increases in the moisture content of the road. In either case, a stable, rot-resistant, water-permeable fabric would be used to separate road ballast from the subsoil. Preliminary evaluation and economic analysis indicate that roads constructed in this way can be cheaper than conventional unpaved roads when subsoil load-bearing characteristics are poor.

Construction and testing of a prototype road is anticipated in 1979. The paper describes the theoretical analysis, preliminary results, and economic analysis of the idea.

INTRODUCTION

Fugitive emissions from vehicular movement on unpaved industrial haul roads are a major source of respirable emissions in urban areas. Current control methods, which include water wetting, treatment with surface agents, soil stabilization, paving, and traffic control, have thier own merits and limitations. Environmental problems could result from surface agents (such as oil) leaching into streams. Safety problems could result from slippery and dangerous road conditions. High initial cost and subsequent maintenance and repair costs make otherwise effective control measures (such as paving) impractical.

A new concept for emissions control has been proposed based on the use of a civil engineering fabric, which is synthetic, stable, water-permeable, rot-resistant, and usually employed in road stabilization. Laid below the haul road overburden, this tough fabric, termed "Road Carpet", separates the fine soil particles in the roadbed from the coarse aggregate, as shown in Figure 1. This action prevents the fine material from reaching the road surface so that dust emissions are reduced.

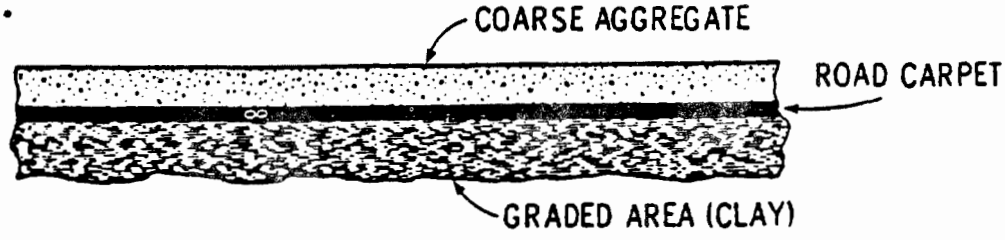

Figure 1. The Road Carpet concept, which spreads the vehicular load, prevents moisture from eroding the graded area, and keeps dirt from reaching the tires where it can be picked up and dispersed.

This report is a summary of work conducted to date on EPA contract 68-02-3107. Further details of the work are available in "Assessment of Road Carpet for Control of Fugitive Emissions from Unpaved Roads", by T. R. Blackwood; report submitted to the U. S. Environmental Protection Agency, Research Triangle Park, North Carolina, March 1979.

GENERAL THEORY OF "ROAD CARPET" OPERATION

The fundamental concept in the use of a fabric roadbed stabilizer, or road carpet, for the control of fine particle emissions from haul roads is the prevention of vortex entrainment and saltation effects by the separation of fine roadbed materials from the coarse aggregate. Large aggregate is prevented from settling, while fines (less than 70 μm) are filtered by gravitation and hydraulic action. Road carpet can be made from spun-bonded, thin-film polypropylene on nylon sheet (Celanese), continuous filament polyester fibers needled to

form a highly permeable fabric (Monsanto Company), or other spun or needle-punched synthetic materials. The mechanical interlocking of fibers makes a formed fabric with the durability and toughness required. Designed for road construction use, this fabric is laid over poor load-bearing soils to help support and contain the overburden aggregate. It spreads the concentrated stress from heavy-wheeled traffic over a wider area, siphons away ground water, and contains fine soil particles in the roadbed that can otherwise contaminate road ballast.

The use of road carpet results in no health or safety hazards or in any other unfavorable environmental impacts. In developing these fabrics, various synthetic polymers, including nylon, propylene, and polyester were screened and evaluated. Fabrics made from any of these products generally are resistant to mildew, mild acids, and alkali, and are rot and vermin proof.

Removal of Fines Contaminating the Ballast

When fine material enters the ballast, from either the aggregate or traffic, rainfall should carry it down to the fabric. If the fines do not pass through the fabric, they will build up and eventually contaminate the ballast. However, preliminary studies indicate that some fines do pass through some of the fabrics. In tests of clay blockage rates with vertical water flow, BIDIM and Cerex fabrics reached a limited blockage of 4 to 18 percent of the fabric area. Other fabrics, as shown in Figures 2 and 3, became essentially plugged with clay and bentonite solutions. These results indicate that the fabric will permit passage of the particles vertically and could be consolidated into the subsurface.

To further evaluate the particle transport characteristics of the fabric, tests were conducted on the horizontal flow through the fabric. The fabric to be tested was placed in the apparatus shown in Figure 4, which resembles a bell jar. A constant head of water was maintained and the horizontal flow measured. In-plane (horizontal flow) transmissability for several fabrics was deduced from these tests and is given in Table 1. In-plane transmissability of water is four to nine times higher for BIDIM than other fabrics. Additional flow studies were conducted with typical road dirt suspended in the water solutions. This composite was suspended in water, and, after settling of the large aggregate (greater than 70 μm), the slurry was sent to the bell jar to measure the in-plane flow of the slurry.

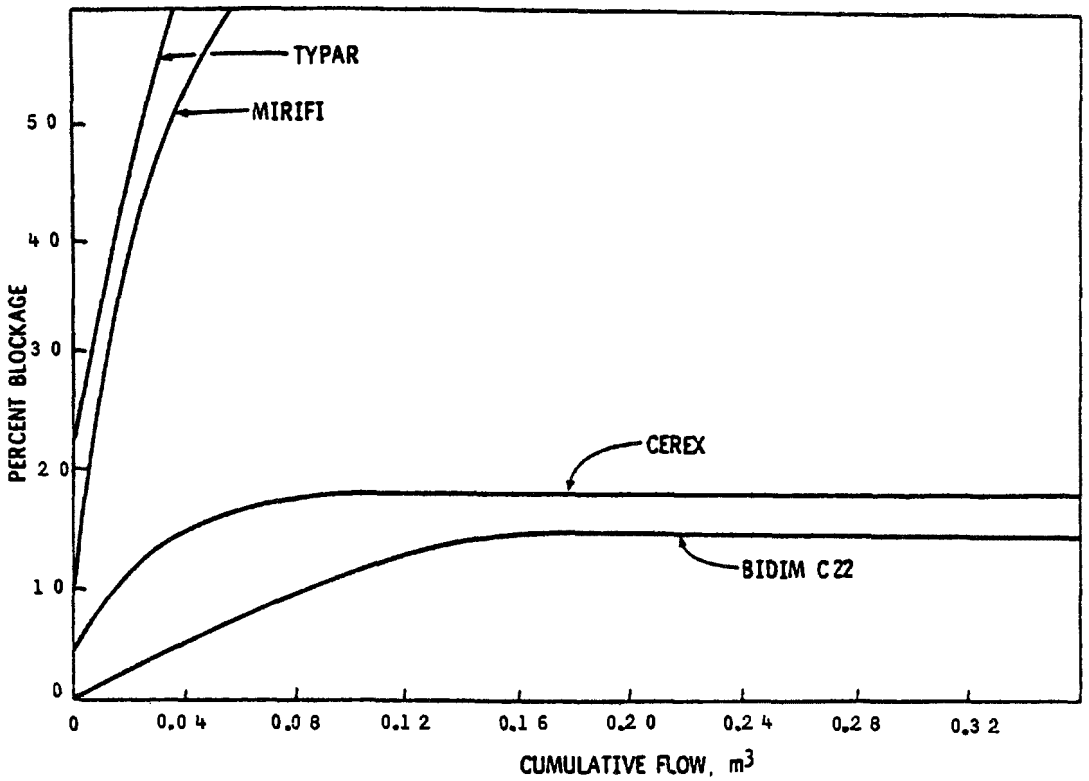

Figure 2. Blockage of fabric due to bentonite clay in water.

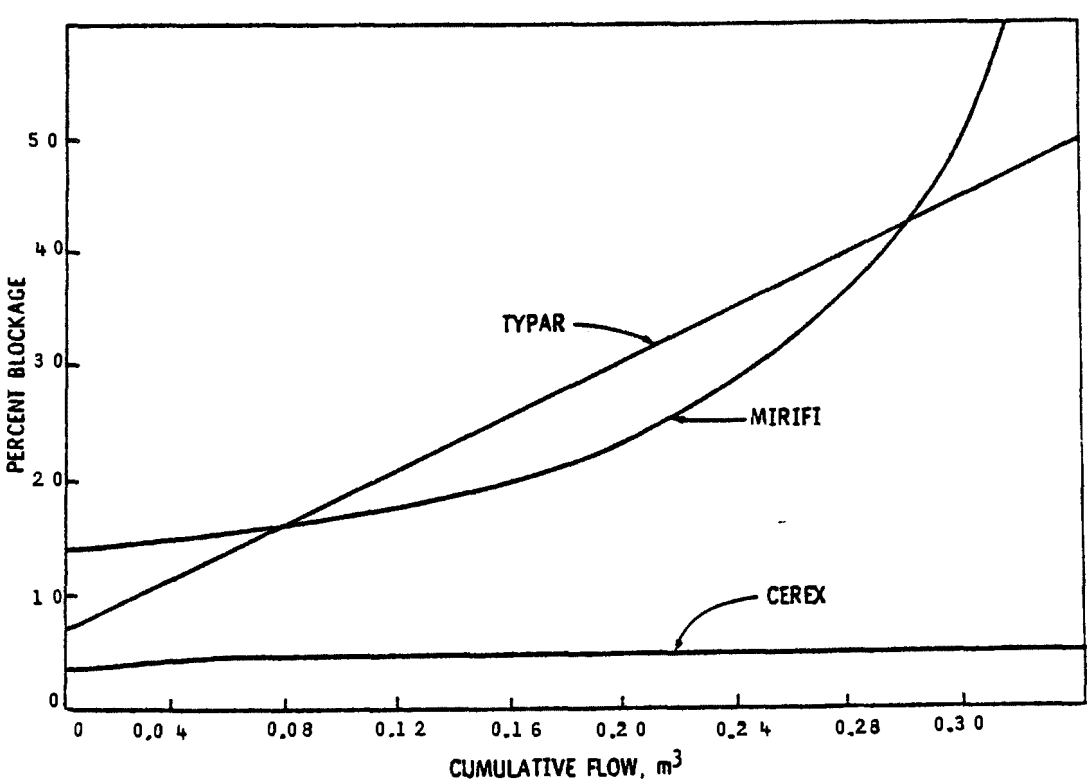

Figure 3. Blockage of fabric due to Hoytville clay in water.

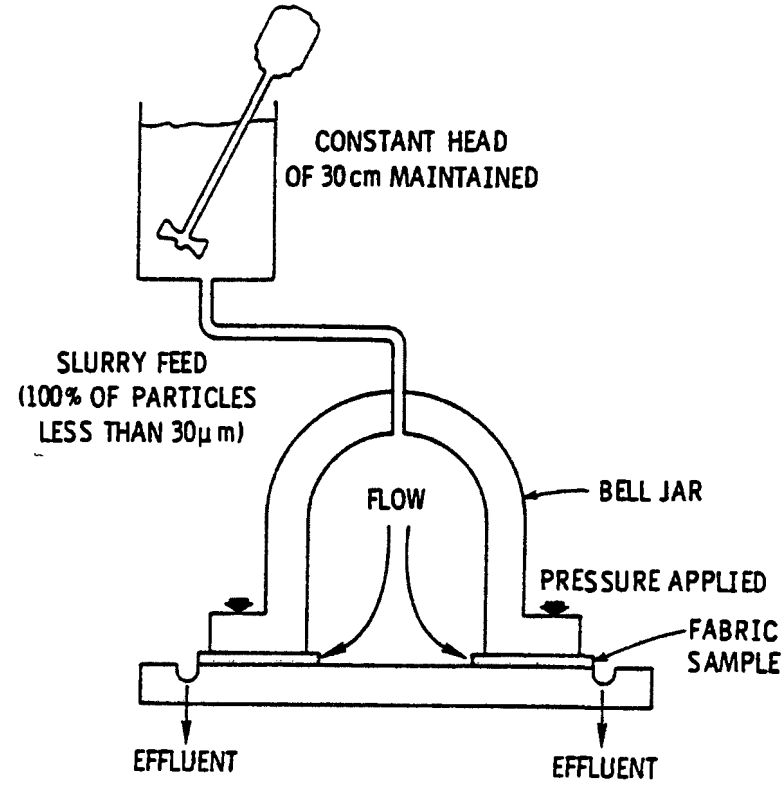

Figure 4. Laboratory Instrument used to evaluate in-plane flow of slurries through fabrics.

Table 1. IN-PLANE WATER TRANSPORT OF FABRICS

Fabric	Transmissability, 10^{-} cm /s
BIDIM C22	16
BIDIM C34	26
BIDIM C38	36
MIRAFI 140	4
TYPAR	1

Table 2 compares the vertical and horizontal flow rates for the BIDIM fabric with and without the presence of solids (i.e., clean water vs. slurry). The horizontal flow is reduced to about 40 percent of the initial clean water flowrate, but the fabric is not completely occluded. It is anticipated that, in the real world, pulsations of flow and channeling may increase the effective flow rate. This was verified in experimental work by momentarily raising the pressure on the fabric. Pulsations resulted from the compression and expansion of the fabric under the load of vehicles. A 17 percent increase in flow was observed due to these pulsations. Channeling is a common phenomenon due to the nonhomogeneity of the aggregate and soil adjacent to the fabric.

Table 2. COMPARISON OF FLOWRATES THROUGH BIDIM FABRIC

Direction	Flowrate, m/min Fabric C-22	Fabric C-34
Vertical:		
Clean water	22	15
Slurry[a]	19	13
Horizontal:		
Clean water	1.7	1.9
Slurry[b]	0.69	0.88

[a]Slurry contains bentonite clay; flowrate is the limit at steady state.

[b]Slurry contains typical road dirt; flowrate is the limit at steady state.

Particle Separation by Size

The holes in the fabric are approximately 70 μm in diameter and will permit passage of particles up to that size depending upon particle shape. Because the fabric does not "blind", the effective size of the holes is not reduced significantly, and all particles smaller than 15 μm (the size of interest) should pass through the fabric vertically. If the soil is soft (cone penetrometer less than 1,000 kPa), these particles would be consolidated with the exisitng soil. When firm soil (soil penetrometer greater than 1,200 kPa) is present, consolidation would be difficult. Because the presence of the fine soil particles does not plug the fabric during horizontal water flow, some if not all of the fines could be purged along with normal water flow. The median particle size that passed through the fabric during the horizontal flow tests was about 3 μm. Particles as large as 20 μm also came through the fabric. This means that only the very small particles would pass horizontally over firm soil; however, some channeling would exist and carry off the intermediate size particles (3 to 15 μm).

ALTERNATIVE CONTROL CONCEPTS

The siphoning action of road carpets such as BIDIM fabric can be applied to maintain a minimum moisture in the orad, as shown in Figure 5. Water passes through the fabric from the upper to the lower drainage pipe. Fines that enter the fabric can be settled out of the recirculating water lines. In dry regions of the United States, this concept would minimize the water used because the losses occur only by evaporation. If the graded surface is porous, a waterproof liner would be laid between the fabric and the graded surface to prevent excessive water loss.

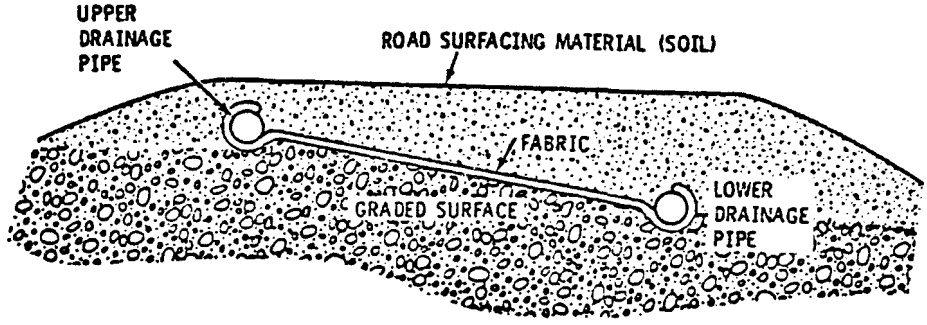

Figure 5. Self-watering road for emission control. Water is pumped from the lower drainage pipe to the upper drainage pipe externally.

ECONOMICS OF THE ROAD CARPET CONCEPT

Capital and operating costs of various control options differ with each alternative. Cost comparisons have been made between the cost of new roads constructed with a fabric base and conventional subsurface preparation.

For very soft soil (cone penetrometer index less than 600 kPa), road construciton cost decreases with increasing fabric thickness because the fabric spreads the stress and can replace 0.5 to 0.75 meters of rock. For soft soil (cone penetrometer index less than 1,000 kPa), the road containing fabric is only 40 to 50 percent cheaper. On firm or existing aggregate-covered roads, the road would cost about 10 percent more. The maintenance cost of a conventional road would be higher than for one containing road carpet; this will offset the difference in capital costs.

For cost comparisons, road width was assumed to be 10 meters. Eighteen metric ton axle loads were assumed for 10:00-20 tires. The design curve for BIDIM fabric is given in Figure 6.

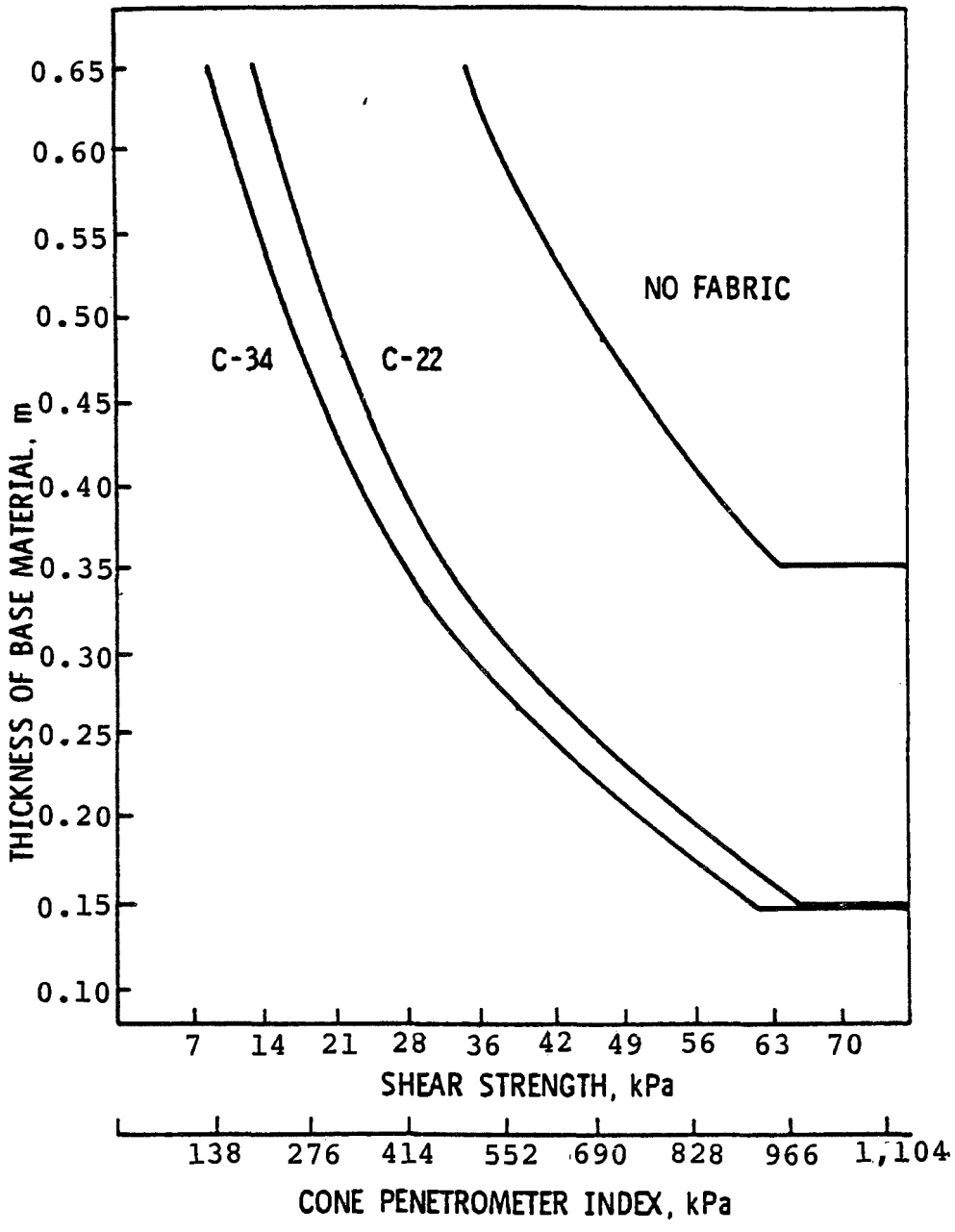

Figure 6. Design curves for 18 metric ton axle load on 10:00-20 tires for BIDIM fabric.

The installed cost of one kilometer of conventional road would be $44,000 on soft soil and $27,000 on firm soil. The main difference is the depth of aggregate required (soft soil needs 0.36 meter and firm soil needs 0.2 meter). Using a fabric costing $0.86 per square meter, the cost of one kilometer is $30,000.

Watering and repair of a conventional road cost about $6,700 per kilometer per year. Oiling of the road instead of watering would cost about $6,200.

The amoritized costs for conventional control measures and for the road carpet are summarized in Table 3. The life expectancy of the fabric in the road is unknown; experience indicates that 12 years would not be an unreasonable estimate. A haul road may last for the life of the plant (25 years) with proper maintenance.

Table 3. AMORTIZED COSTS OF DUST CONTROL ON UNPAVED ROADS (1979)

Type of road and/or dust control	Cost,$/km
Unpaved road on firm soil (no control); $27,400 over 25 years (17% interest)	4,750
Watering and ballast replacement	6,750
Oiling and ballast replacement	6,200
Ordinary road with watering and ballast replacement	11,500
Ordinary road with oiling and ballast replacement	10,950
Fabric unpaved road; $30,000 over 12 years (17% interest)	6,000
Ballast replacement	1,600
Fabric road with ballast replacement	7,600

The road constructed with fabric is cheaper than one which is watered or oiled. Better data would be required on ballast replacement and watering costs due to the high inflation that is presently occurring. With conventional roads, a higher percentage of the yearly cost is required for perpetual care. This would make an even higher capital cost more attractive, if the life expectancy were better than anticipated.

DEVELOPMENT OF A SAMPLING TRAIN FOR THE ASSESSMENT OF PARTICULATE FUGITIVE EMISSIONS

Roland L. Severance, Jr.
and
Henry J. Kolnsberg

TRC - THE RESEARCH CORPORATION of New England
125 Silas Deane Highway
Wethersfield, CT 06109

ABSTRACT

A prototype portable Fugitive Assessment Sampling Train, designed to obtain large samples of particulate emissions generated by sources whose configurations preclude sample collection before the diffusion of the emissions into the ambient atmosphere, has been successfully fabricated and tested.

The prototype FAST utilizes a combination of commercially available and specially designed equipment to collect a 500 milligram particulate sample in an eight-hour period at locations downwind of most industrial fugitive sources. The particulate sample is separated into inhalable and respirable fractions and provides sufficient material for a complete Level 1 assessment including bioassays. A quantity of organic species larger than C_6, sufficient for mass spectrometry analysis is collected on a bed of adsorbent resin.

The establishment of design criteria and operating parameters, selection and design of hardware components, and the fabrication and initial testing of the FAST are discussed. The results of calibration tests and an initial field trial are presented and a plan for additional development is outlined.

DEVELOPMENT OF A SAMPLING TRAIN FOR THE ASSESSMENT OF PARTICULATE FUGITIVE EMISSIONS

INTRODUCTION

A considerable portion of the air-polluting particulate matter and organic vapor emissions from industrial and energy-related processes is generated by sources that do not permit the capture of their emissions for measurement purposes before their diffusion into the ambient atmosphere. Obtaining samples of such fugitive emissions of sufficient size to perform statistically significant analyses of their concentration, particle size distribution, physical characteristics, chemical composition or biological activity presents a problem not readily solved using existing devices and traditional sampling techniques.

Standard high volume samplers, for example, can provide some information about the average particulate matter concentration at a sampling site over a long sampling period, but do not usually provide samples large enough for other than total mass determinations. Cascade impactors can provide particle size distribution information for a relatively small sample and multiple-cyclone separators can collect a fair-sized particulate matter sample in a few size ranges to provide essentially the same information. Grab sampling of gases or vapors for subsequent gas-chromatographic analysis can provide data on the chemical composition and approximate or relative concentration of these emissions, but is subject to the influence of interaction between emissions or aging of the samples. No single sampler exists than can collect a particulate matter sample large enough or a vapor sample stable enough to provide information in all areas.

This paper describes the progress made to date in the development of a Fugitive Assessment Sampling Train (FAST) designed to fill the requirements for a sampler capable of providing a large sample of particulate matter emissions from the atmosphere in a relatively short sampling period. A smaller organic vapor sample is obtained from the sampled stream.

SYSTEM DESIGN AND DEVELOPMENT

The development effort is being conducted by TRC-THE RESEARCH CORPORATION of New England as one task of a contract for the development of fugitive emissions measurement methods with the Process Measurements Branch of the United States Environmental Protection Agency's Industrial Environmental Research Laboratory at Research Triangle Park, North Carolina. Discussions between TRC personnel and the EPA Project Officers resulted in a target design specification for an ideal sampling train as the development starting point. The ideal sampler was described as being able to obtain, from the ambient air in the vicinity of an industrial fugitive emissions source, a 500 milligram sample of suspended particulate matter and a

similar-sized sample of organic vapors in an eight-hour sampling period. The particulate matter sample would be separated into respirable (smaller than 3 micrometer) and non-respirable (larger than 3 micrometer) fractions. The sample size was selected to correspond to the then-considered minimum for complete Level 1 analysis including bioassay. The sampler was also to be self-contained and portable; it would require minimum power and, using commercially available components wherever possible, cost less than $10,000 to fabricate in the prototype version.

An extensive computerized literature search and review was conducted in the hope of obtaining sufficient information on ambient concentrations of industrial fugitive emissions as particulate matter and organic vapors to prepare a realistic system design specification for the FAST. While this search and review revealed almost no data on ambient concentrations, it did provide a wealth of information on emission rates from a wide variety of industrial processes. A series of calculations based on the atmospheric diffusion equations in Turner's Workbook[1] for a range of atmospheric, topological and wind conditions was then performed to relate the published emission rates to ambient concentrations.

The calculations were made using the basic equation for the concentration of gases and particulates at a ground level receptor due to diffusion in the atmosphere from a ground level source,

$$\chi = Q/\pi\kappa\mu,$$

where

χ = pollutant concentration at the sampler, gm/m^3
Q = source emission rate, gm/sec
κ = product of standard deviations of vertical and horizontal pollutant distribution, m^2
μ = wind speed, m/sec

rearranged to express the source strengths as:

$$Q = \pi\chi\kappa\mu$$

The product of the standard deviations, κ, is a function of both the downwind distance of the sampler from the source and the atmospheric stability category, itself a function of wind speed and solar conditions. Values of κ for distances of 100 to 500 meters and atmospheric stability categories A to D, covering all pertinent daylight conditions, were determined from tabular and graphic presentations in Reference 1. Values for μ corresponding to the middle of the wind speed range for each stability category were used with each κ value to calculate source strengths. The pollutant concentration, χ, at the sampler was assumed to be 200 micrograms per cubic meter,

a value higher than most urban atmospheric concentrations but considerably lower than most individual point source plumes. Values of distance, stability category, K and μ used in the calculations are listed in Table 1 along with the calculated values of Q.

The calculations show that the assumed 200 microgram per cubic meter concentration can be obtained from sources emitting as little as 0.6 kilograms per hour at a distance of 100 meters.

Emission rates for some typical industrial processes or operations are listed in Table 2 for average-sized installations.[2,3] A comparison of the values of the rates for these processes with the rates calculated for the proposed sampling showed that the desired sample would be obtained from any of these processes with judicious positioning of the sampler between 100 and 500 meters downwind of the source.

The 200 microgram per cubic meter concentration was then used to determine the sampling rate required to obtain a 500 milligram sample in an eight-hour period of 5.2 cubic meters per minute (184 CFM) as the initial system design parameter. A Roots lobe-type vacuum blower, capable of moving the required volume of air against a pressure drop of about 10 cm Hg, was selected as the particulate sampling prime mover. A system of drive belts and pulleys was selected to operate the blower at the required 3800 RPM from a three horsepower drive motor. The drive system also provides enough flexibility to adjust the speed and the sampling rate up to about 20% if required.

To provide the separation of the particulate matter sample into respirable and non-respirable fractions, an Air Correction Design 6UP Sanitary Cyclone Separator was selected. Its design capacity of 6.3 cubic meters per minute (222 CFM) provides a D_{50} at about 2 to 3 micrometers at a pressure drop of about 0.6 cm Hg. The cyclone was selected as preferable to filter-type collectors since the sample is removed from the sampling stream and minimizes the degradation in sampling rate or effectiveness caused by the deposition of particulate matter on flow-through filters.

The inlet to the sampler was designed with fixed louvers to reject particles larger than 100 micrometers from the sample since such large particles do not ordinarily remain suspended for any appreciable distance from the source. The inlet is about 75 centimeters (30 inches) square, and effects an inlet samping velocity of only about 0.15 meter (0.5 foot) per second.

Consultations with Mr. Kenneth Cushing of the Southern Research Institute, under contract to the Process Measurements Branch in the area of particulate matter sampling, indicated that Reeves-Angel 934AH glass fiber filter material would be about 99.95% effective in collecting the fraction of the particulate matter sample down to about 0.3 micrometers passed through the cyclone. A circular format was selected for the filter material to provide the most even distribution of the sample on the filter surface and minimize the pressure drop buildup. A circular filter holder was

designed to accommodate a 929 square centimeter (1 square foot) filter, limiting the pressure drop across the unloaded filter to 3.7 cm Hg.

To provide stable samples of airborne organic vapor emissions, it was decided to utilize an adsorbent resin in a removable canister that could be easily transported from the sampling site to a laboratory for extraction and analysis of the sample. Dr. Philip Levins of Arthur D. Little, Inc., under contract to the Process Measurements Branch in the organics sampling area, provided consultation to TRC on the resin. The best available resin, XAD-2, which is almost 100% effective in retaining organic vapors C_6 and higher, was determined to require a canister containing about 75 kilograms to provide a 500 milligram sample. This was prohibitive from the standpoints of size and cost, and the design criterion was revised to obtain the minimum sample required for a Level 1 assessment of 14 milligrams. This sample size requires only 2.1 kilograms of resin and a sampling rate of only 0.14 cubic meters per minute (5 CFM). A canister was designed and an oil-less Gast vacuum pump selected to draw the organics sampling stream from the main stream after the particulate matter is removed.

The system design was reviewed and approved, and the procurement and fabrication efforts started. At this time, the EPA's Health Effects Research Laboratory suggested that an additional size fraction of the particulate matter sample be included to help in the assessment of the inhalable (less than 15 micrometer) portion of the emissions. It was decided to add a battery of six single stage Sierra Instrument impactors to the system to effect this additional fractionation between the inlet and the cyclone. These impactors were designed as the initial stage of a multistage impactor to provide a D_{95} for 15 micrometer particles. At the FAST design sampling rate, they would result in a pressure drop of only 0.05 cm Hg, and could therefore be added without affecting the system design.

The final system design is shown schematically in Figure 1. Design flow rates and pressure drops for each system element are shown enclosed in brackets. Samples retained by each element are shown in parentheses.

The procured and fabricated elements of the prototype system were then loosely packaged onto a space frame about 75 cm (2.5 feet) square by 183 cm (6 feet) high to allow easy access to the elements during development testing. The main sampling blower and the organic vapor sampling pump were separately mounted to improve the system's portability and permit the location of the blower and pump exhausts away from the sampling inlet.

After a successful operational test and a few modifications to the system were completed at TRC, the FAST was shipped to the Southern Research Institute's laboratory for calibration testing of the particulate sampling section. Tests were run by Southern using monodisperse ammonium fluorescein aerosols provided by their vibrating orifice aerosol generator at 3, 10 and 15 micrometers. The test results for the cyclone, shown in Figure 2 as points plotted on the manufacturer's design curve, are in very good agreement. The test results for the impactor, also shown in Figure 2, indicate good agreement with the design curve for smaller particles but are

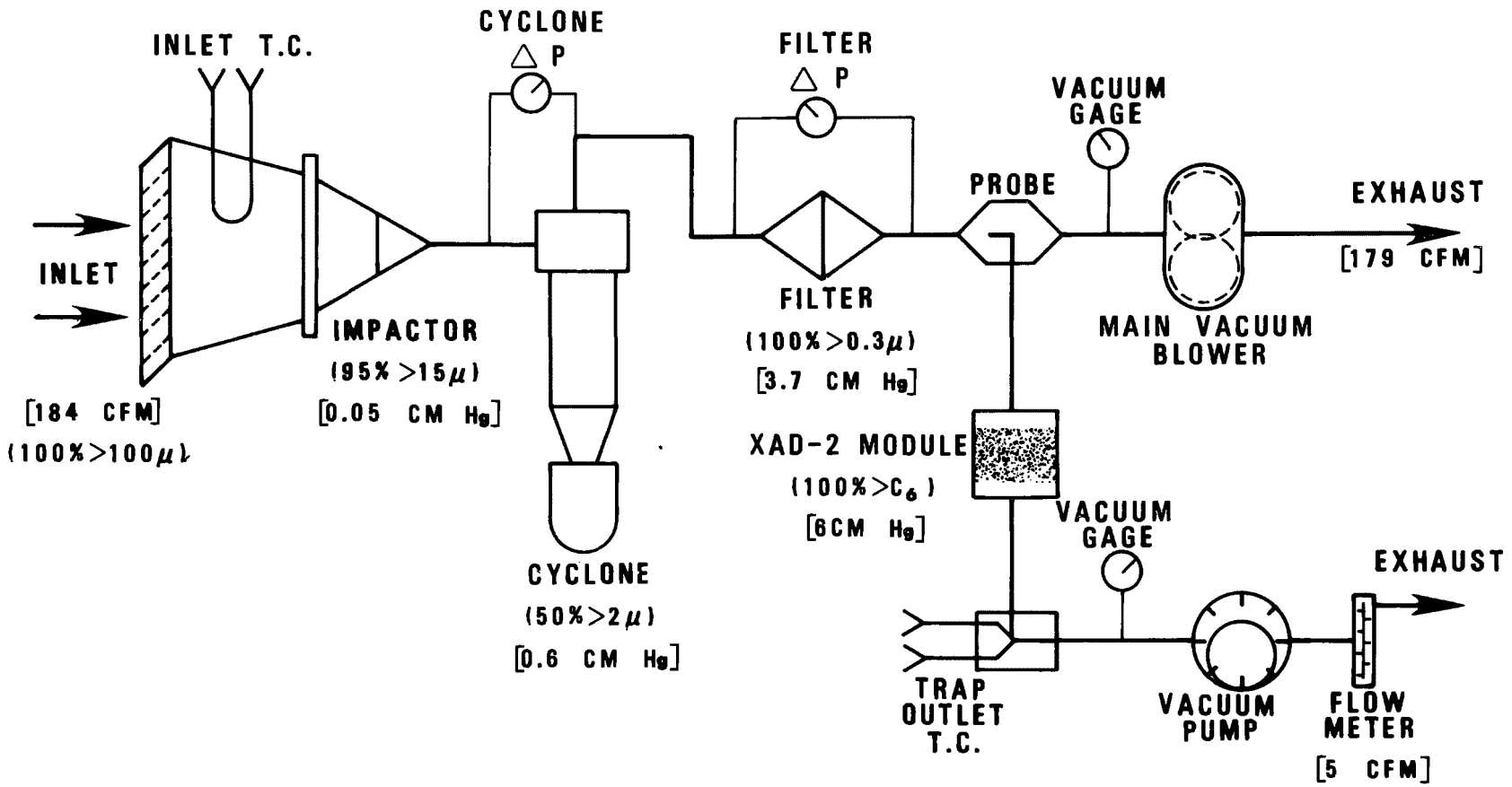

Figure 1. Fugitive assessment sampling train design operating condition

considerably lower than expected for the 15 micrometer particles of major concern.

Since it was felt that this discrepancy was caused by bouncing of the larger particles off the glass fiber substrate used in the impactors, a test was run using a grease substrate in an attempt to reduce the bounce. This resulted in a slight improvement in performance, but not to a level considered satisfactory for further development. A joint effort by TRC and Southern Research has been initiated to design and fabricate an elutriator to replace the impactor as the 15 micrometer fractionator. The elutriator will consist of a vertical array of horizontal plates, the spaces between the plates each forming a small settling chamber. Gravitational effects on the larger particles within each chamber will overcome the velocity effects and cause the larger particles to settle on the surface of the lower plate. Smaller particles will remain entrained in the sampling stream to be collected in the cyclone or on the filter.

SYSTEM TESTING

The initial field test of the FAST was conducted at the Southern Research Institute facility in Birmingham, Alabama, sampling the ambient air in a general industrial area. While it was recognized that the concentration of particulate matter in the ambient could be expected to be considerably lower than the FAST design concentration of 200 micrograms per cubic meter, it was felt that a good comparison of the FAST effectiveness relative to that of a standard hi-vol sampler and an indication of the system's operational capabilities could be obtained by extending the test run to obtain a sample approximating the desired 500 milligrams.

The FAST and a standard hi-vol sampler were run simultaneously and continuously for a period of about 34 hours. The particulate catches from the FAST impactors, cyclone and filter were, respectively, 360, 117 and 185 milligrams. The total 662 milligram sample, which did not include any of the material deposited on the interior surfaces of FAST, represented an indicated average ambient particulate concentration of 62 micrograms per cubic meter with a size cut-off of 100 micrometers. The average ambient particulate concentration indicated by the hi-vol sample of 281 milligrams was 82 micrograms per cubic meter with a theoretical size cutoff of about 120 micrometers.

A calculation using the plots of collection efficiency as a function of particle size (Figure 2) generated in the calibration tests was performed to determine an approximation of the distribution of the sample into the three size categories theoretically separated by the FAST. The results showed that about 44% of the sample was in each of the 0-2 and 2-15 micrometer size ranges and the remaining 12% in the 15-100 micrometer range. This is quite consistent with many existing urban aerosol studies which show that the mass of fine particles (>2 micrometers) is almost equal to the mass of all larger particles.

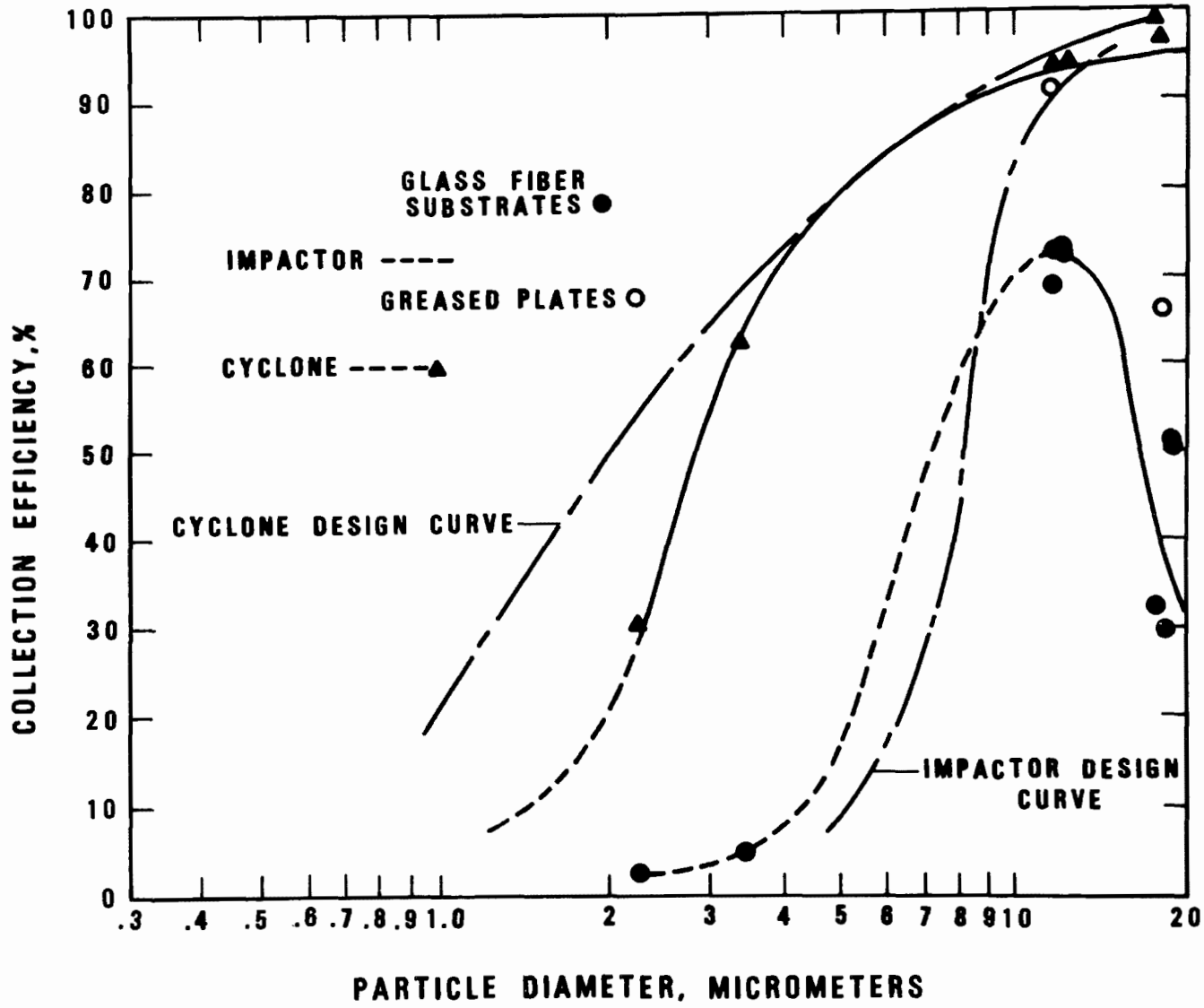

Figure 2. Collection efficiency as a function of particle diameter for the FAST impactor and cyclone

This initial field test indicated that the FAST is capable of collecting a representative sample in excess of its design target without operational problems. Pressure gauges in the system indicated no change in the pressure drop through the cyclone for the duration of the test, an increase in pressure drop across the filter of only 1.1 cm Hg and no change in the pressure drop across the main blower, indicating that the components of the system were operating well within their specifications with no measurable change in the sampling rate.

Arrangements have been completed to conduct a second field test of the prototype FAST at a coke oven battery where the emissions will be more representative of the conditions for which the system was designed. The FAST and a standard hi-vol sampler will be located on a platform at the oven roof level at one end of the battery. They will sample the particulate and gaseous emissions generated by the periodic operation of pushing the finished, hot coke out of the ovens into open railroad cars for transportation to the quenching operation. The battery includes 65 ovens, located between about 10 to 90 meters from the sampler platform. A pushing operation at one of the ovens occurs at an average interval of 15 minutes and lasts for about one minute, moving about 15 tons of coke. The particulate emissions, estimated at between 10 and 30 grams per second per ton of coke and including particles of every size, should provide a good test of the FAST capabilities.

SYSTEM MODIFICATIONS AND FURTHER DEVELOPMENT

The effort to complete the design of the settling chamber elutriator as a replacement for the marginally acceptable impactors as the 15 micrometer fractionator has been continued during the field testing program. The initial design, based on providing a D_{50} for 15 micrometer particles with an assumed density of 1.8 grams per cubic centimeter, contains 66 chambers each about 0.6 cm (0.25 inch) high, 46 cm (18 inches) wide and 20 cm (7.75 inches) deep in the flow direction. This configuration will result in a sampling stream velocity of about 0.47 meters (1.5 feet) per second through the elutriator and a pressure drop on the order of 0.01 cm Hg, only about one fifth of the pressure drop of the impactors. The design also includes a simple mechanism to install cover plates over the open faces of the elutriator while it is in place in the FAST. This feature will permit the removal of the elutriator with its sample intact for transfer to a laboratory for analysis of the sample.

After the completion of the field test at the coke oven battery, the impactors will be replaced with the elutriator and any additional modifications indicated as desirable during the test will be made. The FAST will then be recalibrated and tested at a minimum of two field sites, incorporating desirable modifications as indicated. Data on the operation and effectiveness of the FAST will be obtained at as many source/emissions combinations as program constraints will allow to provide information for the preparation of a procedures or technical manual describing the system andd its application in situations representative of general industrial

conditions. The manual will be published as a volume in the EPA's Environmental Technology Series and distributed to concerned members of government, industry and environmental consultants for their review. A program for additional development of the FAST will then be designed to respond to comments and suggestions of the reviewers.

CONCLUSIONS

The efforts to date in the development of this Fugitive Assessment Sampling Train have been quite successful and the results of the initial tests most encouraging. The completion of the planned development effort is expected to provide a useful tool for obtaining rapid, reasonable assessments of fugitive particulate and organic emissions from a wide variety of industrial sources.

REFERENCES

1. Turner, D.B., Workbook of Atmospheric Dispersion Estimates, Revised. U.S. Environmental Protection Agency, 1970.

2. TRC - THE RESEARCH CORPORATION of New England. Controlled and Uncontrolled Emission Rates and Applicable Limitations for Eighty Processes. Final report, EPA contract 68-02-1382, September 1976.

3. PEDCo Environmental, Inc. Technical Guidance for Control of Industrial Process Fugitive Particulate Emissions. EPA-450/3-77-010, March 1977.

Table 1. CALCULATIONS OF SOURCE STRENGTHS

Receptor Distance (m)	Stability Category (ref. 1)	K (m^2)	Wind Speed μ (m/sec)	Emission Rate Q (g/sec)	Emission Rate Q (Kg/hr)
100	A	410	1.0	0.257	0.925
	B	230	2.5	0.361	1.30
	C	140	4.0	0.352	1.27
	D	44	6.0	0.166	0.600
200	A	1600	1.0	1.01	3.64
	B	770	2.5	1.21	4.35
	C	340	4.0	0.855	3.08
	D	140	6.0	0.528	1.90
300	A	3700	1.0	2.32	8.35
	B	1600	2.5	2.51	9.07
	C	700	4.0	1.76	6.34
	D	290	6.0	1.09	3.92
400	A	7100	1.0	4.46	16.0
	B	2800	2.5	4.40	15.8
	C	1300	4.0	3.27	11.8
	D	490	6.0	1.85	6.66
500	A	10200	1.0	6.41	23.1
	B	4200	2.5	6.59	23.7
	C	1900	4.0	4.77	17.2
	D	700	6.0	2.64	9.50

Table 2. INDUSTRIAL PROCESS EMISSION RATES

Emission Source	Type[a]	Rate, Q[b] (Kg/hr)	Reference
Metal degreasing	HC	1.9	2
Beverage can coating	HC	5.6	2
Carbon black manufacture	HC	52.0	2
Nylon fiber production	HC	2.4	2
Cotton ginning	P	13.7	2
Cast iron foundry	P	2.9	2
Iron and steel scarfing	P	7.1	2
Asphalt batching	P	27.0	2
Steel production - BOF	P	16.3	3

[a]HC = hydrocarbon; P = particulates

[b]most common control applied - 90% control assumed where no data available.

SECONDARY NEGATIVE ELECTRON BOMBARDMENT FOR PARTICULATE CONTROL

By

W. E. (Bill) Stock PE, CSP, CHCM

OSHA-Region IX

San Francisco, California 94102

ABSTRACT

The most startling aspect of this "new" system is that it is not new at all! At least to those firms that have used it for the past 12 or 15 years to solve severe problems of airborne particulates. Other systems work at trying to correct the symptoms - while negative electron bombardment attacks the cause of the problem.

This "Air Charger" system releases high speed electrons through a glass enclosure - provided to keep the unit clean. Unlike primary ionizers which begin to lose their charge as soon as they are emmitted - secondary ionization negative electron emmissions have more power at a distance than at the source.

Unlike other air systems - that collect part of the dust, odor, smoke, bacteria etc., that must pass through their device - NONE of the air or contamination to be treated needs to pass through the "Air Charger." The secondary ionization system does not attempt to collect anything. This system claims success with most contaminants in the air, not just the particulates. Effective control has been demonstrated for dust; microorganisms (bacteria, virus, fungus, mold); odors; static electricity; and low carbon gases.

SECONDARY NEGATIVE ELECTRON

BOMBARDMENT FOR PARTICULATE CONTROL

INTRODUCTION

The decade of the seventies has been tremendous change in our attitudes and efforts toward improving the quality and quantity of life of our nations greatest resource - its people. This phenomena is not sacred to our country either. For example, the government of South Africa has recently initiated an in-depth, modern, mandatory safety and health program in their diamond mines. Many other countries are struggling with environmental pollution problems similar to our own.

The role of our government has expanded rapidly - some of you may think much too rapidly - into areas of environmental legislation, standards, control and research.

A decade ago EPA and OSHA were only embrionic brain children of some far-sighted, thinking, and concerned people - in and out of government. These people recognized the potential for harm in the myriad of vapors, fumes, mists, gases and particulates, with which we are polluting our environment. In light of the hindsight we now have regarding asbestos, kepone, black lung, brown lung, lead, arsenic, mercury, carbon monoxide, and oxides of nitrogen - perhaps we should have started much sooner.

Ten years ago even progressive States with professional safety departments, good safety standards, and nominal enforcement - dare I say like California - had precious little health awareness, information, or expertise.

With the advent of EPA and the Federal Clean Air Act of 1970; and OSHA - The Occupational Safety and Health Act of 1970; the United States entered into a new era in seeking to assure a better environment for all of us, and our children and their children.

I know that EPA has challenges on a broad front old and new processes, the proliferation of new chemicals, and the need for new technologies and solutions.

I want to thank the EPA staff at Research Triangle Park, and the Denver Research Institute for encouraging me to write this paper. Kudos also to my supervisors in Region IX OSHA, whose desire is to investigate the new and innovative in the search for ideas and technology that will provide safer and more healthful places where people work.

The mandate of Congress through the OSH Act is to provide workers with employment, and places of employment that are - as far as possible - safe and healthful. That is quite a challenge for the management of business and industry; for workers; and for the people in OSHA.

There have been allegations that as employers have complied with OSHA to make the interior environment more healthful, they have been dismayed to find EPA standing at the door saying NO! Don't pollute the outside environment! It seems our problems and solutions are inter-related.

NOVEL TECHNOLOGY

I have written this paper for two reasons. First, I believe many people are looking for answers and solutions to particulate problems. Secondly, I have the opportunity to present the first professional paper on a most novel technology.

Negative electron bombardment is not new in the sense of time. This system has been used by a large number of firms over the past fifteen years.

In my efforts to get a handle on the potential for this "Air Charger" system in the workplace, I contacted many users - in all kinds of applications - such as banks, glass plants, foundries, fish packing plants, hospitals, and hotels.

Regulatory agencies are often accused of requiring engineering controls that either are not available, not practicable, or feasible. Sometimes this appears to be true. However, perhaps one way to get some of us off top-dead-center, is to force the issue of technological change. Too often safety considerations are left to chance - not choice. Also, many firms do not want to be "guinea pigs" for new ideas or concepts.

The basic questions we asked those who have used this system were, "does the system operate as claimed?", and "in what area does it provide feasible engineering controls?" and "what research or test data is available?" Last of all, we were interested in the scientific aspects of the system.

ELECTRON BOMBARDMENT

Most of us will accept the fact that an average cubic foot of air contains particulates of various kinds and concentrations. The problem lies in the fact that micron, and sub-micron particulates tend to stay in suspension. A rule of nature is that particles with the same electrical charge repel each other, and opposite charged particles attract each other. The principle behind negative electron bombardment is to change the electrical charge or polarity of a given physical area. Particulates within this area will then be positively displaced to the lowest possible level, usually the floor.

The present state of the art for particulate control is to collect the particulate as near as possible to its point of origin - and then transport it through a collection system - to a place of discharge and/or collection. Selection of suitable control equipment involves at least two basic considerations. Which system or combination of systems will meet the technical requirements of the process - including the physical properties of the parti-

culates, such as the size, shape, density, electrical charge, and surface properties. Then, which type will do the job at the lowest overall cost.

The cost of a typical particulate collection system is considerable, plus the high amount of energy required for its operation. An electron bonbardment system appears to meet the basic requirements, with the claim of significant energy savings, even though the system operates 24 hours a day. The system operates on 110 volts, at 20 amps or less for the largest units. The system also appears to be compatible with the conventional systems and has been shown to make them more effective, and efficient. I understand that a large Denver plant is presently testing the electron bombardment system in conjunction with its sophisticated collection system. Apparently, electron bombardment can be utilized to reduce the load on an existing overloaded system - or might permit expanding plant operations without modifying or adding to the present systems. Owners, operators, and plant engineers have told me this system operates at a fraction of the cost of other systems.

INDUSTRY EXAMPLES

Workers Safety and Health is my primary concern. Several industries have special problems of particulate control. Among these are lead and arsenic, cotton, grain elevators and foundries. Research is needed in these and other industries to provide current scientific data.

I will present some data from employers files which will give an indication of the potential in the electron bombardment "Air Charger" system.

A glass maufacturing plant in the Los Angeles area has the production capacity of 400 tons of raw materials daily. The plant, which employs hundreds of workers, had been cited by Local and Regional air pollution agencies. Within a short time - they report - their overall particulate count was reduced by 67%, with no more air pollution violations.

A brass and bronze foundry, also in the Los Angeles area has used the "Air Charger" system for a number of years. The plant is approximately 120 ft by 180 ft by 30 ft high. Management reports a 92% reduction in 10+ micron particles, 89% reduction in 5+ micron particles, and 81% in 1+ micron particles. Employees report that the air is cleaner and that odors - that formerly smelled four blocks away - were no longer a problem within the foundry.

A battery plant that has recently been testing this system, reports that the lead-in-air concentration was reduced from .5 to .002 Mg/M^3.

A suger refinery in the San Francisco Bay area reported the results of a recent three months test as follows: 40% reduction of 10+ micron particles, 41% reduction of 5+ micron particles, and 53% of 2+ micron particles.

As a last example, a grey iron foundry in the Bay area, presently being

tested, indicates the following average results after sixty days of operating the electron bombardment system: 40% reduction of 10+ micron particles, 88% reduction of 5 micron particles, 83% reduction of 2 micron particles, 82% reduction of 1 micron particles, and 76% of .5 micron particles.

Lint and airborne textile particulates, as well as silica have reportedly been reduced in the 90% to 95% range.

The time required to neutralize a given area and get the optimum negative charge apparently varies with a given load of particulates. Information we have accumulated indicate most badly polluted areas will be controlled in three to four months.

CONCLUSION

The negative electron bombardment system of particulate reduction and control is certainly novel. It is NOT new. It is reported to be cost effective. It is NOT a cure all. Many firms are using it successfully as a primary system, and it also appears to be effective as a secondary system. Apparently the charged particulates that collect on the floor are not able to become airborne again, thus making clean-up easier and faster.

I want to make one point clear! This paper is not - in any way - to infer that OSHA endorses any product or system. The OSHA National Office has not done an evaluation of this system. Due to the fact that the system has been used by a large number of California plants and businesses, we in Region IX have taken the opportunity to acquire information regarding the system. We have reviewed many testimonials but our search is for scientific data, based on valid sampling techniques and accurate laboratory analysis. Some of this type of data is becoming available and based on preliminary findings, subject to continued evaluation, it appears that the negative electron bombardment system may provide a method of feasible engineering control for many industries presently plagued by particulate contamination.

END

HIGH TEMPERATURE AND HIGH PRESSURE SAMPLING DEVICE USED FOR PARTICULATE CHARACTERIZATION OF A FLUIDIZED BED COAL GASIFICATION PROCESS

S. Tendulkar, J. Pavel, P. Cherish
Westinghouse Electric Corporation
Advanced Coal Conversion Department
Box 158, Madison, Pennsylvania 15663

ABSTRACT

In the Westinghouse Coal Gasification Process Development Unit (PDU) being operated by the Westinghouse Advanced Coal Conversion Department at Madison, Pennsylvania, a high-temperature, high-pressure sampling train is being used downstream of the roughing cyclone to sample particulates. It is important in such a system to know the quantitative mass loading, the size distribution, and other characteristics of particulates downstream of the roughing cyclone if one is to determine the material balance in the pilot plant, as well as the efficiency of the cyclone. However, the hardware, procedures, and methodologies to sample particulates in high-temperature, high-pressure environments do not exist in standard form or approach, such as an off-the-shelf package, since the application to coal gasification is unique. This paper describes the experimental particulate and gas sampling train for extractive sampling, the operational difficulties, and a comparison of mass loading and particulate characteristics with dump samples collected from the downstream quench water scrubbing system. Samples were collected from over 12 different PDU test runs, each lasting from 1 to 2 weeks, that were conducted in 1978.

SECOND SYMPOSIUM ON THE TRANSFER AND UTILIZATION
OF PARTICULATE CONTROL TECHNOLOGY

Denver Research Institute
University of Denver
Denver, Colorado
July 23, 1979

HIGH TEMPERATURE AND HIGH PRESSURE SAMPLING DEVICE USED FOR PARTICULATE CHARACTERIZATION OF A FLUIDIZED BED COAL GASIFICATION PROCESS

INTRODUCTION

Since 1974, the Westinghouse Advanced Coal Conversion Department has been developing a fluidized bed coal gasification process which produces low and medium Btu fuel gas. Figure 1 shows the 15 ton-per-day Westinghouse Process Development Unit (PDU) at the Waltz Mill, Pennsylvania Site, which was constructed by Bechtel and is being operated by Westinghouse under DOE sponsorship.

The Westinghouse single-stage coal gasification process utilizes the direct feed of coal as shown in Figure 2. The gasifier, which has four primary zones wherein combustion, gasification, ash agglomeration and ash/char separation take place, is capable of converting all varieties, sizes and ranks of coals to useful and environmentally acceptable fuel gases. A significant accomplishment of the Westinghouse gasifier is its ability to handle highly caking coals, such as Pittsburgh seam coal. The Westinghouse system produces either low-Btu or medium-Btu product gas by using air plus steam for the former and oxygen plus steam for the latter as the combustion medium. Over 4,000 hours of hot operation has been accumulated on the PDU with a full year's experience accumulated for each type of operation. Both air and oxygen tests are continuing to gather additional design data. The process development unit, which is operated at the temperature and pressure of a commercial unit, provides the chemical reaction data and operating experience required to provide the data base for the design of a commercial scale coal gasification unit.

At the PDU, a roughing cyclone is used to capture a portion of the fines which are elutriated from the fluidized beds. The remainder of these fines are captured by a series of water scrubbers. This paper deals with the system developed by Westinghouse to sample and characterize the fines escaping the roughing cyclone.

HARDWARE DESCRIPTION/DESIGN

To determine the cyclone efficiency, quantitative mass loading, size distribution and other characteristics of particulates downstream of a roughing cyclone, a simple probe was developed on site for extractive sampling.

Figure 3 shows the particulate sampling system presently installed in the Westinghouse Process Development Unit. Particulates are sampled via a 3/8 inch stainless steel tube which extends to the center of an 18-inch, refractory-lined process pipe. The process conditions at this point are 1500°F to 1800°F at 100 to 250 psig. Line velocity is 25 to 50 feet per second. The sample probe is oriented parallel to the process gas flow. The sample stream leaves the process pipe through a coaxial heat exchanger and proceeds through a small minicyclone where the primary, that is greater than 90 percent, gas/solids separation occurs. This minicyclone is made of stainless steel with a barrel diameter of approximately 2 inches. The separated solids fall into a catch pot which is located at the bottom of the minicyclone.

Processing of the sample after it leaves this cyclone can be accomplished in three ways. A 2-micron sintered metal filter element can be used to collect solids which escape the primary sampling cyclone. Another option is to pass the sample through the Total Condensible Analyzer (TCA). In the TCA, the gas sample is passed through a glycol heat exchanger where the moisture and other condensible compounds in the gas are condensed. The liquid is collected by a catch pot and desiccant. Small particulates which may have escaped the minicyclone are also collected in the liquid and can be recovered by filtering. In the third option, the gas can be passed through two water-filled miniscrubbers. These scrubbers are used primarily to analyze for trace quantities of water soluble compounds, such as ammonia or alkali metals, that may be present in the gas. Particulates escaping the minicyclone are also collected in these miniscrubbers. With the configuration presently installed, the usual sampling procedure calls for operating the miniscrubber and TCA apparatus in parallel. In this manner, measurements of the moisture content and trace compounds can be made simultaneously with the particulate loading measurement.

After the sample gas leaves the miniscrubber or TCA, the gas is throttled and metered. A standard rotameter is used to monitor the sample flow rate, which is established at a value that achieves a nominal, isokinetic condition in the sample line. The sample flow rate required to achieve a nominal isokinetic condition is calculated on the basis of a measured total process flow rate and nominal line sizes. The total cumulative sample flow is measured using a positive displacement dry gas meter.

Design of the probe was based primarily on temperature considerations. To prevent the condensation of tars, which could be present in the product gas, temperatures in the sample line must be maintained above 600°F. The upper temperature of the sample is limited to 1000°F, based on valve specifications. To maintain temperatures in this range, the sample probe is surrounded by a concentric tube which keeps the hot sample line from directly contacting other cooler parts of the refractory-lined process pipe. This outer tube also serves as the shell side of a single pass, coaxial flow heat exchanger. Gaseous CO_2 is used as a coolant. Sample temperatures are controlled to approximately 650°F as they enter the minicyclone.

The present configuration evolved from earlier designs which suffered from a number of difficulties, primarily safety-related. The gas being sampled is a hot combustible fuel gas. Thus, a leak in the sample system is a safety hazard from the standpoint of ambient carbon monoxide or hydrogen sulfide concentrations, combustion of the leaking gas, or excessive sample temperatures which would result if a high leak rate persisted. As a result, the sample line must be routinely inspected for the possibility of failure from erosion, corrosion, or other causes.

In the original configuration, a heated oven was used to maintain the minicyclone and sample lines at constant temperatures. Since detection of leaks from lines within the oven was difficult, the oven was removed. Early runs of the system without this oven were unacceptable since temperature at the minicyclone had dropped to beneath a dew point of the product gas, approximately

250°F, and plugging of the minicyclone resulted. To correct this problem, the minicyclone was close-coupled to the process line and directly connected to the coaxial heat exchanger. With this arrangement, the minicyclone is heated sufficiently by the sampled gas itself so that condensation is avoided.

The heat exchanger is all-welded construction and extends from the process pipe to the two shut-off valves immediately upstream of the minicyclone. This concentric tube gives double protection against erosion failure of the sample line. If the pressure in the shell side of the heat exchanger cannot be vented to zero, then an erosion failure of the sample line is indicated, and sampling can be suspended. Should a leak occur downstream of the heat exchanger, two block valves permit isolation of the system for repair.

The original design employed an O-ring arrangement to seal the catch pot at the base of the minicyclone. However, the O-ring was difficult to install in this arrangement and seal leaks resulted. A conventional flange and gasket has since replaced the O-ring which, while more inconvenient to install, has proven to be safe and leak-free.

APPLICATION OF DATA

The data obtained from particulates downstream of the roughing cyclone are used primarily in analyzing the performance of the Westinghouse coal gasification process. Tests at the PDU have been conducted with a variety of coal feedstocks, such as Pittsburgh coal, Indiana coal, and Western Kentucky coal. Data are obtained on mass loading, cyclone efficiency, size distribution, and proximate and ultimate analyses.

Quantitative mass loading and cyclone efficiencies data were obtained for each set point in the steady state period of the gasifier test. Some of the results are shown in Table 1. Mass loading and solids analysis data are used routinely for heat and material balance calculations of the Westinghouse process. These data can also be used for sizing the fines handling equipment downstream of the gasification process. Since Westinghouse is not a manufacturer of cyclone systems, the data gathered on cyclone collection efficiency is used only for our own in-house understanding of hot cyclone operation.

The Coulter Counter Model TAII is used in the Westinghouse system for particulate analysis for size distribution. Particle size measurement by Coulter Counter technique has been widely used in industry and laboratories for several years. Basically, this apparatus determines the size and number of particles suspended in a conductive liquid by forcing the suspension to flow through a small aperture which generates a resistance pulse in proportion to the volume of particles, or the volume of electrolyte displaced. The electrodes are immersed in a conductive fluid on opposite sides of the aperture.

As particles pass through the aperture, the current is momentarily altered, and detection is by a pulse in a discriminating circuit. The magnitude of the pulse height is proportional to the resistance change, and

TABLE 1

QUANTITATIVE MASS LOADING IN GASIFIER TESTS

	Tests				
Parameter	TP-017	TP-018-5	TP-019-1	TP-019-2	TP-019-3
Air/Oxygen Used	Air	Oxygen	Oxygen	Oxygen	Oxygen
Coal Used	Pittsburgh	Pittsburgh	Rosebud	Indiana	W. Kentucky
Freeboard Temperatures (°F)	1651-1852	1780-1835	1495-1540	1721-1767	1779-1808
Freeboard Velocities (fps)	0.91-1.70	1.13-1.28	0.76-0.82	1.22-1.29	1.53-1.77
Cyclone Penetration (lb/hr)	74-130	26-86	57-85	73-114	24-98
Cyclone Efficiencies (%)	51-76	54-80	50-89	61-74	70-94

directly proportional to the volume of the particle. Below the 1.3 micron size, the Coulter Counter has experimental difficulties and electronic noise interference.

A complete analysis divided into 16 size channels is given in one scan. Complete data in the form of volume percent are given automatically. Particle size distribution on a weight basis is obtained by assuming that all observed particles are spheres of equal density. Since the particle density is assumed to be the same for all size fractions, the fractional volume distribution and fractional mass distribution are equivalent. It is claimed that the technique is independent of shape, density, or refractive index of the particles. Calibration is carried out with standard Dow polystyrene, latex particles, or N.B.S. glass beads.

Typical curves for size distribution are shown in Figures 4, 5, and 6 for different gasifier tests with different feed stock material. These graphs indicate that weight mean particle size is about 20 microns and that particles greater than 10 microns in size were in the range of 80 to 85 percent. Similar results were obtained with other gasifier tests.

The size distribution of particulates collected from the extractive sampling train at nominal isokinetic conditions are compared with the particulates obtained from the Total Condensible Analyzer (TCA) along with particulates from the dump liquid samples from the quench water scrubbing system. The Coulter Counter Analysis shows all three particulates samples from the different locations were similar in size distribution as shown in Figure 4. From this same figure, it is evident that fragmentation did not occur in hot particulates in the product gas when quenched with water.

PROXIMATE AND ULTIMATE

Proximate and ultimate analyses of the samples collected downstream of the roughing cyclone suggest that these are similar in composition to the char--basically a devolatilized and partially gasified coal particle. The results are tabulated in Table 2 for different coals used in the single-stage gasifier test.

SUMMARY

The high temperature, high pressure sampling device developed by Westinghouse is routinely used on the PDU to sample and characterize particulates escaping the roughing cyclone. Specifically, the system is designed to accomplish the following objectives:

- To achieve a better closure on material balance data for gasifier tests.
- To investigate mass collection cyclone efficiency and to identify future modifications for improved design.
- To understand physical and chemical characteristics of particulates to aid design of downstream equipment in commercial applications.

TABLE 2

CHARACTERISTICS OF CYCLONE PENETRATION PARTICULATES (AS RECEIVED)

PARAMETER	TEST TP-017 Air Blown	TP-018-5 Oxygen Blown	TP-019-1 Oxygen Blown	TP-019-2 Oxygen Blown	TP-019-3 Oxygen Blown
Feedstock Material	Pittsburgh Coal	Pittsburgh Coal	Rosebud Coal	Indiana Coal	W. Kentucky Coal
Weight mean Diameter (μm)	22	18	19	20	22
Less than 10 μm by wt. (%)	20	25	28	16	14
Proximate wt. (%)					
Moisture	2.39	1.12	1.72	3.92	3.22
Volatile matter	3.35	2.88	5.79	Trace	3.98
Fixed Carbon	75.55	66.96	54.46	71.67	66.23
Ash	18.71	29.04	38.03	24.41	26.57
Ultimate wt. (%)					
Carbon	75.00	66.96	56.51	68.82	65.86
Hydrogen	0.77	0.53	0.52	0.83	0.50
Oxygen	2.71	1.15	1.74	4.20	3.93
Nitrogen	0.92	0.55	0.42	0.51	0.69
Sulfur	1.89	1.77	2.78	1.17	2.45
Ash	18.71	29.04	38.03	24.41	26.57
Calorific Value (Btu/lb.)	11,360	9845	7890	----	9902

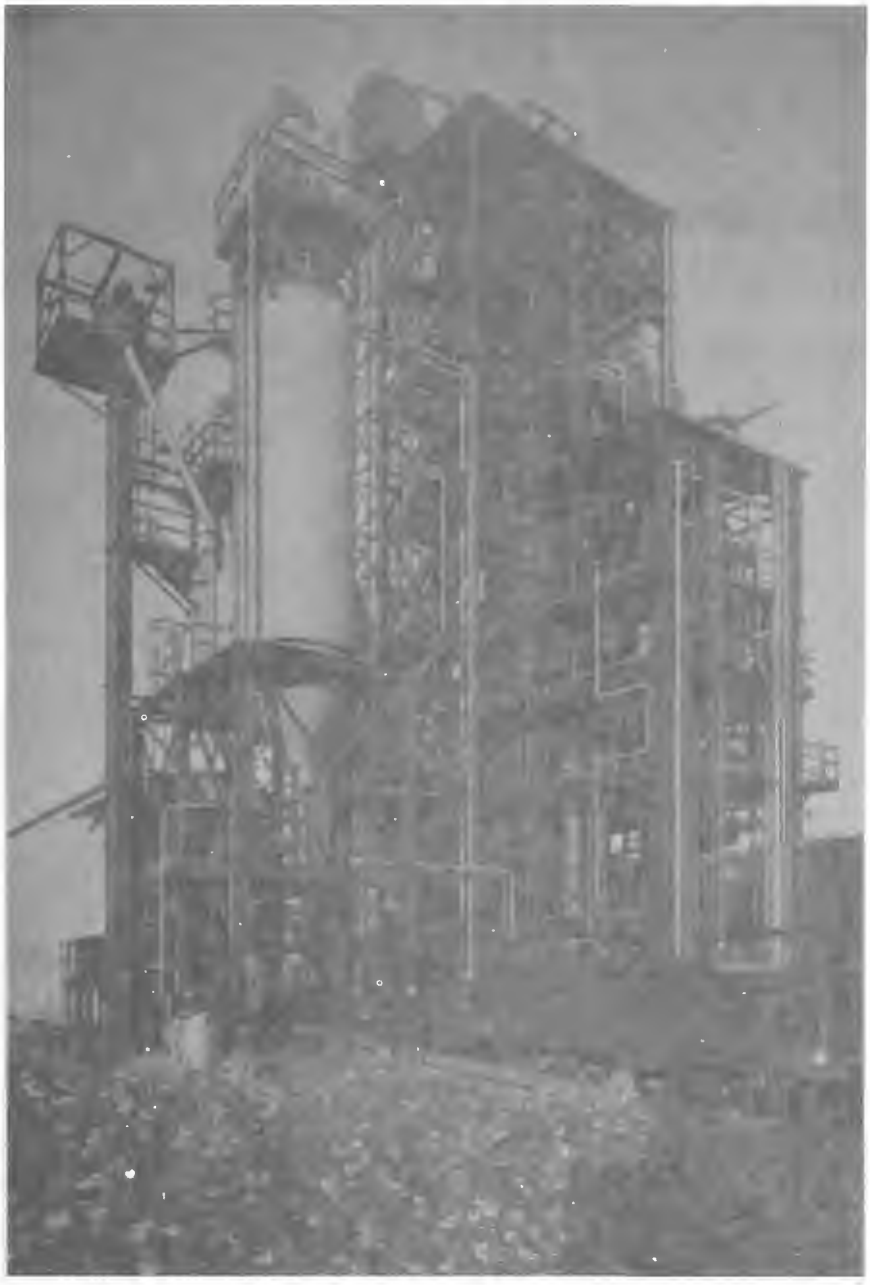

Figure 1. Westinghouse 15 Ton/Day Process Development Unit

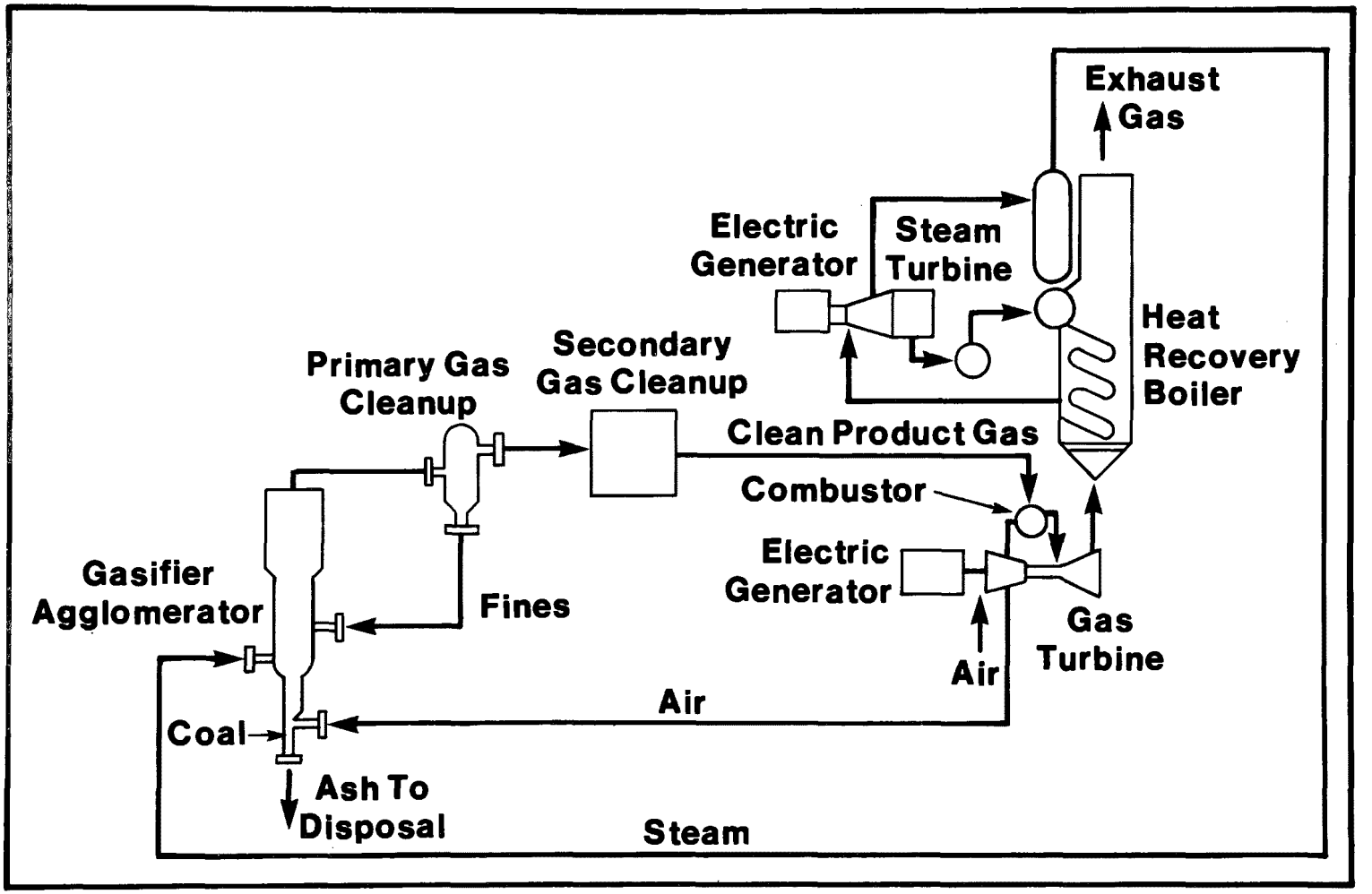

Figure 2. Westinghouse Single-Stage Coal Gasification Combined Cycle System

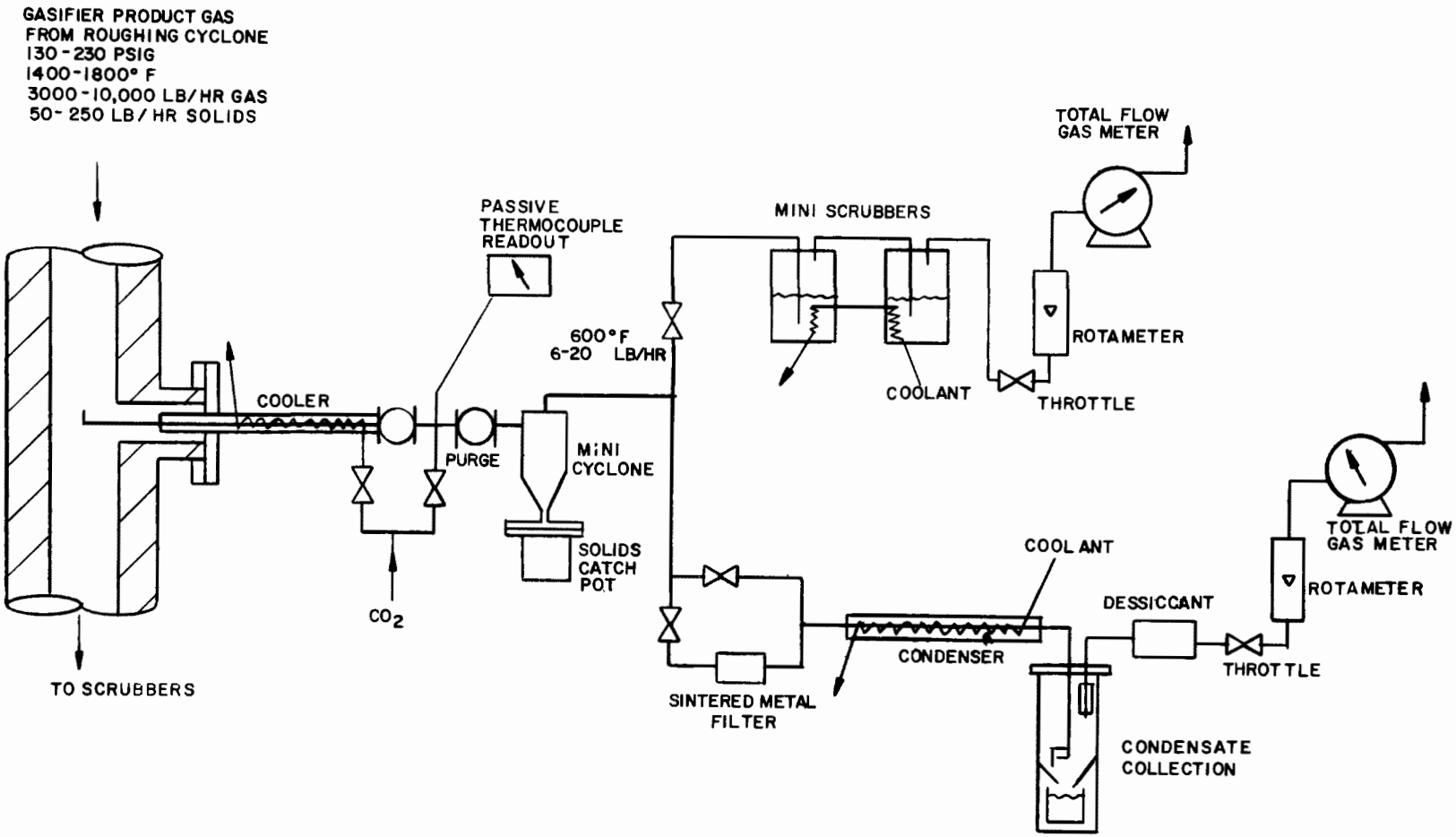

Figure 3. Westinghouse Coal Gasification High-Temperature, High Pressure Particulate Sampling and Characterization System

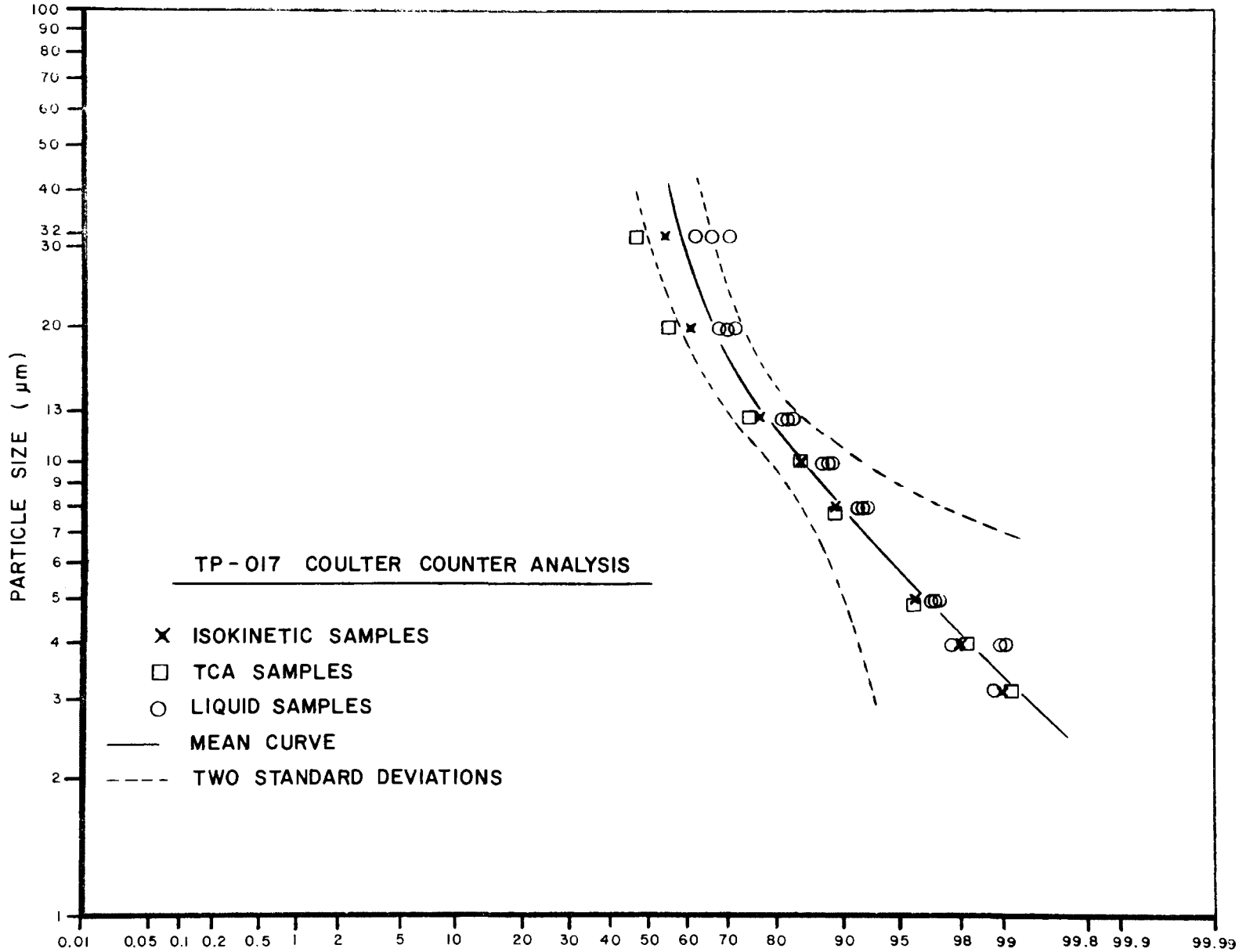

Figure 4. Cyclone Penetration Particulate Size Distribution Data (Coulter Counter Analysis) Test TP-017

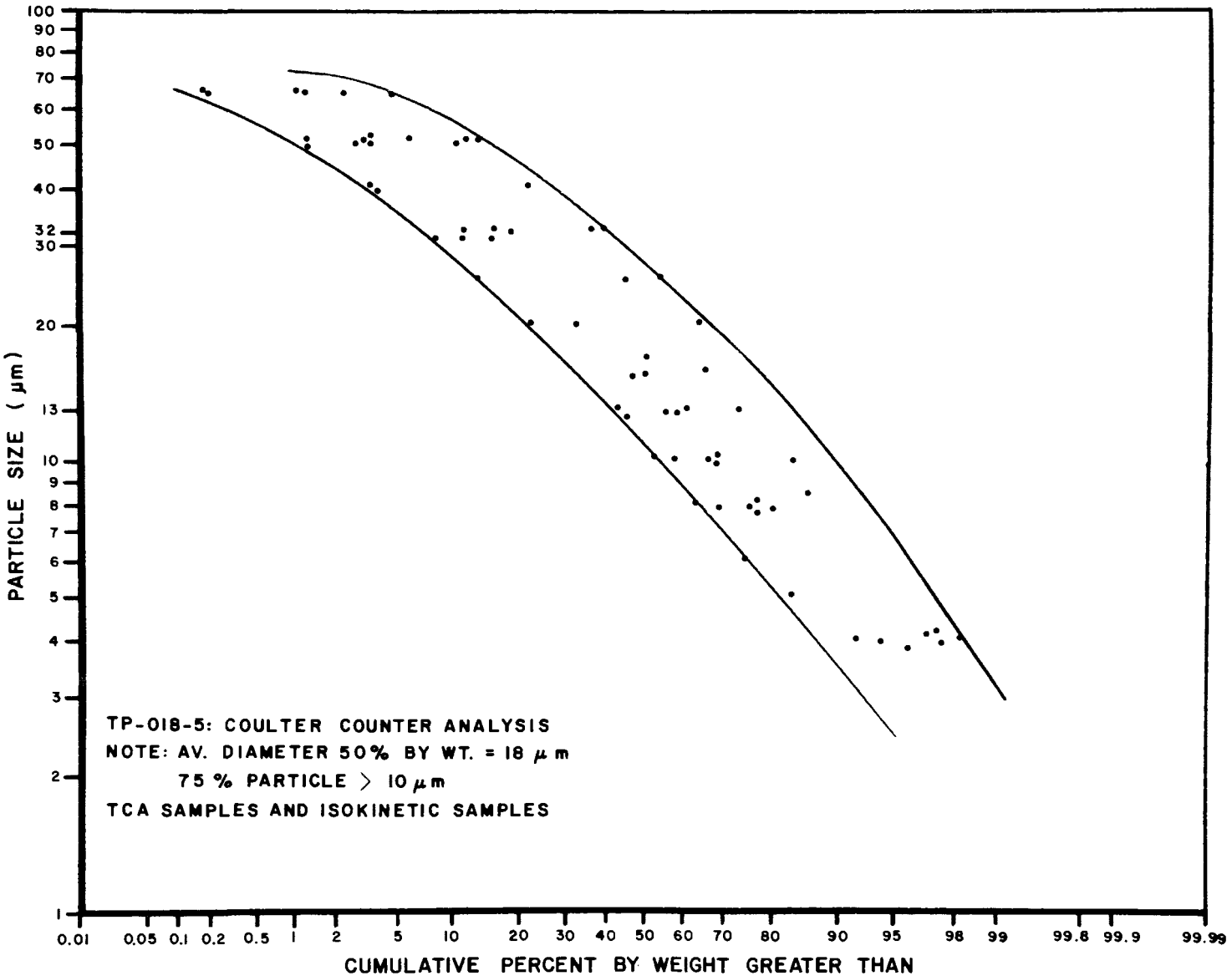

Figure 5. Cyclone Penetration Particulate Size Penetration Data (Coulter Counter Analysis) TP-018-5

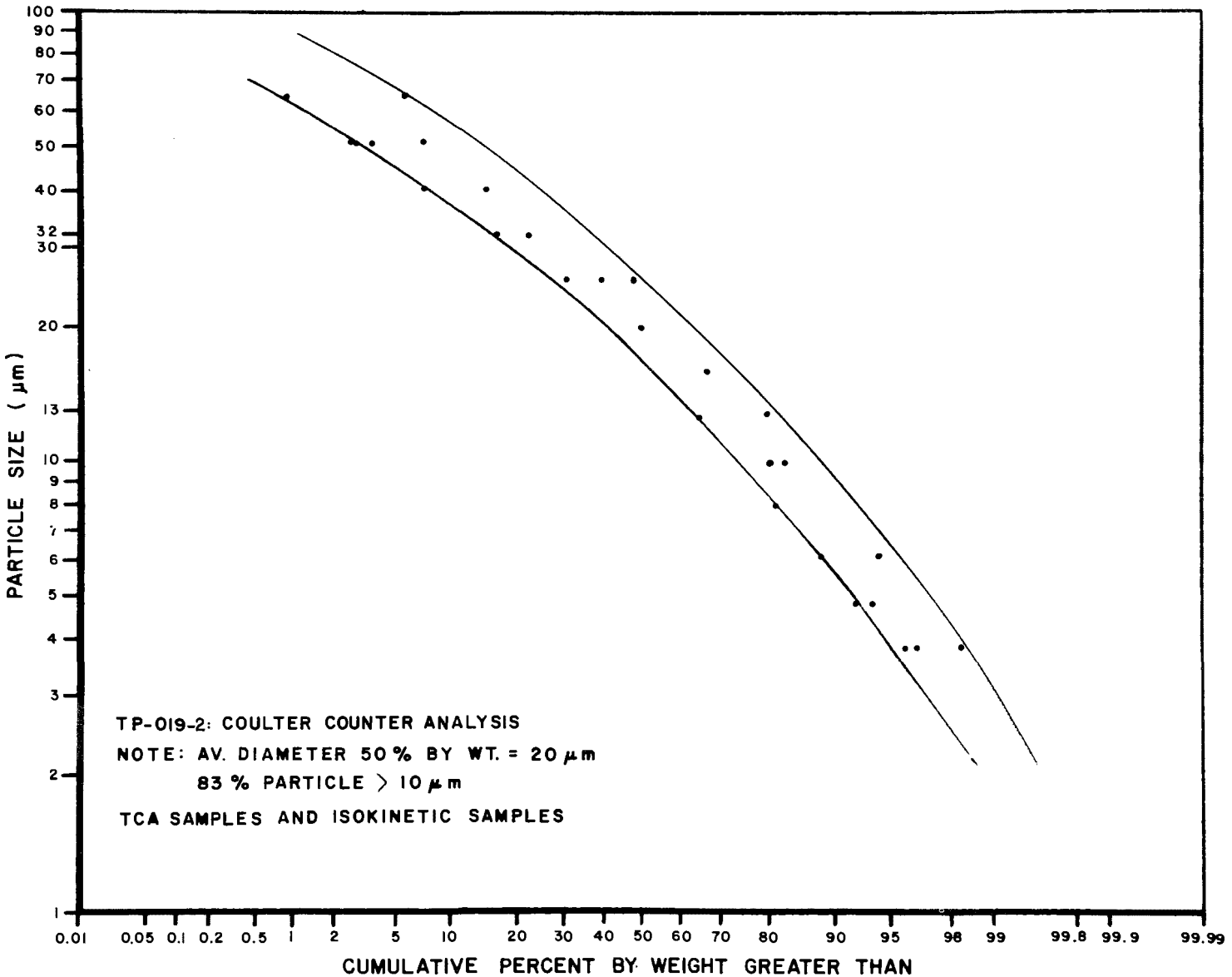

Figure 6. Cyclone Penetration Particulate Size Distribution Data (Coulter Counter Analysis) TP-019-2

ON-STREAM MEASUREMENT OF PARTICULATE SIZE AND LOADING

By:

E.S. VanValkenburg
Leeds & Northrup Company
North Wales, Pa. 19454

ABSTRACT

Leeds & Northrup has developed means for on-line measurement of the effectiveness of particulate clean-up devices in high temperature, high pressure, gas streams. This instrumentation was originally designed for continuous monitoring of particulate loading into the turbine on pressurized fluidized bed combustion systems. The work was sponsored by DOE/ERDA to provide a means for investigating effects of particle loading (quantity and size distribution) on turbine blade erosion.

The resultant prototype instrument measures the in-situ volumetric loading in the range of 0.01 to 10 ppm and particle size varying from 0.8 to 30 micrometers diameter. This instrument has been tested on coal combustion systems at Argonne National Laboratory and Curtiss-Wright Corporation. The paper describes the basic instrument, presents data from the field tests and describes how such instrumentation can be used in various particulate control processes.

ON-STREAM MEASUREMENT OF PARTICULATE SIZE AND LOADING

INTRODUCTION

An on-stream particulate analysis instrument has been developed by Leeds & Northrup Company under DOE sponsorship for in-situ measurement of particle loading and size in the product gas streams of advanced combustion systems. A prototype instrument has been designed and constructed to evaluate this means of measuring particles on fluidized bed combustion systems and field tests have been conducted with this unit at Argonne National Laboratory (ANL) and on a small gas turbine at Curtiss-Wright Corporation (CWC).

This particulate instrumentation is based on Leeds & Northrup's prior research in low-angle forward scattering of light by micron size particles suspended in fluid streams. When such particles are optically illuminated, the scattered light intensity at any given angle is a function of the size, shape and index of refraction of the particles. In the case where the wavelength is small in comparison to the size of the particles, the spatial distribution of the scattered light in the far field is dominated by the volume and size characteristics of the particles. The design of the on-stream instrument is based on utilization of simple diffraction theory to convert measurements of the composite Fraunhofer diffraction pattern for a large number of particles into meaningful data which characterize the size distribution and concentration of the suspended particles.

This type of instrumentation is needed to evaluate the performance of secondary particle clean-up devices and to measure the size distribution and concentration of particles at the inlet to gas turbines in direct combustion coal-fired systems. The latter application requires instrumentation amenable to measurement of particles in high temperature (1500-2000F) pressurized (up to 10 atmospheres) gas streams and be adaptable to rather large diameter gas ducts. The prototype instrument meets these requirements and accommodates gas ducts up to one foot internal diameter. This method of measurement can be extended to accommodate pipe up to two meters i.d.

INSTRUMENT DESCRIPTION

A schematic diagram of the optical train of the instrument is shown in Figure 1. This instrument consists of optical elements mounted to an optical bench which extends under a horizontal run of the combustion system duct. (The duct is not shown in the schematic, only its vertical center line). The illumination source is a helium cadmium laser mounted to the underside of the optical bench. Folding optics, attached to the left end of the optical bench,

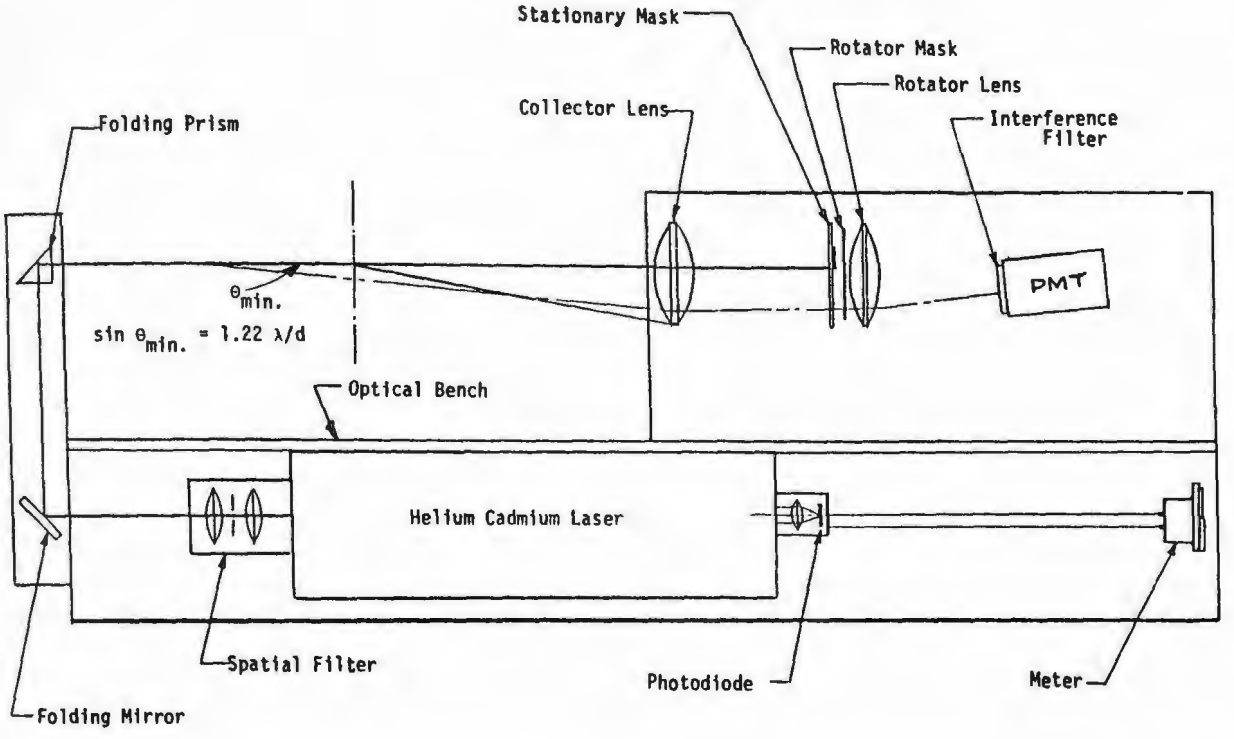

Figure 1 Instrument schematic

Figure 2 Prototype particulate instrument.

direct the laser beam across the duct where particles in the gas stream, which are illuminated by the beam, scatter the light. The scattered flux is collected by a lens and focused on a set of function masks. The portions of flux, which are transmitted through the function masks, are focused by a second lens on to the photomultiplier detector.

A photograph of the prototype instrument is shown in Figure 2. This instrument consists of the optical subsystem assembly, an electronics package, laser power supply, and a digital line printer. All units, except the printer, are contained in NEMA-12 class enclosures to meet industrial environmental requirements. The laser and receiving optics units contain thermostat controlled heaters so that the optical subsystem may be installed on gas ducts which are either indoors or exposed to the weather out-of-doors.

The electronics package includes a microcomputer, visual display and all the operating controls. This unit can be located up to 200 feet from the optical subsystem. The digital printer is used to log the output measurements and can be located remotely from the electronics package, if desired.

The opening on the optical subassembly from the folding optics on the left to the collection lens bezel is 30 inches. The vertical clearance above the optical bench to the laser beam center line is 9 1/2 inches. These dimensions were chosen to accommodate a 12-inch i.d. duct with a tee section viewing port extending on each side of the duct.

Mechanical adjustments are provided on the folding optics for alignment of the optical train to the duct windows after the instrument is installed. The instrument can be mechanically mounted to the duct through the load carrying base structure.

All particles illuminated by the laser beam scatter flux off the beam axis. For particles in the size range of interest, most of the scattered flux is in the near forward direction. We collect that flux and through an optical process, convert that data into information concerning the particle size distribution and loading. The particle loading output is calibrated to be direct reading in parts per million by volume, i.e., ratio of total volume of particles per unit volume of gas.

The angular distribution of scattered light in the Fraunhofer diffraction plane is a function of the number and sizes of the scattering objects. If the objects are spheres and the illumination is monochromatic, the angular extent of the diffraction pattern is given by:

$$\sin \Theta = 1.22 \lambda/d, \tag{1}$$

where Θ = half angle to the first minimum of the pattern, λ = wavelength of the light source and d = particle diameter. Thus, large particles produce a narrowly defined flux pattern, while smaller particles diffract flux over wider angles but with lower flux intensity. The total intensity (F_i) of the scattered flux is given by:

$$F_i = K\Sigma n_i d_i^2, \tag{2}$$

where K is a calibration constant and n_i is the number of particles of diameter d_i.

If a specially designed transmission filter is placed in the Fraunhofer plane of the collection lens, the intensity of the transmitted scattered flux can be made proportional to various powers of the particle radius (a). In particular, a set of masks is defined to yield signals proportional to the second, third and fourth powers of the particle radii.

The transmission characteristics of these mask functions are optimized to yield a uniform response over the total range of particle sizes to be measured. These masks are assembled on a rotating disk such that the three functions are separated in angular extent and allow serial extraction of each of the desired signals. Computations of the particle size distributions and total volume of the particles are implemented as follows.

For a collection of particles, the optical signal from each portion of the mask can be expressed as a summation of particle radii raised to the appropriate power for each mask segment. This summation can be written in integral form when the particle distribution is expressed as $D_N(a)$, the number density distribution by particle radius, so that $D_N(a)da$ is the fraction of particles with radii between a and a + da. For example, the flux, S_3, passing through the 3rd power mask is shown by Wertheimer and Wilcock[1] to be

$$S_3 = K_3 E \int_0^\infty a^3 D_N(a)da \tag{3}$$

where K_3 is an instrumental constant, and E is the intensity of the probe beam. S_3 is thus proportional to the total volume of particulate in the beam.

Similarly, the flux passing through the second power and fourth power masks may be written, respectively, as

$$S_2 = K_2 E \int_0^\infty a^2 D_N(a)da, \tag{4}$$

$$S_4 = K_4 E \int_0^\infty a^4 D_N(a)da, \tag{5}$$

where K_2 and K_4 are instrumental constants.

The first moment of the volume distribution, called the volume mean radius $\bar{a}_v$, is thus given by

$$\bar{a}_v = \int_\sigma^\infty a D_v(a)da = \frac{\int_0^\infty a^4 D_N(a)da}{\int_0^\infty a^3 D_N(a)da} = \frac{K_3 S_4}{K_4 S_3} \tag{6}$$

Thus, the volume mean radius of the particles is given by the ratio of the signals from the fourth and third power apertures, apart from an instrumental constant. Since this is a true volumetric size measurement, the constant can be chosen such that

$$2\,\bar{a}_v = MV \tag{7}$$

where MV is the mean mass diameter, the calibration constant K_3/K_4 is determined

by the dimension of the 3rd and 4th power masks and is independent of the intensity of the laser beam. The concentration of the particles does not affect the measurement so long as it is not high enough to cause multiple scattering.

Another way of describing a particle size distribution is the area distribution $D_A(a)$, where $D_A(a)da$ is the fraction of the total surface area contributed by particles in the range a to a + da. Then the area mean radius $\bar{a}_A$ is given by

$$\bar{a}_A = \int_0^\infty aD_A(a)da = \frac{\int_0^\infty a^3 D_N(a)da}{\int_0^\infty a^2 D_N(a)da} = \frac{K_2 S_3}{K_3 S_2} \tag{8}$$

Thus, the ratio of the signals from the third and second power apertures is proportional to the area mean radius and this measurement is independent of the particle concentration. Further, the constant can be chosen such that $2\bar{a}_A$=MA which is volume-surface mean diameter.

In addition, it is possible to obtain from the three output signals the standard deviation σ_A of the area distribution, which is defined for normal distributions to be:

$$\sigma_A^2 = \overline{a_A^2} - (\bar{a}_A)^2 = \bar{a}_A (\bar{a}_V - \bar{a}_A) \tag{9}$$

Finally, in the case of log normal distributions, the mass mean diameter and the volume-surface diameter define the geometric median diameter.[2] From the Hatch-Choate transformation equations:

$$\log MV = \log dgm + 1.151 \log^2 \sigma g \tag{10}$$

and

$$\log MA = \log dgm - 1.151 \log^2 \sigma g, \tag{11}$$

where dgm is the geometric median diameter and σg is the geometric standard deviation. Thus, for log normal distributions:

$$2 \log dgm = \log MV + \log MA \tag{12}$$

or

$$dgm = \sqrt{MV \times MA}. \tag{13}$$

The prototype on-stream particle instrument provides the following data outputs:

dV = volume of particles in ppm
MV = mean volume diameter in microns ($2\overline{a_V}$)
MA = mean area diameter in microns ($2\overline{a_A}$)
WA = width of area distribution in microns ($2\sigma_A$)
dgm= median particle diameter for log normal distributions.

PERFORMANCE DATA

A photograph of the optical assembly installed on a one inch i.d. pipe at the Argonne facility is shown in Figure 3. After initial alignment, the laser beam is fully enclosed with a shroud from the instrument to the sample cell ports. Thus, there is no laser radiation danger to personnel as long as the equipment is maintained in this buttoned-up state. No realignment of the optics was required during the two month test period at ANL.

A close-up of the ANL sample cell is shown in Figure 4. Two sets of air purge lines were provided by ANL to generate air curtains across each of the viewing port quartz windows. These optical quality windows were coated to eliminate reflection at the laser wavelength (442 nm). The windows were cleaned weekly but daily background measurements with clean air flowing in the duct show insignificant particle deposits between cleanings.

The Leeds & Northrup instrument was operated solely by ANL personnel for the evaluation tests after a one week training period. There were no electronic malfunctions during the course of the tests. The only problem encountered was an unexpected reduction in laser power. However, this didn't inhibit operation of the instrument even though the power dropped over a period of a few weeks from 20 to 8 mW.

The piping arrangement at Argonne permitted measurement of particles after the secondary cyclone and after the metal filter which is downstream from the cyclones. Flue gas flow was directed to the particle instrumentation by valves to enable measurement of particles at either the input to or output from the metal filter.

Argonne provided an extractive probe upstream of the optical windows that allowed particle size analysis on sampled material with cascade impactors. In addition, steady state grab samples were obtained with Gelman membrane filters.

The results of three combustion tests utilizing Sewickley coal and Greer limestone are presented in Table I and Figures 5-8. Table I gives a comparison of size measurements made with the Leeds & Northrup instrument, called MICROTRAC, with the reduced data from the Anderson Cascade Impactor samples.

The average mean volume diameters, $\overline{MV}$, for the impactor samples were calculated from truncated log normal distributions obtained via the Anderson Impactor. Since the MICROTRAC has a linear size response for particles one micron in diameter and larger, and an attenuated response to submicron size particles, the lowest channel (submicron region) data points from the impactor were not used. This provides directly comparable data over the size range 1-20 microns. The average mean area diameters, $\overline{MA}$, were similarly calculated from the Anderson Impactor data. The differences between the direct reading, on-line observations via MICROTRAC and the impactor data are tabulated.

The median diameter, 50th percentile for log normal distributions can be expressed as Median Diameter = $\sqrt{\overline{MV} \times \overline{MA}}$. The results of this computation are shown in the bottom three rows in Table I.

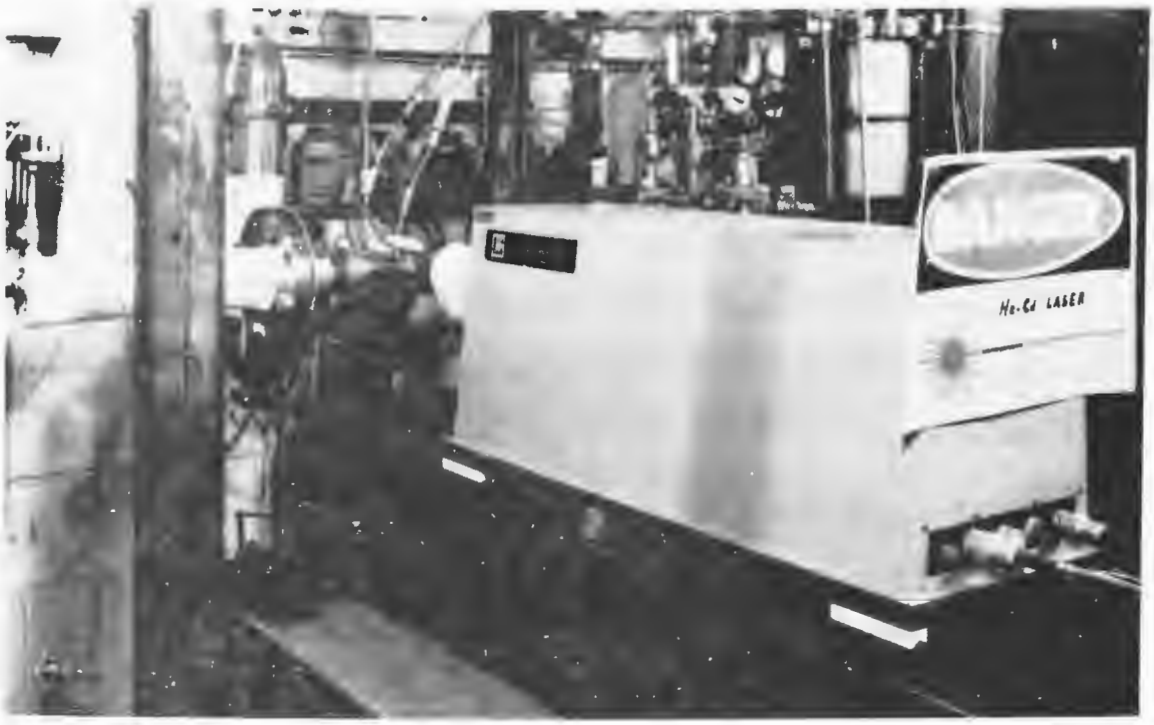

Figure 3 Optical assembly installation at ANL.

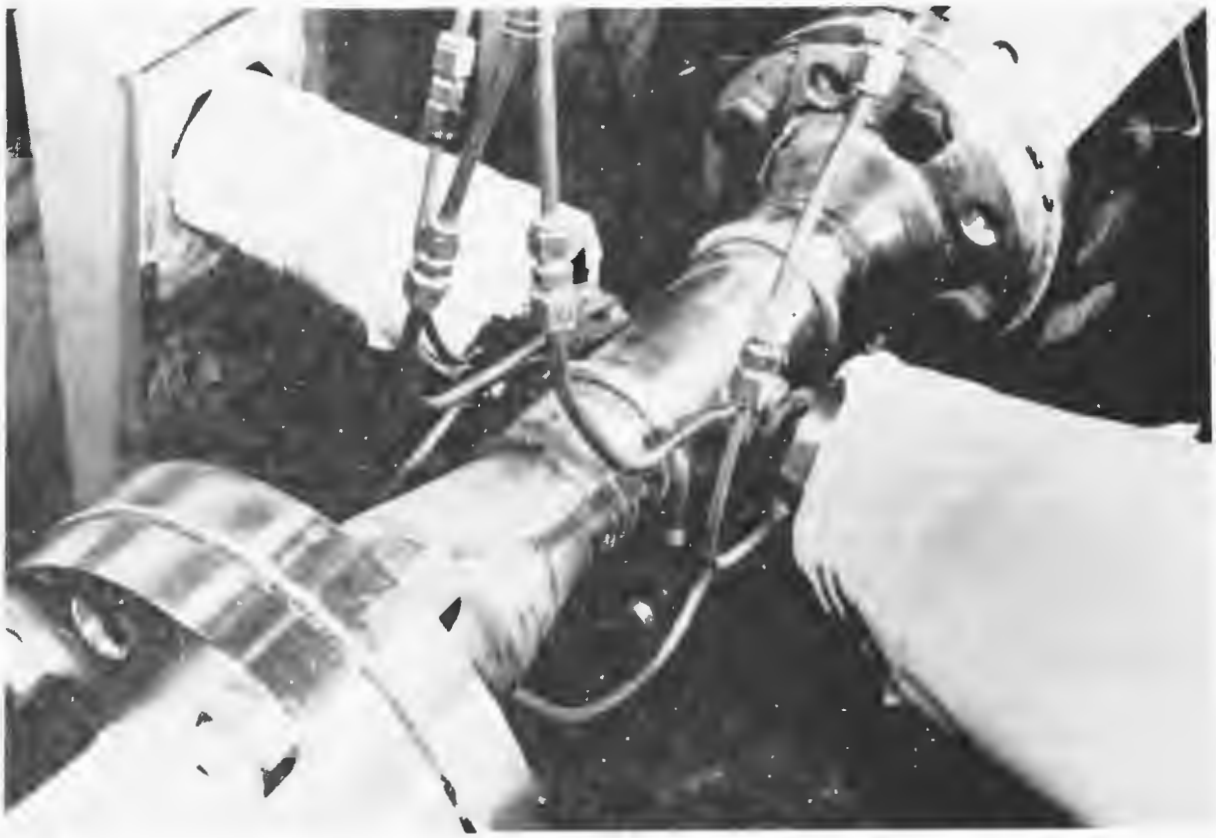

Figure 4 Close-up view of ANL Sample Cell.

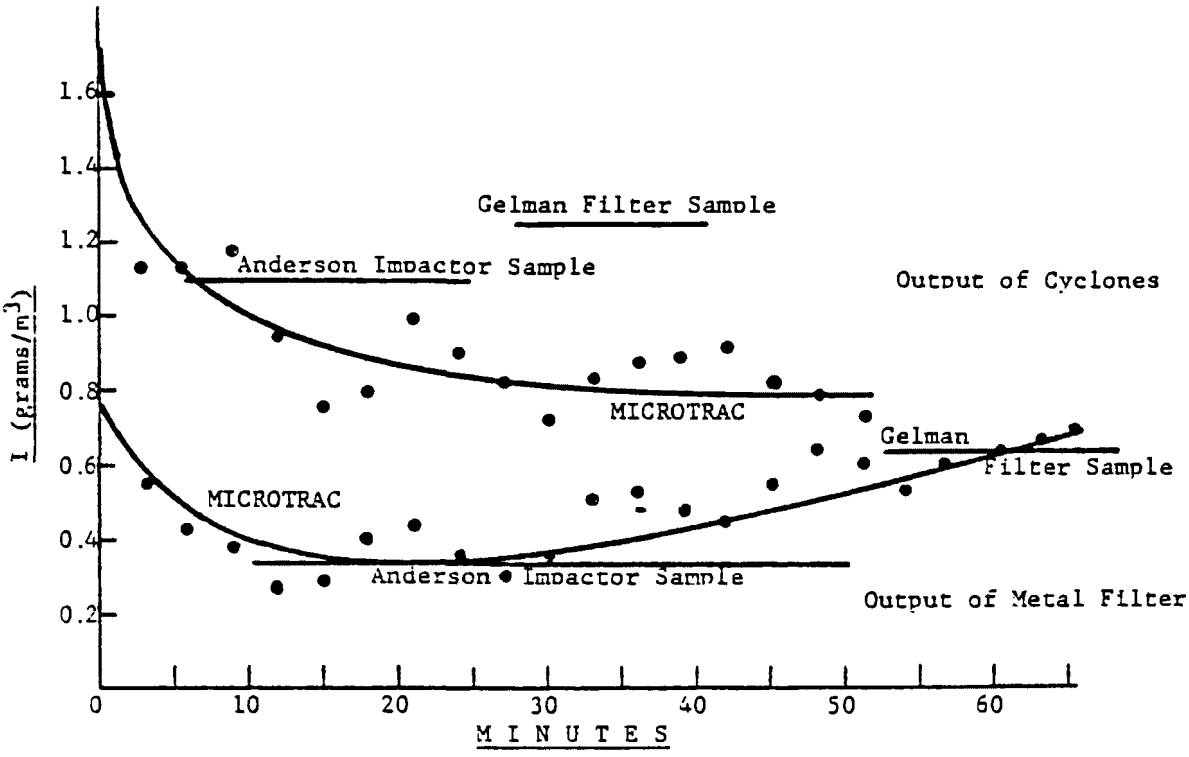

Figure 5 Particulate loading experiment no. 4.

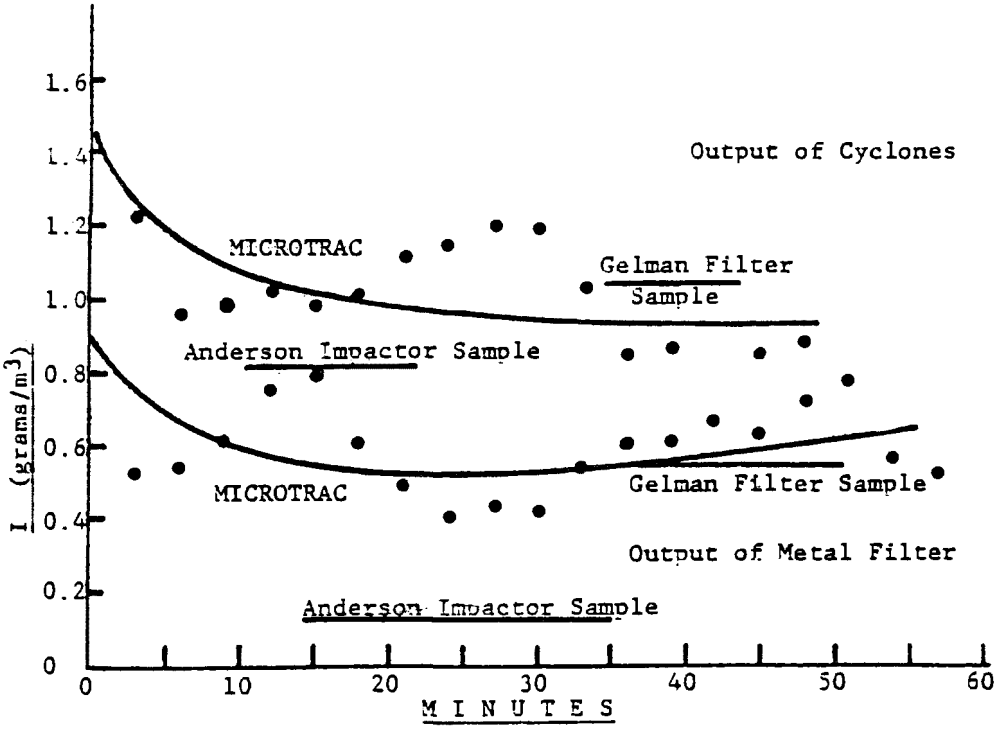

Figure 6 Particulate loading experiment no. 6.

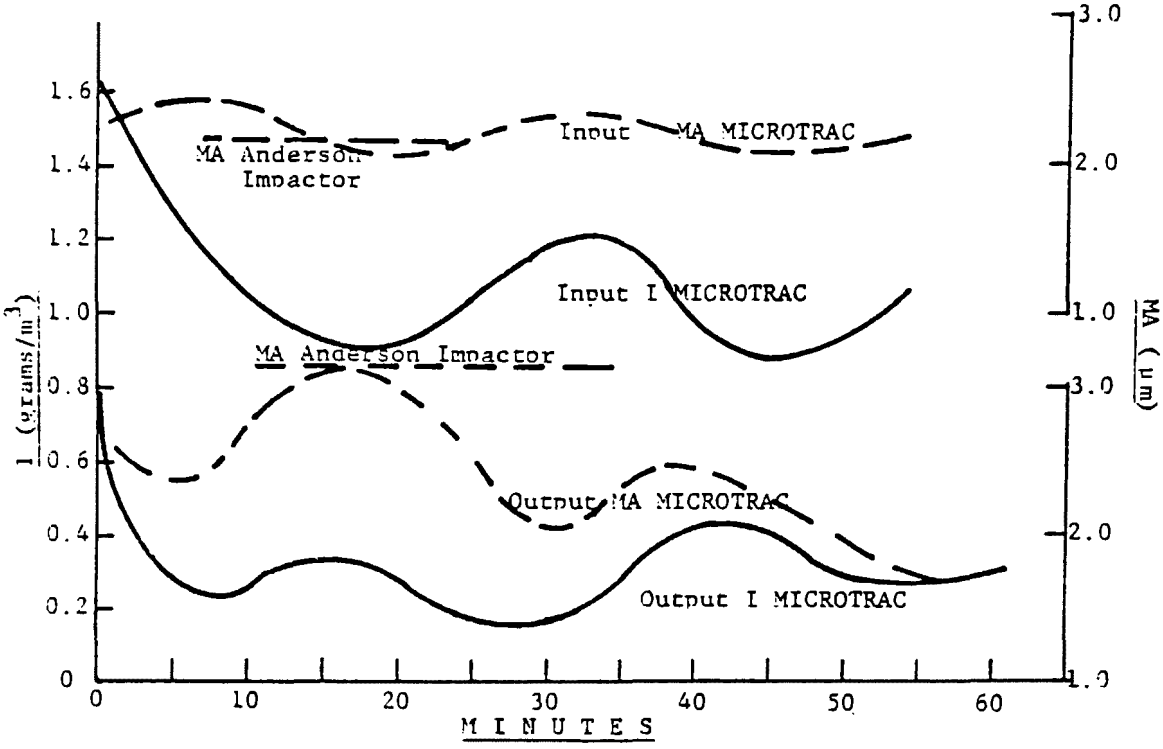

Figure 7 Size and loading experiment no. 4.

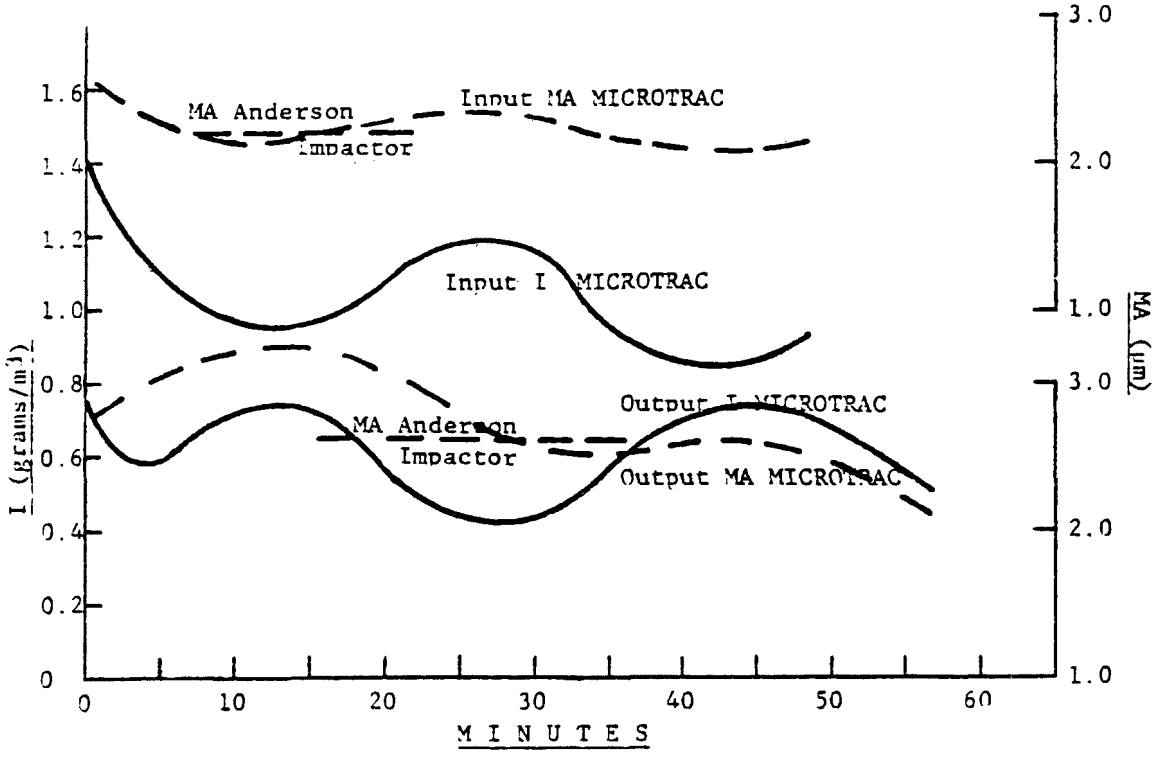

Figure 8 Size and loading experiment no. 6.

Table I. Particle Sizing in Microns

Test	L&N No. 4		L&N No. 5		L&N No. 6	
Measurement	In	Out	In	Out	In	Out
Calculated $\overline{MV}$ Anderson Impactor Sample	5.77	4.64	5.39	7.44	5.33	4.74
MICROTRAC $\overline{MV}$	2.92	5.13	3.91	5.45	3.62	4.39
Difference $\Delta\overline{MV}$	+2.85	-0.49	+1.48	+1.99	+1.71	+0.35
Calculated $\overline{MA}$ Anderson Impactor Sample	2.98	2.34	2.08	3.04	2.20	2.58
MICROTRAC $\overline{MA}$	2.15	2.39	2.26	2.64	2.19	2.71
Difference $\Delta\overline{MA}$	+0.83	-0.05	-0.18	+0.40	+0.01	-0.13
50 Percentile Anderson Impactor Sample	4.15	3.29	3.35	4.75	3.42	3.50
50 Percentile MICROTRAC (dgm)	2.50	3.50	2.97	3.79	2.82	3.45
Difference	+1.65	-0.21	+0.38	+0.96	+0.60	+0.05

These results indicate good agreement between optical scattering and cascade impactor methods for particle sizing. In all but one case, the difference is less than one micron.

Two interesting characteristics are observed, however. The MICROTRAC size measurement tends to indicate slightly smaller size for the median diameter and the MICROTRAC shows the average size of particles coming out of the final filter to be larger than at the input. In one of the three tests, the impactor data also shows the output particle size to be greater than the input. This anomaly will be explained later in discussion of test chronology.

The loading data as functions of time are shown in Figures 5-8 for two operational tests. The in-situ volumetric loadings, as outputted by the MICROTRAC instrument, are converted to standard pressure/temperature conditions by the following equation:

$$I\ (\text{Grams/m}^3) = \frac{D(1 + 0.00367T)dV}{P} \qquad (14)$$

where D = density of particulate (gm/cc)
T = gas temperature, nominally 160C
P = gas pressure, nominally 3 atms.
dV = instrument output in ppm.

The density of the material samples in these tests was 1.2 gm/cc.

The data from MICROTRAC are shown as dots for unit intervals of time. The loading is always high at the beginning of each run due to material loosened in setting the duct valves. It takes about 15 to 20 minutes for this to be purged out of the gas stream.

The MICROTRAC loading data show slow oscillatory variations. Initially, we thought that this might be instrumental error caused by change in laser beam intensity. However, observations of particle size as a function of time show similar variations and these data are, independent of laser intensity. Therefore, we conclude that these oscillations are characteristic of the Argonne/Combustor process.

Smooth lines are drawn through the MICROTRAC data points to show the loading trends. In addition, the loading values obtained by the cascade impactor and the membrane filter samples are shown. The horizontal location and length of lines for the extracted sample loadings indicate approximate time and duration for collection of each of these samples. The vertical locations of these lines designate the sample loading measurements for those intervals.

A significant part of the variance between MICROTRAC and the extracted samples may be due to non-uniformity of loading across the duct or, probably more likely, due to problems of achieving isokenetic sampling with the extractive probe. A particular advantage of the MICROTRAC type of instrument is that it measures all particles passing through the laser beam and the gas flow is not influenced in any way by this method of measurement.

Figures 7-8 show the time variations of the mean area diameter (MA) superimposed on the loading functions. It is noted that the size variations tend to follow closely the loading variations. Thus, it is concluded that the size of particles is a major contributor to the total loadings in this process.

Furthermore, the amplitude of variation in MA is consistently largest at the beginning of the metal filter output measurements and the mean size tends to decrease with time. This is characteristic of the performance of the ANL metal filter. The efficiency of filtration improves as particulate builds up in the filter media.

It is also observed in these data, that the MA variations at the input to the final filter are less than at the output. The test sequence at ANL specified first measurement of the particulate at the output of the metal filter, then at the input. For all three combustion tests, the output measurements were made in the morning, a few hours after start-up, and the input measurements occurred in the afternoon. One can now only hypothesize that this combustion system requires a long time to stabilize and that the metal filter output variations would have been smaller had the test sequence been reversed. This also explains why the average size over the total measurement time was larger at the output than the input. For example, at the end of the L&N-5 metal filter output run, the average MA was 1.73 microns and the input average particle diameter, measured two to three hours later, was 2.26 microns. These results indicate the desirability of having two MICROTRAC instruments to enable simultaneous measurements at the input and output of the final filter in order to obtain complete characterization of a combustor/filtration process.

After completion of the tests at ANL, the prototype instrument was returned to L&N where the calibration of the particulate loading output was rechecked. For a calibrated sample of 10.0 ppm diamond dust of nominal 3 microns diameter, the instrument read 10.11 ppm, while the standard deviation of this calibration procedure is 0.18 ppm. Thus, the calibration constant for dV did not change in a measurable degree during two months of operation.

PILOT PLANT INSTALLATION

The prototype instrument was installed in July, 1978 at the inlet of a gas turbine on the Curtiss-Wright Corporation fluidized-bed combustion system. The pipe diameter at this location is 4 inches i.d. The quartz windows on each side of the pipe are 4 inches in diameter and purged with instrument air.

During initial tests a film of oil from the compressed air supply was deposited on each window. However, the instrument functioned well and the median size of particulate was observed to vary from 6.5 to 6.9 micrometers and the loading varied from 0.84 ppm to 0.23 ppm (by volume). The actual particulate loading may have been somewhat less due to build-up of dust deposit on the windows caused by the oil films.

Upon conclusion of this series of tests, Curtiss-Wright added oil coalescing filters on the air purge supply which has corrected this problem.

The next series of tests, involving operation of the small gas turbine, is now in process.

While waiting for further operational tests, we investigated means for scale-up of this type of instrumentation to commercial size installations. The results of this study follow.

INSTRUMENT SCALE-UP TO COMMERCIAL SIZE PLANTS

The primary limiting factor in scale-up for on-stream measurement of particulate in high temperature gas is the distance over which the smallest particles can be detected. For any size of collecting optics some of the scatter flux is vignetted by the lens (i.e., falls outside the field of view of the lens). Thus, given size of the collection lens and diameter of a pipe, there is a maximum distance from the lens for which the smallest particles can be detected.

This distance (L_V) is defined by the following approximation:

$$L_V \triangleq \frac{\pi \ell_d d}{2\lambda K} \tag{15}$$

where ℓ_d is the lens diameter and K is determined experimentally for the -3db point on the volume response. For λ = 442 nm and particles of 0.5 micron diameter, θ_V (scatter angle to first minimum) is about 12.5^o and K = 0.854.

Thus, for across-the-pipe measurement, there is a limiting distance (L_V) over which particles of interest can be measured. See Figures 9 and 10. If one wants to measure all particles larger than one micron at 0.8 meter from the collection lens, a lens diameter of 20 cm is required as seen from the solid lines in Figure 10.

Somewhat larger lens can be used but larger apertures increase demand on purge gas which is undesirable. Alternatively, it is possible to design an asymmetrical lens which, in effect, will double the scatter collection aperture for a given window diameter. This is the maximum optical gain achievable and is shown by the dashed lines in Figure 10. This type of lens will permit measurement of particles one micron and larger in size from the center line to the wall for pipes up to 2 meters i.d. Assuming the loading to be uniform across the diameter of the gas stream, the total loading can easily be calculated.

We conclude that on-stream measurements on pipes larger than 2 meters i.d. will require isokenetic sampling to permit the measurements to be made on smaller size pipe and connect the sample gas stream back into the main pipe downstream of the measurement.

CONCLUSIONS AND FUTURE PLANS

Leeds & Northrup Company has demonstrated that it is technically feasible to measure particle size and loading on-stream in high temperature pressurized systems. Furthermore, this method of measurement is capable of being scaled up to commercial size installations. What remains to be determined is whether the optical quality of the windows can be maintained in large pipes for long time intervals. Thus, further investigation is needed on development of air-purge

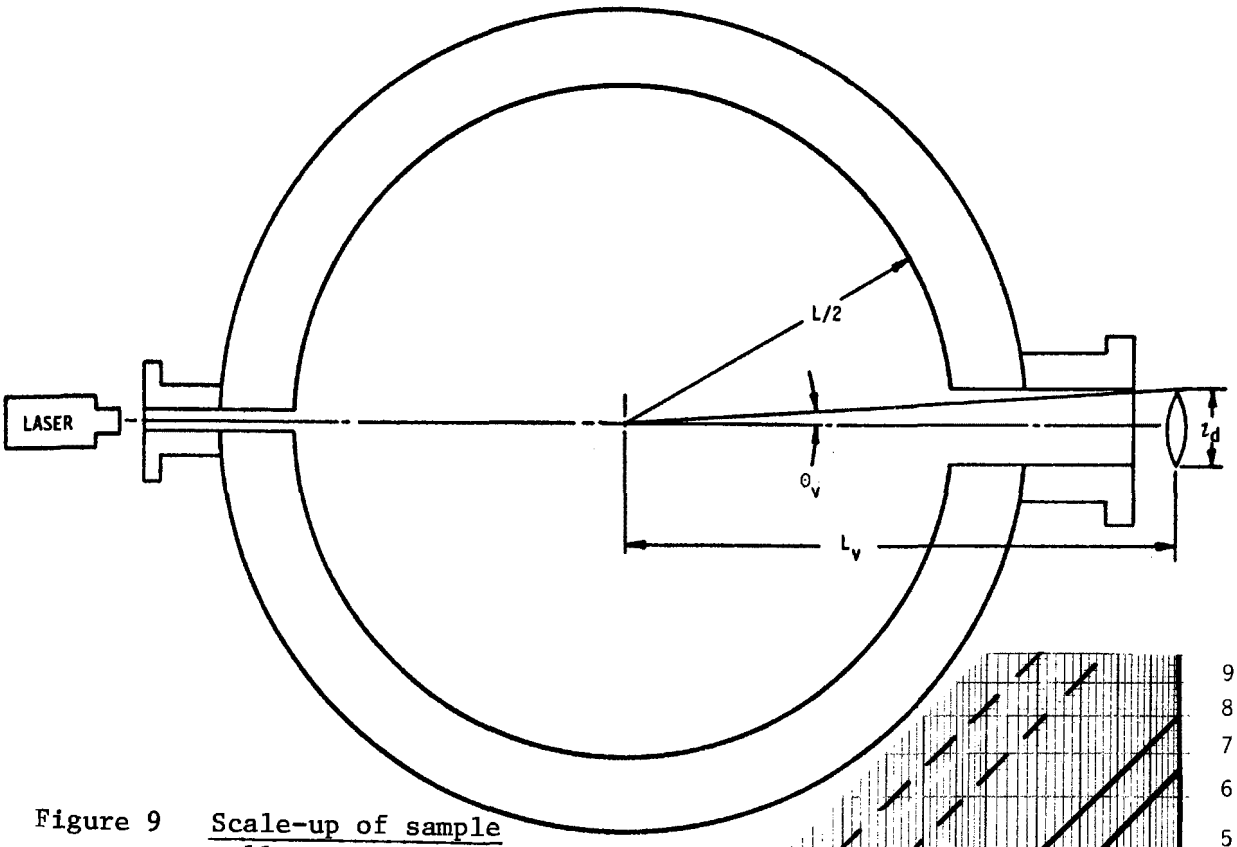

Figure 9 Scale-up of sample cell.

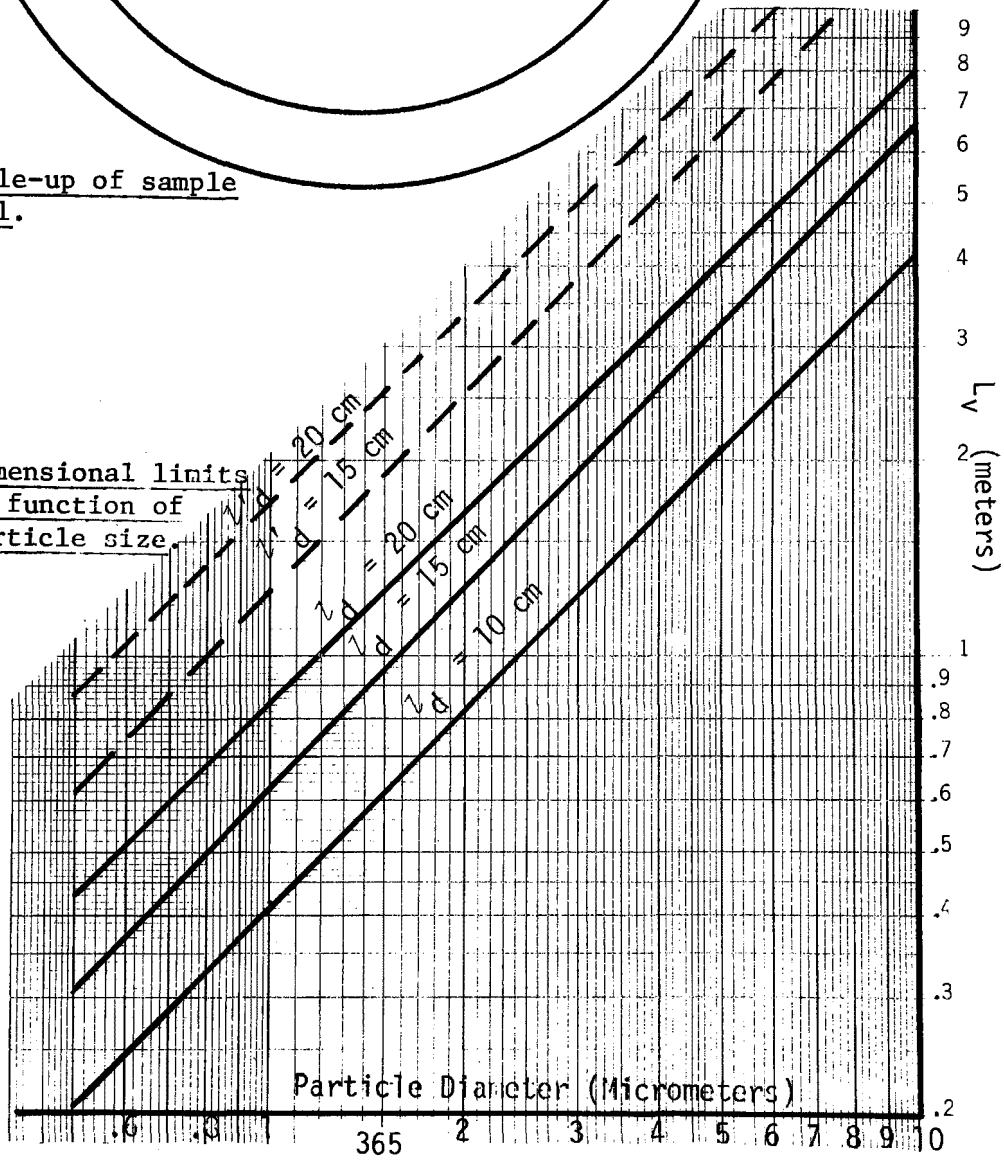

Figure 10 Dimensional limits as function of particle size.

meter. For baseline conditions, virtually all the particulate emissions are generated in this size range. This baseline distribution is in great contrast with coal fired boilers where the mass mean particle diameter typically ranges between 10 and 20 micrometers. It is also important to note that the submicron peak is at a size region which can contribute significantly to plume opacity due to the light scattering characteristics of these particle sizes.

A typical photomicrograph of baseline particulate matter in Figure 1-2 shows spherical shaped particles with a relative size uniformity consistent with the size distribution results. Chemical analysis indicates mostly sulfate compounds with smaller quantities of carbon and oil ash mineral constituents.

Poor Fuel Atomization: Deteriorated fuel atomization resulted in the generation of a substantial mass of large particulates (greater than 10 micrometer diameter) as indicated in Figure 1-1. The fine submicron distribution and composition was essentially unaltered compared to baseline. Significantly, no changes in stack opacity were noted despite an up to a 10-fold increase in total particulate emissions. Photomicrographs of the large particles as typified by Figure 1-3 indicate irregularly shaped, porous particles with sponge-like appearance. Surface analysis of individual large particles indicated mostly carbon, but with an abundance of sulfur and oxygen (sulfate) and lesser quantities of trace elements. However, particle depth analysis illustrated in Figure 1-4 revealed that the dominant portion of the sulfate was contained in a surface layer while the bulk of the particles consisted mainly of carbon.

These results indicate that reducing the fuel atomization quality produces large particulates which appear to be derived from the carbonization of large fuel droplets which neither completely vaporize nor burn out in the furance. Thus, the presence of large porous carbonaceous particulates in the emissions from an oil-fired boiler may indicate the existence of an atomization deficiency or mismatch between the furnace burnout characteristics and the type of atomizer used. Measurements of the type made in this study might be utilized as a diagnostic procedure in situations where excessive particulate emissions are encountered.

Reduced Excess Air: Referring again to Figure 1-1, the low excess air test conditions produced a particle size distribution very similar to baseline, but the generation of a small quantity of large particles was apparent. Chemical analysis showed a measurable increase in carbon compared to baseline measurements. Nevertheless, it appears that the particulate matter is fundamentally similar in size to that produced under baseline conditions and that carbon soot generated during low excess air operations does not necessarily produce larger size particles. This conclusion may not be applicable to extreme low excess air conditions (smoking) where large carbonaceous particles might be expected. Unlike poor fuel atomization, increases in-stack opacity were noted during reduced excess air conditions.

Summary: A summary of the overall particulate matter emission rates and composition for the three Ravenswood Unit 10 test conditions is shown in

REFERENCES

1. Wertheimer, A.L. and W.L. Wilcock. Measurement of Particle Distributions Using Light Scattering. Applied Optics 15: 1616-1620 June 1976

2. Stockham, J.D. and E.G. Fochtman. Particle Size Analysis. Ann Arbor Science Publications, 1977. p.8.

ANALYSIS OF SAMPLING REQUIREMENTS FOR CYCLONE OUTLETS

by

Michael Durham
DRI Electronics
University of Denver
Denver, Colorado 80208
(303)753-2241

and

Dale Lundgren
Dept. of Environmental Engineering
A.P. Black Hall
University of Florida
Gainesville, Florida 32611
(904)392-0846

A comprehensive analysis of intertial effects in aerosol sampling was combined with a thorough study of swirling flow patterns in a stack following the exit of a cyclone in order to determine the errors involved in sampling particulate matter from a tengential flow stream. Aerosol sampling bias was analyzed by comparing samples taken from a 10 cm wind tunnel at duct velocities varying from 550 to 3600 cm/sec. Experiments were performed at four sampling angles: 0, 30, 60 and 90 degrees and for particles 1 to 19.9 micrometers in diameter. A mathematical model was developed and tested which predicts the sampling error when both nozzle misalignment and anisokinetic sampling velocities occur simultaneously. A three-dimensional or five-hole Pitot Tube was used to map cross-sectional and axial flow patterns in a stack following the outlet of a cyclone. Using information found in this study, a simulation model was developed to determine the erros involved when making a Method 5 analysis in a tangential flow stream.

ANALYSIS OF SAMPLING REQUIREMENTS FOR CYCLONE OUTLETS

INTRODUCTION

Obtaining a representative sample of particulate matter from a stack following the outlet of a cyclone poses a difficult problem when standard sampling methodology is used. The swirling flow pattern produced by the cyclone is well maintained in a circular stack so that the air flows in spiral or helical paths up the stack. Since the gas stream flows at an angle to the stack axis, sampling errors are induced due to the inertia of the particles and the limitations of the velocity measuring instrument presently being used.

The analysis of sampling errors induced by cyclonic flow was approached from two directions in this study. One approach involved an investigation of aerosol sampling bias due to anisokinetic sampling velocities and misalignment of the nozzle with respect to the flow stream as a function of particle and flow characteristics. The second part of the study involved an accurate mapping of the flow patterns in a tangential flow system. The information obtained in the two parts of the study were then combined to simulate the errors that would be encountered when making an EPA Method 5 (1971,1977)[1,2] analysis in a tangential flow stream.

Review of the Literature on Anisokinetic Sampling

In order to obtain a representative sample of particulate matter from a moving fluid it is necessary to sample isokinetically with the inlet velocity equal to the free stream velocity and the nozzle aligned parallel to the flow stream (Wilcox,1957).[3] Most of the early research in this area has been concerned with the sampling errors when the ratio of the free stream velocity to the inlet velocity is other than unity. Several authors (Watson,1954; Badzioch,1959; Davies,1968; Lundgren and Calvert,1967)[4-7] found that the amount of error was a function of the velocity ratio, particle inertia, and nozzle velocity and could be best characterized by the dimensionless inertial impaction parameter or Stokes number, K, defined as:

$$K = C\rho_p V_0 D_p^2 / 18\eta D_i \qquad (1)$$

where

C = Cunningham's correction for slippage

ρ_p = particle density

V_0 = particle velocity

D_p = particle diameter

η = viscosity of the gas

D_i = nozzle diameter

Extensive experimental studies were performed by Belyaev and Levin(1972,1974)[8,9] in which flash illumination photographic techniques were used to study the trajectories of particles approaching and entering a sampling nozzle. The results shown in Figure 1 and described by equations 2 and 3 illustrate the relationship between Stokes number and the aspiration coefficient (ratio of the sample concentration to the true concentration) as a function of the velocity ratio ($R=V_0/V_i$).

$$(2) \qquad A = C_i/C_0 = 1 + (R-1)\beta(K,R)$$

$$(3) \qquad \beta(K,R) = 1 \quad \frac{1}{1 + (2+0.617/R)K}$$

The curves confirm the results of Dennis et al.(1957)[10] and Whiteley and Reed(1959)[11] that for small Stokes numbers the aspiration coefficient approaches 1 for all velocity ratios (R), and for large Stokes numbers it approaches R.

The sampling bias due to misalignment of the nozzle with the flow stream is similar to that caused by superisokinetic sampling (R<1). When the nozzle is at an angle to the flow stream, the projected area of the nozzle is reduced by a factor equal to the cosine of the angle. Even if the nozzle velocity is equal to the flow stream velocity an aspiration coefficient less than or equal to unity will be obtained because some of the larger particles will be unable to make the turn into the nozzle with the streamlines. Mayhood and Langstroth, as reported by Watson(1954)[4], and Glauberman(1962)[12] experimentally found that the amount of sampling error increased proportional to the particle size and the angle of misalignment. An equation derived by Lundgren et al.(1978)[13] describes the sampling bias that would occur when both the nozzle is misaligned with the flow stream and the velocity ratio is other than unity:

$$(4) \qquad A = 1 + (R\cos\Theta-1)\beta'(K,R,\Theta)$$

Where β' is a function of the velocity ratio, Stokes number, and the angle of misalignment. To satisfy the boundary conditions, β' must approach zero for small Stokes numbers and must approach 1 for large Stokes numbers. This means when the velocity ratio is equal to 1, the curve for the aspiration coefficient will approach $\cos\Theta$ at large values of K.

Review of the Literature on Tangential Flow

The swirling flow in a stack following the outlet of a cyclone, combines the characteristics of vortex motion with axial motion along the stack axis. Since this represents a developing flow field, the swirl level decays and the velocity profiles and static pressure distributions change with axial position along the stack (Baker and Sayre,1974).[14] Velocity vectors in tangential or vortex flows are composed of axial, radial, and tangential or circumferential velocity components (see Figure 2). The relative order of magnitude of the velocity components varies across the flow field with the possibility of each one of the components becoming dominant at particular points (Chigier,1974).[15]

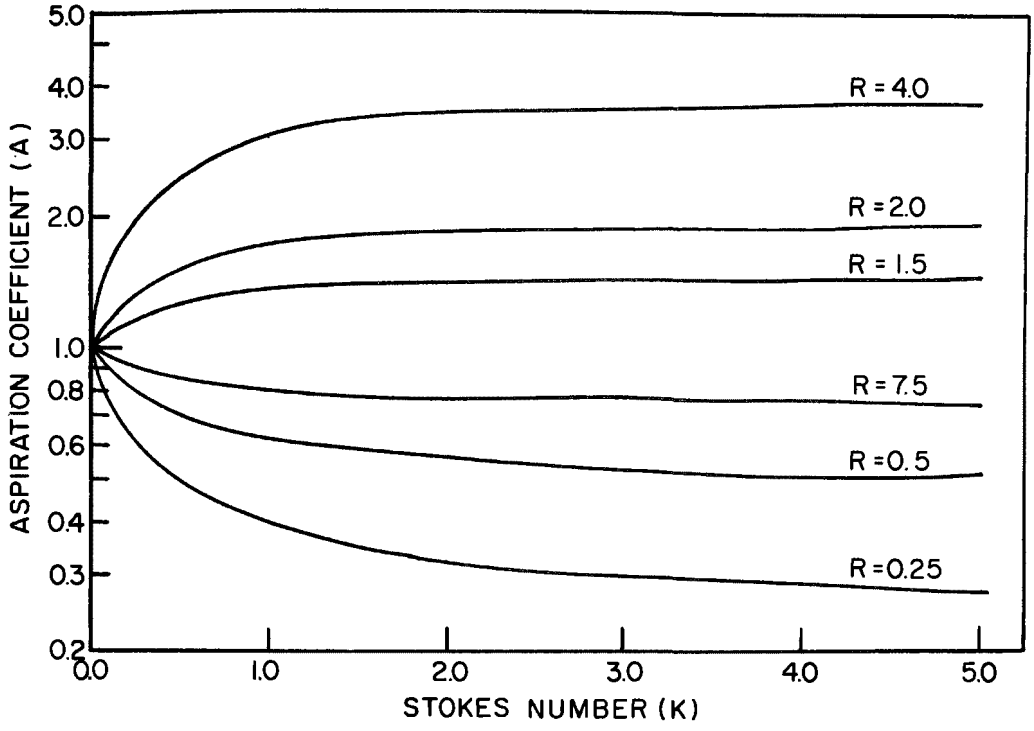

Figure 1. Sampling efficiency as a function of Stokes number (K) and velocity ratio ($R=V_o/V_i$).[8,9]

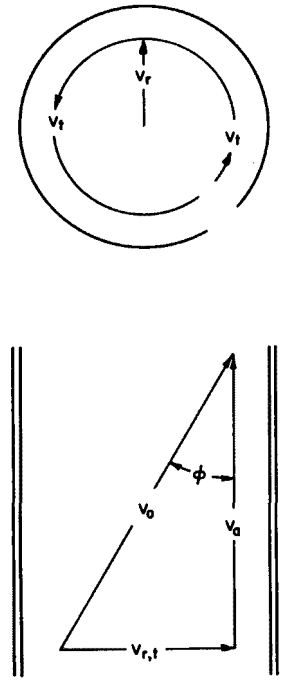

Figure 2. Velocity components in a swirling flow field.

The established vortex flows are generally axisymmetric but during formation of the spiraling flow the symmetry is often distorted.

Two distinctly different types of flow that are possible in a swirling flow field are known as free vortex and forced vortex flows. When the swirling component of flow is first created in the cyclone exit, the tangential profile of the induced flow approahces that of a forced vortex. As the forced vortex flow moves along the axis of the stack, momentum transfer and losses occur at the wall which cause a reduction in the tengential velocity and dissipation of angular momentum. This loss of angular momentum id due to viscous action aided by unstable flow and fluctuating components. Simultaneously, outside the laminar sublayer at the wall where inertial forces are significant, the field develops toward a state of constant angular momentum. This type of flow field with constant angular momentum is classified as free vortex flow. The angular momentum and tangential velocities of the flow decay as the gas stream flows up the stack. However, Baker and Sayre(1974) found that even after 44 diameters the tangential velocity is still quite significant when compared to the axial velocity. Therefore, satisfying the EPA Method 5 requirement of sampling 8 stack diameters downstream of the nearest upstream disturbances will not eliminate the effect of sampling in tangential flow.

Types of errors that would be expected to be introduced by tangential flow are nozzle misalignment, concentration gradients and invalid flow measurements. The sampling error caused by nozzle misalignment was described previously. Concentration gradients occur because the rotational flow causes the larger particles to move toward the walls of the stack, causing higher concentrations in the outer regions. Mason(1974)[16] ran tests at the outlet of a small industrial cyclone to determine the magnitude of errors induced by cyclonic flow. He found that flow angles as high as 70° existed in the stack and sampling with the nozzle parallel to the stack wall produced an error of 52.7%. However, particle size distribution tests showed no significant effect of a concentration gradient across the traverse.

The errors in the measurement of velocity and subsequent calculations of flow rate in tangential flow are due primarily to the crudeness of the instruments used in source sampling. Because of the high particulate loadings that exist in source sampling, standard pitot tubes cannot be used to measure the velocity. Instead, the S-type pitot tube must be used since it has large diameter pressure ports that will not plug. Although the S-type pitot tube will give an accurate velocity measurement, it is somewhat insensitive to the direction of the flow (Hanson and Saari,1977; Brooks and Williams,1975; Grove and Smith,1973; Hanson et. al.,1976; and Williams and DeJarnetter,1977).[17-21] Although the S-type pitot tube is very sensitive to pitch direction, the curve for yaw angle (Figure 3) is symmetrical and somewhat flat for an angle of 45° in either direction. Because of this insensitivity to direction of flow in the yaw direction, the S-type pitot tube cannot be used in a tangential flow situation to align the nozzle to the direction of the flow, or to accurately measure the velocity in a particular direction.

The velocity in a rotational flow field can be broken up into three components in the axial, radial, and tangential directions (see Figure 2). The magnitude of the radial and tangential components relative to the axial components will determine the degree of error induced by the tangential flow. Neither the radial nor the tangential components of

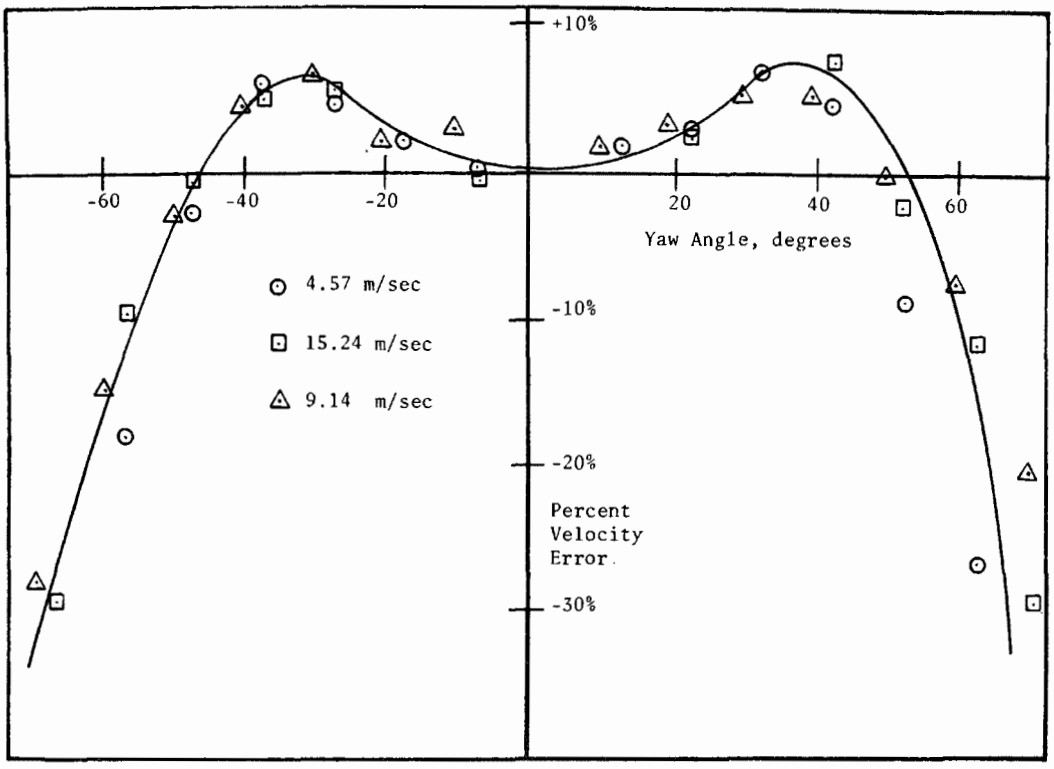

Figure 3. Velocity error vs. yaw angle for an S-type pitot tube.[20]

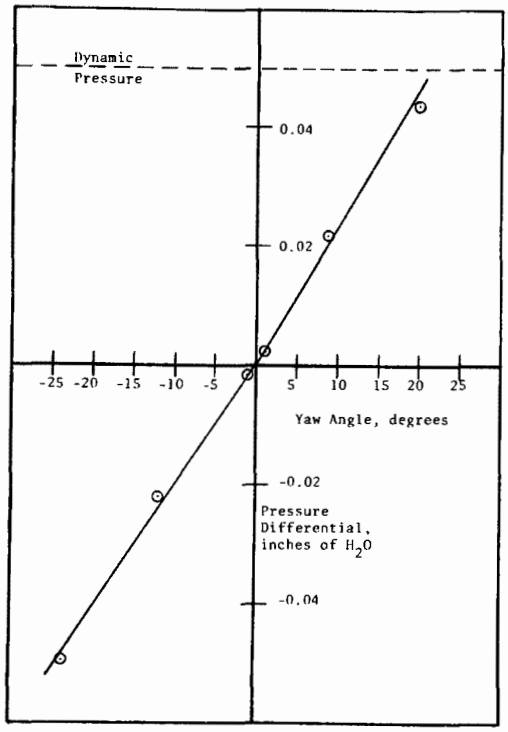

Figure 4. Five-hole pitot tube sensitivity to yaw angle.[20]

velocity affect the flow rate through the stack, but both affect the velocity measurement made by the S-type pitot tube because it lacks directional sensitivity.

Two common types of pressure probes capable of measuring velocity accurately in a tangential flow stream are the 5-hole and the 3-hole pitot tubes. The 5-hole or three dimensional directional pressure probe is used to measure yaw and pitch angles, and total and static pressure. Five pressure taps are drilled in a hemispherical or conical probe tip, one on the axis and at the pole of the tip, the other four spaced equidistant from the first and from each other at an angle of 30-50° from the pole. Each probe requires calibration of the pressure differentials between holes as a function of yaw and pitch angles. Figure 4 shows the sensitivity of a typical 5-hole pitot tube to yaw angle. Because of its sensitivity to yaw angle, it is possible to rotate the probe until the yaw pressures are equal, measure the angle of probe rotation (yaw angle) and then determine the pitch angle from the remaining pressure differentials. Velocity components can then be calculated from the measured total pressure, static pressure, and yaw and pitch measurements. The 3-hole pitot tube is similar except that it is unable to detect pitch angle.

EPA Criteria for Sampling Cyclonic Flow

The revisions to Reference Methods 1-8 (1977)[2] describe a test for determination of whether cyclonic flow exists in a stack. The S-type pitot tube is used to determine the angle of the flow relative to the axis of the stack by turning the pitot tube until the pressure reading at the tube pressure openings is the same. If the average angle of the flow across the cross section of the stack is greater than 10°, then an alternative method to Method 5 should be used to sample the gas stream. The alternative procedures include installation of straightening vanes, calculating the total volumetric flow rate stoichiometrically, or moving to another measurement site at which the flow is acceptable.

Straightening vanes have shown the capability of reducing swirling flows; however, there are some problems inherent in their use. One is the physical limitation of placing them in an existing stack. Another is the cost in terms of energy due to the loss of velocity pressure when eliminating the tangential and radial components of velocity. Since the vortex flows are so sensitive to downstream disturbances, it is quite possible that straightening vanes might have a drastic effect on the performance of the upstream cyclonic control device which is generating the tangential flow. Because of these reasons the use of straightening vanes is unacceptable in many situation.

Calculating the volumetric flow rate stoichiometrically might produce accurate flow rates but the values could not be used to calculate the necessary isokinetic sampling velocities and directions. Also, studies reported here have shown that the decay of the tangential component of velocity in circular stacks is rather slow and therefore it would be unlikely that another measurement site would solve the problem.

EXPERIMENTAL DESIGN

Since cyclonic flow leads to probe misalignment it was necessary to first determine the relationship between sampling bias and the angle of the nozzle to the flow stream. This was accomplished by sampling monodisperse particles, 1-20 micrometers in diameter, flowing through a 10 cm. wind tunnel shown in Figure 5. Two simultaneous samples were taken, one parallel to the duct and the other at an angle of 30, 60, or 90 degrees to the axis of the duct. The sampling rates were identical so that the concentration difference between the two represented the inertial sampling bias. Preliminary tests with both nozzles sampling isokinetically and parallel to the flow proved that the concentration at the two traverse positions was identical. Particle diameter, duct velocity, and nozzle diameter were varied to produce a range of Stokes numbers from 0.007 to 2.97. In order to determine the effect of simultaneous probe misalignment and anisokinetic sampling rates, additional tests were performed in which the control nozzle sampled at an isokinetic rate parallel with the flow stream while the test nozzle sampled at an anisokinetic sampling rate and at an angle to the duct axis.

The system used to map the flow pattern in a tangential flow stream is shown in Figure 6. It consisted of a 34,000 liters per minute industrial blower, a section of 15 cm. PVC pipe containing straightening vanes, a small industrial cyclone collector, followed by a 6.1 meter length of 20 cm. PVC pipe. The 150 cm. long cyclone was laid on its side so that the stack was horizontal and could be conveniently traversed at several points along its length. A change in flow through this system was produced by supplying a restriction to the inlet of the blower.

To measure the velocity in the stack, a United Sensor type DA 3-dimensional directional pitot tube was used. The probe is 0.32 cm. in diameter and is capable of measuring yaw and pitch angles of the fluid flow as well as total and static pressure. The yaw angle is a measure of the flow perpendicular to the axis of the stack and tangent to the stack walls, while the pitch angle is a measure of the flow perpendicular to the axis of the stack and perpendicular to the stack walls.

RESULTS

Analysis of the Inertial Sampling Bias

The results of the tests to determine sampling bias as a function of angle of misalignment and Stokes number are shown in Figure 7. For all three angles, the curves approach a theoretical limit of $\cos\theta$.[13] However, the Stokes numbers where the curves closely approach their limits decrease with increasing angles. This is due to an effective decrease in nozzle diameter produced by the angle of misalignment. An equation was developed to account for this and produces an "adjusted Stokes number" (K') defined by:

$$K' = Ke^{\frac{0.022\theta}{375}} \qquad (5)$$

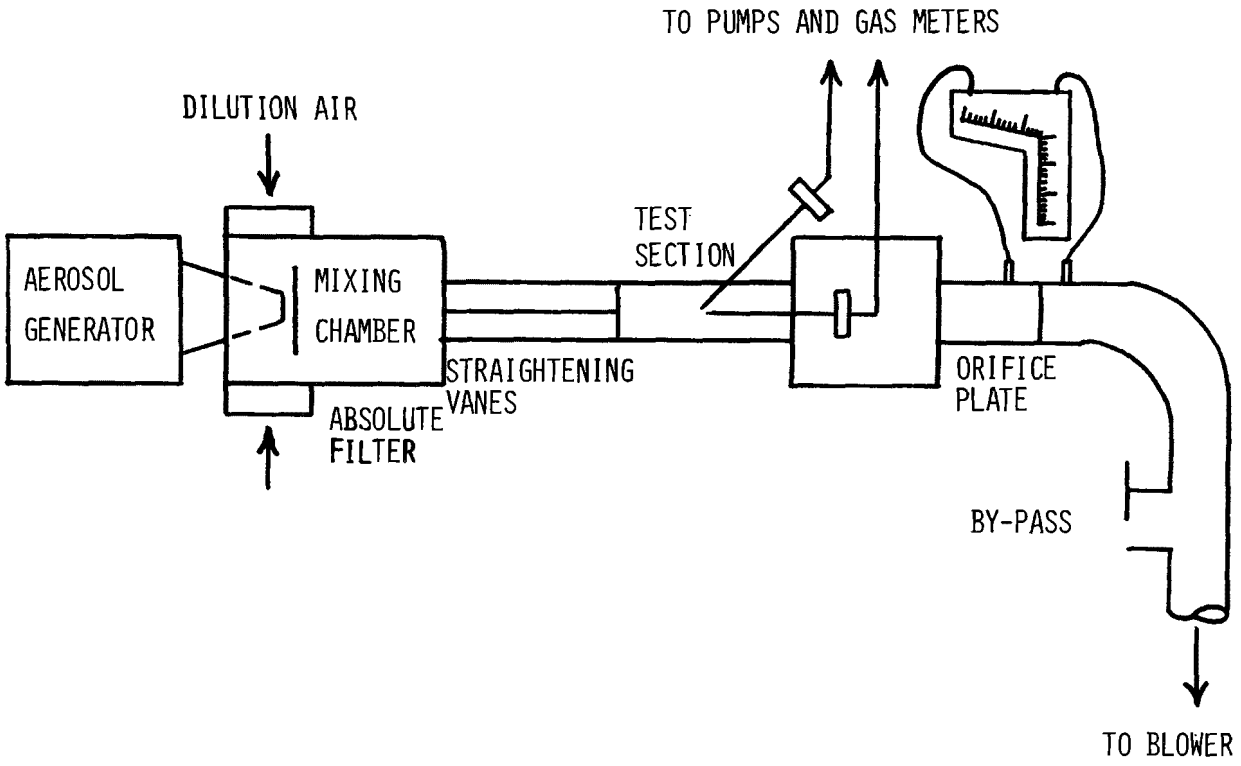

Figure 5. Experimental system to determine inertial sampling bias.

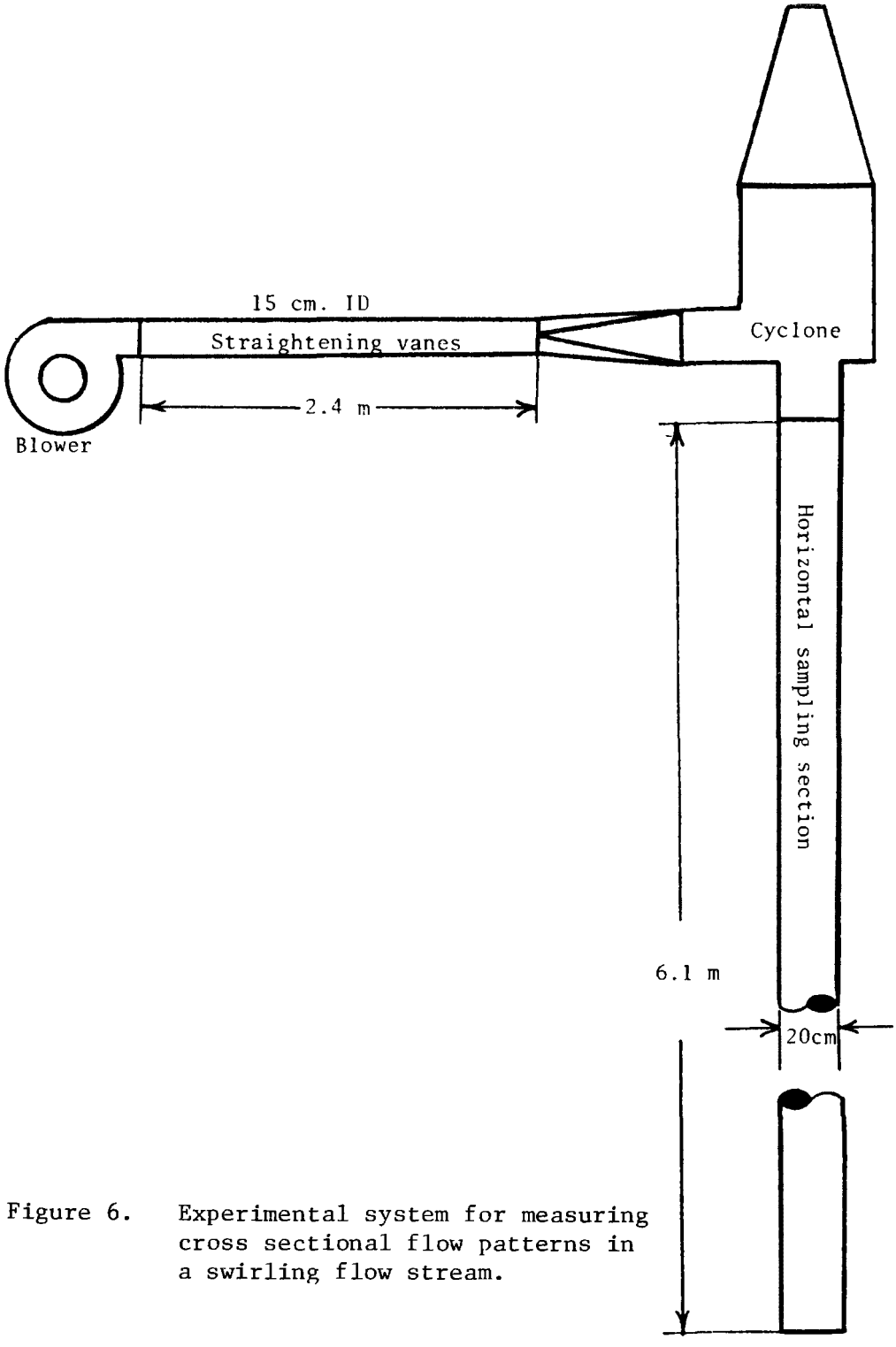

Figure 6. Experimental system for measuring cross sectional flow patterns in a swirling flow stream.

Using this correction an equation was empirically derived for β' to be used in equation 4 for R=1:

$$(6) \qquad \beta'(K',\theta,R=1) = 1 - \frac{1}{1 + 0.55K'e^{0.25K'}}$$

This equation is plotted along with the experimental data in Figure 7.

Further testing was performed to develop an equation to describe the sampling bias for $R \neq 1$ and $\theta \neq 0$. The equation would incorporate the work of Belyaev and Levin(1972,1974)[8,9] for $\theta=0$ and $R \neq 1$ and the results for R=1, $\theta \neq 0$ described by equation 6. The following equation was found to best fit the data:

$$(7) \qquad \beta'(K,R,\theta) = \frac{\beta(K',R)}{\beta(K',R=1)} \times \beta'(K',\theta,R=1)$$

where

(8) $\beta(K',R)$ is defined by equation 3

$\beta(K',R=1)$ is defined by equation 3 evaluated at R=1

$\beta'(K',\theta,R=1)$ is defined by equation 6

Equation 7 is plotted along with the data for R=0.5 and 2.0, and $\theta=60°$ in Figure 8.

Analysis of Cyclonic Flow Patterns

Eight traverse points for the velocity measurements were selected according to EPA Method 1. Measurements were made using the 5-hole pitot tube at two flow rates and at five axial distances from the inlet--1D, 2D, 4D, 8D and 16D, where D is the inner diameter of the duct. At each point in the traverse, the pitot tube was rotated until the pressure differential between the yaw pressure taps was zero. This angle was recorded as the yaw angle and the pressure readings from all five pressure taps were recorded for later calculation of total and static pressure, and pitch angle.

During the initial traverse, a core area was discovered in the center of the duct where the direction of the flow could not be determined with the pitot tube. The core area was characterized by negative readings at all five pressure taps which did not vary much with rotation of the probe. The location of the core area was measured at each location along the duct axis and recorded.

Table I shows an example of the calculated results of the velocity measurements at eight diameters downstream of the cyclone for the lower flow rate. The angle ϕ represents the angle of the flow relative to the axis of the duct. The Reynolds number of the system calculated on a basis of average axial flow rates of 11,260 and 15,500 liters per minute were 80,000 and 111,000 for the low and high flow rates respectively. The velocity measurements at the other traverse points for both flow

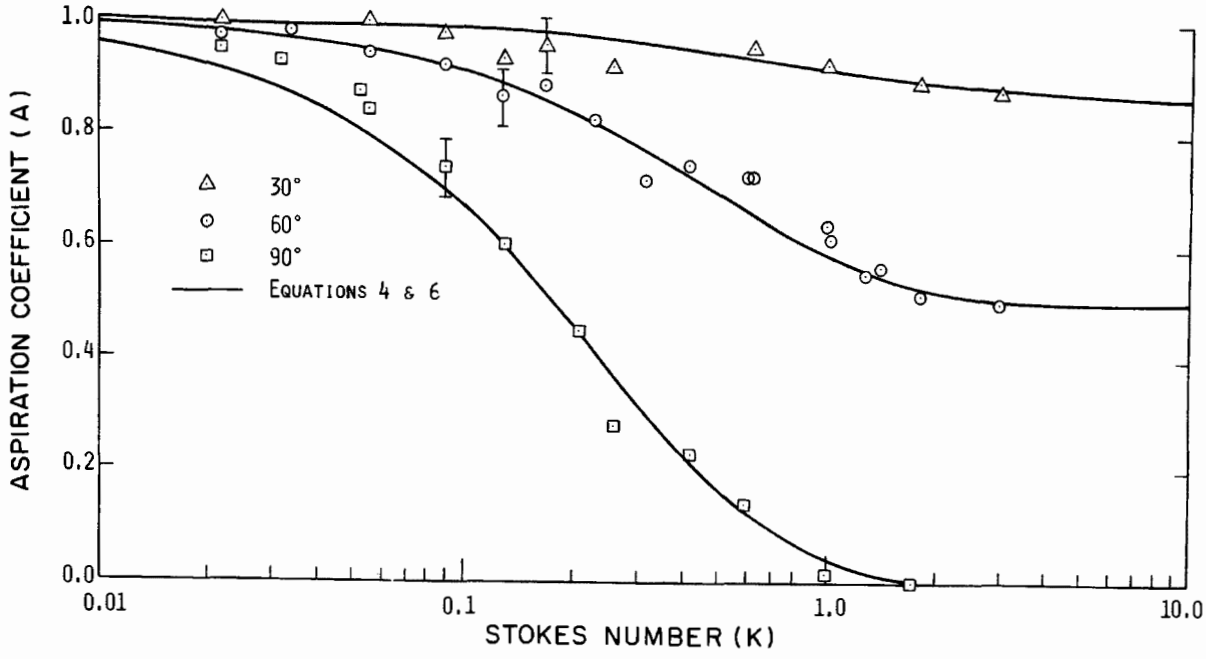

Figure 7. Aspiration coefficient vs. Stokes number--empirical equation and experimental data for 30, 60, and 90 degrees.

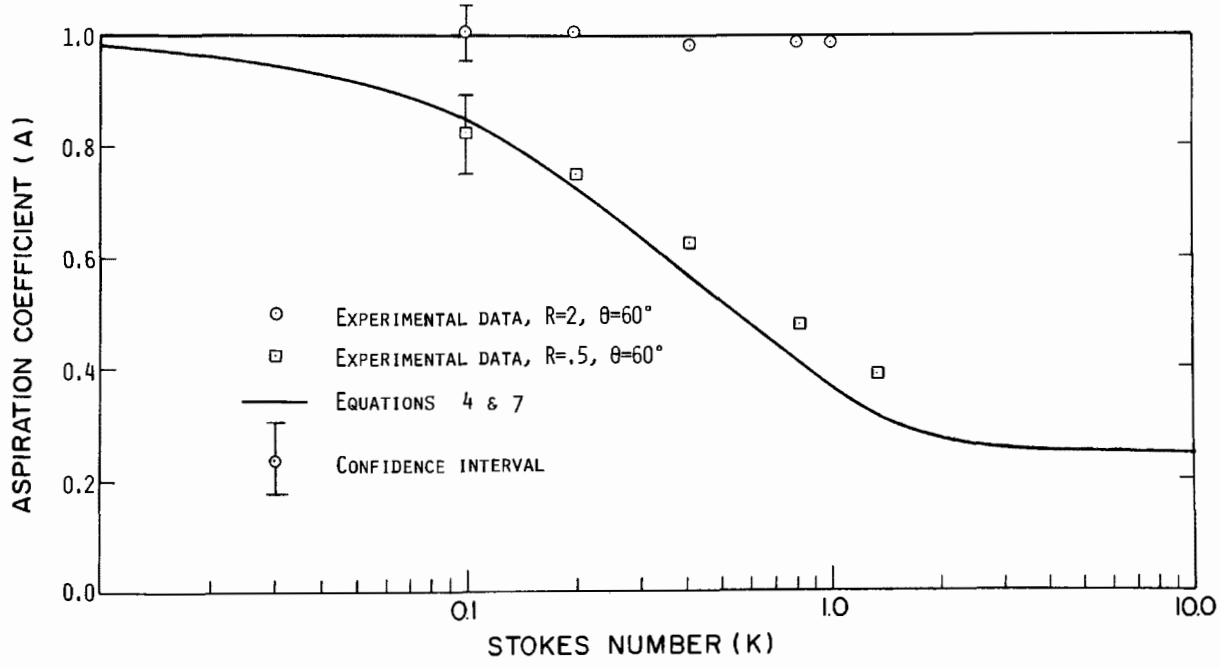

Figure 8. Sampling efficiency vs. Stokes number at 60^{o} misalignment for R = 2.0 and 0.5.

rates and all five axial distances showed approximately the same characteristics. The pitch angle increased from the core area to the duct wall. The yaw angle and the combined angle ϕ decreased from the core area to the walls. At the inlet and up to eight diameters downstream, angles as high as 70° were found near the core area of the flow field. The total velocity, axial velocity, and the tangential velocity all showed the same cross-sectional flow pattern. The velocities were minimum at the core, increased with radius and then slightly decreased near the walls. These patterns are similar to those found in the swirling flow generated with fixed vanes (Baker and Sayre,1974).[14]

In order to observe the changes in the flow as a function of axial distance from the inlet, the cross-sectional averages of the angle ϕ and the core area were calculated and presented in Figure 9. Both parameters are indicators of tangential flow and show a very gradual decay as was expected from the reported tests (Baker and Sayre,1974).[14] The curves have the same shape for both flow rates.

Plotted in Figure 10 is the location of the core area with respect to the duct center. It can be seen that the swirling flow is indeed not axisymmetric and the location of the core area changes with axial distance. A similar flow pattern was found for both flow rates.

EPA Method 5 Simulation Model

A model was developed and tested which describes particle collection efficiency as a function of particle characteristics, angle of misalignment, and velocity ratio. Together with the measurement of velocity components in a swirling flow field it was possible to analyze emission rate errors that would occur when performing a Method 5 analysis of the effluent stream following a cyclone.

For this simulation analysis, the volumetric flow rate and isokinetic sampling velocities were calculated from velocity measurements obtained at the eight diameter sampling location using an S-type pitot tube. The angle ϕ, velocity ratio, and particle velocity were determined from velocity measurements made at the same location using the 5-hole pitot tube. The particle characteristics were obtained from particle size distribution tests made by Mason(1974)[16] on basically the same system. From a particle distribution with a 3.0 micrometer MMD and geometric standard deviation of 2.13, 10 particle diameters were selected which each represent the mid-points of 10% of the mass of the aerosol. The density of the particles was assumed to be 2.7 g/cm^3. The nozzle diameter was selected using standard criteria to be 0.635 cm (¼ inch). In the model it was assumed that the nozzle would be aligned parallel with the axis of the stack, and therefore, $\theta=\phi$. Using these parameters, the average aspiration coefficients were determined at each traverse point using the ten particle diameters. Since the sampling velocity would determine the volume of air sampled at each traverse point, the total aspiration coefficient for each flow rate was determined by taking an average weighted according to sample velocity.

The total aspiration coefficients calculated in this manner for the low and high flow rates were 0.937 and 0.906 respectively. There are two reasons for the relatively low amounts of concentration error found in this analysis. One reason is that the two mechanisms causing sampling error, nozzle misalignment and anisokinetic sampling velocities, caused

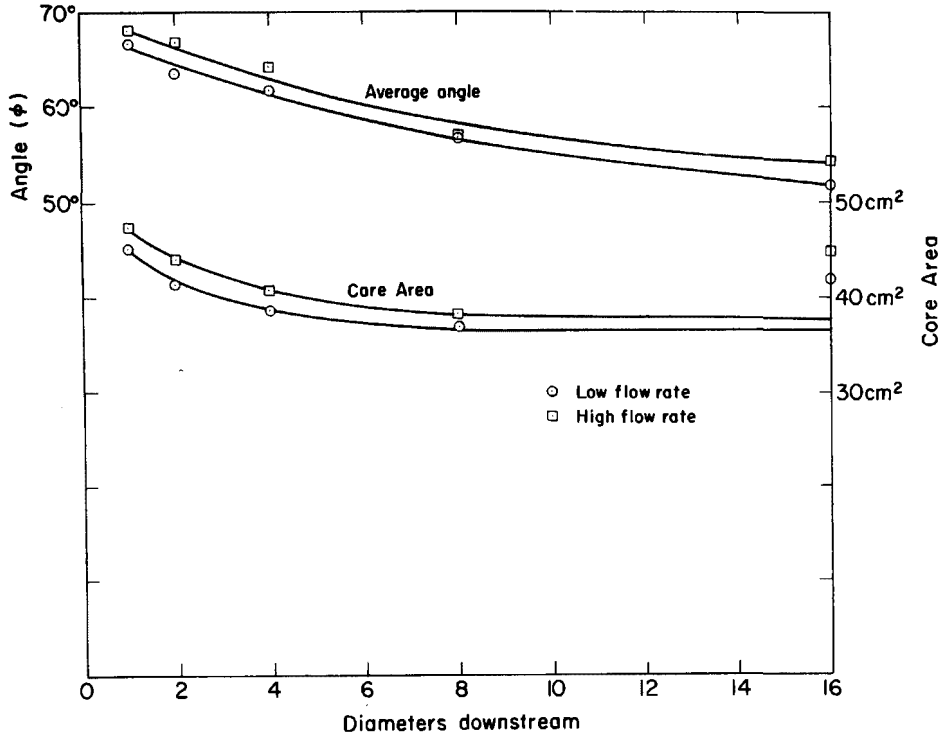

Figure 9. Decay of the angle θ and core area along the axis of the duct.

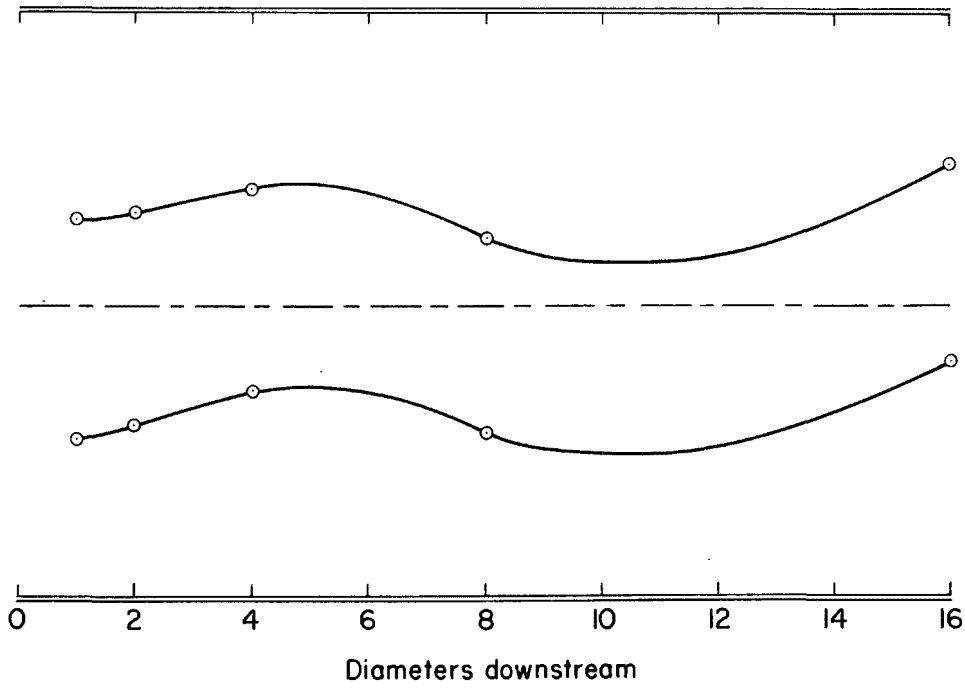

Figure 10. Location of the negative pressure region as a function of distance downstream from the cyclone.

errors in the opposite direction. The S-type pitot tube detected a velocity less than or equal to the actual velocity which would lead to subisokinetic sampling producing an increased concentration. The nozzle misalignment when sampling parallel to the stack wall would produce a decreased concentration. So each of these errors have a tendency of reducing the other error.

Another reason for the small errors was the small size of the aerosol. The Stokes numbers for over 50% of the particles were less than 0.2 and 0.3 for the low and high flow rates respectively. These values lead to small sampling errors, even when isokinetic sampling conditions are not maintained.

In order to see how much greater the error would be for larger particles, a similar analysis was performed using a distribution with a 10 micrometer mass mean diameter and a 2.3 geometric standard deviation. This was the distribution obtained at the outlet of a cyclone in a hot-mix asphalt plant (Danielson,1973).[22] Because of the larger diameter particles, the sampling efficiency was reduced to 0.799 for the high flow condition.

The volumetric flow rates determined from the S-type pitot tube measurements were compared with the flow rates calculated from 5-hole pitot tube measurements. The axial flow rates using the 5-hole pitot tube data is calculated by multiplying the average axial velocity by the inner duct area minus the core area. The flow rates using the S-type pitot tube data were determined using two different methods varying in how the negative velocity at port 4 was handled.

In the first method, the negative velocity was not used to determine the average axial velocity. The volumetric flow rate was calculated by multiplying the average axial velocity by 7/8th of the inner cross-sectional area. In the second method, the negative value was used in the determination of the average velocity and the entire inner duct was used to determine the flow rate.

The errors for both sampling efficiency and flow rate determination are presented in Table II for the three simulated conditions. The sampling errors and flow rate errors are in opposite directions so that when the two values are combined to determine emission rate, the overall effect is reduced.

SUMMARY

Flow patterns found in a stack following the exit of a cyclone are such a nature that makes it extremely difficult to obtain a representative sample with the present EPA recommended equipment. Angles in excess of 70° relative to the stack axis are found in some parts of the flow. Since large scale turbulence, such as swirling flow, is inherently self-preserving in round ducts, it decays very slowly as it moves up the stack and therefore sampling at any location downstream of the cyclone will involve the same problems.

Because of its yaw characteristics the S-type pitot tube is not suitable for measuring the velocity or the direction of the flow following a cyclone. However, pitot tubes based on the 5-hole and 3-hole designs

Table I. Five-hole pitot tube measurements made at 8 diameters downstream of the cyclone.

Point	ϕ	Total Velocity cm/sec	Axial Velocity cm/sec	Tangential Velocity cm/sec
1	***	***	***	***
2	61.0	1414	685	1212
3	70.3	1436	484	1346
4	+++	+++	+++	+++
5	63.9	1396	614	1250
6	53.0	1326	798	1019
7	47.0	1289	879	818
8	46.4	1231	849	758

*** Point No. 1 was too close to the wall to allow insertion of all five pressure taps.

+++ Point lies inside the negative pressure section.

Table II. Results of the cyclone outlet simulation model for three conditions.

Particle Size Distribution	Flow Condition	Concentration, Measured/True	Flow Rate[a], Measured/True	Flow Rate[b], Measured/True	Emission Rate[a], Measured/True	Emission Rate[b], Measured/True
MMD 3 μm σg = 2.13	Low	0.937	1.31	1.19	1.23	1.11
MMD 3 μm σg = 2.13	High	0.906	1.34	1.22	1.21	1.10
MMD 10 μm σg = 2.3	High	0.799	1.34	1.22	1.07	0.975

[a] Negative velocity was not used in the calculation of average velocity.

[b] Negative velocity was used in the calculation of average velocity.

are useful tools in determining the velocity components in a tangential flow field. The 5-hole pitot tube has the advantage of giving pitch information as well as yaw angle. However, in a cyclonic flow stream, the yaw angle is of much greater magnitude than the pitch angle and therefore, the pitch angle can be ignored with small error. In the situation modeled, if pitch angle were ignored, the calculated flow rate would be in error by less than 6%.

RECOMMENDATIONS

EPA recommends that if the average angle of flow relative to the axis of the stack is greater than 10 degrees, then EPA Method 5 should not be performed. Since the maximum error in particle sampling has been found to be $|1-R\cos\theta|$, the 10 degrees requirement is unduly restrictive and a 20 degrees limitation would be more appropriate. For a 20 degrees angle the velocity measured by the S-type pitot tube would be approximately the same as the true velocity (i.e., R=1). Therefore, the maximum error would be $1-\cos 20°$ or 6% for a very large aerosol.

When cyclonic flow does exist in a stack, EPA recommends either straightening the flow or moving to another location. Because of the physical limitations of these suggestions a better approach would be to modify Method 5 so that it could be used in a tangential flow stream. By replacing the S-type pitot tube with a 3-hole pitot tube, the direction of the flow could be accurately determined by aligning the nozzle and the velocity components could be measured for a correct calculation of volumetric flow rate. The sampling rate would be calculated on a basis of the total velocity of the flow. However, the volumetric flow rate through the stack would be calculated on a basis of only the axial component of velocity (i.e. $V_a = V_t\cos\theta$). In addition to the 3-hole pitot tube, the modification would have to include a protractor to measure the flow angle, and a method of rotating the probe without rotating the entire impinger box.

ACKNOWLEDGEMENT

This research was partially supported by a grant (Grant No. R802692-01) from the Environmental Protection Agency (EPA), and was monitored by EPA's Project Officer Kenneth T. Knapp.

REFERENCES

1. "Test Methods and Procedures. Method 5 - Determination of Particulate Emissions from Stationary Sources." Federal Regulations, 40 CFR 60.85.

2. Revision to Reference Method 1.8. Federal Register, Volume 42, Number 160, Thursday, August 18 (1977).

3. J. D. Wilcox, "Isokinetic Flow and Sampling of Airborne Particulates." Artificial Stimulation of Rain, p. 177 (1957).

4. H. H. Watson, "Erros Due to Anisokinetic Sampling of Aerosols." Am. Ind. Hyg. Assoc. Quart., 15:1 (1954).

5. S. Badzioch, "Collection of Gas-Borne Dust Particles by Means of an Aspirated Sampling Nozzle." Br. J. Appl. Phys., 10:26 (1959).

6. C. N. Davies, "The Entry of Aerosols into Sampling Tubes and Heads." Br. J. Appl Phys., Ser. 2, 1:921 (1968).

7. D. A. Lundgren and S. Calvert, "Aerosol Sampling with a Side Port Probe." Am. Ind. Hyg. Assoc. J., 28(3):208 (1967).

8. S. P. Belyaev and L. M. Levin, "Investigation of Aerosol Aspiration by Photographing Particle Tracks Under Flash Illumination." Aerosol Science, 3:127 (1972).

9. S. P. Belyaev and L. M. Levin, "Techniques for Collection of Representative Aerosol Samples." Aerosol Sci., 5:325 (1974).

10. R. Dennis, W. R. Samples, D. M. Anderson and L. Silverman, "Isokinetic Sampling Probes." Ind. Eng. Chem., 49:294 (1957).

11. A. B. Whiteley and L. E. Reed, "The Effect of Probe Shape on the Accuracy of Sampling Flue Gases for Dust Content." J. Inst. Fuel, 32:316 (1959).

12. H. Glauberman, "The Directional Dependence of Air Samplers." Am. Ind. Hyg. Assoc. J., 23:235 (1962).

13. D. A. Lundgren, M. D. Durham and K. W. Mason, "Sampling of Tangential Flow Streams." Am. Ind. Hyg. Assoc. J., 39:640 (1978).

14. D. W. Baker and C. L. Sayre, "Decay of Swirling Turbulent Flow of Incompressible Fluids in Long Pipes." Flow: Its Measurement and Control in Science and Industry, Volume 1, Part 1, Flow Characteristics, Instrument Society of America (1974).

15. N. A. Chigier, "Velocity Measurement in Vortex Flows." Flow: Its Measurement and Control in Science and Industry, Volume 1, Part 1, Flow Characteristics, Instrument Society of America (1974).

16. K. W. Mason, Location of the Sampling Nozzle in Tangential Flow. M. S. Thesis, University of Florida, Gainesville, Florida (1974).

17. H. A. Hanson and D. P. Saari, "Effective Sampling Techniques for Particulate Emissions from Atypical Stationary Sources." EPA-600/2-77-036, U.S. Environmental Protection Agency, Research Triangle Park, N.C. (1977).

18. E. F. Brooks and R. L. Williams, "Process Stream Volumetric Flow Measurement and Gas Sample Extraction Methodology." TRW Document No. 24916-6028-RU-00, TRW Systems Groub, Redondo Beach, California (1975).

19. D. J. Grove and W. S. Smith, "Pitot Tube Errors Due to Misalignment and Nonstreamlined Flow." Stack Sampling News, November (1973).

20. H. A. Hanson, R. J. Davini, J. K. Morgan and A. A. Iversen, "Particulate Sampling Strategies for Large Power Plants Including Nonuniform Flow." EPA-600/2-76-170, U.S. Environmental Protection Agency, Research Triangle Park, N.C. (1976).

21. F. C. Williams and F. R. DeJarnette, "A Study on the Accuracy of Type S Pitot Tube." EPA 600/4-77-030, U.S. Environmental Protection Agency, Research Triangle Park, N.C. (1977).

22. J. A. Danielson, "Air Pollution Engineering Manual." Environmental Protection Agency, OAQPS,AP40, Research Triangle Park, N.C. (1973).

ELECTROSTATIC EFFECTS ON SAMPLING THROUGH UNGROUNDED PROBES

By:

W. B. Giles and P. W. Dietz
General Electric Company
Mechanical Systems and Technology Laboratory
Corporate Research and Development
Schenectady, New York 12309

ABSTRACT

When a sampling probe is inserted into a particle laden gas stream, the particles can exchange charge with the probe on impact. If the probe is electrically insulated from the duct, large potentials can develop and the resultant electric field can influence the sample by repelling charged particles.

In the present paper, a model is developed for this electrostatic sampling error and experimental data is reported to support the model.

Electrostatic Effects on Sampling Through Ungrounded Probes

INTRODUCTION

The problems associated with sampling charged, particulate suspensions have been highlighted by the development of new and/or improved pollution control technologies which employ electrostatic forces to enhance collection efficiencies. Efficiency measurements on devices such as the charged-droplet scrubber, the electrostatic precipitator, the electrofluidized bed and the electrostatically-augmented fabric filter, require that samples be taken from the charged, particulate suspension. Several of the problems inherent to this process are documented;

- The concentration profile of the dust within the main duct is effected by the extend of charge on the particles. Even in turbulent flow, the concentration is higher near the walls than along the centerline (i.e. Soo (1971)[1], (1964)[2], (1964)[3], (1965)[4]).

- Charged suspensions tend to precipitate along the walls of the sampling lines. Space charge precipitation can reduce the total loading and shift the size distribution (Melcher (1974)[5]).

- The calibration curves of sampling instruments such as impactors and cyclones can be shifted when charged particles are being collected (Cushing et. al. (1978)[6].

In the present article, a new source of sampling error is identified; dust-induced probe voltage. In laboratory experiments involving high voltages, the materials of construction are often electrical insulators. In this case, the potential of the sampling probe can become raised to a level significantly higher than the surrounding ducting. The electric fields which result from this voltage will strongly influence the sampling process.

COLLECTION MODEL

When a sampling probe is electrically insulated from the surrounding ducting, a significant sampling error can result. As the particles pass the probe, some fraction of them impact the walls and exchange charge. The charge that is accumulated on the probe must travel to ground. The only path available for this current is through the insulating probe support. Since this has a high resistance, even small currents can result in appreciable probe voltages. As the probe voltage increases, the electric field around the probe intensifies and the incoming, are repelled. The result is a systematic sampling error.

The present analysis considers a conducting probe of radius R_s in a conducting duct of radius R_t (see Figure 1). The probe is electrically isolated from the ducting by an insulating support which has resistance R. The flow through the duct is at velocity U, and the probe will be assumed to be approximately isokinetic. The particles are assumed to be monodisperss spheres with radius r_p, charge q, mass density ρ_p and number density n.

An electric field in the vicinity of the probe tip will cause the particles to migrate relative to the average fluid velocity with a particle velocity, U_p, which is given by the product of the electrical mobility of the particle, $b = \frac{q}{6\pi\mu r_p}$, and the electric field, E, as

$$U_p = U - bE \tag{1}$$

Thus, the ratio of what is actually sampled to what would be sampled if charges were not present (β) is given by

$$\beta = \frac{U - bE}{U} \tag{2}$$

and the sampling error is

$$\text{Error} = |\beta - 1| = \frac{bE}{U} \tag{3}$$

The current to the probe is composed of two components: the current due to particles impacting the exterior of the probe and that due to the sampled particles. For most probes, the component of current impacting the probe will be dominant and is given by

$$i = U\pi A\alpha n(\Delta q) \tag{4}$$

where A is the cross-sectional area of the probe presented to the flow, Δq is the charge transfer per particle impact with the probe and α is the fraction of incoming particles that impact the probe. The collection parameter, α, is a function of particle size and density, probe size, electric field, gas velocity and viscosity (Tardos et. al. (1978)[7], Gutfinger and Tardos (1978)[8], Nielsen and Hill (1976)[9], Nielsen and Hill (1976)[10]).

The voltage of the probe relative to the duct wall is

$$V = iR \tag{5}$$

The electric field in the vicinity of the leading edge of the probe can be approximated by that of a sphere of radius R_s. Thus, the electric field is given by

$$E = \frac{CV}{4\pi\varepsilon_o R_s^2} \tag{6}$$

where C is the capacitance of the sphere relative to ground. If the diameter of the probe is small compared to that of the duct, then the capacitance of probe is that of an isolated sphere

$$C = 4\pi\varepsilon_o R_s \tag{7}$$

where ε_o is the permittivity of free space.

Thus

$$E = \frac{V}{R_s} \tag{8}$$

and the sampling error is

$$\text{Error} = \gamma \tag{9}$$

where

$$\gamma \equiv \pi b R \frac{A}{R_s} \alpha n \Delta q \tag{10}$$

Also, the probe voltage is given by

$$V = \frac{U R_s \gamma}{b} \tag{11}$$

EXPERIMENTS

A 1/8-inch diameter sampling probe was centrally located within a 5-inch diameter galvanized duct. The probe was electrically isolated from the duct by a plexiglas spacer. Preclassified (4-8μ) A.C. Fines were introduced upstream by a blown bed. A Sedigraph (5000 D) analysis of these test particles was performed and the results are shown in Figure 2.

The experiments consisted of sampling 0.1 cfm for Royco analysis. With the duct grounded and the probe flating, repeatable data were obtained for the size distribution (see Figure 2) independent of the flow rate. However, this differed significantly from the Sedigraph results.

When the probe is electrically connected to the duct, the results agreed with the Sedigraph (see Figure 2). If the probe and duct were raised to a high potential together, no shift in the size distribution was observed.

Typical dust loadings for these tests was 0.02 - 0.05 grains/ft^3.

Probe voltages were observed to be of the order of 200 volts at 720 cfm. These voltages increased with increasing flow rate or increasing dust loading.

DISCUSSION

A model has been developed in this paper for the error in the number of particles that are sampled from monodisperse, charged, particulate suspension. While this result cannot be directly applied to the results of the Royco analysis, several features of the model warrant discussion.

- Inertial interception of particles by the probe is characterized by the Stokes number (Tardos et. al. (1978)[7], Gutfinger and Tardos (1978)[8]).

$$St = \frac{2\rho_p U r_p^2}{9\mu R_s}$$

where ρ_p is the density of particle, r_p is the radius of the particle and μ is the gas viscosity. For the range of flows considered here, the Stokes number is greater than one and, thus, the impaction parameter is approximately unity. In this regime, Equation 9 predicts that the sampling error will be independent of flow rate. This result is in agreement with data (see Figure 2).

- In the absence of experimentally measured values of the particle charge, typical values can be computed from the formula for the saturation charge of a particle in a uniform field (Whipple and Chalmers (1944)[11]).

$$q_s = 12\pi\varepsilon_o r_p^2 E_c$$

where $E_c \approx 10^6$ V/m. Using a mean particle diameter of 6μ (see Figure 2), a dust loading of 0.04 grain/ft^3, and typical resistances of between 10^{10} and 10^{12}, sampling errors of between 0.3 and 30% are predicted. Obviously, since several of the key variables are not known to better than an order of magnitude, this result is somewhat arbitrary. Nonetheless, this result does bracket the errors observed in experiments.

- Equation 11 predicts that the probe voltage will increase with flow rate. This result is also supported by experiments.

- The Royco data in Figure 2 indicates that when electrostatic effects are present, all particles greater than 15μ are excluded from the probe. Since this represents approximately 1% of the particles (by number), the error is approximately 0.01. Substituting this value of γ into Equation 11 yields a probe voltage of 170 volts for a flow rate of 720 cfm. This result compares well with the 200 volts measured in the lab.

- The probe voltage increases with increasing dust loading as predicted by Equation 11.

- Voltage effects due to space charge were neglected. If a probe is used to sample a dense, charged particulate suspension, electric fields resulting from the space charge can distort the sample.

- Since the charge on particles is typically proportional to the square of the radius, the largest particles will have the highest mobility. Thus, in a polydispersed system, one would expect the largest error to appear for the larger particles. Data presented in Figure 2 support this statement.

CONCLUSION

Sampling of electrically charged particles is found both by analysis and

by experiment to be susceptible to large errors. The magnitude of these potential errors are such that seriously erroneous assessments of particulate control equipment could result. The procedure for avoiding these errors, once identified, is simple: ground the probe to the ducting. It is not sufficient to ground the probe without also grounding the duct.

ACKNOWLEDGEMENT

This work was supported by the U. S. Department of Energy under Contract No. EX-76-C-01-2357 issued by the Fossil Energy Program. George C. Weth of BOE/FE is gratefully acknowledged as the program editor.

REFERENCES

1 S. L. Soo, "Dynamics of Charged Suspension" in International Reviews in Aerosol Physics and Chemistry, Vol. 2, ed. G. M. Hidy and J. Brock Pergamon Press, New York (1971).

2 S. L. Soo, G. J. Trezek, R. C. Dimick and G. F. Hohnstreiter, "Concentration and Mass Flow Distributions in a Gas-Solid Suspension" I&EC Fundamentals 3(2), 98 (1964).

3 S. L. Soo, "Effect of Electrification on the Dynamics of a Particulate System" I&EC Fundamentals 3(1), 75 (1964).

4 S. L. Soo, "Dynamics of Multiphase Flow Systems", I&EC Fundamentals, 4(4), 426 (1965).

5 J. R. Melcher and K. S. Sachar, "Charged Droplet Scrubbing of Submicron Particulate" Environmental Protection Seires EPA-650/2-74-075 (1974).

6 K. M. Chushing, W. Farthing, L. G. Felix, J. D. McCain, W. B. Smith, "Particulate Sampling Support: 1977 Annual Report" Interagency Energy-Environment Research and Development Program Report EPA-600/7-78-009 (1978).

7 G. I. Tardos, N. Abuaf and C. Gutfinger, "Dust Deposition in Granular Bed Filters: Theories and Experiments," J. APCA 28(4), 354 (1978).

8 C. Gutfinger and G. I. Tardos, "Analytical and Experimental Studies on Granular Bed Filtration" EPA Symposium on the Transfer and Utilization of Particulate Control Technology, paper C6/4, Denver (1978).

9 K. A. Nielsen and J. C. Hill, "Collection of Inertialess Particles on Spheres with Electrical Forces" I&EC Fundamentals 15(3) 149 (1976).

10 K. A. Nielsen and J. C. Hill, "Capture of Particles on Spheres by Inertial and Electrical Forces" I&EC Fundamentals 15(3), 157 (1976).

11 F. J. W. Whipple and J. A. Chalmers, "On Wilson's Theory of the Collection of Charge by Falling Drops", Roy. Met. Soc. London Quart. Journal 70, 103 (1944).

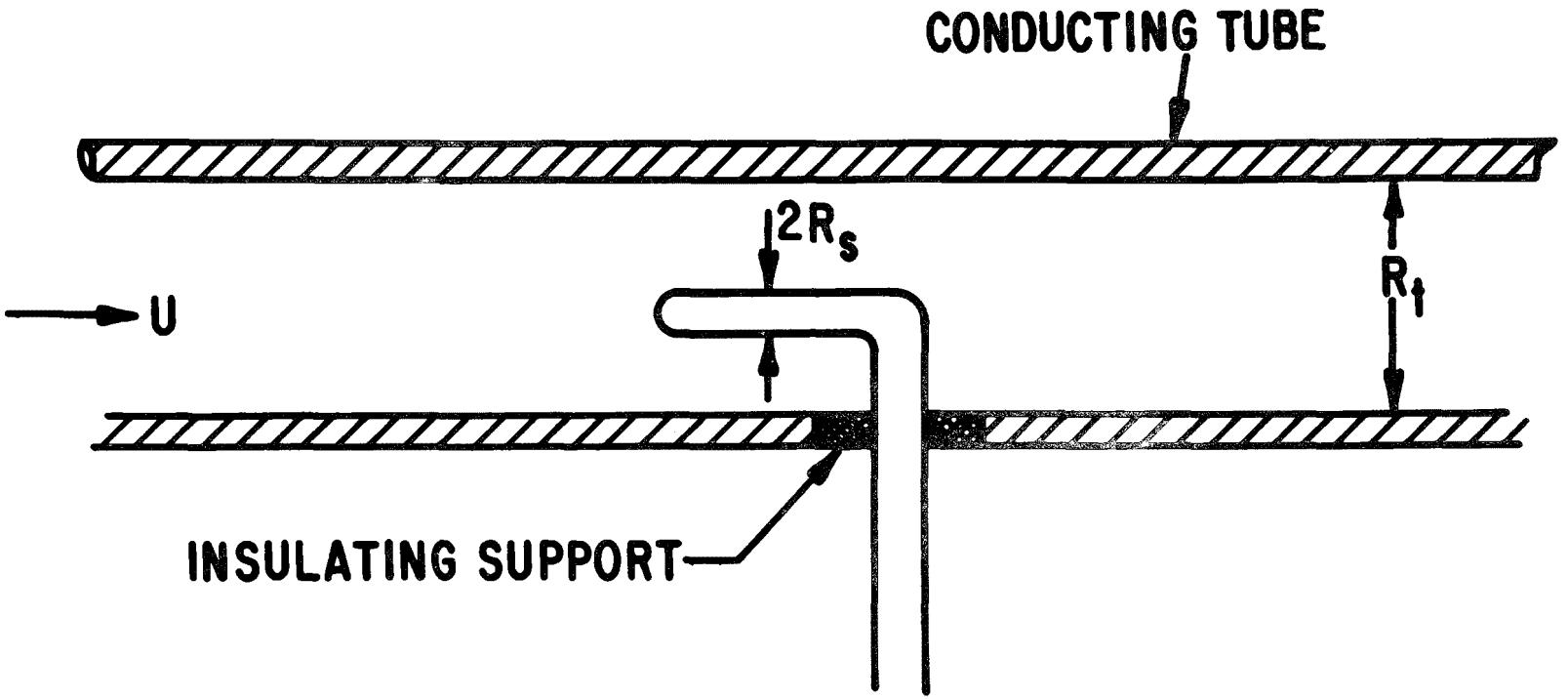

FIGURE 1 SIMPLIFIED DUCT/TUBE GEOMETRY USED FOR ANALYSIS

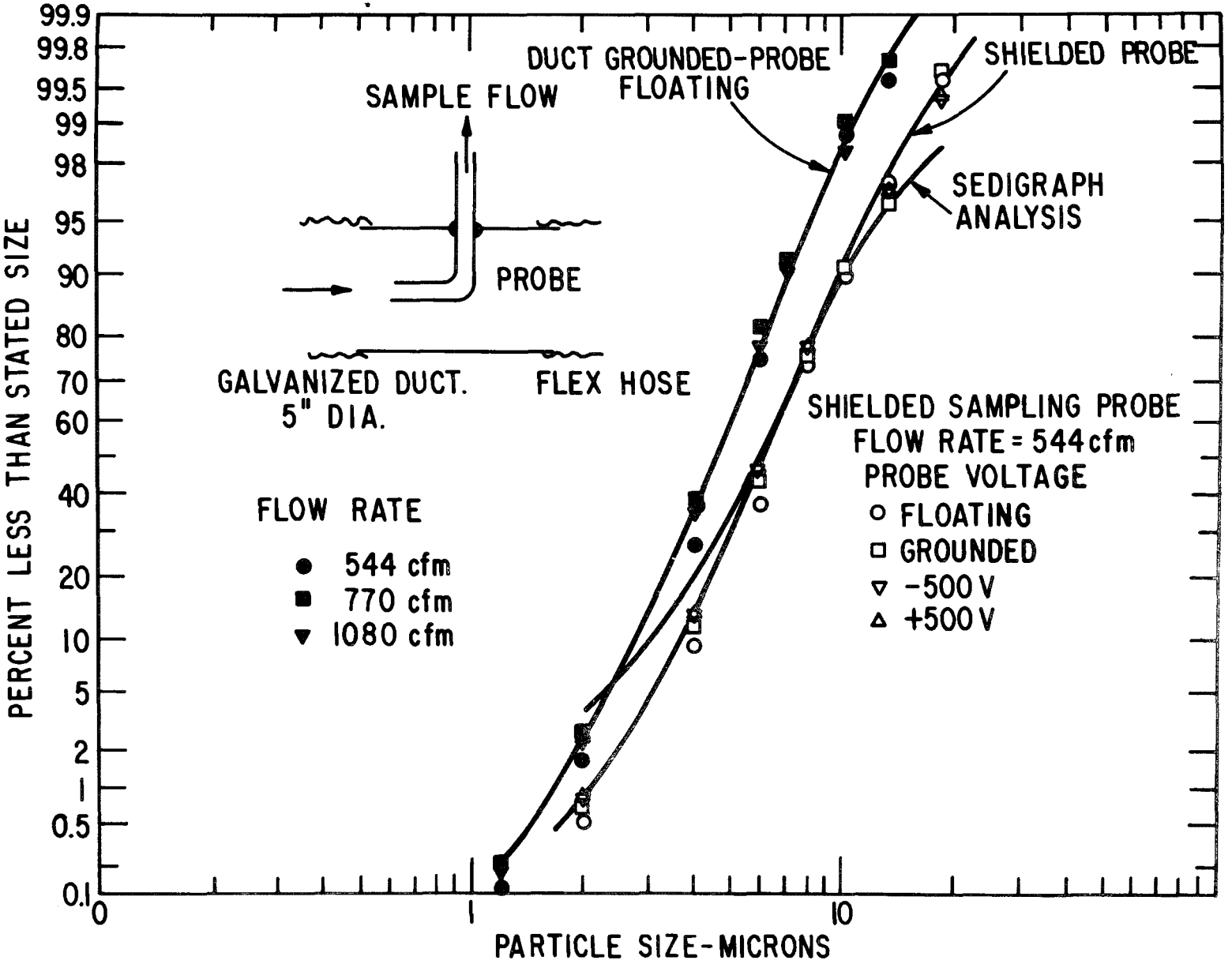

FIGURE 2 INFLUENCE OF ELECTROSTATICS ON SAMPLING USING 4-8 μA.C. FINES

OPTICAL PARTICULATE SIZE MEASUREMENTS USING A SMALL-ANGLE NEAR-FORWARD SCATTERING TECHNIQUE

By:

James C. F. Wang
Combustion Research Division 8353
Sandia Laboratories, Livermore, CA 94550

ABSTRACT

Techniques for measuring particle size distributions in the range of 1 to 50 μm based on light scattering principles were reviewed and examined to define appropriate diagnostic tools for applications in combustor environments of advanced power systems. Light scattering at forward small angles (1 to 5°) was identified as one of the most promising optical techniques based on a systematic theoretical investigation using Mie calculations. To verify the theoretical predictions, a laboratory bench experiment was initiated in this near-forward small-angle configuration using monodispersed and polydispersed particles of known physical properties of different refractive indices and sizes.

I. INTRODUCTION

Fundamental to the use of coal and alternate fuels is the achievement of combustor effluent cleanup to meet environmental regulations, gas turbine product specifications, and other quality standards set by commercial and industrial users. Particulate emission control is one of the most challenging tasks in recent developments of advanced fossil fuel combustion systems. The lack of accurate, real-time particulate diagnostic techniques for the combustion systems is a major complicating factor in the development of these advanced power systems and cleanup processes. The need for appropriate particulate diagnostics for fossil fuel combustion systems is urgent and necessary, especially those with capabilities of non-intrusive, in-situ, and real-time monitoring. Particle size distribution, mass loading density, and other critical physical and chemical properties of the particulates in the effluent of combustors and/or cleanup equipment comprise the key information needed to guide the development of advanced power systems.

Presently, the particle diagnostic techniques can be grouped into three categories: (1) physical sampling, (2) optical scattering, and (3) photographic techniques. The physical sampling technique has been used extensively by users in industry and with utility companies to characterize the effluents from their boilers or furnaces. It is the only means of providing collected samples of particles for the detailed analyses of their physical and chemical properties. The measurements obtained from the physical sampling methods, however, may be biased or dubious because of the inherent shortcomings associated with the sampling process. (Vitols (1966)[1]) For example, it is intrusive and requires off-line data analyses. The sample collected may not represent what is in the measured flow. Thus, a real-time, non-intrusive, and in-situ particulate diagnostic technique is required to complement the measurements by the physical sampling technique and even to replace it in some applications.

In principle, both optical and photographic (including holographic) techniques can provide non-intrusive measurements of particle size and/or mass loading density. The photographic methods, however, also require off-line data analysis which is usually tedious and time consuming. (Holtham (1974)[2]) To obtain real-time monitoring capability, the optical techniques appear as the most promising candidates. There are, however, many assumptions and statistical interpretations involved in relating the measured optical signal to the size and number density of the particles. The accuracy of the measurements by optical

methods depends on how much is known a priori about the particulates and the flow environment and how good are the assumptions related to a particular application. The high-temperature, high-pressure, and high-dust-loading conditions encountered in almost every fossil fuel combustion system provide further challenges to the designers of optical particle counters for real-time, in-situ measurements.

The objective of this paper is to concentrate on surveying various optical scattering characteristics and their applicability to the broad range of particle size, chemical composition, and mass loading density generally encountered in an advanced fossil fuel combustion system. Single particle scattering measurement is emphasized because it can provide accurate size distribution information instead of mean size only. A bench scale experiment based on the small-angle near-forward scattering principle is described. One should keep in mind, however, that there is no single instrument expected to satisfy the entire size or composition range of interest or applications anticipated.

II. LIGHT SCATTERED BY A SPHERE

When light strikes a particle, a portion of the light energy is absorbed and the rest is scattered by the particle or its surface irregularities. The extent of the absorption and scattering depends on the wavelength of the incident light, λ, and the nature of the particle (e.g., refractive index m, radius r, and shape). For a sphere of radius comparable or large relative to the wavelength of the incident light, the light scattering pattern can be predicted by Mie theory. (Mie(1908)[3]) The Mie function is an exact solution to Maxwell's wave equation for the scattering of electromagnetic radiation by a spherical particle. It consists of a series of spherical harmonic terms with the coefficients containing the refractive index and size parameter, $\alpha = 2\pi r/\lambda$, of the particle.

For unit intensity incident light polarized in the directions perpendicular or parallel to the scattering plane, the expressions for the scattered light intensity respectively, are:

$$I_1 = \frac{\lambda^2}{4\pi^2 r^2} \left|S_1(\theta, m, \alpha)\right|^2 \sin^2\phi \quad , \tag{1}$$

$$I_2 = \frac{\lambda^2}{4\pi^2 r^2} \left|S_2(\theta, m, \alpha)\right|^2 \cos^2\phi \quad , \tag{2}$$

where S_1 and S_2 are complex amplitude functions of the Mie scattering functions and are sums of spherical Bessel functions of the first and second kind. A sketch of the Mie scattering geometry is shown in Figure 1. The scattering plane is the plane containing the incident light ray (direction of propagation) and the scattering vector; ϕ is

the azimuthal angle measured from the plane of polarization to the scattering plane and θ is the scattering angle measured from the direction of propagation to the direction of observation in the scattering plane. The Mie theory is quite general in that it is applicable on the one hand to particles in the Rayleigh region ($r<<\lambda$) and on the other hand to large particles up to the size where classical geometric optics can be applied. It is applicable to both absorbers and dielectrics.

For very small particles ($r < 0.1\ \lambda$), the Mie function simplifies to yield the Rayleigh equation (Van de Hulst (1957)[4]). It is usually written in the following form for unpolarized light as,

$$I = \frac{8\pi^4}{R^2} \frac{m^2-1}{m^2+2} \frac{r^6}{\lambda^4} (1 + \cos^2 \theta) \quad , \tag{3}$$

where I is the intensity of light scattered by a sphere of radius r at an angle θ to the incident light beam. R is the distance from the particle to the point of observation. I is composed of two polarized components with intensities I_1 and I_2. Figure 2 shows a typical Rayleigh scattering pattern from a particle of 0.1 μm diameter. The intensity of the vertical polarized light, I_2, is the first term in the last bracket and represents a uniformly distributed pattern from 0° to 360°. The intensity of the horizontal polarized light, I_1, peaks in the forward (0°) and the back (180°) scattering directions and is zero at 90°. The Rayleigh scattering intensity shows a sixth power dependence on the radius of the particle. As the size of the particle decreases, the scattered light becomes undetectable very quickly. Thus, scattering from a group of these small particles has to be used instead of the scattering from a single particle.

III. CHARACTERISTICS OF LIGHT SCATTERING PHENOMENA

The scattering intensity from particles is a function of the wavelength of the incident light and characteristics of the particle such as its refractive index, size, and shape. The Mie function provides a quite general theoretical prediction of the scattering intensity from spherical particles. By using the Mie scattering function as a reference and employing proper calibration with known particles, one can use the light scattered from a medium as a means to obtain information about the state of the medium, such as the size of the discrete particles in the medium. There are, however, many assumptions and statistical interpretations involved in relating the measured scattering intensity to the size of the particle. One instrument may be useful in one application, but not so useful in others. In order to select an appropriate light scattering optical arrangement for a specific application, the characteristics and limitations of the light scattering phenomena have to be understood. Some of the observations based on the calculated results from Mie function are summarized

in the following paragraphs.

A typical Mie scattering pattern is shown in Figure 3 for a sphere of 2 μm diamter and incident light wavelength of 0.647 μm. It is an absorbing particle with refractive index, m = 1.56 - 0.62i which represents a soot-like material. The oscillatory pattern in the forward direction varies as a function of the size, shape, orientation, and refractive index of the particle. For non-absorbing particles, the oscillatory pattern exists also in the backscattering direction (Figure 4). This pattern is called Tyndall spectra and has been used as a means to determine the size of the particle. (Sinclair and LaMer (1949)[5]) This becomes impractical for particles of a broad range of chemical composition, shape, and number density.

Another well-known characteristic of the Mie scattering response at a fixed angle is its oscillatory behavior vs. particle size. Figure 5 shows a typical Mie response curve for a monochromic light scattered from soot-like particles in the range of 0.3 to 100 μm. The nonunique relation between the scattered light intensity and the size of the particle is attributed to the diffraction phenomena from a monochromic light source. A much smoother response curve will be obtained from a white light source or a light source with combination of some preferable wavelengths. The response curve can also be smoothed via spatial integration of the scattered light over the solid angle subtended by the collector. Examples of multiple wavelengths and spatial integration on the Mie scattering response curve are discussed in Section IV. The Mie scattering response curve at a fixed angle is a strong function of the refractive index of the particles, except inside the forward Fraunhfer diffraction lobe close to the incident light direction.

The scattered light intensity from a particle depends on the intensity of the incident light at the location of the particle. The intensity of a well collimated white light beam or a laser usually has a Gaussian distribution across the cross section of the beam. If only the average incident light intensity is monitored, the scattered light intensities measured from a small particle at the center of the beam (high incident intensity region) and a large particle at the edge of the beam (low incident intensity region) will be similar. Thus, a serious ambiguity in particle size determination based on the absolute scattered intensity is introduced. This is called the "edge effect" or "non-uniform intensity" ambiguity. An illustration of the edge effect is shown in Figure 6. Without proper correction for this effect, the measurement accuracy on particle sizes cannot be defined. Various means for overcoming this ambiguity have been proposed and exercised in some applications. If one uses the intensity ratio arrangement (Hodkinson (1966)[6]), the local incident light intensity will be cancelled and the measurement will become independent of the incident light edge effect. A two-spot or donut-shaped incident light source has been suggested to provide a check on those particles passing through the

center of the light beam (uniform intensity region), thus minimizing the edge effect ambiguity. (Foxvog (1977)[7]) For simple scattered light intensity measurements, an inversion procedure can be used to deconvolute the measured scattered light histogram based on the geometry of the optics and light intensity distribution, and thus obtain a more accurate particle-size histogram. (Holve and Self (1979)[8])

Another problem arises because the Mie scattering function is derived for a spherical particle, whereas in most fossil fuel combustion environments, particulates are irregularly shaped with random orientation. The particle composition is generally unknown and sometimes varies with time. If a particle counter is designed based on the Mie scattering response curve of particles with a fixed refractive index and a calibration using a few standard particles, it may not provide accurate measurements in the combustor exhausts. Theoretical predictions similar to the Mie function have not been established for irregular shaped particles. Recently, limited calculations on spheroid particles were reported (Latimer, et al (1978)[9]) and showed a strong dependence of the scattering pattern on the shape and orientation of the spheroid. Fortunately, isometric particles (i.e., with no great inequality between their different dimensions) of many shapes have scattering patterns similar to spheres of equal volume. (Hodkinson (1966)[10]) In addition, scattered light intensity inside the forward Fraunhofer diffraction lobe is recognized as being least sensitive to the shape and orientation of the particles. (Ellison (1957)[11], Hodkinson (1963)[12])

IV. SMALL-ANGLE NEAR-FORWARD SCATTERING (SANFS) EXPERIMENT

Based on discussions in Section III, light scattered within the forward Fraunhofer diffraction lobe is found least sensitive to the refractive index and shape of the particle. Typical computed Mie scattering responses for spheres in the range of 0.3 to 100 μm diameter at 2° from the forward direction are shown in Figure 7. For both nonabsorbing and absorbing particles, the scattering responses agree closely. The inherent Mie scattering oscillation in the response curves begins at about 20 μm diameter particles and limits the useful range of this optical arrangement to less than 5 μm. The amplitude of this oscillatory response can be reduced and the useful size range for particle measurements can be extended by using a large collection lens and a multiwavelength light source. Figure 8 shows computed Mie scattering responses for a detector with collection angle covering 0.57° to 5.7° in the forward direction. A light trap is assumed at the center of the collection lens to stop the incident laser light from entering the photodetector. By introducing three wavelengths from a typical argon/krypton ion laser, namely 0.647, 0.514, and 0.488 μm, the Mie scattering responses are further smoothed as shown in Figure 9. A nearly monotonic relation between the scattered light intensity and the particle diameter up to 100 μm can be approximated.

Based on the calculations shown in Figures 8 and 9, a bench scale

experiment has been assembled at Sandia to test the concept of this small-angle near-forward scattering arrangment (SANFS). A schematic of the experiment setup is shown in Figure 10. A 5-mW He-Ne laser is used as the light source. A beam expander and focusing lens combination is designed to focus the laser beam to approximate 40 μm diameter at the measurement volume. The incident beam intensity I_0 is monitored by a photodiode from the light split at the beam splitter.

The collection optics consist of a F/10 collection lens, a 10 mm diameter mirror mounted at the center of the lens, and two photodetectors. The mirror at 45° to the incident beam direction is used as the light dump for the scattering detector. One of the photodetectors measures the reflected incident light from the 10-mm mirror and provides information on the attenuation of the incident light, I_A. The other photodetector measures the collected scattered light in the small-angle near-forward direction (0.57° to 2.86°). A 100-μm-diameter aperture is used in front of the scattering light photodetector to reduce the depth of view along the laser beam at the focal point to about 500 μm length. This allows the single-particle counting capability of the SANFS optical arrangement to be extended to a number density in the flow of 10^6 particle/cm^3.

A block diagram of the data acquisition and analysis procedure is shown in Figure 11. The essential data management center is the PDP11/34 minicomputer. The measured intensities of the incident and the attenuated light, I_0 and I_A, respectively, are stored in the memory of the minicomputer via a constant A/D sampling process. The ratio I_A/I_0 is computed and stored continuously with the light scattering data. The signatures of the scattering light from particles passing through the measuring volume are detected by an RCA 33000A photomultiplier and digitized by a Nicolet Model 204 digital scope. The digitized signatures are then transferred to the minicomputer which constructs histograms of the ratio of signature pulse height to incident light and the particle transient time (pulse width of the particle signature). The histogram of particle size is constructed by deconvoluting the measured laser beam incident intensity distribution at the measuring volume from the pulse height histogram. (8) Particle velocity is obtained from the histogram of the particle transient time.

Parallel to the Nicolet digital recording of the particle signature in real-time, a Traco Northern pulse-height analyzer is used to establish a pulse height histogram of particle signatures on-line. This is used as a real-time particle-size distribution monitor. The actual particle size information can be obtained by storing the pulse-height histogram on the PDP11 minicomputer and processing the data through the same deconvolution procedure for the Nicolet scope recorded data off-line.

Two monodispersed particle generators are used as the calibrated particle source for the bench test. The TSI-model 3050 Berglund-Liu

Vibrating orifice aerosol generator provides monodispersed liquid droplets of 10 to 40 μm and solid particles of 1 to 10 μm. The PMS-Model PG-100 particle generator can produce monodispersed latex polystyrene particles at low number density in the range of 0.05 to 3 μm. Combination of these two generators can provide a wide range of particles of different sizes and compositions to verify the Mie scattering responses of the SANFS optical arrangment.

An atmospheric combustor exhaust simulator (ACES) facility is being constructed as the test bed for the SANFS optical arrangement. A schematic of the facility is shown in Figure 12. It is designed to provide a high-temperature atmospheric pressure air flow up to 1200°C and 60 m/s. Particulates from the Exxon Miniplant Pressurized Fluidized Bed demonstration facility will be injected into the hot air stream to provide a particle laden flow environment. Windows are provided on ACES for optical diagnostic tests. An isokinetic sampling system will be installed immediately downstream from the optical section to collect dust samples for detailed analyses on the particulates. Comparison of the measurements from the SANFS detector and those from the isokinetic sampling system will be used as the means to evaluate the performance of the SANFS arrangement.

V. CONCLUSIONS

Particulate diagnostics using the optical light scattering principle can provide an on-line real time monitoring of particle size distributions in the combustion systems. For a medium with particles of a broad range of size, shape, composition, and mass loading density such as those generally encountered in a fossil fuel combustion system, the small angle near forward scattering arrangement appears to be the most appropriate candidate among various optical arrangements. The Mie scattering response is found least sensitive to the refractive index of the particle within the forward Fraunhofer diffraction lobe. By introducing a multiwavelength light source and an on-axis collection lens, the scattering light response becomes a reasonably smoothed monotonic curve based on Mie theory calculation. A bench test experiment for the small angle near forward scattering optical arrangement is currently underway to verify the calculated Mie scattering response. The feasibility test for the fossil fuel combustion applications in the atmospheric combustor exhaust simulator is scheduled after the present bench test experiment.

REFERENCES

1. Vitols, V., "Theoretical Limits of Errors Due to Anisokinetic Sampling of Particulate Matter," J. Air Pollution Control 16, 79 (1966).

2. Holtham, G. A., "Sizing Aerosals in Real Time By Pulsing UV Laser Machine," in The Proceedings of a Seminar on Aerosal Measurements, edited by W. A. Cassatt and R. S. Maddock, (NBS Special Publication 412), p. 97 (1974).

3. Mie, G., "Beitrage Zur Optik Truber Medien Speziell Kolloidaler Mattalosungen," Ann. der Physic, 28, 377 (1908).

4. van de Hulst, H. C., Light Scattering By Small Particles, John Wiley & Sons, Inc., New York, NY (1957).

5. Sinclair, D. and La Mer, V. K., "Light Scattering As a Measure of Particle Size in Aerosals," Chem. Rev., 44, 245 (1949).

6. Hodkinson, J. R., "Particle Sizing by Means of the Forward Scattering Lobe," Appl. Optics, 5, 839 (1966).

7. Faxvog, F. R., "New Laser Particle Sizing Instrument," International Automotive Engineering Congress and Exposition, Detroit, MI, (Feb. 28-March 4, 1977), paper 770140 (1977).

8. Holve, D. and Self, S., "An Optical Particle-Sizing Counter for In-Situ Measurements," Appl Optics, 18, 1632 (1979).

9. Latimer, P., Brunsting, A., Pyle, B. E., and Moore, C., "Effects of Asphericity on Single Particle Scattering," Appl Optics, 17, 3152 (1978).

10. Hodkinson, J. R., "The Optical Measurement of Aeosals," Aerosol Science, Chap. X, edited by C. N. Davis, Academic Press, New York, NY (1966).

11. Ellison, J., McK., "Extinction of Light By Suspension of Silica," Proc. Phys. Soc., B70, p 102 (1957).

12. Hodkinson, J. R., "Light Scatterings and Extinction by Irregular Particles Larger than the Wavelengths," Proc. Interdisciplinary Conf. Electromagnetic Scattering, p. 87, edited by M. Kerker, Pregammon Press, Oxford (1963).

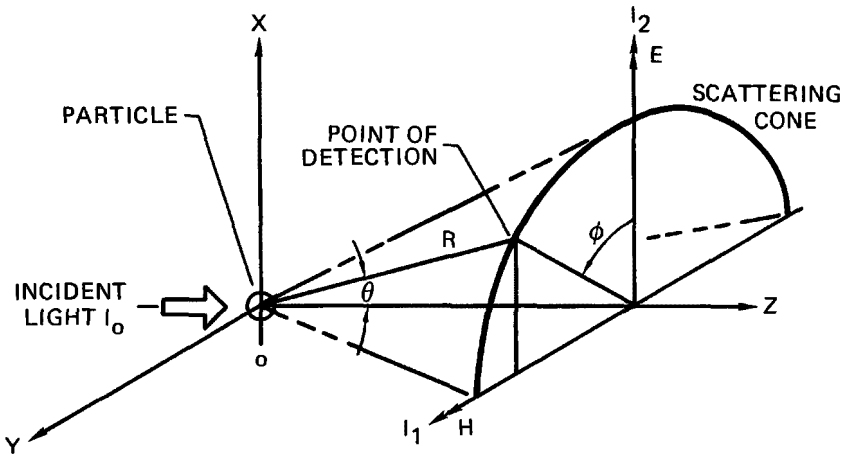

Figure 1. Schematic Of Light Scattering Geometry

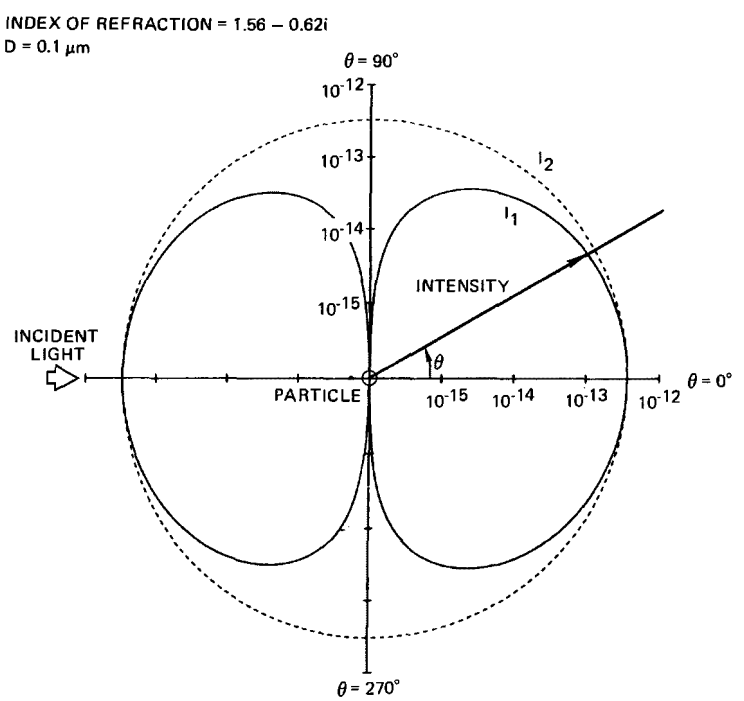

Figure 2. Typical Rayleigh Scattering Intensity Pattern (λ = 0.647 μm)

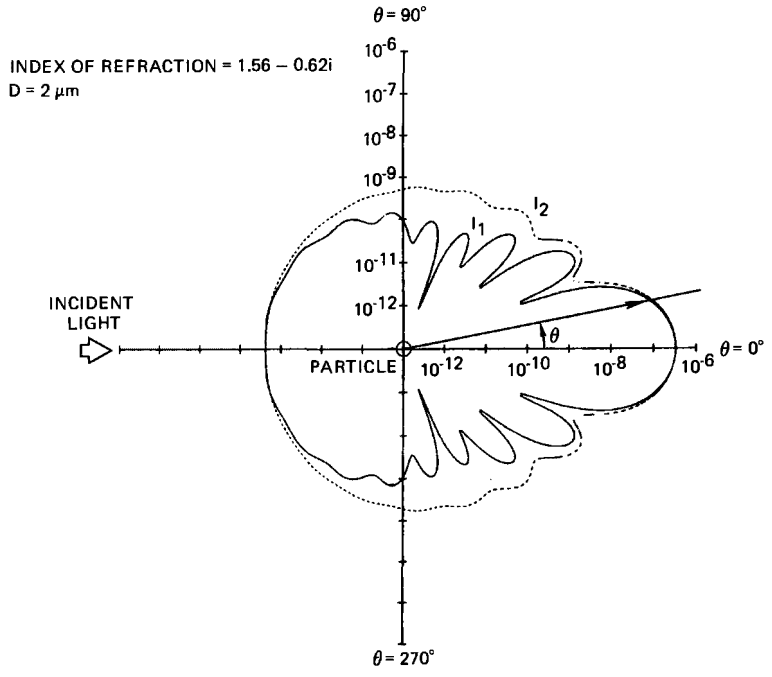

Figure 3. Typical Mie Scattering Intensity Pattern From An Absorbing-Sphere (λ = 0.647 μm)

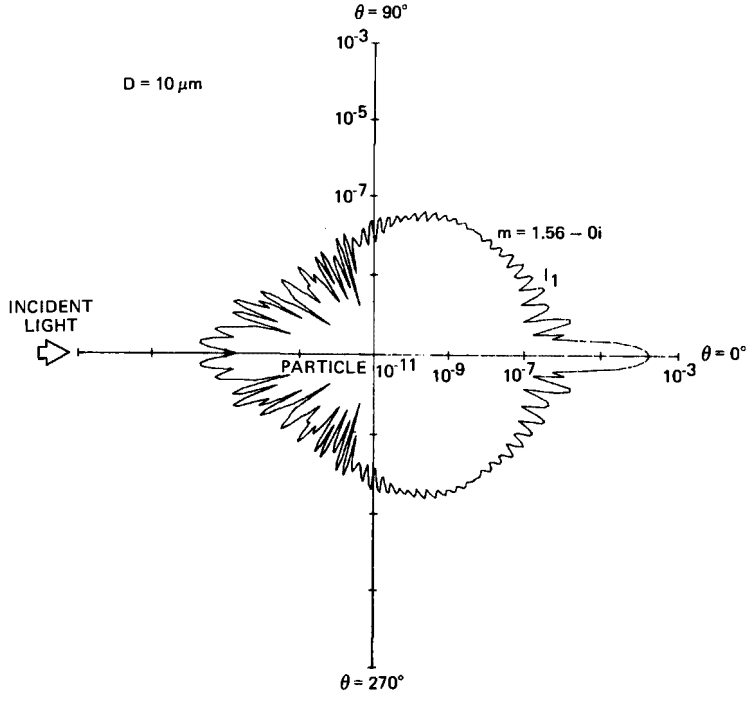

Figure 4. Typical Mie Scattering Intensity Pattern From A Nonabsorbing Sphere (λ = 0.647 μm)

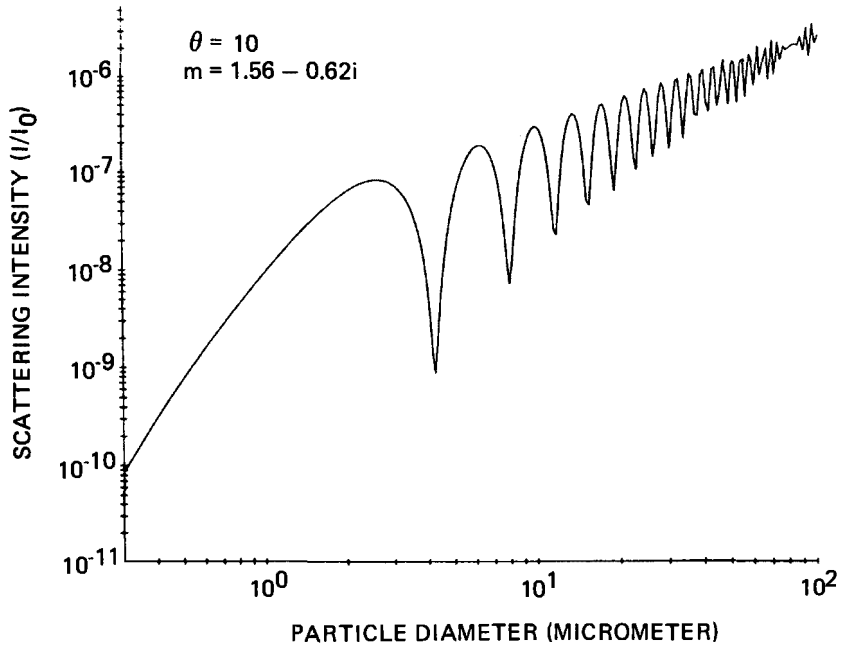

Figure 5. Typical Oscillatory Response Curve of Mie Scattering With Respect to Particle Size (λ = 0.647 μm)

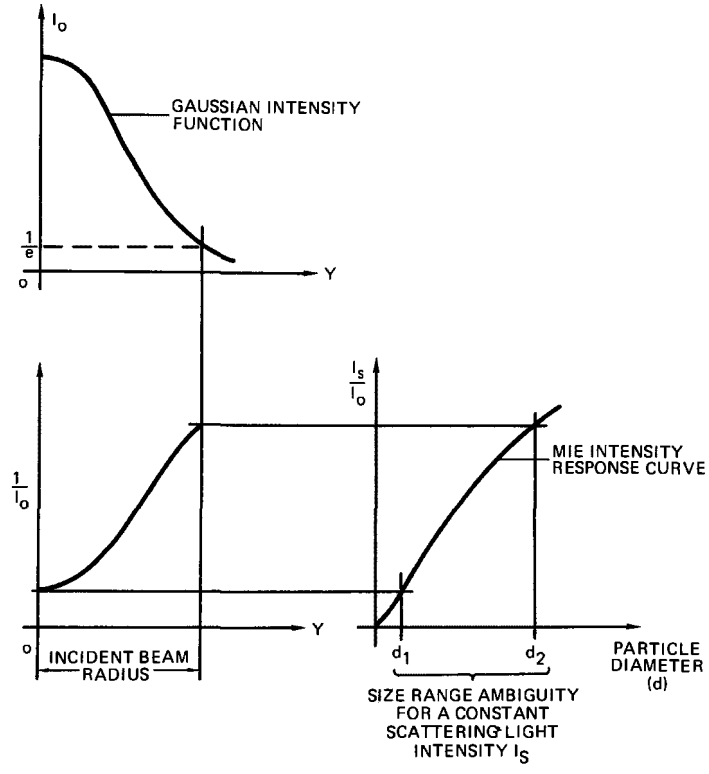

Figure 6. Illustration of Size Ambiguity Due To Nonuniform Incident Beam Intensity

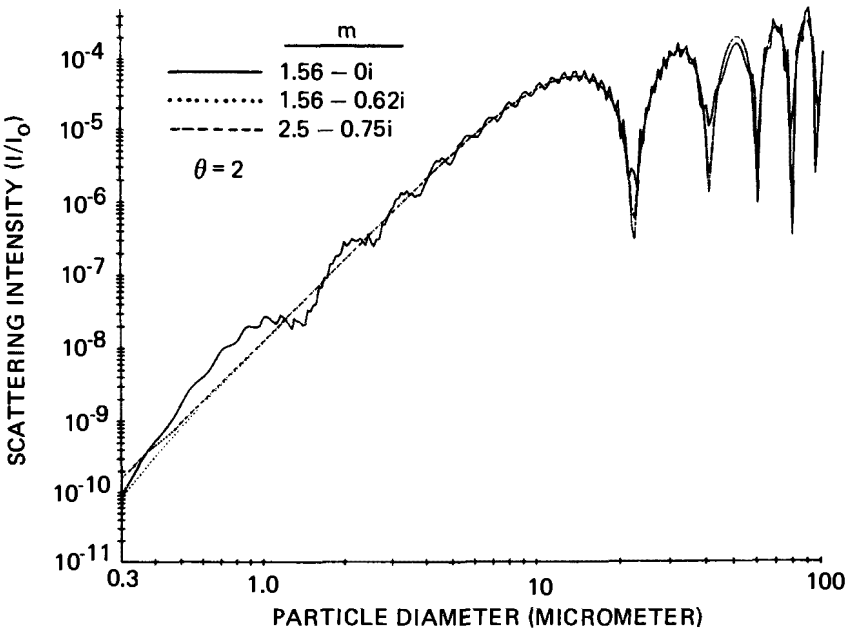

Figure 7. Calculated Mie Scattering Response Curve at Θ = 2° and λ = 0.647 μm

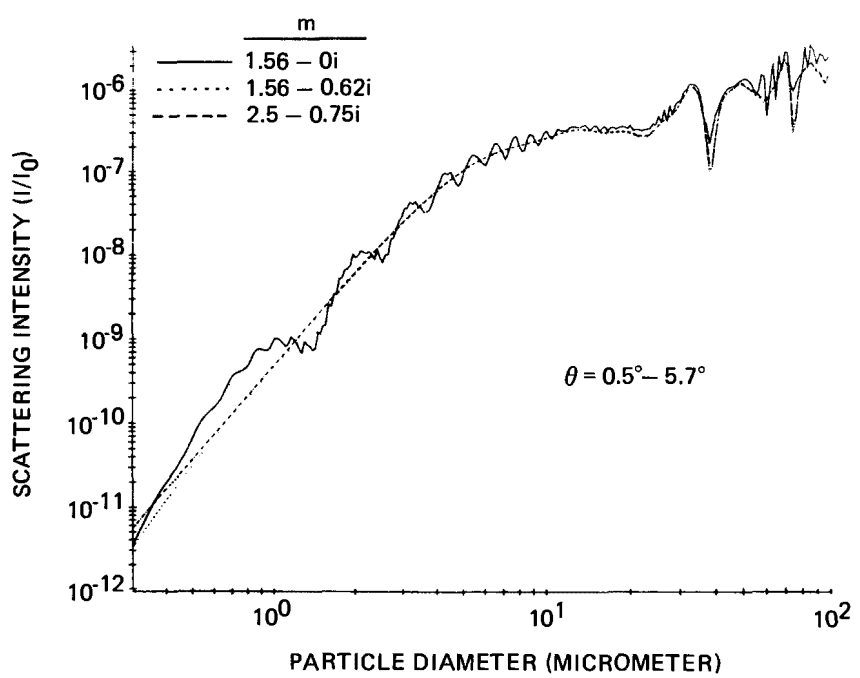

Figure 8. Calculated Mie Scattering Response Curve At Small-Angle Near-Forward Direction and λ = 0.647 μm

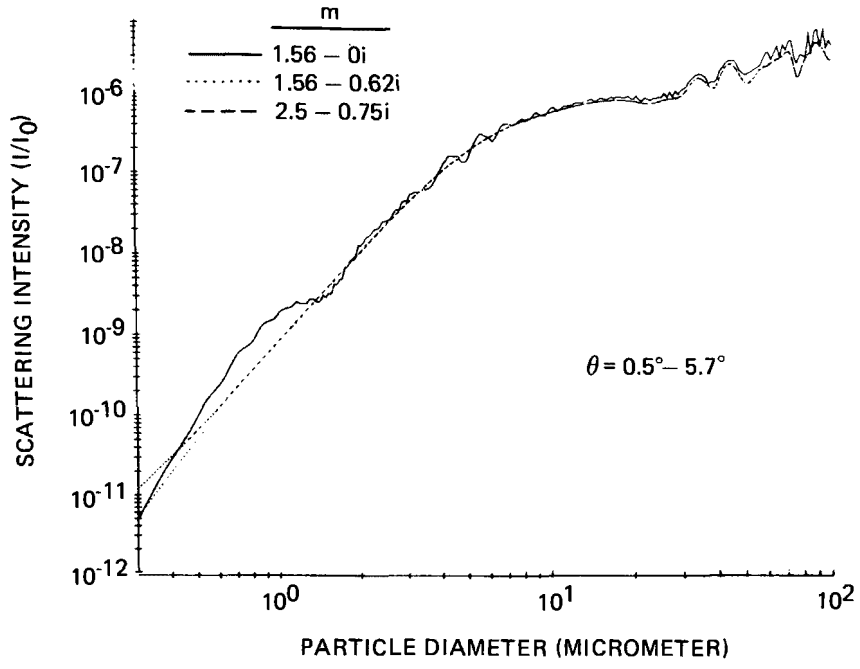

Figure 9. Calculated Mie Scattering Response Curve At Small-Angle Near-Forward Direction Using Three Wavelengths (λ = 0.647, 0.5145, and 0.488 μm)

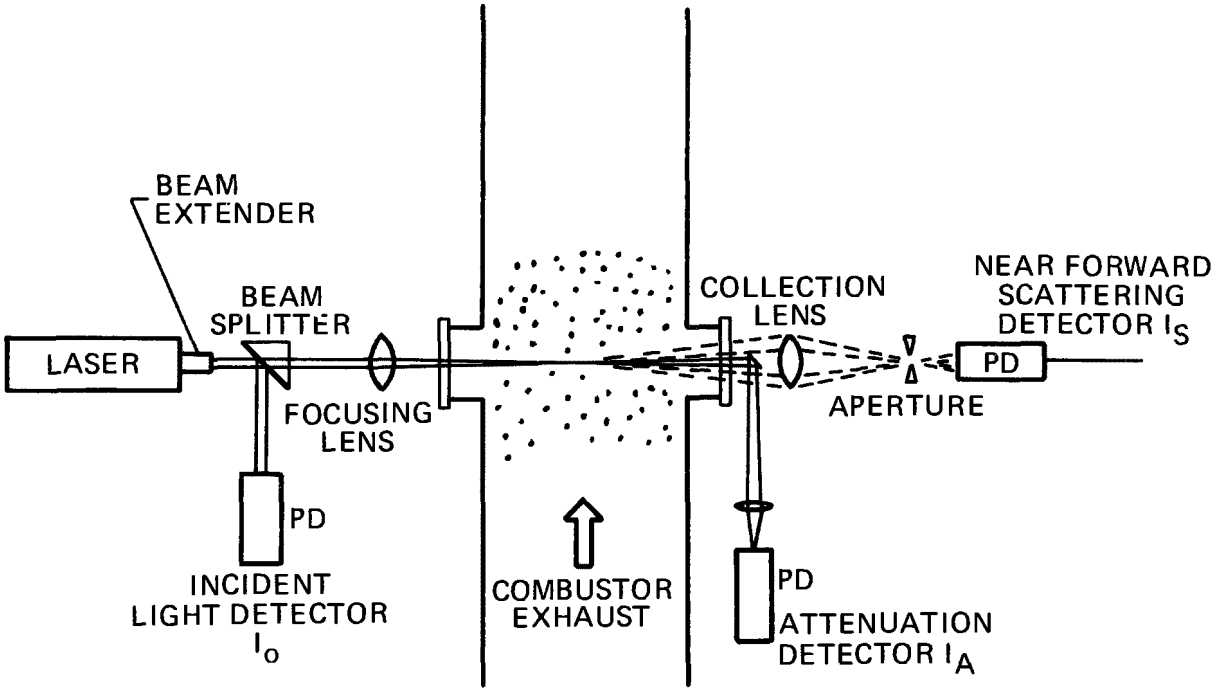

Figure 10. Schematic of the Small-Angle Near-Forward Scattering Experiment (SANFS)

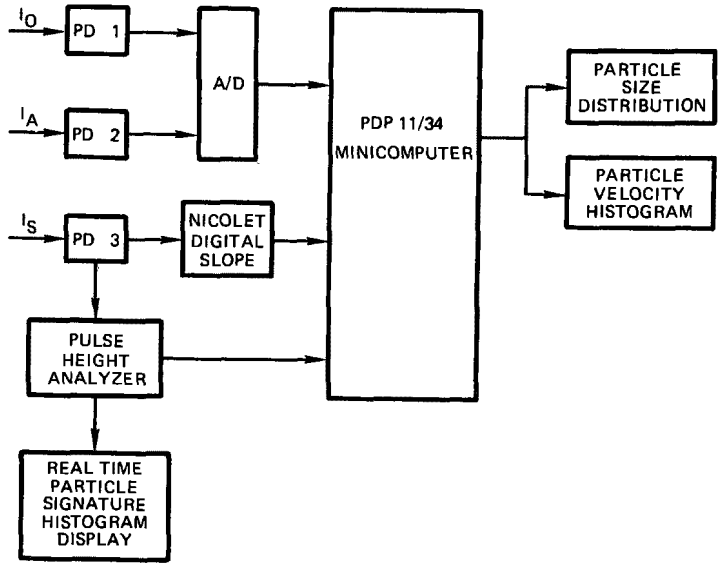

Figure 11. Block Diagram of SANFS Experiment Data Acquisition System

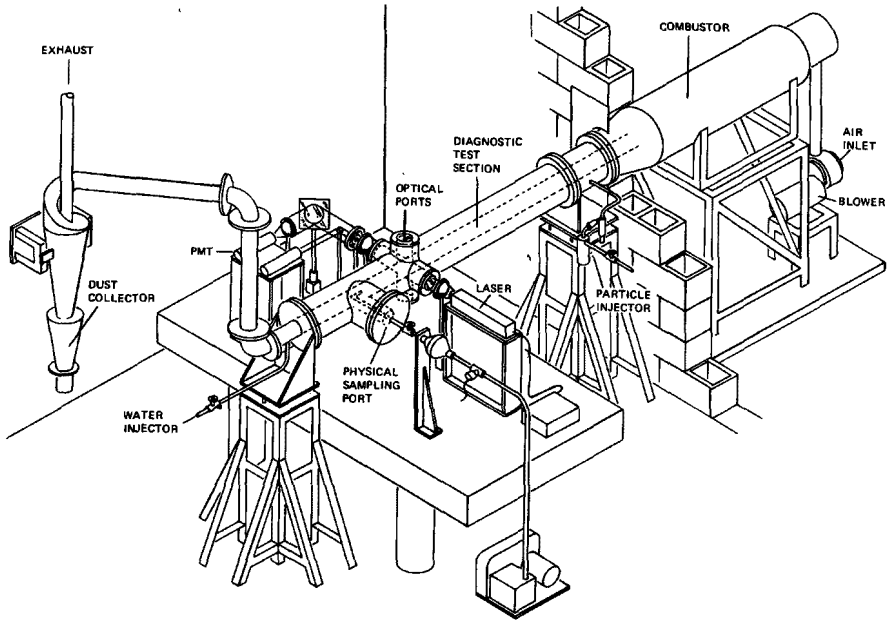

Figure 12. Sketch Of The Atmospheric Combustor Exhaust Simulator (ACES) Facility

IN-STACK PLUME OPACITY FROM ELECTROSTATIC PRECIPITATOR SCRUBBER SYSTEMS

by

L. E. Sparks, G. H. Ramsey, and B. E. Daniel

Introduction

Particulate air pollution control regulations generally limit both the mass of particulate matter that can be emitted and the opacity of the plume. It is generally assumed that the two regulations are compatible; i.e., if a plant meets the mass emission standard it will also meet the plume opacity standard. However, this assumption may not be justified for electrostatic precipitator (ESP) scrubber systems.

Recent theoretical results and laboratory scale experiments with a particulate control system, which consisted of an ESP followed by a scrubber, indicate that the mass emissions required to meet a given opacity limit may be very much lower than the mass emission standard.[1] Also, recent compliance tests of the ESP/Scrubber System at Southwestern Public Service Company's (SWPS) Harrington Unit 1 showed a mass emission of about 19.4 ng/J (0.045 lb/10^6 Btu) and an opacity of over 30%: this is in line with results of Sparks et al.[1] The mass emission is well under the current New Source Performance Standard (NSPS) of 43 ng/J (0.1 lb/10^6 Btu) but the opacity exceeds the standard of 20%. Other similar situations have been reported.

The recent revisions to the New Source Performance Standards (NSPS) which mandate SO_x removal for almost all plants will likely lead to increased use of ESP scrubber systems. Thus, the mass emission plume opacity relationship from such systems are of concern both to EPA and the utility industry.

In this paper we will review the previous theoretical and experimental studies of the opacity from ESP scrubber systems and present preliminary data from an ongoing pilot scale study of the problem.

Possible Reasons for Excessive Opacity

Several possible explanations of the high opacity at Harrington and other plants with high opacity have been suggested. The most plausible

are creation of submicron particles due to:

1. Inefficient entrainment separation.
2. Reactions of SO_2 or SO_3 with water in the plume.
3. Water condensation.

Although these factors may be important in some situations, the work reviewed in this paper indicates that high opacity for a given mass concentration is an intrinsic property of the emissions from ESP scrubber systems--at least when the scrubber is downstream from the ESP.

Previous Work

IERL-RTP Pilot Plant Studies - Sparks et al.[1] and Ramsey et al.[2] presented the results of a pilot scale study of particle collection by an ESP followed by a venturi scrubber. Their data demonstrate that existing mathematical models for ESP and venturi scrubber adequately describe the performance of ESP scrubber systems. Thus the models can be used to model the particle collection efficiency of such systems.

Sparks et al. also showed that the overall particle collection efficiency of ESP scrubber systems is very high and predicted that the particle size distribution from an ESP scrubber system should be nearly monodisperse.

Figures 1, 2, and 3 from Sparks et al. show the theoretical arguments for both the expected high overall collection efficiency and the nearly monodisperse emissions for ESP scrubber systems.

Figure 1 shows the penetration as a function of particle diameter for a moderately efficient ($\sim$ 92%) ESP. Note the broad peak on the curve which covers the $\sim$ 0.5 to 2 μm diameter range. Also note the reasonably low penetration for particles less than 0.2 μm in diameter. Figure 2 shows the penetration as a function of particle diameter for a moderate pressure drop scrubber ($\sim$ 23 cm H_2O ΔP). Note that the penetration is above 10% for particles less than 1 μm in diameter but is less than 1% for particles larger than $\sim$ 2.5 μm.

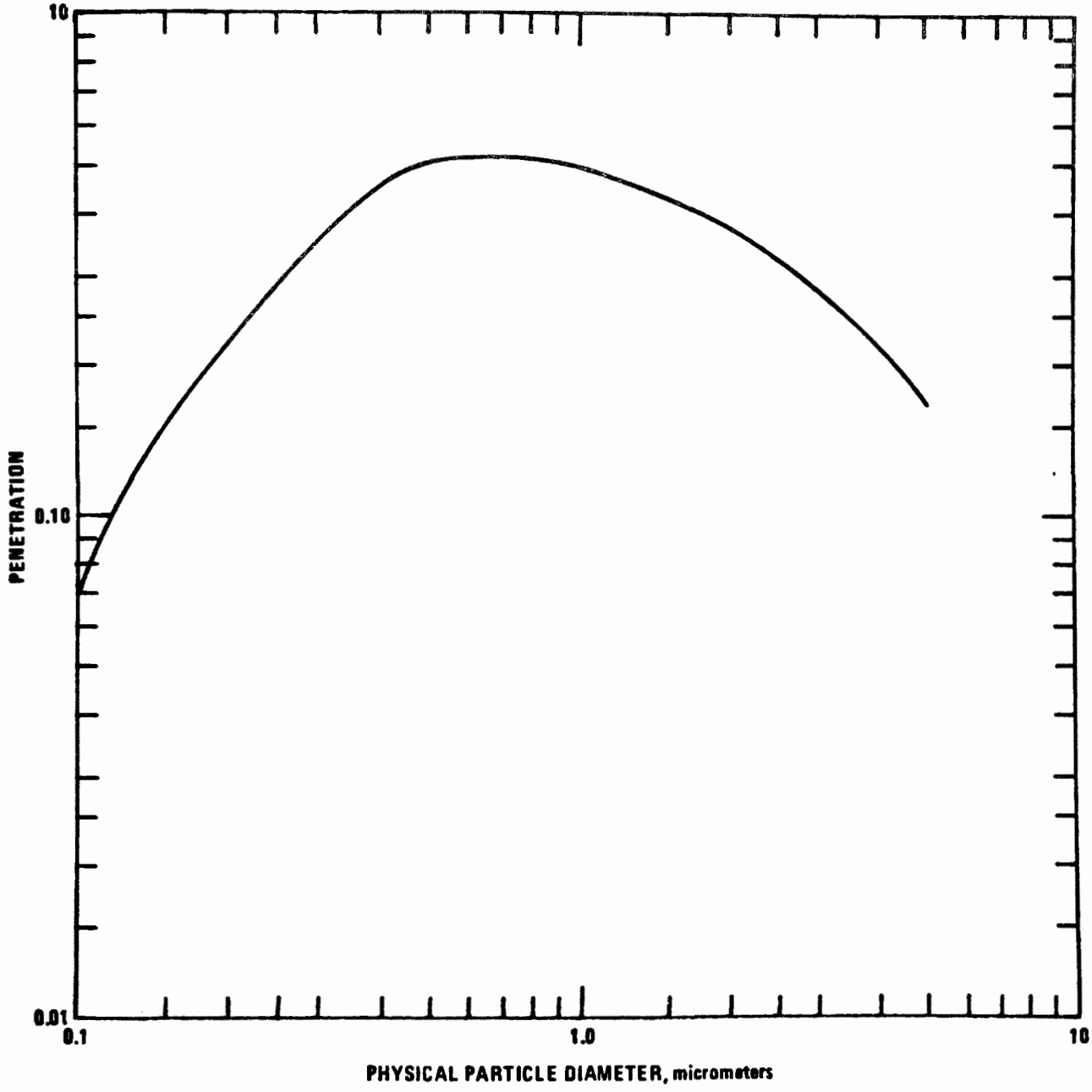

Figure 1. Graded efficiency curve for ESP with penetration of 0.0771.

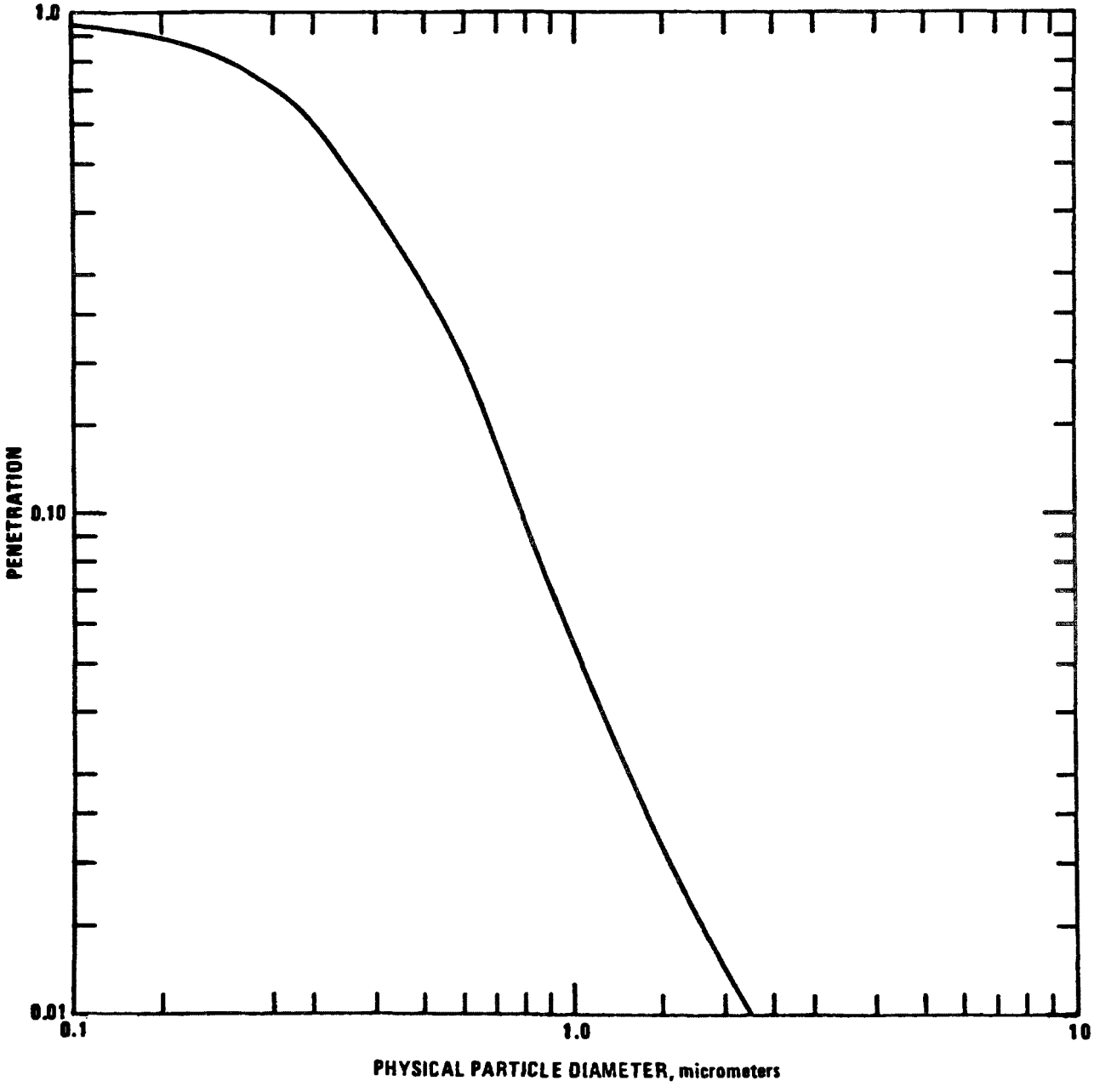

Figure 2. Penetration versus particle diameter for scrubber with pressure drop = 23 cm H_2O, density = 2.4 g/cm^3

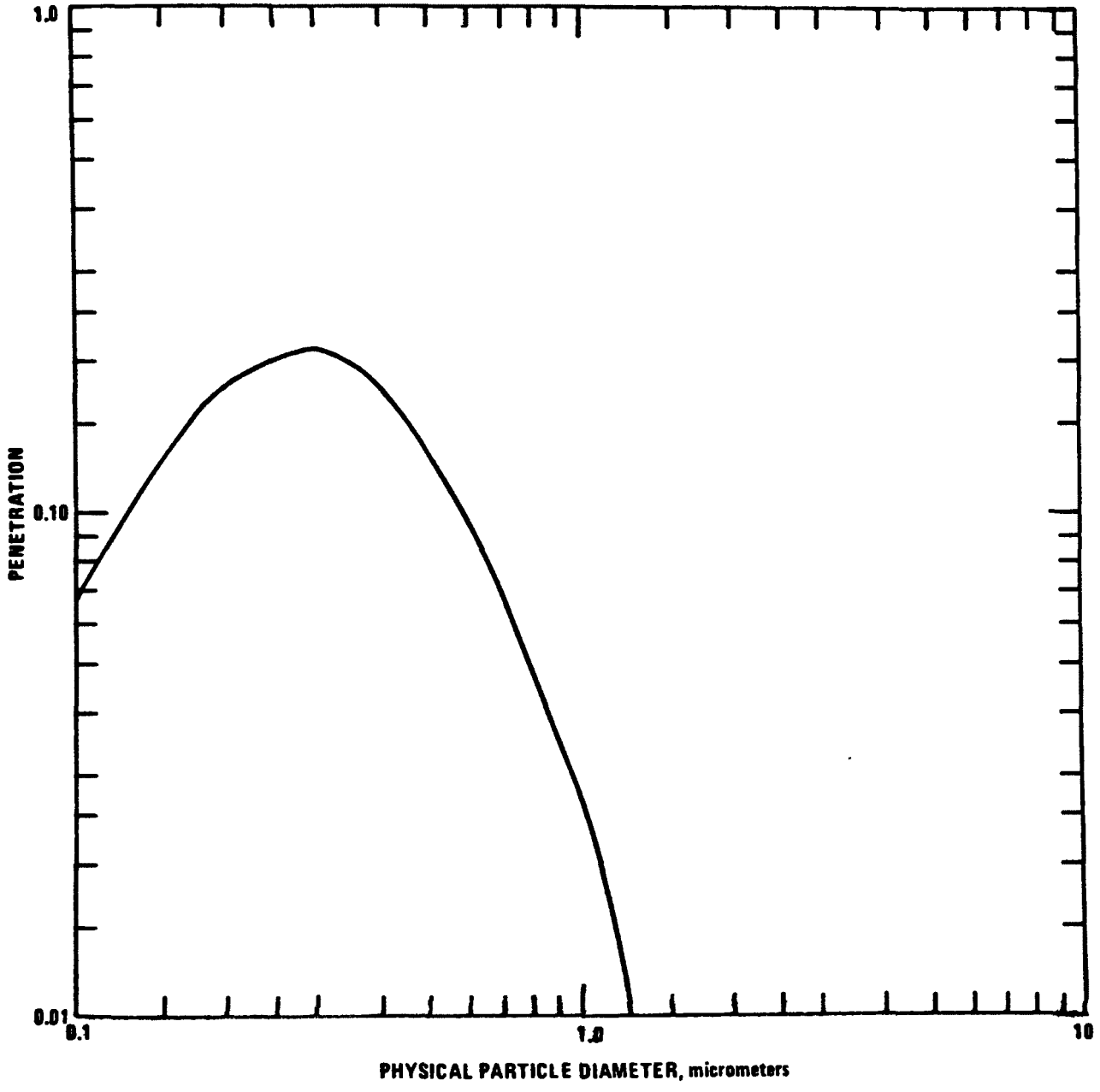

Figure 3. Graded penetration curve for ESP scrubber system - ESP penetration = 0.0771 scrubber, pressure drop = 23 cm H_2O.

The penetration as a function of particle diameter for the ESP scrubber system is obtained by multiplying the two curves together. The result is shown in Figure 3. Note the sharp peak in the 0.3 - 0.5 μm diameter region. This sharp peak means that the mass emissions from the system are fairly monodisperse and are in the optically active size band. If this system were on a typical power plant the mass emissions would be less than 15 ng/J.

Sparks et al. used the results of Ensor[3] to estimate the opacity from ESP scrubber systems for various operating conditions. These results are shown in Table 1.

Theoretical Study of Harrington Unit 1 - As mentioned in the introduction, Southwestern Public Service Company's (SWPC) Harrington Unit 1 is able to comply with the mass emission regulation but cannot meet the opacity limit. EPA's Division of Stationary Source Enforcement (DSSE) requested that we model the situation at Harrington Unit 1 to determine the nature of the problem. Mass emission, opacity, particle size distribution, and ESP scrubber design and operation data were provided by SWPS for the modeling.

The results of the modeling study were reported by Sparks[4] and are reviewed below.

The situation at Harrington Unit 1 was that the mass emissions were less than 20 J/ng and the opacity was in excess of 38%. The ESP scrubber system which was designed for particulate collection thus met the NSPS for the plant but failed to meet the 20% opacity limit.

Because the plant burns low sulfur western coal, sulfuric acid mist was rejected as a reason for the high opacity. Also, the low mass emissions were inconsistent with inefficient mist elimination. Therefore, it seemed likely that the high opacity was a particle size distribution effect. Sparks' calculations showed that the expected plume opacity based on the expected particle size distribution was very close to the measured opacity (see Table 2). The outlet mass concentration plume opacity relationship for Harrington Unit 1 is shown in Table 3.

Experimental Study - The theoretical studies reviewed in the previous sections offer strong support for the idea that ESP scrubber systems

Table 1. ESTIMATED LIGHT TRANSMISSION AND IN-STACK PLUME OPACITY FOR ESP SCRUBBER SYSTEMS

ESP Penetration	Scrubber Penetration	System	Transmission I/I_o	Opacity $1-I/I_o$
0.0030	1.0	ESP alone	0.85	0.15
0.0165	0.182	ESP & Scrubber	0.63	0.37
0.077	0.039	ESP & Scrubber	0.70	0.30
0.187	0.016	ESP & Scrubber	0.73	0.27
0.330	0.009	ESP & Scrubber	0.76	0.24
1.0	0.003	Scrubber alone	0.80	0.20

All systems produce outlet emission of 13 ng/J.

Table 2. COMPARISON OF PREDICTED AND MEASURED EMISSIONS AND OPACITY FOR HARRINGTON UNIT 1

	Measured	Predicted
Emission, ng/J	19.4	17.8
Opacity, %	37	35
Scrubber Pressure Drop, cm H_2O	18	18
Scrubber Efficiency	0.62	0.65

Table 3. CALCULATED EMISSIONS AND OPACITY AT VARIOUS SCRUBBER PRESSURE DROPS FOR EXISTING MARBLE BED SCRUBBER[a] AT HARRINGTON UNIT 1

Scrubber Pressure Drop, cm H_2O	Penetration	Efficiency	Emission ng/J	Opacity %
19	0.350	0.650	17.8	35
32	0.278	0.722	14.2	30
48	0.226	0.774	11.5	25
64	0.192	0.808	9.8	20
167	0.101	0.899	5.1	12

[a]All calculations based on f = 0.2, ρ_p = 2.4 g/cm^3, and m = 1.38 - 0.02i

give high opacity for a given mass emission. However, experimental data are needed to confirm the study. Therefore, a major experimental study is underway at IERL-RTP to develop data necessary to confirm the theory. The study is just started and only preliminary data are available.

The experimental facility for this study is the same as that used by Sparks et al.[1] The optical properties of the emissions from the ESP and the scrubber were measured with a Meteorology Research, Inc. (MRI) Plant Process Visiometer (PPV). The PPV was zeroed and calibrated each day.

The particle size distribution at the ESP inlet, outlet, and scrubber outlet were measured with calibrated MRI cascade impactors. Cascade impactor data were reduced as described by Lawless[5] and Sparks.[6] A TRS-80 microcomputer was used for data reduction. Software for data reduction was written by Denver Research Institute.

A typical particle size distribution for the scrubber outlet is shown in Figure 4. Note the sharp peak at 1 m.

The PPV reading in relative units versus outlet mass concentration for a high efficiency ESP is shown in Figure 5. The same curve for the ESP scrubber system is shown in Figure 6. Note the high PPV reading for relatively low emissions in Figure 6. These data, although not fully analyzed, are consistent with the theoretical results of previous studies.

Summary

Both theoretical and experimental results demonstrate that high in-stack plume opacity for a given mass emission is a property of ESP scrubber systems. Thus, if an ESP scrubber system is designed for particulate control, it must be designed to give about one-half the mass emission of an ESP alone or a scrubber alone if the opacity and mass emission standard must both be met.

References

1. Sparks, L. E., Ramsey, G. H., and Daniel, B. E., "Particle Collection by a Venturi Scrubber Downstream from an Electrostatic Precipitator," EPA-600/7-78-193 (NTIS No. PB 288-203), U. S. Environmental Protection Agency, Research Triangle Park, N. C., October 1978.

2. Ramsey, G. H., Sparks, L. E., and Daniel, B. E., "Experimental Study of Particle Collection by a Venturi Scrubber Downstream from an Electrostatic Precipitator." Proceedings of Symposium on Transfer and Utilization of Particulate Control Technology, Vol. III, EPA-600/7-79-044, NTIS No. PB 295-228, U. S. Environmental Protection Agency, Research Triangle Park, N. C., February 1979.

3. Ensor, D. S., "Smoke Plume Opacity Related to the Properties of Air Pollutant Aerosols," Ph.D. Dissertation, University of Washington, 1972.

4. Sparks, L. E., "In-Stack Plume Opacity from Electrostatic Precipitator/Scrubber System at Harrington Unit 1. " EPA-600/7-79-118, U. S. Environmental Protection Agency, Research Triangle Park, N. C., May 1979.

5. Lawless, P., "Analysis of Cascade Impactor Data for Calculating Particle Penetration," EPA-600/7-78-189, NTIS No. PB 288-649, U. S. Environmental Protection Agency, Research Triangle Park, N. C., September 1978.

6. Sparks, L. E., "Cascade Impactor Data Reduction with SR-52 and TI-59 Programmable Calculators", EPA-600/7-78-226, NTIS No. PB 290-710, U. S. Environmental Protection Agency, Research Triangle Park, N. C. November 1978.

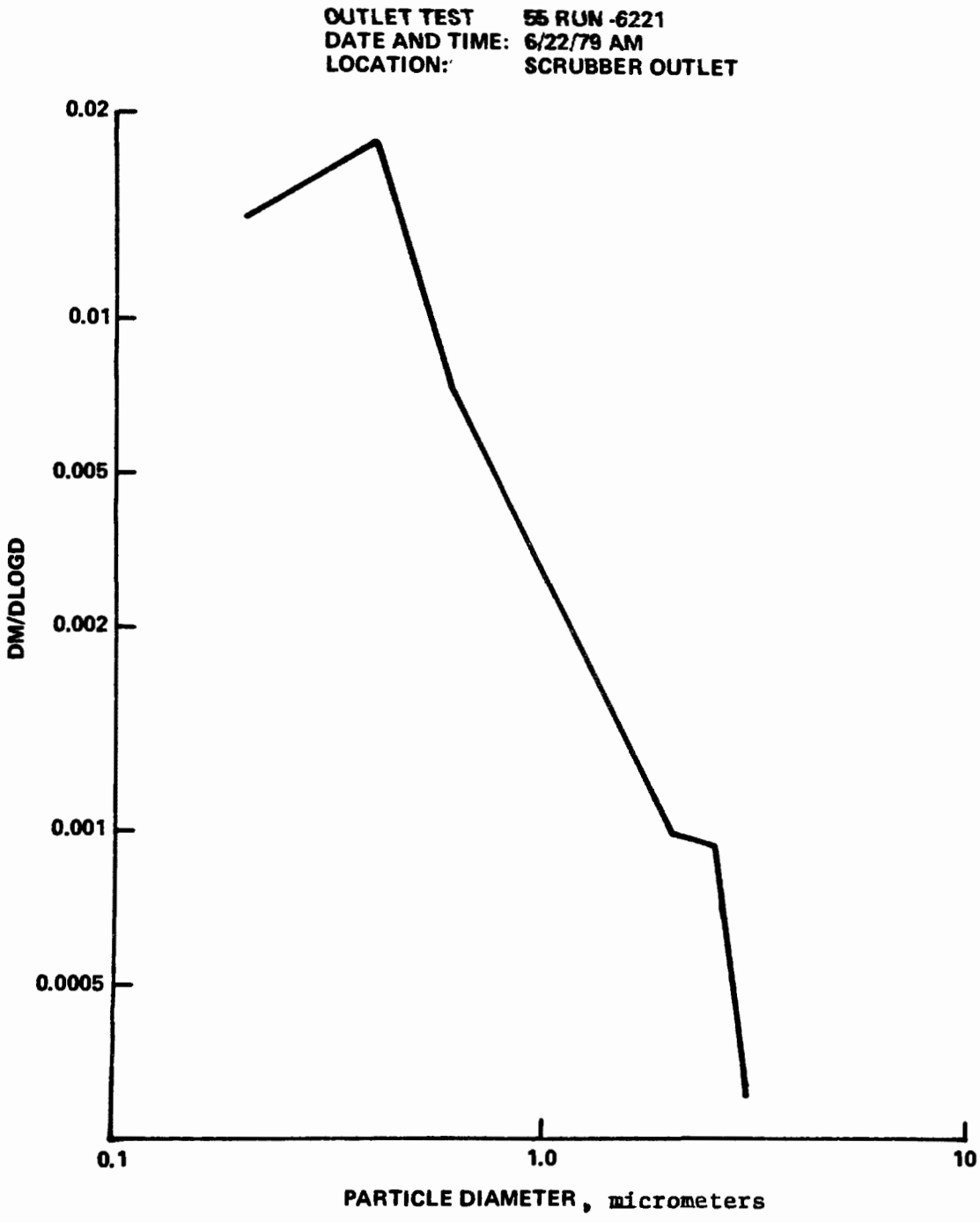

Figure 4. Scrubber outlet particle size distribution for ESP scrubber experiments.

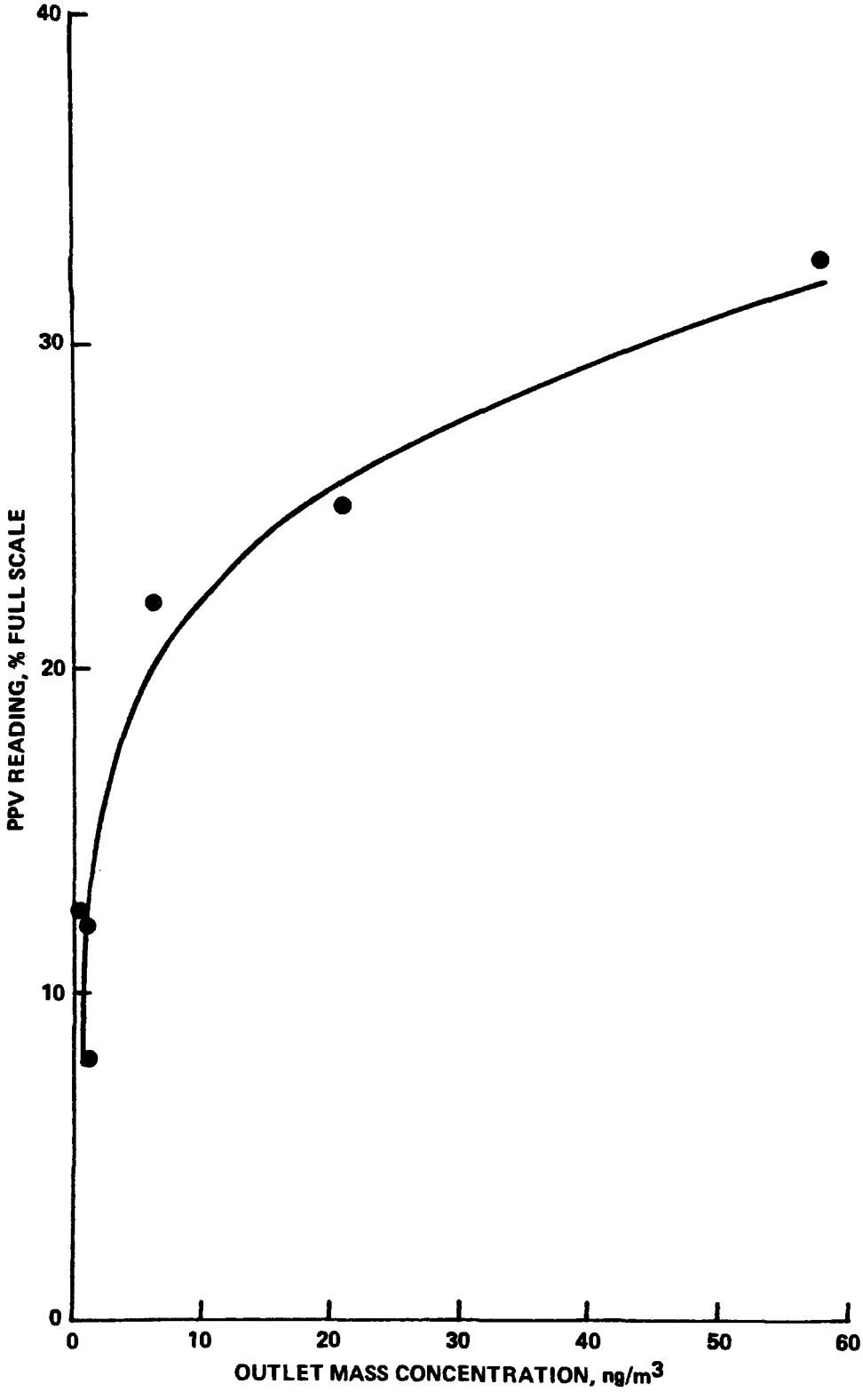

Figure 5. Relative PPV reading versus outlet mass concentration for ESP.

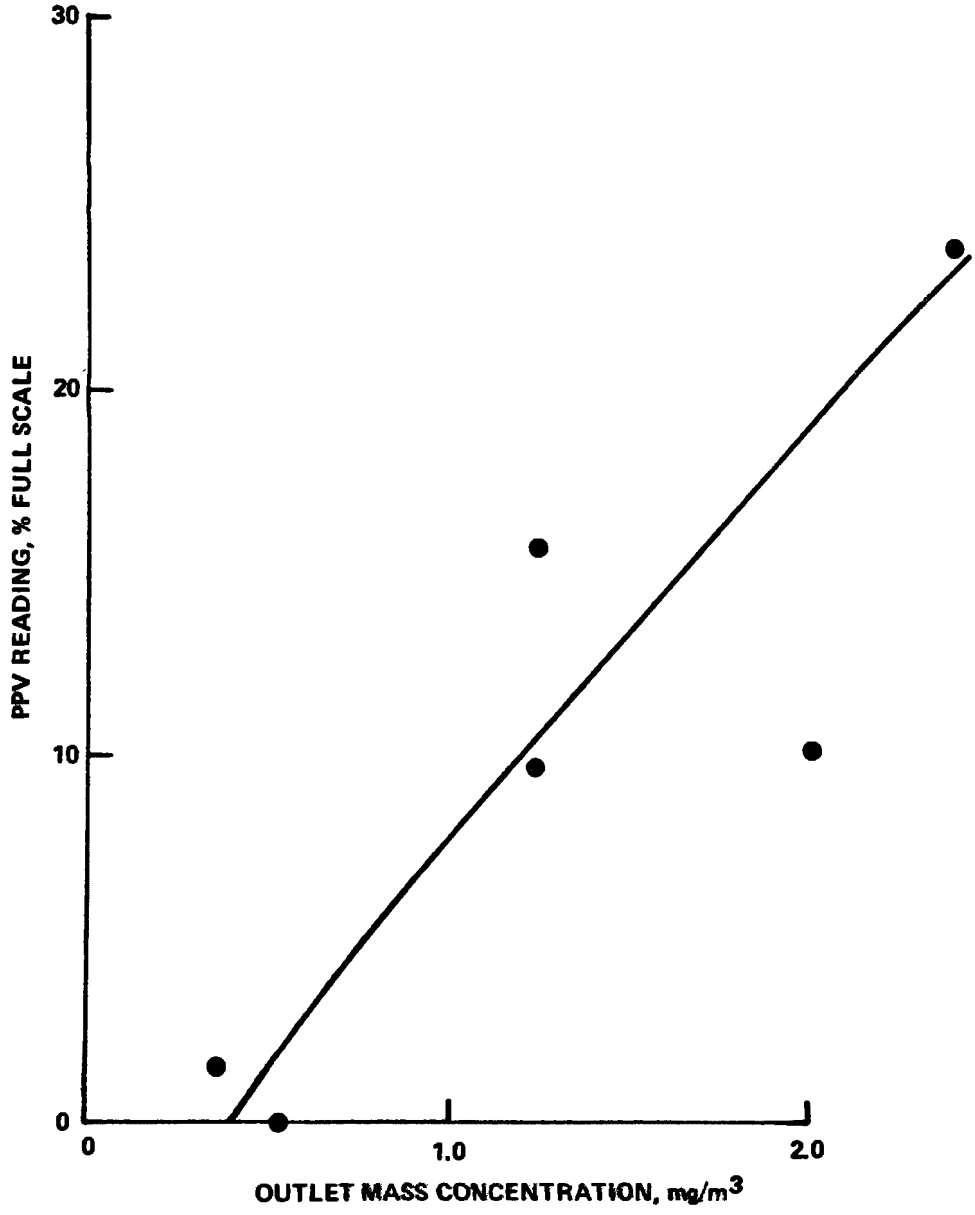

Figure 6. Relative PPV reading versus outlet mass concentration for ESP Scrubber experiments.

TI-59 PROGRAMMABLE CALCULATOR PROGRAMS FOR IN-STACK OPACITY

By:

Stanton J. Cowen
David S. Ensor
Atmospheric Research Group
Altadena, California 91001

and

Les E. Sparks
U.S. Environmental Protection Agency
Office of Research and Development
Industrial Environmental Research Laboratory
Research Triangle Park, North Carolina 22711

ABSTRACT

A description of Texas Instrument, Inc., TI-59 programmable calculator programs used to conveniently calculate in-stack opacity is presented. The effect of particulate control devices on in-stack opacity can be predicted by using these programs. The size distribution data input can be either in log-normal or histogram format. The opacity is calculated by using Deirmendjian's approximation to Mie series to obtain extinction efficiencies. Also, an alternative opacity program employing the exact Mie series solution is available. The running time for this program is approximately 8 hours while the running time for the approximate program is 60 minutes. The accuracy of these programs is generally much better than the measured data input.

For presentation at EPA Particulate Control Symposium, Denver, Colorado, 23 July 1979.

MRI 79 Pa-1703

TI-59 PROGRAMMABLE CALCULATOR PROGRAMS FOR IN-STACK OPACITY

INTRODUCTION

Predicting opacity for stationary sources of air pollution is an important tool for the design of control devices in order to meet government-mandated opacity limitations. Plume opacity may present significant problems to industrial sources because it can be relatively difficult to control. Also, opacity regulations are relatively easy to enforce. Smoke inspectors are trained to associate plume opacity with in-stack transmittance. The use of these inspectors to legally enforce opacity regulations has been demonstrated many times. Accurate opacity predictions are especially useful for designing particulate control equipment to meet opacity standards.

The ability to make opacity predictions on a large-scale computer, based on log-normal particle size distribution, has been developed by Ensor and Pilat (1). Transforming this computer program into a form easily computed on a programmable calculator is a major part of this paper. This program specifically calculates in-stack opacity as measured by stack opacity monitors. The development objectives of these calculator programs performed with a Texas Instrument TI-59 programmable calculator with a PC-100A printer, are as follows (mention of brand names does not imply endorsement by either EPA or MRI):

1. The program should predict opacity for any particle size distribution, log-normal or otherwise.
2. The program should be easy to use, providing rapid calculation of opacity with error equivalent to that found in measurement methods of aerosol properties.
3. To determine their effect on opacity, the programs should easily interface with calculator programs for particulate control devices (scrubbers and precipitators) such as those developed by Sparks (2).
4. The program should predict opacity for many different kinds of aerosols, either absorptive or nonabsorptive to light.

BACKGROUND

In-Stack Versus Plume Opacity

This calculation of opacity refers basically to in-stack measurements. This program will not give valid predictions if condensibles (excluding water)

$$Sp = \frac{\frac{3}{2} \int_0^\infty d_p^{\,2}\, Q\,(d_p, \lambda, m)\, n\,(d_p)\, d\, d_p}{\int_0^\infty d_p^{\,3}\, n\,(d_p)\, d\, d_p} \qquad (2)$$

This Sp is actually the reciprocal of the parameter, K, described by Pilat and Ensor (3).

d_p = particle diameter
Q_{ext} = light extinction efficiency; a function of only particle size and index of refraction
λ = wavelength of incident light
$n(d_p)$ = number particle size distribution
m = particle index of refraction

The solution to this integration, using Simpson's Rule on a programmable calculator, is all that is required to compute opacity. The major assumptions are spherical particles and no multiple particle scattering. At small forward scattering angles, as measured by a transmissometer, the extinction efficiency of the particle is relatively insensitive to particle shape. The mass concentrations at the outlet of a highly efficient control device are too low for the occurrence of multiple scattering.

Extinction Efficiency

Since one of the design criteria for the calculator program was fast computation, an approximation for the extinction efficiency (Q_{ext}) was required. This part of the program, if calculated by exact Mie formulation, takes 8 hours. The approximation, derived by Deirmendjian (4), is written as follows:

$$Qext\,(\rho, m) = 2 - \frac{4 \cos g}{\rho} \exp(-\rho \tan g) \sin(\rho - g) \qquad (3)$$

$$+4\left(\frac{\cos g}{\rho}\right)^2 [\cos 2g - \exp(-\rho \tan g) \cos(\rho - 2g)] \times (D-1)$$

for $m = a - bi$

when $|m-1| \to 0$

where $\rho = 2 \frac{\pi d_p}{\lambda} (a-1)$

$g = \arctan b/(a-1)$

are present. For example, the condensation of sulfuric acid drops in the plume causes a dramatic increase in opacity as measured by a trained observer. Water condensation in a plume is not considered a pollutant, and the observer is trained in detection techniques for a wet plume. The possibility of moisture condensation can be calculated given the following data and a psychometric chart: stack gas temperature, ambient temperature, wet-bulb temperature, and ambient relative humidity. Observers are taught to read the plume at the exact point of departure from the stack. In this manner water condensation occurring downwind as seen in a "detached plume" will not be mistaken for a high opacity level.

Theory of In-Stack Opacity

Opacity is defined as the amount of light extinction caused by aerosols over a given path. Beer's law describes this familiar relationship:

$$\text{Opacity} = 1 - I/I_o = 1 - \exp - [b_{ext} L]$$

I = transmitted light
I_o = incident light
b_{ext} = extinction coefficient
L = path length

The extinction coefficient equals the sum of the scattering coefficient (b_{scat}) plus the absorption coefficient (b_{abs}). Thus, the transmitted light theoretically has not been scattered or absorbed by particles. In practice, the decrease in light intensity is compensated partly by light scattering of particles at small angles in the forward direction.

The theoretical analysis of opacity in terms of basic aerosol properties has been formulated by Pilat and Ensor (3). The following equation is equivalent to this formulation:

$$b_{ext} = \frac{M\ Sp}{\rho} \qquad (1)$$

M = aerosol mass concentration (g/m^3)
Sp = specific extinction coefficient (m^2/cm^3)
ρ = particle density (g/cm^3)

Thus, the specific extinction coefficient (Sp) is the ratio of the extinction coefficient (b_{ext}) to the specific particle volume (m/ρ). Sp is simply a function of the wavelength of incident light, particle index of refraction, and particle size. It can be calculated by Mie theory as shown by Pilat and Ensor (3):

COMPARISON OF FAST IN-STACK OPACITY PROGRAMS

The two opacity programs are compared in Table 5 for a refractive index equal to 1.5. This table is presented in the same format as Table 4 with the specific extinction coefficient (Sp) data for various size distributions. Only the index of refraction is changed.

The average relative error for the log normal size data (opacity program) is 4.1 percent with maximum value of 9.5 percent. The running time for this program is approximately 15 minutes. The greatest contribution to error here is the extinction efficiency approximation. Accuracy cannot be improved by using more increments. However, the opacity from the size distribution σ_g = 6 and D_g = 4 can be improved by extending the range of integration up to a particle diameter of 80 micrometers.

The average relative error for the incremental size distribution (opacity program) is 12.3 percent with a maximum error of 23.5 percent. The running time for this program is approximately 35 minutes. The primary cause of error arises from using crude size distribution interpolation. The second major cause of error is the approximation used to calculate the extinction efficiencies. The extent of this error is identified by comparison with the log-normal case.

Use of Opacity Programs

The calculator programs presented in this paper provide a convenient and useful prediction of in-stack opacity. The use of venturi scrubbers and electrostatic precipitators in controlling in-stack opacity can also be predicted.

Analyses of both the calculation of in-stack opacity and measurement of opacity parameters show that error in the calculator programs is similar to or less than the measurement error of approximately 20 percent. Thus the programs provide the most practical means to calculate in-stack opacity. They are also designed to handle almost all sizes and optical properties of aerosols.

For more detailed description of program operations and listings, consult the EPA report which is the source of this paper, TI-59 Programmable Calculator Programs for In-stack Opacity, Venturi Scrubbers, and Electrostatic Precipitators, EPA-600/8-80-024.

Table 4 COMPARISON OF APPROXIMATE TI-59 CALCULATIONS OF Sp WITH EXACT VALUES

$m = 1.96 - 0.66\ i \qquad \lambda = 0.55\ \mu m$

σ_g	D_g	Exact Sp	Approximate Calculation (Histogram Size Data)	Approximate Calculation (Log-normal Size Data)	Long Calculation (Log-normal Size Data)
2	1	5.08	5.76	6.63	5.16
4	1	6.05	10.47	10.79	6.15
6	1	6.02	10.61	12.51	6.07
2	2	2.41	2.73	2.35	2.54
4	2	3.88	5.54	6.18	3.90
6	2	4.34	9.17	8.26	4.39
2	3	1.54	1.60	1.42	1.60
4	3	2.83	3.80	4.25	2.89
6	3	3.44	6.06	6.32	3.56
2	4	1.12	1.12	1.02	1.15
4	4	2.22	2.90	3.2	2.31
6	4	2.86	4.18	5.18	3.05

1. Data entry

2. 1st integration

$$\int_{0.02}^{2} d_p^{\,3}\, n(d_p)\, d\, d_p \qquad \Delta d_p = 0.099 \qquad (12)$$

3. 2nd integration

$$\int_{2}^{40} d_p^{\,2}\, Q\, n(d_p)\, d\, d_p \qquad \Delta p = 1.9 \qquad (13)$$

4. Calculation of opacity and specific extinction coefficient

The main function of this program is the relatively quick (less than 1 hour) approximate determination of in-stack opacity for size distributions in histogram format. This opacity program can also be used to examine the effect of high efficiency particulate control devices.

The calculated specific extinction coefficient (Sp) may <u>not</u> be correct because of the extinction efficiency approximation when a particle index of refraction is <u>not</u> in the following ranges:

$1.0 \leq$ real part ≤ 1.5
$0.0 \leq$ imaginary part ≤ 0.25

Table 4 shows that relative errors may vary from 1 to 100 percent for a carbonaceous aerosol ($m = 1.96 - 0.66i$). This table compares the exact Sp derived numerically on a computer to the three opacity programs for various size distributions. Overall, the magnitude of these errors for the approximate programs allows only a very rough estimate of in-stack opacity for highly absorptive aerosols. Therefore, using the long opacity program is highly recommended for this type of aerosol. Although this program requires approximately 8 hours, the error is less than 5 percent. Once initiated, this program runs automatically so other work can be performed simultaneously.

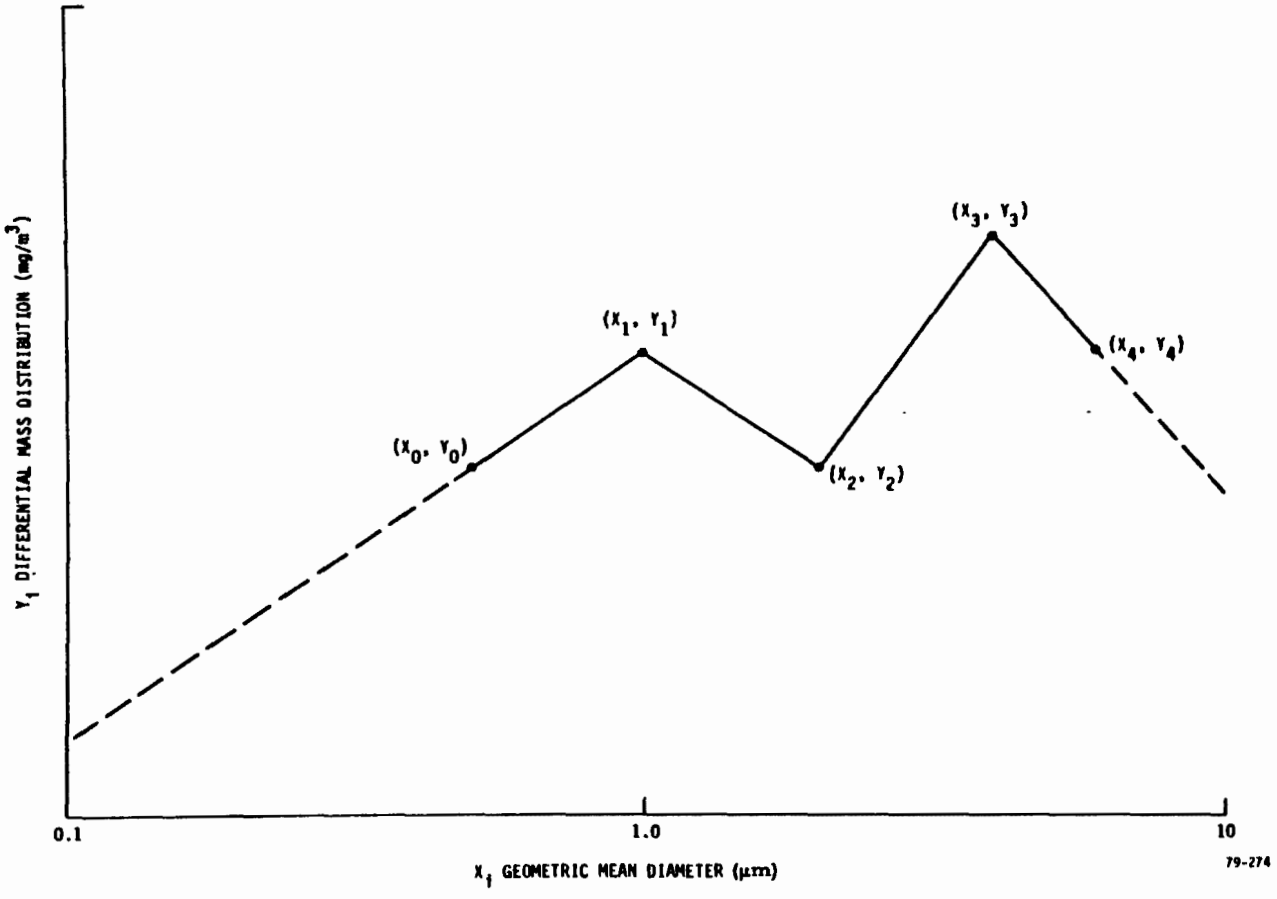

Figure 2 Linear interpolation of particle size distribution.

2. Calculation of differential mass distribution, Y_i

$$Y_i = \frac{f_i}{\log\left(\frac{D_{50_{iti}}}{D_{50_i}}\right)} \qquad (11)$$

where f_i is the fractional mass loading on impactor stage with cut point D_{50_i}

The interpretation required for points between the experimental values is simply linear (Figure 2). Points outside the range of experimental values are assumed to reside on a linear extension of the boundary lines as shown by the dashed lines.

A result of this size distribution interpolation is the generation of negative values of the differential mass distribution. The negative values were assumed equal to zero because they have no physical meaning.

This method of finite difference differentiation, although a crude approximation, is the best technique for this program, especially considering the limited number of available program steps. This method also allows a maximum of 10 D_{50}'s to be used, so that the data from a low pressure impactor with 10 stages can be used. The error in this program, generated partly by the finite difference, is moderately larger than that produced by the log-normal opacity program.

The differential mass distribution is converted to the differential number distribution before the continuous Simpson's Rule integration is applied. The integrals solved in this program are identical to those contained in the log normal opacity program. This program can also be divided into four basic operations:

This program can estimate in-stack opacity for a given facility. It can also be used with the control device model programs to estimate design for opacity. The effect on particle size distribution on the specific extinction coefficient and opacity can be examined by varying the values of particle size distribution, σ_g and d_g. Also, the effect on opacity variables such as particle density, stack diameter, and mass grain loading can be examined for a given size distribution.

This program can also determine the opacity for bimodal log-normal size distributions. The steps for this calculation are as follows:

1. Determine the specific extinction coefficient, Sp, for each mode using standard program operation.
2. Clear calculator display.
3. Sum these specific extinction coefficients.
4. Enter the sum from Step 2.
5. Push subroutine 620.

The printed result will show the new specific extinction coefficient, Sp, and in-stack opacity (OP%).

This program will produce incorrect results for standard deviation approaching 1.0; i.e., monodisperse aerosols. This logarithm equals zero, and the subsequent division by zero is undefined. The limit for the standard deviation depends upon the geometric mean and the range of particle diameters. Generally, standard deviations greater than 1.009 should provide correct calculations. A flashing display indicates error; however, this is not a serious problem because real aerosols are not monodisperse.

Approximation Opacity Program With Histogram Size Distribution Input

This program uses the opacity formulation with histogram size data input. Light extinction efficiency is calculated using Deirmendjian's approximation. The advantage of this program is that it allows opacity calculation for aerosol masses with size distributions not conforming to log-normal size distributions. This program is especially designed to handle cascade impactor data, although any size distribution data in histogram form can be used.

The following manipulations of size distribution are performed:

1. Calculation of the geometric mean diameter, X_i (10)

$$X_i = (D_{50_{i+1}} \quad D_{50_i})^{\frac{1}{2}}$$

where D_{50} is the impactor diameter cut point; i.e., the diameter of particles collected with 50 percent efficiency on that stage

$$n(d_p) = \frac{1}{(2\pi)^{\frac{1}{2}} \ln\sigma_g d_p} \exp\left[\frac{-\ln^2 (d_p/d_g)}{2 \ln^2 \sigma_g}\right] \quad (5)$$

where d_p is the particle diameter, σ_g is the geometric standard deviation, and d_g is the geometric mass mean diameter. This function is substituted into the integral to calculate the specific extinction coefficient (Sp), and the Simpson's Rule (continuous) approximation is applied to obtain the two integral solutions. The integration program is provided by the master library module for all integrations in this paper. The extinction efficiency is calculated using Deirmendjian's approximation of the Mie series. This program can be divided into four basic operations:

1. Data entry (6)

2. 1st integration

$$\int_{d_1}^{d_n} d_p^{\,3}\, n(d_p)\, d\, d_p \quad (7)$$

3. 2nd integration

$$\int_{d_1}^{d_n} d_p^{\,2}\, Q\, n(d_p)\, d\, d_p$$

4. Calculation of opacity and specific extinction coefficient

Each integral above is calculated twice at two ranges of particle diameters as follows:

1. $$\int_{0.02}^{4} \Delta d = 0.199 \quad (8)$$

2. $$\int_{4}^{40} \Delta d = 1.8 \quad (9)$$

Table 3 CALCULATOR PROGRAM SUMMARY

Program	Calculation	Input Required	Can Be Used With
1. Approximate opacity (log-normal)	In-stack opacity on log-normal distribution	Stack diameter, mass concentration, density, index of refraction, wavelength, geometric mass mean diameter, geometric standard deviation	ESP, Scrubber Program with log-normal distribution
2. Approximate opacity (histogram)	In-stack opacity on histogram distribution	Stack diameter, mass concentration, density, index of refraction, wavelength histogram distribution (mass fractions at particle diameter)	ESP, Scrubber Program with histogram distribution
3. Extinction efficiency approximation	Approximates light extinction efficiency for spherical particle	Particle diameter, index of refraction wavelength	
4. Long extinction efficiency	Light extinction efficiency for spherical particles	Particle diameter, index of refraction wavelength	
5. Long opacity (log-normal)	In-stack opacity on log-normal distribution	Same as approximate opacity (log-normal)	

The scattering part of the index of refraction can be measured by comparison with oils of known indices of refraction on a high contrast microscope, if the resulting aerosol is solid. If the material is liquid, the refractive index can be determined by measuring the change in position of the image of an object viewed through the liquid of known depth. Also, a commercial Abbe refractometer can be simply used to measure the refractive index of organic fluids.

The density of the aerosol particles is measured with a Micromeritics Helium Pycnometer. Change in the volume of gas displaced by the sample is proportional to change in pressure using a nonabsorbing gas such as helium. By using a standard of known volume as a reference, the sample volume can then be calculated. An analytical balance is then used to weigh the sample to determine density. If the aerosol is liquid, a bottle pycnometer is simply used to determine the volume and weight of a sample. The experimental error is approximately 5 to 10 percent, depending on the accuracy of the balance used to weigh the samples.

The combined error from the measurement of particle size, density, refractive index, and mass concentration results in an opacity prediction that contains 15 to 20 percent error. Thus, the use of the calculator program is ideal for this type of computation. The accuracy obtained on a large-scale digital computer would not be warranted for this type of measurement error.

OPACITY CALCULATOR PROGRAMS

The calculator programs were performed using a Texas Instruments TI-59 programmable calculator with a PC-100A printer. The opacity programs are summarized in Table 3, which shows the calculation results, data input, and compatible calculator programs. The user has a choice of three different in-stack opacity programs, depending upon the particle size distribution and the particle index of refraction. The programs either specify "log-normal" for log normally distributed particle size or "histogram" for nonlog-normal distributions. The third program is specifically for determining in-stack opacity for particles with an index of refraction outside the ranges outlined for the use of approximate extinction efficiency calculation. This program would apply if the real part of the refractive index were greater than 1.5 or less than 1.0 and if the imaginary part were greater than 0.25. The major drawback of this particular program is the running time--approximately 8 hours. The reason for this long calculation is the use of Bessel series to solve the Mie equations for extinction efficiency, which requires many iterations. The programs using the Deirmendjian approximation require only 30 to 60 minutes.

Opacity Program with Log-Normal Size Distribution

This program computes in-stack opacity for an aerosol mass with a log-normal particle size distribution. This size distribution is represented as follows:

reentrainment. Wall losses can be mitigated by removing the aerosols from the walls and depositing them on the appropriate stages. The effects of particle reentrainment on opacity prediction for a large-scale pulverized coal-fired boiler with a cold-side electrostatic precipitator were insignificant for the facility under investigation (Iowa Public Service, George Neal Unit #3), see Table 2. However, particle size measurement on a source with a much higher proportion of submicron aerosol will have a much larger impact on opacity prediction if particle reentrainment occurs.

Table 2 EFFECTS OF PARTICLE SIZING ON CALCULATOR OPACITY

Particle Sizing [a] Instrument Used	Corrections Made	Opacity (%)
Cascade impactor	None	18.3
Cascade impactor and electrical mobility analyzer	None	21.0
Cascade impactor and electrical mobility analyzer	Assume 75% reentrained particles on lowest impactor stage and 20% reentrained particles on other stages	19.5

[a] Using cascade impactor solely excludes submicron aerosol. The electrical mobility analyzer provides this measurement.

Another important parameter required for predicting opacity is the particle index of refraction. The absorption part of the refractive index has successfully been measured with the Integrating Plate Method on ambient aerosols [Lin et al., (5), Weiss et al., (6)]. The applicability of this method to emission aerosols is unknown since little data exists on their absorption properties. Bulk absorption is found by comparing the transparency of a clean Nuclepore filter with the same filter plus a layer of aerosol. An opal glass is used to integrate the light so it can all be detected by the photodiode. Light extinction from absorption is then calculated by:

$$I_t'/I_t = \exp(-b_{ABS}\chi) \qquad (4)$$

where I_t' is transmitted light intensity with aerosol deposition, I_t is transmitted light intensity without aerosol deposition, χ is the path length of sample volume with a cross-sectional area equal to the filter, and b_{ABS} is light extinction from absorption. The experimental error is approximately 10 percent as calculated by Weiss et al. (6).

Table 1 STACK OPACITY DATA

Stack Aerosol Size Distributions[a]

Actual Diameter (μm)	Size Distribution No. 1 Sp = 4.549 Percent within interval	Partial[b] Sp	Size Distribution No. 2 Sp = 1.65 Percent within interval	Partial Sp
0.123 - 0.215	1.887	0.0443	14.0	0.2027
0.215 - 0.328	1.887	0.0903	0.0	0.0581
0.328 - 0.433	0.943	0.2954	0.117	0.0127
0.433 - 0.573	18.868	1.6719	0.415	0.0531
0.573 - 0.758	14.151	1.2661	2.002	0.2086
0.758 - 1.002	1.887	0.2638	4.204	0.2391
1.002 - 1.524	14.151	0.3452	9.375	0.2617
1.524 - 2.317	14.151	0.3007	9.912	0.2099
2.317 - 4.053	18.868	0.1942	21.093	0.2644
4.053 - 6.164	1.887	0.0271	12.708	0.0836
6.164 - 9.375	9.434	0.0342	9.837	0.0423
9.375 -12.398	1.887	0.006	5.151	0.0142

Stack Diameter (meters)	Opacity (%)	Opacity (%)
6.9	56.9	26.3
3.05	31.1	12.6
6.10	52.5	23.6
9.15	67.3	33.3
12.20	77.4	41.7

Other important data:

Aerosol index of refraction:	1.54 - 0.02i
Aerosol specific gravity:	2.6 g/cm^3
Wavelength light:	0.56 μm
Pressure:	695 mm H_g
Temperature:	132° C
Mass concentration:	0.0698 g/m^3

[a] These particle size distributions do not necessarily represent real data. The purpose is only to show the effects of particle size on opacity.

[b] The partial Sp indicates the individual contribution of light extinction for particle size range; i.e., $\sum_i$ Partial Sp_i = Sp

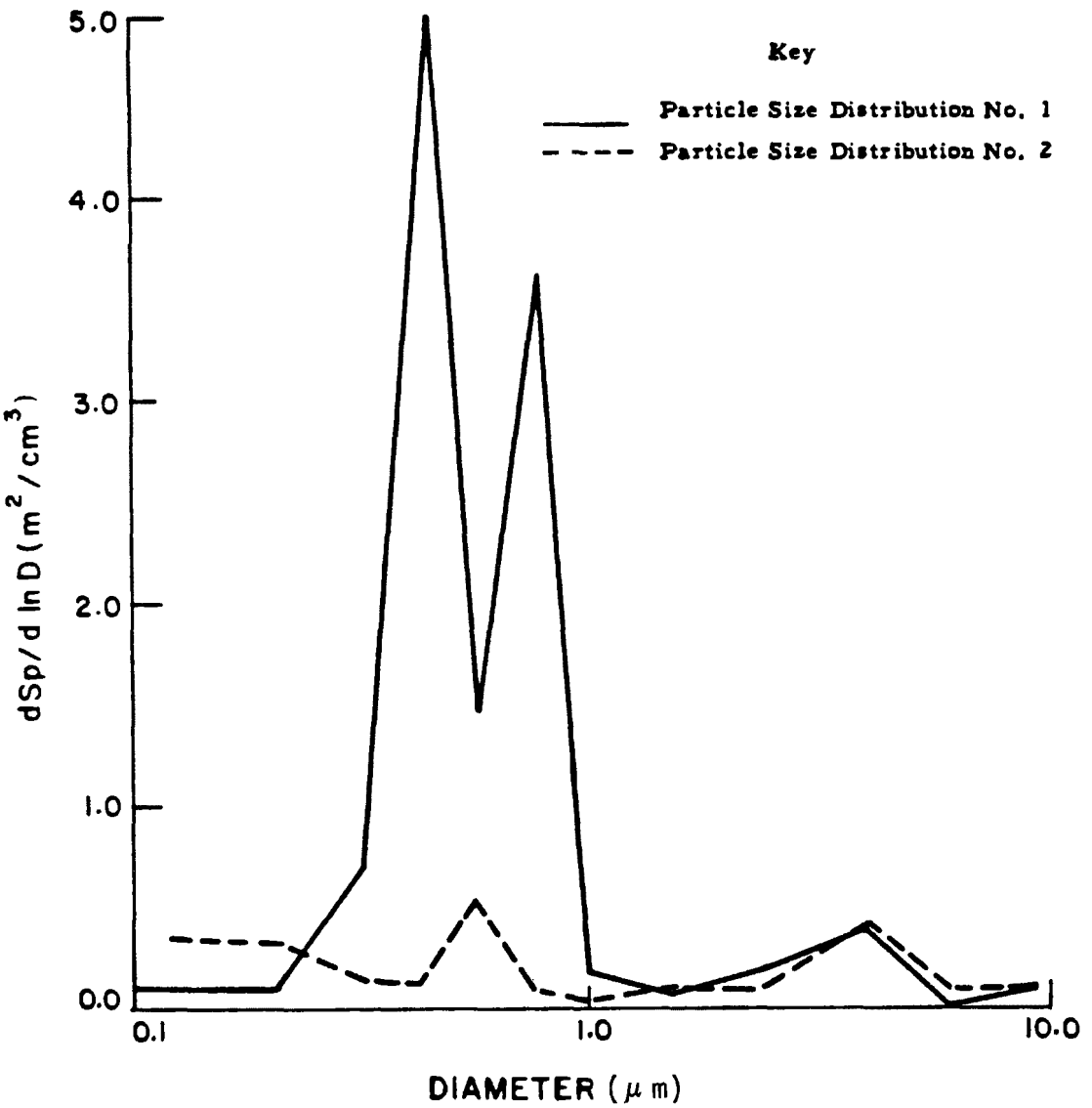

Figure 1 Differential specific extinction coefficient distribution with particle size.

a = real part of the index of refraction
b = imaginary part of the index of refraction
(D-1) = an empirical correction factor.

The extinction efficiency approximation is restricted in that the particle index of refraction must fall in the following ranges:

$$1 < a \leq 1.5$$
$$0 \leq b \leq 0.25$$

Otherwise the actual Mie theory calculation must be used. (An additional program was developed for this reason.) However, this calculation may last up to 8 hours on a programmable calculator.

Data Required to Predict Opacity

Based on the theoretical analysis, the following data are needed to make opacity predictions:

1. Particle size distribution
2. Particle index of refraction
3. Particle density
4. Particulate mass concentration in-stack
5. Stack diameter

The most sensitive of these parameters is the particle size distribution. This can be demonstrated clearly by comparing graphs of $dSp/d\ell nD_p$ vs ℓnD_p (Figure 1). The areas under each curve are equal to specific extinction coefficient (Sp) and are approximately proportional to the opacity. The particle size distribution is the only parameter that is different for the two curves (Table 1). The opacities for these two distributions differ by a factor of two as a result of these differing particle sizes. The particle size range that scatters light most efficiently per unit mass is approximately 0.1 to 1 micrometer based on a wavelength of 0.5 micrometer.

Instruments used to measure particle size distribution are cascade impactors, cyclones, and particle optical counters. If submicron particles are more than 20 percent of the total particulate mass, an electrical mobility analyzer should be used to measure the size range, 0.01 to 0.3 micrometer.

Since particle sizing is so critical in predicting opacity accurately and the cascade impactor is a main source of sizing information for particles whose diameters exceed 0.5 micrometers, it is useful to outline some of the major errors involved with impactor sampling. In general, an error of less than 10 percent in the D_{50} had an insignificant effect on predicted opacity. Random errors include construction tolerance (diameter of jets), gas flow rate (jet velocity), and weighing. Random errors are generally less than 5 percent, except for the weighing error on the low load bottom stages, which can be significant. The main systematic errors are wall losses and particle

Table 5 COMPARISON OF APPROXIMATE TI-59 CALCULATIONS OF Sp WITH EXACT VALUES

$m = 1.5 \qquad \lambda = 0.55\ \mu m$

σ_g	D_g	Exact Sp m^2/cm^3	Approximate (Log-normal Size Data)	Approximate (Histogram Size Data)
2	1	4.99	4.82	4.92
4	1	3.67	3.73	3.95
6	1	3.06	3.23	3.38
2	2	2.62	2.51	2.99
4	2	2.88	2.87	3.21
6	2	2.62	2.77	2.88
2	3	1.64	1.56	1.91
4	3	2.31	2.316	2.6
6	3	2.27	2.44	2.55
2	4	1.17	1.11	1.31
4	4	1.91	1.94	2.17
6	4	2.0	2.19	2.47

REFERENCES

1. Ensor and Pilat. Comparison Between the Light Extinction Aerosol Mass Concentration Relationship of Atmospheric and Air Pollution Emission Aerosols. Atmos. Envir. 5:209-215, 1971.

2. Sparks, L.E. SR-52 Programmable Calculator Programs for Venturi Scrubbers and Electrostatic Precipitators. EPA-600/7-78-026,(NTIS PB 277-672), March 1978.

3. Pilat and Ensor. Plume Opacity and Particulate Mass Concentration. Atmos. Envir. 4:163, 1970.

4. Deirmendjian, D. Electromagnetic Scattering on Spherical Polydispersion. New York, American Elsevier Publishing Company, 1969.

5. Lin et al. Absorption Coefficient of Atmospheric Aerosol: A Method for Measurement. Applied Optics. 12:1356-1363, June 1973.

6. Weiss et al. Studies of the Optical, Physical and Chemical Properties of Light Absorbing Aerosols. (Presented at the Conference on Carbonaceous Aerosols, Lawrence Berkeley Laboratory, Berkeley, California, March 20-22, 1978).

UTILIZATION OF THE OMEGA-1 LIDAR IN EPA ENFORCEMENT MONITORING

Arthur W. Dybdahl and Frank S. Mills
Remote Sensing Section
National Enforcement Investigations Center
Office of Enforcement
U.S. Environmental Protection Agency
Denver, Colorado 80225

ABSTRACT

The EPA-NEIC Omega-1 Lidar is being proposed for use as an alternate method to Method 9 for the monitoring of the opacity of particulate emissions from stationary sources. This lidar is mobile and can be placed in a desired testing position and in full operation within 5 to 10 minutes. It is capable of collecting plume opacity data at a measurement rate of 1 measurement/second for hours if required. The data recording/processing system has been augmented to provide rapid analysis/reduction of the lidar data in a mechanism most useful in enforcement use. The lidar system has been subjected to extensive performance evaluation and calibration tests. Over 7,000 data points have been recorded and analyzed. The results of these tests shall be presented. A description and summary of the lidar's field use shall also be given.

INTRODUCTION

The EPA-NEIC has acquired a mobile lidar (laser radar) for use as an alternate method to Reference Method 9 (40CFR60) for the measurement of the opacity of particulate emissions from stationary sources. In this paper we describe briefly the lidar concept as it applies to the measurement of smoke plume opacity, and the techniques used for data analysis and calibration. The EPA-NEIC Omega-1 is discussed along with the results of its performance evaluation and calibration tests, and future plans for using this lidar as a tool in the EPA enforcement program.

PRINCIPLE OF THE MEASUREMENT

The lidar is an instrument which is used to remotely measure properties of the atmosphere. A very short, intense pulse of light from a laser is transmitted through the atmosphere. Aerosols and molecules in the path of the laser beam scatter some of the light out of the beam. A telescope, mounted in the lidar so that its field-of-view is parallel to that of the laser beam, collects the light which is scattered straight back to the lidar. A detector, usually a photo-multiplier tube (PMT), is used to convert the backscattered light collected by the telescope to an

electronic video signal which can be displayed on an oscilloscope and processed further as desired. Figure 1 shows an oscilloscope trace of a backscatter signal for clear air.

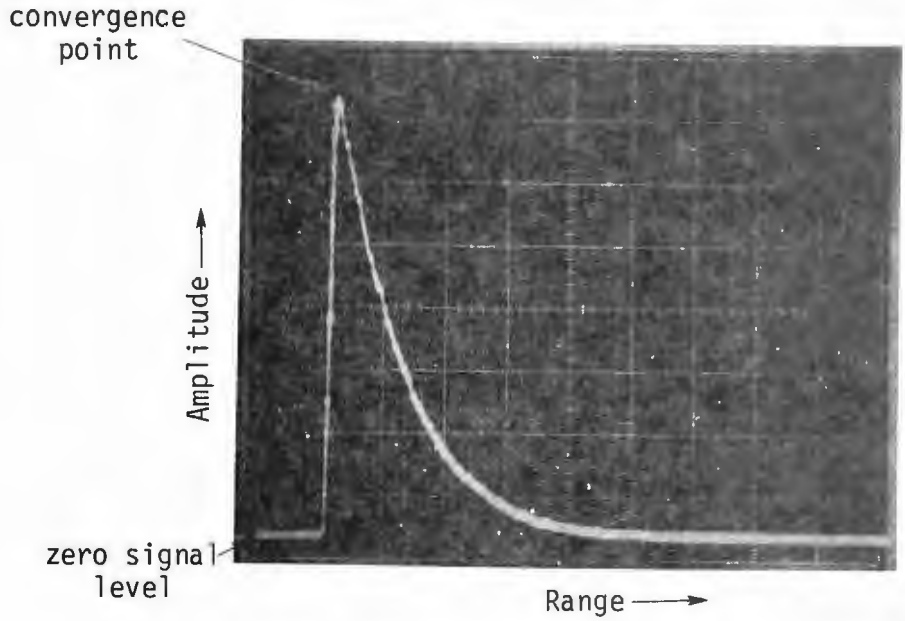

Figure 1 Linear Channel Video Signal Clear Air (Uncorrected for $1/R^2$)

The oscilloscope records the amplitude of backscatter signal as a function of time or, equivalently, range along the lidar's line-of-sight. The backscatter signal is zero until the laser beam enters the field-of-view of the telescope. The signal rises rapidly to a peak which corresponds to the spatial point where the telescope's field-of-view completely overlaps the laser beam which is about 80 meters from the lidar. The signal then decreases in amplitude or falls off as $1/R^2$, where R is range along the lidar line-of-sight, in accordance with the lidar equation [1, 2].

The backscatter return signal can be corrected for the $1/R^2$ fall-off resulting in a signal trace which is ideally flat beyond the point of convergence. Now any attenuation of the laser energy by the atmosphere either by scattering or absorption will show up in the $1/R^2$ corrected trace as a slight decrease in amplitude from the flat line. This property of the return signal permits the direct measurement of plume opacity as described below.

To measure the opacity of the particulate emissions from a given smoke stack, the lidar is aimed so that the laser beam passes through the smoke plume just above the orifice or opening of the stack. The backscatter return signal which results from the laser being fired through a particulate plume, is shown in Figure 2. The spike in the return is the backscatter signal from the smoke plume. Its amplitude is much greater than that of the atmospheric return because the particulate density is much greater in the plume than in the surrounding air. Figure 3 shows the return in Figure 2 corrected for $1/R^2$ falloff. The return is flat in the region before the plume and after the plume, indicating that there is no measurable attenuation from this atmospheric path. There is the strong spike from the plume return and then a drop in the signal level after the plume compared with that before the plume. This is caused by the optical attenuation of the laser beam by the smoke plume.

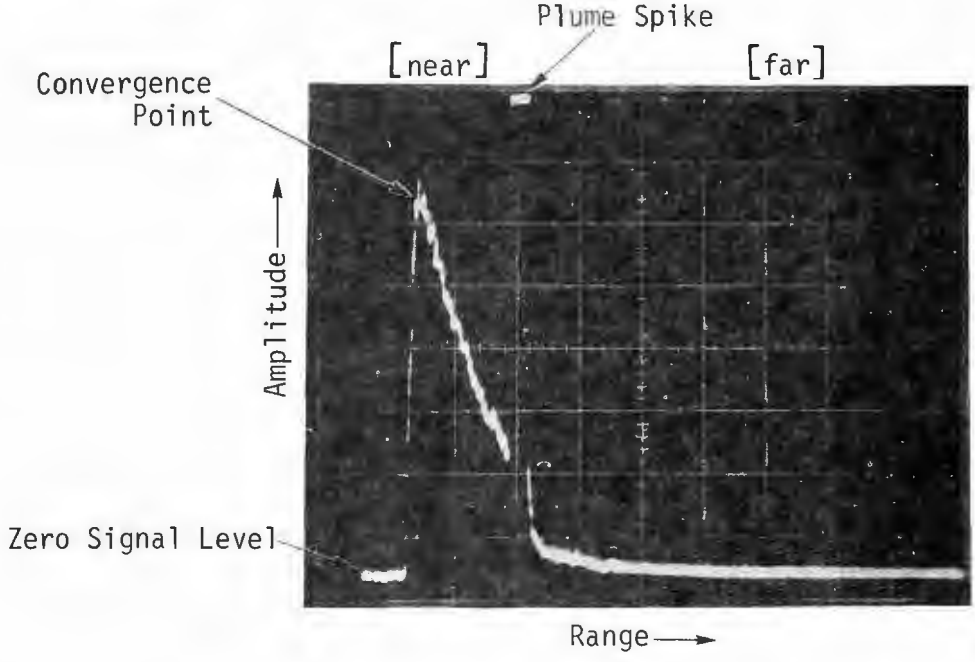

Figure 2 Linear Channel Video Signal, 40% Opacity (Uncorrected for $1/R^2$)

If I_n is the signal level before the plume (near-region) and I_f is the signal level after the plume (far region) [Figure 3], then the transmittance, T, of the plume is given by

$$T = \left[\frac{I_f}{I_n}\right]^{1/2} \qquad (1)$$

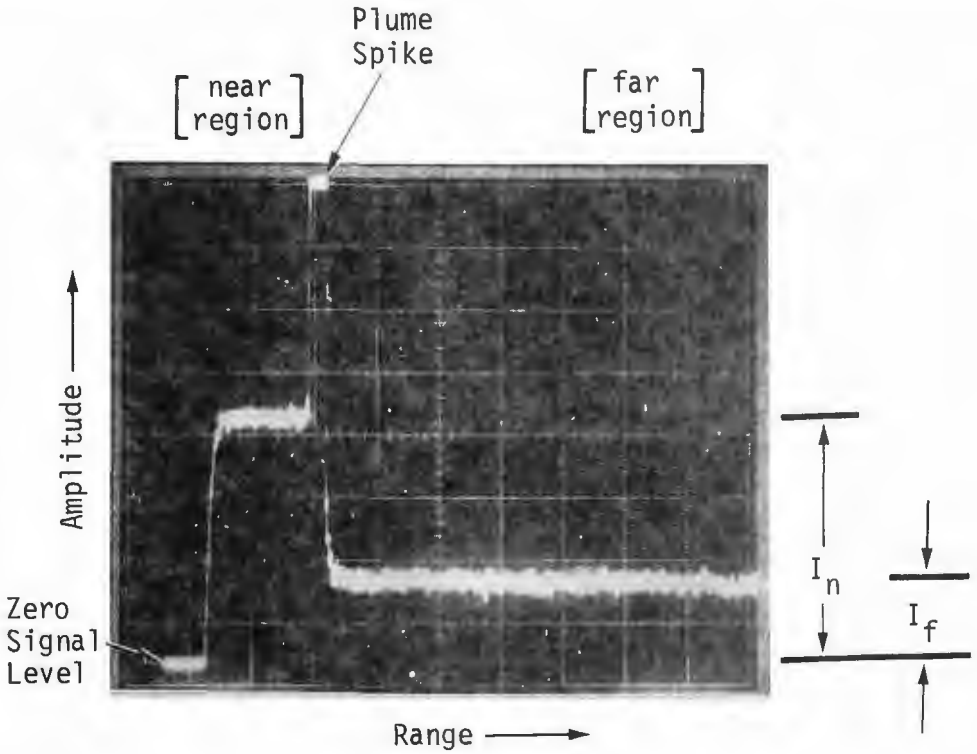

Figure 3 Linear Channel Video Signal,
40% Opacity (Corrected for $1/R^2$)

The square root enters equation (1) because the backscatter signal level is attenuated twice, once when the laser beam passes through the plume, and again when the backscattered light from the far-region passes through the plume returning to the lidar receiver. The opacity value, O_p, is then given by

$$O_p = (1 - T) \times 100\% \qquad (2)$$

or

$$O_p = \left[1 - \left[\frac{I_f}{I_n} \right]^{\frac{1}{2}} \right] \times 100\% \qquad (3)$$

If the ambient atmosphere in front of and beyond the plume is not clear but hazy, the backscatter signal before and after the plume will not be flat as shown in Figure 3; but will have a negative or downhill slope. In this situation the values I_n and I_f must be adjusted to account for this negative slope or the opacity calculated by equation (3) will include the opacity of the atmosphere between the points where I_n and I_f are measured as well as the opacity of the plume.

One way to correct for the atmospheric attenuation is to make a reference measurement by aiming the lidar at a point upwind from the smokestack so that the plume is not in the lidar's line-of-sight. The amplitude R_n of the reference return signal is measured at the same point in time that I_n is measured in the plume return signal. Similarly, the amplitude R_f of the reference signal is measured at the same point that I_f is measured in the plume return signal. The corrected opacity is then given by

$$O_p = \left[1 - \left(\frac{I_f \, R_n}{I_n \, R_f} \right)^{1/2} \right] \times 100\% \qquad (4)$$

In the above description, I_n, I_f, R_n, and R_f are described as point measurements. In practice these values are averages in a small range (time) interval in order to reduce the effect of noise in the return signal on the accuracy of the opacity calculation.

Since the lidar method of measuring opacity does not depend on lighting conditions or background contrast conditions, it can be used in situations where Method 9 cannot; for example, nighttime and measurement of white smoke against a white background. (The lidar method does not have the inherent negative bias of Method 9.) The main requirement is that there be an unobstructed line-of-sight from the lidar to the plume, and a region of clear air in front of and behind the plume where I_n and I_f can be measured. The lidar method cannot be used in conditions of heavy precipitation or fog, and it cannot look directly into the sun.

DESCRIPTION OF THE OMEGA-1 LIDAR

A block diagram of the Omega-1 Lidar is shown in Figure 4. The lidar consists of an optical transmitter, optical receiver, and associated signal processing electronics. The optical transmitter is a pulsed ruby laser which can generate pulses with a maximum energy of 3 joules and a duration of approximately 15 nanoseconds at a pulse repetition frequency of up to 1 pulse per second. The light pulses have a wavelength of 6943 A (red light) and are approximately 5 meters in length. The pulses are transmitted through the atmosphere in a highly collimnated, very narrow beam. The backscattered light is collected by a 20.3cm Schmidt-Cassegrain telescope and detected by a special PMT that converts the optical signal into an electronic signal which can be further amplified or processed as desired.

There are two gate generators adjustable in time, duration, and amplitude which can be used to adjust or modulate the gain of the PMT to suppress or reduce some features of the plume return signal such as the plume spike while leaving other areas of the return signal unchanged.

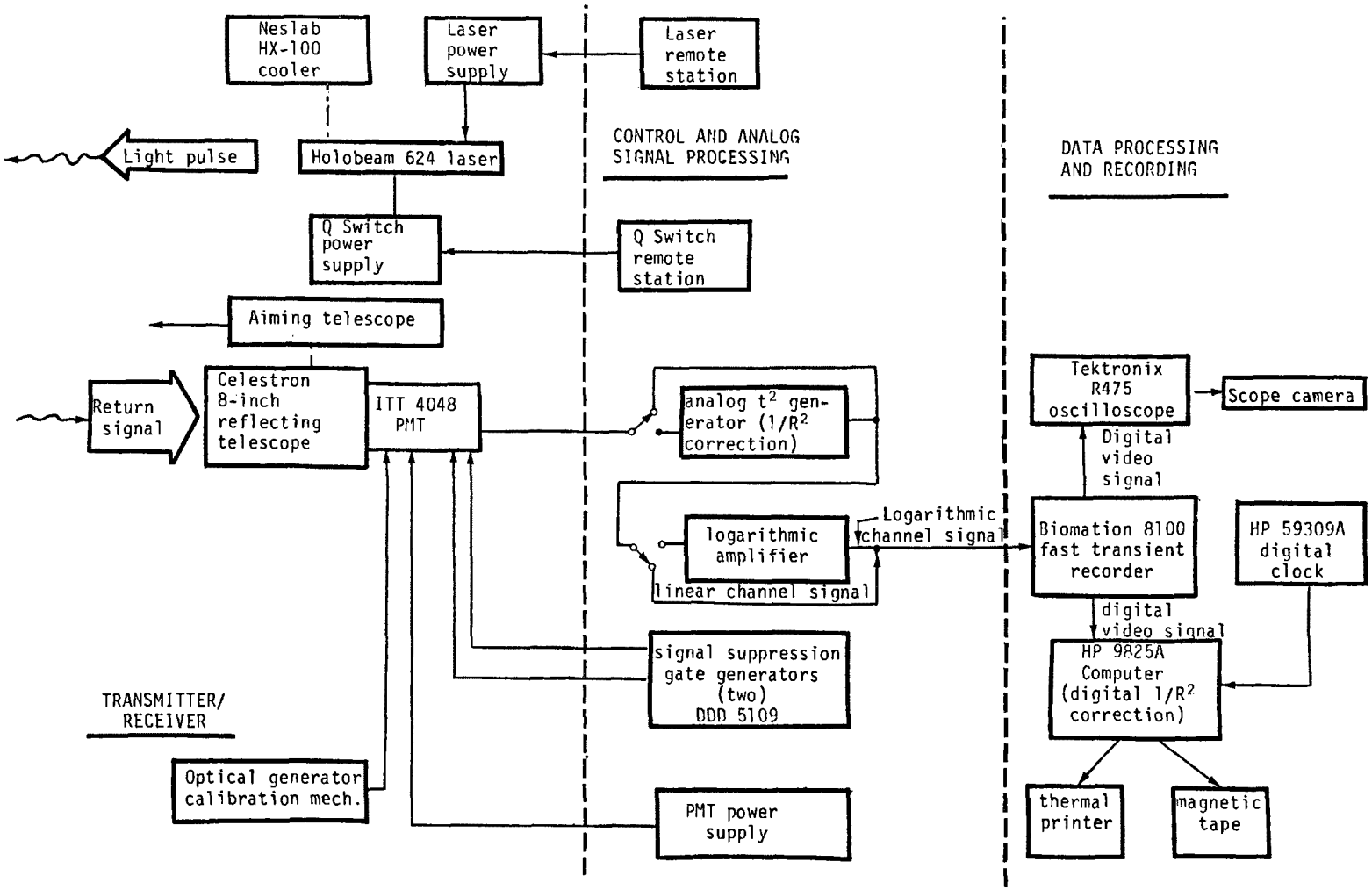

Figure 4 Schematic diagram of the Omega-i Lidar system

The analog signal processing electronics has two data processing channels and three processing options available which may be used as needed. The two data processing channels are the linear channel and the logarithmic channel. The three processing options are: 1) no processing, that is the signal is passed unchanged, 2) analog $1/R^2$ correction, and 3) logarithmic amplification.

Option 1) is used for measuring opacities of 60% or less in relatively clean air. Option 2) analog $1/R^2$ correction is not used for opacity measurements since the accuracy of the correction is not as good as can be obtained with digital correction in the computer. Option 3), logarithmic amplification, compresses the dynamic range of the return signal by amplifying low level signals and deamplifying high level signals as can be seen in Figure 5 which is a plume return signal of 80% opacity, corrected for $1/R^2$. For the same return processed by the linear channel, I_f would be almost at the zero level and very difficult to measure accurately. The logarithmic channel then is used in cases where the return signal has a large dynamic range such as high plume opacity (greater than 50%) or very hazy ambient air conditions. The analog signal processing electronics then permit measuring plume opacity accurately under a wide variety of conditions from low opacity to high opacity and a wide range of atmospheric attenuation conditions.

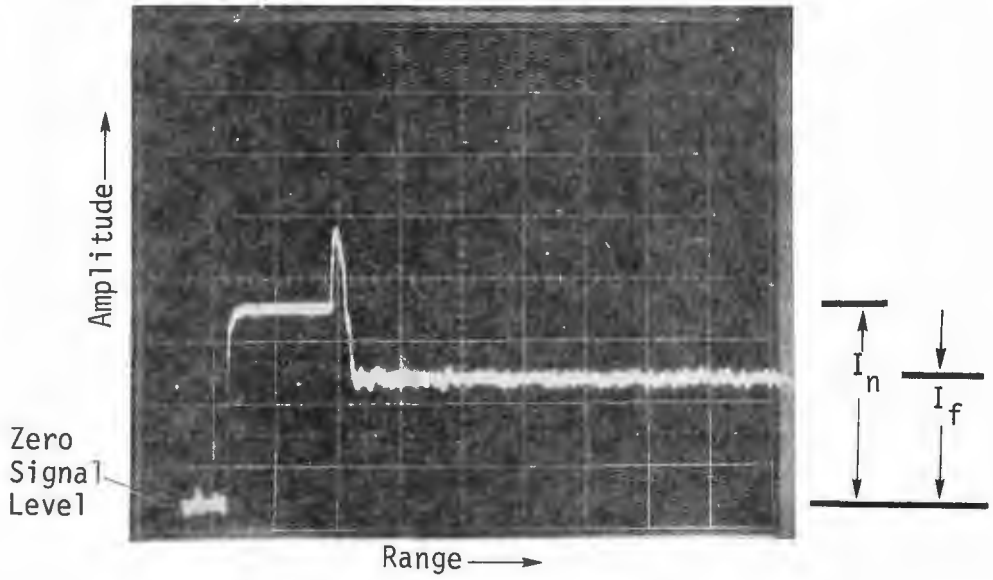

Figure 5 Logarithmic Channel Video Signal, 80% Opacity (Corrected for $1/R^2$)

The analog signal is converted to digital form by a Biomation 8100 waveform recorder, which samples the analog signal at 10 nanosecond intervals, converts it to digital form and stores it in a 2048 word buffer memory. (The abscissa of Figure 5 divided into 2048 increments or words.) The signal is then read from the Biomation buffer memory into the computer. The waveform recorder also has an analog output which allows the signal stored in the buffer memory to be displayed continuously on the oscilloscope.

The computer stores the return signal on magnetic tape along with auxiliary information such as time of day to the nearest second, video signal channel used, gate generator settings and other information. The data on tape can then be processed later using either the lidar computer or the NEIC PDP 11/70 computer.

Besides storing the return on tape, the lidar computer can also do preliminary data processing so that proper lidar operation can be verified and corrective measures taken if required.

CALIBRATION AND DATA ANALYSIS

Lidar calibration and linearity are checked using an optical generator which optically generates synthetic plume returns with known opacity values. Fiber-optic bundles are used to carry these signals from the light emitting diodes (LED's) where they are generated, to the PMT. Thus the proper operation of the entire receiver from the PMT to the computer output can be verified in a short time in the field.

Data analysis can be done either in the field as data is being taken at a later time, or both. The same analysis is performed in either case. First, the signal is corrected according to the analog signal processing which has occurred. If the gates have been used to suppress part of the signal, the signal is restored. If the logarithmic channel has been used, the return signal is converted to linear form. Finally the return signal is corrected for $1/R^2$ decay by multiplying each digital interval by R^2.

Before a series of opacity measurements, the lidar operator, viewing a typical plume return signal on the oscilloscope, selects a point in the near region of the return signal where I_n will be measured and a point in far region where I_f will be measured. These points, called "pick points," are selected in areas of the return which are clear of influence from the plume or heavy ambient particulates. Then the lidar is aimed at a point outside and upwind of the plume but close to it, and a reference (measurement) return signal from the ambient air is recorded. The values R_n and R_f at the near and far pick points are calculated as the average of ten signal sample intervals starting at the pick point. This corresponds to an overall interval of 100 nanoseconds in time or 15 meters in range. The standard deviation values for R_n and R_f are also calculated.

For each opacity measurement, the return signal is first corrected for the channel used, etc., as described previously. Then I_n and I_f and their respective standard deviations are calculated using the same procedure that was used for R_n and R_f. The opacity is then calculated using equation (4). The values of I_n and I_f, the respective standard deviation values of I_n and I_f, the plume opacity and its overall standard deviation are printed out by the computer.

This measurement is repeated at about 10 second intervals over a period of 6 minutes and the average opacity for the 6-minute period is calculated from the individual measurements. The total measurement period and frequency may vary depending on whether a federal, state or local regulation is being enforced.

Any opacity data which is expected to be used in an enforcement proceeding would be analyzed later, either on the lidar computer or the NEIC PDP 11/70 computer, to be certain that the opacity values are as accurate as possible.

PERFORMANCE EVALUATION AND FIELD TESTS

Confidence in the accuracy of the lidar opacity measurement depends on being able to verify the linearity and repeatability of all the electronics in the receiver from the PMT to the computer. The key component in the chain of electronics is the PMT. Extensive tests have been conducted using the optical generator to determine the linear operating range of the PMT and to verify its stability. These tests are repeated periodically to verify that the tube characteristics have not changed.

Proper operation of the linear and logarithmic channels, and the Biomation waveform recorder is checked periodically using known electronic test signals. Finally, as an additional safeguard, the waveform recorder is returned to the factory for calibration at least once each year.

To evaluate the performance of the complete lidar system, a number of field tests have been performed using a variety of sources.

One series of tests was performed using an aerosol chamber at SRI International. The particulate loading within the aerosol chamber could be controlled both for particle size distribution and opacity. The lidar was aimed through the chamber to measure the opacity of the particulate-laden air. There were air curtains at both ends of the chamber to prevent particulates in the chamber from diffusing out through the ends. A white light transmissometer was installed in the chamber along a path as close to the lidar line-of-sight as practicable.

For a total of 251 measurements in 30 runs at different opacities, the mean difference between the opacity as measured by the lidar and the opacity measured by the transmissomter was +0.3%, with an overall standard deviation of 6%. The standard deviation of the lidar data was 3.1% over the entire opacity range from about 0% to 95%, and the standard deviation from other sources was 5%.

Using the optical generator as the source for the plume return signals, the entire Omega-1 Lidar receiver and processing electronics were subjected to a detailed performance evaluation test. The linear channel measured opacity over the entire range from 0% to 85% with a mean difference of +0.2% and maximum standard deviation of 0.6% based upon 2,880 data values. The logarithmic channel measured opacity over the range from 20% through 85% with a mean difference range from +0.1 to -0.3% with a maximum standard deviation of 0.5% based upon 2600 data values.

The Omega-1 Lidar has also been used to monitor various types of stationary sources including a cement manufacturing plant, refineries, a glass plant, a steel plant (roof monitors), power plants, and a smoke generator.

The smoke generator is located at Camp George West in Golden, Colorado, and is used by EPA and the State of Colorado to certify visible emissions observers in accordance with Reference Method 9. It is a good test source, since the smoke opacity can be varied from 0% to 100% for both white and black smoke.

Over 30 test runs have been made using both white and black smoke. Each run was made with the smoke conditions maintained as nearly as possible in a steady state. For a given run the average opacity measured with the lidar agrees with the average opacity measured by the white light transmissometer in the smoke generator to within 1%. However, it is not unusual for individual readings made at the same time to differ by 5% or more. This is understandable, since the opacity of the smoke from the generator is not constant but varies about an average value. Since the lidar makes an instantaneous measurement of opacity (15 to 30 nanoseconds measurement time), while the transmissometer makes a measurement with an integration time of 5 to 7 seconds, the corresponding individual measurements could not be expected to agree continually.

Future plans are to conduct more tests using both the smoke generator and a variety of industrial sources under various atmospheric conditions in order to build a data base to further establish the lidar as a reliable method for measuring plume opacity day and night.

The calibration tests and the field tests have clearly shown that the lidar mechanism or technique is an excellent instrument for opacity measurement. This technique is being proposed as an Alternate method to Reference method 9.

REFERENCES

1. R.T.H. Collis, Applied Optics 9, 1782 (1970)
2. A.W. Dybdahl, The Use of Lidar For Emissions Source Opacity Determination, U.S. Environmental Protection Agency-NEIC Technical Report, In Publication.

EFFECTS OF PARTICLE-CONTROL DEVICES ON ATMOSPHERIC EMISSIONS OF MINOR AND TRACE ELEMENTS FROM COAL COMBUSTION

By
J.M. Ondov, A.H. Biermann

Lawrence Livermore Laboratory
University of California
Biomedical Sciences Division
Livermore, California 94550

ABSTRACT

In this paper we compare emissions of elements in total suspended particles and in discrete particle size intervals from five coal utility boilers, equipped with either cold- or hot-side electrostatic precipitators (ESPs) or high-energy, venturi wet scrubber systems. Coal and ash samples collected from emission-control systems and samples of atmospheric discharges were analyzed by instrumental neutron activation analysis, atomic absorption spectroscopy, and x-ray fluorescence. Emissions of Cr, Mn, Zn, and Co were enhanced probably because of corroded internal metal surfaces of the scrubbers. Concentrations of several potentially toxic elements, including Br, As, Se, Sb, U, V, and Cr, in aerosol particles emitted from the scrubber were as much as 170 times greater than in aerosol particles from the ESP. Also, the scrubber emitted a greater proportion of aerosol mass in particles of respirable sizes than did units equipped with cold-side ESPs. We conclude that the wet scrubber systems tested would be less effective in reducing the potential hazard associated with the elements cited above than a cold-side ESP of comparable overall efficiency. Based on their relative concentrations in total suspended aerosol particles and in discrete size fractions, it appears that Se, Mo, and Cr, and to a lesser extent As, Ba, Ga, U, V, and In, may be less effectively collected by the hot-side ESP than by the cold-side ESPs tested.

INTRODUCTION

According to the 1977 EPA National Emissions Report, conventional power plants fired by pulverized coal are the largest single anthropogenic source of atmospheric fine particles. Associated with particles from coal combustion are potentially toxic and carcinogenic trace elements, heavy metals, and naturally occurring radionuclides. Studies in our laboratory (Ondov et al., 1979; Ondov et al., in press; Coles et al., 1978; Coles et al., 1979)[1-4], and others (Klein et al., 1975; Gladney et al., 1976; Andren and Klein, 1975; Kaakinen et al., 1975)[5-8] of trace elements associated with emission of fine particles from utility coal plants equipped with cold-side electrostatic precipitators (ESPs) indicate that emissions of Se, Hg, As, W, and U may be large relative to other sources in cities (Gordon, 1977; Ondov et al., 1977)[9,10] and large also with respect to their natural fluxes (Bertine and Goldberg, 1971; Andren and Klein, 1975)[11,12]. Given the predicted two-fold increase in utility coal use by 1985 and recent evidence of inorganic mutagens in coal fly ash (Chrisp et al., 1978)[13], the control of these substances is of special concern.

Properties such as the gas temperature and efficiency-vs-particle-size characteristics of emission-control systems may be expected to alter both the quantity and composition of atmospheric emissions drastically. For example, commercial wet scrubbers designed for particle removal rely principally on impaction and interception mechanisms and theoretically should not efficiently remove submicron particles (McIlvaine, 1974; Stern, 1968; Calvert et al., 1975; Hesketh, 1975)[14-17]. During combustion, many potentially toxic substances, e.g., As, Se, U, V, Cd, and Pb, are volatilized and later condense on particles, resulting in an inverse-square relationship between concentration and particle size (Biermann and Ondov, in press)[18]. Thus, larger fractions of these substances are expected to escape collection by a venturi wet scrubber system. Similarly, at the higher temperatures at which hot-side electrostatic precipitators operate, we expect that somewhat larger quantities of the more volatile species may remain in the vapor phase and therefore escape precipitation. In general, the list of volatile elements in coal combustion, e.g., Hg, Se, As, Cd, Pb, Cl, U, and S, include more of the highly toxic elements than the list of relatively nonvolatile elements, e.g., Si, Al, Ca, Na, Fe, Ti, and lanthanides (Schroeder, 1971)[19]. Therefore, the relative efficiencies of various alternative particle-control technologies should be carefully evaluated.

In this paper, we describe our recently published work on the elemental emissions and particle-size distributions of the elements from two power units equipped with high-energy, variable throat, venturi wet scrubbers and a unit equipped with a cold-side ESP. Because all of the units were in use

at the same power plant, burned the same low-sulfur, high-ash coal, and had boilers with similar fly-ash elutriation and particle-size characteristics, we can evaluate the relative effectiveness of the two types of control devices for trace element removal by comparing their emissions. We also include data from two other western coal-fired power plants that used either a high-efficiency cold- or hot-side ESP. We, therefore, discuss emissions from a total of five boilers at three separate plants, designated as Plants A, B, and C.

"Work performed under the auspices of the U.S. Department of Energy by the Lawrence Livermore Laboratory under contract number W-7405-ENG-48."

EXPERIMENTAL

Power Units

At Plant A, a 430-MW(e) unit equipped with a cold-side ESP with total particle removal efficiency of 99.8% was studied. At Plant B, three separate units designated as Units 1, 2, and 3 with maximum steam capacities of 160, 203, and 654 kg/s, respectively, were tested. Units 1 and 2 were equipped with high-energy, venturi wet scrubbers designed to remove 99.2% of the incident aerosol. Unit 3 was equipped with a cold-side ESP that operated at 97% efficiency. A 350-MW(e) unit with a hot-side ESP of 99.8% design efficiency was tested at Plant C. Stack and precipitator gas temperatures of the three ESP-equipped units were 114 and 110°C at Plants A and B, and 400 and 139°C at Plant C. The gas temperatures at the sampling location at the outlet of the mist eliminators of the venturi wet scrubber systems were about 54°C. Additional design and operating parameters for the three units at Plant B are listed in Table 1.

Low-sulfur, western coal was burned in each of the units. Ash contents of coal burned at Plants A, B, and C were 9.2, 23.9, and 21.7%, and sulfur contents were 0.46, 0.52, and 0.94%, respectively.

Sampling and Analyses

Total aerosol and size-segregated fly-ash samples were collected in-stack at each of the plants using a modified, EPA-method-5-type sampling system. Samplers were mounted at the in-stack end of the sampling probe permitting in-stack particle collection. Filter samples were obtained with fluoropore or Nuclepore filters with pore diameters of 1.0 and 0.4 μm, respectively. Size-segregated fly-ash samples ranging from ≤ 0.1 to ≥ 30 μm were obtained with 8- and 12-stage University of Washington Mark III and Mark V inertial cascade impactors. Polycarbonate or Kapton impaction substrates were coated with grease to improve collection efficiency. Records of plant-operating data collected hourly included gross generating load, coal consumption, and proximate analyses. Energy-conversion efficiencies (determined monthly), status of ESP sections, and scrubber venturi pressure (hourly) were obtained from plant personnel. Velocity, temperature, and pressure of the stack gas were monitored continuously during each sampling. Samples of coal, ESP fly ash, bottom ash, and scrubber slurry were also taken during the stack fly-ash collections at each of the plants.

At Plants A and C, 15 and 14 particulate samples were collected at the stack sampling locations over a one-week period during which the units operated at full capacity. At Plant B, cascade impactor and filter samples

were collected at the outlets of the scrubber mist eliminators during a two-week period in June and in-stack at the 61-m level of the ESP-equipped unit during a one-week period in July 1975. Sample collections from the scrubber occurred several months after scrubber maintenance. Additional samples were collected from scrubber Unit 1 and the ESP unit along with concurrent inlet and outlet testing during a third period in February 1976 shortly after scrubber maintenance. A total of 88 filter and cascade impactor samples were collected during these periods.

During the sampling period in June, Units 1 and 2 operated at 90 to 100% full capacity and the differential venturi pressures of each of the scrubber systems was about 35 mm Hg. During February, the measured removal efficiency of toal suspended partides (TSP) of scrubber Unit 1 was 99.7 $\pm$ 0.1% at a differential venturi pressure of 36.8 mm Hg.

Gross load of the ESP-equipped unit varied from 70 to 95% full capacity during the sampling period in July, but was constant during each test. During most of the test period, 4 of the 32 precipitator sections were inoperative. However, compliance with emission standards (213 ng/J) and precipitator efficiency were maintained by operating at reduced loads. Under the test conditions, precipitator efficiency for the removal of TSP was estimated at about 97%. In February, the ESP suffered failures that resulted in a 10- to 20-fold increase in emissions; hence, only the results of inlet testing on this unit are reported.

Coal, stack fly ash, bottom ash, and ash collected by the particle-control devices at each of the plants were analyzed for up to 43 elements by instrumental neutron activation analysis, Ni and Pb in bulk coal and fly ash samples by energy-dispersive x-ray fluorescence analysis, and Cd and Be by atomic absorption spectroscopy using a heated graphite analyzer. Details of these analyses were described previously (Heft, 1977; Bonner *et al.*, 1975; Ragaini *et al.*, 1976)[20-22]. Results from each of these techniques were verified with NBS standard reference materials (SRM) 1632 (coal) and 1633 (coal fly ash), which were analyzed along with the samples, and through interlaboratory comparisons of results on SRM samples (Ondov *et al.*, 1975).[23]

DISCUSSION

Comparison of Emissions from Scrubber- and ESP-Equipped Units at Plant B

Scrubber Emissions. In Table 2, we compare emissions of trace elements collected during the June and February sampling periods at Plant B. To account for differences in the coal consumption, electric power production, and efficiency of energy conversion for each unit, the emission data were normalized to the heat input into the boiler as described elsewhere (Ondov et al., 1979).[1]

As shown in Table 2, emissions of most elements from scrubber Units 1 and 2 were similar during the June 1975 sampling, despite the differences in generating loads of 30%. Thus, normalization to gross heat consumption accounts successfully for differences in coal consumption of these units.

Emissions of most elements from scrubber-equipped units during the June 1975 period, however, were about 1.5 to 5 times greater than those from scrubber Unit 1 during the February 1976 period. Coal composition during the three sampling periods was nearly identical as shown in Table 3. The greater emissions in June might have resulted from entrainment problems with the mist eliminators or high content of dissolved solids in the recycled scrubbing solution. We note that the unit was, however, operating within compliance (TSP emission $\leq$ 21.5 ng/J) during this period.

ESP and Scrubber Efficiency. Curves of particle-collection efficiency vs particle size for the ESP and Unit 1 scrubber were constructed from the data from concurrent inlet-outlet sampling during February. As shown in Figure 1, the collection efficiency of the scrubber unit for supermicron particles is >99%, but below 1 μm drops off rapidly with decreasing particle size. The aerodynamic 50% cut-off diameter for the scrubber was about 0.75 μm, and its efficiency for TSPs was 99.7 $\pm$ 0.1%. The negative efficiency for the collection of very small particles is attributed to mist entrainment and flash volatilization of liquid droplets that contain dissolved and suspended solids.

Unfortunately, the mechanical failures noted earlier prevented measuring optimum ESP performance. The ESP efficiency curve, however, agreed qualitatively with that typical of a cold-side ESP shown in Figure 2. These curves are characterized by high collection efficiencies of both supermicron and submicron particles, with a shallow minimum for particles in the 0.1- to 1.0-μm range. Thus, we would expect submicron particles to penetrate the scrubber more effectively than the ESP.

Many potentially toxic trace substances become highly concentrated on fine particles derived from coal combustion because of volatilization and surface-condensation mechanisms or as a result of residence in fine mineral grains in coal. Curves of concentration enrichments vs particle size of typical elements in fly ash collected from the ESP unit are shown in Figure 3. Concentrations of elements in fly ash that show some surface-deposition component are often 10 to 50 times greater in submicron particles than in particles >10 μm in diameter. Curves of concentration enrichment vs particle size for Sb, As, Mo, V, In, and Ga are similar to those of Se, W, U, and Ba shown in the figure. Because of these enrichments on fine particles and the poor removal efficiency of the scrubbers for fine particles, these elements should penetrate the scrubber more effectively than the ESP.

As noted earlier, the emissions or penetrations of trace substances from the two units are comparable if the particle-size distributions from the two types of control devices are also similar.

Particle Size Distributions at the Inlet. Size distributions of particles entering both a scrubber system (Unit 1) and the ESP were measured with cascade impactors during the February experiment. The distributions of Sc, an element whose distribution is independent of particle size and shown in Figure 4, indicate that normalized rates of mass flow (mass/unit heat input) and particle-size distributions are nearly the same for particles < 2 μm. The considerable discrepancy in the curves at larger particle sizes probably results from problems associated with turbulence and severe losses on walls of the impactor. The data reflect single-point sampling in turbulent inlet ducts and, hence, difficulties in obtaining truly isokinetic and representative sampling. As indicated by the dark and light symbols in the figure, the results of two successive measurements of particles in both control devices generally differed at sizes ≥ 5 μm. Based on the engineering parameters, the normalized fly-ash input (mass/gross boiler heat input) should be equal to that of the ESP. Because the composition of the coal burned during each sampling period was essentially identical, emissions normalized to gross boiler heat input may be compared directly.

Emisssion and Penetration of Elements. Particle-size distributions of several elements in aerosols discharged from the scrubber- and the ESP-equipped units are shown in Figure 5. In the figure, emission rates normalized to the boiler heat inputs are plotted vs the aerodynamic diameters of particles on individual impactor stages and back-up filters as determined from particle sizing from scanning electron micrographs.

In the scrubber experiment in June, $\geq 90\%$ of the mass emission of most elements occurred in particles of diameters ≤ 1 μm. Several elements, however, including Co, Cr, Fe, Mn, Cl, Br, Na, K, and Ca, often had appreciable or even major portions of their mass in aerosols of large sizes. Therefore, these elements are most probably contained in the liquid droplets. Scanning electron microscope analyses of dried impactor substrates collected in June revealed only submicron fly-ash particles on the uppermost (large particle) stages. However, on filter and impactor

substrates collected in February, fly-ash particles with physical diameters as large as 6 μm were present. These larger particles suggest that the scrubber (Unit 1) was less efficient in removing supermicron particles of the fly ash in February than in June. Despite this apparent decrease in collection efficiency of supermicron particles, the normalized elemental emission rates of the scrubber-equipped unit in June were 1.5 to 5 times higher than in February. As shown in the figure, the increased emission rates in June were generally confined to submicron-size particles. Evaporation of the liquid in entrained droplets can lead to the formation of submicron particles. Hence, the greater emissions in June may have resulted from entrainment problems.

By comparing the emission rates of elements established for particles collected on the back-up filters, we estimate that during the sampling period in February, when the scrubber was operating nearly optimally, it permitted six times more particulate material to penetrate than did the ESP.

In Table 4, we list the ratios of the penetrations of trace elements through the scrubber-equipped unit to those through the ESP-equipped unit for all particle sizes. The penetration ratios are nearly identical to the ratios of the emission rates from the two units except that they account for the small differences in elemental concentrations in coal, as well as for differences in the generating capacity and quantity of coal burned.

Based on the efficiencies of the two devices for TSPs, we would expect the penetration ratios to all be 0.087 if the elements were distributed uniformly among the particles of different sizes. As shown in Group 1 of Table 4, the penetration ratios for several trace elements are much greater than 0.087.

The concentrations of most of the elements listed are highly enriched on particles leaving the boiler as a result of volatilization and surface-deposition mechanisms. Calcium and strontium, however, are generally not enriched on small particles by vapor deposition, but are components of the limestone added to reduce SO_2 emissions. Therefore, the concentrations of these elements are probably enhanced via mist entrainment and droplet evaporation, as both of these mechanisms may lead to the formation of fine particles. Because the scrubbing solution is recycled, elements that can be leached from fly-ash particles, such as Cl, Br, and Se, may also be enhanced by these mechanisms.

Substantial fractions of Se occur in the vapor phase at inlet-gas temperatures (Ondov *et al.*, 1977)[10]. Thus, the very large relative emission of Se probably results from both scrubbing and condensation occurring at the lower gas temperature at the scrubber sampling location (54 vs 110°C in the ESP stack).

Scrubber emissions of Cr and Mn, and to some extent Zn and Co (Group 2), were also enchanced relative to the TSP. Emission of these elements seems to be enhanced by corrosion of metal surfaces inside the scrubbers. Although independent evidence supports this conclusion, the magnitude of the enhancement might be in error because of possible contamination by corrosion of the stainless steel samplers.

Matrix elements such as Fe, Al, and Sc, (Group 3) as well as total particulate mass, were emitted in greater quantities per unit heat input from the ESP unit than from the scrubber unit because of their predominant association with large (MMADs of about 10 μm) silicate fly-ash particles, which the scrubber removed efficiently.

Under the conditions of operation in February, scrubber emissions of trace elements in each of the groups on a per joule basis were actually less than those from the ESP. However, as noted earlier, the ESP that was tested at Plant B was somewhat undersized and not nearly as efficient as larger, more modern units such as the one used at Plant A. The ratios of the concentrations of elements in particulate emissions from the scrubber- and ESP-equipped units given in of Table 4 indicate the relative emission rates of elements that would be obtained if the overall mass-removal efficiencies of the two devices were equal. In this case, the venturi scrubber tested would clearly be less effective in removing the elements listed than a cold-side ESP. Based on the behavior of Pb, Cd, and S during coal combustion, we can assume that these elements also effectively penetrate the scrubber. In general, more of the elements that are toxic to humans are also those that were found or are expected to penetrate the scrubber effectively. Therefore, we conclude that the venturi scrubber system tested would be less effective in reducing the potential inhalation hazard of trace elements than an ESP of comparable overall efficiency.

Effects of a Hot-Side ESP

Considerations of Vapor Pressure and Chemical Forms. As suggested earlier, some of the more volatile, trace-element species may escape precipitation at the high temperatures at which hot-side ESPs operate. The volatility of the trace elements may depend on its chemical form in coal, the kind of reactions during combustion, the nature of particle surfaces, and the magnitude of surface area.

Complete data regarding the actual chemical forms of trace elements in coal and combustion products do not presently exist. X-ray diffraction studies of coal fly ash (Johnson, 1979)[24] and stoichmetric considerations of possible anions indicate that the largest portions of essentially all of the major elemental components occur as oxides, along with some sulfates and chlorides. Therefore, trace elements may also occur in these forms. At trace levels, however, the relative abundances of halogens, sulfur, nitrogen, and other anionic species are much greater, and a greater variety of covalent and ionic species may be important. Also, the final chemical form may be governed by complex competitive reactions.

The oxides and carbonates of Hg are not stable at high temperatures; hence, Hg may well be emitted as the metal. Based on selective chemical reactions and the solubilites of individual Se compounds, Andren and Klein (1975)[7] deduced that essentially all of the Se in coal fly ash obtained from the Allen Steam Plant was present as Se metal as opposed to selenium dioxide or the selenate or selenite anions. They postulated that the high abundance of the elemental form might result from the reduction of Se in the

oxide or oxyanion forms to the elemental state by SO_2. In the laboratory ashing of coal, As typically volatilizes, probably as As_2O_3, in high Ca coals, but is largely retained as arsenate or arsenite in low Ca coals (Betnell, 1962)[25]. Calcium is presumed to compete with arsenic in reaction with SO_2 on particle surfaces. Therefore, other trace elements might also be reduced to the elemental state by SO_2.

In Table 5, we list the equilibrium vapor pressures (expressed as μg of the element per m^3 of gas) of several trace elements and their compounds at precipitator and stack-gas temperatures measured at Plants A, B, and C. Also listed are the maximum possible vapor concentrations of the elements that would occur if all of the element introduced into the furance were vaporized, except for the quantity measured in bottom ash. These data were computed from the elemental concentrations in coal, the coal feed rates, and volumetric flow rates of the gas. The vapor concentrations were obtained by interpolation or extrapolation of vapor pressure data (Weast, 1975)[26]. If we compare the expected vapor pressure with the maximum possible concentrations, we can estimate the portion of the element or its compound that might be expected to remain in the vapor phase at the specified temperatures.

These data indicate that both Hg and $HgCl_2$ should exist totally in the vapor phase at precipitator and stack-gas temperatues at each of the plants. This is consistent with the mass balance reported by Billings and Matson (1972)[27], who found that more than 90% of the Hg emission from a coal-fired power plant was emitted in the gas phase. The Hg balance at Plant C (Table 6) indicates that about 94% of the Hg was emitted in the gas phase.

Similarly, the vapor pressure of elemental Cd is much larger than the maximum available concentration at Plant C and that at Plants A and B is nearly equal to the maximum possible concentration. Thus, if Cd were emitted in the elemental state, it would be expected to escape precipitation at both plants. Cadmium oxide, however, is much less volatile than elemental Cd. If present in this form, only 0.1% of the Cd would escape in the vapor phase at Plant C, and essentially all of it would have condensed before precipitation at all three plants. Cadmium chloride would be expected to penetrate the hot-side precipitator, but quantitatively condense on particles after gas temperature is reduced by passing through the air preheater.

Elemental Pb, Co, and Mo are much less volatile than Cd and would not have significant fractions in the vapor phase at any of the temperatures. Elemental As, $PbCl_2$ and MoO would each exist in the vapor phase only in the hot-side precipitator. Arsenic trioxide and $SbCl_3$ would be volatile at all of the temperatures. Nearly all of the Sb present as Sb_2O_3 would be volatile at 400°C, and large fractions would volatilize at the other temperatures; Se is predicted to exist totally in the vapor phase at all of the temperatures as the oxide and in the elemental form at 400°C and 139°C. If all of the Se at Plants A and B were in the elemental form, then about 15 and 13% of it, respectively, would be in the vapor phase at the stack temperatures.

We note that at 139, 114, and 110°C, the maximum possible vapor concentrations of Se, Cd, and Sb are near the saturation vapor pressures of elemental Se, elemental Cd, and Sb_2O_3. If these were indeed the chemical forms, the relative proportions of the vapor and particulate components would be quite sensitive to the magnitude of their concentrations in the coal, i.e., a greater proportion of the element might be collected by a given precipitator simply because its vapor concentration would be high enough to cause condensation on particles before reaching the ESP.

Mass Balances of Volatile Elements

In Table 6 are listed the flow rates of several trace elements in coal and ash streams from each of the three plants. By comparing the sum of the flow rates of elements in each of the ash streams with the flow rates of elements in the coal stream, we can estimate the portion that might be in the vapor phase. The problem with this technique is that even for elements for which the analytical uncertainty is quite good, the overall uncertainty in the unaccounted-for fraction is typically greater than 7% of the original flux in coal and generally quite large with respect to the fraction unaccounted for. Of the 15 or more elements for which a mass balance was constructed, only Hg, Cl, and Se seemed to have truly detectable vapor-phase components on the basis of these data. The vapor concentrations of As, Sb, Mo, W, U, Cd, Pb, and Cr appear to be less than 12%. Given the extremely high efficiencies of the control devices (99.8%), it is clear that a vapor-phase component of only a few tenths of a percent would be large relative to the portion emitted on particles. Therefore, vapor-phase components must be measured directly.

The mass-balance data are consistent with the occurrence of Hg as the element and Cd and Pb as the oxides. At Plant C, nearly all of the Se, As, and Sb were predicted to be volatile at the stack-gas temperature on the basis of either the oxides or the elemental forms. The much lower fractions of these elements predicted by the mass balances and confirmed for Se by direct measurement of vapor at Plant C in later experiments may suggest that significant portions of these elements are present as the nonvolatile oxyanions, e.g., selenate/selenite, arsenate/arsenite, and antimonate. It seems that about 35% of the Se is emitted in the vapor phase at Plants B and C despite the considerably higher temperature at Plant C, where we predicted that all of the Se would be in the vapor phase on the basis of elemental Se. It would seem, therefore, that more of the Se at Plant C is in a nonvolatile anionic form compared with Plant B. This may be due, in part, to the higher Ca:Se ratio in the coal of Plant C, i.e., 8,000:1 compared to a ratio of about 3,500:1 at Plant B, which, according to the hypothesis of Andren and Klein, would be conducive to the occurrence of selenate/selenite.

It is quite possible, however, that the vapor pressures of these species are reduced by chemisorption on fly ash or carbonaceous particles. This seems possible especially in light of the high concentrations of Se and Br on large particles at all of the plants studied and as seen in the plot of relative concentration vs particle size shown for Plant A aerosols in Figure 6.

Here we see that the concentrations of Se and Br were present in both small and large particle sizes at all of the plants studied and correlate roughly with the distribution of surface area as determined by nitrogen adsorption of sized fly-ash fractions collected at Plant A. The concentration of carbon increased in successively larger particle fractions of Plant A fly ash; hence, the increase in surface area may be the result of a greater abundance of highly porous carbonaceous particles, which effectively adsorb Br and Se vapors. Electron spectroscopy studies of fly ash from Plant A indicate that carbon is present primarily in the graphitic or simple aliphatic forms. We have determined the surface areas of particles at Plant A before and after removing carbon by combustion in an oxygen atmosphere. From this experiment, we infer that significant portions of the total surface area of all particles eluted from the boiler were due to carbon, which occurred in the fly ash at Plant A at concentrations of about 4%. We believe, therefore, that the quantity of carbonaceous particles and hence the carbon combustion efficiency may be important in controlling the vapor pressure of trace species in gases from coal combustion.

Finally we note that the vapor fraction of Se at Plant A, corresponding to about 40 $\mu g/m^3$ is somewhat larger than the 15 $\mu g/m^3$ that we predicted on the basis of elemental Se alone. Therefore, some of the Se at Plant A might be in the form of selenium dioxide.

Concentration Enrichments. On the basis of vapor pressure data, we predict that Cd, Pb, Mo, As, Se, and Sb might have significant vapor-phase components in the hot-side ESP and would condense on particles at the cooler temperature of the stack gas. These elements, therefore, would penetrate the ESP more effectively than the nonvolatile components, their concentrations becoming enriched. Alternately, if appreciable components of the element did not condense or adsorb on particles at the stack-gas temperature, then their concentrations might be deficient on particles relative to those collected at the lower stack-gas temperature of the plants with cold-side ESPs. After atmospheric release, these vapor components may be expected to condense or adsorb on particles at the much lower ambient atmospheric temperatures.

As suggested by Davison et al. (1974),[28] the concentration of an element in fly-ash particles may be expressed in terms of its volume and surface-associated components. The concentration of an element distributed throughout the volume of the particles is uniform with respect to size. The concentration of the element associated with the surfaces of particles, however, varies inversely with particle radius. In these data, we determined that the power of the radius in the concentrations-vs-size relationship is two (Biermann and Ondov, in press)[18]. This is the relationship expected for the deposition of vapor to the surface of particles in aerosols governed by slipflow mechanics. Given this relationship, log plots of concentration vs particle diameter should be linear, with the magnitude of the slope proportional to the depth of the surface layer. The large negative slopes of Se, W, U, and Ba shown in Figure 3 for six replicate concentration-vs-size profiles of elements emitted in aerosol particles at Plant B indicate large surface components

for these elements. The elements Sb, As, V, Pb, Cd, and In (not shown) also display this behavior. The concentration of Fe and Na, as well as Al, Sc, K, Mg, lanthanides, and other elements that are not volatilized in the furnace are associated predominantly with the volume component. We also note that preliminary calculations indicate that the considerable deviation from linearity in the 2 to 8 μm region of the curves is a result of coagulation between highly enriched fine particles of the accumulation mode and the larger particles (MMAD ~ 10 μm at Plant B), that comprise the major mass emission mode.

The five replicate plots of relative concentration vs particle size shown in Figure 7 for Mo in stack-emitted aerosol particles at Plant C also indicate a large vapor-deposited component for this element as did plots of W, Zn, Co, and Cr. The concentrations of As, Ba, Ga, U, V, and In, by contrast, are much more uniform with respect to size as would be the case if vapor components of these elements had not yet condensed or adsorbed onto particle surfaces.

In Table 7 we compare the relative penetrations of several elements measured on particulate emissions from Plants A, B, and C, as well as those from the Allen Steam Plant (Klein et al., 1975)[5] and the Chalk Point Plant (Gladney et al., 1976)[6], two other plants equipped with cold-side ESPs. The penetration of an element is defined as the rate of atmospheric emission divided by the input flow rate of the element in coal, i.e., data in Column 6 of Table 6 divided by the data in Column 3. The relative penetrations are defined as the ratios of the penetrations of an element to that of an element whose concentration is uniform with respect to particle size, in this case, Sc. This normalization accounts for differences in precipitator efficiencies, elemental concentrations in coal, and coal feed rates at each of the plants. Because of the double normalization, the relative penetration of an element is identical to and may be interpreted as an enrichment factor.

Of the 14 elements listed, only three, Cr, Mo, and Se, seem to have higher penetrations at Plant C and hence are more highly enriched on aerosols emitted than those emitted at plants with cold-side ESPs. The observed enrichments of Mo and Se can be easily explained in terms of condensation or adsorbtion of MoO and elemental Se vapors, as discussed above. The enrichment of Cr might possibly be due to the volatile chloride, or oxychloride, however, definitive data are not available.

Two elements, Sb and As, seem to have somewhat lower concentrations on stack aerosols from Plant C. The concentrations of Br and Cl on stack aerosols are often much less than 1, presumably because these elements do not condense or effectively adsorb on particles at stack temperatures. As discussed above, As_2O_3 and Sb_2O_3 are highly volatile, but would be expected to be deficient on stack aerosols from Plants A, B, and C. The lower concentrations of these elements on particles at Plant C might occur because greater portions of the As and Sb are in the oxide forms than at Plants A or B. Or perhaps because As_2O_3 vapors are not as readily adsorbed on particles at the higher gas temperature of the hot-side ESP.

SUMMARY AND CONCLUSIONS

In comparisons of emissions from three separate coal utility units in use at a single western plant, the concentrations of Se, Sb, W, As, Mo, V, U, Ba, Co, Cr, and possibly Pb and Cd in particles emitted from two high-energy venturi wet scrubber systems were significantly greater than concentrations in particles emitted from the unit equipped with a cold-side ESP. We conclude that the wet scrubber system tested would be less effective in reducing the potential hazard associated with these elements than a cold-side ESP of comparable overall efficiency.

Based on their relative concentrations in total suspended aerosol particles and in discrete size fractions, we conclude that Se, Mo, Cr, and, to a lesser extent As, Ba, Ga, U, V, and In, may be less effectively collected by the hot-side ESP than by the cold-side ESP units that we tested. Mass balances and limited vapor determinations of trace elements indicate that, except for Hg, Se, and Cl, the vapor components of the elements are quite small relative to the total quantities available in coal, but may easily be large relative to the quantities emitted on particles. The vapor components of Se, Cd, As, Mo, and Sb at three coal-fired power plants were small also relative to the vapor pressures predicted for their volatile oxide or elemental forms. We suggest that further evaluation of control technologies will require additional research to characterize factors governing the fractionation of elements between volatile and nonvolatile forms and the dynamics of vapor deposition onto particle surfaces.

Table 1. OPERATING CONDITIONS OF A VENTURI WET SCRUBBER AND COLD-SIDE ESP.

Parameter	Scrubber units #1	#2	ESP unit
Flow rate of flue gas at inlet (m^3/s)[a]	254	322	1026
Temperature[b] (^oC)	129	129	117
Suspended particle concentration at inlet ($\mu g/m^3$)	20.2	20.2	23.0
SO_2 concentration at inlet (ppm)	650	650	800
Efficiency of particulate removal (%)	99.2[c] (99.7 $\pm$ 0.1)[d]	99.2	97[e]

[a]Nominal value at 21°C. [b]Measured at location of outlet sampling.
[c]Nominal values. [d]Measured during February sampling episode.
[e]Estimated from elemental penetrations and plant-design data.

Table 2. NORMALIZED EMISSION RATES OF SEVERAL ELEMENTS IN PARTICULATE EMISSIONS FROM TWO SCRUBBER-EQUIPPED ELECTRICAL GENERATING UNITS (pg/J).[a]

Element	June		February
	Unit 1	Unit 2	Unit 1
Al	1320 ± 120	1130 ± 160	680 ± 0.018
La	0.46 ± 0.04	0.45 ± 0.02	0.275 ± 0.018
Na	230 ± 20	219 ± 12	170 ± 8
Fe	455 ± 40	425 ± 14	239 ± 28
V	16.6 ± 0.8	19.9 ± 1.2	9.4 ± 1.0
As	13.5 ± 0.4	9.2 ± 0.4	5.24 ± 0.016
Se	20.5 ± 1.0	21.0 ± 1.6	12.9 ± 0.4
Ba	450 ± 40	580 ± 60	97.9 ± 0.8

[a]Data listed are median values of up to 8 and 14 samples from Units 1 and 2 in June and up to 23 samples from Unit 1 in February. The uncertainties reflect only those in the elemental analyses at the 95% confidence.

Table 3. CONCENTRATIONS OF SEVERAL ELEMENTS IN COAL BURNED DURING SAMPLING PERIODS (μg/g)[a].

Elements	June 75		July 75		Feb. 76	
Al	30100 ± 4990	(7)	30300 ± 3600	(15)	29500 ± 2390	(7)
La	13.0 ± 1.0	(7)	14.3 ± 0.8	(15)	13.4 ± 0.8	(7)
Na	2970 ± 370	(7)	2940 ± 160	(15)	2930 ± 248	(7)
Fe	5940 ± 740	(7)	5720 ± 380	(15)	6470 ± 570	(7)
V	22.9 ± 3.0	(4)	22.1 ± 3.2	(9)	24.9 ± 3.1	(4)
As	2.03 ± 0.43	(7)	2.73 ± 0.71	(11)	2.84 ± 0.84	(6)
Se	1.41 ± 0.11	(7)	1.55 ± 0.15	(15)	1.74 ± 0.25	(7)
Ba	466 ± 108	(7)	418 ± 88	(14)	420 ± 167	(7)

[a]Averages and standard deviations; number of samples given in parentheses.

Table 4. RATIOS OF EMISSION RATES OF ELEMENTS FROM A VENTURI WET SCRUBBER AND AN ELECTROSTATIC PRECIPITATOR (FEBRUARY SCRUBBER DATA: JULY ESP DATA)

Element	Penetration ratio[a] Median	Penetration ratio[a] Range	Concentration ratio[b] Median	Concentration ratio[b] Range
	Group 1			
Br	15 ± 0.04	5.4 - 63	170 ± 0.5	66 - 250
Se	1.9 ± 0.1	1.2 - 5.5	22 ± 3	15 - 22
Sb	0.58 ± 0.02	0.39 - 2.1	6.7 ± 0.7	4.8 - 8.4
W	0.36 ± 0.03	0.25 - 1.1	4.1 ± 0.6	3.0 - 4.4
As	0.32 ± 0.01	0.22 - 1.7	3.7 ± 0.4	2.7 - 6.8
Mo	0.31 ± 0.04	0.13 - 1.2	3.6 ± 0.6	1.6 - 4.8
V	0.21 ± 0.02	0.13 - 0.69	2.4 ± 0.4	1.6 - 2.8
Ca	0.22 ± 0.015	0.13 - 0.67	2.5 ± 0.3	1.6 - 2.7
U	0.14 ± 0.01	0.065 - 0.45	1.6 ± 0.2	0.79 - 1.8
In	0.14 ± 0.01	0.080 - 0.65	1.6 ± 0.2	0.98 - 2.6
Ba	0.12 ± 0.005	0.060 - 1.0	1.4 ± 0.2	0.73 - 4.0
Ga	0.11 ± 0.01	0.061 - 0.42	1.3 ± 0.2	0.74 - 1.7
Sr	0.10 ± 0.04	0.042 - 0.42	1.1 ± 0.4	0.51 - 1.7
	Group 2			
Cr	1.03 ± 0.06	0.046 - 29	12 ± 2	0.56 - 120
Mn	0.48 ± 0.02	0.042 - 13	5.5 ± 0.6	0.51 - 52
Zn	0.11 ± 0.01	0.049 - 3.7	1.3 ± 0.2	0.060 - 15
Co	0.064 ± 0.003	0.020 - 1.8	0.74 ± 0.08	0.24 - 7.2
TSP	0.087 ± 0.009	0.082 - 0.25	≡1.0 ± 0.1	≡1.0 - 1.0
	Group 3			
Mg	0.08 ± 0.03	0.02 - 0.5	0.9 ± 0.2	0.2 - 2.0
Na	0.077 ± 0.003	0.025 - 0.27	0.89 ± 0.10	0.30 - 1.1
Zr	0.05 ± 0.02	0.03 - 0.3	0.6 ± 0.2	0.4 - 1.2
Fe	0.057 ± 0.004	0.030 - 0.54	0.66 ± 0.09	0.37 - 2.2
Ti	0.047 ± 0.011	0.024 - 0.25	0.54 ± 0.14	0.29 - 1.0
Al	0.043 ± 0.001	0.017 - 0.34	0.49 ± 0.05	0.21 - 1.4
La	0.033 ± 0.003	0.010 - 0.11	0.38 ± 0.05	0.12 - 0.44
K	0.031 ± 0.009	0.012 - 0.17	0.36 ± 0.11	0.15 - 0.68
Ce	0.028 ± 0.002	0.016 - 0.092	0.32 ± 0.04	0.20 - 0.37
Th	0.025 ± 0.001	0.011 - 0.094	0.29 ± 0.03	0.13 - 0.38
Sc	0.025 ± 0.001	0.013 - 0.95	0.29 ± 0.03	0.16 - 0.38

[a]Uncertainties are derived from analytical uncertainties only.
[b]Emission ratio normalized to mass emission rates. [c]Group 3 also includes the elements Nd, Eu, Yb, Sm, Dy, and Lu.

Table 5. VAPOR PRESSURES OF SEVERAL VOLATILE ELEMENTS AND THEIR COMPOUNDS AT PRECIPITATION AND STACK-GAS TEMPERATURES, $\mu g/m^3$

	Plant C			Plant A, B		
	Maximum available conc	ESP 400°C	Stack 139°C	Maximum available conc	ESP 114°C	Stack 110°C
Mo	190-300	2.2×10^{-22}	5.6×10^{-45}	-; 180	9.7×10^{-49}	2.2×10^{-49}
MoO_3		139	1.2×10^{-7}		3.6×10^{-9}	2.0×10^{-9}
Hg	10 ± 4	1.7×10^{10}	1.9×10^{7}	7.7; 5.3	6.2×10^{6}	5.1×10^{6}
$HgCl_2$		9.6×10^{10}	1.3×10^{7}		3.0×10^{6}	2.4×10^{6}
Se^o	96 ± 12	1.5×10^{7}	148	100; 120	21.6	15.5
SeO_2		2.8×10^{10}	1.4×10^{6}		2.8×10^{5}	2.1×10^{5}
As^o	360 ± 60	1.2×10^{7}	3.9	37; 200	0.33	0.21
As_2O_3		2.8×10^{9}	3.9×10^{5}		8.8×10^{4}	6.8×10^{4}
Sb^o	50 ± 7	2.4	4.7×10^{10}	9.9; 43	1×10^{-11}	6×10^{-11}
Sb_2O_3		9.7×10^{5}	47		9.0	6.8
$SbCl_3$		1.6×10^{11}	5.2×10^{8}		2.0×10^{8}	1.7×10^{8}
Cd	23 ± 11	7.7×10^{6}	70	~10; ~5	10	7.3
CdO		2.4×10^{-2}	1.2×10^{-3}		1.6×10^{-15}	2.7×10^{-16}
$CdCl_2$		8.8×10^{4}	2.5×10^{-2}		2.0×10^{-3}	1.3×10^{-3}
Pb	1050 ± 150	4.4	6.5×10^{-9}	180; 700	2.2×10^{-10}	1.2×10^{-10}
PbO		0.25	3.4×10^{-12}		5.2×10^{-14}	2.6×10^{-14}
$PbCl_2$		1.5×10^{5}	3.0×10^{-2}		2.3×10^{-3}	1.5×10^{-3}
Co	215 ± 41	$\ll 1$	$\ll 1$	49; 130	$\ll 1$	$\ll 1$
$CoCl_2$		6.0×10^{4}	6.8×10^{-2}		6.9×10^{-3}	4.7×10^{-3}
Al	2.8×10^{6}	$\ll 1$	$\ll 1$	4×10^{5} 2×10^{6}	$\ll 1$	$\ll 1$
Al_2O_3		$\ll 1$	$\ll 1$		$\ll 1$	$\ll 1$
$AlCl_3$		25	5×10^{-5}		6×10^{-6}	4×10^{-6}

Table 6. FLOW RATES OF SEVERAL ELEMENTS IN COAL AND ASH STREAMS AT THREE COAL-FIRED POWER PLANTS, g/h[a]

	Plant	Coal	ASH			Fraction unaccounted for %
			Boiler	ESP	Stack	
Sc	A	215 ± 13	43 ± 0.2	171 ± 9	0.28 ± 0.13	≡0 ± 7[b]
Hg	C	3.2 ± 0.7	0.039 ± 0.016	0.16 ± 0.06	-	~ -94
Cl	A	10700 ± 2600	1100 ± 480	1960 ± 270	6 ± 3	-70 ± 25
	C	14300 ± 2600	350 ± 60	6600 ± 5500	5.5 ± 0.9	-50 ± 40
Se	A	216 ± 13	7 ± 7	177 ± 3	1.3 ± 0.4	-14 ± 6
	B	76.4 ± 7.8	< 2.5	38.6 ± 35	5.8 ± 0.2	-36 ± 11
	C	150 ± 20	6.1 ± 0.3	84.4 ± 8.3	8.3 ± 0.6	-34 ± 14
Br	C	33.8 ± 6.0	2.9 ± 0.5	29.5 ± 6.2	0.042 ± 0.006	-4 ± 24
As	A	86 ± 13	8.0 ± 1.2	76 ± 7	0.99 ± 0.26	-1 ± 17
	B	134 ± 35	14.6 ± 2.8	120 ± 5.6	15.3 ± 0.3	+11 ± 27
	C	554 ± 94	19.8 ± 3.3	642 ± 69	1.45 ± 0.26	+20 ± 20
Sb	A	23.5 ± 1.6	2.8 ± 0.2	22.4 ± 2.6	0.31 ± 0.01	+8.5 ± 12
	B	28.2 ± 2.4	1.8 ± 0.2	20.9 ± 3.0	2.15 ± 0.04	-12 ± 13
	C	83.7 ± 11.7	3.4 ± 0.3	73.6 ± 5.5	0.13 ± 0.01	-8 ± 15
Mo	B	128 ± 27	16.6 ± 5.5	119 ± 30	6.5 ± 0.8	11 ± 33
	C	310 - 480	27.9 ± 6.4	409 ± 34	1.1 ± 0.4	-8 to +40
W	B	39 ± 12	10 ± 3.9	19.9 ± 4.0	2.8 ± 0.2	-17 ± 33
	C	130 ± 34	7.45 ± 2.4	119 ± 19	0.35 ± 0.05	-2.5 ± 30
U	B	91.1 ± 9.4	16.9 ± 0.6	76.2 ± 6.5	3.3 ± 0.15	+6 ± 11
	C	395 ± 47	27.1 ± 3.2	364 ± 28	0.45 ± 0.03	-0.9 ± 14
Cd	C	23 ± 11	1.6 ± 0.9	~21	-	-1.7 ± 5
Pb	B	500 ± 60	75 ± 11	590 ± 40	-	+30 ± 15
	C	1640 ± 230	82 ± 15	1640 ± 160	-	+5 ± 17
Co	A	123 ± 6	20.7 ± 4.1	107 ± 9	0.59 ± 0.07	+4 ± 9
	B	98 ± 12	16.9 ± 0.7	73.4 ± 5.4	2.4 ± 0.04	-5 ± 13
	C	351 ± 41	31 ± 4	304.7 ± 1.6	0.42 ± 0.12	-4 ± 12
Cr	A	1140 ± 49	201 ± 2	952 ± 69	5.0 ± 1.1	1.6 ± 7
	B	256 ± 14	50 ± 1.7	210 ± 6	9.6 ± 0.4	+5 ± 6
	C	1050 ± 140	78.8 ± 5.7	909 ± 42	5.1 ± 3.6	-5 ± 14

[a]Uncertainties reported are the standard deviation of replicate analyses or the uncertainty of a single analysis, whichever is greater.
[b]Uncertainties in the fraction unaccounted for are the square root of the sums of the uncertainties of coal and fly-ash streams squared.

Table 7. RELATIVE PENETRATIONS OF ELEMENTS AT SEVERAL COAL-FIRED POWER PLANTS[a]

Element	This Work			Other Cold-Side ESPs	
	Hot-side	Cold-side			
	Plant C[a]	Plant B[b]	Plant A[c]	Allen[d]	Chalk Point[e]
As	(4.4 ± 1.3)	7.9 ± 4.1	6.6 ± 0.6	6	6.3
Ba	2.0 ± 0.9	2.7 ± 1.1	2.5 ± 0.3	0.7	0.9
Co	2.1 ± 0.5	1.7 ± 0.4	2.3 ± 0.1	1.4	1.0
Cr	8.7 (3.4 - 15)	2.6 ± 0.4	2.5 ± 0.2	3.0	1.1
Ga	2.8 ± 0.9	3.0 ± 1.0	4.3 ± 0.8	-	1.2
In	3.4 ± 1.1	3.7 ± 1.0	5.5 ± 1.1	-	-
Mo	5.4 ± 0.4	3.5 ± 1.7	1.8 ± 0.7	-	-
Sb	(2.9 ± 0.3)	5.3 ± 1.0	7.0 ± 1.0	6.7	4.0
Se	100 ± 16	5.3 ± 1.2	3.0 ± 0.7	5.5	5.7
V	2.5 ± 0.5	2.5 ± 0.8	2.0 ± 0.7	2.5	0.75
W	5.0 ± 1.6	4.9 ± 3.0	-	-	-
Zn	3.0 ± 0.2	4.3 ± 1.1	4.3 ± 0.6	7.8	1.5
U	2.0 ± 0.1	2.5 ± 0.6	3.3 ± 0.2	-	-
Sc	1	1	1	1	1
ESP Efficiency	99.8	97	99.8	99.5	97

[a]Median of seven determinations ± the quartile spread. [b]Based on a single value when the plant operated at 83% capacity. [c]Median and quartile spread of three values. [d]Data of Klein et al., Reference 5. [e]Data of Gladney et al., Reference 6.

REFERENCES

1. Ondov, J.M., R.C. Ragaini, and A.H. Biermann. Elemental Emissions From a Coal-Fired Power Plant: Comparison of a Venturi Wet Scrubber System With a Cold-Side Electrostatic Precipitator. Environ. Sci. Technol. 13, 598-607, 1979.

2. Ondov. J.M., R.C. Ragaini, and A.H. Biermann. Emissions and Particle-Size Distributions of Minor and Trace Elements At Two Western Coal-Fired Power Plants Equipped With Cold-Side Electrostatic Precipitators. Environ. Sci. Technol. in press.

3. Coles, D.G., R.C. Ragaini, and J.M. Ondov. Behavior of Natural Radionuclides in Western Coal-Fired Power Plants. Environ. Sci. Technol. 12, 442-466, 1978.

4. Coles, D.G., R.C. Ragaini, J.M. Ondov, G.L. Fisher, D. Silberman and A. Prentice. Chemical Studies of Stack Fly Ash from a Coal-Fired Power Plant. Environ. Sci. Technol. 13, 455-459, 1979.

5. Klein, D.H., A.W. Andren, J.A. Carter, J.F. Emery, C. Feldman, W. Fulkerson, W.S. Lyon, J.C. Ogle, Y. Talm, R.I. Van Hook, and N. Bolton. Pathways of Thirty-seven Trace Elements Through Coal-Fired Power Plant. Environ. Sci. Technol. 9, 973-979, 1975.

6. Gladney, S., J.A. Small, G.E. Gordon, and W.H. Zoller. Composition and Size Distribution of In-Stock Particulate Material at a Coal-Fired Power Plant. Atmos. Environ. 10, 1071-1077, 1976.

7. Andren, A.W. and D.H. Klein. Selenium in Coal-Fired Stream Plant Emissions. Environ. Sci. Technol. 9, 856-858, 1975.

8. Kaakinen, J.W., R.M. Jorden, M.H. Lawasani, and R.E. West. Trace Element Behavior in Coal-Fired Power Plant. Environ. Sci. Technol. 9, 862-869, 1975.

9. Gordon, G.E. Study of the Emissions From Major Pollution Sources and Their Interaction. Progress Report Nov. 1972 to October 1974, Univ. Maryland, College Park, Md. 1977.

10. J.M. Ondov, R.C. Ragaini, and A.H. Biermann. Characterization of Trace Element Emissions in Aerosols Emitted From Coal-Fired Power Plants. In: Proceedings 3rd International Conference on Nuclear Methods in Environmental and Energy Research, Colombia, Mo., 1977.

11. Bertine, K.K. and E.D. Goldberg. Fossil Fuel Combustion and the Major Sedimentary Cycle. Science 173, 233-235, 1971.

12. Andren, A.W. and D.H. Klein. Trace Element Discharges from Coal Combustion for Power Production. Water Air Soil Pollut. 5, 71-77, 1975.

13. Chrisp, C.E., G.L. Fisher, and J.E. Lammert. Mutagenicity of Filtrates from Respirable Coal Fly Ash. Science 199, 73-75, 1978.

14. McIlvaine Scrubber Manual, Vol. II p. 5-11 McIlvaine Co., Northbrook, Ill., 1974.

15. Stern, A.C., Air Pollution, Vol. III, Academic Press, New York 1968, p. 437-495.

16. Calvert, S., J. Goldshmide, D. Leith, and D. Mehta. In: Wet Scrubber System Study, Scrubber Handbook, Vol. I, Environmental Protection Agency, Rept. R2-118a, 1975. p. 5-81.

17. Hesketh, H.E. In: 68th Annual Meeting of the Air Pollution Control Association, Boston, Paper No. 75-50.6, 1975. p. 1-21.

18. A.H. Biermann and J.M. Ondov. Application of Surface Deposition Models to Size Fractionated Coal Fly Ash. Atmos. Environ. in press.

19. Shroeder, H.A. Metal in the Air. Environment 13 (#18), 18-24, 29-32 (1971).

20. Heft, R.E. "Absolute Instrumental Neutron Activation Analysis at Lawrence Livermore Laboatory," Presented at the Third International Conference on Nuclear Methods in Environmental and Energy Research, Columbia, Mol., October 10-13, 1977.

21. Bonner, N.A., F. Bazan, and D.C. Camp. Chem. Instr. 6, 1-36, 1975.

22. R.C. Ragaini, R.E. Heft, and D. Garvis. Neutron Activation Analysis at the Livermore Pool-type Reactor for the Environmental Research Program," Lawrence Livermore Laboratory, Rept. UCRL-52092, 1976.

23. J.M. Ondov, Zoller, W.H., Olmez, K., Aras, N.K., Gordon, G.E., Ranticelli, L.A., Able, K.H., Filby, R.H., Shah, K.R., and Ragaini, R.C. Anal. Chem. 47, 1102-1109, 1975.

24. Johnson, Q. Lawrence Livermore Laboratory, Livermore, Calif., private communication, 1979.

25. Betnell, F.V. Br. Coal Util. Res. Assoc. Mon. Bull. 26, 406-430 (1962).

26. Weast, R.C. Ed., Handbook of Chemistry and Physics, 55th ed. Chemical Rubber Co., Cleveland, Ohio, 1975. p D162-7.

27. Billings, C.E. and W.R. Matson. Mercury Emissions from Coal Combustion. Science 176, 1232-1233, 1972.

28. Davison, R.L., D.F.S. Natusch, J.R. Wallace, and E.A. Evans, Jr. Environ. Sci. Technol. 8, 1107-13, 1974.

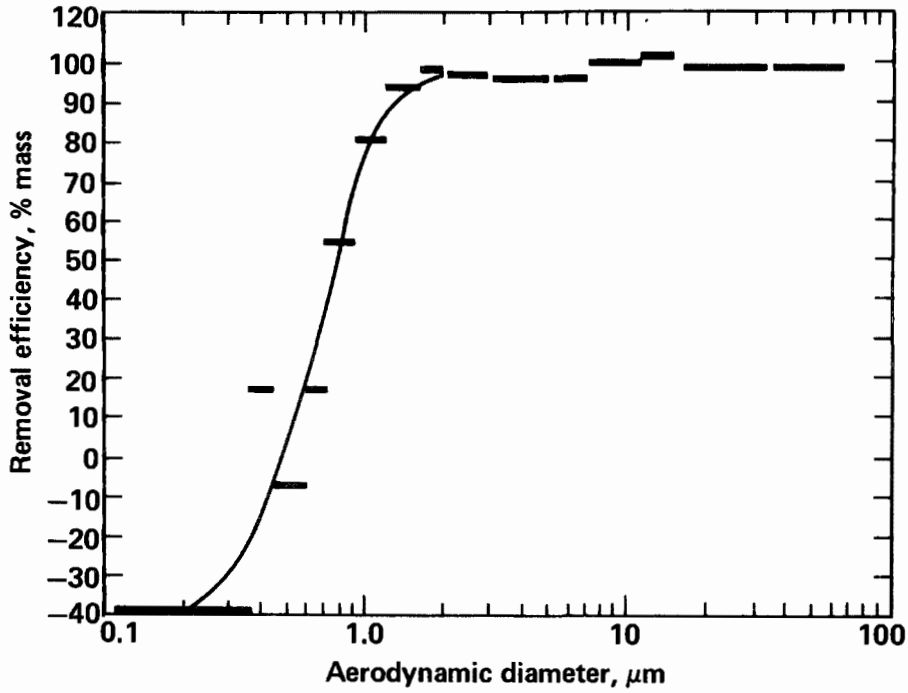

Figure 1. Removal efficiency vs particle-size curve determined for a high-energy, venturi wet scrubber.

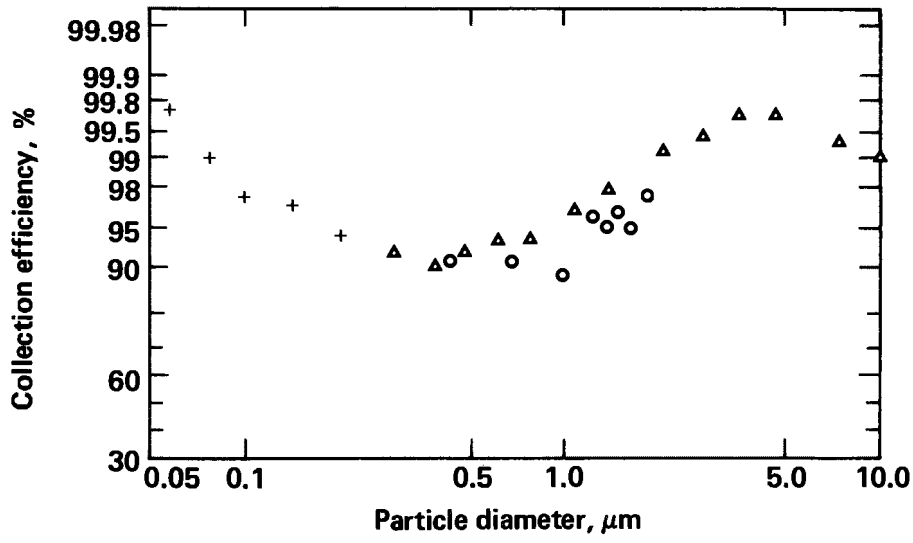

Figure 2. Removal efficiency vs particle-size curve of a cold-side ESP reported in McCain et al. J. Air Pollut. Contr. Assoc. 25, 117-21 (1975). Reprinted with permission; copyright 1975 Air Pollution Control Association.

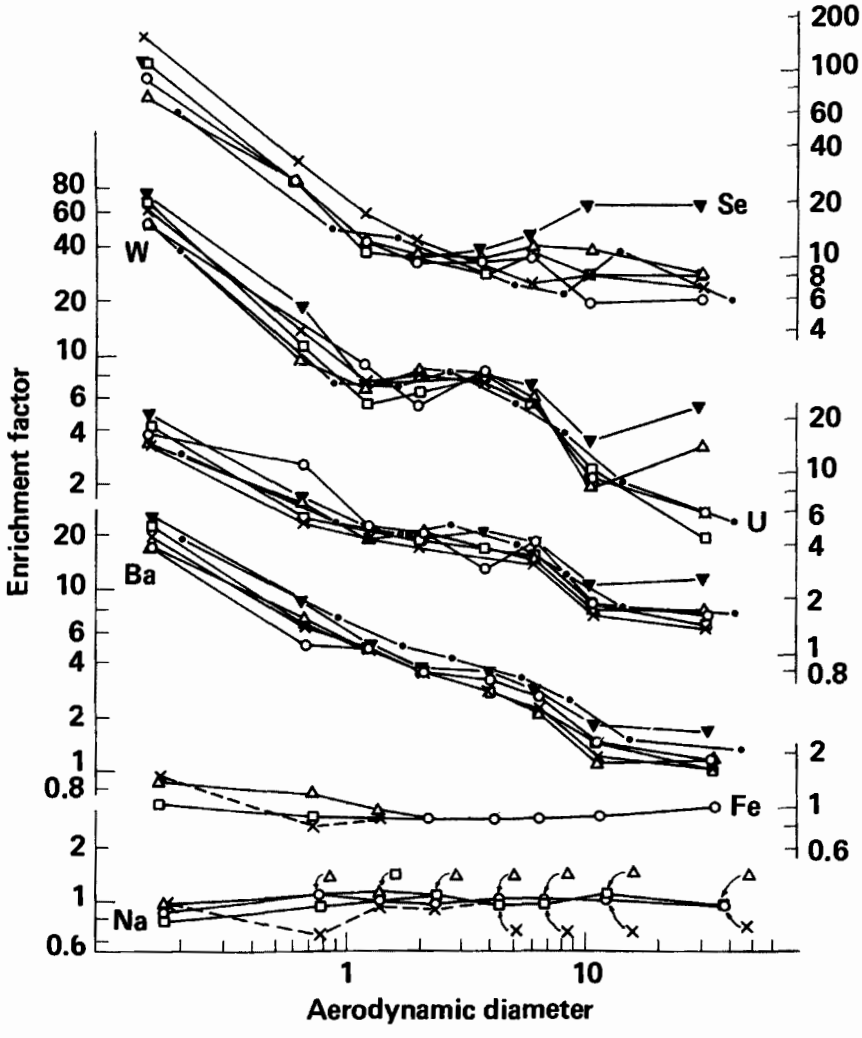

Figure 3. Concentration relative to coal vs particle-size curve for several elements contained in fly ash emitted from the ESP Unit 3.

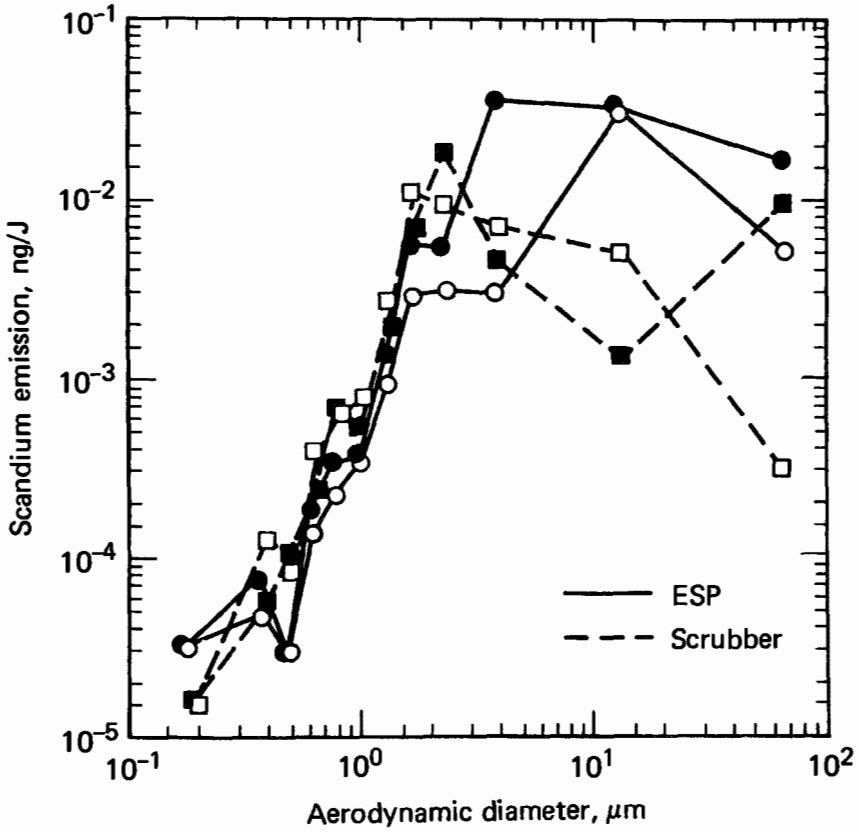

Figure 4. Emission rate of Sc in aerosols collected at the inlet of the precipitator and wet scrubber.

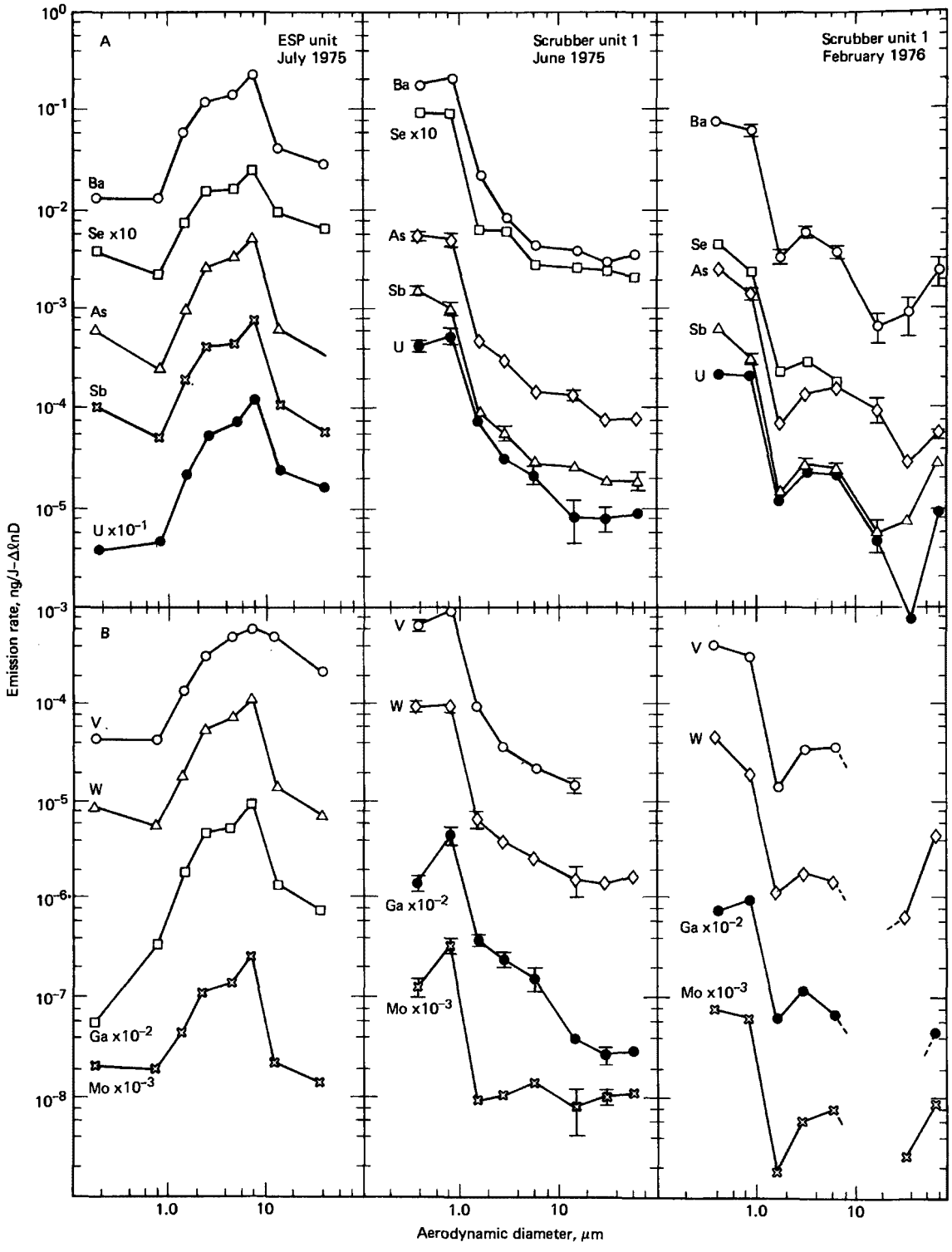

Figure 5. Particle-size distributions of elements emitted from power units equipped with a cold-side ESP and a venturi wet scrubber. The concentration data of individual elements are expressed as emission rate per joule of heat input to the boiler to allow comparison of the two units. The data are normalized to log size intervals (D=particle diameter).

COMPARISON OF ESP AND VWS EMISSIONS

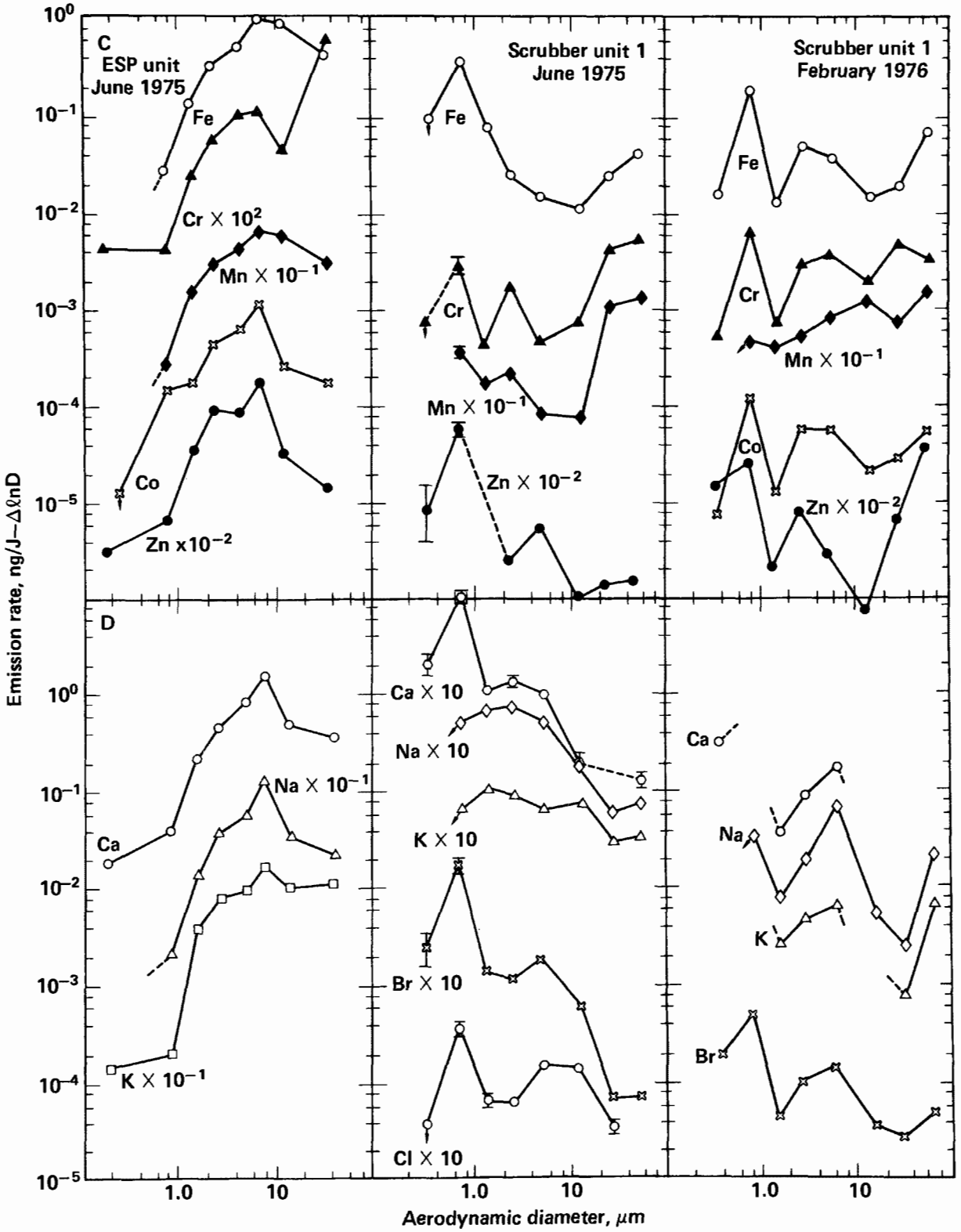

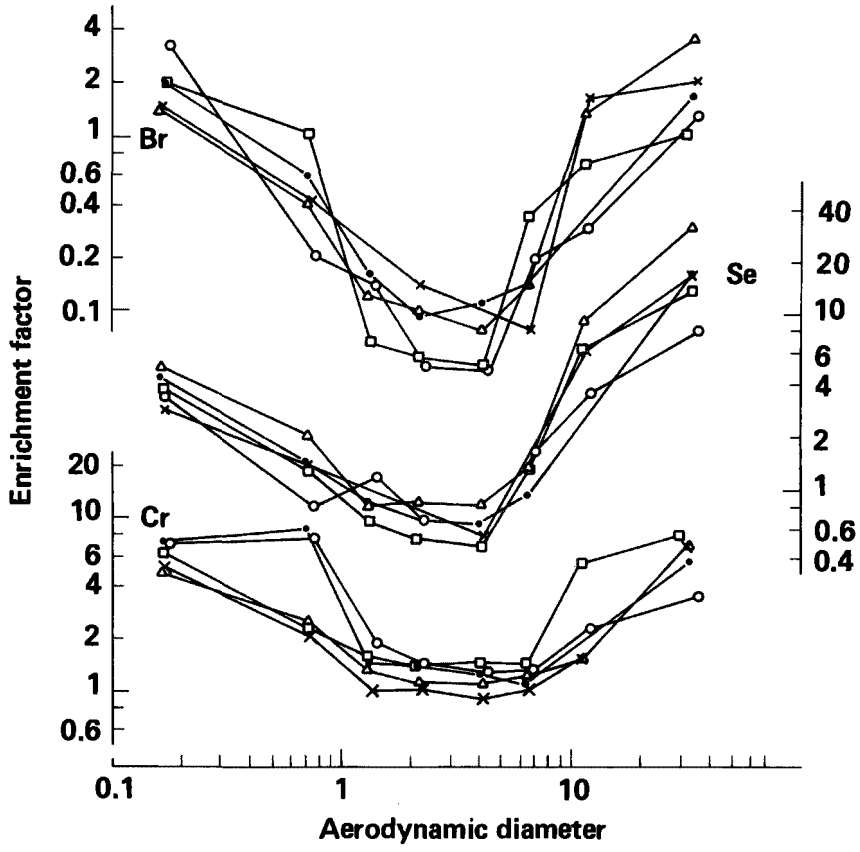

Figure 6. Relative concentrations of three elements in discrete size fractions of stack fly ash from Plant A.

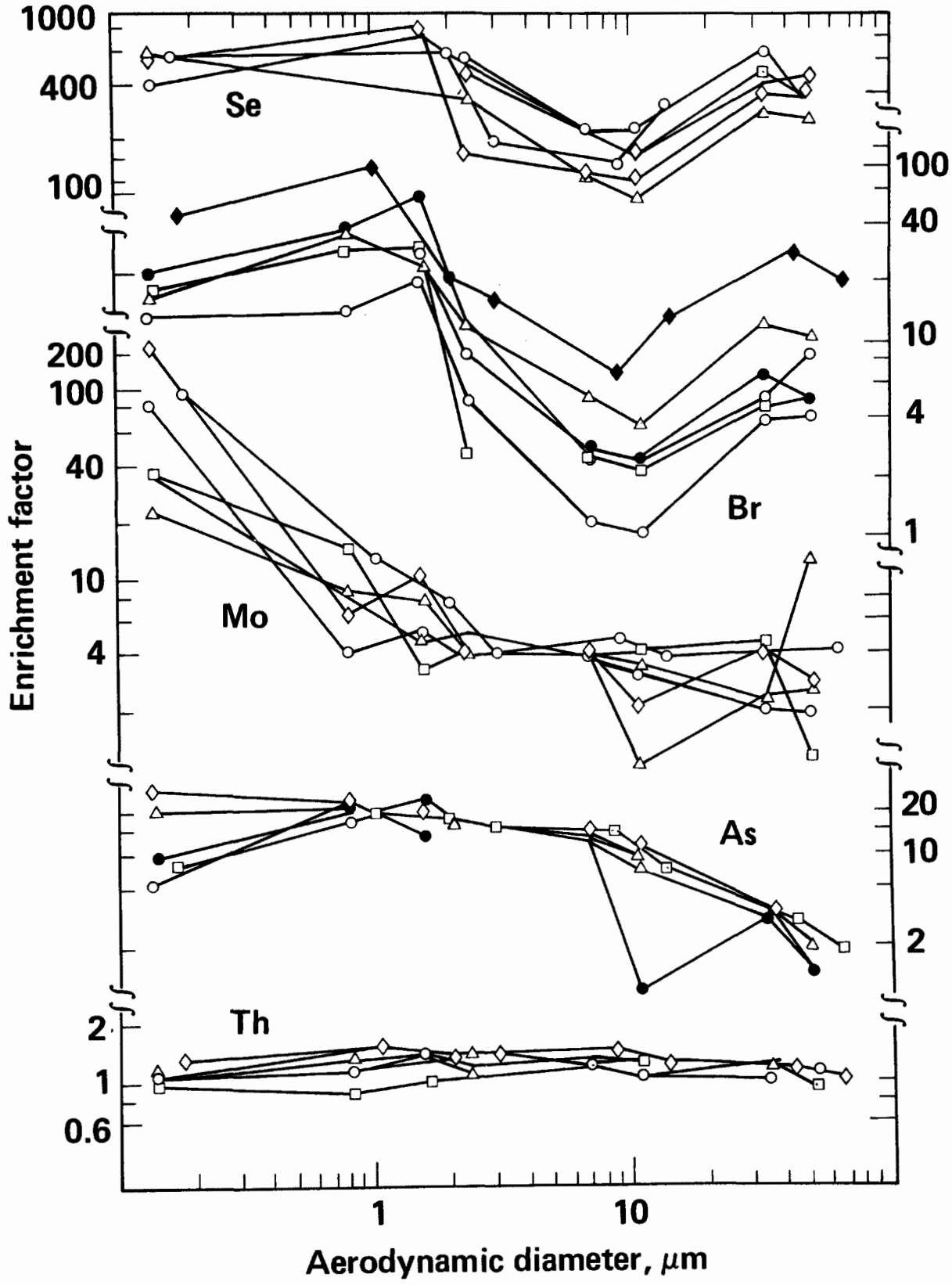

Figure 7. Relative concentration (enrichment factor) vs size profiles of fine elements associated with aerosol particles emitted from Plant C.

A SOURCE IDENTIFICATION TECHNIQUE FOR AMBIENT AIR PARTICULATE

By:

Edward J. Fasiska, Ph.D., Philip B. Janocko, and David A. Crawford
Materials Consultants & Laboratories, Inc.
1567 Old Abers Creek Road
Monroeville, Pa. 15146

Subsidiary of: Science Management Corporation

"A powerful analytical technique
which is revolutionizing air
particulate analysis in the
environmental field."

This paper describes an impressive technique for identifying particulate matter in ambient air samples, and then tracing these particles to their sources. The system, Electron Beam Particulate Analysis (EBPA), utilizes electron microscopy, x-ray analysis and electron beam image analysis, combined with sophisticated computer technology, to analyze and compare particles in seconds. This technique is extremely important in light of EPA requirements for air quality which must be met by every state with proposed standards for fine inhalable particulates.

The first section presents an overview of the air particulate problem. Then a brief description of the evolution of this extraordinary technique is given, followed by a step-by-step discussion of the operation of the system. Finally, a practical application of the system is presented through a description of an air particulate study that was conducted in the Pittsburgh area, the first study in the country to separate traditional sources of particulate matter from non-traditional sources.

A SOURCE IDENTIFICATION TECHNIQUE FOR AMBIENT AIR PARTICULATE

AIR PARTICULATE PROBLEM

One of the most serious and difficult to control pollutants in the United States is air particulate. Approximately 40 states currently exceed Environmental Protection Agency (EPA) standards for allowable levels of particulate matter (e.g. dust, smoke and soot) in ambient air. These standards are based on the total weight of particulate matter per cubic meter of air, regardless of the type of particles involved. The maximum permissable annual average concentrations of total suspended particulate (TSP) are 75 micrograms per cubic meter to protect public health and 60 micrograms per cubic meter of air to protect welfare.

In the past, it has been particularly difficult to enforce ambient air standards because no routine analytical technique existed to chemically analyze TSP on a particle-by-particle basis. Now, however, the Electron Beam Particulate Analyzer can be used to take "fingerprints" of the chemistries, morphologies and sizes of the particles and to track their probable origins.

EVOLUTION OF THE EBPA

The Electron Beam Particulate Analyzer actually combines three basic analytical instruments synergistically to produce its highly complex particulate analyses (Figure 1). The first, and most familiar tool is the scanning electron microscope (SEM). The SEM was developed ten years ago as the natural offspring of the original transmission microscope, and quickly proved itself to be a revolutionary microscopy technique because of its capability to produce high-magnification, three-dimensional images.

It was soon discovered that the combination of the SEM with the Energy-Dispersive X-ray Analyzer (EDAX), a micro chemical analysis technique permitted instantaneous chemical analysis of particles and features as small as fractions of a micron of virtually anything observed on the SEM viewing screen. This technology permitted a "new" look at the materials on a three-dimensional micro scale with the advantage of concurrent micro chemical analysis. The capabilities of the SEM/EDAX have expanded since their initial combination with increasing spatial resolution and the development of sophisticated quantitative computerized analysis systems.

The Electron Beam Image Analyzer was mated with the SEM and EDAX to make the EBPA complete. This instrument digitizes the motion of the electron beam as opposed to the SEM which systematically scans the beam. This allows the position of the beam to be completely controlled by a mini computer. With the aid of contrast conditions induced by differences in chemistries of particles, a description of particle size, shape and retrieval. The image

analyzer of the EBPA is one of the key components and was developed by Lemont Scientific.

The combination of the SEM, EDAX and Image Analyzer, and its application to air particulate analysis, represents a major breakthrough in the environmental field. This instrumentation package was originally synthesized by Dr. Richard Lee at the U. S. Steel Research Laboratories (Figure 2). The EBPA has been described by the authors as perhaps the most powerful analytical composite to impact the materials science field in a decade.

As a result, in a matter of seconds, morphological and size data can be collected and stored in a computer memory on a particle-by-particle basis. Thousands of analyses can be performed very rapidly, with the resulting data stored for future reduction, refinement and cataloging into various categories of size, shape and chemistry. It should be emphasized that, because of the large number of particles analyzed and because of the random distribution of air particulate, the analytical results determined by these systems are statistically equivalent to those that would be derived if all particles on a sample were analyzed. EBPA makes it possible not only to quantitatively analyze a micro particle, but also to compute the number of such particles, their average size and shape distributions, the average particle size, their weight percentages of the total sample, and many other characteristics of the particulate samples. In other words, EBPA functions as the bookkeeper of the particle information for future retrieval and analysis.

BASIC EBPA OPERATION

The basic operational steps of the EBPA are as follows:

- Generation of a search grid system
- Detection of particles intersecting the search grid system
- Size and shape analyses of particles
- Chemical analyses of particles

Generation of a Search Grid System

The normal electron beam scanning motion in the SEM is very similar to the motion of the electron beam in a conventional television set. A digital scan generator is used to convert this motion to a stepping motion with regular intervals and the spacing between grid points is chosen in such a manner as to intersect a representative fraction of the particles on the SEM viewing screen. After the grid is defined, a computer instructs the electron beam to pause at each grid point while a particle detection function is performed.

Detection of Particles Intersecting the Search Grid System

The particles are detected on the grid points by monitoring a back-scattered electron signal. A signal above an adjustable threshold value indicates the beam is on a particle. If the signal is below the threshold value the computer selects the next coordinate of the grid.

Size and Shape Analysis of Particles

After a particle is located, a subroutine is used to drive the beam in a preset pattern to determine the particle size and shape. The preset pattern consists of 4 pairs of diagonals; each of which is terminated when a grid point is monitored and found to be off the particle. The pattern is repeated twice: once to locate the particle, and once to determine the lengths of the diagonals through its centroid. The maximum, minimum, and average diagonals are stored and the electron beam is positioned to chemically analyze the particle.

Chemical Analyses of Particles

The chemical analysis of the particle is performed by a computer command which positions the electron beam at the measured centroid of the particle for a preset time. The electron beam excites x-rays characteristic of all the elements present in the particle. All elements present in the particle above atomic number eight (oxygen) in the periodic table may be detected simultaneously. Their signal levels are stored in the memory of the computer for subsequent retrieval.

Data Reduction and Particle Type Classification

After all size, shape and chemical data for the samples are collected, and stored (typically thousands of particles per sample), software is used to separate the particles into different types, based on preset chemistries. Forty-five to fifty particle types are identified in a typical study. Using the measured sizes of the particles and their known densities, the results of an analysis can be reported in terms of the number of each particle type, volume and weight percentages, and particle size distribution for each chemical particle type, or for all particle types combined. Because the analysis is totally objective, human judgment errors are eliminated. Also, since thousands of particles are analyzed, favorable statistics are generated, reducing the uncertainties of the final results.

With the basic operational procedure of EBPA in mind, it should be of interest to the reader to examine a practical application of the system. A pilot study of air particulate in the City of Pittsburgh was recently conducted, and a description of the background and implementation of this effort follows.

STUDY OF AIR PARTICULATE IN PITTSBURGH

The Clean Air Act Amendments of 1977 stimulated a study of air particulate in Pittsburgh, a highly industrialized city. These amendments require each state exceeding primary and secondary standards for TSP to revise its State Implementation Plan. States must devise control strategies for obtaining ambient air TSP standards for traditional sources of particulates by January, 1979. The amendments further require states to develop control strategies to for non-traditional sources of particulates by January 1, 1982. One difficulty in complying with this mandate lies in the ability to discriminate between

traditional and non-traditional sources of particulate. By definition, traditional sources are emissions from industrial background sources such as street dust, automotive particles, field soil, insects and pollen; all of which are beyond the area of the control agency.

The pilot air particulate study of the Pittsburgh Area work was done by Materials Consultants and Laboratories, DeNardo and McFarland Weather Services and United States Steel Research Laboratories and included the following elements:

- Choosing two hi-vol stations representing ambient air in one typical industrial and one typical non-industrial area and reference samples from local meteorological data, topography maps, and a known emissions inventory survey.
- Field hi-vol sample collection of the ambient air and reference samples.
- Interpretation of the particulate analytical results, including type and size distribution of various particle types (e.g., quartz, clays, various oxides, organic species, etc.) their numbers, weight percentages and volume percentages.
- Combining final particulate analysis with meteorological data.
- Conclusions outlining the contributions of traditional and non-traditional sources to the air particulate monitored in Allegheny County and, more specifically, industry's contribution to ambient air particulate quality.

One of the monitoring sites was a high-density industrial area of Pittsburgh, located near the Monongahela River, and the other site was in a rural area southwest of the Pittsburgh airport with no known industrial sources in the vicinity. Sampling was conducted under specific meteorological conditions which were later incorporated into study results. A total of eight industrial and two rural samples were taken under various meteorological conditions.

During the course of the study, 25 specific particle types were identified and analyzed; however, with the current EBPA system, 53 particle types were isolated. The types of particles found ranged from the anticipated common materials such as power plant flyash, quartz, road salt, eight unique clay minerals, slag and iron oxides, to more exotic particle types such as titanium-rich compounds. From these 25 particle types, the traditional and non-traditional fractions of the total particulate were estimated on the basis of known environmental chemistries of particular industries. Surprisingly, the percentage of weight of the particulates broken down by sources indicated that a range of 40 to 70 percent of the particulates were from traditional sources in the heavily industrialized area, depending upon meteorological conditions. In the rural site, the breakdown of traditional source particles ranged from 26 to 39 percent of the filter weight. The bar graph entitled "Pittsburgh Air Particulate Source Distribution" (Figure 3) represents an average of eight samples taken under four different meteorological conditions

at the rural site.

For the first time in Pittsburgh, or for that matter anywhere in the United States, statistically valid distributions of traditional and non-traditional source particles have been determined. The results are very important to the Allegheny County Air Pollution Control Bureau because they indicate that non-traditional sources consitute approximately half of the particulates measured at the industrial site. The results also indicate that steel companies in the industrialized area normally contribute about one fifth of the total particulate weight present in ambient air under average meteorological conditions.

As expected, the traditional component of air particulate was significantly higher in the industrial area (55 per cent), as compared to the rural area (38 per cent). In both the industrial and rural areas, the main contributors to air particulate were power plants and the steel industry. The overwhelming portion of the non-traditional particulate matter was contributed by road dust and soil.

The study also found unusually high concentrations of calcium-sulfur rich particles at the industrial sites under poor atmospheric dispersion conditions. The light wind speeds present during these tests indicated that the sources of these particles were not in the immediate vicinity, but rather, emitted from distant sources. It has been postulated that some fraction of these particles might have originated from lime scrubbers which were installed on power plants to reduce gaseous sulfur dioxide emissions. The calcium-sulfate particulate could be emitted in the water droplets of the emitted vapors and subsequent evaporation of the water could cause the calcium-sulfate particles to be suspended in the atmosphere.

Another important finding of this study was the precent weight distribution by particle size and number of particles in each size range. These data indicated that the bulk of the mass, or the weight of particulates, was clearly associated with the "larger" particles. In other words, about 75 percent of the total TSP weight was represented by particles greater than 10 micrometers, but these particles made up only about one percent of the total particles by number of particles. The significance of this particle size distribution is that industrial concentration in Pittsburgh could be reduced by 40 percent from the 1977 annual TSP average of 101.6% ug/m^3 (geometric mean) by simply controlling the large particles at their sources. However, the emphasis of proposed EPA TSP guidelines will be on the smaller particle sizes, since they are considered respirable. This concentration on the smaller, respirable particles is related to their high potential as a health hazard. EPA is currently using a new air particulate sampler called the dichotomous sampler. This sampler collects and separates the particulate into two aerodynamic size ranges: 0-2.5 micrometers and 2.5-15 micrometers. Again, this is an attempt to gather information on the respirable fraction of the particulate. Materials Consultants and Laboratories is currently examining several dichotomous air samples for EPA to determine the feasibility of using the EBPA to give a more detailed particle type breakdown. The Pittsburgh study results, however, indicate that these smaller particles will be very difficult to control because of their large numbers and small size.

The overall conclusion of this study was that, before particulate concentrations in Pittsburgh can be reduced to meet the present ambient air standards, control strategies must be developed to deal with the non-traditional source particles and especially to control large size particles (15 microns or greater).

It should be emphasized that this pilot study was preliminary in nature and a more comprehensive analysis of some fifty air filters representing Pittsburgh air particulate from a network of sampling stations around Pittsburgh has just been completed by Materials Consultants and Laboratories. The data interpretation of this study is scheduled for completion in late June, 1979. In the new study, 16 elements are being monitored as opposed to 9 in the feasibility study. Further, 53 particle types have been isolated as opposed to 23 in the original study.

The results of the work have far-reaching implications for the future, not only for controlling air pollution in Pittsburgh, but for the entire nation. Now every state and city can determine the sources of particulate matter in the air and take steps to control these sources in compliance with EPA regulations and to the benefit of the health and welfare of residents.

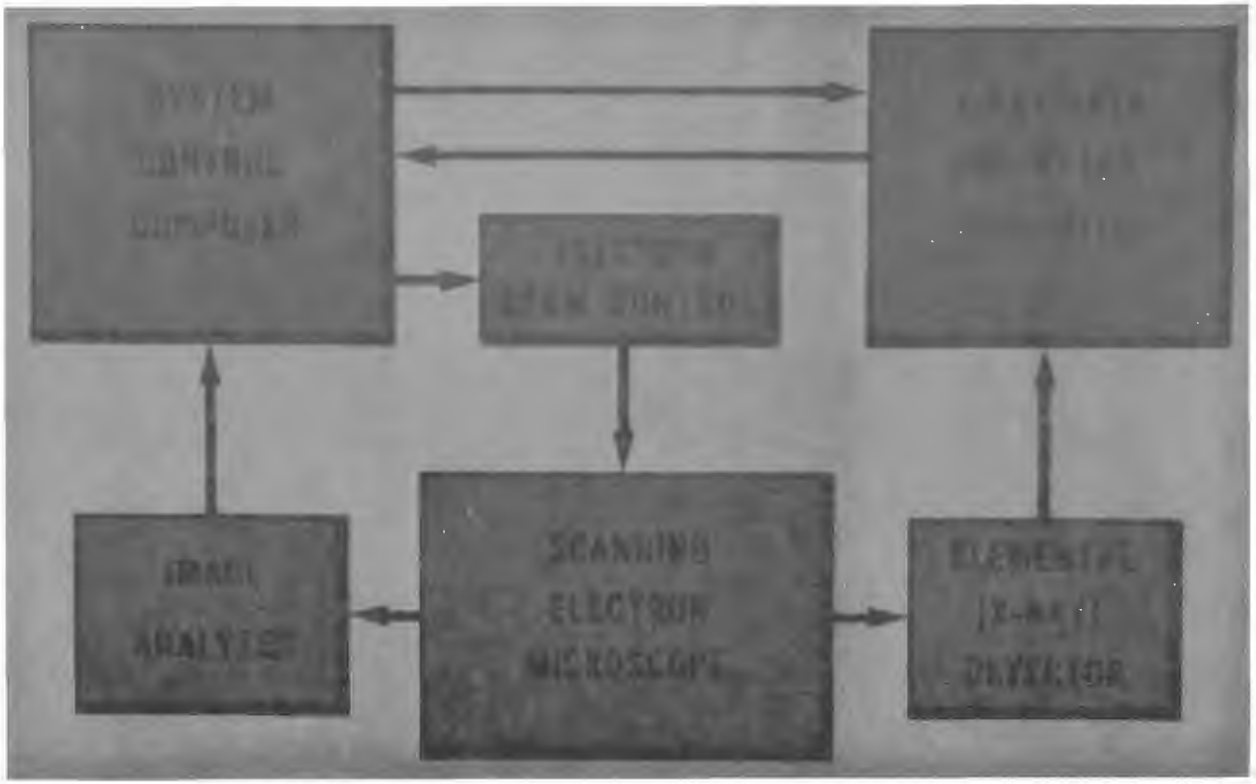

AIR PARTICULATE ANALYZER

Figure 1

Air particulate analyzer.

Figure 2

Air particulate analyzer
instrumentation.

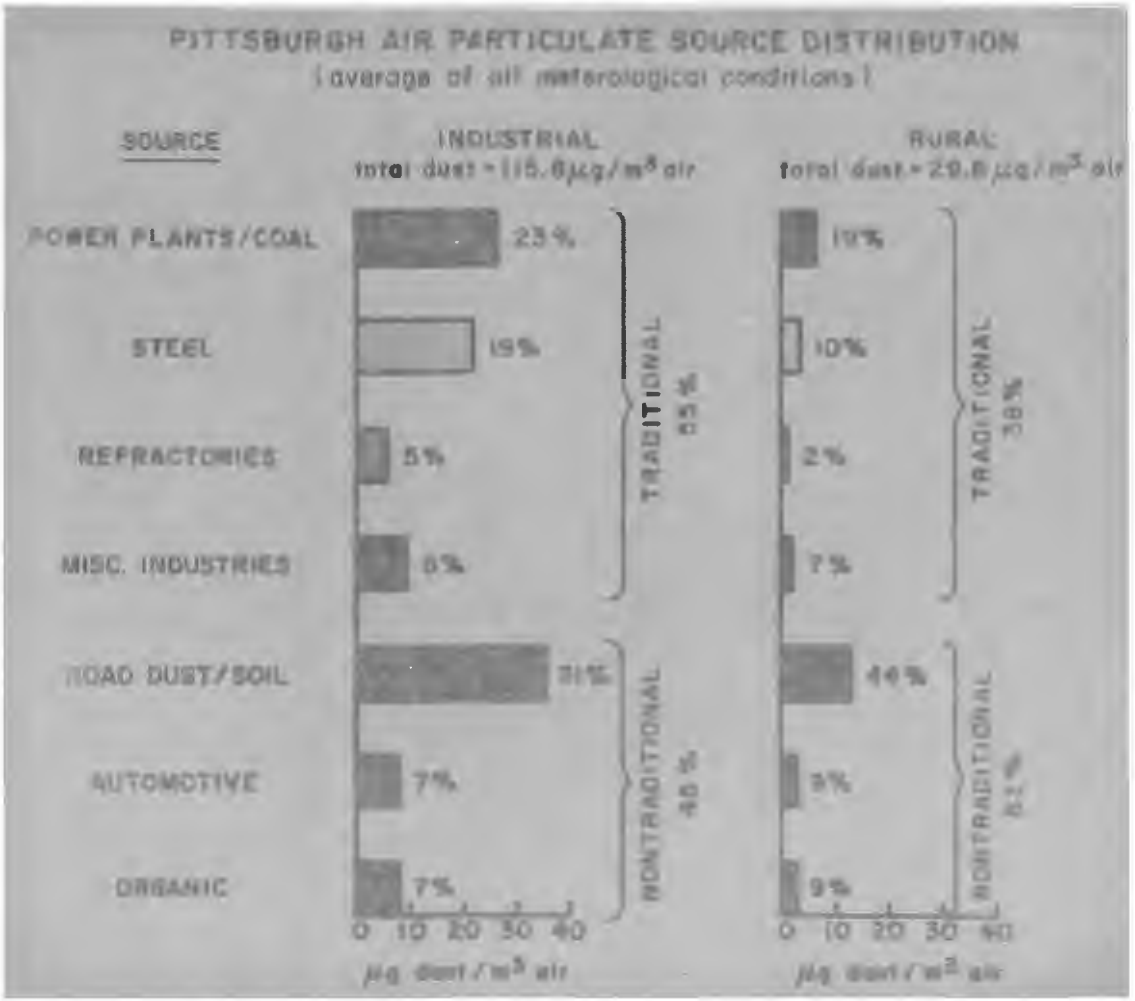

Figure 3

Pittsburgh air particulate source distribution.

PARTICLE SIZE MEASUREMENTS OF AUTOMOTIVE DIESEL EMISSIONS

by

Joseph D. McCain
Southern Research Institute
2000 Ninth Avenue, South
Birmingham, Alabama 35205

and

Dennis C. Drehmel
Industrial Environmental Research Laboratory
Environmental Protection Agency
Research Triangle Park, North Carolina 27711

Presented at

The Second Symposium on the Transfer and Utilization of Particulate Control Technology, Denver, Colorado, July 23-27, 1979

Introduction

The federally mandated fuel economy standards for passenger automobiles have resulted in considerable impetus being given to the introduction of substantial numbers of diesel powered automobiles into the passenger car fleet. The diesel engine has long been acknowledged as being "dirtier" than the spark ignition gasoline engine (by factors of 30 to 50 in particulate emissions). The diesel particulate emissions are primarily carbonaceous, but 10 percent to 50 percent by weight of the material is adsorbed higher molecular weight organics, a significant portion of which may be polycyclic aromatics.[1] Preliminary results of Ames microbial mutagenicity bioassay tests have indicated the possibility that these particulates may be carcinogenic.

Possible solutions to the diesel particulate problem are combustion modification or the use of aftertreatment devices in the exhaust gas stream to collect and/or render the material innocuous. Such treatment may be mandatory if the emissions do prove to represent a significant carcinogenic risk. Selection of candidate aftertreatment devices requires knowledge of the chemical and physical properties of the particles. These include particle morphology, particle size distribution, bulk densities of the collected material, and particulate mass concentration and emission rates in the exhaust gas stream. Because the organic fraction of the particles appears to be adsorbed on the surfaces of graphitic carbon base particles, the temperature history of the gas stream may be important. If the sorption process takes place at elevated temperatures, then collection of the particulate at the normal, relatively hot, exhaust gas temperatures may be sufficient. However, if the sorption takes place only during and after cooling of the exhaust stream to near ambient conditions, the hot particle collection will not result in the removal of the organic fraction.

The study reported here represents the first of a planned series of experiments to characterize the exhaust emissions from the point of view of aftertreatment exhaust gas cleanup and to collect samples for bioassays to determine whether the biological effects of particles collected at exhaust line temperatures are the same as those collected after dilution and cooling by ambient air.

Test Program

The tests described here were performed November 27 through December 1, 1978, at a U. S. EPA facility located at Research Triangle Park, North Carolina. A 1979 Oldsmobile 88 with a 350 Cubic Inch Displacement (CID) diesel engine was operated on a

Burke E. Porter No. 1059 Chassis Dynamometer. The dynamometer was programmed to emulate the Clayton roadload curve for water-brake dynamometers used for vehicle certification. Test conditions included the 13 minute Fuel Economy Test (FET) combined city-highway test cycle, 97 kmph highway cruise, 56 kmph highway cruise, and 56 kmph no load conditions. However, conditions were not equivalent to those required by EPA for vehicle certification and the test results should not be compared to those acquired by official certification methods and conditions.

Sampling and measurement methods included Andersen cascade impactors, conventional filtration techniques followed by condensers and organic sorbent traps, optical single particle counters, electrical mobility methods, and diffusional methods. All samples were taken directly from a modified exhaust pipe which was run out from under the chassis and alongside the passenger side of the automobile to permit reasonable access to the exhaust stream.

Andersen Model III cascade impactors with glass fiber impaction substrates and backup filters were used to obtain total particulate loadings and particle size distributions on a mass basis over the size range from about 0.4 μmA to 5 μmA. The impactors were operated in an oven close-coupled to the exhaust pipe. During runs at a steady engine load (56 kmph and 97 kmph), the oven was maintained at the same temperature as the exhaust gas temperature at the sampling point. During the 13 minute FET cycle testing, the impactors and ovens were maintained at about the average exhaust gas temperature for the cycle, 175°C.

In addition to the cascade impactors, a Thermosystems Model 3030 Electrical Aerosol Analyzer (EAA) was used to determine concentrations and size distributions of particles in the size range of 0.01 μm to 0.5 μm. Particle concentrations ranging from 0.3 μm to 2.5 μm were monitored using a Royco Model 225 optical particle counter. The Southern Research Institute SEDS III sample extraction, conditioning, and dilution system was used as an interface between the exhaust system and the EAA and particle counter. This system provides a mechanism for the removal of condensible vapors from the sample gas stream at elevated temperatures followed by quantitative dilution to particle concentrations within the operating ranges of the measurement instruments.

Figure 1 is a diagrammatic sketch of the layout of the exhaust system and measurement instrumentation during the tests.

The vehicle operating conditions were selected to provide samples collected at elevated exhaust gas temperatures prior to cooling for the same engine cycle as the very large (10 kg) sample collected for bioassay work. This 10 kg bioassay sample was being collected using the FET test cycle using a standard "constant volume" automatic dilution tunnel. The hot samples collected were to be used for Ames tests to provide some indication

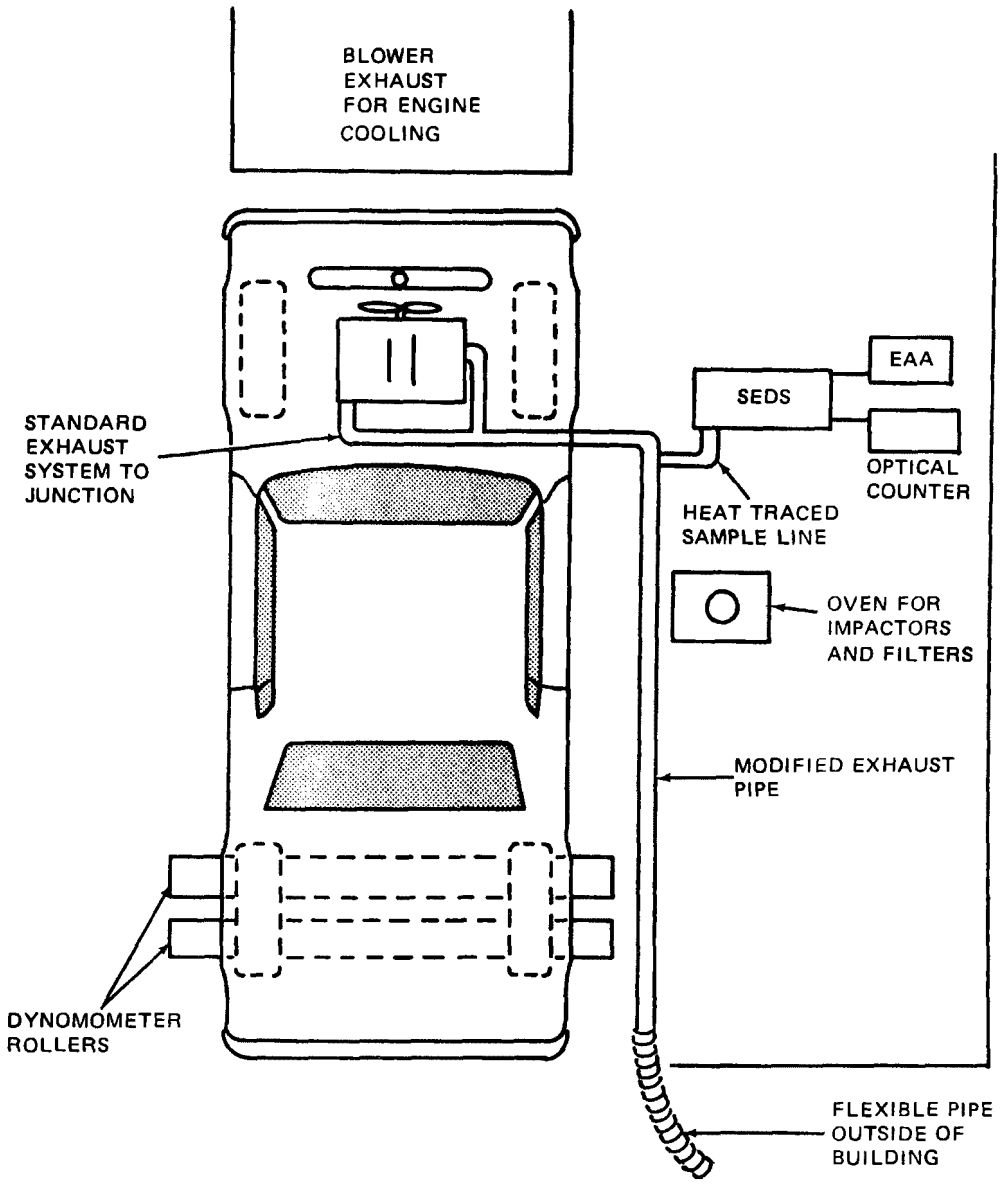

Figure 1. Modified exhaust pipe and test equipment layout for diesel emission testing.

of the relative mutagenicity of material collected at the exhaust line temperatures and material collected after cooling and dilution. This information is intended to provide some insight into whether hot collection of the particles will remove the carcinogenic component of the exhaust. In the program as originally conceived, samples were to be taken at a number of points between the exhaust manifold and the tailpipe to provide samples collected over a range of temperatures and engine loads. These would have provided information on changes in particle size distribution and composition as the exhasut gases were cooled. Time limitations in preparing for the tests rendered it impossible to carry out the proposed plan. However, it was found that a considerable swing in gas temperature did occur with changes in engine load. However it is not possible to differentiate between engine load/speed induced and temperature induced concentration and composition changes in the data obtained during this test.

Overall particulate loadings, engine gas flows, and sampling temperatures for the cascade impactor samples are given in Table I. Particle size distributions for the various conditions are given in Figures 2, 3, 4 and 5. Each figure in this series contains a plot of cumulative percentage smaller than the indicated diameter versus diameter from the impactor data alone and that obtained by integrating the distributions from the electrical aerosol analyzer up to 0.5 μm and continuing the integration from 0.5 μm to 10 μm with the impactor data. A particle density of 1.0 g/cm^3 was assumed for the integrations of the EAA data. The overall size distributions from 0.01 μm to 10 μm obtained in this fashion agree very well with those obtained from the impactors alone.

The variability in particulate concentrations through the FET cycle is illustrated in Figure 6. This shows particle concentrations versus time in three particle size intervals through several test cycles. These data were obtained using the optical particle counter.

The particulates collected at exhaust gas temperatures were found to be approximately 15 percent by mass organics. The results of the biotesting of the samples from the impactors, filters, and organic vapor traps will be reported elsewhere.

Conclusions

Typical particulate concentrations at exhaust line conditions for the Oldsmobile 350 CID diesel engine were found to be about 50 mg/NCM. Aerodynamic mass median diameters were about 0.3 to 0.5 μm with larger medium diameters being obtained from higher

TABLE I. RESULTS OF CASCADE IMPACTOR SAMPLING

Operating mode	Average exhaust volume flowrate (m^3/s)	Average exhaust temperature at sampling location ($^\circ C$)	Particulate loading (mg/NCM)	Aerodynamic mass median particle diameter (μmA)
FET cycle	0.051	177	68	0.26
97 kmph	0.057	218	55	0.54
56 kmph (with load)	0.033	149	45	0.46
56 kmph (no load)	(Not Available)	129	39	0.33

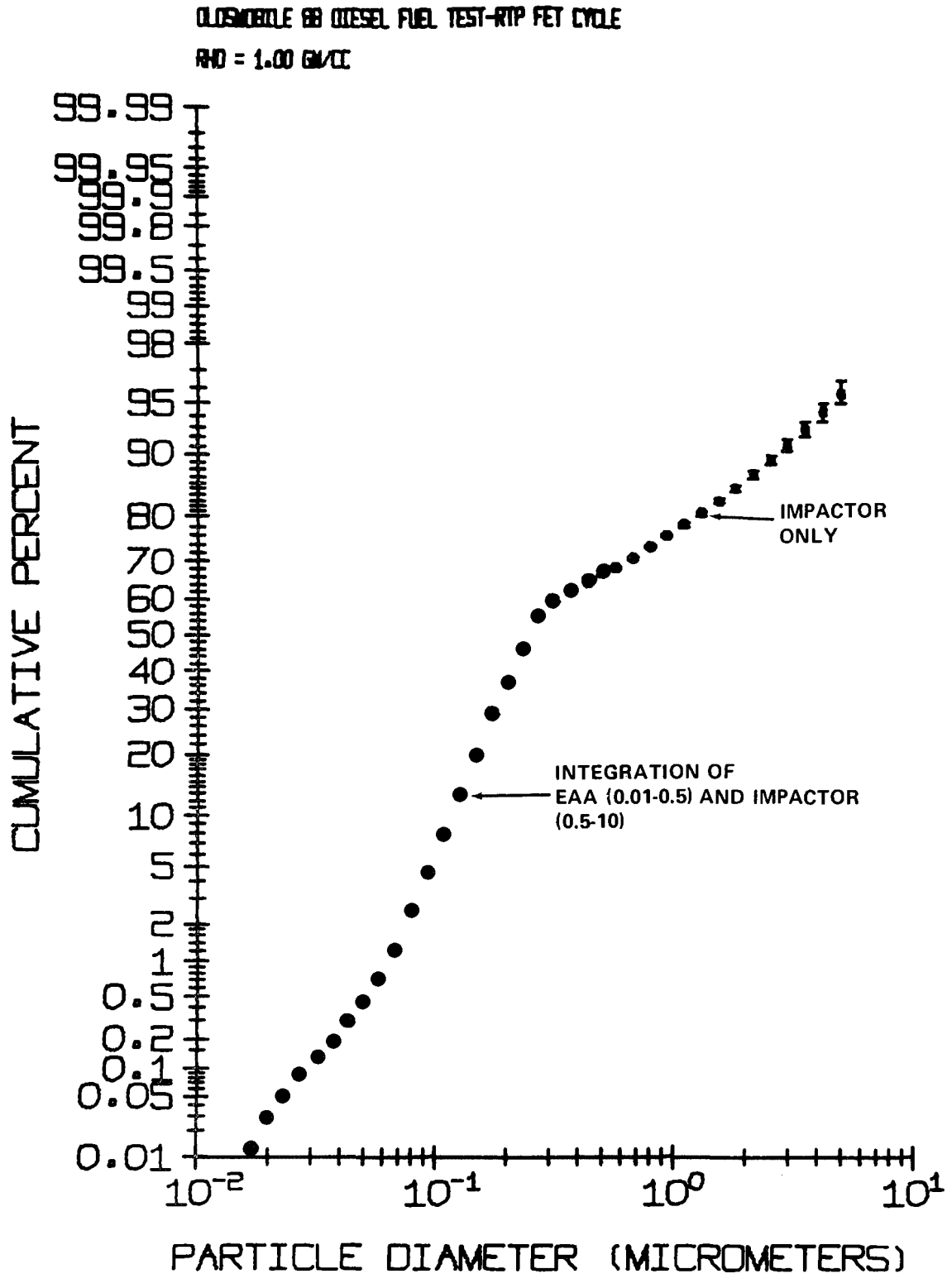

Figure 2. Particle size distribution for FET-cycle.

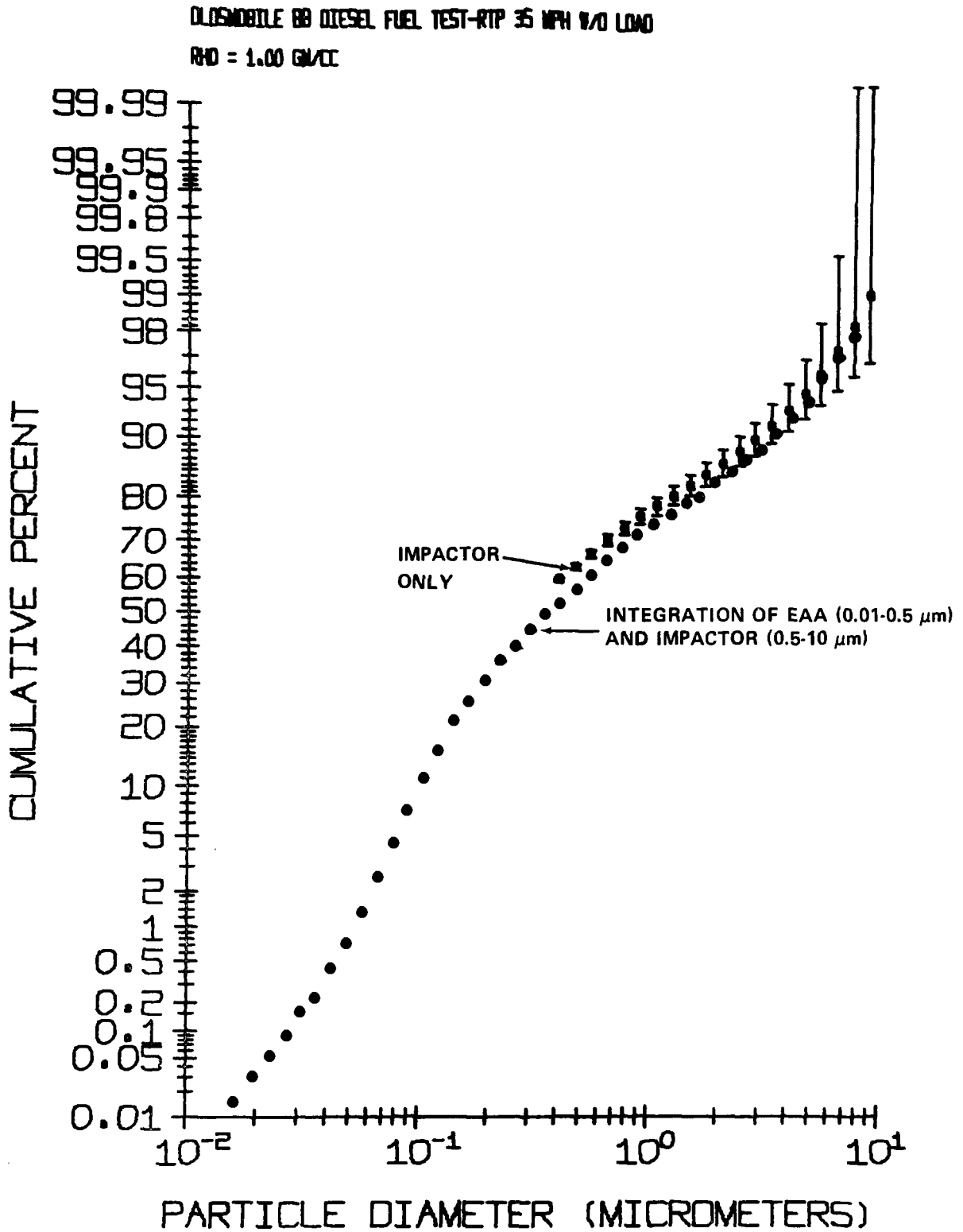

Figure 3. Particle size distribution for 35 mph no load condition.

DATE 4/10/79 RUN TIME 15:35:6

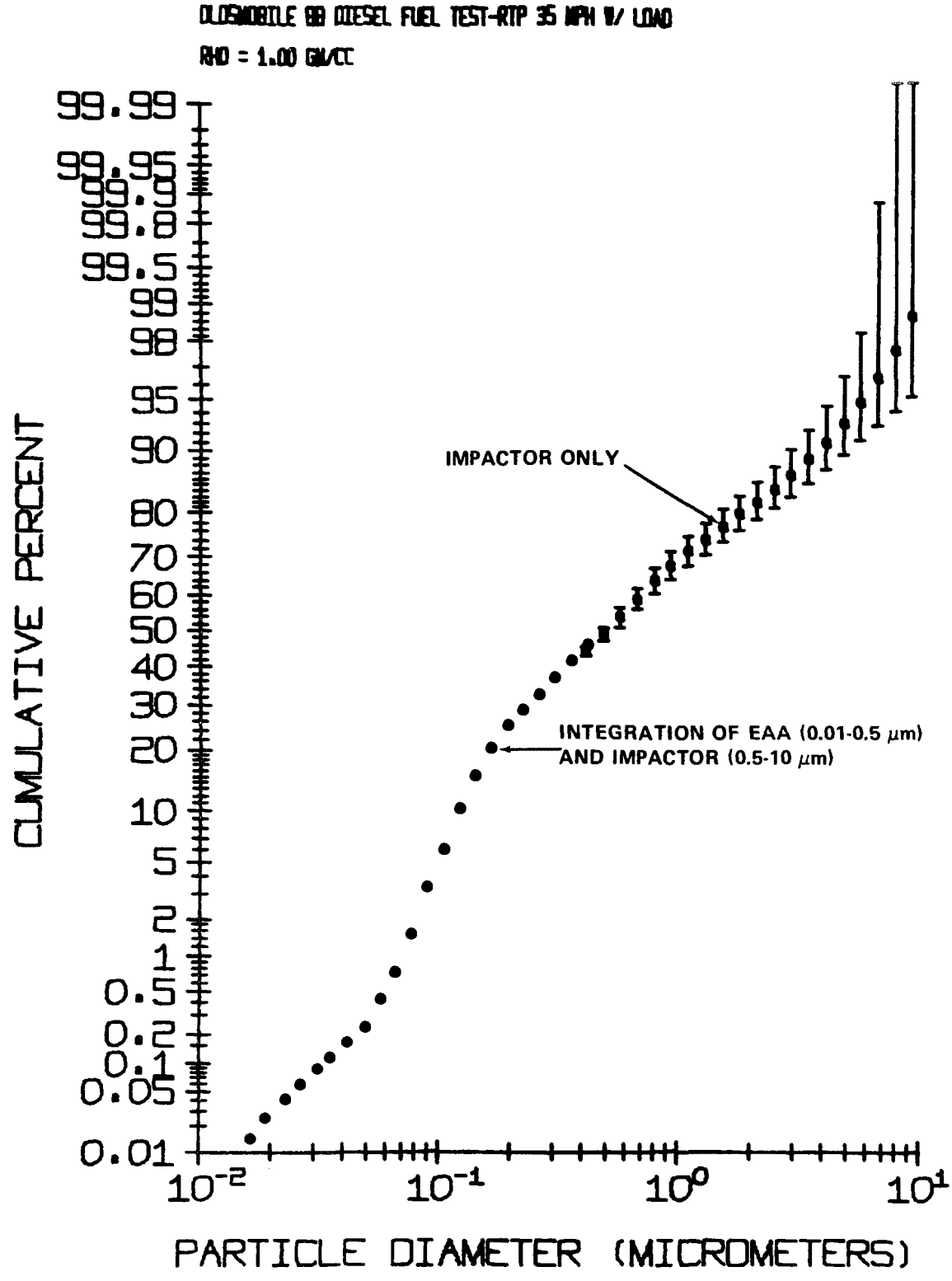

Figure 4. Particle size distribution for 35 mph with load condition.

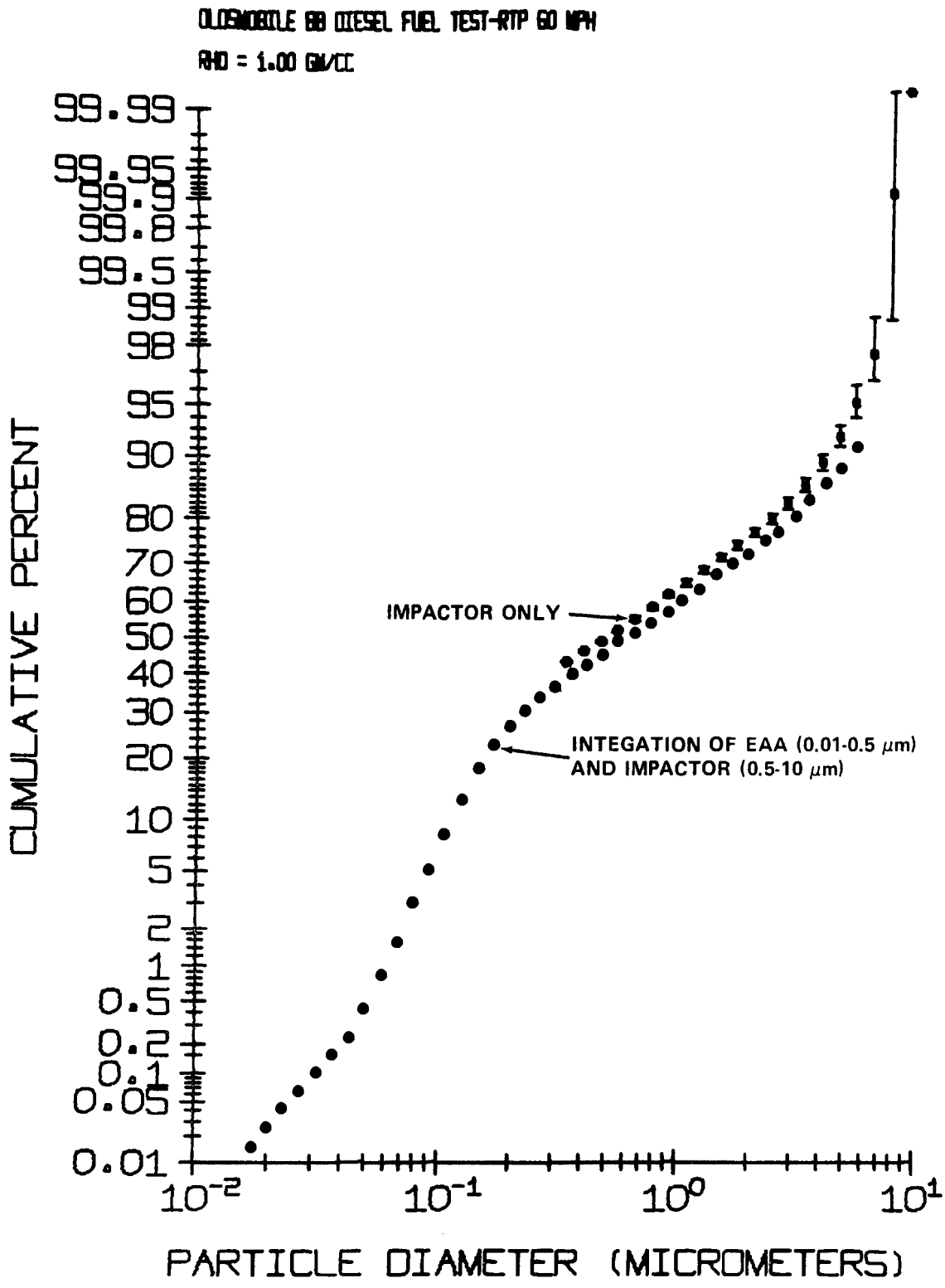

Figure 5. Particle size distribution for 60 mph condition.

DATE 4/11/79 RUN TIME 8:11: 3

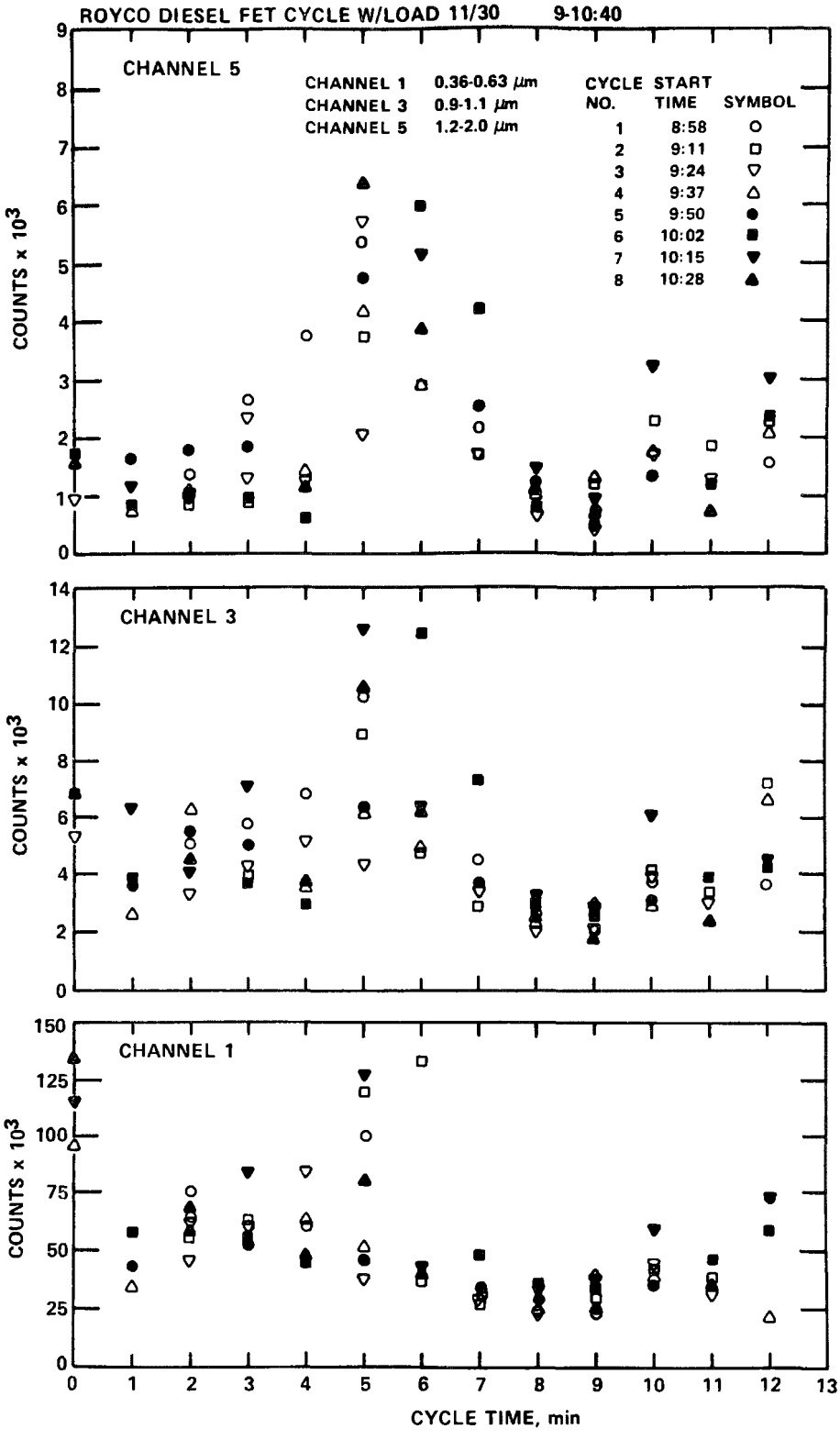

Figure 6. Relative concentration versus time for three particle size ranges during several FET cycles.

engine speed/load conditions under steady state operating conditions. The results reported here are qualitatively similar in size distribution to those found by other investigators in measurements of emissions from heavy duty diesel engines insofar as the impactor data are concerned.[2,3]

References

1. Blacker, S.M. EPA Program to Assess the Public Health Significance of Diesel Emissions. Journal of the Air Pollution Control Assoc. Vol 28, page 769, August 1978.

2. Lipkea, W.H., J.H. Johnson, and C.T. Vuk. The Physical and Chemical Character of Diesel Particulate Emissions - Measurement Technique and Fundamental Considerations. SAE Paper # 780108, presented at the SAE Congress and Exposition, Detroit, Michigan, February 27-March 3, 1978.

3. Springer, K., and R. Stahman. Removal of Exhaust Particulate from a Mercedes 300D Diesel Car. SAE Paper # 770716, presented at the SAE Off-Highway Vehicle Meeting and Exhibition, Mecca, Milwaukee, Wisconsin, September 12-15, 1977.

CONTROL STRATEGIES FOR PARTICULATE EMISSIONS FROM VEHICULAR DIESEL EXHAUST

M. Greg Faulkner
John P. Gooch
Jack R. McDonald
Southern Research Institute
2000 Ninth Avenue South
Birmingham, Alabama 35205

and

James H. Abbott
Dennis C. Drehmel
Industrial Environmental Research Laboratory
U.S. Environmental Protection Agency
Research Triangle Park, North Carolina 27711

ABSTRACT

The advantages and disadvantages of several possible control strategies for particulate emissions from vehicular diesel exhaust are discussed. The evaluation of the potential usefulness of the various control strategies is based on available data concerning the mass loading and particle size distribution and on anticipated control standards. Several studies have been made on devices for removing particulate emissions from vehicular diesel exhaust. These studies, which include the techniques of filtration, wet scrubbers, and electrostatic precipitation, are summarized. A comparison of the various control devices is made based on such factors as size, expected efficiency, and maintenance requirements.

INTRODUCTION

As a result of the federal government's requirement that the average fuel mileage of U.S. auto manufacturers be at least 11.6 kilometers per liter (27.5 miles per gallon) by 1985, there is increased interest in the use of diesel engines for light-duty vehicles because of the diesel's superior fuel economy. Unfortunately the diesel engine produces a high level of combustion byproducts which are potentially hazardous, and therefore the Environmental Protection Agency has proposed emission standards which would require up to 70% particulate removal efficiencies for some current models.

Several approaches for controlling particulate emissions are under investigation by automobile researchers, including fuel modification, combustion modification, and after-treatment of the exhaust in a control device. The purpose of

the work presented here was to examine the potential applicability of stationary source particulate control technology to diesel particulate control. The control mechanisms which were examined included electrostatic precipitation, filtration, and wet scrubbing. The removal of particulate by catalyzed or uncatalyzed oxidation is another after-treatment concept which is being investigated elsewhere, but which may ultimately need to be considered as a disposal strategy in connection with particulate removal by a filtration or electrostatic precipitation device.

Figure 1 shows the physical characteristics of the particulate. Consideration of these characteristics yields some insight into the difficulty of designing a practical control device. The size distribution of the material has a mass median diameter of about 0.3 μm, which is in the particle size range at which conventional control devices are least effective. If suitable collection is achieved, the bulk density of the soot is only about 0.1 gm/cm^3 which creates a storage and disposal problem. For example, if 90% particulate control is achieved on an Olds 350 diesel, about 20 liters of material would be accumulated in 5,000 kilometers if no compaction occurred. The flow rate of 0.14 actual cubic meters per second (300 acfm) is a worst case value derived from the displacement of an Olds engine. Actual values appear somewhat smaller than this.

The approach used in the present work was to use existing theories for the fundamental collection processes to identify control concepts which appear to provide an effective means for capturing diesel exhaust particulate without adversely affecting engine performance. Based on favorable projections for filtration and electrostatic precipitation devices, new filtration, electrostatic precipitation, and electrostatic/filtration control devices were designed which could be utilized on a light-duty diesel vehicle. Also, a literature survey was performed to determine which control devices had been previously employed and the degree of success achieved.

FILTRATION

Several authors have reported on the use of filtration as a means of collecting diesel exhaust particulate. Springer and Stahman[3] tested a total of 48 combinations of devices and identified a best system for particulate removal. This system, which consisted of two filters packed with alumina-coated steel wool, initially reduced the exhaust particulate by 64%. However, the collection efficiency decreased rapidly with distance, accompanied by a sharp increase in system backpressure. The high backpressure of the system had no great effect on the fuel economy of the test vehicle, but the acceleration rate, already a weak point on diesels, was reduced by 20%.

Sullivan, et al,[5] examined six different filter materials in a study concerned with emission of underground diesel engines. Although good collection efficiencies were reported, relatively high backpressures were experienced and the rate of increase of backpressure was too high for automotive use. General Motors[6] has also tested a number of filter materials including both paper and metal mesh filters. The paper filters exhibited high collection efficiencies, but with unacceptable backpressures, while the metal mesh filters had more reasonable backpressures but showed efficiency degradation and carry-over of agglomerated particulate.

Individual particle size[1]	0.01 μm
Agglomerated particle size[2]	
mass median diameter	0.3 μm
% less than 1 μm	70
Exhaust temperature[3]	
Manifold	190 - 275°C
Muffler	164 - 210°C
Bulk density[4]	0.12 g/cm^3
Gas flow rate (assumed)	0.14 actual m^3/s
Mass loading[4]	0.07 g/actual m^3

Figure 1. Physical characteristics of the particulate.

The Eikosha Company[7] in Japan has been conducting developmental work on a particulate collection device called an Aut-Ainer intended for use on both gasoline and diesel vehicles. Figure 2 shows one of these. The initial concept for this device was to provide for the collection of emissions by condensation growth with collection on a mesh material. The original system consisted of a number of expansion chambers followed by regions filled with metal mesh to serve as a collection media. A ram air cooling tube was also provided down the center on the device. This device has been carried through a number of stages of development using an empirical approach.

At the current stage of development, the device attains a collection efficiency of about 70% for diesel particulate when the system is clean. However, it is necessary to provide for cleaning at intervals of 2,000 kilometers of operation. In the absence of cleaning, the collection sites become covered with the very low density soot particles after which reentrainment occurs. Therefore, the device initially acts as a collection device until reentrainment occurs, at which time the characteristic behavior changes to that of an agglomerator.

The recognition of this fact led the developers to investigate adding a post-collection device as a means for collecting this reentrained material. Two methods are currently under investigation, each of which involves the use of a collector operating on a side stream consisting of about 10 to 15% of the total flow through the system. The method shown in Figure 2 uses a cyclone to divert the particulate to a collection bag. The other method uses a rotating particle catching wheel which passes through a backflow of air where the particulate is blown into the collection bag. This portion of the system still needs a lot of work but the approach does show promise. Further study is needed to devise a more reliable method for diverting the reentrained material into the post-collection device.

Filtration theory attempts to predict overall particle removal in a filter based on an understanding of the interaction of particles with a single filter element, which may consist of a fiber, granule, or previously collected particle. The currently available filtration theory was employed to estimate the performance of various filter designs.* The approach used was to select a reasonable filter volume and path length, and then to examine the performance of filters half and double the volume, with half and double the path length. Both fiber bed and granular bed filters were considered, and the porosity of each was fixed at a reasonable value. The fiber and granule diameter were fixed, and the properties of the gas and aerosol were fixed at a base case condition of 200°C, with 0.14 actual m^3/s transporting 0.07 g/m^3 of particulate with an mmd of 0.20 μm.

The analysis resulted in the selection of a fibrous filter for further study.* The filter is shown in Figure 3. This device is approximately the same size as a regular muffler. The packing material is a 10 cm thick mat of 10 μm diameter fibers with a porosity of 99%. The filter shown in Figure 3

*This task was performed by Dr. David Leith under subcontract to Southern Research Institute.

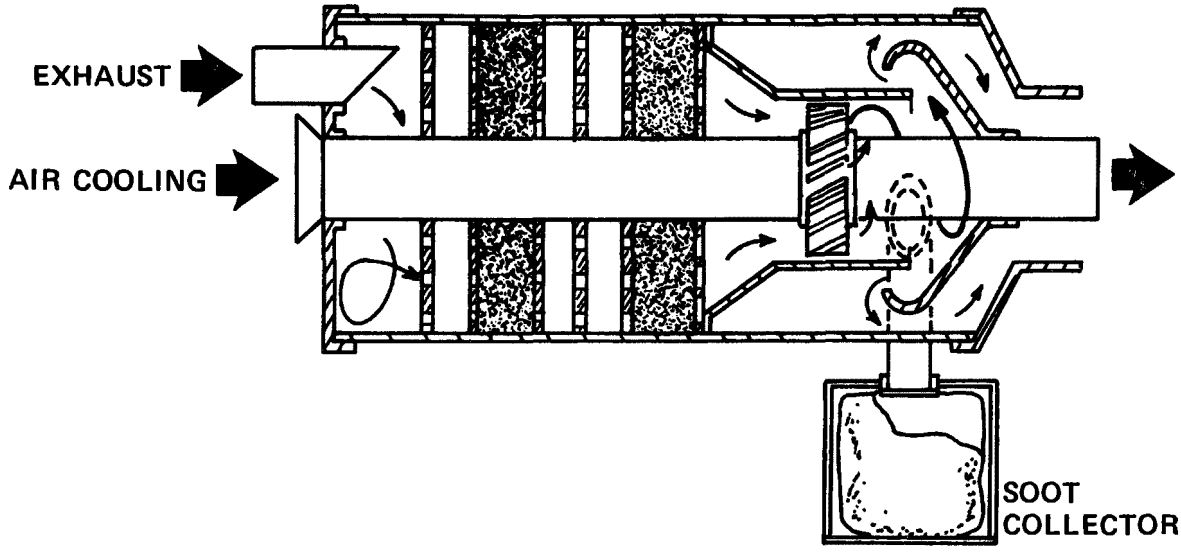

Figure 2. Aut-ainer filter with cyclone soot collector.

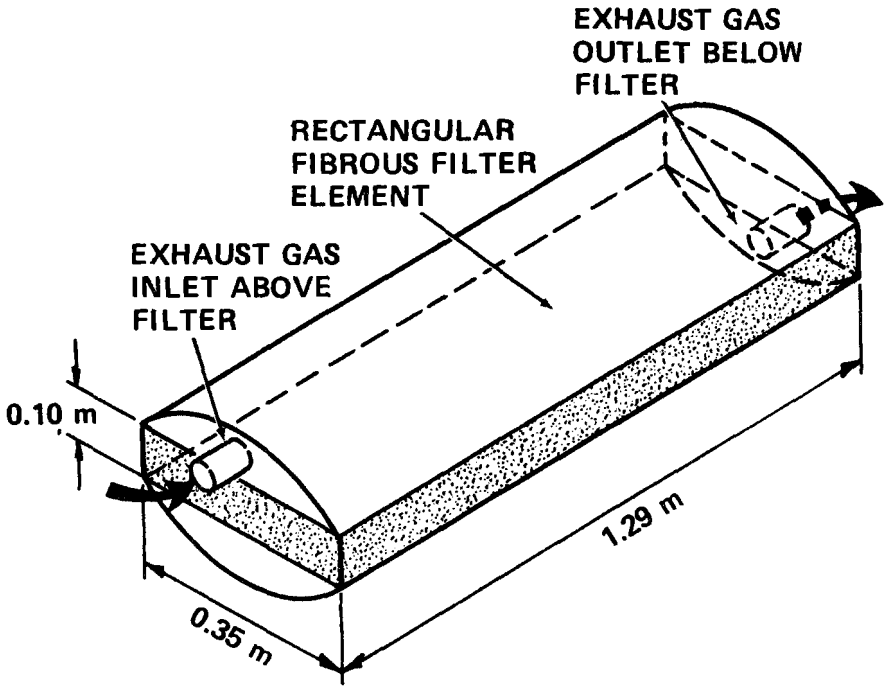

Figure 3. Prototype fibrous filter.

has a cross-sectional area of about .5 m^2. This will allow a great reduction in the gas velocity which will reduce reentrainment. The large area will also increase the lifetime of the device by making it more difficult for the collected particulate to seal over the face of the filter. The estimated pressure drop is 730 Pa or about 7.6 cm of water.

Figure 4 shows the theoretical efficiency of this filter design. Note that the collection is good in the diffusional region and in the impaction region, but that a large dip occurs in the region of the 0.3 μm mass median diameter of the diesel particulate. Integrating this curve over the size distribution gives 82% efficiency. As the filter loads with particulate, a change in the collection mechanisms will occur due to the fact that particulate will be collected on particulate coated fibers rather than clean fibers. Although there are no numerical theories to describe this phenomena, it is expected that the dip in the efficiency curve in Figure 4 will be reduced somewhat.

The theory also cannot predict the effects of condensation of hydrocarbons or H_2O. There should be a lot of condensation on cold starts when the hot exhaust hits a cold filter. Particle reentrainment is another topic not treated by theory. It is expected that the large cross section and consequently low superficial velocity of the proposed filter will reduce reentrainment but there is no way to determine the quantity and size distribution of the emerging particulate without building and testing a prototype filter. Post-collection devices, such as those mentioned for the Aut-Ainer, can be easily applied to this design if necessary. This design should also provide a convenient geometry for the incineration of collected particulate.

Unfortunately, the literature survey on filtration devices did not reveal data on collection efficiency as a function of particle size or on the applicability of existing filtration theory to the various devices which have been tested. Consequently, it is not possible to directly relate the proposed fibrous filter prototype to the prior studies without additional experimentation.

ELECTROSTATIC PRECIPITATION

The electrostatic precipitation process consists of the fundamental steps of particle charging, particle collection, and the removal of the collected material from the collection and discharge electrodes. The particle charging process is accomplished through the creation of an electric field and a corona current by applying a large potential difference between a small radius electrode and a much larger electrode where the two electrodes are separated by a region of space containing an insulating gas. Particle charging is essential to the precipitator process because the electrical force which causes a particle to migrate toward the collection electrode is directly proportional to the charge on the particle. The most significant factors influencing particle charging are particle diameter, applied electric field, current density, and exposure time. Particle collection rates for a given value of particle charge are a function of particle size, the electric field in the region of the collection electrode, gas flow rate, gas viscosity, and electrode geometry. Removal of the collected material is usually accomplished by mechanical vibrations of the collection and discharge electrodes, but irrigated electrode systems are also

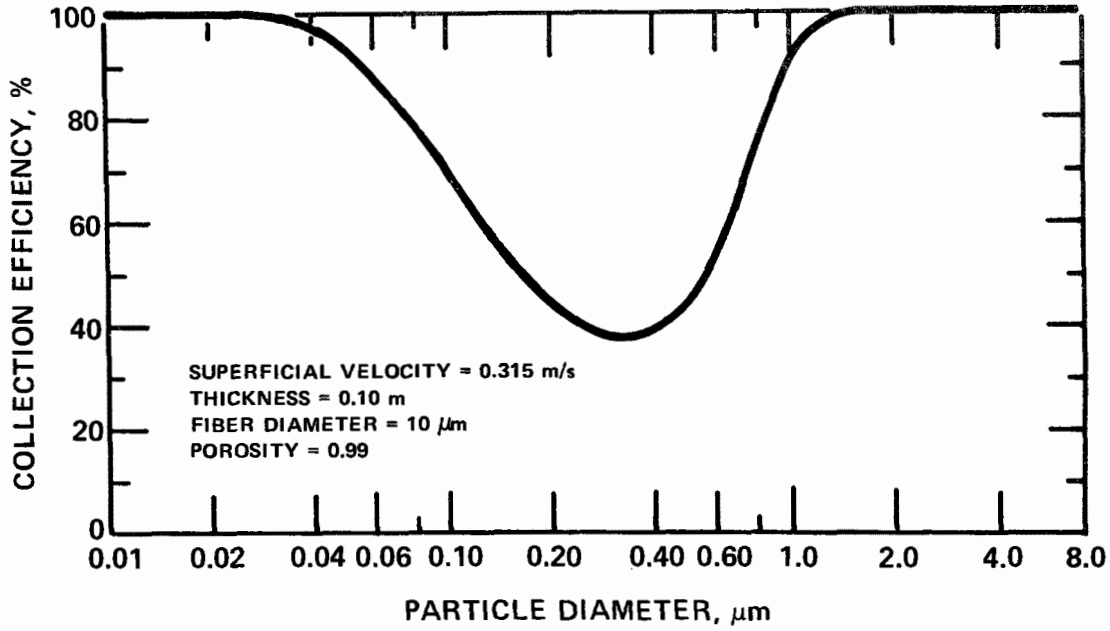

Figure 4. Fibrous filter efficiency versus particle diameter.

in use which employ sprays of liquid to clean the electrodes. The electrical resistivity of the particulate matter for dry applications strongly influences the collection efficiency which can be achieved with a given electrode geometry.

An electrostatic control device for diesel particulate has the potential advantage of providing high efficiency collection of small particles with low backpressure and low energy consumption. However, there are two serious problems which must be overcome before such a device becomes practical - particle reentrainment and current leakage through conductive films on high voltage insulators. Reentrainment stems from high gas velocity and discharge of conductive particles. Conductive films are a direct result of the deposition of conductive particles on the insulators.

Only two reports of electrostatic devices applied to diesel engines have been located. Both devices showed marginal performance before ceasing to function due to a conductive path problem. The marginal performance can be attributed to design problems. The conductive path problem represents a major obstacle which must be overcome before electrostatic devices can be used successfully.

However, due to the effectiveness of electrostatic particle collection, two prototype devices have been proposed for construction and evaluation. Both devices separate the particle charging and particle collection step as a result of the special requirements needed for diesel particulate collection. Figure 5 is a conceptual sketch of a device which employs a periodic wet flushing scheme to thoroughly clean the collected particulate from all internal surfaces of the system.* A vertically oriented, cylindrical geometry appears best suited to such a cleaning method, and optimum from the standpoint of structural strength. A two-stage device was selected to provide a maximum collecting surface within the space limitations of a vehicular installation. The exhaust gas from the engine enters the electrostatic precipitator (ESP) tangentially so as to avoid immediate impaction on the high voltage insulators. The cyclonic motion of the gas in the first stage (upper half) of the ESP has little effect on particulate collection by impaction, since most of the particles are very fine; however, the circular path allows for adequate charging time for the particles before they enter the collecting stage.

Particle charging is achieved by means of an electrical corona discharge from flat, star-shaped electrodes mounted on the axial rod extending downward from the insulator at the top of the device. A corona ball on the end of the rod suppresses discharges to the grounded plates in the collecting stage. This structure is preferred over a more conventional fine wire corona discharge electrode because of its ruggedness.

The collecting stage consists of a set of concentric cylinders. In sequence of decreasing diameter, the odd numbered cylinders are connected to electrical ground and the even are connected to the output of a high voltage power supply. The high voltage cylinders are connected together by a metal bus bar and nested between the grounded insulators. Insulating spacers between

---

*This device was designed by Dr. Duane Pontius of Southern Research Institute.

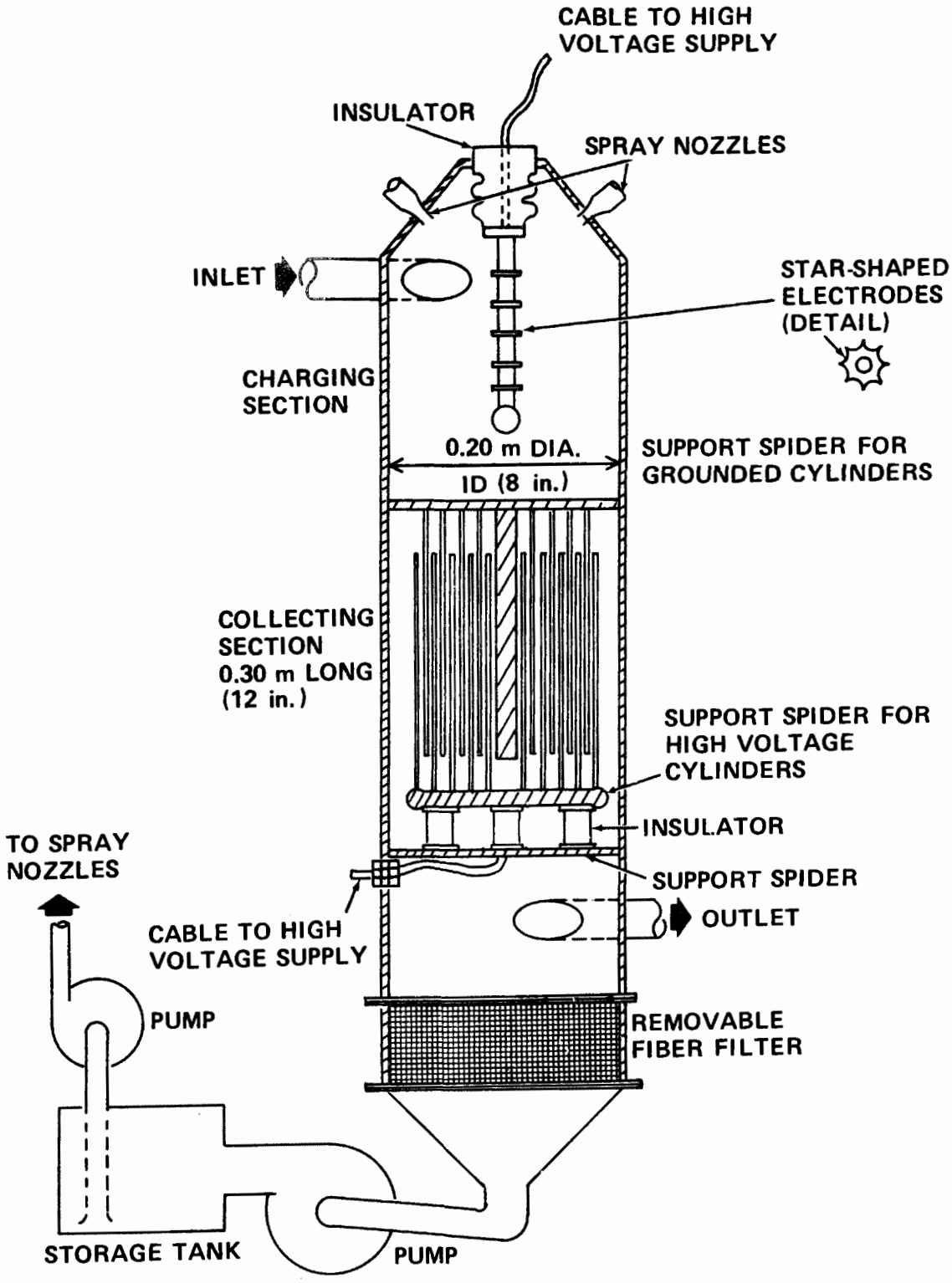

Figure 5. First prototype electrostatic precipitator for collecting diesel particulate.

cylinders are avoided in order to minimize leakage resistance due to fouling by low resistivity material. Three stand-off insulators are used to support the entire array of high voltage cylinders.

The ESP is to be cleaned periodically by spraying a nonvolatile liquid through the nozzles at the top of the device. The liquid is pulled through a filter at the bottom of the ESP and then pumped into a storage tank for the next cleaning cycle. The period between flushing operations would probably be governed by the length of time required for the particulate buildup on the insulators to develop a significant current leakage path between high voltage components and ground. Provisions would be required to bypass the ESP during the cleaning operation, which might take 30-60 seconds.

The .2 m diameter and .15 m long charging region and the 1.5 square meter collection area of this device allow an estimation of collection efficiency to be made using mathematical relationships which describe the particle charging and collection process. If favorable electrical conditions can be maintained, the collection efficiency of 0.30 μm diameter particles from an exhaust gas stream of 0.14 m^3/s is estimated to be 80%.

The electrostatic/filtration device* shown in Figure 6 is a radial flow device which uses dielectric filter material in the collection region. This device has the following features:

(a) two stage operation, thus minimizing ozone generation and power consumption,

(b) adapts high velocity gas in small diameter ducts to low radial velocities for collection, thereby reducing reentrainment,

(c) highly efficient for the submicron particle size range,

(d) can utilize a combination of mechanical collection forces as well as coulombic, dielectrophoretic, and image electrical forces,

(e) convenient geometry for using electrified media in the collection stage and readily adaptable to removable cartridge form.

It is believed that the most effective form of collector would involve a gradation using three collection zones. The first would be a mechanical impaction collector utilizing the high velocity jets of gas produced by the inner perforated screen that changes the gas flow from the axial to the radial direction. The second zone could be a relatively coarse fibrous bed of collection media with superimposed electrostatic field. The final zone would be a finer graded bed of fibrous media with superimposed electrostatic field.

---

*This device was designed by Dr. Peter Castle under subcontract to Southern Research Institute.

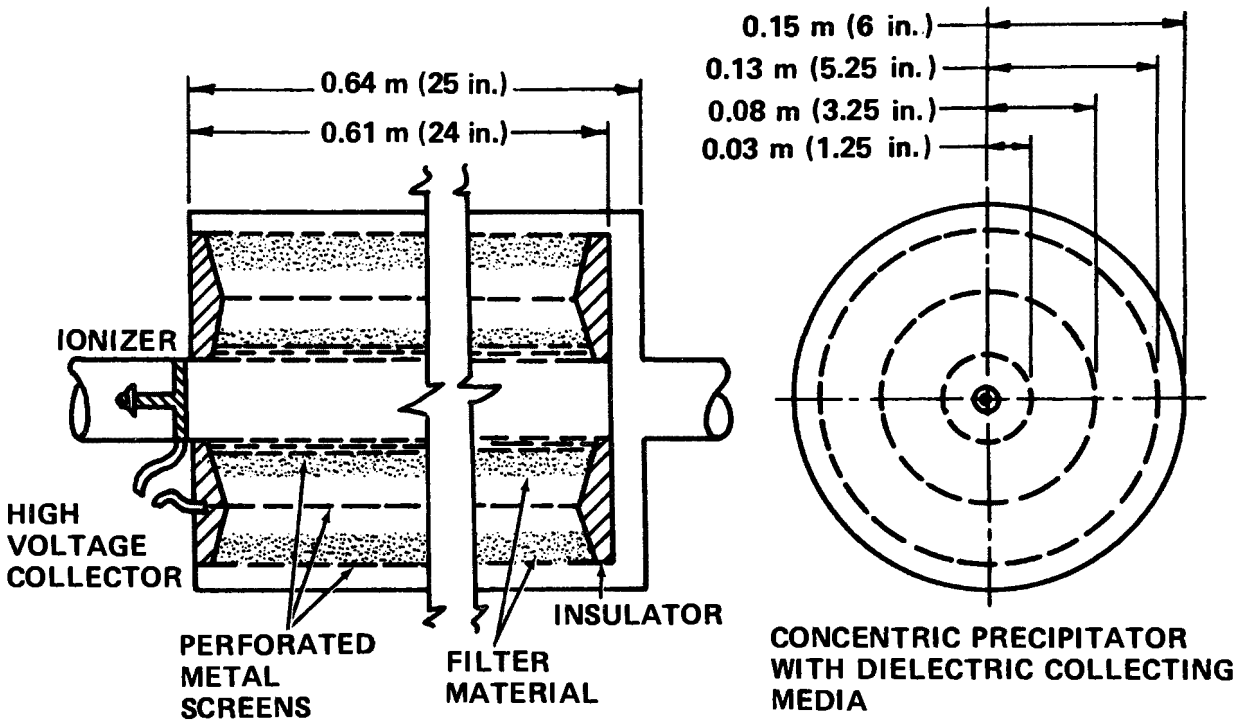

Figure 6. Second prototype electrostatic precipitator for collecting diesel particulate.

The efficiency of this device is harder to predict. If the effects of the dielectric material are neglected and the particles are assumed to have acquired the same charge as in the electrostatic device just mentioned (admittedly a bad assumption), then by using the metal collection plate area of 1.2 m^2 an efficiency of 0.7 can be calculated. The effect of the dielectric material will be to increase the collection efficiency. Figure 7 shows the results of using various geometries of dielectric material in a similar device described by Inculet and Castle.[8] Note that the collection efficiency for the device was improved with any dielectric inserted and that the most efficient case was for a fibrous bed similar to that proposed here.

This device does have two possible design drawbacks. The first of these is the susceptibility to conductive contamination on the insulators. This will probably be worse on the ionizer and may necessitate the use of a different type of ionizer. The second is the increase in backpressure that will result when the dielectric fiber bed becomes loaded with particles. The magnitude of this problem can only be determined experimentally.

WET SCRUBBER

The collection of particulate by wet scrubbing is accomplished through various mechanisms, including inertial impaction, gravitational collection, diffusion, electrostatic collection, and thermophoreses and diffusiophoresis. Mathematical descriptions of these mechanisms were employed to calculate particle collection efficiencies in various scrubber designs which might be employed for collection of diesel particulate.* The general conclusion derived from these calculations was that wet scrubbers are not suitable for removing particulate from diesel exhaust.

Under the constraint of a 25.4 cm (10-inch) water head, scrubbers are not efficient enough in removing the fine particles present in diesel smoke. A possible exception is the charged droplet scrubber, but it is not clear that this device would be preferable to some other type of electrostatic device.

The above conclusions are reinforced by consideration of the rate of water loss by evaporation in a wet scrubber. Diesel exhaust entering a scrubber at 200°C at a rate of 8.49 m^3/min (300 ft^3/min) will contain about 3% by volume water vapor as the result of fuel combustion in the engine. This rate corresponds to the flow of 118 g/min of water vapor. On leaving the scrubber at 50°C with water vapor at the saturation level (concentration, 12.17% by volume), the gas stream will carry water vapor away at the rate of 530 g/min. Thus, water will be lost at the rate of 412 g/min. This is equivalent to about 0.412 ℓ/min or 0.109 gal/min. For comparison, the rate of fuel consumption may be calculated by assuming that the exhaust flow rate corresponds to a highway speed of 96 km/h and that the fuel consumption rate is 10.5 km/ℓ or 0.15 ℓ/min. The conclusion, therefore, is that water would be consumed at 2.7 times the rate of consumption of diesel fuel.

---

*These calculations were performed by Dr. Mike Pilat under subcontract to Southern Research Institute and by Dr. Ed Dismukes of Southern Research.

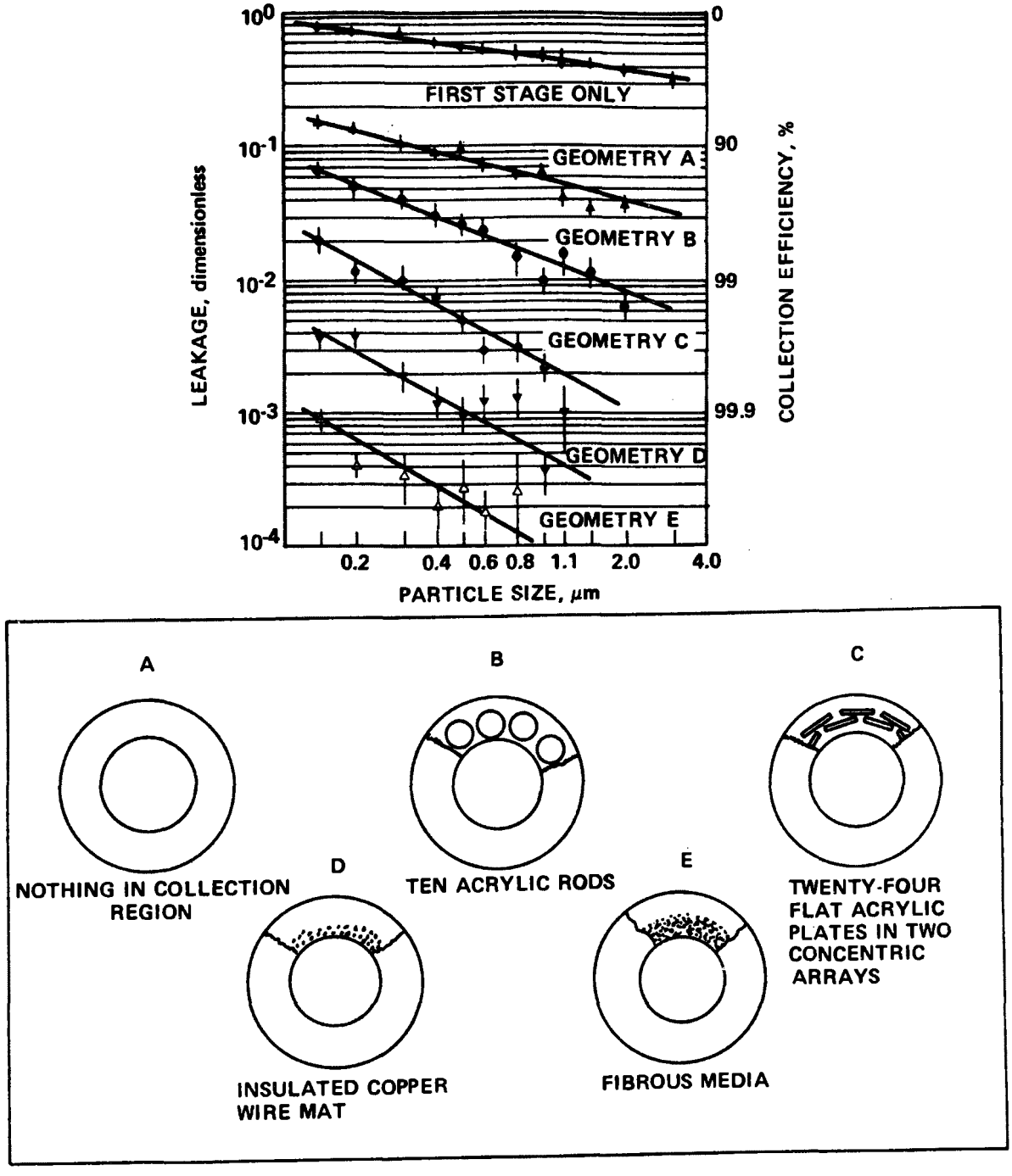

Figure 7. Collection efficiency of a concentric precipitator with dielectric collection media.[8]

CONCLUSIONS

From the preceeding discussion it is possible to draw some conclusions regarding the applicability of scrubbers, electrostatic devices, and filters to the problem of controlling diesel particulate emissions. The first of these, scrubbers, can be eliminated from further consideration due to the large size required to obtain adequate efficiencies at reasonable backpressures and to the high rate of water consumption.

Electrostatic devices merit further consideration for the important reasons that they present very little backpressure to the system and that they maintain a relatively high collection efficiency over the 0.1 to 0.8 μm particle size range. To offset this, they have the severe disadvantage of dysfunction due to conductive particle contamination. Further research will have to be performed to design a system which can eliminate this difficulty. A lesser problem is that of disposal of the collected particulate. A method must be developed whereby the device may be cleaned and the collected particulate properly and safely disposed of as a matter of routine maintenance.

The third mechanism, filtration, demonstrates the same problem of disposal of the collected particulate. Another problem area is the possibility of high backpressure. Although it is possible to design a device of appropriately low backpressure when new, only experimentation will determine the amount of particulate the filter can collect without elevating the backpressure beyond allowable limits and adversely affecting engine performance. The problem of surface seal over can be avoided by utilizing a filter with a large face area such as the proposed prototype. The advantage of filtration is that it is a mechanically simpler concept. Filters, while not necessarily simple to design, are simpler to build and maintain in the field than electrostatic devices and as a consequence should be cheaper and more convenient in use.

Both electrostatic devices and filtration devices show promise of becoming workable solutions to the diesel exhaust problem. However, more research is needed on both types of device. The prototypes described need to be fabricated and tested on actual diesel exhaust streams. Determinations of collection efficiency as a function of particle size and of overall efficiency would be useful in the study of the collection mechanisms involved which should in turn lead to the development of improved collection devices. Testing of prototype devices will also yield additional insight into the particular problems which affect each device.

Additional study is also needed on the effects of gas stream temperature on the hydrocarbon portion of the particulate. A study by Black and High[9] indicates that most of the condensation and subsequent adsorption of vaporous hydrocarbons occurs in the last meter of the vehicle's tail pipe. This implies that a temperature reduction in the exhaust system would increase the amount of hydrocarbons which condense and can therefore be collected as particulate. Supportive evidence has been given by Masuda[10] who reports that Eikosha has seen a 20% by volume increase in collected particulate occur when the cooling air flow on the Aut-Ainer filter was increased.

REFERENCES

1. Lipkea, W. H., J. H. Johnson, and C. T. Vuk. The Physical and Chemical Character of Diesel Particulate Emissions - Measurement Technique and Fundamental Considerations. SAE Paper #780108, presented at the SAE Congress and Exposition, Detroit, Michigan, February 27 - March 3, 1978.

2. McCain, J. D., D. C. Drehmel, and J. H. Abbott. Characteristics of Particulate Emissions for a Light Duty Automotive Diesel Engine. Presented at the Second Symposium on the Transfer and Utilization of Particulate Control Technology, Denver, Colorado, July 23-27, 1979. Proceedings to be published by U.S. Environmental Protection Agency, Research Triangle Park, N.C.

3. Springer, K., and R. Stahman. Removal of Exhaust Particulate from a Mercedes 300D Diesel Car. SAE Paper #770716, presented at the SAE Off-Highway Vehicle Meeting and Exhibition, Mecca, Milwaukee, Wisconsin, September 12-15, 1977.

4. Frey, J. W., and M. Carn. Physical and Chemical Characteristics of Particulate in a Diesel Exhaust. American Industrial Hygiene Association Journal, 28(5):468-478, September-October, 1967.

5. Sullivan, H., L. Tessier, C. Hermance, and G. Bragg. Reduction of Diesel Exhaust Emissions (Underground Mine Service). Prepared for the Department of Energy, Mines and Resources, Ottawa, by the Mechanical Engineering Department of the University of Waterloo, Waterloo, Ontario, May 1977.

6. General Motors Response to EPA Notice of Proposed Rulemaking on Particulate Regulation for Light-Duty Diesel Vehicles, April 19, 1979. Available from General Motors Corporation.

7. Personal communication between Grady Nichols, Southern Research Institute and Eikosha Company.

8. Inculet, I. I., and G. S. P. Castle. A Two-Stage Concentric Geometry Electrostatic Precipitator with Electrified Media. ASHRAE Journal, 13(3): 47-52, March 1971.

9. Black, F., and L. High. Diesel Hydrocarbon Emissions, Particulate and Gas Phase. EPA Symposium on Diesel Particulate Emissions Measurement Characterization. Ann Arbor, Michigan, May 1978. Proceedings available from U.S. Environmental Protection Agency, Research Triangle Park, N.C.

10. Personal communication with Senichi Masuda.

AN EVALUATION OF THE CYTOTOXICITY AND MUTAGENICITY OF ENVIRONMENTAL PARTICULATES IN THE CHO/HGPRT SYSTEM

Neil E. Garrett, George M. Chescheir, III, and Nancy A. Custer
Cellular Pathology and Biochemistry Section, Northrop Services, Inc., Research Triangle Park, N.C. 27709

John D. Shelburne and Catherine R. De Vries
Department of Pathology, Duke University Medical Center and Veterans Administration Hospital, Durham, N.C. 27710

Joellen L. Huisingh and Michael D. Waters
Biochemistry Branch, U.S. Environmental Protection Agency, Research Triangle Park, N.C. 27711

ABSTRACT

The cytotoxicity and mutagenicity of fly ash collected from an electrostatic precipitator were investigated using Chinese hamster ovary (CHO) cells. Cellular toxicity was determined by measurement of cell viability by trypan blue dye exclusion, cell number by optical enumeration, cellular adenosine triphosphate (ATP) by luminescence assay, and clonal growth. Cellular ATP was a sensitive biochemical indicator of toxicity at particle concentrations of 1000 µg/ml. CHO cells readily phagocytized fly ash particles. Internalization of fly ash was confirmed by light and electron microscopic observation. Fly ash was frequently observed in association with the cell nucleus and its effect on nuclear DNA was evaluated by measurement of mutation at the gene locus coding for the enzyme hypoxanthine-guanine phosphoribosyl transferase (HGPRT). The mutation frequency was increased in cultures exposed to 100-200 µg/ml of fly ash.

INTRODUCTION

The emmision of particulate matter into the atmosphere is a serious environmental problem. The magnitude of the problem relative to particles from stationary fuel combustion sources has been discussed by Abbott and Drehmel (1979)[1]. The cytotoxicity, mutagenicity or carcinogenicity of industrial particulates from coal combustion processes are largely unknown. It has been reported that many carcinogens and potential carcinogens are apparently preferentially concentrated on the surface of respirable coal fly ash particles some which may pass through conventional particulate control devices, enabling them to come into intimate contact with lung tissue when inhaled. Recently it has been shown that extracts of well defined respirable fly ash particles are mutagenic in Salmonella typhimurium (Chrisp et al., 1978; Fisher et al., 1979)[2,3]

We have previously reported on the utilization of the rabbit alveolar macrophage and Chinese hamster ovary (CHO) cell systems for the evaluation of the toxicity of particulates (Garrett et al., 1979)[4]. In this paper we report further studies of the phagocytosis of fly ash particles by CHO cells, the intracellular localization of particulate, and subsequent toxic and mutagenic effects.

MATERIALS AND METHODS

Polystyrene latex particles (1.1 μ) were obtained from Dow Corning. Fly ash particles were obtained from the Illinois Institute of Technology Research Institute. The fly ash was collected from an electrostatic precipitator, size-fractionated and designated 0-2, 2-5 and 5-8 μ (Yamate and Ashley, 1975)[5]. Fly ash was fractionated using a Bahco Microparticle Classifier. Particulate samples were stored in desiccators containing Drierite to prevent absorption of moisture and were weighed in a vented glove box on a Perkin-Elmer microbalance.

Culture of Cells

The Chinese hamster ovary (CHO) cell line was obtained from the American Type Culture Collection and maintained in medium supplemented with fetal calf serum (virus and mycoplasma screened). Exponentially growing cells were removed after washing the cultures three times with phosphate-buffered saline and once with 0.25% trypsin. Cells were resuspended in Ham's F-12 media supplemented with 10% fetal calf serum and antibiotics and the suspensions were added to dishes for studies of phagocytic activity, microscopy, toxicity, and mutagenicity.

Electron Microscopy

CHO cells were plated in plastic petri dishes and allowed to grow to near confluency and incubated with 2-5 micron fly ash particles. Cells in monolayer were then fixed overnight in 2.5% glutaraldehyde in Millonig's phosphate buffer. After 1 hour post-fixation with 1% osmium tetroxide in s-collidine buffer, the monolayers were stained en bloc with 0.5% uranyl acetate in water, dehydrated in a graded series of ethanol, and embedded in Epon 812. One micron sections were cut with a diamond knife, stained with uranyl acetate and lead citrate, and examined at 80KV on a JEOL 100B transmission electron microscope.

Toxicity Assay

Two ml of cell suspension (1×10^6 cells/ml) in media containing 10% fetal calf serum were added to individual wells of Costar 6-well cluster dishes. Samples were added to each of three cluster dish wells containing cells. Five replicates of control cultures without sample were also made. The dishes were incubated on a rocker platform for a 20-hour period at 37°C in a humidified atmosphere with 5% CO_2 in air.

After incubation cells were collected by trypsinization and aliquots of the cell suspension were used for assay of cell ATP by luminescence assay (Waters et al., 1975)[6], viability by trypan blue exclusion, and cell number by optical enumeration with a hemocytometer. In some experiments cells were washed by low-speed centrifugation and total protein was determined using the method of Lowry et al. (1951)[7]. Phagocytic activity was measured as previously described (Waters et al., 1975)[6].

Assay of Mutation

Mutation was assayed by the method of O'Neill et al. (1977)[8]. Cells were cultured in Ham's F-12 media containing 5% extensively dialysed fetal calf serum (F12FCM5). Cultures in 75 cm^2 flasks were washed three times with Puck's saline G. After trypsinization 0.5×10^6 cells were counted and added to Corning 75 cm^2 flasks and incubated at 37°C. After a 24-hour growth period, the sample was added to the medium and the cultures incubated for 20 hours. Treated flasks were washed three times with saline G, and the cells were trypsinized and enumerated. For determination of initial cell survival, aliquots of the cell suspension were added to media in 25 cm^2 flasks to yield 300 cells/flask. The flasks were incubated for 7 days and then fixed and stained.

For determination of mutation induction the treated cells were subcultured every 48 hours. The flasks were washed, trypsinized the cell number determined, and 1 x 10^6 cells were added to 75 cm^2 flasks. After 8 days of culture cells were plated for selection and cloning efficiency. The cells were washed, trypsinized and the cell number determined. For cloning efficiency cells were suspended in hypoxanthine-free media and aliquots of 200 cells were added to 25 cm^2 flasks. For selection of mutants 2 x 10^5 cells were added to 75 cm^2 flasks containing F12FCM5 media without hypoxanthine and with 10 μM 6-thioguanine. Flasks were incubated at 37°C for 7 days and then fixed and stained.

RESULTS

Polystyrene latex is often used as a model particulate in studies of phagocytosis. The time course of phagocytosis of 1.1 μ latex spheres is shown in Figure 1A. Extracellular latex was dissolved with xylene using the method of Gardner et al. (1973)[9]. Identical results were obtained if the extracellular latex was not dissolved in xylene (Figure 1B). These results suggest that latex attached to the surface of the cells is rapidly internalized. CHO cells were also shown to be capable of ingesting latex 5.7 μ and 10.1 μ in diameter.

Having shown that CHO cells are capable of ingesting model latex particles by dissolving external latex with xylene, we exposed the cells to fly ash particles collected from an electrostatic precipitator. Internalization of fly ash was studied using light and electron microscopy. Both living cells examined in vitro by phase contrast microscopy and sections of fixed and embedded cells revealed large numbers of fly ash particles in the cytoplasm (Figure 2). By phase contrast these particles were frequently noted to be closely arranged around the nucleus. Electron microscopy confirmed that the fly ash particles were in the cells and that often they were closely apposed to the nucleus (Figure 2). Often a limiting membrane could be seen around each particle or group of particles. Many particles either sectioned poorly or appeared to have fallen out of the section. Except for the presence of fly ash particles, the treated cell cytoplasm, and nuclei resemble intact control cells.

Although the toxic effects of particulates may not be visible with light or even electron microscopy, particulate matter may exert cytotoxicity after gaining access to the cell interior. We examined the cytotoxicity of three particulates including fly ash after a 20-hour exposure to CHO cells(Table 1). Cellular ATP determined by luminescence assay and cell viability determined by exclusion of the dye trypan blue were sensitive indicators of damage caused by silica(Cab-O-Sil). Total cell protein and cell

number were also significantly depressed. Cell viability or ATP was not affected by a 20-hour exposure to 0.45 μ titanium dioxide particles. The number of CHO cells was less than the control which reduced the viability index, and possibly indicates an effect on cell division. In addition, the total cellular protein was slightly affected. Fly ash exerted only a minimal effect on cell viability, but ATP was depressed. Cell number was slightly reduced which lowered the viability index.

Since fly ash particles gravitated toward the perinuclear region, it is conceivable that this close apposition to the nucleus could permit diffusion of material from the particle surface into CHO cell nuclei and subsequently produce damage to DNA or nucleoprotein. It has been established that most chemical carcinogens cause mutation or DNA damage. Experiments were conducted to measure mutation at the specific gene locus coding for the enzyme hypoxanthine-guanine phosphoribosyl transferase(HGPRT). It may be seen in Figure 3(A,B) from two independent experiments that more mutants were found in cultures treated with increasing concentrations of the particles. A decrease in mutation frequency occurred if the concentration of fly ash was increased above 100 μg/ml apparently due to toxic effects of the particles. The particles caused essentially no effect on the long-term survival of the cells (Figure 3 C,D). Although the mutagenic effects of fly ash are small we have consistently observed a higher level of mutation in the treated cultures.

DISCUSSION

This report provides biological data illustrating the effects of model particulate compounds and coal fly ash on Chinese hamster ovary (CHO) cells in culture. The CHO cell system has been used previously for testing environmental chemicals (Wininger et al., 1978)[10], for evaluation of particulate materials (Garrett et al., 1979)[4], and for studying both cytotoxicity and mutagenicity of environmental agents (Hsie et al., 1978)[11].

As shown in this report and in our previous work (Garrett et al., 1979)[4] CHO cells are phagocytically active. These cells rapidly accumulate fly ash particles. Fly ash was frequently observed in close association with the cell nucleus. The close apposition of the fly ash particles to the cell nucleus may be due to the geometry of the CHO cells in culture. The possible effects of particulate materials on the structure and function of the nucleus are unknown, although it has been reported that whole particles of asbestos (Huang et al., 1978)[12] are weakly mutagenic in Chinese hamster lung cells. Free asbestos fibers have been demonstrated in the cytoplasm of Type II lung pneumocytes (Suzuki et al., 1972)[13]. Since relatively large protein molecules and messenger RNA

(Blackburn, 1971)[14], can apparently penetrate the nuclear envelope, material dissociating from phagocytized particles may be expected to be found within the cell nucleus. A juxta-nuclear position of ingested particulate matter would facilitate the transfer of dissociable substances to cell DNA, possibly causing mutation or cell transformation.

In our experiments, fly ash was not extremely cytotoxic. Cell viability was only slightly affected after a 20-hour exposure to the particulate although total cellular ATP was significantly depressed (66% of control). Damage to DNA was determined by measurement of mutation induction at the hypoxanthine-guanine phosphoribosyl transferase (HGPRT) locus (O'Neill et al., 1977)[8]. Fly ash increased mutation several fold over baseline values.

The experiments reported here have shown that in vitro studies at the cellular level with the CHO system can be used as a first stage in the evaluation of the toxicity and mutagenicity of whole particulates from coal-energy related processes. The cellular pathology data may be coupled with other chemical and biological research to improve pollutant control devices by detecting and ranking toxicity of the particles from stationary fuel combustion sources.

REFERENCES

1. Abbott, J.H. and D.C. Drehmel. Control of Particulates from Combustion. In: Proceedings of the Symposium on the Transfer and Utilization of Particulate Control Technology. U. S. Environmental Protection Agency, Research Triangle Park, N.C. EPA-600/7-79-044b, Vol. 2, pp 383-405, 1979.

2. Chrisp, C.E., G.L. Fisher and J.E. Lammert. Mutagenicity of Filtrates from Respirable Coal Fly Ash. Science. 199: 73-75, 1978.

3. Fisher, G.L., C.E. Chrisp, and O.G. Raabe. Physical Factors Affecting the Mutagenicity of Fly Ash from a Coal-Fired Power Plant. Science. 204: 879-881, 1979.

4. Garrett, N.E. et al. The Use of Short Term Bioassay Systems in the Evaluation of Environmental Particulates. In: Proceedings of the Symposium on the Transfer and Utilization of Particulate Control Technology. U. S. Environmental Protection Agency, Research Triangle Park, N.C. EPA-600/7-79-044d, Vol. 4, pp 175-186, 1979.

5. Yamate, G. and H. Ashley. Preparation and Characterization of Finely Divided Particulate Environmental Contaminants for Biological Experiments. IIT Research Institute, Chicago, Illinois, IITRI Report No. C6321-5, September 1975.

6. Waters, M.D. et al. Toxicity of Platinum (IV) Salts for Cells of Pulmonary Origin. Environmental Health Perspectives. 12: 45-56, 1975.

7. Lowry, O.H. et al. Protein Measurement with the Folin Phenol Reagent. J. Biol. Chem. 193: 265-275, 1951.

8. O'Neill, J.P. et al. A Quantitative Assay of Mutation Induction at the Hypoxanthine-Guanine Phosphoribosyl Transferase Locus in Chinese Hamster Ovary Cells (CHO/HGPRT System): Development and Definition of the System. Mutation Res. 45: 91-101, 1977.

9. Gardner, D.E. et al. Technique for Differentiating Particles that are Cell-Associated or Ingested by Macrophages. App. Microbiology. 25: 471-475, 1973.

10. Wininger, M.T., F.A. Kulik, and W.D. Ross. In Vitro Clonal Cytotoxicity Assay Using Chinese Hamster Ovary Cells (CHO-K1) for Testing Environmental Chemicals. In Vitro. 14: 381, 1978.

11. Hsie, A.W. et al. Quantitative Mammalian Cell Genetic Toxicology: Study of the Cytotoxicity and Mutagenicity of Seventy Individual Environmental Agents Related to Energy Technologies and Three Subfractions of a Crude Synthetic Oil in the CHO/HGPRT System. In: Application of Short-term Bioassays in the Fractionation and Analysis of Complex Environmental Mixtures. U. S. Environmental Protection Agency, Research Triangle Park, N.C. EPA 600/9-78-027, pp 292-315, 1978.

12. Huang, S.L. et al. Genetic Effects of Crocidolite Asbestos in Chinese Hamster Lung Cells. Mutation Res. 57: 225-232, 1978.

13. Suzuki, Y., J. Churg, and T. Ono. Phagocytic Activity of the Alveolar Epithelial Cells in Pulmonary Asbestosis. Am. J. Path. 69: 373-379, 1972.

14. Blackburn, W.R. Pathobiology of Nucleocytoplasmic Exchange. In: Pathobiology Annual. Volume I. H.L. Ioachim (Ed.). New York, Appleton. Century-Crofts, 1971, pp. 1-32.

Table 1. EFFECTS OF SILICA, TITANIUM DIOXIDE, AND FLY ASH ON CHO CELLS AT 1000 µg/ml.

Particle	% Viability	Viability Index	% of Control ATP (fg/cell)	% of Control Cells/ml	% of Control Protein
Silica (M-5)	1.7±1.9	0.5±0.6	4.3±5.1	49.7±22.7	67.8±13.7
Titanium dioxide (0.45µ)	97.8±2.2	66.5±12.2	106.9†	67.9±11.6	87.4±45.4
Fly ash (0-2µ)	82.9±4.1	59.5±9.2	66.2±9.3	71.5±7.7	98.4±19.7

Data are average of 2 experiments (6 replicates).

† 3 replicates

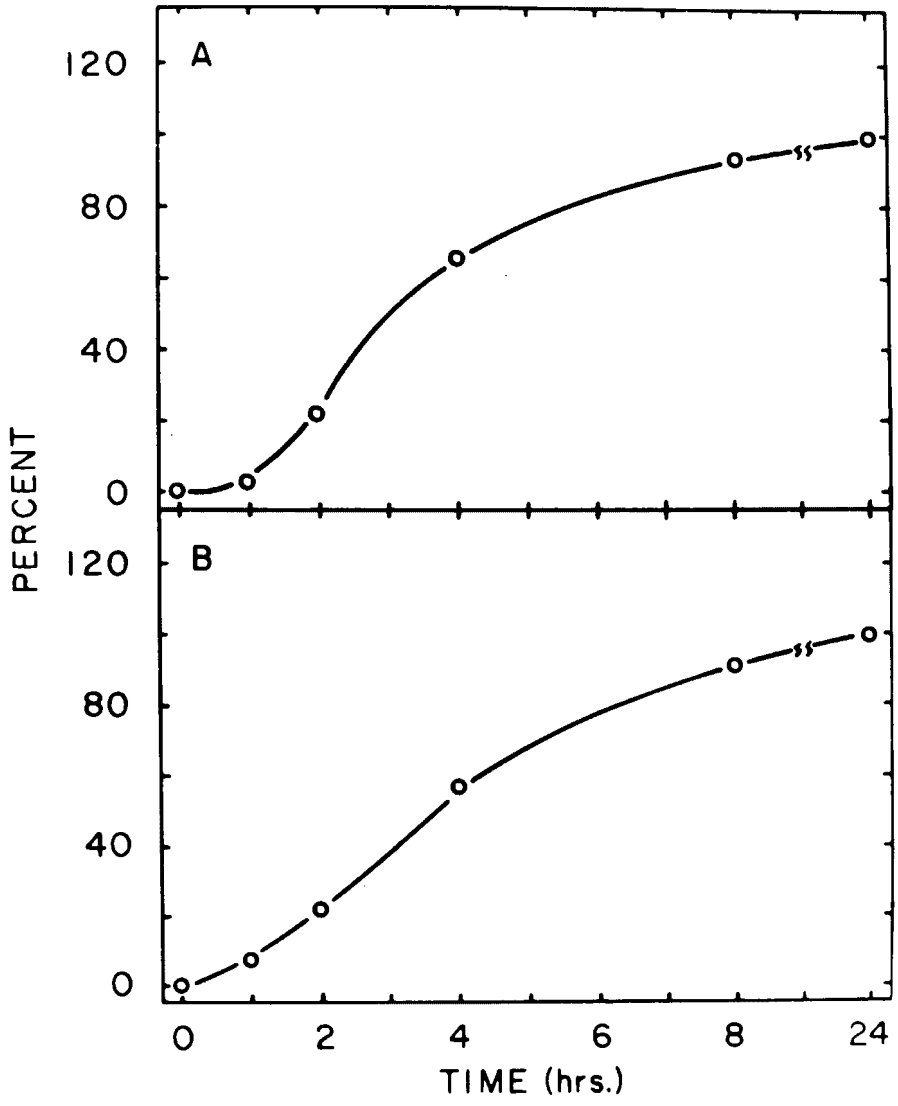

Figure 1. Phagocytosis of 1.1 μ polystyrene latex spheres by CHO cells. A. Extracellular latex was dissolved with xylene. B. Extracellular latex was not dissolved.

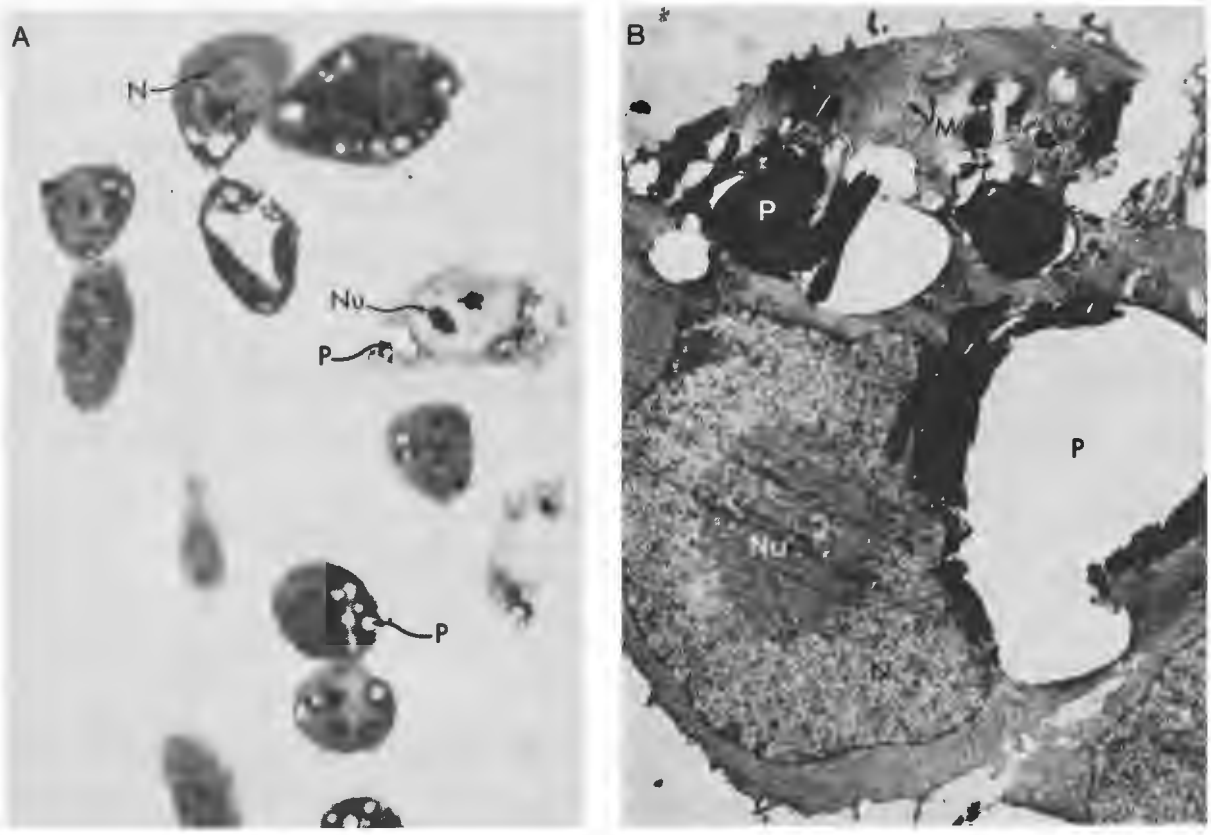

Figure 2. CHO cells after exposure to 2-5 μ fly ash particles. A. Light micrograph: Numerous fly ash particles (P) are visible in the cytoplasm. No evidence of necrosis is seen. Nucleoli (Nu) are present. (The width of this micrograph is 77 microns and the magnification is 100X). B. Electron micrograph: Numerous fly ash particles (P) in the cytoplasm, one of which is immediately adjacent to the nucleus (N). This nucleus exhibits a prominent nucleolus (Nu). Mitochondria (M) are intact. (The width of this micrograph is 10.9 microns and the magnification is 7,100X).

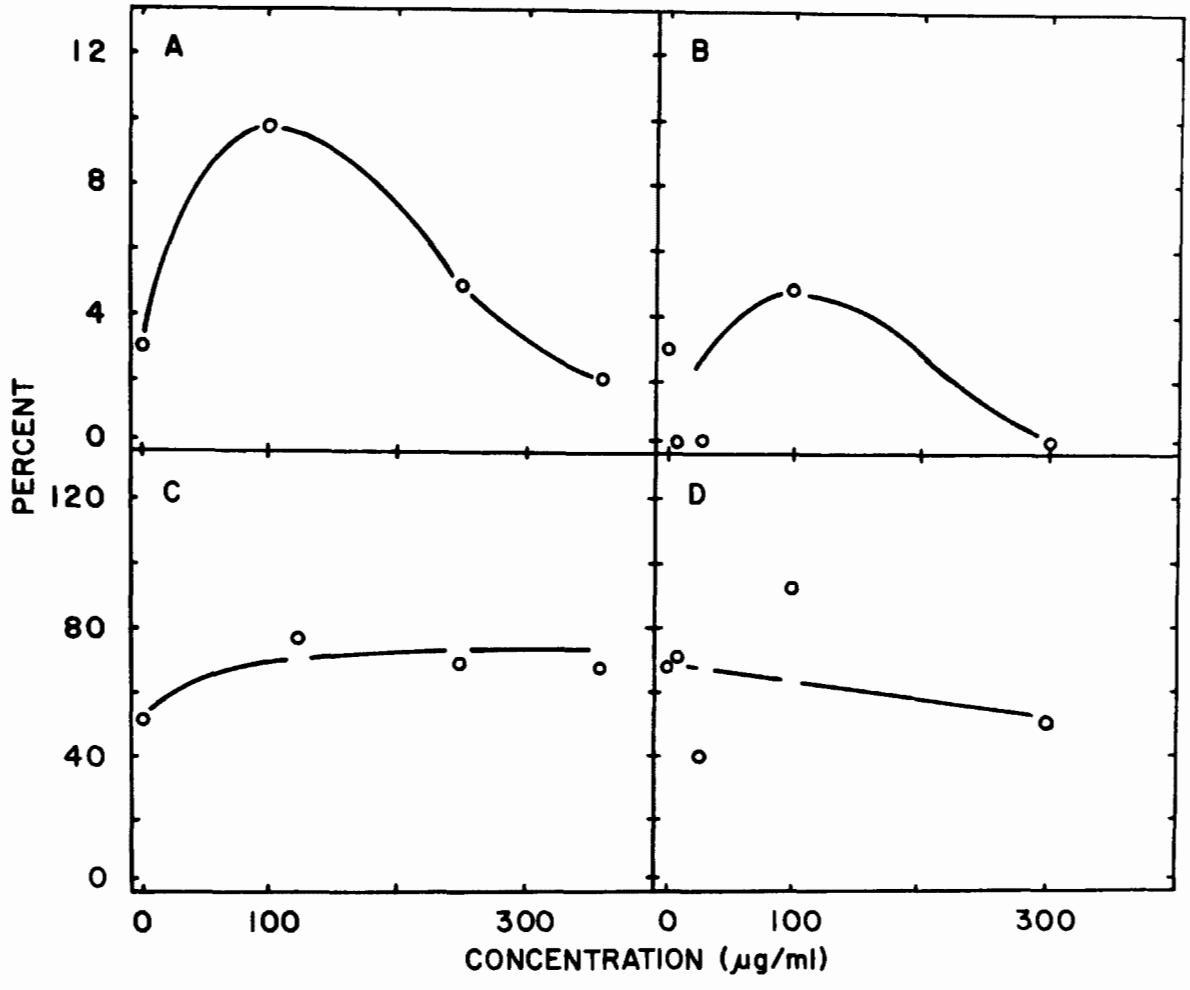

Figure 3. Mutagenic and toxic effects of fly ash in the CHO/HGPRT system. Mutagenicity (A,B) is expressed as percent of a positive control. A. Mutagenicity of 2-5 µ fly ash. B. Mutagenicity of 0-2 µ fly ash. C. Long-term survival of cells treated with 2-5 µ fly ash. D. Long-term survival of cells treated with 0-2 µ fly ash.

AUTHOR INDEX

TECHNICAL REPORT DATA
(Please read Instructions on the reverse before completing)

1. REPORT NO.	2.	3. RECIPIENT'S ACCESSION NO.
EPA-600/9-80-039d	IERL-RTP-1064	

4. TITLE AND SUBTITLE
Second Symposium on the Transfer and Utilization of Particulate Control Technology (Denver, July 1979) Vol. IV. Special Applications for Air Pollution Measurement and Control

5. REPORT DATE
Sept. 1980 Issuing Date.

6. PERFORMING ORGANIZATION CODE

7. AUTHOR(S)
F.P. Venditti, J.A. Armstrong, and Michael Durham

8. PERFORMING ORGANIZATION REPORT NO.

9. PERFORMING ORGANIZATION NAME AND ADDRESS
Denver Research Institute
P.O. Box 10127
Denver, Colorado 80210

10. PROGRAM ELEMENT NO.
EHE624

11. CONTRACT/GRANT NO.
R805725

12. SPONSORING AGENCY NAME AND ADDRESS
Industrial Environmental Research Laboratory
Office of Research and Development
U.S. Environmental Protection Agency
Research Triangle Park, NC 27711

13. TYPE OF REPORT AND PERIOD COVERED
Proceedings; 6/79-6/80

14. SPONSORING AGENCY CODE
EPA/600/13

15. SUPPLEMENTARY NOTES IERL-RTP project officer is Dennis C. Drehmel, MD-61, 919/541-2925. EPA-600/7-79-044a thru -044d are proceedings of the 1978 symposium.

16. ABSTRACT

The proceedings document the approximately 120 presentations at the EPA/IERL-RTP-sponsored symposium, attended by nearly 800 representatives of a wide variety of companies (including 17 utilities). The keynote speech for teh 4-day meeting was by EPA's Frank Princiotta. The meeting included a plenary session on enforcement. Attendees were polled to determine interest areas: most (488) were interested in operation and maintenance, but electrostatic precipitators (ESPs) and fabric filters were a close second (422 and 418, respectively). Particulate scrubber interest appears to be waning (288). Major activities of attendees were: users, 158; manufacturers, 184; and R and D, 182. Technical presentations drawing great interest were the application of ESPs and baghouses to power plants and the development of novel ESPs. As important alternatives to ESPs, baghouses were shown to have had general success in controlling coal-fired power plant emissions. When operating properly, baghouses can limit emissions to <5 mg/cu nm at pressure drops of <2 kPa. Not all baghouse installations have been completely successful. Both high pressure drop and bag loss have occurred (at the Harrington Station), but these problems appear to be solved.

17. KEY WORDS AND DOCUMENT ANALYSIS

a. DESCRIPTORS	b. IDENTIFIERS/OPEN ENDED TERMS	c. COSATI Field/Group
Pollution Dust Aerosols Electrostatic Precipitators Filters Fabrics Scrubbers Flue Gases	Pollution Control Stationary Sources Particulate Baghouses	13B 07A 11G 21B 07D 13I 14G 11E

18. DISTRIBUTION STATEMENT	19. SECURITY CLASS *(This Report)*	21. NO. OF PAGES
Release to Public	Unclassified	557
	20. SECURITY CLASS *(This page)*	22. PRICE
	Unclassified	

EPA Form 2220-1 (Rev. 4-77) PREVIOUS EDITION IS OBSOLETE ☆ U.S. GOVERNMENT PRINTING OFFICE: 1980--657-165/0160